Technical Report

TR-11-01

Long-term safety for the final repository for spent nuclear fuel at Forsmark

Main report of the SR-Site project

Volume II

Svensk Kärnbränslehantering AB

March 2011

Svensk Kärnbränslehantering AB
Swedish Nuclear Fuel
and Waste Management Co

Box 250, SE-101 24 Stockholm
Phone +46 8 459 84 00

ISSN 1404-0344
SKB TR-11-01
ID 1271591
Updated 2015-05

Long-term safety for the final repository for spent nuclear fuel at Forsmark

Main report of the SR-Site project

Volume II

Svensk Kärnbränslehantering AB

March 2011

Keywords: Safety assessment, Long-term safety, Final repository, Spent nuclear fuel, Forsmark.

A pdf version of this document can be downloaded from www.skb.se

Update notice

The original report, dated March 2011, was found to contain both factual and editorial errors which have been corrected in this updated version. The corrected factual errors are presented below.

Updated 2015-05

Location	Original text	Corrected text
Page 363, Figure 10-44	Wrong data used in figure	Figure updated with correct data
Page 365, Figure 10-47	Wrong data used in figure	Figure updated with correct data
Page 513, Figure 10-148	Wrong data used in figure	Figure updated with correct data
Page 519, Figure 10-153	Wrong data used in figure	Figure updated with correct data

Updated 2012-12

Location	Original text	Corrected text
Page 383, Table 10-4 heading text	/Åkesson et al. 2010/.	/Åkesson et al. 2010a/.

Updated 2011-12

Location	Original text	Corrected text
Page 403, last paragraph, line 6	...time, four tunnel intersecting...	...time, five tunnel intersecting...
Page 403, last paragraph, line 11	...only four positions...	...only five positions...
Page 403, Figure 10-73	300 tonnes in 25 % of 1,000,000 years 300 tonnes in 100 % of 1,000,000 years	Figure 10-73 updated 220 tonnes in 25 % of 1,000,000 years 220 tonnes in 100 % of 1,000,000 years

Updated 2011-10

Location	Original text	Corrected text
Page 294, paragraph 1, line 7	Chapter 4	Chapter 5
Page 318, paragraph 4 last line	Section 15.4	Section 15.5
Page 330, last paragraph	...and generic stress-transmissivity models,	...and fracture normal stiffness data given in the **Data report,**
Page 334, Figure 10-21, last line in figure text	Figur 6-18	Figur 6-21
Page 337, paragraph 8, last line	Section 15.4.	Section 15.5.15
Page 347, Figure 10-31	$\log_{10}$ m(Fr) (yrs/m)	Figure 10-31 updated $\log_{10}$ (Fr) (yrs/m)
Page 389, second last paragraph, last line	Section 10.3.10.	Section 10.3.11.
Page 417, paragraph 2, line 1	According to the maximum chloride concentration of any time frame is < 0.4 M in the Forsmark groundwater.	According to Table 10-6, the maximum chloride concentration of any time frame is < 0.4 M at repository level in the Forsmark groundwater
Page 424, paragraph 2, line 1	...the initial thermal period,	...the initial temperate period,
Page 424, paragraph 3, line 1	...during the thermal period.	...during the temperate period.
Page 430, paragraph 1, line 8	Section 15.4	Section 15.5.15
Page 430, paragraph 5, last line	Section 15.4.	Section 15.5.15.
Page 436, paragraph 9, line 3	...erosion, few, if any, deposition holes will reach advective...	...erosion, no deposition holes will reach advective conditions...
Page 436, paragraph 10, line 5	...could be lost,	... could be lost in a million year perspective,
Page 454, second last paragraph, last line	Section 3.4.1	Section 10.4.1
Page 459, paragraph 1, line 5	...in the range 40-45 GPa, presented in the Site description, the results...	...in the range 40-45 GPa, suggested to be valid for large scale models of the bedrock surrounding the Forsmark site, the results...
Page 463, paragraph 3, line 1	...hydraulic jacking is...	...hydraulic jacking in front of an advancing ice sheet is...
Page 512, last paragraph, line 2	...network of deformation zones.	...network of fractures.

Updated 2011-10 continued

Location	Original text	Corrected text
Page 525, paragraph 1, line 1 and 2	...during the advance or retreat of an ice sheet in highly transmissive deformation zones cannot be discarded.	...in highly transmissive deformation zones during the advance or retreat of an ice sheet cannot be discarded.
Page 526, last paragraph, line 7	Furthermore, the backfill	Furthermore, the repository closure, which, in accordance with the reference design, is similar to the backfill in the deposition tunnels,
Page 529, paragraph 3, last line	...canister integrity	...canister integrity since no deposition holes will be located there.
Page 537, paragraph 5, line 1	...buffer swelling pressure is sufficiently high around a canister.	....buffer density is high.
Page 537, paragraph 5, line 3	...density range, the swelling pressure criterion is judged to be fulfilled with ample margin, also for groundwater salinities that can be expected during the reference glacial cycle, see Section 10.4.8.	...density range, this safety function is fulfilled.
Page 537, paragraph 5, line 6	For a deposition hole that has experienced loss of buffer mass due to erosion/colloid release and to the extent that advective conditions prevail, this safety function can, however, not be guaranteed.	For a deposition hole that has experienced substantial loss of buffer mass due to erosion/colloid release, this safety function can, however, not be guaranteed.
Page 538, paragraph 6, last line	...estimated to be 43 MPa.	...estimated to be 43.5 MPa.
Page 538, last paragraph, last line	...safety function R3a...	...safety function R3b...
Page 540, paragraph 4 (c), line 2	...periods of glacial conditions...	...periods of temperate and glacial conditions...
Page 541, paragraph 6, line 1	...preliminary quantitative evaluations...	...quantitative evaluations...
Page 542, paragraph 1, line 1	...the buffer swelling pressure is high.	...the buffer density is high.
Page 542, paragraph 1, line 2	...buffer density, the swelling pressure criterion is fulfilled with ample margin, also for groundwater salinities that can be expected during the assessment period, see Section 10.4.8.	...buffer density, this safety function is fulfilled.
Page 542, paragraph 1, line 5	…experienced loss of buffer mass due to erosion/colloid release and to the extent that advective conditions prevail, this safety function can, however, not be guaranteed.	...experienced substantial loss of buffer mass due to erosion/colloid release, this safety function can, however, not be guaranteed.
Page 542, paragraph 5, line 2	...with ample margin for the reference glacial cycle.	...with ample margin.
Page 543, paragraph 4	Between zero and two canisters....	On average less than one canister...
Page 548, paragraph 1, line 1	...and towards the South-East of the candidate repository	...and south-east of the candidate repository
Page 548, paragraph 3, line 3	...less than 200 mg/L	...less than 200 µg/L

Contents

Volume I

Volume II

Volume III

10 Analysis of a reference evolution for a repository at the Forsmark site

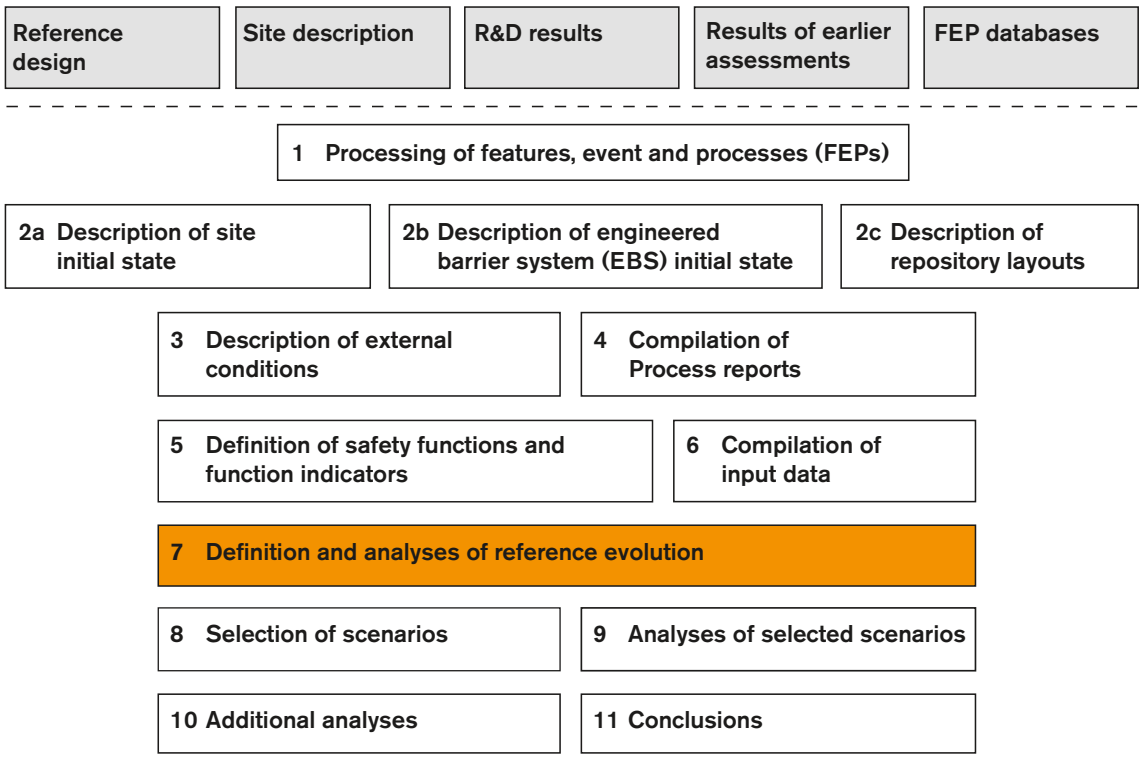

Figure 10-1. *The SR-Site methodology in eleven steps (Section 2.5), with the present step highlighted. This chapter deals with the definition of the reference evolution and with the analysis of the containment potential. Retardation is treated in Chapter 13 (step 9 in the figure).*

10.1 Introduction

This chapter describes a reference evolution of a KBS-3 repository at the Forsmark site over the entire one million year assessment period. The purpose is to gain an understanding of the overall evolution of the system, for the scenario selection and scenario analyses that follow in Chapters 11, 12 and 13. The ambition is to assess the impacts of processes affecting the containment safety functions and to describe a reasonable evolution of the repository system over time. The reasonable evolution is an important basis for the definition of a main scenario, see Chapter 11 and, for details, Section 12.1.2.

Focus is on the containment capacity; consequences in terms of radionuclide releases are not analysed. Chapter 13 describes radionuclide transport and dose consequences for canister failure modes identified in all scenarios, of which the main scenario is closely related to the reference evolution described below.

Two cases of the reference evolution are analysed.

1. A base case in which the external conditions during the first 120,000 year glacial cycle are assumed to be similar to those experienced during the most recent cycle, the Weichselian. Thereafter, seven repetitions of that cycle are assumed to cover the entire 1,000,000 year assessment period. The base case is analysed in Sections 10.2 through 10.5.
2. A global warming variant in which the future climate and hence external conditions are assumed to be substantially influenced by anthropogenic greenhouse gas emissions. This analysis is related to that of the base case and is presented in Section 10.6.

For both cases, the initial state described in Chapter 5 is assumed and all internal processes are handled according to the specification given in the **Process report**, as summarised in Chapter 7.

In order to fulfil its needs, the chapter covers a substantial number of issues and subject areas to a rather detailed level, where the level of detail is to a large extent a reflection of the safety relevance of the issue in question. In fact a large part of all the analyses conducted within the SR-Site project are summarised and put into perspective in this chapter. Also, for reasons explained below, the chapter is divided into different time frames. This structuring makes the chapter longer since the same process needs to be discussed at several occurrences. However, it is preferred, since it helps to demonstrate the comprehensiveness of the analysis and compliance with regulatory criteria, as well as making the approach transparent.

10.1.1 Detailed prerequisites

Initial state of engineered barriers

The initial state encompasses the entire repository with all 6,000 deposition holes and the initial state relates to the conditions expected in the entire ensemble of deposition holes. The initial state, as given in Chapter 5, is the expected result of the production of the engineered components of the repository, including the application of relevant control procedures (see further Section 5.1.1). For example, the initial state of the canister includes welding defects (Table 5-9 in Section 5.4.3) and variations in initial buffer density that were derived taking imperfections in deposition hole geometry, variations in raw material composition and imperfections in the manufacturing process into account (Table 5-13 in Section 5.5.3).

Possible deviations from the initial state given in Chapter 5 are further addressed in the selection of scenarios in Chapter 11.

Geosphere and biosphere initial state

The initial state for the geosphere and the biosphere is that given by the site descriptive model, including uncertainties and possible variants as described in Chapter 4 and quantified for the purposes of SR-Site in the **Data report**. The site-specific layouts are those described in Section 5.2.2.

Process system

The set of processes governing repository evolution is handled according to the information given in the **Process reports** for the fuel/canister, the buffer/backfill/closure, the geosphere and the biosphere. Uncertainties in process understanding and/or model representation are handled according to the procedures established in those reports.

It should be noted that all identified processes are considered in the evolution. If, after consideration, a process is excluded, this exclusion is justified in the **Process report**. The handling is summarised in Table 7-2 through Table 7-6 in Chapter 7. Data uncertainty as identified in the **Data report** is also considered.

External conditions – base case

As mentioned in Section 6.2, it is not possible to predict a single future climate evolution in a long-term perspective with enough confidence for a safety assessment. It is very likely though that the repository site in the long-term will experience periods of all the identified climate domains and all the associated transitions. The reference evolution should, therefore, include periods of temperate conditions including shore-level displacement, both regression and transgression, at different rates, as well as permafrost and glaciation of different extent and also the possible transitions between the domains. A relatively well known evolution including all the mentioned components is the one covered by the Weichselian glacial and the Holocene interglacial, i.e. the evolution from the end of the Eemian (Marine Isotope Stage 5e, see Figure 10-96, Section 10.4.1) at about 120,000 years ago to the present time. In this assessment, this last glacial cycle has been chosen to constitute a reference evolution of climate-related conditions at the Forsmark site.

The selected external conditions of the reference evolution are regarded as one example of a credible development during a glacial cycle. The description in the reference evolution is not an attempt to predict a "most probable" future development. Instead the purpose of the reference evolution is to construct a scientifically reasonable starting point for the analysis of potential climate related impacts on repository safety. It is only necessary to capture the major aspects of the last glacial cycle, since even if for instance the ice sheet development were to be constructed in more detail for the site, the impact of any future glaciation will differ at such a detailed level. Instead, the reference glacial cycle is complemented by additional climate cases that describe more extreme conditions, with for example larger and smaller ice sheets.

The analysis of the evolution is initiated by a 1,000 year long period within which the development is based on extrapolation of current evolution and trends. Thereafter, the analysis is based on a repetition of conditions reconstructed for the Weichselian glacial cycle as it evolved from 120,000 years ago until the present day. At 120,000 years ago, the climate-related conditions are, in a broad sense, considered to have been similar to those existing at the present. For the remainder of the assessment period, this 120,000 years long glacial cycle is assumed to be repeated.

The reason for choosing the reconstruction of Weichselian conditions as the reference evolution is twofold. Firstly, it is the best known of the past glacial cycles and the evolution and variability of climate-related conditions can be investigated by reference to associated geological information. Secondly, the available geological information makes it possible to test or constrain the supporting analysis and modelling efforts aimed at process understanding and the studies of the, often complex, coupled processes related to climate changes. For more information on the approach of using reconstructed last glacial cycle conditions as one example of a future development of climate related issues at Forsmark, see the **Climate report**.

External conditions – global warming variant

An additional factor related to future climate evolution is introduced by the impact and duration of human influence on climate due to emissions of greenhouse gases. Therefore, as a variant of the evolution based on the repetition of the last glacial cycle, a global warming variant comprising a 50,000 year long period of temperate domain, followed by the first, relatively mild, 70,000 years of the base case is analysed, see further Section 10.6 and the **Climate report**, Section 5.1. In addition, a complementary case with more severe global warming is described and analysed, see the **Climate report**, Section 5.2.

10.1.2 Structure of the analysis

The presentation of the analysis of the base case of the reference evolution is divided into four time frames:

- The excavation/operational period, Section 10.2.
- The first 1,000 years after closure and the initial period of temperate domain from the reference glacial cycle, Section 10.3.
- The remaining part of the glacial cycle, Section 10.4.
- Subsequent glacial cycles up to one million years after closure, Section 10.5.

In Section 10.6, the global warming variant is analysed over an entire glacial cycle.

For each time frame, issues are presented in the following order:

- Climate issues.
- Biosphere issues.
- Thermal, mechanical, hydraulic and chemical issues in the geosphere.
- Thermal, mechanical, hydraulic and chemical issues for the engineered barrier system (canister, buffer, backfill and other repository components).

The commentary on each time frame concludes with a discussion of the expected status of the safety function indicators defined in Chapter 8 during and at the end of the time frame.

A considerable part of the material presented results from simulation studies. An overview of these studies is given in the assessment model flow chart, AMF, for the excavation/operation period, the first 1,000 years after closure and a continued warm period, Section 7.5 and Figure 7-3. Table 7-7 explains how the modelling activities in the AMF are documented and the processes that are handled by each model. An AMF for permafrost and glacial conditions is given in Figure 7-4, with the associated Table 7-8.

Figure 10-2 shows the safety functions of the repository system and the safety function indicators used to evaluate whether the safety functions are maintained, as defined in Chapter 8. The safety functions in Figure 10-2 are referred to in the following sections, to explain the safety-related purposes of the analyses undertaken in the evaluation of the reference evolution.

Figure 10-2. *Safety functions (bold), safety function indicators and safety function indicator criteria. When quantitative criteria cannot be given, terms like "high", "low" and "limited" are used to indicate favourable values of the safety function indicators. The colour coding shows how the functions contribute to the canister safety functions Can1 (red), Can2 (green) or Can3 (blue). See Section 8.3 for details.*

10.1.3 Hydrogeological modelling in SR-Site

The systems approach in hydrogeological modelling used by SKB in the **Site description Forsmark** and in SR-Site is to divide the geosphere into three hydraulic domains denoted by HCD, HRD and HSD, where:

- HCDs (Hydraulic Conductor Domains) represent the deterministically modelled deformation zones.
- HRDs (Hydraulic Rock mass Domains) represent the less fractured bedrock in between the deformation zones.
- HSDs (Hydraulic Soil Domains) represent the regolith (Quaternary deposits).

Figure 10-3 shows an overview of the three flow modelling studies made with respect to the safety functions related to the bedrock domains, i.e. HCDs and HRDs /Svensson and Follin 2010, Joyce et al. 2010, Vidstrand et al. 2010/. The modelling methodology, numerical setups including description of utilised data, and summary of results in an SR-Site context of these studies are provided in /Selroos and Follin 2010/. A summary of the results is given in Sections 10.2.3, 10.3.6 and 10.4.6.

Any release of radionuclides reaching the surface system from the bedrock will be directed to the deeper parts of the regolith (i.e. HSD). From there, radionuclides will be distributed up to and within the surface ecosystems by near-surface groundwater and surface water flow systems. In order to support the modelling of radionuclide transport in the surface system, detailed hydrological modelling of the surface system during periods with temperate and periglacial climate conditions has been conducted by /Bosson et al. 2010/. A summary of the results is given in the **Biosphere synthesis report**. Studies of the effects of groundwater withdrawal during the excavation and operational phases on hydrological and near-surface hydrogeological conditions (including groundwater in the HSD) are reported by /Mårtensson and Gustafsson 2010/. These results are used as an input to analyses of ecological and other types of consequences during the mentioned phases, as a basis for the Environmental Impact Assessment (EIA) /SKB 2010a, Werner et al. 2010/.

Figure 10-3 indicates the time period handled by each bedrock flow modelling study and where the results are presented in the present report. The three studies employ different computer codes and modelling teams. The studies conducted by /Svensson and Follin 2010/ and /Vidstrand et al. 2010/ are made with DarcyTools, whereas the study by /Joyce et al. 2010/ is made with ConnectFlow. The studies share the same systems approach and hydrogeological input to support conceptual integration, to allow for consistency checks of the reported flow simulations and to provide a good modelling strategy.

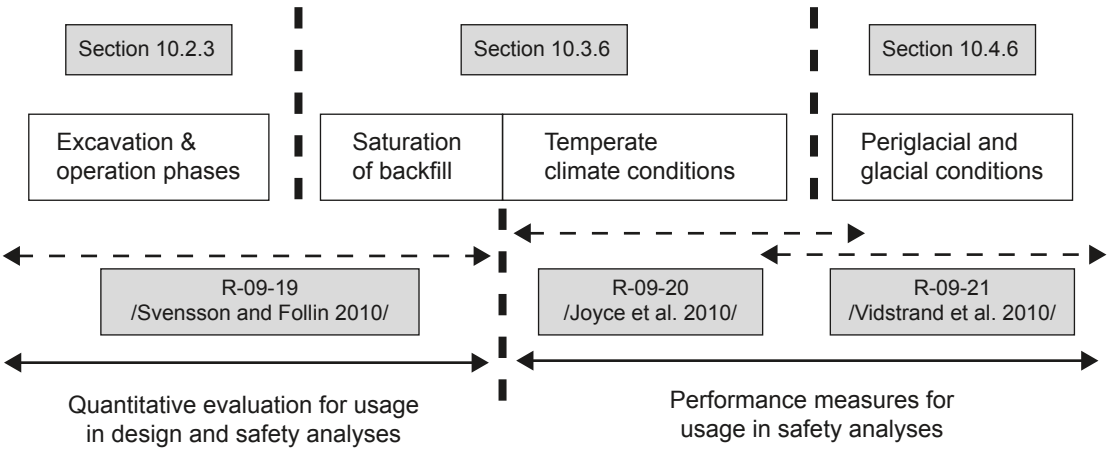

Figure 10-3. *Overview of flow modelling made with respect to the safety functions related to the bedrock.*

In Figure 10-4, the relation between the hydrogeological model presented in the **Site description Forsmark** and in more detail in /Follin 2008/, i.e. the Base model simulation, and the models used in SR-Site are exemplified. The term 'SDM-Site' in Figure 10-4 and in the discussions on hydrogeology in the present report is used synonymously with the **Site description Forsmark**.

A Hydrogeological base case model is derived within the temperate phase modelling. This model is essentially identical to the SDM-Site model, which also was derived using the modelling tool ConnectFlow, but with slight modifications to incorporate features specific to SR-Site. This model is in turn exported to the other two phases, and modified on two accounts. First, modifications are made specific to the other modelling tool DarcyTools, and second, modifications and/or additional parameterisations are made specific to the problems addressed. Within these other phases, the central cases studied are denoted Base cases in order to clearly distinguish them from the central ConnectFlow case (hydrogeological base case) used within the temperate period simulations.

The spatial distribution of waters of different salinities is modelled during all phases since the variation in fluid density affects the flow field and the interactions between waters of different chemical compositions. In particular, the transport of fresh water from the top boundary down to repository depth and the upconing of saline water from below are analysed in detail. The transport of fresh water from the surface during the Temperate and Glacial time periods is important to describe since dilute water conditions over a long period of time affects repository performance.

SDM-Site concluded that the occurrence of horizontal sheet joints of high transmissivities in the uppermost 100 m of bedrock have a profound effect on the percolation depth of the fresh water recharge that started approximately 1,100 years ago as a result of the ongoing shoreline displacement process during Holocene time. In effect, the salinity of the fracture water in the uppermost 100 m of bedrock is generally lower than the salinity of the fracture water below this depth. The increase in fracture water salinity is fairly moderate between –100 and –800 m elevation, where the fracture water salinity is approximately 1% by weight (c. 10 g of total dissolved solids per litre). Below this elevation, the fracture water salinity could be expected to increase significantly with depth. In SR-Site, the salinity at the elevation –2,000 m is set to be about 7% by weight based on data acquired in the 1,660 m deep borehole KLX02 at Laxemar, see /Selroos and Follin 2010, Vidstrand et al. 2010/ for details.

The chemical composition of near-surface groundwater samples gathered in the uppermost 100 m of bedrock reveals that chemical reactions (water-rock interactions) have a profound effect on the composition of the infiltrating rain water. Therefore, the chemical composition of rain water considered in the palaeohydrological groundwater flow modelling is substituted by a modified water composition called Altered Meteroric water. The characteristic composition of this reference water is described in /Laaksoharju et al. 2008/ and in /Salas et al. 2010/.

Besides reactions, the transport of Altered Meteoric water is also affected by matrix diffusion. The matrix porewater data used for modelling come from three boreholes drilled in the target volume, see Section 4.8.2 (or /Laaksoharju et al. 2008, Waber et al. 2009/ for details). The key bedrock matrix

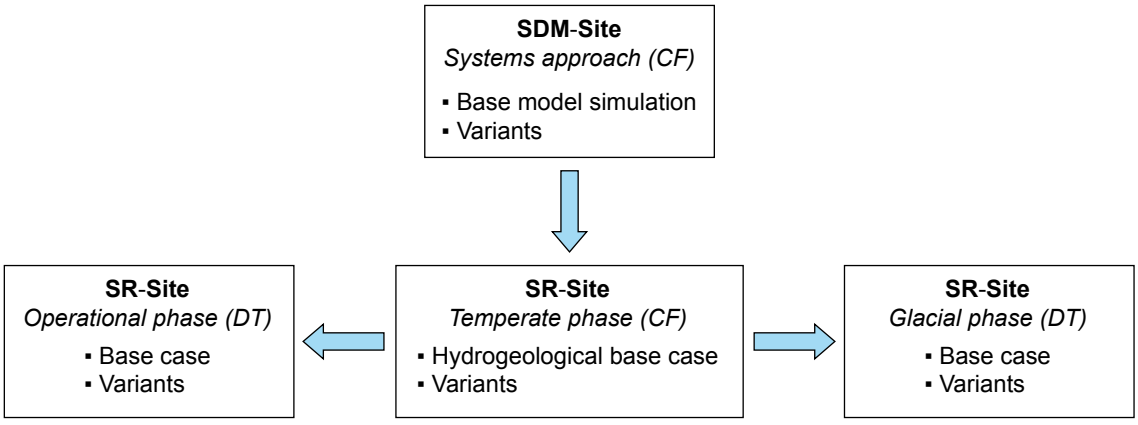

Figure 10-4. *Relation between SDM-Site model, Hydrogeological base case, Base cases and variants. CF and DT denote ConnectFlow and DarcyTools, respectively.*

transport properties governing the penetration length (depth) of a non-sorbing fracture water component are the effective diffusivity and matrix porosity. Albeit an important process for radionuclide transport modelling, particularly for sorbing radionuclides, the penetration into the matrix of Altered Meteoric (or Glacial) water from a flowing fracture nearby is probably not very deep during a glacial cycle. During a period of about 10,000 years, the penetration into the matrix of Altered Meteoric (or Glacial) fracture water could be expected to be on the metre scale, see /Selroos and Follin 2010/.

The interaction between the fracture water salinity and the matrix porewater salinity is also dependent on the spacing between the flowing fractures. At Forsmark, the intensity (frequency) of conductive (flowing) fractures vary considerably with depth within the target volume, see the **Data report**; the fracture intensity is very high above –100 m elevation, whereas it is very low below –400 m elevation. The two types of water, the fracture water and the matrix porewater, should be more alike in the densely fractured bedrock close to surface than in the sparsely fractured bedrock at repository depth, and this is also what the data show as described in the references cited above. At even larger depths, the water circulation is low and the system may become diffusion controlled. Hence, the fracture water and the matrix porewater are more alike.

SDM-Site concluded that the initial hydrochemical conditions of the fracture water at the start of the flow simulations at 8000 BC can be modelled by mimicking the present-day depth trends in matrix porewater salinity within the target volume and outside this volume, respectively, see Section 4.8.2 and /Follin 2008/ for details. This simplification is accepted in SR-Site since the key changes in the top boundary conditions during Holocene time between 8000 BC and 2000 AD are sufficient to create differences between the fracture water and matrix porewater that resemble the observed differences /Follin 2008/. The key hydrological changes are the intrusion of Littorina Sea water, that began approximately 6500 BC, and the subsequent flushing by Altered Meteoric water that started approximately 900 AD, see /Follin 2008/ for details. In principle, these palaeohydrological phenomena have a greater effect on the near-surface fracture water salinity than on the matrix porewater salinity at repository depth.

10.2 The excavation and operation phases

The analyses for the excavation, construction and operation phases of the repository have mainly focused on disturbances of the mechanical, hydrological and chemical conditions induced by the excavation/operational activities.

The duration of this stage can be assumed to be several tens up to a hundred years, depending on the progress of the excavation/operational activities and the total number of canisters to be disposed.

10.2.1 Thermal evolution of the near field

The undisturbed rock temperature at repository depth is around 11.2°C, see the **Data report**, Section 6.2. As the rock is excavated, this temperature will be slightly affected by ventilation of the excavated volumes. This effect is small and of negligible significance compared with the thermal impact of the residual radioactivity of the gradually deposited spent nuclear fuel. This will alter the rock temperature for thousands of years and is, therefore, handled in more detail in Section 10.3.4, which is part of the description of repository evolution during the initial period of temperate climate after closure.

Since the repository is gradually excavated and operated, the thermal impact of the residual radioactivity will also be potentially important during the excavation/operational phase. The safety relevant issue is, however, the peak temperatures over time. According to the thermal analyses by /Hökmark et al. 2010, THM-report Chapter 5/, peak buffer temperature is underestimated by less than 0.2°C if simultaneous deposition is assumed, compared to a case where canisters are deposited in an sequential fashion (i.e. panel by panel) at a rate of 2 or 4 days per canister. However, certain deposition sequencing, although possibly non-practical, may result in higher temperatures for a few canisters. This issue is further discussed in Section 10.3.4.

Identified uncertainties and their handling in the subsequent analysis

As already stated, the discussion on thermal evolution during the excavation phase is found in Section 10.3.4.

10.2.2 Mechanical evolution of near-field rock due to excavation

The rock mass at repository depth is under a pre-stressed condition, namely the in situ rock stress. Repository excavation, i.e. removal of rock, creates a localized readjustment of the in situ stresses. This raises several rock mechanics concerns for the construction work, such as the risk of breakouts into excavated volumes, spalling and/or key block instability. These engineering-related rock mechanics issues are evaluated within the framework of the repository design work and reported in the design report /SKB 2009b/, and are to a large extent not of importance for long term safety. However, as further discussed in Chapter 5 and fully assessed in the **Underground openings construction report**, the design and construction of the underground openings must follow specific design premises provided from a long term safety perspective /SKB 2009a/.

The following mechanical processes related to the excavation and the open phase could have potential safety implications (the safety functions refer to Figure 10-2):

- Development of an Excavation Damaged Zone (EDZ) and other impacts on rock permeability (safety function R2ab, see Figure 10-2).
- Spalling, (safety function R2b and also safety functions of the buffer that either directly or indirectly depend on buffer density).
- Reactivation of fractures (safety function R2ab and R3b).
- Induced seismicity (safety function R3bc).

These issues are assessed in the **Underground openings construction report** and the resulting initial state is summarised in Section 5.2.3. However, for transparency the safety relevant conclusions are repeated in the following subsections, together with the assessed implications for the safety functions.

Deposition hole EDZ and spalling

Drilling of deposition holes is not judged to result in any significant damages to the surrounding intact rock. As stated in Section 5.2.3 and in the **Underground openings construction report**, Chapter 6, findings from a comprehensive literature study /Bäckblom 2009/ suggest that for mechanical full face down-hole drilling techniques in competent rock the depth of damaged zone (EDZ) is limited to less than a few centimetres in the rock surrounding the deposition hole. The hydraulic conductivity in such a zone is in the order of 10^{-10} m/s or less. Hence there is high confidence that competent rock conditions prevail for the reference design and consequently that the EDZ axial transmissivity in deposition holes would be less than 10^{-10} m^2/s. However, the magnitude of the connected effective transmissivity may be altered due to occurrences of spalling.

If the initial, pre-excavation, stresses are sufficiently high, spalling may occur during the operational phase in response to the stress redistribution caused by excavation. The **Underground openings construction report** states, based on analyses by /Martin 2005/ and a three dimensional elastic stress analysis, presented in the repository design report /SKB 2009b/, that in the case of the "most likely" stress model, some 100–200 deposition holes (out of 6,000) would experience a spalling depth (overbreak) that exceeds 5 cm, provided the deposition tunnels are aligned between 0 and 30 degrees to the maximum horizontal stress. Due to uncertainty in stress an alternative, "unlikely maximum" stress model is also considered. For the "unlikely maximum" stress model, the deposition tunnel must be aligned parallel to the maximum horizontal stress, but the number of deposition holes that can sustain a spalling depth in excess of 5 cm is approximately the same.

If spalling were to occur prior to waste emplacement, the current reference method stated in the **Underground openings construction report**, would be to remove loose rock debris from localised spalling on the rock walls. Larger overbreak would need to be filled with, for instance, pieces of bentonite or with bentonite pellets before or during installation of the bentonite buffer. The ultimate contingency action is to reject the deposition hole. Thereby it should be ensured that deposition holes will always have negligible EDZ prior to waste emplacement. In conclusion, there are no safety related impacts of the few cases of spalling prior to canister emplacement expected provided the action envisaged in the **Underground openings construction report** is implemented.

New fracturing induced near the tunnel by the excavation work – formation of an "EDZ"

The possibility that the damage done to the rock using the drill-and-blast excavation method will result in zones of increased axial permeability has long been considered. For SR-Site the EDZ is defined as *the part of the rock mass closest to the underground opening that has suffered irreversible deformation where shearing of existing fractures as well as propagation or development of new fractures has occurred*, since this is the long term safety relevant issue of concern for repositories in crystalline rock. It is recognised that other definitions of the EDZ exist that may be more appropriate for other disposal concepts. Clearly, there may also be reversible effects that, together with pure hydrodynamical changes, may impact on the inflow to open tunnels. However, these "skin effects" are of limited importance for the long term safety functions since they only relate to conditions when the repository is open.

As stated in Section 5.2.3 and in the **Underground openings construction report**, Chapter 6, it is possible to control the drill and blasting of the tunnels such that a continuous fracturing along the axial direction of the tunnel will not develop. This was already stated in SR-Can based on experience from the excavation of the TASQ tunnel at Äspö HRL /Olsson et al. 2004/ and has been further confirmed by the intermediate results from the demonstration trial of smooth blasting techniques at the Hard Rock Laboratory in Äspö /Olsson et al. 2009, Ericsson et al. 2009/. These indicate that blast induced fractures in the rock side-walls are dominantly radial and that such fractures will not be continuous along the axial direction of the tunnel over any significant distance, see Figure 10-5. Furthermore, available literature suggests that the hydraulic conductivity in drilled and blasted tunnels is in the order of 10^{-8} m/s /Bäckblom 2009/ although this conductivity could possibly be very local and may not necessarily be created by the excavation activities. However, existing fractures parallel to the tunnel may be reactivated as discussed in the next section.

It is concluded that there is ample evidence that the fractures induced by the drill-and-blast construction work, will not result in a connected zone along the tunnel with a transmissivity above the maximum allowed transmissivity as set out in the design premises. In fact, data suggest that a continuous EDZ would not develop at all. However, given that the occurrence of the EDZ currently can only be assessed

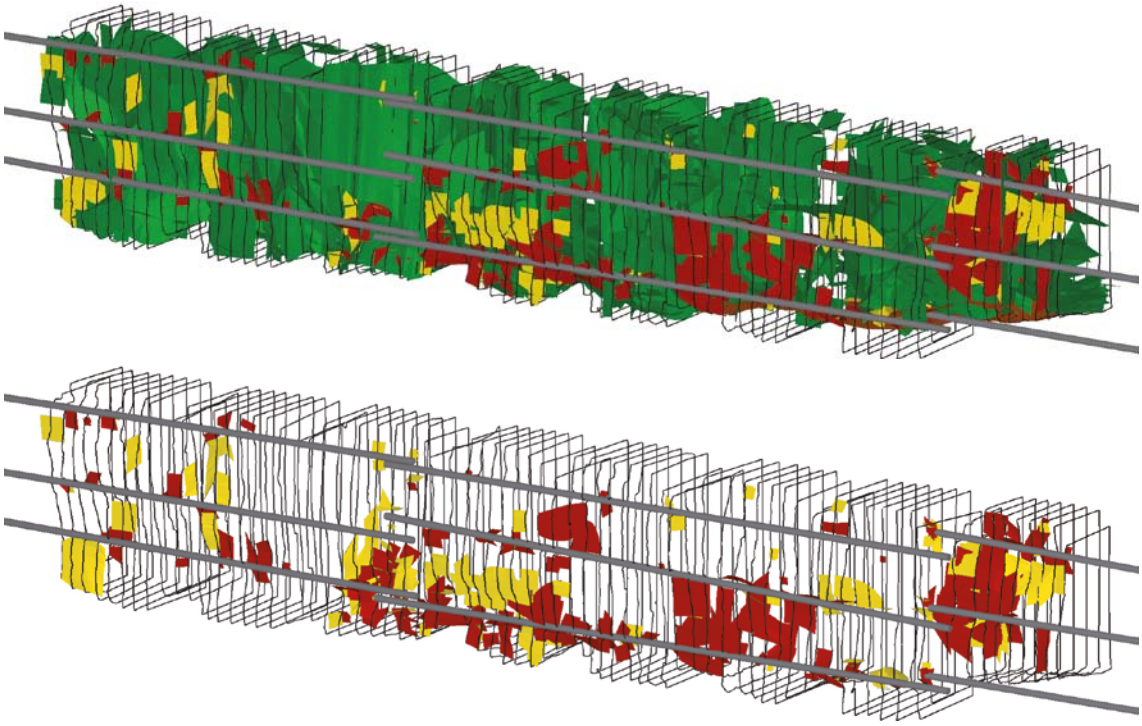

Figure 10-5. *Top: Boreholes, slabs and all interpreted fractures (Natural, Blast and Blast-induced). Bottom: Ditto but with only Blast and Blast-induced fractures. Reproduced from /Olsson et al. 2009, Figures 7-9 and 7-10/. The length of the test area is 8 m and the height is 1.5 m.*

by indirect measurements, it seems justified to consider an EDZ according to the design premises, i.e. with an axial transmissivity of 10^{-8} m^2/s as a basic assumption for further analyses. Furthermore, it also seems justified to explore how transmissive an EDZ needs to be in order to significantly impact other safety functions as well as exploring the impact of no axially continuous EDZ at all. A more rigorous discussion of these matters, together with input data for SR-Site, is found in the **Data report**, Section 6.5.

Reactivation of fractures

The stress redistribution resulting from the tunnel excavation may reactivate some existing near-field fractures. The process has been modelled in a set of numerical analyses /Hökmark et al. 2010/, building on the experience of a similar approach used for SR-Can /Hökmark et al. 2006/. In short the three-dimensional discontinuum programme 3DEC is used to determine stress redistribution effects in fractured near-field rock, and then the results are used to estimate possible permeability changes caused by shear and extensional fracture deformations. The numerical analysis covers a series of events ranging from excavation of the tunnel to the mechanical effects of glacial loading with the boundary stresses resulting from large-scale three-dimensional simulations of mechanical ice/crust/mantle interactions. Relevant changes, i.e. changes that extend more than a couple of metres from the openings, only occur after the thermal load is applied, e.g. starting from the initial temperate phase. More details of the modelling are thus provided later, e.g. starting from Section 10.3.5.

The analysis shows that the normal stress on fractures parallel to the tunnel and close to the tunnel wall or to the tunnel floor will decrease to a few MPa over significant distances, whereas fractures intersecting the tunnel at an angle of a few tens of degrees will show significant stress reductions only very close to the tunnel. However, since gently dipping fractures already have relatively low normal stress, the impact on relative transmissivity of a horizontal fracture is quite small, see Figure 10-6 (left). Furthermore, in reality, large fractures that connect to the flowing fracture network will not be persistently parallel to the tunnel where there are deposition holes, especially since deposition holes intersected by fractures intersecting more than four deposition holes will be rejected according to the EFPC, see Section 5.2.2. For steeply dipping fractures almost parallel to the tunnel, the transmissivity change is, at most, a factor of 6–7 on the intersecting fracture, Figure 10-6 (right), but it is confined to a limited area. This means that this effect can be discarded, or at least captured within the EDZ assumption of 10^{-8} m^2/s along the tunnel.

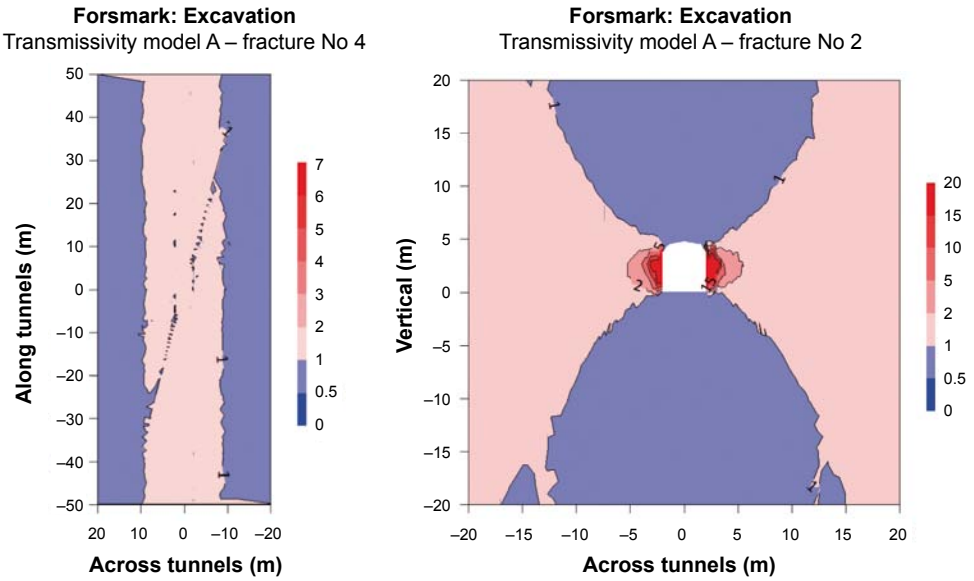

Figure 10-6. *Relative transmissivity change due to stress impact from the tunnel boundary in a fracture (left) parallel to the tunnel floor and (right) a vertical fracture intersecting the tunnel at a small angle. See Figure 10-19 for an illustration on how the modelled fractures intersect the deposition tunnel. Modified after Figures 8-16 and 8-12 in /Hökmark et al. 2010/.*

Induced seismicity

The excavation activities may, induce seismicity through the generation of new fractures or reactivation of pre-existing fractures. However, as argued in the **Geosphere process report**, neither of these possibilities needs further consideration in SR-Site. As further discussed in the **Geosphere process report**, Section 4.3.7, seismic events that could impair the integrity of the already deposited canisters, would require an induced earthquake of approximately magnitude 5. To host such an earthquake, the structure must have a rupture area exceeding a square kilometre and it is unlikely that such a structure would remain undetected after tunnel mapping. Furthermore, there is no evidence that present-day deviatoric stresses in Swedish bedrock at repository depth are sufficient to power seismic events of magnitude 5.

Identified uncertainties and their handling in the subsequent analysis

The discussion above is used to draw a set of conclusions regarding the uncertainties and their subsequent handling in the SR-Site analyses related to the mechanical evolution during the excavation phase.

- There are no safety related impacts of the few cases of *spalling prior to canister emplacement* expected provided the action envisaged in the **Underground openings construction report** is implemented. Heating from already deposited canisters may increase stress and cause spalling in and additional loss of holes prior to canister emplacement. This allows the exclusion of the phenomenon in question in the risk calculation.
- There is ample evidence that an *EDZ formed during excavation* will be kept below the maximum allowed transmissivity as set out by the design premises and data suggest that a continuous EDZ would not develop at all. However, given that the occurrence of the EDZ currently can only be assessed by indirect measurements, it seems justified to consider an EDZ according to the design premises, i.e. with an axial transmissivity of 10^{-8} m^2/s as a basic assumption for further analyses. Furthermore, it also seems justified to explore how transmissive an EDZ would need to be in order to significantly impact other safety functions as well as exploring the impact of no axially continuous EDZ at all. A more rigorous discussion on these matters, together with input data for SR-Site, is found in the **Data report**, Section 6.5, which propagates this uncertainty into a set of distinct calculation cases for the hydrogeological assessment.
- *Reactivation of fractures* caused by the stress redistribution only results in insignificant increases of transmissivity in near-field fractures, apart from very locally close to the tunnel. These limited fields of increased transmissivity will have little importance, unless the fracture is located close to the tunnel floor and approximately parallel to it. However, in reality large fractures connected to the flowing fracture network will not be persistently parallel to the tunnel where there are deposition holes, especially since deposition holes intersected by fractures intersecting more than four deposition holes will be rejected according to the EFPC. This means that this effect can be discarded, or at least captured within the EDZ assumption of 10^{-8} m^2/s along the tunnel.
- *Induced seismicity*: The implications of induced seismicity can be excluded in the risk calculation.

10.2.3 Hydrogeological evolution

During the excavation and operational phases, the tunnels will be at atmospheric pressure and the inflow of water to the open repository will depend on the hydraulic properties of the intersecting, water conducting fractures. The inflow may result in a redirection of flow and in changes of the groundwater flow pattern, potentially resulting in drawdown of the water table, infiltration of near-surface waters into the deeper parts of the bedrock, and in upconing of saline water from depth. The actual impacts primarily depend on the permeability distribution of the rock, the repository layout and on the tightness of the underground construction, which in turn depends on the grouting efficiency. In order to assess the magnitude of these impacts, groundwater flow simulations, based on the hydrogeological models developed as part of the **Site description Forsmark**, are performed. The overall objective is to assess the effects of an open repository on site hydrogeochemical and hydrogeological conditions, i.e. safety functions R1 and R2 in Figure 10-2.

The expected effects of the operational phase with relevance for long-term safety are related to changes in groundwater flow and chemistry. Inflow rates into tunnels and deposition holes during the operational phase are relevant both for construction issues and long-term safety. Near-surface effects such as lowering of the groundwater table are of primary interest for the environmental impact assessment.

Methodology

The groundwater flow modelling of the excavation and operational phases conducted by /Svensson and Follin 2010/ using the DarcyTools modelling tool has the following key components.

- An unstructured grid that allows for a spatially varying resolution of the computational grid. For SR-Site, a fine resolution is used in the proximity of the repository.
- A tunnel routine that allows for detailed inflow simulations to the repository, including analyses of grouting efficiency and canister failures.
- A phreatic surface algorithm that allows for a spatially varying elevation of the groundwater table. For SR-Site, the disturbance of the water table (drawdown) as a function of the grouting efficiency is analysed.
- Variable-density flow. For SR-Site, the potential for upconing of more saline water present at depth is analysed.
- An approach for studying the saturation of backfilled tunnels. For SR-Site, the hydration process of the initially unsaturated backfill material is analysed in several ways. The results reported by /Svensson and Follin 2010/ are presented in Section 10.3.6.
- Spatially varying equivalent continuous porous medium (ECPM) properties. For SR-Site, the ECPM properties were derived through up-scaling of deformation zone and discrete fracture network (DFN) realisations generated in the groundwater flow modelling of temperate climate conditions using the ConnectFlow modelling tool /Joyce et al. 2010/, see Section 10.3.6.

The traditional approach in ECPM modelling is to assign a low value of the hydraulic conductivity to all parts of the computational grid that do not contain fractures. Besides using the ECPM model grid, /Svensson and Follin 2010/ also provide results for an alternative approach where grid cells not intersected by fractures are deleted, i.e. an equivalent discontinuous porous medium (EDPM) is created. /Selroos and Follin 2010/ conclude that the EDPM model grid is of particular interest for the inflow rejection calculations, see below for details.

Performed analyses and usage within SR-Site

The different cases that /Svensson and Follin 2010/ performed with relevance for the excavation and operational phases are listed below. It is indicated where the results produced by each case are used within the subsequent analyses in SR-Site.

- **Drawdown of the groundwater table, infiltration of shallow surface water, and upconing of deep saline groundwater.** The operational phase of the repository with tunnels at atmospheric pressure, i.e. water will flow into the tunnels, implies a drawdown of the groundwater table with a possible change of water composition at repository depth. Upconing may also change water composition at repository depth. The drawdown results are used as an input to analyses of ecological and other types of environmental consequences during the mentioned phases, see Section 10.1.3. The upconing results are used as an input to analyses of the groundwater chemistry at repository depth during the mentioned phases, see Section 10.2.5.
- **Inflow calculations.** Since the tunnels are maintained at atmospheric pressure during the operational phase, the natural hydraulic gradients are affected and redirected towards the tunnels. Depending on which tunnels are kept open and which are closed, and also depending on the grouting efficiency achieved, the inflow distribution and magnitude will vary in space and time. The results of these analyses are used primarily within Repository Engineering /SKB 2009b/, but also in the assessment of buffer and backfill (mechanical) erosion during backfilling of the deposition holes and tunnels, see Section 10.2.4.

- **Inflow rejection criteria.** The deposition holes associated with the highest groundwater flow (Darcy flux) during saturated conditions yield the most severe consequences in terms of erosion of the buffer and copper corrosion, see Sections 10.3.11, 10.3.13, 10.4.8 and 10.4.9. Since some degree of correlation in flow characteristics exists between the open conditions and later saturated conditions and it is desirable to avoid deposition hole positions with high Darcy fluxes during saturated conditions, an assessment is conducted concerning the merits of applying inflow rejection criteria during the operational phase, see /Selroos and Follin 2010/ for details. The potential benefits of inflow rejection criteria are further discussed in Section 14.3.

Drawdown of the groundwater table, infiltration of shallow surface water, and upconing of deep saline groundwater

Three different stages of operation, A–C, are considered, see Figure 10-7. The three stages are run in sequence, where the first stage, stage A, lasts for 15 years, stage B lasts for 15 years and stage C lasts for 20 years. Hence, the total operational time is 50 years. The different stages imply that different parts of the repository are kept open while the other parts are not yet excavated or are already backfilled. Furthermore, for each stage, three different levels of grouting efficiency are assessed. These are:

- Level I: The hydraulic conductivity of all cells in contact with the repository has a maximum value of 10^{-7} m/s.
- Level II: The hydraulic conductivity of all cells in contact with the repository has a maximum value of 10^{-8} m/s.
- Level III: The hydraulic conductivity of all cells in contact with the repository has a maximum value of 10^{-9} m/s except where the modelled ungrouted hydraulic conductivity is 10^{-6} m/s or greater. At these positions the hydraulic conductivity has a maximum value of 10^{-8} m/s.

Results are produced for all combinations above. However, here only a set of key illustrations are presented for operation stage C and grouting level II.

Operation stage C implies the largest inflows and hence the strongest perturbation of the initial salinity field. Also, since operation stage C is the last stage, the chemical conditions have already to some extent been perturbed during the first two operational stages. The modelled drawdown is relatively small with maximum values around one metre except for the central area (CA) of the repository, where a drawdown of around ten metres is obtained /Svensson and Follin 2010/.

Comparing the salinity for conditions prior to the construction of the repository with conditions during operation stage C, it is observed that a dilution occurs around most parts of the repository. That is, fresh water is drawn towards repository depth due to the lowering of the groundwater table. A corresponding upconing occurs, but water with higher salinity is found only around the central area with ramp and shafts. It is also noted that surface water with a higher salt content may infiltrate into the bedrock from the brackish Baltic Sea.

The recharge area for water entering the repository is assessed by backward particle tracking. The results in /Svensson and Follin 2010/ indicate that most of the recharge to the repository is located right above the facility, i.e. within a small radius of influence as expected.

The deep repository for spent nuclear fuel and the SFR[15] facility will likely be in operation simultaneously. /Svensson and Follin 2010/ simulate various operational cases of the two repositories as a means to investigate their hydraulic contact. In summary, during the time when both repositories are in operation, the recharge area of the deep repository does not include the SFR facility. This is due to several reasons, e.g. the SFR facility is located beneath the sea floor, the existence of the thick, steeply dipping, regional Singö deformation zone that strikes perpendicular to the cross-section between the two repositories, and the fact that a water divide forms due to the pumping needed to keep both repositories open.

[15] The SFR facility for low and intermediate waste is located outside the target area approximately one kilometre to the north of the final repository at approximately 50–100 m depth below the Baltic Sea.

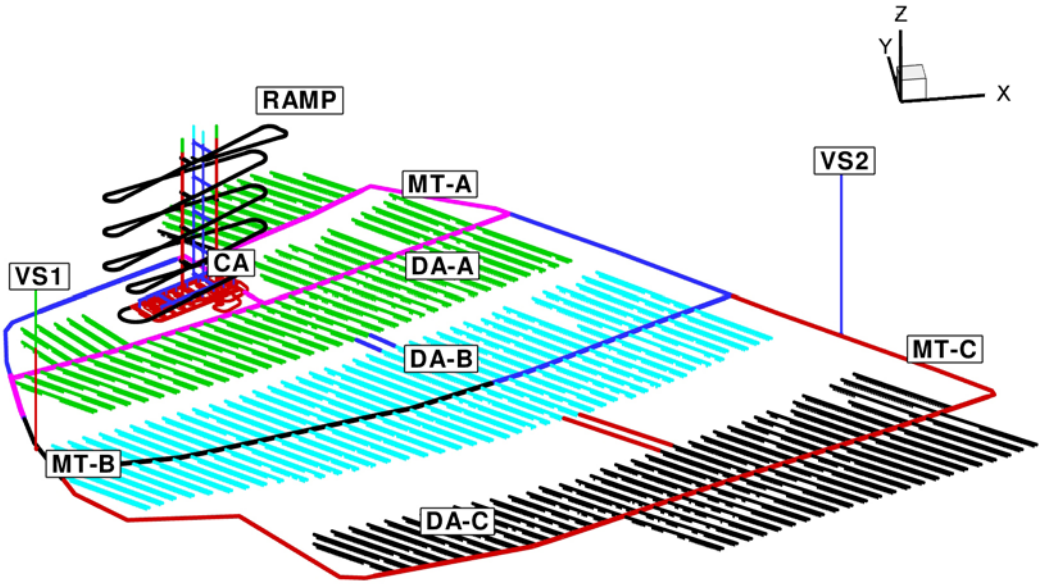

Figure 10-7. *Definition of different parts of the studied repository layout. The modelling considers three operational stages (A–C) and three possible grouting levels for each stage. The three stages are indicated by green, turquoise and pink colours. DA = deposition area, MT = transportation and main tunnel, VS = ventilation shaft, CA = central area.*

Inflow calculations

The calculated inflow during the different operational stages and grouting levels using the ECPM model grid are presented in Table 10-1. The total inflows vary from 8 to 51 L/s depending on the stage of operation (A–C) and the level of grouting efficiency (I–III), For the case discussed above, i.e. operation stage C and grouting level II, the inflow is 28 L/s. The inflows mainly occur at the boundaries of the repository. This is due to the fact that the largest gradients are found at the boundaries between the repository and the outside rock volumes. Also of interest to note is that for grouting level I, i.e. the lowest grouting efficiency, the main inflows occur in the ramp. The ramp penetrates the transmissive sheet joints encountered at shallow depths in Forsmark /Follin 2008/; hence, large inflows occur for the case with a low grouting efficiency.

The sensitivity to inflow is tested by applying a second realisation of the underlying fracture network combined with heterogeneous deformation zones, see /Svensson and Follin 2010/ for details. In this comparison, grouting level II is used in combination with the condition that the whole repository is kept open. It is noted that in the base case realisation, each deformation zone has a unique but homogeneous value of hydraulic conductivity including a constant depth trend. Thus, the resulting values using the second realisation are not directly comparable to Table 10-1. The base case realisation yields a total inflow rate of 31.2 L/s, whereas the second realisation yields a total inflow rate of 33.4 L/s. The magnitude of the total inflow rates as well as the variability in inflow rate between the two realisations is considered small.

Inflow rejection criterion

According to the design premises /SKB 2009a/ “The total volume of water flowing into a deposition hole, for the time between when the buffer is exposed to inflowing water and saturation, should be limited to ensure that no more than 100 kg of the initially deposited buffer material is lost due to piping/erosion. This implies, according to the present knowledge, that this total volume of water flowing into an accepted deposition hole must be less than 150 m^3”.

Table 10-1. Calculated inflow rates (L/s) to different parts of the repository for three levels of grouting efficiency (I–III) and three stages of operation (A–C). CA = central area, DA = deposition area, MT = transportation and main tunnels, VS = ventilation shaft.

Part of repository	Grouting level I			Grouting level II			Grouting level III		
	Operation stage			Operation stage			Operation stage		
	A	B	C	A	B	C	A	B	C
CA	4	4	5	2	2	2	1	1	1
DA-A	6	–	–	4	–	–	3	–	–
DA-B	–	8	–	–	6	–	–	3	–
DA-C	–	–	9	–	–	8	–	–	4
RAMP	16	17	17	6	6	6	2	2	2
MT-A	6	6	7	4	4	5	2	2	2
MT-B	–	1	1	–	1	1	–	0	0
MT-C	–	–	9	–	–	5	–	–	2
VS1	1	1	1	1	1	0	0	0	0
VS2	–	2	2	–	1	1	–	0	0
Total	33	39	51	17	21	28	8	8	11

In the reference design, see Section 5.2.3, it is judged that this design premise is met if

- Potential deposition holes with inflows greater than 0.1 L/min are avoided (inflow criterion #1 in /Svensson and Follin 2010/).

As explained above, it is also of interest to evaluate to what extent high inflow rates during the operational phase are correlated to deposition holes with high Darcy fluxes during saturated conditions. If this is the case, avoiding deposition holes with high inflow rates would also have potential advantageous implications for long term safety. In order to investigate this, the EDPM approach in /Svensson and Follin 2010/ is used. The inflow rejection criteria are applied for the inflow calculations for the operational phase analyses described above, and then recording the impact on the distribution of equivalent flow rates and flow-related transport resistance for the remaining deposition holes.

Figure 10-8 shows the positions of the deposition holes failing inflow criterion #1 using the base case realisation and the EDPM model grid. The number of failing deposition hole positions is 88 out of 6,916.

In /Selroos and Follin 2010/, an analysis is conducted to assess whether the inflow rejection criteria are able to identify deposition hole positions with unfavourable characteristics for long term safety; i.e. deposition holes with a high Darcy flux during saturated conditions. Based on the correlation found between deposition hole inflows during open repository conditions and the Darcy flux at deposition hole positions during saturated conditions, it is concluded that inflow rejection criteria should be able to identify deposition holes with unfavourable characteristics for long term safety. Furthermore, the inflow rejection criteria appear as a good complement to the EFPC criterion in terms of identifying hydraulically unfavourable deposition hole positions. The outcome of this analysis is further assessed in Section 14.3.

Identified uncertainties and their handling in SR-Site

General uncertainties related to the hydrogeological modelling, specifically the use of discrete fracture network (DFN) modelling within hydrogeological modelling, are discussed in more detail in the **Data report** (Section 6.6) and in /Selroos and Follin 2010/. Here, a set of conclusions regarding the uncertainties in the hydraulic evolution during the excavation and operational phases and their subsequent handling in the SR-Site analyses are drawn based on the discussion in the above sub-sections.

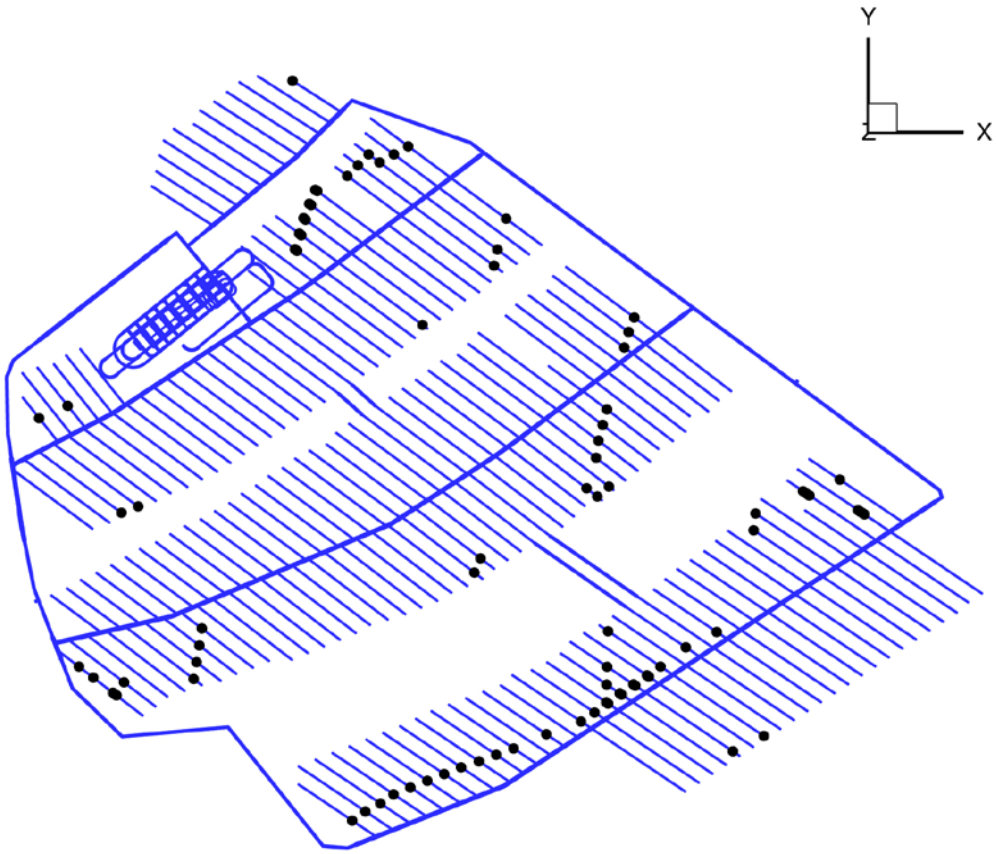

Figure 10-8. *Illustration of the 88 deposition hole positions, out of 6,916 deposition hole positions, failing inflow criterion #1 in /Svensson and Follin 2010/ using the equivalent discontinuous porous medium (EDPM) approach for the base case realisation.*

Drawdown of the groundwater table, infiltration of shallow surface water and upconing of deep saline groundwater

The results of the analysis of drawdown of the water table, infiltration of shallow water and upconing of saline water from depth are used for assessing the chemical evolution in and around the repository during the operational period, see Section 10.2.5. The results are also used as a starting point for assessing the groundwater flow during resaturation, see Section 10.3.6.

Detailed calculations of the near-surface effects of an open repository are carried out with MIKE SHE /Mårtensson and Gustafsson 2010/ as part of the analyses of ecological and other types of consequences during the mentioned phases, as a basis for the Environmental Impact Assessment (EIA) /SKB 2010a, Werner et al. 2010/, see Section 10.1.3. Based on this comparison, it is noted that the near-surface effects, including the changes in advective (fracture water) salinity around the repository reported by /Svensson and Follin 2010/ may be too large. In conclusion, in the subsequent SR-Site analyses, no further action to handle these uncertainties is needed as the calculated water chemistry perturbation is exaggerating the probable effect of salinity dilution.

Inflow to the repository

The calculated inflow to the repository is used as the input for assessing the evolution, mainly piping and erosion of the buffer and the backfill on the already sealed deposition tunnels during the operational phase, see Section 10.2.4. The inflows are also used as input for assessing the saturation of buffer and backfill, see Section 10.3.8.

The tunnel routines implemented in the DarcyTools modelling tool have been verified against an analytical solution and shown to be accurate within 10% /Svensson and Follin 2010/. However, the ECPM approximation may imply an overestimation relative to the discrete system. A comparison has also been performed between DarcyTools and the MIKE SHE modelling tool for a tunnel located

in a porous medium. The difference in total inflow to the open repository is also here found to be within 10% /Mårtensson and Gustafsson 2010/. In the subsequent SR-Site analyses, no further action is needed as the calculated water inflow likely is an overestimation of the true inflow.

Inflow rejection criterion

/Selroos and Follin 2010/ conclude that the EDPM approach described in /Svensson and Follin 2010/ should be applied in subsequent SR-Site analyses when inflow rejection criteria are evaluated.

The potential benefits in applying hydraulically based deposition hole rejection criteria are discussed in Section 14.3 and the findings made there are in turn used as input for the discussion on the need to revise the design premises in Section 15.5.

10.2.4 Evolution of buffer, backfill and plug

During the operational phase the already installed buffer, backfill and plugs may be affected by the groundwater flow seeping into the open repository. This affects the safety functions in the following way:

- When the canisters have been emplaced and the deposition tunnels have been backfilled, a plug is placed at the end of deposition tunnel (see Figure 5-22). The plug is required for the backfill in the deposition tunnel to maintain its barrier function. The performance of the plug affects the flow of water in the backfill and potentially the buffer during the operational phase of the repository when high hydraulic gradients are present. A well-performing plug is needed to ensure that the safety functions related to buffer and backfill density, swelling pressure and hydraulic conductivity (Buff1, Buff2, Buff3, Buff5, Buff6 and BF1) are upheld.
- As long as the buffer and the backfill have not developed a sufficient swelling pressure there is a potential for piping and associated erosion effects in these components. Piping may lead to erosion of bentonite. Erosion is a redistribution of material within the repository. This may lead to a lowered density in certain parts of the buffer and backfill and will affect the safety functions related to buffer and backfill density (Buff1, Buff2, Buff3, Buff5, Buff6 and BF1).
- The swelling properties of bentonite make the buffer and backfill material swell and close open gaps or channels to form a more homogeneous buffer or backfill. Homogenisation of buffer and backfill is crucial to fulfil the safety functions related to buffer and backfill density (Buff1, Buff2, Buff3, Buff5, Buff6 and BF1).
- The reference bottom plate consists of a low pH-cement concrete slab, and a lower and upper copper plate (see Figure 5-23). The only purpose of the bottom plate in the deposition holes is to facilitate the installation of the canister and the buffer. As soon as the buffer is installed in the deposition hole, no more performance is expected from the bottom plate. This, however, does not mean that the bottom plate can be neglected in the long term assessment of the repository.

These issues are assessed in the following subsections.

Water saturation of the plug and its sealing ability

The purpose of the plug is to seal the deposition tunnel and keep the backfill in place during the operational phase until the transport tunnels have been backfilled and water saturated, and have regained their hydrostatic water pressure. It should also limit the flow of water out from the backfilled deposition tunnel to the transport tunnel in order to minimise the effects of piping and subsequent erosion. The design of the plug is presented in Figure 5-22, Section 5.7.2. The discussion in this section concerns the performance of the current design of the plug, but was not covered in the **Buffer, backfill and closure production report** forming the basis for the reference design in Section 5.7.

The water saturation of the bentonite seal in the plug has been modelled /Åkesson et al. 2010a/. In these models the seal, with a thickness of 0.7 m and located between the concrete plug and the filter, was made of bentonite blocks and pellets in a similar configuration to the backfill. Under the condition that there is good availability of water at the plug, either natural or artificial, then the saturation process is a fairly simple one-dimensional hydration problem. If the pellets filling the seal were to seal quickly, then the hydration would only occur from one side, and this process would take around twenty years. If, on the other hand, there were a sustained piping through the pellet filling, then the hydration would be two-sided, resulting in a saturation time of around five years.

To define the required plug performance, the maximum allowed cumulative leakage through the plug is considered to be a certain fraction of the available pore volume of the pellet-filled slots in the entire tunnel. A value of 10% is used as an example in SR-Site. Moreover, although the seal constitutes the main resistance, it will require access to water and time to develop a high flow resistance. During this period the sealing ability will rely on the plug itself (or actually the low transmissivity between the concrete and the rock). These circumstances thus imply a relation between: i) the maximum allowed leakage, ii) the flow resistance of the plug and, iii) the time needed for the seal to become functional.

The analysis of needed sealing abilities for the plug and the bentonite /Åkesson et al. 2010a/ shows that an aperture smaller than ~5 μm in the contact zone between the concrete plug and the rock surface is required in order to obtain a sufficiently high flow resistance in the concrete plug/rock interface itself if the entire water pressure gradient is taken by the concrete plug without considering the sealing ability of the clay seal. A larger aperture can nevertheless be acceptable if the hydraulic conductivity of the pellet-filled slot in the clay seal is taken into account. If this conductivity is lower than approx. 10^{-10} m/s, then there is no need to rely on the plug/rock interface. It is noted that this value is much higher than the hydraulic conductivity at the expected density of the homogenised seal.

Piping erosion

An additional hydraulic issue during the operational phase concerns piping and associated erosion effects in the buffer and backfill. Water inflow into the deposition hole will take place mainly through fractures and will contribute to the wetting of the buffer. However, if the inflow is localised to fractures that carry more water than the swelling bentonite can adsorb, there will be a water pressure in the fracture acting on the buffer. Since the swelling bentonite is initially a gel, which increases its density with time as the water goes deeper into the bentonite, the gel may be too soft to stop the water inflow. The results may be piping in the bentonite, formation of a channel and a continuing water flow and a consecutive erosion of bentonite particles. There will be a competition between the swelling rate of the bentonite and the flow and erosion rate of the buffer. This is further discussed in the **Buffer, backfill and closure process report**.

Piping will take place and the pipes remain open if the following three conditions are fulfilled at the same time:

1. the water pressure p_{wf} in the fracture, when the water flow is prevented, is higher than the sum of the counteracting total pressure from the clay and the shear resistance of the clay,
2. the hydraulic conductivity of the clay is so low that water flow into the clay is sufficiently prevented so as to keep the water pressure at p_{wf},
3. there is a downstream location available for the flowing water and the removal of eroded materials in order for the pipe to stay open.

Erosion will take place if the drag force on the clay particle from the water movement is higher than the sum of the friction and attraction forces between the particle and the clay structure.

Erosion can occur both as a consequence of channels caused by piping and over the long-term at the interface between the clay and the fractures in the rock. Since the water flow rate in the latter case is very low, erosion will only be important for colloids leaving the clay gel that has penetrated into the fractures.

The consequence of piping will be a channel leading the flowing water out to dry or unfilled parts of the repository. Since the clay swells, the channel will reduce in size with time, but on the other hand the erosion will counteract and tear off bentonite particles and thus increase the size of the channel. There is thus a competition between swelling clay and eroding clay. If the inflow is low and the increase in water pressure slow the pipe may seal before water pressure equilibrium has been reached.

The consequence of piping is always that there will be erosion of material that has been torn off from the pipes. That material is transported in the pipes out into either a stagnant part of the backfill where the eroded material may settle or out from the backfill into the open transport tunnel.

After completed water saturation and homogenisation of the buffer and backfill and re-establishment of the hydrostatic water pressure, the water pressure can be separated from the swelling pressure according to the effective stress theory. The pipes or openings caused by the erosion will thus be healed and a swelling pressure established if the density and resulting swelling pressure are high enough to overcome the internal friction. After the initial stage, there is very little risk that piping will occur again, since piping requires a strong and fast increase in water pressure gradient locally in the rock at the contact with the buffer or backfill.

Problem description

There are some general understandings of how flowing water interacts with bentonite after installation at repository depth that are important for the behaviour of the buffer material in the deposition hole after exposure to the natural ground water inflow.

- Before swelling the pellet filling cannot stop the water inflow since the water pressure that will occur if the water inflow is stopped is in the order of several MPa and the swelling pressure of the pellet filling is initially only about 100 kPa.
- It will take several years for the buffer and even more for the backfill to generate a swelling pressure that is high enough to stop the water inflow.
- The consequence of this is that, when the tunnel is filled with water after installing the plug, new channels that distribute the water to empty parts will steadily be formed until the slots are filled with water. When the slots are filled the water pressure in the tunnel will start to rise and the hydraulic gradients will be taken by the plug instead of by the bentonite and the inflow will be strongly reduced.
- Since the pellet filling cannot stop the water inflow there may consequently be channels in the pellet filling in the deposition hole leading to the tunnel. However, this will only be the case if there is an inflow of water in the deposition hole.
- Numerous measurements of water flowing in channels in bentonite pellets or on the surface of bentonite blocks show that the discharging water contains bentonite collected on the way through the channels due to erosion. Water flowing in channels out from the deposition hole will thus transport bentonite from the deposition hole into the backfill.

Since piping and subsequent erosion cannot be prevented by the pellet filling in the buffer or the backfill it is important to try to estimate the amount of bentonite material lost by erosion especially from the buffer in a deposition hole.

In SR-Can the loss was estimated with a simple expression based on a description by /Börgesson and Sandén 2006/. A loss of 1–10 g dry mass of bentonite per litre eroding water was used as an estimate.

Hydromechanical modelling of erosion processes expected during the operational phase has not been done due to lack of models and tools. However, measurements show that limits can be set to the effect of the erosion. An empirical model of the erosion rate has been developed and is used to estimate the erosion for different cases.

Erosion estimates in deposition holes

The erosion from a deposition hole out to the tunnel and to some extent possibly out through the plug is to a large degree a function of the total volume of eroding water. If the water inflow is strong, water will at first fill up the open pore space in the pellet filling both in the buffer and in the backfill before any significant amount of water is absorbed by the buffer or backfill blocks since there is no resistance against water flow in the pellets while the very low hydraulic conductivity in the blocks limits the water uptake rate in the blocks. Thus the volume of the open pore space available for water in the pellet filling is an important parameter, but also the unsaturated voids in the blocks and the possible leakage through the plug is of relevance. The voids in the blocks cannot be neglected if the total inflow to the tunnel is relatively low.

According to the **Buffer production report** and the **Backfill production report** the total empty pore volume in the buffer and the backfill in a 300 metres long tunnel with 50 deposition holes is ~1,050 m^3. Some leakage through the plug cannot be ruled out, depending on the tightness of the plug. It is presently not known how tight these plugs can be made. As an illustration, it is assumed that additionally 20% of the total volume in the tunnel will leak out through the plug. This yields a *total possible water volume that could flow into the tunnel,* V_t, of ≈ 1,250 m^3.

A large number of erosion tests have been performed. The results from some of these are presented in /Sandén et al. 2008/. Different materials, flow rates and flow lengths have been used for the tests but all those tests were done with horizontal flow directions. A number of additional tests have recently been performed in order to simulate erosion in a deposition hole that mainly takes place in the vertical direction in the pellet filling /Sandén and Börgesson 2010/. Based on the tests an exponential erosion model has been suggested /Sandén et al. 2008/ and /Sandén and Börgesson 2010/. According to the model the accumulated mass of eroded bentonite is related to the accumulated mass of eroding water. Based on the tests an exponential erosion model described by the equation below has been suggested:

$m_s = \beta \cdot (m_w)^{\alpha}$

where

m_s = accumulated mass of eroded bentonite (g)

m_w = accumulated mass of eroding water (g)

β = 0.02–2.0 (general), 0.02–0.2 (vertical piping) = parameter defined by the level of erosion at a certain accumulated water flow

α = 0.65 = parameter defined by the inclination of the straight line relation between m_s and m_w.

As stated above a total volume of about 1,250 m^3 = $1.25 \cdot 10^9$ g water is expected to flow into the tunnel before it is filled with water and sealed including possible leakage through the plug. In an extreme case where all water to the entire tunnel comes from one single deposition hole the eroding mass of bentonite will according to the model be 16.4–164 kg of bentonite. For deposition holes where the inflow is at the limit value for acceptance in accordance with the design premises (see Section 5.2.1) of 150 m^3 the models yields an erosion of 4–41 kg of bentonite. In fact, most of the inflow of water into a deposition tunnel will occur through the periphery of the tunnel itself and not through the deposition holes. The reasons for this are that the volume and surface area of the tunnel are much larger, which means that it is more likely to intersect fractures and that the deposition holes should preferably be placed in location with limited inflow of water.

For the case when the total inflow of water to a deposition tunnel (including deposition holes) is very low, or not measurable, it is difficult to claim that the accumulated inflow to a single deposition hole will be less than 150 m^3. However, in this case the first condition for piping, described in the first paragraph in this section, will not be fulfilled and neither piping nor erosion will occur. The bentonite will have time to absorb all water that enters the deposition hole and the water pressure p_{wf} in the fracture will remain low. The lower inflow limit, when piping cannot occur is still not clearly defined.

Eroded mass in a deposition tunnel

The erosion model described above can be used for the deposition tunnel as well. With a total volume of 1,250 m^3, the largest possible erosion will be 1,640 kg. Erosion in the backfill will basically mean that material is redistributed within the tunnel itself. According to Table 5-21 the total mass of backfill in a 300 m tunnel will be ~10,200 tonnes. Considering the large mass of backfill in the tunnel, a redistribution of 1,640 kg is assessed to have no impact at all on the backfill performance.

Homogenisation after loss of bentonite mass

The swelling properties of bentonite make the buffer and backfill material swell and close open gaps or channels to form a more homogeneous medium. Homogenisation of buffer and backfill is crucial to fulfil the safety functions related buffer and backfill density (swelling pressure and hydraulic conductivity).

Erosion caused by piping will not be prevented by the bentonite as long as water flow and high water pressure gradients persist in the deposition tunnel. This will be the case until the flow and gradients are limited by the tunnel plug. If the erosion is strong, large openings of missing bentonite may locally be formed. The swelling and sealing of bentonite cannot take place unhindered since there is a resistance to swelling caused by friction both internally in the bentonite and between the bentonite and the surrounding fixed walls represented by the rock surface and in some cases the canister.

In order to investigate how well the buffer material seals the openings resulting from the mentioned processes a number of finite element calculations with the code Abaqus have been performed /Åkesson et al. 2010a/.

As described above, erosion during and after installation of the buffer may cause significant loss of bentonite under unsatisfactory conditions.

Two different geometrical cases have been considered:

- The bentonite is lost in the shape of a half torus at the rock surface.
- The bentonite is lost in the shape of a half sphere at the rock surface.

The half torus shape around the deposition hole has been selected to maximise the mass loss around the canister. A more likely geometry would be a vertical half pipe going up towards the deposition tunnel. The geometry and the element mesh of the half torus case are shown in Figure 10-9. This geometry has been used to study the influence of:

- The water supply; water can be supplied from the rock surface, the inside space and the backfill.
- The radius of the half torus, which was varied from 0.034 m to 0.134 m (15–240 kg). (Note that the estimation of buffer loss due to piping erosion shows that for the maximum allowed inflow to the deposition hole (150 m^3) an erosion of up to 41 kg can occur).
- Combinations of the above.

The results from the variations of the water supply show that the final swelling pressure varies very little as a function of the water supply. However, the time for saturation and sealing of a pipe with radius of 67 mm (61 kg) varies from 2.2 years for the case where the water is supplied from rock surface, the inside space and the backfill to 42 years when water is only supplied from the backfill. The final swelling pressure in the original hole (pipe) is around 1.2 MPa. Variations of the radius of the half torus also yielded very similar final swelling pressures, even though 240 kg of bentonite is lost when the radius is increased.

As an illustration of the significance of the piping geometry, a case where water enters the deposition hole at one point, at e.g. a fracture intersection, and where the erosion is very local around the inflow spot, which could be imagined as a loss of bentonite in a half sphere like configuration, has been evaluated (Figure 10-10). This is a more severe case than the torus case since bentonite is lost locally instead of distributed around the canister.

The results show that the swelling process is similar to the case with the half torus. Due to the friction against the rock there is very little swelling along the rock surface. Instead, the bentonite between the canister and the hole swells and seals the hole. Due to the rather thin buffer left between the canister and the spherical hole, the resulting void ratio after completion is rather high (> 1.5), which yields a swelling pressure below 1 MPa in about 1/3 of the buffer. This piping geometry would then violate the safety function criteria for the buffer. However, this case does not reflect a possible piping situation, since there is no exit point for the flow. It is noted that, even though the safety function is violated, the mass loss is not sufficient to lead to advective conditions (see Section 10.3.9).

Hydraulic interaction bottom plate/package

In order to achieve a sufficiently flat bottom of the deposition hole, a bottom plate is installed in each deposition hole (Section 5.7). In the case where water can enter the deposition hole under the bottom plate, there might be a possibility that the water pressure generated may be sufficient to lift the entire buffer-canister package.

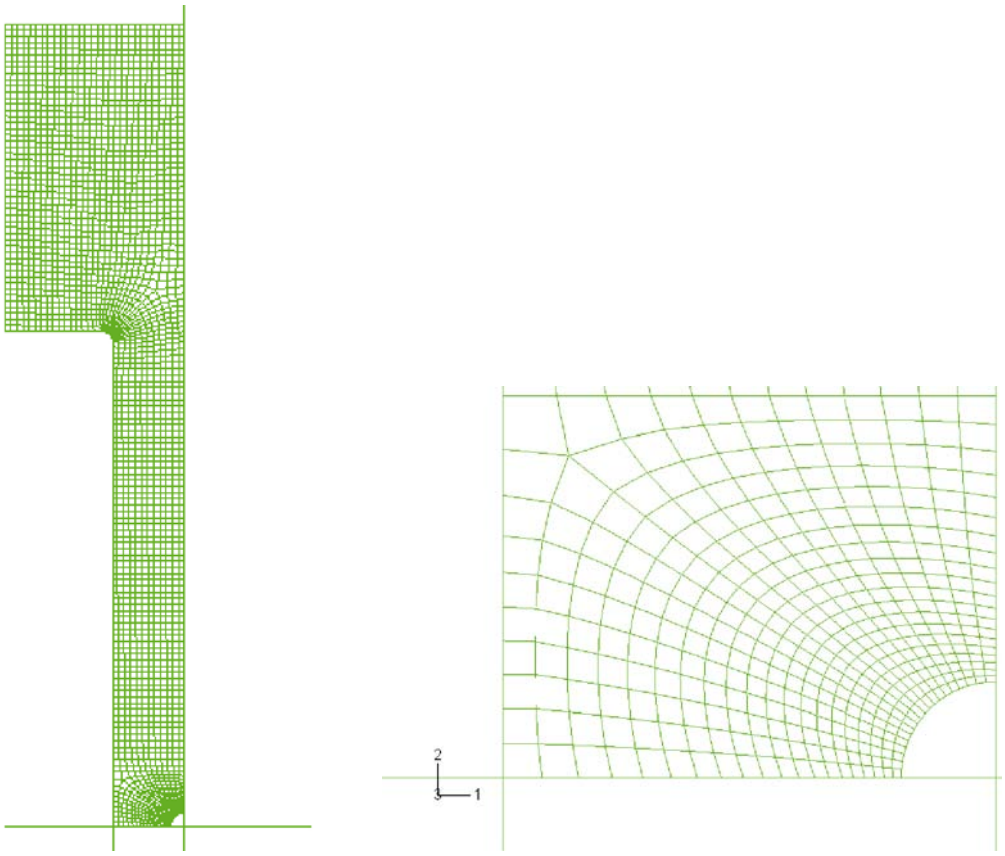

Figure 10-9. *Element mesh of the calculation of a case with a half torus and radius 0.067 m. The mesh is axially symmetric around the left side and the bottom plane is a symmetry plane. The whole mesh and an enlargement of the part with the empty torus are shown /Åkesson et al. 2010a/.*

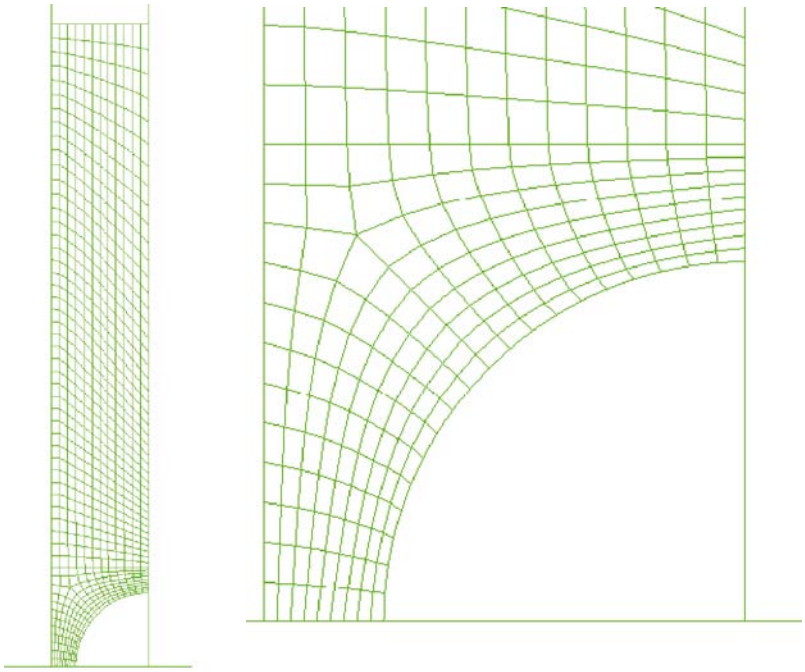

Figure 10-10. *Element mesh for the case with a half sphere with radius 0.263 m. The mesh is axially symmetric around the bottom side. The whole mesh and an enlargement of the empty part are shown /Åkesson et al. 2010a/.*

/Åkesson et al. 2010a/ have studied the potential lifting of the buffer/canister package during the period from the termination of the drainage to the installation of the backfill. This was done for a case in which a water-bearing fracture intersects the deposition hole beneath the bottom plate. In the **Buffer, backfill and closure process report**, it was observed that the contact zones between the concrete and both the copper plate and the rock are not tight, and that this implies that a water pressure can act on the entire surface area.

This is a complex process which is related to the phenomenon of piping and a key issue is how fast the build-up of the swelling pressure can be. The assumption that pellets cannot stop inflowing water until all slots are filled due to piping is pessimistic in other cases, such as for the tunnel plug, but it disregards the build-up of pore pressure upstream. So in this case it is optimistic since such a build-up is unfavourable.

A tailored solution has been developed based on the following assumptions:

1. The hydration varies with time and distance from the bottom plate.
2. The build-up of swelling pressure is proportional to the hydration.
3. The water pressure beneath the package equals the swelling pressure at the bottom.

The build-up of the lifting forces is concurrent with the build-up of the frictional forces along the rock wall. Details of the calculations can be found in /Åkesson et al. 2010a/. These calculations indicate that the time to reach lifting conditions is approximately one week. And the model also suggests that an inflow higher than approximately 100 litres per day will avoid lifting conditions, due to the rapid build-up of the frictional force along the rock wall. The time-scales to reach lifting conditions at low inflows are given directly by the adopted swelling pressure evolution, and the weight of the package, which corresponds to a pressure of 0.2 MPa. The swelling pressure should therefore not be allowed to reach this level as long as the backfill has not been installed.

The empirical data on the initial swelling pressure build-up in large-scale experiments is quite scattered. The chosen swelling pressure evolution in the presented model can nevertheless be regarded to be fairly rapid. This suggests that there should not be any risk of lifting conditions before the installation of the backfill, if a bottom plate is used in a deposition hole with a water-bearing fracture beneath. Still, due to the uncertainty in data, and to some extent also in conceptual understanding, it has not been possible to make any definitive judgment concerning the use of the bottom plate in such holes.

Identified uncertainties and their handling in the subsequent analysis

The function of the plug is to limit the flow of water out from the backfilled tunnel. The primary reason for this is to minimise the effect of piping and subsequent erosion in the buffer and backfill. A certain sealing capability is needed either from the concrete plug or from the bentonite seal within the plug. Modelling has shown that it will take 5–20 years to saturate the bentonite seal within the plug with good availability of water. This means that either the plug/rock interface or the pellet filling in the seal need to limit the flow during that period. In the former case, the required aperture is rather small, while in the latter case the required hydraulic conductivity of the pellets filled slot is relatively high. Two uncertainties related to the sealing ability should be noted. The first concerns the sealing ability of the bentonite seal in a situation where the hydraulic pressure on one side of the seal (4.6 MPa) significantly exceeds the swelling pressure (~2 MPa). It is currently not known if the risk of piping can be neglected in such a situation. The second point is that eroding bentonite is expected to increase the flow resistance of the downstream concrete plug/rock interface. This process is not well known and has not been addressed. The plug design will under all circumstances be adjusted to meet the requirements and failed plug performance is not assessed in SR-Site. This is further discussed in Section 15.5.11. Piping and subsequent water flow from a fracture into a deposition hole and further out into the deposition tunnel cannot be excluded if the inflow rate is higher than the rate of water absorption of the buffer material, since the pellet filling and the bentonite blocks cannot stop the water inflow until the deposition holes and the tunnel are water filled and the hydraulic gradient occurs over the end plug. Erosion tests have shown that the dry mass of eroded bentonite can be modelled as a function of the total volume of inflowing water according to the model discussed in this section, which yields a loss of 41 kg of dry bentonite mass if the inflow requirements on the deposition holes are fulfilled. The model is purely empirical and it is difficult to theoretically derive a model. However, many geotechnical models are empirical (e.g. strength and friction angle relations) for the same reason and have successfully been used for numerous geotechnical design works.

The analysis of homogenisation processes occurring in the buffer after erosion yielding a half torus-shaped pipe indicates a strong decrease in density and swelling pressure in the analysed volume due to the friction in the bentonite. However, the swelling pressure after complete homogenisation is above 1 MPa for the analysed cases with torus radius varying from 3.4 cm to 13.4 cm. The influence of the radius seems to be insignificant due to the long distance to the bentonite boundaries. For the cases when the piping occurs as a half torus (or half pipe) the conclusion is thus that more 100 kg of dry bentonite may be lost from one deposition hole due to erosion without violating the safety function of the buffer. However, the uncertainty in the assessment of the eroded volume needs to be considered when revising the design premises in order to determine the acceptable inflow to deposition holes, see further Section 15.4.

It is expected that most of the inflow of water into a deposition tunnel will occur through the wall of the tunnel itself and not through the deposition holes. The largest possible erosion will be 1,640 kg. Erosion in the backfill will basically mean that material is redistributed within the tunnel itself. Considering the large mass of backfill in the tunnel a redistribution of 1,640 kg can be assumed to have no impact on the backfill performance.

It is evident from the studies described above that additional assessments and possibly development work are needed for the bottom plate. There are uncertainties regarding the current design that are unresolved. These are connected to the thickness and the compressibility of the bottom plate and to the possibility for a lifting of the buffer/canister package before the backfill is in place. However, the safety function indicator criteria for the swelling pressure in the buffer will be maintained. The possibility for lifting of the buffer/canister package is related to the properties of the pellets and may put a stricter requirement on the inflow into the deposition hole, especially into the floor of the deposition hole. These negative effects of the bottom plate are not considered further in SR-Site, but are given as feedback to the need for further design work, see Section 15.5.10.

10.2.5 Chemical evolution in and around the repository

Introduction

During the excavation and relatively long operational period, hydraulic conditions will change as described in Section 10.2.3. The changed hydraulic conditions may alter the groundwater composition around the repository. Some of these changes will be induced by the presence of the repository, but also shore-level displacements and climatic variations may cause more limited alterations. As a consequence, the salinity in some parts of the repository may decrease due to an increased infiltration of dilute waters of meteoric origin, whereas in other regions the corresponding up-coning or the infiltration of Baltic seawater might instead induce an increase in salinity. This involves the safety function indicators R1b and R1c in Figure 10-2, and in extreme cases it might affect the swelling of the backfill, see Section 10.3.9 or enhance colloidal erosion of the buffer during deposition, see Section 10.3.11.

In addition to the groundwater changes caused by hydrological processes, other chemical aspects need to be considered during this period. It is to be expected that the excavation will be accompanied by grouting, and the chemical influence of the grout on groundwater must be considered. In general, cementitious grouts will increase the pH of the water, involving the safety function indicator R1e. During the operational phase, the role of stray materials must be assessed, as well as that of any other process that could possibly change the chemical conditions in the repository, such as the precipitation or dissolution of minerals, corrosion of metal in rock-bolts, etc. These processes might, for example, affect the safety function indicators R1d and R1e in Figure 10-2, that is, the generation of colloids and the sorption properties of minerals.

When deposition tunnels are backfilled and plugged, air will be trapped in the porous buffer and backfill, and processes consuming oxygen must be evaluated. Air will also cause some initial corrosion of the copper canisters until anoxic conditions are reached. All these chemical processes are related to the safety indicators Can1 (copper canister thickness) and R1a (reducing conditions) in Figure 10-2.

Other chemical processes taking place in the buffer and backfill occur on longer time scales than the relatively short operational phase, and they are discussed in Section 10.3.10.

Natural groundwater conditions at the site

The chemical characteristics of groundwater at Forsmark prior to the construction of the repository are set out in detail in the **Site description Forsmark** and supporting documents /Laaksoharju et al. 2008/. A brief account is provided in Chapter 4.

Salinity (upconing effects)

The groundwater salinity and composition in the vicinity of the repository will be affected during the excavation and operational phases because of the inflow into open tunnel sections. This will cause an unnatural infiltration of meteoric and Baltic seawater, and as a consequence of groundwater drawdown and upconing may occur. This phenomenon has been observed for example in some boreholes at Äspö. In extreme cases, if the groundwaters at larger depth have high salinities, the upconing of these waters might decrease the swelling pressure of the backfill, safety function indicator R1b. However, no such highly saline groundwaters have been found at the deepest sampling points at Forsmark. A quick inflow of Baltic seawater would increase the potassium concentrations of the groundwaters, involving the safety function indicator R1d in Figure 10-2.

The inflow to the tunnels will be reduced by injecting grout into the surrounding fractures. This will prevent the depression of groundwater levels near the ground surface and the corresponding inflow of meteoric water and seawater, as well as the upconing of saline waters.

The hydraulic effect of grouting has been modelled, see Section 10.2.3. The results obtained using the code DarcyTools indicate that limited upconing and limited changes in salinities are to be expected during construction and operation of a repository located at Forsmark. Further details are given in Section 10.2.3 and references therein.

Once the repository has been backfilled and closed it is expected that groundwater salinities will return to normal conditions after some time. For example saline groundwaters that had moved upwards due to upconing will then sink due to their higher density.

Redox conditions

Even with moderate inflows to the open tunnels, see Section 10.2.3, large amounts of superficial waters are predicted to percolate when considering the whole period of repository operation. Infiltrating waters will initially be equilibrated with oxygen in the atmosphere, whether they are marine, lake, stream or meteoric in origin. It could be contended that the redox stability of the rock volume on top of the repository area might be challenged at the time of repository closure by the large amounts of infiltrating O_2-rich waters.

However, microbial oxygen consumption takes place in the overburden and in the first metres of rock, as well as in lacustrine, fluvial and marine sediments. Therefore infiltrating waters are free of dissolved O_2. Oxygen consumption in saturated soils is well documented, see for example /Drew 1983, Silver et al. 1999, Pedersen 2006/. The Äspö Redox Zone experiment /Banwart 1999, Molinero-Huguet et al. 2004/ also showed that microbial respiration in the upper metres of a fracture zone effectively consumes the oxygen in infiltrating waters. In addition, groundwater samples from Äspö /Banwart et al. 1999, Luukkonen 2008/ and Stripa /Nordstrom et al. 1989/ are always found to contain dissolved Fe(II) indicating that groundwaters remain reducing even after prolonged periods of inflow into the tunnels.

Concerning nitrate and nitrogen compounds, unpublished indications from Äspö suggest that although during the excavation period nitrogen compounds may accumulate in the groundwater draining into the tunnel and in the waters percolating through rock debris, these waters are pumped out, and fracture groundwaters appear to be unaffected.

In conclusion, the reducing capacity of transmissive fracture zones is not affected during the excavation and operational periods, because consumption of oxygen in infiltrating waters takes place in soils, sediments as well as in the upper metres of fractures by microbial processes.

Effects of grout, shotcrete and concrete on pH

Injection of grout into fractures surrounding the repository tunnels will be necessary to avoid inflow of groundwater. Traditionally, cement-based grout is used when excavating tunnels. Standard Portland cement paste has porewater that is highly alkaline (pH ≈ 12.5). In order to avoid detrimental effects from porewater diffusing out of the cement matrix, cement recipes with porewaters having pH ≤ 11 will be used in the vicinity of deposition tunnels, see the **Underground openings construction report**. It is to be expected that the development of recipes for such materials will be an ongoing process both at SKB and elsewhere during the whole period of repository operation. Although the effects of these porewaters are much smaller, they must be considered, because it is possible that relatively large quantities of cement will be used in some repository areas. In general only limited amounts of grouting will be needed at Forsmark due to the low permeability of the rock.

The distribution of shotcrete and concrete in the repository will probably be spatially limited and their potential impact during the excavation and operational phases will be restricted. The exact shotcreting needs will not be known until the construction itself. Most of the leaking porewaters from these materials will be mixed with groundwater infiltrating into the tunnel and pumped away. A small part of the cement materials will be in contact with the backfill, and cement porewaters could migrate and diffuse into the bentonite. As long as low-alkalinity cement materials are used, the consequences on the performance of the backfill may be neglected.

On the other hand, grout could have a large impact on the geosphere conditions, as it is widely and diffusely distributed in the fracture system. Grouting is, however, necessary to avoid a large groundwater drawdown (increased meteoric water influx) and the corresponding up-coning of saline waters. Grouting is also needed for construction purposes; the ingress of water needs to be limited for the engineering installation and for worker safety. Two types of grout are envisaged in the vicinity of the deposition tunnels in the final repository, (see the **Underground openings construction report**): low-pH cement based grouts and suspensions of nano-sized silica particles (silica sol). The solidified silica sol grout is similar in its properties to the silica present in large quantities in the rock and fracture fillings, and may, therefore, be ignored in a long-term safety context. Cement-based grouts on the other hand have chemical properties quite different from the surrounding rock, and their effects have to be considered.

Boreholes crossing cement grouted fractures at the Olkiluoto site in Finland have yielded waters with elevated pH values since sampling started /Arenius et al. 2008/. The more limited experience from Äspö (only available as unpublished progress reports and technical notes) shows that a pulse of alkaline solution (pH up to 11.3) may be detected in the immediate vicinity of the grouted fractures during the first few days after injection. This pulse of alkaline waters is believed to be due to two factors: porewater released while the liquid grout solidifies; and erosion and dilution of grout by flowing groundwater in the outer edge of the grouted volume. These effects in the grouted fractures at Äspö were transitory, and after a few days the chemical composition of the groundwater returned to its original state (pH ≈ 7.5). The pH values were sufficiently low as to indicate that substantial dilution had occurred. The data from Olkiluoto indicates that the intensity of this short alkaline pulse will be decreased by the use of "low-pH" cement. Because of its short duration, the effects of a pulse with pH ≈ 11 are negligible.

After the excavation and operational phases grout will start to react with circulating groundwater, and a slightly alkaline plume will develop downstream in the grouted fractures /Luna et al. 2006/. This process is, however, relatively slow and it is, therefore, discussed in Section 10.3.7 in connection with the evolution of the repository during the initial temperate period after closure.

Precipitation/dissolution of minerals

During the operational phase, inflow of groundwater into the tunnel and mixing of groundwaters of different origin within rock fractures will result in precipitation or dissolution of minerals. These processes could only indirectly affect the safety function indicators. Precipitation and dissolution may be observed at the tunnel walls of the Äspö Hard Rock Laboratory (HRL). Simulations indicate that calcite and iron(III)oxyhydroxide may precipitate at the tunnel/backfill boundary /Domènech et al. 2006/ but that this process does not influence the performance of the repository negatively.

Effects of organic materials and microbial processes

Remaining organic materials in the repository include microbial biofilms, plastics, cellulose, hydraulic oil, surfactants and cement additives. Most of these organic compounds can be degraded by microorganisms, initially via aerobic degradation pathway as long as there is oxygen, and later via anaerobic biodegradation pathways. The degradation products will increase the reducing capacity of the near field of the repository. The largest pool of organic material is potentially the organic carbon in the bentonite clay, which according to specifications is less than 0.25 weight %, although the design criterion is < 1%, see the **Buffer production report**. This organic material is assumed to be mostly humic and fulvic acids. It is not known how much of it will be subject to biodegradation. It is unlikely that such material will dissolve in the groundwater unless the bentonite loses its swelling capacity. There will be a potential for formation of organic material by autotrophic microorganisms using the energy in H_2 that can be produced in anaerobic corrosion of steel constructions like rock support left in the rock at closure of the repository. Apart from the possibility of acting as reductants in aerobic or anaerobic biodegradation, organic materials might also be detrimental during later periods in enhancing the potential for radionuclide transport in groundwater after repository closure, for example by the formation of organic complexing compounds and organic colloids (safety function indicator R1d in Figure 10-2).

An inventory of organic materials and an assessment of their impact on microbial processes has been prepared /Hallbeck 2010/. This study concluded that it is to be expected that microbial degradation of organic materials will contribute to: a) quick consumption of any oxygen left in the repository; and b) by a combination of processes, involving anaerobic degradation and sulphate-reduction, sulphide production in the vicinity of the deposition holes. Some of the sulphide could reach the canister and may cause corrosion.

The maximum amount of organic carbon including that in the bentonite in the different parts of a repository in Forsmark is $3.9 \cdot 10^5$ kg in the deposition holes, $2.0 \cdot 10^6$ kg in the deposition tunnels and $3.4 \cdot 10^6$ kg in other areas. As noted above, the real amount of organic carbon in the bentonite is not known with any precision, and furthermore it is deemed as highly improbable that all of it could be used by microbial sulphate reduction given its non-reactive nature. As mentioned above, the organic material in the buffer probably consists to a large extent of humic and fulvic acids whose molecules are too large to be used by bacteria as a carbon source. In the deposition holes, the bentonite density is such that microbial sulphate reduction sustained by the organic matter in the bentonite is not expected to take place to any great extent (see Section 10.3.13). If the bentonite buffer were to be eroded away then the corresponding amounts of organic matter would also be eroded and although microbial sulphate reduction would then become possible, the dissolved organic carbon in the incoming groundwater would have to be used.

If all the organic carbon in the deposition tunnels, $2.0 \cdot 10^6$ kg as noted above, were to dissolve in their pore space ($3.7 \cdot 10^5$ m^3) it would result in an unlikely dissolved organic carbon concentration (DOC) of 0.45 mol/L. However, as mentioned above most of this organic carbon is present as organic matter in the bentonite, and these organics are deemed to be insoluble. The amount of organic carbon with the bentonite excluded is $5.2 \cdot 10^3$ kg in the deposition tunnels and $7.2 \cdot 10^3$ kg in the other areas /Hallbeck 2010/, which if all of it were to be used for microbial sulphate reduction, the resulting sulphide, if evenly distributed, would correspond to about 35 mol per canister. If the organic matter in the backfill bentonite could be used for microbial sulphate reduction, then, assuming a 0.25% content, about 13,600 mol of sulphide could be made available per canister.

Rock bolts and other iron components will remain in the deposition tunnels, and the highest theoretical concentration of sulphide that can be produced with H_2 from anaerobic iron corrosion via acetogenesis and sulphate-reduction in Forsmark is about 353 mol per canister as calculated from the amounts of steel in Table 2-15 in /Hallbeck 2010/. Calculations on the sulphide produced from biodegradation of biofilms with sulphate-reduction in Forsmark give 0.17 mmol/L in deposition tunnels (about 11 mol per canister) /Hallbeck 2010/. These are highly uncertain values and are based on the presumption that no cleaning of the rock surfaces is undertaken before closure. Steel corrosion will proceed slowly and the total values are reported here for reference only. It is to be expected that the hydrogen produced by corrosion will diffuse and be mixed with circulating waters, and that only a small fraction will reach any deposition hole. If the corrosion products are not dispersed, then there is no contribution to dissolved sulphide because steel corrosion also produces iron(II) which reacts with sulphide, and the overall reaction becomes: $Fe(s) + 0.25\ SO_4^{2-} + 2H^+ \rightarrow 0.25\ FeS(s) + 0.75\ Fe^{2+} + H_2O(l)$.

In conclusion, the largest pool of organic carbon in the repository is the organic matter included in the bentonite. Organic matter could contribute to canister corrosion if it was available for microbial sulphate reduction, and this is further evaluated in Section 10.3.13. The organic matter in the deposition holes can be ruled out, but that in the backfill could potentially be used in microbial sulphate reduction.

Interactions with SFR

The conclusions from the study /Svensson and Follin 2010/ are that an expanded SFR in operation appears to have little or no impact on the groundwater inflow rates to a final operating repository in the target volume at Forsmark. The case with SFR closed (but existing in the model) and a deep spent fuel repository open has not been fully analysed in /Svensson and Follin 2010/, but the simulations indicate that some pressure response is transmitted from the deep repository to boreholes close to SFR. Thus, some interactions between a closed SFR and an operating deep repository cannot be excluded.

Although the plans at present are that SFR will be kept open during the life span of the deep repository, the possibility of early closure cannot be ignored. If that was to happen, anaerobic microbial processes in the BLA vault of SFR, that contains large amounts of cellulose and other organic compounds, would result in porewaters that could have a large content of organic matter. These organic matter rich porewaters could then find their way to the operating deep repository, where microbial sulphate reduction would generate locally high sulphide concentrations.

Even if microbial consumption of the organic matter along the pathway between SFR and the deep repository and mixing of groundwaters are disregarded, the consequences for the performance of the canisters can be neglected. This is due to the short time period involved (at most ~100 years) and to the fact that during this period all canisters will be surrounded by an intact buffer that will act as a diffusion barrier.

Oxygen consumption in backfill

Air will be trapped in the porous buffer and backfill when deposition tunnels are plugged. Most of the oxygen in this air will be in the backfill because of its larger volume. This oxygen can diffuse to the canister surface and cause some initial corrosion until anoxic conditions are achieved, and, therefore, it is valuable to estimate the reducing capacity of the backfill. Both chemical processes and microbial activities are expected to consume oxygen.

Numerical calculations /Grandia et al. 2006, Yang et al. 2007/ coupling chemical processes consuming oxygen with the hydrodynamic saturation of the backfill have been used to estimate the time scale for reaching anoxic conditions in the tunnels of the repository. These studies show that several inorganic O_2 consumption processes may take place with the accessory minerals present in the bentonite in the buffer and in the backfill. These reactions are, in order of decreasing rate, the dissolution of Fe(II)-containing carbonates, the oxidation of pyrite, and the oxidation of Fe(II)-bearing silicates such as mica and montmorillonite. The calculated oxygen consumption times are highly dependent on the postulated value for the surface area of the reacting minerals. Nevertheless, it may be concluded that anoxic conditions are likely to be reached after a period of the order of one month after the backfill becomes completely water saturated. As noted in Section 10.3.8, it may take several thousand years for the repository to reach full saturation. The density of the backfill is low enough to allow some microbial activity, at least before it is fully saturated in all parts, and the effect of microbial activity will be to shorten the time to reach anoxic conditions in the backfill. Diffusion of oxygen to the surrounding granite would also be an effective mechanism for oxygen consumption by aerobic bacteria populations that could develop in the backfill/granite interface. The REX experiment in the Äspö HRL showed that oxygenated water in contact with a granite surface will be reduced in a few weeks.

In the Prototype Repository Project at the Äspö Hard Rock Laboratory, a programme is in progress for sampling and analysing gases at different locations in the buffer and backfill. One of the specific aims is to monitor the consumption of oxygen /Pedersen et al. 2004/. The two sections of the Prototype Repository were sealed in September 2001 and September 2003, respectively. Results have been published for the samplings in 2004 and 2007 /Eriksson 2007/. The resulting oxygen content in the gas phase ranged from almost zero to that present in the atmosphere, although there is a general decreasing trend with time. However, for technical reasons the backfill is not completely

water saturated in all parts, and the two sections are not fully sealed off, which prevents the drawing of unequivocal conclusions about the processes responsible for the decrease of oxygen. These data, however, provide further indications that the oxygen consumption will be rapid.

In conclusion, both inorganic reactions and microbial processes will quickly consume O_2 in the air trapped in the backfill, which has the largest pore volume in the deposition tunnels. The majority of the oxygen in the backfill will react before it can diffuse into the buffer and reach the surface of a canister.

Colloid formation

During the excavation and operational phases, substantial amounts of colloids may be formed due to microbial activities, and microbes themselves may act as colloids. In addition, bentonite erosion by fresh waters may generate colloids as may the precipitation of amorphous Fe(III) hydroxides, etc. These colloids are expected to be short-lived, mainly because colloids will aggregate and sediment in moderately saline waters, see for example /Degueldre et al. 1996/.

Other processes contributing to the elimination of colloids are microbial decomposition of organics, and the re-crystallization and sedimentation of amorphous materials.

In conclusion, possible increased formation of colloids during the excavation and operational phases is not expected to affect the performance of the repository in the long-term, because the colloid concentrations will quickly resume the natural values under the saline water conditions that will prevail.

Canister corrosion

During the operating period the canister will be subject to atmospheric corrosion, at slightly elevated temperatures, and most probably at a varying relative humidity (canisters stored in and cooled by circulating indoor air). Under these conditions, /King et al. 2010/ estimated the maximum corrosion attack to be less than 1 μm even after a storage period of two years.

The total extent of corrosion under aerobic conditions will be limited by the available amount of oxygen, i.e. the oxygen trapped in the repository after closure. After backfilling the tunnels, the available trapped oxygen can be calculated to be about 475 moles oxygen gas per canister. Due to the large difference in volume between the buffer in one deposition hole and the amount of backfill that can be assigned to each deposition hole, only a small part of the oxygen (21 moles) comes from the buffer, and the remainder from the backfill. The entrapped 475 moles of oxygen gas corresponds to a corrosion depth of 768 μm if evenly distributed on the canister surface, or 5.5 mm if the oxygen is assumed to attack the lid and topmost 10% of the canister height. It is pessimistically assumed that copper is only oxidised to Cu_2O.

However, of the available amount of oxygen in the buffer and backfill, only a very small fraction, if any, is expected to reach the canister. The oxygen will most likely be consumed by reactions with accessory minerals. The density of the tunnel backfill is low enough to allow microbial activity and this will also limit the amount of oxygen available for corrosion. As concluded in the previous subsection, the majority of the oxygen in the backfill will react before it can diffuse into the buffer in the deposition hole and reach the surface of the canister.

Pessimistic estimates can be made for the possible corrosion depth from entrapped oxygen if these other oxygen consuming processes are disregarded. Evenly distributed corrosion over the canister surface may be a reasonably pessimistic assumption for the oxygen from the buffer, although it is probably more realistic to assume that half of the oxygen will diffuse towards the oxygen-free rock. The corrosion from the oxygen in the buffer corresponds to a corrosion depth of 34 μm if all oxygen diffuses inward or 17 μm if half of the oxygen is diffusing outwards.

For the oxygen in the backfill different assumptions could be made that take into account the diffusion of the oxygen. Provided there is a sufficient consumption of oxygen in the rock, the amount of oxygen that could reach the canister will be only the fraction diffusing to the top of the deposition hole. This area (c. 2.4 m^2) is only about 2% of the area of a 6 m tunnel section (the tunnel length assigned to one canister). If it is further assumed that this would only corrode the topmost 10% of the canister (lid and 10% of the canister height) the corrosion depth would be 106 μm.

Another approach would be to compare the diffusion time for oxygen in the backfill with the total time before anoxic conditions are reached in the repository. With a pessimistic assumption of 300 years /Wersin et al. 1994a/ before the oxygen is consumed by mineral reactions and microbial activity, the diffusion length will be in the order of one metre. Assuming the oxygen in a 3 m cylinder of backfill on top of the deposition hole reaching the canister would correspond to a corrosion depth of 260 μm over the topmost 10% of the canister.

During the time period when the oxygen potential is sufficiently high, pitting corrosion is conceivable. Experimental studies of copper corrosion under repository conditions show, however, that the corrosion will have the appearance of uneven general corrosion, and thus that mechanistic models that include the possibility of pit stifling are more appropriate than statistically based models e.g. using pitting factors. The experimental data indicate that the unevenness around the average corrosion depth may be in the order of ±50 μm, see further the **Fuel and canister process report**, Section 3.5.4.

In conclusion, the corrosion depth from the atmospheric and initially entrapped oxygen is expected to be less than 500 μm at the most, and will thus have a negligible impact on the minimum copper coverage of the canisters.

Identified uncertainties and their handling in the subsequent analysis

Several uncertainties are identified when considering the different chemical aspects of the evolution of the repository during the operational period:

- There is a large degree of uncertainty in the detailed salinity distribution around the repository. However, the salinity will not become so high or so low as to affect the performance of the repository during this period or when considering its future evolution. The distributions of salinity, pH and other groundwater characteristics obtained from the modelling of the temperate conditions at 2000 AD, described in Section 10.3.7, is wide enough to include the small changes caused by the operation of the repository.
- The corrosion effects of sulphide produced by microbial activity with organic matter in bentonite and man-made materials, and anaerobic corrosion of steel as an energy source is further discussed in Section 10.3.13. The corrosion depth from the atmospheric and initially entrapped oxygen is expected to be less than 500 μm, and will thus have a negligible impact on the minimum copper coverage of the canisters.

10.2.6 Effects of operational activities on completed parts of the repository

SR-Can stated that “The rock mechanics analyses only suggest very local impacts from the excavation work. The open repository simulations suggest that resaturation starts very soon in the repository parts that are back-filled and sealed. Consequently, it seems clear that the continued operation and excavation of the repository would not imply any detrimental impacts on the completed part of the repository. However, this issue needs careful analysis both for safety assessment purposes and for establishing the appropriateness of working procedures at the underground construction and detailed characterisation stage.”

In the repository design, a minimum of 80 m separation between a deposition tunnel under construction and a backfilled deposition tunnel is applied. A study has been conducted /Jonsson et al. 2009b/ exploring whether this separation is sufficient to ensure there will be no vibration damage from the blasting over such a distance. According to /Jonsson et al. 2009b/ the most vulnerable stage from a vibration point of view is when the bentonite buffer is placed in the deposition hole but the canister has not yet been placed. During this stage, a hollow column of bentonite blocks remains free to vibrate inside the deposition hole. A three dimensional model in 3DEC, capable of capturing the dynamic behaviour of the bentonite buffer was set up and calibrated to recorded vibrations from the TASQ tunnel at Äspö HRL. It was concluded that when conducting blasting activities at 30 m distance with 4 kg of loading, the bentonite buffer will likely encounter a displacement which is less than 0.5 mm.

These analyses confirm the conclusion suggested in SR-Can that the continued excavation and operation of the repository, provided the blasting activities are separated a minimum of 80 m away from the completed parts, will not imply any detrimental impacts on the completed part of the repository. Furthermore, analyses suggest that this minimum distance can probably be shorter without any loss in safety.

As stated in Section 10.2.4 piping followed by erosion of buffer and backfill in already deposited tunnels cannot be ruled out in SR-Site. About 100 kg of dry bentonite may be lost from a deposition hole by erosion without jeopardizing the function of the buffer. The potential effect is substantial, but the case of point erosion rather unlikely. This situation is handled by avoiding potential deposition hole positions with too high an inflow, and need thus not be further considered in the risk assessment. Since the inflow to the backfill cannot be higher than the available void volume in the deposition tunnel, the largest possible erosion of the backfill will be 1,640 kg. Considering the large mass of backfill in the tunnel, about 34,000 kg per m tunnel (see Table 5-21), a redistribution of 1,640 kg can be assumed to have no impact at all on the backfill performance.

10.2.7 Summary of the excavation/operation phase

Summary of system evolution

The state of the repository system at the start of the excavation/operational phase is the initial state described in Chapter 5.

The evolution of the system during this phase is dominated by the excavation/operational activities. The evolution is thus different in nature from that at later stages, since the latter is essentially driven by naturally occurring processes. In principle, this evolution also depends on how the repository excavation and emplacement proceeds, but this is not specified in the current phase of the repository layout and design work. Several conclusions can be drawn without this more detailed specification.

The duration of this stage can be assumed to be several tens up to a hundred years depending on the progress of the excavation/operational activities and the total number of canisters.

Radiologically, the radiation intensity from each deposited canister will decrease during this period. This has a direct impact on the residual radioactive decay heat from the deposited canisters.

The thermal evolution will be dominated by the heat output from the canisters and some parts of the engineered barrier system will reach their peak temperatures during the excavation/operational phase as this occurs after typically a few tens of years. This evolution is treated in more detail in the next section, as it continues for thousands of years and as the local peak temperatures are insensitive to details of the operational sequence. See Section 10.2.1.

The mechanical evolution is dominated by the excavation of the host rock. An obvious mechanical impact is the creation of rock cavities for the repository. According to Section 10.2.2, the following conclusions regarding additional mechanical consequences can be drawn.

- There are no safety related impacts of the few cases of spalling prior to canister emplacement expected provided the actions envisaged in the **Underground openings construction report** are implemented. This allows the exclusion of the phenomenon in question in the risk assessment.
- There is ample evidence that a potential EDZ formed during excavation will be kept below the maximum allowed transmissivity as set out by the design premises and data suggest that a continuous EDZ would not develop at all. However, given that the occurrence of the EDZ currently can only be assessed by indirect measurements, it seems justified to consider an EDZ according to the design premises, i.e. with an axial transmissivity of 10^{-8} m^2/s as a basic assumption for further analyses. Furthermore, it also seems justified to explore how transmissive an EDZ needs to be in order to significantly impact other safety functions as well as exploring the impact of no axially continuous EDZ at all.
- Reactivation of fractures caused by the stress redistribution only results in insignificant increases of transmissivity in near-field fractures, apart from fractures that are parallel, and very close, to the tunnel. However, in reality fractures will not be persistently parallel to the tunnel where there are deposition holes, especially since deposition holes intersected by fractures intersecting more than four deposition holes will be rejected according to the EFPC criterion. This means that this effect can be discarded, or at least captured within the EDZ assumption of 10^{-8} m^2/s along the tunnel.
- Induced seismicity: The implications of induced seismicity can be excluded in the risk calculation.

Hydraulically, the evolution is dominated by upconing and drawdown effects of the repository excavation. The hydrogeology studies presented in Section 10.2.3 show that salinities generally will decrease at repository level due to the drawdown of shallow waters, apart from a few locations where salinities slightly increase due to upconing. The inflow to the repository is very small, but it should be noted that groundwater will seep into the already plugged deposition tunnels, thus affecting the potential for piping and erosion of the buffer and the backfill in these tunnels.

The drainage of water into the opened part of the repository affects the hydraulic evolution of the buffer, backfill and plug in already deposited tunnels. The plug needs to be able to limit the flow of water out from the backfilled tunnel, primarily to minimise the effect of piping in the buffer and backfill. Modelling has shown that it will take 5–20 years to saturate the bentonite seal within the plug. This means that either the plug/rock interface or the pellet filling in the seal need to limit the flow during that period. Precise requirements on the seal capacity are not yet defined but the plug design will under all circumstances be adjusted to meet the requirements when specified. Since the only function of the plug is to ensure the initial state before closure, failed plug performance is not assessed in SR-Site.

- Piping and subsequent water flow from a fracture into a deposition hole and further out into the deposition tunnel cannot be excluded if the inflow rate is higher than the rate of water absorption of the buffer material, since the pellet filling and the bentonite blocks cannot stop the water inflow until the deposition holes and the tunnel are water filled and the hydraulic gradient is taken by the end plug. Erosion tests have shown that the dry mass of eroded bentonite can be modelled as a function of the total volume of inflowing water.
- The calculations of the swelling and homogenisation of a half torus resulting from erosion show that the swelling yields a strong decrease in density and swelling pressure in the eroded volume due to the friction in the bentonite. About 100 kg of dry bentonite may be lost due to erosion without jeopardizing the function of the buffer. This situation is handled by avoiding deposition holes with too high an inflow, see Section 5.2.1, and is not further assessed in SR-Site. However, the uncertainty in the assessment of the eroded volume needs to be considered when revising the design premises for acceptable inflow to deposition holes, see further Section 15.5.

During the excavation/operational phase, the chemical evolution mainly arises from the disturbance to the natural conditions caused by the presence of the repository. According to the results presented in Section 10.2.5, the following conclusions can be drawn.

- There is a large uncertainty in the detailed salinity distribution around the repository. However, the salinity will not become so high or so low as to affect the performance of the repository during this period or when considering its future evolution. The distributions of salinity, pH and other groundwater characteristics obtained from the modelling of the temperate conditions at 2000 AD, described in Section 10.3.7, is wide enough to include the small changes caused by the operation of the repository.
- A short alkaline pulse in the groundwater from low-pH cement, shotcrete and concrete is likely to form, but its effects will be negligible.
- An increased precipitation of calcite and iron(III)-oxyhydroxides will occur at the tunnel wall during operations, but this process is evaluated as being of no consequence for the performance of the repository.
- Organic stray materials will be consumed by microbes, with the main effects being an increased rate of oxygen consumption and possibly also of sulphate reduction. The largest pool of organic carbon in the repository is the organic matter included in the bentonite. This could contribute to canister corrosion if it could be made available for microbial sulphate reduction. This is considered in the canister corrosion assessment during the initial temperate period, see Section 10.3.13.
- An increased formation of colloids during the excavation and operational phases will not affect the performance of the repository in the long-term, because the colloid concentrations will quickly resume their natural values.
- Oxygen left in the repository will be consumed by either chemical processes or microbes; the majority of the oxygen in the backfill, which has the largest pore volume in the deposition tunnels, will react and thus not diffuse into the buffer and reach the surface of the canister.
- Canister corrosion depths from the atmospheric and initially entrapped oxygen are expected to be less than 500 μm at the most, and will thus have a negligible impact on the minimum copper coverage of the canisters.

Safety function indicators at the end of the excavation/operation phase

Due both to the gradual excavation of the repository and the spatial variability of rock conditions, the state of the system at the end of the excavation/operational phase will vary e.g. between deposition holes.

Also, several safety function indicators are defined only for a water saturated repository, meaning that several safety function indicators are not meaningful to discuss at this stage.

Therefore, the detailed discussion of safety functions and status of safety function indicators is postponed until the end of the account of the initial temperate period, see Section 10.3.16. There also, the development during the excavation/operational phase is taken into account.

10.3 The initial period of temperate climate after closure

10.3.1 Introduction

The initial period of temperate climate can be expected to last several thousand years after repository closure. From a compliance point of view, the initial 1,000 years after closure are of particular interest, since SSM's regulations require a more detailed account of repository evolution for this period. Since many of the initial phenomena in the repository system occur within a 1,000 year period, a more detailed account of this time period is automatically obtained as every phenomenon is studied on the timescale appropriate to its nature. Examples of such phenomena are the resaturation of the host rock, the saturation of the buffer and the backfill and the thermal transient with its induced mechanical effects. Biosphere development is explicitly divided into an initial 1,000 year period and a subsequent period of development extending to the end of the temperate domain.

10.3.2 External conditions

The development of external conditions over the first 1,000 years after present is based on current knowledge of the Forsmark site and extrapolation of present trends, e.g. of shore-level changes. The development of climate-related processes for the remaining part of the initial period of temperate climate domain is based on model reconstructions of ice sheet-, shore-level-, and permafrost development for the last glacial cycle, including the Weichselian glacial, i.e. from 120,000 years ago up to present, see further Section 10.4.1. In the reference glacial cycle, the initial period of temperate climate domain after repository construction is c. 8,000 years long. For the assessment period of 1 million years, several identical reference glacial cycles, 120,000 years long, are envisaged to follow each other. In this process, each of the following *full* interglacial periods locally defined for Forsmark are ~20,000 years long. During these future interglacials, the repository location is submerged by the Baltic Sea for about half of the time, resulting in the repository being exposed to temperate climate conditions for almost 8,000 years in each interglacial, see the **Climate report**, Section 4.4.4.

In the reference glacial cycle, the long-term climate trend is assumed to be affected only by natural climate variability, and not by anthropogenically enhanced global warming. Therefore, palaeoclimate data depicting natural climate variability and trends can be used to assess the reference glacial cycle climate during the initial 1,000 years of temperate climate conditions. Climate variability in Sweden during the past millennium has experienced changes both in air temperature and precipitation /Moberg et al. 2006/, but the changes have not been large. If applying a 30 year smoothing filter on simulated air temperature data, the results show that, for southern Sweden, including the Forsmark region, annual air temperature variability was up to around ±1 degree C for variations slower than c. 30 years /Moberg et al. 2006, Figure 6-1/. Therefore, in the reference glacial cycle it is assumed that the temperate climate variability, in terms of temperature and precipitation, during the first 1,000 years after present is also relatively small, and, in line with the basic assumption, that climate trends during this period follow the patterns of natural climate variability.

The reference glacial cycle has been produced by applying palaeoclimate interpretations and regional Fennoscandian climatic- and topographical conditions for modelling of ice sheet, permafrost and shore-level changes, see the **Climate report**. This approach, together with a local definition of the ending of the present interglacial, see the **Climate report**, Section 4.5, determines the ~8,000 year

duration of the initial temperate period. This approach also results in the timing and durations of all following periods of climate domains during the reference glacial cycle (Section 10.4.1). In the ice-sheet modelling, a paleotemperature curve obtained from central Greenland is used in the absence of a continuous long-term climate proxy record from Fennoscandia. However, even though the Greenland paleotemperature curve, and its use for Fennoscandian conditions, involve major uncertainties, see the **Climate report**, Appendix 1, this is not a drawback considering the general approach adopted; namely to first develop a reference glacial cycle describing *one relevant example* of a future climate evolution for the coming 120,000 years, and subsequently construct other complementary climate cases covering a broader range of possibilities of future climate developments with a potentially larger impact on repository safety.

A climate case that includes global warming, as a result of an increase in atmospheric greenhouse gases from anthropogenic activity, is described in Section 10.6.

10.3.3 Biosphere

Processes of importance for long-term biosphere development

Long-term landscape development in the Forsmark area is dependent on two main, and partly interdependent factors, *climate variations* and *shoreline displacement*. These two factors in combination strongly affect a number of processes, which in turn determine the development of ecosystems. Some examples of such processes are erosion and sedimentation, groundwater recharge and discharge, soil formation, primary production, and decomposition of organic matter. These processes are discussed in relation to landscape development in more detail in /Lindborg 2010/. According to results from the hydrogeological modelling /Joyce et al. 2010/, discharge of deep groundwater will almost exclusively take place at low points in the landscape, i.e. in lakes, wetlands, streams and in near-shore areas of the sea. Thus the focus in the description of landscape development is on these areas where accumulation of potentially released radionuclides may occur.

Periodically, the shoreline displacement has strongly affected the Forsmark area, both before and after the latest deglaciation. At the time of the latest deglaciation around 8,800 BC, the area was covered by approximately 150 m of glacio-lacustrine water and the nearest shoreline was situated some 100 km west of Forsmark, see Chapter 3 in /Söderbäck 2008/. Thereafter, the isostatic rebound has been continuous and slowly declining. The rate of rebound in Forsmark has decreased from c. 3.5 m/100 years directly after the deglaciation to a present rate of c. 0.6 m/100 years, and it is predicted to decrease further to become insignificant around 30,000 AD (see Figure 10-101).

The present regressive shoreline displacement will continuously bring new areas of the sea floor above the wave base. This will expose sediments to wave erosion and resuspended fine-grained particles will be transported out of the area into the Bothnian Sea, or re-settle on deeper bottoms within the study area /Brydsten and Strömgren 2010/. Accordingly, the relocation of sediments may have important implications for transport and accumulation of radionuclides potentially originating from a future repository.

When new areas of the present seafloor are raised above the sea level, weathering of the calcium-rich Quaternary deposits is initiated. Most of the easily weathered calcite in the upper regolith will be dissolved and washed out within a period of some thousands of years /Tröjbom and Grolander 2010/. This means that the strong influence of the calcium-rich deposits on the terrestrial and limnic ecocystems will be reduced over time. For instance, the oligotrophic hardwater lakes that are characteristic for the coastal area in Forsmark will likely be transformed to more dystrophic (low pH, brown-water) conditions within some thousands years after isolation from the sea, see /Andersson 2010/.

The shoreline displacement will also cause a continuing and predictable change in the abiotic environment, e.g. in water depth and nutrient availability. It is therefore appropriate to describe the origin and succession of major ecosystem types in relation to shoreline displacement. One example of this is the isolation of a sea bay into a lake, followed by the ontogeny of the lake and its development into a wetland. As the lake is ageing, sediment and organic matter are accumulating due to sedimentation and vegetation growth, and eventually all lakes are transformed to wetlands. The rate of sedimentation decreases with decreasing lake volume /Brydsten 2004/, whereas the colonisation of littoral plants

requires shallow water (< 2 metres). Thus, the rate of lake infilling is mainly dependent on lake depth, area and volume /Brydsten and Strömgren 2010/. Mires may also develop on newly emerged land without a preceding lake stage /Kellner 2003/.

The initial 1,000 years after closure of the repository

The vertical component of the shoreline displacement is projected to be nearly 6 m during the next 1,000 years, assuming an almost constant isostatic rebound rate of 6 mm/year /Ekman 1996, Hedenström and Risberg 2003/ and a constant absolute sea level. Based on this scenario, a likely development of the site is described below.

The shoreline displacement will result in a horizontal transfer of the coastline to a location c. 1 km east of the repository at 3000 AD, which means that parts of the present seafloor will become land. Some of the coastal bays will be isolated and transformed to lakes (see Figure 10-11). The ongoing shoreline regression causes a succession pattern, where the shore vegetation, dominated by herbs, sedges and grasses, will be replaced by forest vegetation. The types of dominating vegetation communities during this succession are mainly determined by the composition of the underlying Quaternary deposits, which, in turn, depends on the extent of previous wave exposure of the shallow coast.

The newly isolated lakes will occasionally be affected by flooding with brackish water from the Bothnian Sea during periods of high sea water levels, in the same way that can be seen in low-elevation present-day lakes in the area.

All present-day lakes in the Forsmark area are small and shallow. This means that large parts of the lakes will be transformed to wetlands during the coming 1,000 years /Brydsten and Strömgren 2010/. For example, two of the smaller lakes, Lake Puttan and Norra Bassängen, situated close to the planned repository, are expected to be almost completely transformed to wetlands, whereas a minor part of the larger Lake Bolundsfjärden will remain as open water in the year 3000 AD (see Appendix C for a map of the Forsmark area today).

The human-made, deep inlet canal for cooling water to the nuclear power plants, situated immediately north of the planned repository, will be isolated from the sea around 2500 AD /Lindborg 2010/. If it is left unaltered after decommissioning of the power plants, it will probably remain as a lake far beyond the initial 1,000 years. Moreover, two new, relatively large lakes situated north of the repository and west of the present "Biotest basin", will be isolated from the sea in the latter part of the period (see Figure 10-11).

As the seafloor close to the coast gets shallower, erosion will occur on wave-exposed bottoms. Some sheltered areas inside a developing, denser archipelago will show accumulation for a short period /Brydsten 2009/. The circulation in Öregrundsgrepen is expected to remain essentially the same as today /Karlsson et al. 2010/. The salinity of the Bothnian Sea is expected to decrease slightly to around 4.8‰ during the initial 1,000 years, assuming unaltered runoff to the Bothnian Sea /Gustafsson 2004/.

The potential for sustainable human exploitation of food resources in the area over the coming 1,000 years is not expected to differ much from the situation today. Only minor parts of the newly formed land will have the potential for cultivation due to the boulder-rich sediments in the former sea and lake areas, but also due to problems with draining the low-elevation new areas /Lindborg 2010/. New areas will, however, be available for grazing by livestock.

The potential water supply for humans is expected to be fairly unaltered during this period. Lakes existing in the area today, e.g. Bolundsfjärden and Puttan, contain bad-tasting water due to fringing mires and occasionally high salinity. In the future, the deep canal north of the repository has potential as a freshwater reservoir when the salinity decreases, and also the stream through Bolundsfjärden may potentially be used for freshwater supply. New wells may be drilled in the bedrock or dug in the regolith in the area which is land today, whereas the new land will be too young for wells if current practises are sustained /Kautsky 2001/. However, the water quality of drilled wells in this area is poor and few wells are today used for drinking water /Ludvigson 2002/.

In summary, the biosphere at the site during the next 1,000 years is assumed to be quite similar to the present situation. The most important changes are the natural infilling of lakes and a slight withdrawal of the sea with its effects on the near-shore areas and the shallow coastal basins.

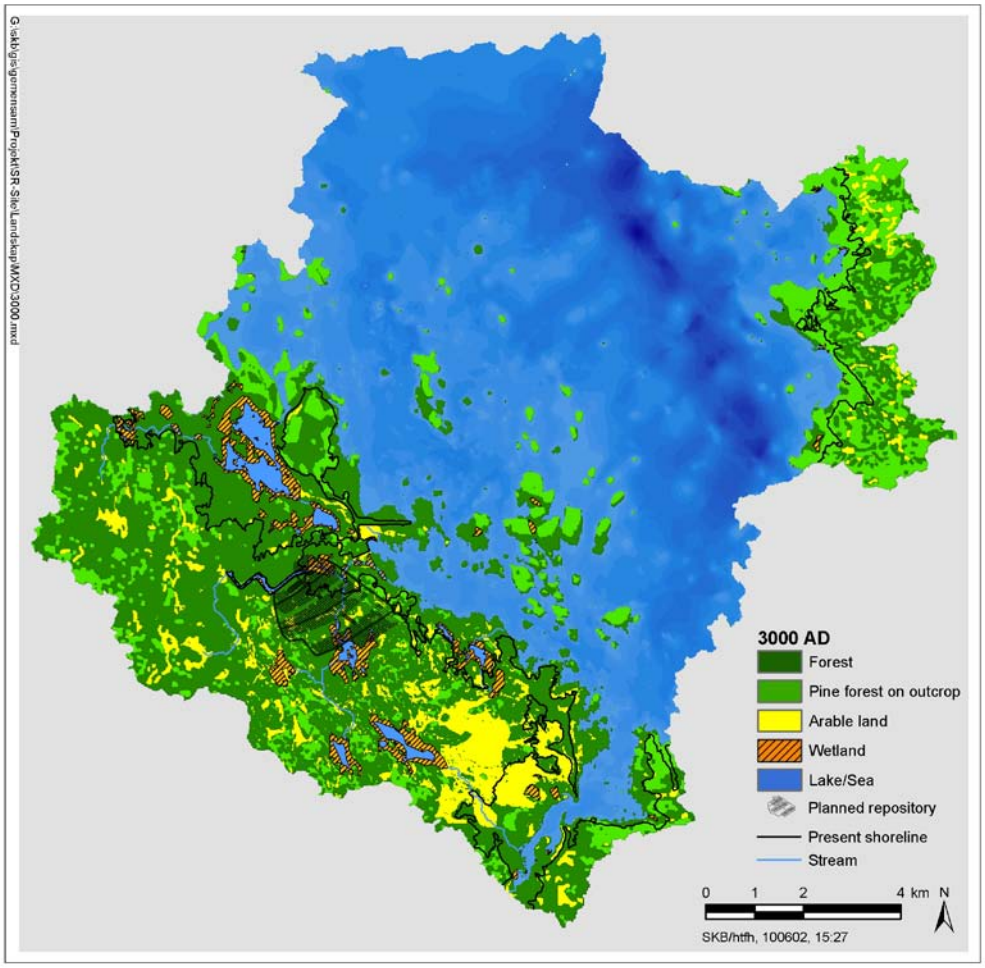

Figure 10-11. *Modelled distribution of vegetation and land use in Forsmark at 3000 AD. All areas that potentially can be cultivated are represented on the map as arable land (see Chapter 4 in /Lindborg 2010/). The present shoreline is marked as a black line and darker shades of blue represent deeper sea.*

Biosphere development after 1,000 years until the end of the initial period of a temperate domain at Forsmark

According to the SR-Site reference glacial cycle, see Section 10.4.1, temperate conditions will persist in Forsmark until c. 10,000 AD. During this period, the regressive shoreline displacement is assumed to continue, but at a gradually declining rate /Lindborg 2010/ (see further Section 10.4.1). Initially, the coastline will be subject to a horizontal transfer of approximately 1 km per 1,000 years. This will strongly influence the landscape, especially during the first part of the period, and eventually it will result in a situation where the planned repository will have an inland rather than a coastal setting (see Figure 10-12).

The strait at Öregrund, south of the modelled area, is expected to be cut off about 3000 AD, and Öregrundsgrepen will turn into a bay. This will affect the water circulation, and, due to the continued narrowing of the bay, the water turnover will be further restricted. However, at the beginning of the period it is not expected to be longer than a couple of weeks, except for minor sub-basins which are near isolation /Karlsson et al. 2010, Engqvist and Andrejev 2000/. During the period from 3000 to 5000 AD, a semi-enclosed archipelago is expected to develop northeast of the repository. Around 5000 AD, many straits in this archipelago will close and a number of lakes will be isolated from the sea.

At 5000 AD, the coastline has withdrawn c. 5 km from the repository. A small stream drains the area above the repository, and some small and shallow lakes are expected to be situated along the stream. This small stream will join a large stream in the south-east at about 5000 AD. This large stream consists of the merged Forsmarksån and Olandsån, draining a large part of Northern Uppland (drainage area $1.3 \cdot 10^3$ km^2). During the period from 3000 AD to 10,000 AD, the Öregrundsgrepen bay gradually shrinks to finally form a short and narrow bay along the island of Gräsö (Figure 10-12).

In the modelled area, a large number of lakes will be isolated from the sea during the period from 3000 AD to 10,000 AD. Most of the new lakes are small and shallow, and are expected to be infilled and transformed into mires within a period of 2,000 to 6,000 years /Brydsten and Strömgren 2010/. Around 10,000 AD, almost all lakes in the area have been infilled and only some initially relatively large and deep lakes near Gräsö island are expected to remain (Figure 10-12).

The salinity of the sea will continuously decrease due to the isostatic rebound of the shallow sills at Åland between the Bothnian Sea and the Baltic Proper. Around 6000 AD, the salinity is expected to have decreased to 3–4‰, which means that an ecosystem similar to that in the Northern Kvark today, with lower abundance of marine species and higher of freshwater species, will develop.

According to /Brydsten 2009/, accumulation of sediments may occur both on bottoms at large water depths and on shallow bottoms that are sheltered from wave exposure inside a belt of the skerries. Erosion occurs mainly on shallow bottoms exposed to waves. Transport bottoms can be found in all places between these two extremes, i.e. at intermediate depth with moderate wave exposure. This means that the seafloor in the model area will show a characteristic evolution over time, beginning with a period of accumulation due to large water depth early after deglaciation. Then comes a period with transport, after which erosion dominates when the water depth decrease even more. Finally, transport and accumulation may occur in sheltered locations during a short period before the sea bottom becomes land. This means that there are very limited parts of the model area that will show continuous accumulation of sediments throughout the whole marine period. The small areas that potentially may show continuous accumulation since the latest deglaciation are situated in the deepest parts of Öregrundsgrepen /Brydsten and Strömgren 2010/.

Much of the newly formed land will be unsuitable for farming due to boulder- and stone-rich deposits, see /Lindborg 2010/, but there are large areas in central Öregrundsgrepen with fine-grained sediments that can be cultivated. Also patches of organic soils on previous lakes/mires may be cultivated, but presumably these soils can be sustainably utilised only for limited periods since compression and oxidation of the organic material will lower the ground surface and cause problems with the draining, see /Lindborg 2010/.

The food productivity in agricultural areas is several hundred times higher than that in aquatic or non-cultivated terrestrial areas /Andersson 2010, Aquilonius 2010, Löfgren 2010/. Since the proportion of land that it is possible to cultivate will increase as new land areas are formed, this means that the potential food productivity in the total modelled area is expected to increase during the period. However, the number of people that potentially can be sustained by food produced within the Forsmark area is strongly dependent on the degree to which land is used for farming.

The availability of freshwater for human supply is expected to gradually increase. As mentioned above, new lakes and streams will form, but most of the lakes will be short-lived due to their shallowness. New groundwater, potentially useful as drinking water, will be available when the shoreline moves eastwards. Among already existing geological formations, the Börstilåsen esker, situated c. 4 km southeast of the planned repository, may provide groundwater of drinking-water quality, but there are no indications in the hydrogeological modelling results that this aquifer will have contact with discharging groundwater from the repository /Joyce et al. 2010/.

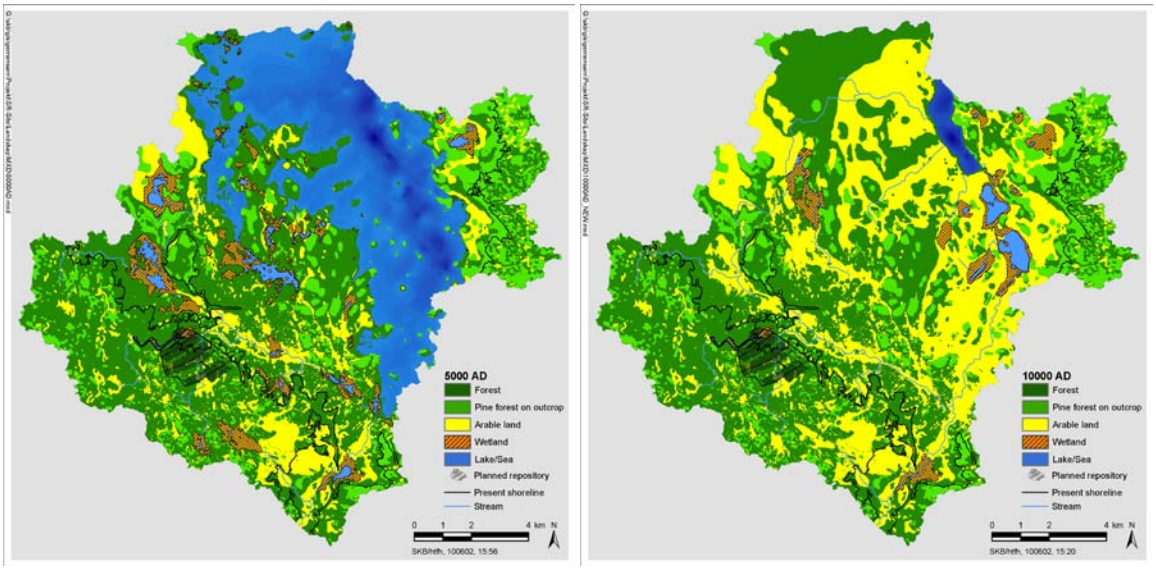

Figure 10-12. *Modelled distribution of vegetation and land use in Forsmark at 5000 AD and at 10,000 AD. All areas that potentially can be cultivated are represented on the map as arable land (see Chapter 4 in /Lindborg 2010/). The present shoreline is marked as a black line and darker shades of blue represent deeper sea.*

Identified uncertainties and their handling in the subsequent analysis

The description of the landscape development during the initial temperate period is associated with three major uncertainties:

1. The configuration of the landscape, e.g. location and size of future lakes and streams, and depth and stratigraphy of regolith layers.
2. The timing of different events, e.g. withdrawal of the sea, and isolation and infilling of lakes.
3. The composition and properties of species and communities inhabiting the future landscape.

Uncertainties in the development of the landscape configuration in Forsmark are not handled explicitly in the modelling. Thus, the modelled landscape development should be seen as an example of a possible future, based on a thorough understanding of present-day geometries and an expected shoreline displacement. The topography is not expected to vary significantly during the period, and the main uncertainties in the future landscape configuration are associated with the location of thresholds for future lakes.

The landscape can be subdivided into drainage areas, delimited by water divides. In the SR-Site assessment, low-lying areas that, according to the hydrogeological modelling /Joyce et al. 2010/, potentially will be affected by discharge of deep groundwater, are identified and thoroughly described over time (see further the discussion of biosphere objects in Section 13.2). Each biosphere object will typically go through a similar succession, from being part of the open sea, over a sea bay phase, to a lake which eventually will transform to a wetland (or agricultural land). Thus, the biosphere objects encompass considerable variation, both in size (the area range is almost two orders of magnitude) and in the timing and rate of succession events.

Uncertainties associated with the depth and development of regolith layers, the infilling of lakes, the future surface hydrology and the properties of species and communities that may inhabit the future landscape, are handled either as parameter uncertainties or in systematic studies of alternative scenarios in the modelling of radionuclide transport and accumulation in the surface system (see Section 13.2). For example, the effects of varying rates of sedimentation and vegetation in-growth on lake ontogeny and on depth of sediments have been studied /Brydsten and Strömgren 2010/.

The annual water balances for a suite of lakes in the area, which vary with respect to size, ontogeny and depth of underlying sediments, have been used to set reasonable boundaries on the hydrology of future lakes. In addition, natural variations of biomass and primary productivity in temperate aquatic

and wetland ecosystems similar to those observed in Forsmark today (or expected to develop in the area) have been used to characterize uncertainties in the properties of communities that may inhabit the future landscape.

In the biosphere assessment, the worst case (i.e. highest risk) for each radionuclide during an interglacial period is selected from a number of biosphere objects in a dynamic landscape, covering landscape configurations from a fully submerged to an entirely terrestrial landscape. Thus, even though the exact future landscape development is difficult to predict, the systematic landscape analysis and the approach for estimating doses encompasses a broad array of future landscape configurations. Further details of the landscape modelling are given in Section 13.2.

10.3.4 Thermal evolution of the near field

Introduction

The thermal evolution of the near field is of importance as general input information to the mechanical, chemical and hydrological processes. The direct safety relevant thermal criterion concerns the buffer peak temperature, safety function indicator Buff4 (Figure 10-2) that requires that this temperature does not exceed 100°C, chosen pessimistically in order to avoid, with a margin of safety, mineral transformations of the buffer.

The thermal evolution of the repository depends on the thermal properties of the rock and the initial temperature at the site being considered, on the repository layout, i.e. canister spacing and tunnel spacing, and the canister power. For the thermal evolution in the interior of the deposition holes the properties of the bentonite buffer and of possible air-filled gaps are additional parameters. These properties depend strongly on the water supply, i.e. on the degree of saturation and may differ from one deposition hole to another depending on the local hydraulic conditions.

The peak buffer temperature occurs some 5-15 years after deposition. At this time, approximately 50% of the local temperature increase is caused by the heat from the canister itself and 50% by the heat contribution from all the other canisters. This means that the local rock heat transport properties are particularly important to the peak temperature for the individual canisters and that, therefore, the low tail of the conductivity distribution, the spatial variability and the scale of variation are important for the dimensioning issue.

The SR-Site assessment of the thermal evolution is based on dimensioning guidelines and calculation schemes established by /Hökmark et al. 2009/ and on results in the Site engineering report /SKB 2009c/ regarding layout D2 for the Forsmark site obtained applying those guidelines as described in the **Underground openings construction report**, see also Section 5.2.2.

As far as demonstrating that the 100°C safety assessment requirement is met for all canisters, the numerical calculations in the Site engineering report /SKB 2009c/ are adequate and sufficient. These calculations do however concern only the first 20 years after deposition and apply only to canisters deposited in rock volumes dominated by low conductivity rocks. They cannot be used to estimate the number of canisters that actually will have peak temperatures close to the design threshold. It should be noted that the majority of the canisters will be deposited in rock with properties approximately equal to the domain mean values and consequently have lower peak temperatures. The dimensioning calculations do not capture the overall large-scale and long-time thermal evolution of the repository host rock. To account for this additional thermal assessments have been made and reported in detail by /Hökmark et al. 2010, Chapter 5/, using data from the **Data report**, Section 6.2.

Distribution of peak buffer temperatures

An estimate of the distribution of peak buffer temperatures in *both dry and wet* deposition holes can be made by use of an analytical solution /Hökmark et al. 2009/ and the distributions of thermal conductivity in each rock domain as provided by the **Data report**, Section 6.2.

In dry deposition holes the maximum buffer temperature is found at the top of the canister where the bentonite is in direct contact with the copper surface, see Figure 10-13 (left). Note that the hottest point on the canister surface is located at canister mid-height. In wet deposition holes, the air-filled

gap between the canister and bentonite blocks will be closed at the time of the peak temperature, and the bentonite will also be in direct thermal contact with the copper shell at points on the vertical canister surface. In this case the maximum buffer temperature will coincide with the hottest point on the canister surface, i.e. at mid-height, see Figure 10-13 (right).

The analytical model does not take spatial variations of the thermal properties into account, i.e. it is assumed that the thermal properties are uniform everywhere. Therefore, the peak buffer temperatures calculated using thermal conductivity values from the low end of the distribution are overestimated, whereas the corresponding temperatures at the high end of the distribution are underestimated. A temperature correction term, T_{corr}, that accounts for the variability of the thermal properties is therefore added. It should be noted that the temperature correction is an approximate way of accounting for the inhomogeneity in rock thermal properties. The method was, however, compared to numerical analyses modelling the spatial variability and the correction was found to forecast the spacing values finally established in the Site engineering report /SKB 2009c/ with good accuracy.

Figure 10-14 shows the peak temperature distribution using the canister spacing in the layout. There are two cases: with and without the temperature correction above. Without the correction there are temperature over- and underestimates, for canisters associated with the low- and high conductivity parts of the distributions, respectively.

On average, less than one canister position, out of 6,000 canister positions, would have a peak buffer temperature larger than 95°C meaning that the design requirement would be satisfied with a margin of 5°C, based on this analysis. A very large majority of the canisters, about 98%, will have a margin of 10°C or more. Furthermore the peak temperatures are overestimated because of the following considerations.

- All canisters are assumed to be deposited with the nominal canister spacing everywhere, whereas some deposition holes in reality will be discarded. Canisters neighbouring rejected positions will have lower temperatures.
- All canisters are assumed to be deposited in the central parts of the deposition areas while in reality about 1,000 canisters will be deposited close enough to the tunnel ends to get reduced peak temperatures.
- All canisters are assumed to be completely dry with a 10 mm air-filled gap between canister and bentonite, while in reality there will be a variation in the degree of saturation. A fraction of the holes will be sufficiently close to saturation that the wet hole model rather than the dry hole model applies, Figure 10-13. This will reduce the peak temperatures.

Importance of deposition sequence

In assessing the peak temperature it is assumed that all canisters are deposited simultaneously. Analytical temperature calculations by /Hökmark et al. 2009/ show that if the canisters are deposited in an orderly fashion (i.e. panel by panel) at a rate of 2 or 4 days per canister, the increase in temperature at the time of peak buffer temperature is less than 0.2°C, and this approximation is justified. However, it is possible to envisage deposition sequences, e.g. when a canister is deposited centrally in a panel where all other positions were deposited several years before, where the resulting temperature would be much higher. Such situations will, however, always be avoided, but this observation highlights the need for careful thermal management of the disposal sequence.

Thermal evolution

/Hökmark et al. 2010, Chapter 5/ numerically assess the thermal evolution of the repository both in the large and near-field scale. In the large-scale, covering the entire repository with surrounding rock, all the canisters are represented by point sources of heat.

Since no information can be given regarding how the loss of canister positions is distributed across the repository region, /Hökmark et al. 2010/ uniformly removed every 8th canister position across the repository in order to achieve the approximate thermal load on a large scale. Contour plots of the

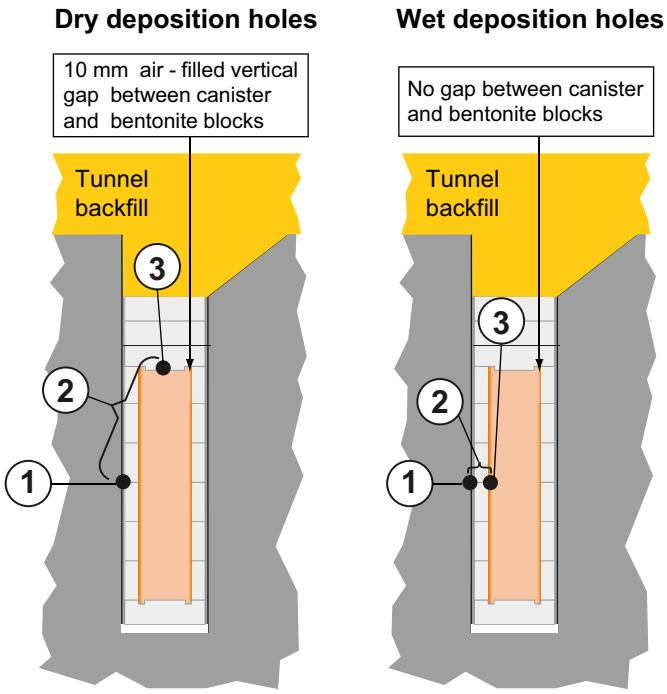

Figure 10-13. Rock wall temperature (1), temperature drop across bentonite (2), maximum bentonite temperature (3) located at the top of the canister in dry deposition holes and at canister mid-height in wet deposition holes. Modified from /Hökmark et al. 2009/.

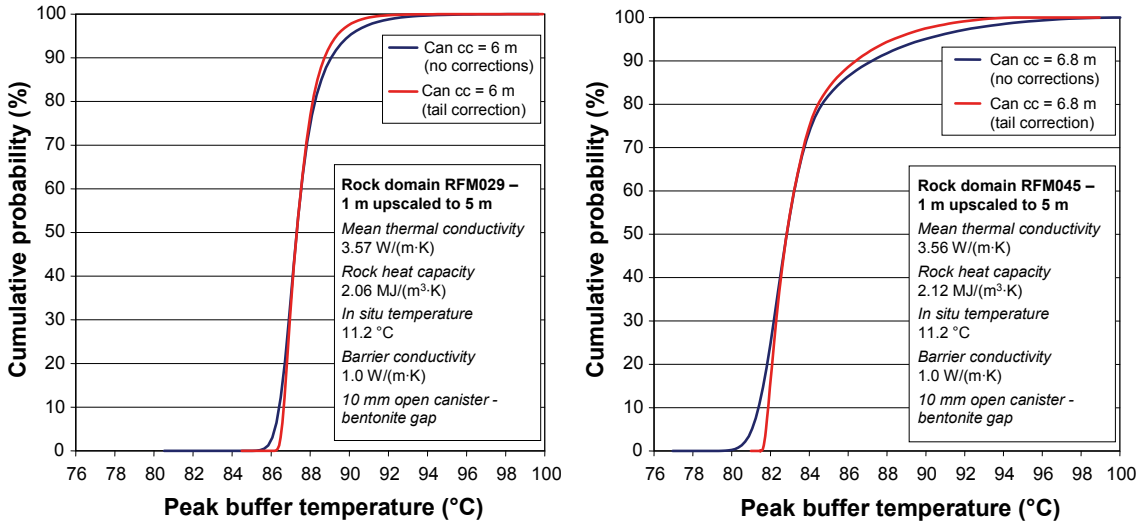

Figure 10-14. Distribution of buffer peak temperature in rock domains RFM029 (left) and RFM045 (right), with and without correction for spatial variability. Modified from /Hökmark et al. 2010, Figure 5-6/.

calculated mean rock temperature increase at repository level after 50 and 1,000 years are shown in Figure 10-15 assuming simultaneous deposition. Corresponding contour plots of the temperature increase valid at other times with and without account being taken of the deposition sequence are provided in /Hökmark et al. 2010/.

In the near-field temperature calculations, i.e. the temperature at the wall of a deposition hole at canister mid-height, surrounding canisters are represented in the same way as in the large-scale calculations but the local canister and its six nearest neighbours (in the same tunnel segment) are replaced by more detailed representations of canisters. Also all available canister positions are assumed to be filled, which consequently may overestimate the temperature.

Figure 10-16 shows the resulting rock wall and buffer temperatures in two different positions, considering both dry and wet deposition holes. The peak buffer temperature occurs approximately 5–15 years after deposition /Hökmark et al. 2010/ and the peak rock wall temperature occurs approximately 50 years after deposition.

Identified uncertainties and their handling in the subsequent analysis

The discussion above can be used to draw a set of conclusions regarding the uncertainties and their subsequent handling in the SR-Site analyses.

- For the *thermal evolution during the initial temperate period* there is an adequate margin to the peak temperature criterion for the buffer, even when the spatial variability of the rock thermal properties is taken into account and with other data essential for computing the result chosen pessimistically. However, the thermal evolution is input to other assessments of the reference evolution. Only a representative thermal evolution without uncertainty is propagated for use in these assessments since the uncertainty in the thermal evolution is sufficiently small that it would not impact these other parts of the assessment.
- It is possible to envisage *deposition sequences*, e.g. when a canister is deposited centrally in a panel where nearby positions were deposited several years before, where the resulting temperature in the buffer would exceed the maximum allowed. Such situations will, however, always be avoided, but this observation highlights the need for careful thermal management of the disposal *sequence.* This will be further considered in providing feedback to current design premises, see Section 15.5.

10.3.5 Mechanical evolution of the rock

After deposition, backfilling and closure, the mechanical evolution, e.g. rock stress changes, rock expansion/compression and fracture aperture reductions/expansions, is controlled by the heat generation from the spent fuel, by the swelling pressure of the bentonite buffer in the deposition holes, and by the gradual restoration of the groundwater pressure, which will locally reduce the effective stress and the fracture shear strength. The timescale for the thermal effects can be predicted in detail as demonstrated in Section 10.3.4 and numerous other analyses of the thermal development of the repository. The time-scale for the development of the swelling pressure depends on the local permeability conditions around the individual deposition hole and on the general repository-scale restoration of the groundwater pressure.

Furthermore, as further explained in the **Geosphere process report**, Section 4.1, the Baltic Shield is continuously subject to a horizontal compression or “ridge push” due to seafloor spreading from the Mid-Atlantic Ridge at the western tectonic plate boundary which initiated approximately 15 million years ago /Muir Wood 1993/. The compression is an important factor for the development of the state of stress currently prevailing in the Swedish bedrock (see Chapter 4) where the maximum principal stress tends to be horizontal and oriented NW-SE, i.e. in the ridge-push direction.

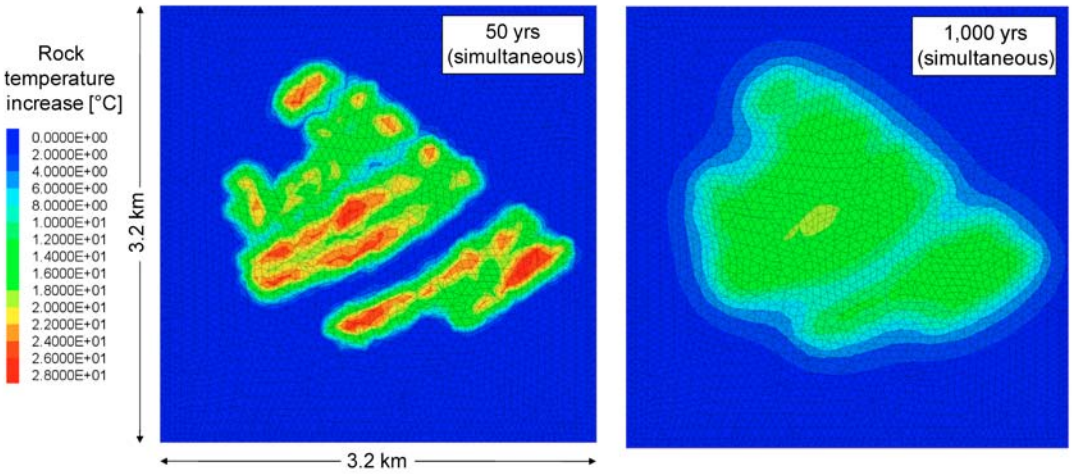

Figure 10-15. *Contour plots of the rock temperature increase at repository level (460 m) at Forsmark. Point sources representing canisters are placed 5 m below. From /Hökmark et al. 2010, Figure 5-12/.*

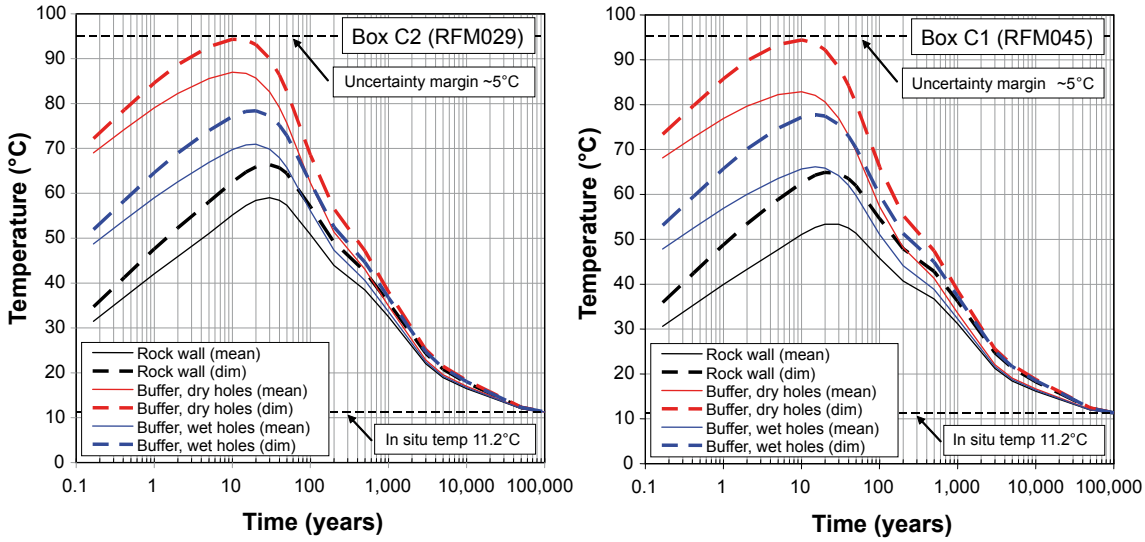

Figure 10-16. *Rock wall temperature at canister mid-height and peak buffer temperature, considering mean and dimensioning ("worst case") thermal conductivity, both dry deposition and wet deposition holes for central locations in rock domain RFM029 (left) and in rock domain RFM045 (right). Note that the shapes of the peak temperature distributions are direct reflections of the shapes of the conductivity distributions, which are different in the two domains. From /Hökmark et al. 2010, Figure 5-15/.*

The following mechanical processes related to the initial temperate period after repository closure, could have potential safety implications.

- Reactivation of fractures in the near field due to thermal load, including fracture aperture reductions due to temperature increase expanding the intact rock, that could affect the mechanical stability (safety function R3bc, see Figure 10-2) and the fracture transmissivity and thus the transport resistance in the near-field rock (safety functions R2ab).
- Reactivation of fractures in the far field that could affect fracture transmissivity and thus the transport resistance (safety function R2a).
- Reactivation due to the crustal strain resulting from the mid Atlantic ridge push that could affect the mechanical stability of the deposition holes (safety function R3bc).
- Fracturing of the rock that could affect the deposition hole geometry (safety function Buff1) and migration between buffer and rock (related to safety function R2a).
- Potential for creep deformation that could affect deposition hole geometry (related to safety functions Buff3 and Buff6). Here the term creep is also used for cases in which the mechanical load is not constant over time, i.e. when the shear strain successively relaxes the stresses.

These issues are assessed in the following subsections.

Modelling approach

Most of the above issues are assessed by integrated numerical modelling /Hökmark et al. 2010/ applying the distinct element code 3DEC (3 Dimensional Distinct Element Code) /Itasca 2007/on a large scale and on near-field models. This modelling produces stress changes resulting from the thermal (and later glacial) loads. These stress changes, in turn, are used to assess potential changes in fracture or fracture zone transmissivity by assuming certain relationships between stress change and transmissivity.

The large-scale model is represented by rectangular blocks with dimensions 8 km·7.4 km·~3 km, see Figure 10-17. Average values of the thermo-mechanical properties judged to be relevant in the entire modelled domain are used to represent the properties of the rock mass as further specified in the **Data report**, Section 6.4. The heat sources are positioned in the models according to Layout D2, where the loss of canister positions is assumed to be uniformly distributed across the repository region. Boundary conditions for the subsequent near-field modelling are obtained from the displacements on pre-defined cut-planes representing the near-field model boundaries and are evaluated as the expansion/contraction relative to the centre of the near-field model as a function of time.

Two types of and sizes of near-field models are used:

- One tunnel segment with seven heat generating canisters (for spalling analyses), but with only three of the deposition holes explicitly included. Model dimensions are 40 m (across tunnels) and 50 m (vertically), see Figure 10-18.
- Five tunnel segments each with 33 potential canister positions (shearing, normal stress variations and transmissivity changes of fractures). None of the deposition holes are explicitly included. Similarly to the approach taken by /Hökmark et al. 2006/ and /Fälth and Hökmark 2007/ the fracture system is stylised considering a model in which the fracture orientations are based on site-data in fracture domain FFM01 /Fox et al. 2007/ and a model with one fracture orientated such that the potential for shear failure is large, see Figure 10-19. Model dimensions are 200 m (across tunnels) and 200 m (vertically).

Based on the transmissivity data for fracture domain FFM01 at Forsmark /Follin et al. 2007b/ and fracture normal stiffness data given in the **Data report**, /Hökmark et al. 2010/ apply two different models for the relation between stress and transmissivity changes, see Figure 10-20. As further discussed in the **Data report**, the strength of the hydromechanical coupling is highly uncertain, but it is judged that the range of these models captures, or at least overestimates, this coupling.

/Hökmark et al. 2010/ also assessed, using analytical solutions of the thermo-mechanical evolution of an elastic medium subject to time dependant thermal loads, whether the calculated stresses depend on the deposition sequence. As with the analyses for the temperatures they show that the assumption that all canisters are deposited simultaneously produces very similar stresses to those produced in the models where the impact of the deposition sequence is considered, unless very specific sequences are used (for instance starting and finishing the deposition in neighbouring tunnels or very nearby deposition areas). Given a proposed deposition sequence, it can easily be checked (e.g. by use of the analytical solution) whether or not the approximation of simultaneous deposition still gives valid results.

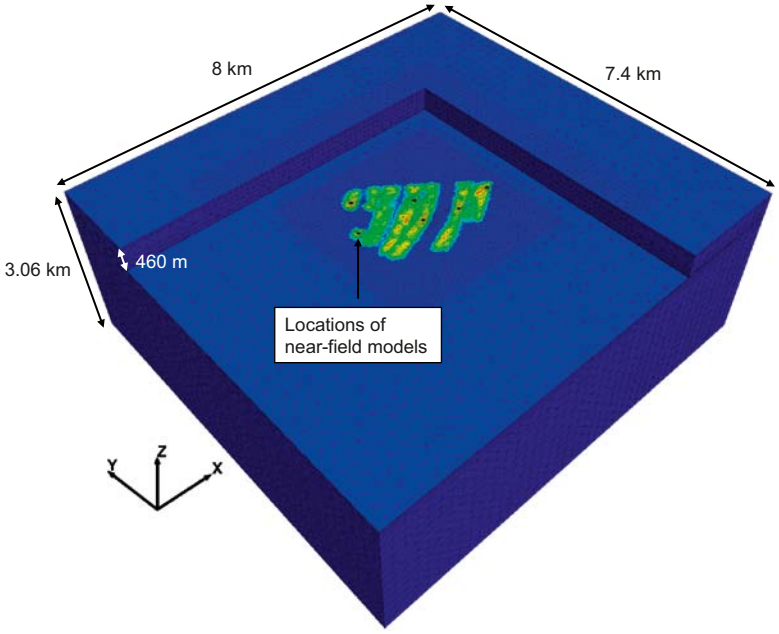

Figure 10-17. *Outline of Forsmark large-scale 3DEC model. Note that parts of the model are hidden from view. (Figure 6-13 in /Hökmark et al. 2010/).*

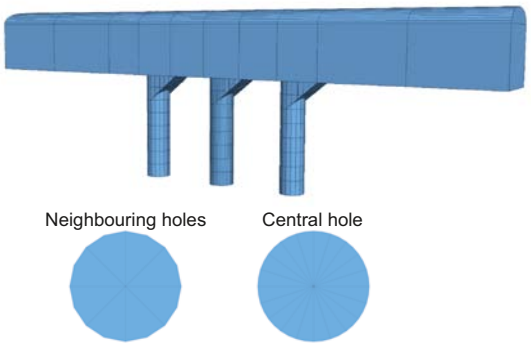

Figure 10-18. *The detailed near-field model representation of three central deposition holes. From /Hökmark et al. 2010/.*

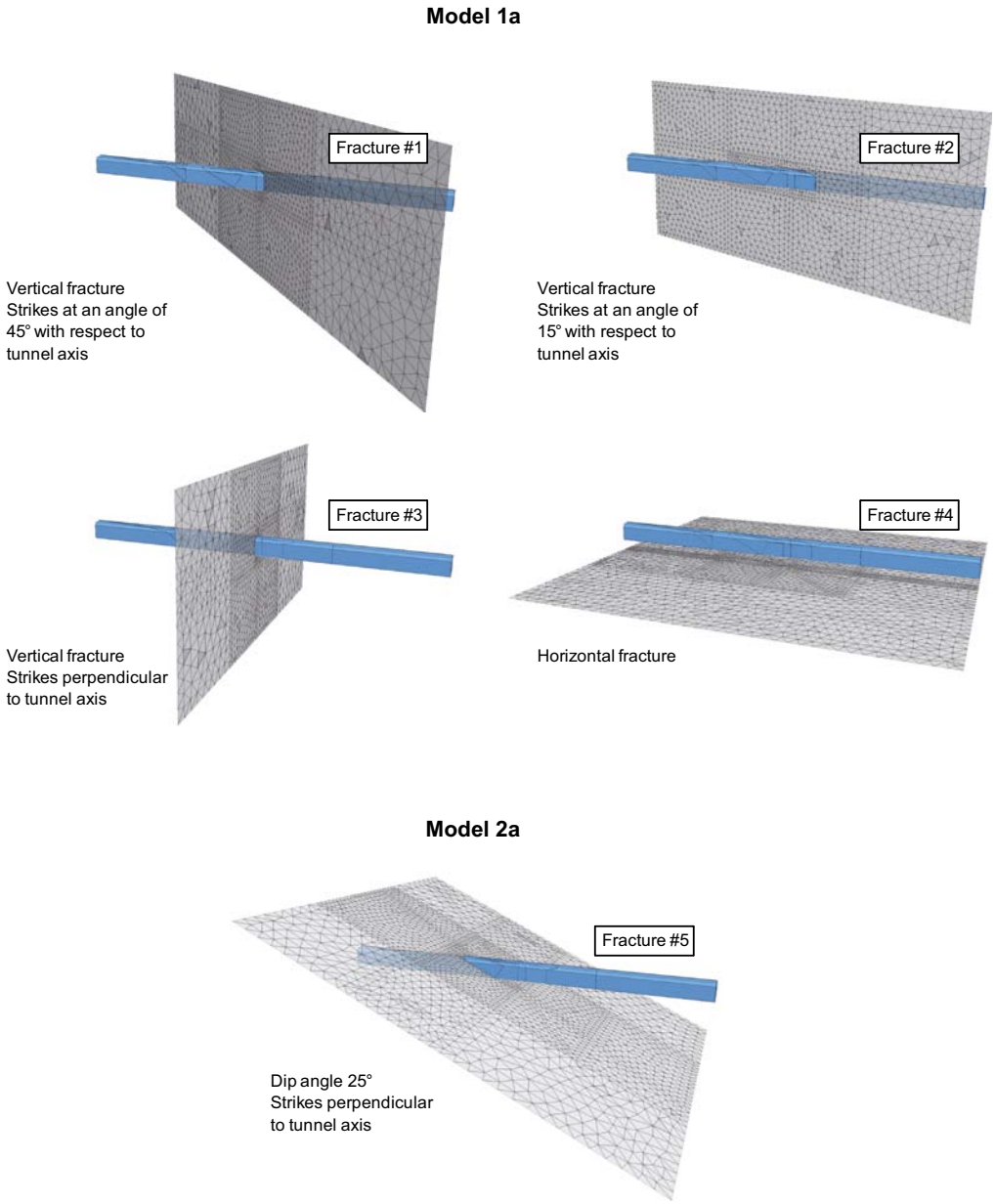

Figure 10-19. *Fracture configurations in the medium size near-field model. All 5 orientations are based on site data, but the orientation of fracture 5 is selected in order to maximize shear failure. The dip direction of fracture 5 is SE and the tunnel trends NW-SE i.e. parallel to the direction of the present day maximum principal stress which is linked to the Atlantic ridge push. From /Hökmark et al. 2010, Figure 8-6/.*

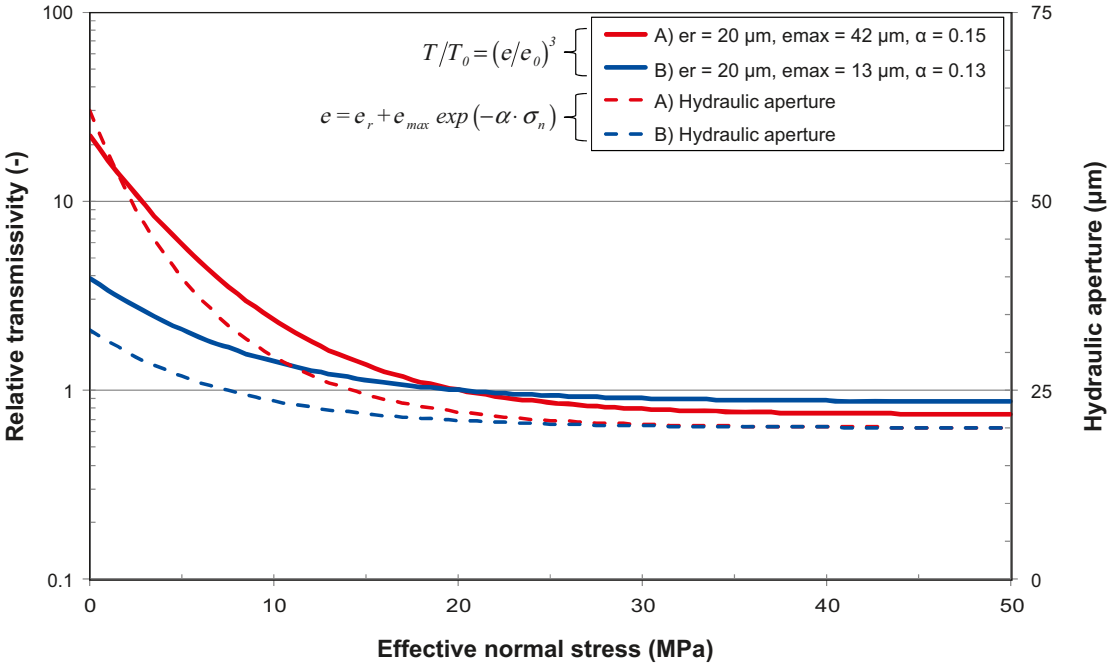

Figure 10-20. *The two stress-transmissivity models (A and B) and related stress-hydraulic aperture models adopted for the Forsmark site. T is transmissivity, e hydraulic aperture and σ_n normal stress. The range of these models captures, or at least overestimates, the stress coupling. From /Hökmark et al. 2010, Figure 4-9/.*

Reactivation of fractures in the far field

A complete set of results from the numerical modelling of the impact of the thermal load is provided by /Hökmark et al. 2010, Chapter 6/. In the far field, the numerical modelling shows that for fractures perpendicular to the major horizontal in situ stress there are only negligible variations in relative transmissivity. For vertical fractures oriented perpendicular to the minor horizontal in situ stress and located above the repository panels, the reductions in effective normal stress in the upper 100 m of rock result in an increase in relative transmissivity by at most a factor 2.5 (model A) and 1.5 (model B). Below a depth of 200 m there are only negligible changes in relative transmissivity for both stress-transmissivity models, see Figure 10-21. Between repository panels and just outside the repository there is a decrease in vertical stress leading to transmissivity increases for sub-horizontal fractures by, at most, a factor 1.5 to 2 at the repository level, depending on which stress versus relative transmissivity curve is used, but there is no such increase inside the panels.

The large scale thermally induced horizontal stresses are aligned with the deposition geometry, i.e. oriented perpendicular and parallel to the deposition tunnels, respectively. Since the tunnels are approximately parallel to the major horizontal stress, the resulting net background stress field is approximately oriented as the *in situ* stress field such that the stability and response of differently oriented fractures can be easily deduced from the results of the large-scale thermo-mechanical models using analytical expressions. However, the analytical expression assumes fractures to be perfectly planar with uniform properties, meaning that effects of large scale undulations, local in-plane asperities and other irregularities that are not captured by the laboratory scale tests used to provide shear strength data to the model are not accounted for. The actual slip will, therefore, probably be less due to the actual fracture cohesion. The analysis, presented by /Hökmark et al. 2010, Sections 7.5 and 8.4/, suggests that fractures dipping approximately 27° in the direction of the major horizontal in situ stress and passing through non-heated regions appear to have the largest potential for instability. For a fracture with 150 m radius at 450 m depth, outside the deposition area, the maximum slip at the fracture centre is less than 27 mm according to the applied analytical expression. Because of the accompanying reduction of the normal stress, the transmissivity is likely to increase. The scope of that increase is, however, very uncertain. Fractures intersecting the heated deposition areas are significantly more stable. For a fracture with 150 m radius at 450 m depth, inside the deposition area, the maximum slip would be around 6–7 mm – again according to the

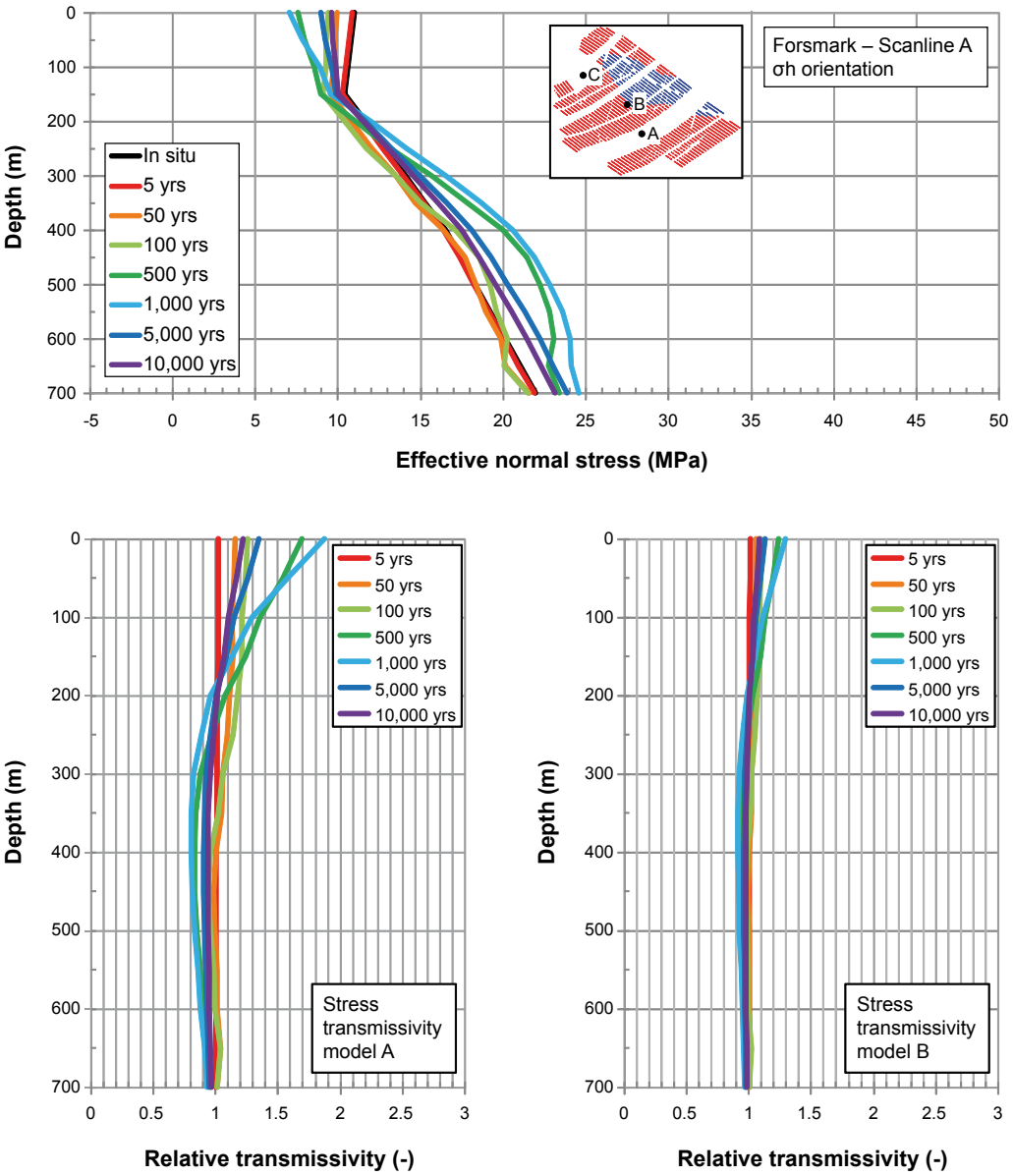

Figure 10-21. *Top: Effective stress along a scan-line in the direction of σ_h. Here compression is positive. Bottom: Relative transmissivity of fractures perpendicular to σ_h. From /Hökmark et al. 2010, Figure 6-21/.*

analytical expression. The slip movement is accompanied by a normal stress increase, due to the heat load, which means that the transmissivity might decrease rather than increase. It should also be noted that the slip, and transmissivity impacts, will be much less for fractures with other orientations.

In conclusion, the transmissivity changes induced by the thermal load are judged too small to require any further consideration in the far-field hydrogeological analyses.

Reactivation of near-field fractures

Results from the intermediate scale near-field model suggest that during the thermal phase the normal stresses for the site specific fracture orientations generally increase, leading to small reductions of the transmissivity of the modelled fractures. Also, the transmissivity increase close to the tunnel resulting from the excavation, see Figure 10-6, is much reduced compared with that during the period of excavation. There may be regions very close to the openings where local transmissivity effects could be significant, for instance because of thermally induced shear displacements along fractures in very low compression. According to /Hökmark et al. 2010/ these effects do, however,

not extend more than about a metre into the rock from the wall. As already judged for the excavation phase these impacts are too local to warrant further consideration. Transmissivity effects in the immediate surroundings of the opening peripheries are judged be adequately covered by the schematic representation of the EDZ.

In general, the shear displacements are small, apart from gently dipping fractures with unfavourable orientations with regard to shear stability. The conclusions are the same as those for the far field.

In conclusion, since the impact on fracture transmissivity during the heating phase is small, and very local to the deposition tunnel, there is no reason to assess the implications of these changes in the hydraulic modelling.

Reactivation due to tectonic compression and/or glacio-isostatic adjustment

The tectonic conditions in the Baltic Shield have been stable for the past 2 million years /Muir Wood 1995/. In addition to ridge push, the shield suffered shorter-term loading and unloading because of repeated glaciations and deglaciations. The potential for future seismicity during the temperate period needs thus to be handled as a part of the assessment of seismicity during the glacial cycle. This is discussed in Section 10.4.5. There, it is shown that between $9.3 \cdot 10^{-6}$ and $2.2 \cdot 10^{-5}$ canisters may be sheared 50 mm or more due to earthquakes within the 1,000-year time frame. In short, while the seismic activity is generally very low in Sweden, earthquakes leading to potential canister damage cannot be totally ruled out even during the temperate period.

Fracturing of the rock – thermally induced spalling

Even if the initial rock stress magnitudes may not be sufficient to produce spalling in deposition holes, there is still the possibility that spalling may occur later due to the additional thermal load. The potential occurrence of spalling is site and repository design specific, as it depends on the *in situ* stress, the strength of the intact rock, its thermo-mechanical properties, and on the repository layout. This is the only fracturing mechanism identified as relevant during the initial temperate period.

/Hökmark et al. 2010/ have revised the assessment of the potential for thermally induced spalling presented in SR-Can, using the detailed near-field model geometry that incorporates one tunnel segment with seven canisters, three of which have explicitly modelled deposition holes, see Figure 10-18. The model calculates the tangential stress at the wall of the deposition hole during the period of thermal load. This stress is compared with the spalling strength of the rock. The latter is assumed to lie somewhere between 52%–62% of the Uniaxial Compressive Strength (UCS) of the rock, cf. Section 6.4 in the **Data report**. The following is found, see also Figure 10-22.

- The spalling strength is likely to be reached in all deposition holes during the thermal phase even when the lower limit of the stress magnitudes and most favourable tunnel orientations are considered. /Hökmark et al. 2010/ also assess the major principal stress at the centre of the tunnel roof. As opposed to the stresses in the deposition hole walls, the stresses at the centre of the tunnel roof will not reach the spalling strength during the heated phase.
- For the most unfavourable stress orientation and upper limit of stress magnitudes, it is possible that the lower limit of the spalling strength (52% of UCS) will be reached from the tunnel floor down to a depth of around 7.9 m (both values of the thermal conductivity) after 50 years. The upper limit of the spalling strength (62% of UCS) will be reached after 50 years, from the tunnel floor to a depth of 7.3 m (mean value of the thermal conductivity) and 7.6 m (dimensioning value of the thermal conductivity), respectively.

In addition, SKB has conducted field tests at Äspö HRL /Glamheden et al. 2010/ to assess the potential for mitigating spalling by adding small counter pressures. However, while the project findings supports the possibility that the counter pressure exerted by bentonite pellets in the slot between buffer and rock wall may suppress the spalling, or at least keep the spalled slabs in place and by this minimize the hydraulic transmissivity of the spalled damage zone, current results are inconclusive. For SR-Site, it is judged necessary to assume that thermally induced spalling is likely to occur, and this needs to be considered when assessing the migration across the rock-buffer interface. This does not mean that efforts to handle and mitigate thermally induced spalling should not continue,

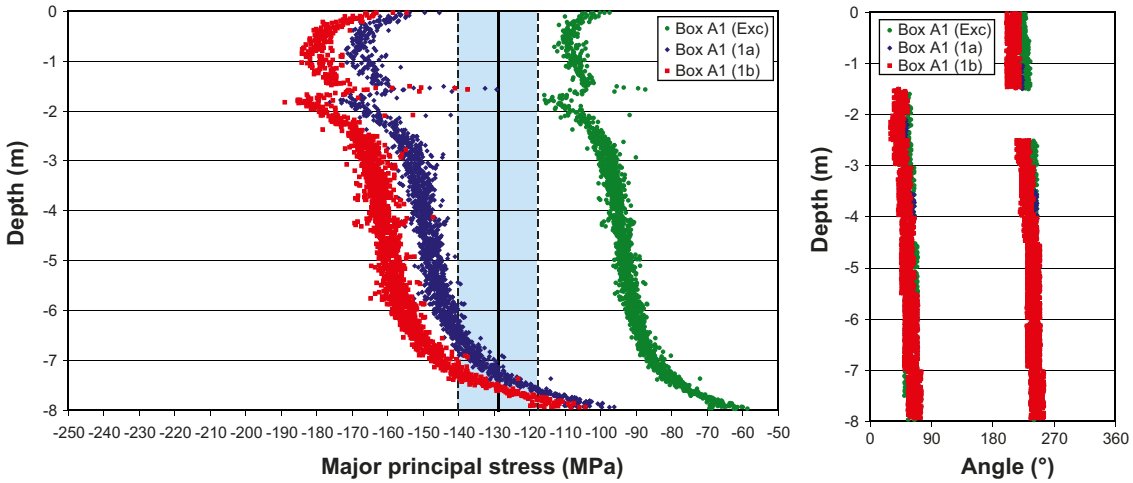

Figure 10-22. *Left: Simulated maximum tangential stress after excavation (green) and 50 years (for two different thermal conductivities- red and blue) along deposition hole wall. Blue area represents spalling strength in fracture domain FFM01 (52–62% of UCS). Right: Location and orientation of maximum stress on deposition hole perimeter. (Figure 9-8 of /Hökmark et al. 2010/).*

since suppressing the spalling will enhance this safety function. There is plenty of evidence in the literature to show that a small amount of confining stress has a significant effect on increasing the compressive strength of a rock, but numerically strict rules for how much counter pressure is needed to suppress the spalling are lacking.

/Hökmark et al. 2010/ also assess whether or not the order of deposition of canisters influences the risk of spalling during the construction of a local tunnel and its deposition holes or if the deposition sequence would influence the magnitudes of the thermally induced stress concentrations. Their results show that the construction-deposition sequence approximation made in all models in their report, i.e. that all excavation work has been completed prior to deposition and that all canisters are deposited simultaneously, is valid unless very specific sequences are used (for instance excavating or depositing late, close to regions of early deposition). Given a proposed construction-deposition sequence, it will easily be checked (e.g. by use of the thermo-mechanical analytical solution demonstrated in /Hökmark et al. 2010/) that these approximations hold also for that specific case.

Potential for creep – time dependent deformation

The concept of creep implies that a material has inherent time-dependent mechanical properties so that movements take place without additional loading, due to already active stresses. The consequence of extensive creep movement along fractures would be that fracture shear stresses would relax and that the stress state would tend to be less deviatoric over time. However, there is no evidence, anywhere in the world where deep mining is carried out in hard rocks that such a condition exists, i.e. substantial deviatoric stresses are recorded at all mine sites. Based on this, it was argued in SR-Can that the relative importance of creep, i.e. in comparison to movements calculated to take place in direct response to changes in mechanical load and pore pressure, are small enough that effects of creep can be neglected.

These conclusions are strongly supported by a recent study by /Damjanac and Fairhurst 2010/ assessing whether there is a lower bound to the long-term strength of rocks. The analysis demonstrates that there is always a stress threshold for confined conditions, because confinement acts to suppress the tensile stresses associated with crack growth. Furthermore, even under unconfined conditions, the internal structure and heterogeneity of the rock, with grains several orders of magnitude tougher than the interface, results in blunting of the fracture tip and arrest of the fracture, even when the fracture toughness is reduced to zero (i.e. assuming that the stress-corrosion activation energy is zero). The actual magnitude of the lower bound to the long-term strength, when the stress-corrosion activation energy is assumed to be zero, will depend on a number of parameters, including pre-existing fracture sizes, their spacing, grain size and magnitude of confining stress.

If spalling occurs and a notch forms, the stress adjustments that can occur at the notch tip may cause additional time-dependent/creep deformations. The monitoring of the unconfined open notch in the APSE Experiment showed that the majority of the new displacements occurred in the existing notch /Andersson 2007/. /Martin and Kaiser 1996/ reported that the displacements for an unconfined spalled zone/notch in the AECL Mine-by Test Tunnel Canada were monitored for a 13 day period and that the creep related displacements amounted to between 0.6 and 1.4% of the total displacements measured over that period. They concluded from their field experiment that changes in the measured displacements over time generally can be attributed to changes in boundary conditions and that these time-dependent displacements occur in the unconfined damaged zone around the test tunnel. As shown by the APSE experiment a small confining stress is often sufficient to suppress spalling /Andersson 2007/. When the spalled notch is confined, any time-dependent deformations are expected to be insignificant, compared with the deformations that formed the notch.

It can also be noted that the effects of fracture creep, in terms of fracture displacement under constant shear load because of time-dependent material strength properties, can be estimated using the modelling approach for fracture reactivation described in /Hökmark et al. 2010/. This would be the same as those of a slow decrease in fracture shear strength, i.e. some additional stress relaxation and a corresponding amount of additional movement. Even if the strength is reduced to zero over the entire fracture plane, only very minor fracture displacements would occur.

Creep deformation and related issues like “sub-critical crack growth” is, therefore, not further considered in SR-Site.

Identified uncertainties and their handling in the subsequent analysis

The discussion above can be used to draw a set of conclusions regarding the uncertainties and their subsequent handling in the SR-Site analyses in relation to the mechanical evolution during the initial temperate period.

- *Reactivation of fractures in the near field* due to thermal load that could affect the mechanical stability and the fracture transmissivity in the near-field rock are excluded from further analysis since the calculated impacts on fracture transmissivity during the heating phase are small, and very local to the deposition tunnel.
- *Reactivation of fractures in the far field* that could affect fracture transmissivity is excluded from further analyses since the calculated transmissivity changes induced by the thermal load are judged too small to require any further consideration in the far-field hydrogeological analyses.
- *Reactivation due to tectonic compression* that could affect the mechanical stability of the deposition holes (safety function R3a) cannot be totally ruled out even during the temperate period. This is further assessed in Section 10.4.5.
- *Fracturing of the rock, i.e. thermally induced spalling*, is likely to occur but the counter pressure exerted by bentonite pellets in the slot between buffer and rock wall, may suppress the spalling, or at least keep the spalled slabs in place and minimize the hydraulic transmissivity of the spalled damage zone. A set of distinct calculation cases, assuming no spalling or spalling in all deposition holes, are propagated for further assessment. This does not mean that efforts to handle and mitigate thermally induced spalling should not continue since suppressing the spalling will enhance this safety function. The potential for spalling may also depend on the deposition sequence, but only for very specific ones. Nevertheless this may need consideration for the detailed design of deposition areas, see further Section 15.5.15.
- There is no potential for *creep deformation* that significantly could affect deposition hole geometry, allowing the exclusion of the phenomenon.

10.3.6 Hydrogeological evolution

In SR-Site, the hydrogeological evolution during the temperate period after repository closure involves two distinct time intervals. The first is that for saturation of the repository once pumping of the open tunnels has stopped. The subsequent time interval deals with the evolution of the saturated repository up till the start of the next glacial period. The actual impacts primarily depend on the permeability

distribution of the bedrock (fracture network connectivity and hydraulic properties of the fractures), the repository layout and the associated permeability of the backfilled tunnels, and the prevailing initial and boundary conditions. At Forsmark, the primary hydraulic driving force for groundwater flow during the temperate period considered in SR-Site is the flushing due to precipitation; the ongoing shoreline displacement implies a continuous change in the flushing pattern. In order to assess the magnitude of these impacts, groundwater flow simulations, based on the hydrogeological models developed as part of the **Site description Forsmark**, have been performed. These models start at 8000 BC, i.e. at a time when the Forsmark area was submerged under approximately 100 m of water.

The overall objective is to assess the effects of a temperate climate on site hydrogeochemical and hydrogeological conditions in the presence of a backfilled repository, i.e. safety functions R1 and R2 in Figure 10-2. The expected effects with relevance for long-term safety are mainly related to the composition of groundwater and the performance measures (PM) of groundwater flow at repository depth and the so-called flow-related transport properties.

Methodology

In order to meet the requirements of SR-Site /Joyce et al. 2010/ adopted a methodology where a mixture of discrete media (DFN) and continuous porous media (ECPM and CPM) flow concepts using the ConnectFlow modelling tool are used in a sequence. Furthermore, due to computational constraints that arise from using large amounts of high resolution data within a large model domain, three "model scales" are used in ConnectFlow; regional scale, repository scale and site scale.

In the *regional-scale* model, variable-density pressure solutions are derived for a transient flow model based on continuous porous media concepts. The advective transport of salt is subject to a dual-porosity rock matrix diffusion (RMD) process. Between 8000 BC and 1000 AD, the repository area is submerged and for a long period covered by marine water (Littorina Sea). Between 1000 AD and 12,000 AD, terrestrial conditions prevail and the groundwater is subjected to a flushing by meteoric water. The shoreline displacement between today and 12,000 AD results in a total vertical displacement of the area of about 40 m upwards. Thus, the modelling methodology used for SR-Site is identical to that used for SDM-Site, except that the regional-scale modelling in SDM-Site halted at 2000 AD.

The usage in SR-Site of the results from the regional-scale flow modelling between 2000 AD and 12,000 AD is based on the assumption that there is no remaining impact from the excavation and operational phases on the groundwater salinity or the variable-density flow during the initial period of temperate climate after closure. Given that this assumption is justified, the regional-scale flow modelling between 2000 AD and 12,000 AD is representative for the initial period of temperate climate after closure. In the reference evolution of SR-Site, the initial temperate period is assumed to end at 8000 AD; thus the hydrogeological modelling covers a slightly longer period. The choice of 12,000 AD is made in order to assess the effects of the shoreline displacement up to the point in time when the shoreline retreats beyond the model domain.

The output from the regional-scale model consists of pressure, salinity, concentrations of groundwater constituents, fractions of reference waters, and fluid density at predefined time slices between 8000 BC and 12,000 AD. The salinity and fractions of reference waters are used as input to the analysis of the chemical conditions in the proximity to the repository during the initial period of temperate climate after closure, i.e. between 2000 AD and 9000 AD (Section 10.3.7), as well as during the submerged conditions following forthcoming periglacial and glacial conditions, i.e. based on results from the modelled period between 8000 BC and 1000 AD (Section 10.4.7). The simulated pressures and densities are used to define initial and boundary conditions of the groundwater flow modelling carried out on the more detailed model scales, i.e. repository scale and site scale, during the initial period of temperate climate after closure, i.e. between 2000 AD and 9000 AD. Thus, the temperate period is assumed to last until 9000 AD in both the hydrogeochemical analyses and the hydrogeological analyses at the most detailed scale.

In the *repository-scale* model, steady state pressure solutions are derived for predefined time slices between 2000 AD and 12,000 AD treated in the regional-scale model. The pressure solutions assume fixed pressures on the model domain boundaries and a fixed, yet spatially varying, density field throughout the model domain. Hence, there is no advective transport of salt and no matrix diffusion in the repository-scale model; i.e. the salinity field is fixed.

The physical dimensions of the repository-scale model domain are limited because of the computational constraints involved. Therefore, three repository blocks are used. For each repository block, the derived pressure solution is based on a discrete fracture network (DFN) medium representation of the fractured bedrock surrounding the repository. It is noted that in the repository-scale model, some of the implemented repository features are modelled in a discrete fashion, i.e. ramp, shafts, central area and transport tunnels, whereas others are modelled as continuous porous media, i.e. deposition holes, deposition tunnels and main tunnels.

The output from the repository-scale model consists of two types of performance measures with regard to safety functions R2a and R2b, see Figure 10-2.

1. Cumulative advective travel times (t_w [T]) and flow-related transport resistances[16] (F [TL^{-1}] of the released particles.
2. Darcy fluxes (q [LT^{-1}]) and equivalent flow rates (Q_{eq} [L^{3}T^{-1}]) at the deposition-hole positions.

The Darcy fluxes and equivalent flow rates are used as input to buffer erosion-corrosion analyses (Sections 10.3.11 and 10.3.13) as well as input for the near-field radionuclide transport calculations (Chapter 13). The advective travel times and flow-related transport resistances are used as input for the far-field radionuclide transport calculations (Chapter 13). In the transport calculations, three release paths, Q1, Q2 and Q3, for radionuclide release are considered, see also Figure 13-12:

1. A fracture intersecting the deposition hole, i.e. the Q1 path.
2. The excavation damaged zone (EDZ), if such a zone exists, located below the floor of the deposition tunnel that runs above the deposition holes, i.e. the Q2 path.
3. A path through the backfilled tunnel and into a fracture intersecting the deposition tunnel, i.e. the Q3 path. The Darcy flux associated with this path is the flux in a fracture intersecting the deposition tunnel.

Individual particles are released for each canister deposition hole and release path, i.e. three particles per deposition hole, see /Joyce et al. 2010/ for details. It is noted that for the Q3 release path, the fracture intersecting the deposition tunnel is identified through particle tracking of a particle released in the tunnel above the deposition hole. The cumulative values of t_w and F of each particle together with its exit location on the side of the repository-scale block are propagated to the site-scale model for continued particle tracking to the biosphere.

The *site-scale* model domain is as large as the regional-scale model domain, but a mixture of the flow concepts described above is used. However, the mixture of flow concepts is a bit different from that of the repository-scale model as the scale is different. It is noted that the flow concepts are formally coupled through an embedding approach where continuity of both pressure and mass flux is ensured by the use of constraint equations, see /Joyce et al. 2010/ for details.

In the site-scale model, steady state pressure solutions are derived for predefined time slices in the same fashion as in the repository-scale model. Thus, there is no advective transport of salt and no matrix diffusion in the site-scale model in contrast to the regional-scale model.

In the repository-scale model, particles are also back-tracked from the deposition hole positions in order to assess recharge pathways. The particle paths extend into the site-scale model in a corresponding manner to the discharge pathways. An assessment of the potential for penetration of dilute waters to repository depth is made by /Joyce et al. 2010, Appendix F/. The assessment is based on the recharge paths and an analytical solution for solute transport.

Performed analyses and usage within SR-Site

Below, the different cases that /Joyce et al. 2010/ performed with relevance for the periods with temperate climate conditions are listed. In addition, the saturation calculation of /Svensson and Follin 2010/ is included. Finally, it is indicated where the results produced by each case are used within the subsequent analyses of SR-Site.

[16] The flow-related transport resistance is an entity, integrated along a flow path, that quantifies the flow-related aspects of the possible retention of a solute transported in fractures. A description of how the flow-related transport resistance is calculated in the present analysis is given in /Joyce et al. 2010/ and summarised in both the **Data report** and in /Selroos and Follin 2010/. A comprehensive, and more general, description of the flow-related transport resistance is given in e.g. /Crawford and Sidborn 2009/.

- **Saturation**. In the simulations of /Joyce et al. 2010/, the back-filled repository is assumed saturated. However, the analysis of the temperate period formally starts when the repository is closed; i.e. prior to full saturation. In order to assess the simplification of assuming full saturation, an assessment of the saturation process is conducted. The results of the saturation calculations are also used in Section 10.3.8.
- **Hydrogeochemical evolution**. The groundwater chemistry, here represented as fractions of different reference waters, is calculated in the regional-scale model utilising a porous medium representation of the discrete fracture network /Joyce et al. 2010/. Due to the shoreline displacement process and infiltration of meteoric water, the groundwater chemistry changes with time. The results are used within the hydrogeochemistry assessment in Section 10.3.7.
- **Discharge locations in the biosphere.** The discharge locations of particles transported advectively through the system from all deposition hole positions are calculated. The analysis is first performed in the site-scale model for every 1,000 years (i.e. from 0 AD to 12,000 AD) in order to support the identification of discharge locations in the biosphere, see Section 10.3.3 for details. Furthermore, discharge locations are calculated in the combined repository and site-scale models including a detailed representation of the repository structures for a few selected snapshots-in-time. These flow paths are used when flow-related migration properties are calculated, see bullet point below. Due to the shoreline displacement process, the discharge locations move in time and generally follow the retreating shoreline.
- **Performance measures.** The main performance measures used in the subsequent radionuclide transport calculations are the Darcy flux (and associated equivalent flow rates) and flow-related migration properties along flow paths. These are calculated for each deposition hole position (Darcy flux and equivalent flow rates) and associated flow path from deposition hole position to the biosphere (flow-related transport resistance and advective travel time). Due to the shoreline displacement, these measures also change with time. The results are used as input for the buffer erosion and canister corrosion analyses (Sections 10.3.11 and 10.3.13) and for radionuclide transport calculations, see Chapter 13.
- **Penetration of meteoric water.** The recharge of meteoric water in combination with the shoreline displacement implies a gradual dilution of the originally more saline water. As dilute water has negative effects on the buffer and backfill stability, it is of interest to assess the possibilities of dilute water reaching repository depth considering the hydrogeological flow and transport conditions. This is done using the flow-related migration properties described above in conjunction with analytical transport estimates. The results are used within the hydrogeochemistry assessment in Section 10.3.7.
- **EDZ, crown space and spalling.** The intended properties of the repository are defined in the **Underground openings construction report** and the **Backfill production report**; however, it is of interest to assess consequences in terms of the performance measures if the intended repository properties are not achieved. The results of these sensitivity analyses are mainly used in Chapter 13.
- **SDM-Site related model variants.** The hydrogeological base case properties of the geosphere are defined through SDM-Site Forsmark /Follin 2008/. However, it is of interest to assess consequences in terms of the performance measures if the geosphere is assumed to be characterised by other cases or properties identified as relevant in the SDM-Site work. The results of these sensitivity analyses are used for the buffer erosion and canister corrosion analyses (Sections 10.3.11 and 10.3.13) and for radionuclide transport, see Chapter 13.
- **Unsealed boreholes.** Boreholes are drilled in close proximity to or into the repository rock volume both during the characterisation phase and during construction. In case the sealing of these boreholes does not function as intended, or if a borehole is abandoned and forgotten, the boreholes may affect the groundwater flow and transport characteristics. Variant cases incorporating completely unsealed boreholes are performed to bound the importance of such boreholes. The results of this analysis are also used as input to the Future Human Action scenario, see Section 14.2.

Saturation

The time scale of saturation is estimated using the DarcyTools code based on the methodology described above /Svensson and Follin 2010/. The inflow is calculated separately for each operational stage A–C; for an explanation of the different phases, see Section 10.2.3.

In Figure 10-23, the inflow is shown as a function of time for stage A. A high initial inflow rate is followed by an asymptotic regime where the inflow gradually decreases. Based on the calculations, /Svensson and Follin 2010/ conclude that it will take several hundred years for the repository to reach full saturation. The temperate period is on the order of 10,000 years, hence this initial period of unsaturated conditions covers only a small part of it, and the assumption of saturated conditions within the rest of the simulations of the temperate period can be defended.

In order to study differences in saturation characteristics between different parts of the repository, an analysis is made where slow, intermediate and fast tunnel sections, in terms of saturation, are identified based on the pressure distribution after 100 days of saturation. The result is shown in Figure 10-24 in terms of integrated inflow per metre of tunnel. Approximately 4.1 m^3/m of water is needed to fully saturate the void space of the backfill in the tunnels. The results indicate that after 50 years the fast tunnel section has reached 3.7 m^3/m, whereas the slow tunnel section has reached 2.9 m^3/m. The intermediate tunnel section has reached 3.1 m^3/m.

The water that saturates the backfilled repository structures originates predominantly from the top of the model domain. The reasoning behind this conclusion is twofold. First, the only available free source of water in the model is the recharge at the surface. This enters the model either as net precipitation (meteoric water with an altered chemical composition) or as water from the Baltic Sea (sea water with an altered chemical composition). Second, the permeability of the bedrock is much lower below repository depth than above. In principle, the contrast in kinematic porosity between the backfill and the bedrock suggests that the entire volume of mobile water in the bedrock above repository depth equals the volume of water required to reach full saturation.

Hydrogeochemical evolution

The evolution of groundwater flow and hydrogeochemistry for the temperate period from 8000 BC to 12,000 AD is modelled (note that results only up till 9000 AD are used in the geochemical analyses, see Section 10.3.7). The initial condition is expressed in terms of reference waters which are assumed to contribute to the groundwater composition in the Forsmark area. The chosen initial condition is Deep Saline water at depth, with the less saline groundwater above being a mixture of Deep Saline water, Old Meteoric waters and Glacial Melt water.

Figure 10-25 shows the location of a slice through the regional-scale model domain; in Figure 10-26, the distribution of Altered Meteoric water at 2000 AD and 9000 AD is shown for this vertical slice. The important deformation zones ZFMA2 and ZFMENE0060 in the region of the repository and the repository structures are also shown for context.

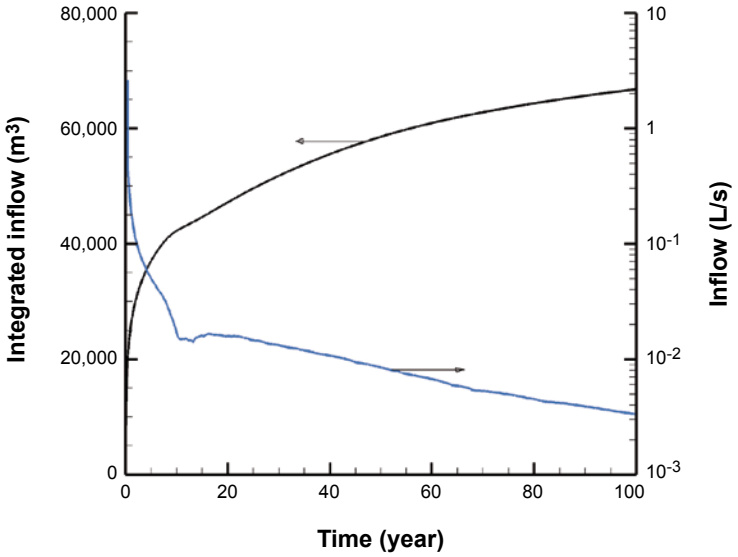

Figure 10-23. *Inflow rate [L/s] and cumulate inflow [m^3] for operational stage A.*

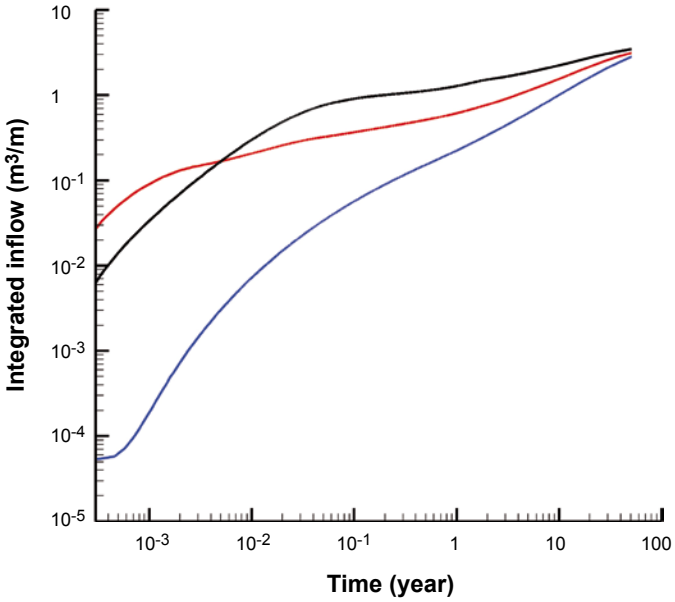

Figure 10-24. *Integrated inflow [m^3/m] for three tunnel sections with different saturation rates; black = fast, red = intermediate, and blue = slow.*

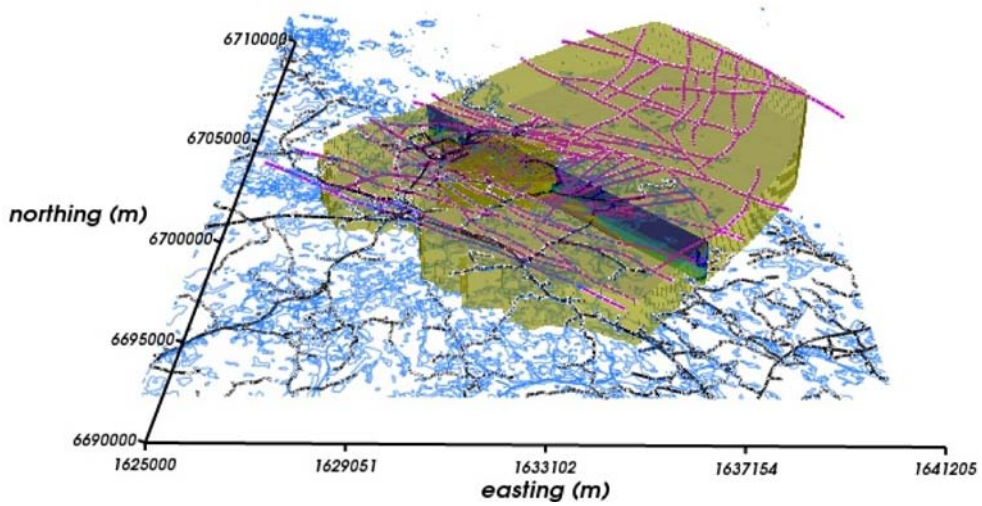

Figure 10-25. *The location of the north-west to south-east vertical slice used in the fractional distribution plots in Figure 10-26.*

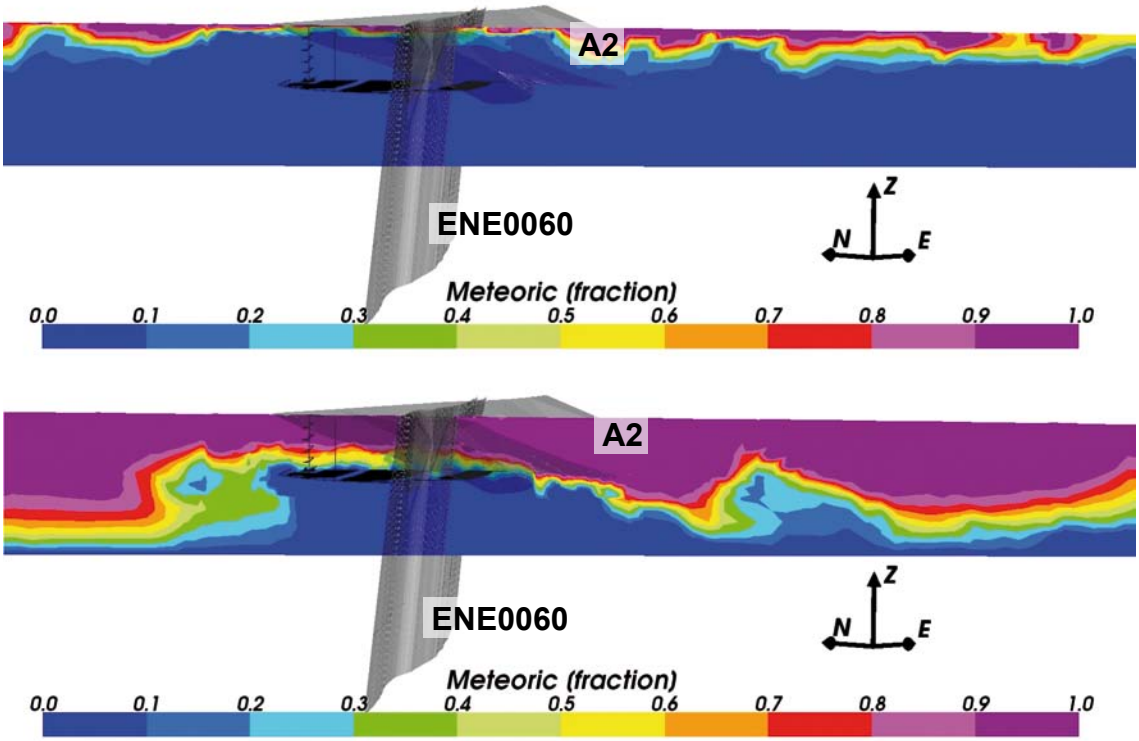

Figure 10-26. *Vertical slices (north-west to south-east) of the fractional distributions of the Altered Meteoric water for the regional-scale model. From the top: Distributions at 2000 AD and 9000 AD. The model depth is 1,200 m.*

In Figure 10-26, the distribution of concentrations of Altered Meteoric water at 2000 AD is comparable to that found in the Site descriptive model, with concentrations (maximum concentration fraction of over 0.9) highest at the very top of the slice. The depth of the highest concentrations increases steadily from 2000 AD through to 9000 AD until it reaches the full depth of the model. Thus, it can be concluded that the domain over time will also be subject to more dilute water conditions at depth. This will have implications on repository performance as discussed below.

Discharge locations in the biosphere

Figure 10-27 shows the discharge point evolution in time. Particles are released in steady-state velocity fields at times from 0 AD to 12,000 AD in the site-scale model. The repository is included in a simplified manner expressed as equivalent fractures. The discharge points of particles released at earlier times (0 AD, 1000 AD and 2000 AD) are located onshore near the repository and show a very slight migration toward the 2000 AD shoreline with release time. The near-future exit points (3000 AD, 4000 AD and 5000 AD) follow the retreating shoreline. The far-future exit points (6000 AD through to 12,000 AD) congregate on the north-eastern model boundary. This may be interpreted such that the model domain should be extended further to the northeast. However, the boundary is consistent with the boundary of the SDM-Site model /Follin 2008/ and also corresponds to a bathymetric depression in the terrain. Thus, extending the model domain would not necessarily change the discharge location pattern. Furthermore, as discussed in Section 13.2.2, a minor change in discharge locations would not affect the derived biosphere discharge areas used in subsequent dose calculations.

In /Joyce et al. 2010/, it is shown that the Darcy flux in the starting locations, and properties along the flow paths (travel time and flow-related transport resistance) are essentially unchanged between different release times.

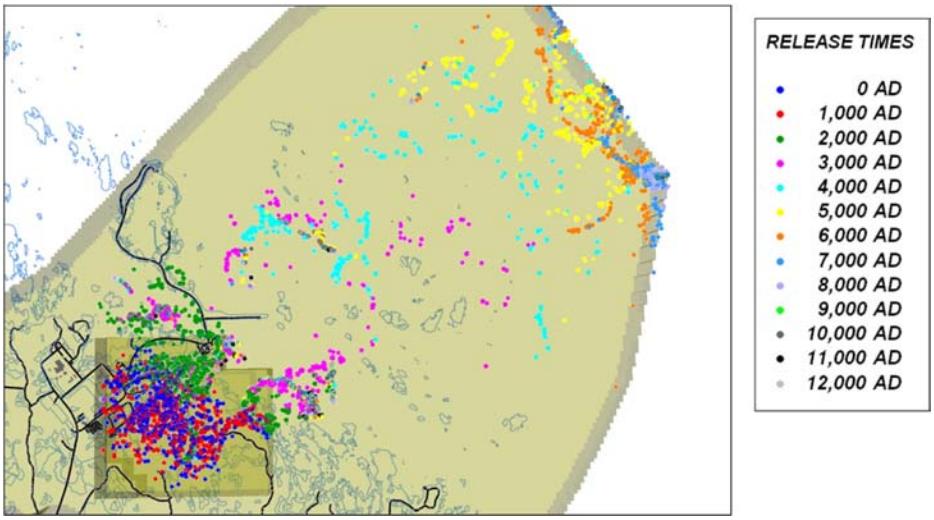

Figure 10-27. *Discharge locations for particles (Q2 path) successfully reaching the top boundary of the site-scale hydrogeological base case model (89%–97%) for releases every 1,000 years from 0 AD to 12,000 AD. The model domain is shown in beige.*

Performance measures

The performance measures are calculated for four steady-state velocity fields at different times; these are 2000 AD, 3000 AD, 5000 AD and 9000 AD. A multitude of results are available in /Joyce et al. 2010/ for multiple times and realisations representing the hydrogeological base case presented. In addition, the effect of branching along flow paths is assessed in a variant calculation by the use of multiple particles per start position. Furthermore, results can be analysed in terms of spatial variability among different particle start locations within the same realisation. Here, only a small subset of the results is presented for illustrative purposes.

In Figure 10-28, the flow-related transport resistance (F) is shown at the starting location for the released particles; i.e. the final F value at the end of the path is shown at the start location. No clear trend of more or less favourable conditions within the repository is readily discerned.

As indicated above when assessing discharge locations, flow paths tend to become longer as the shoreline is displaced. This generally implies longer travel times and larger flow-related transport resistance values with time as indicated in Figure 10-29.

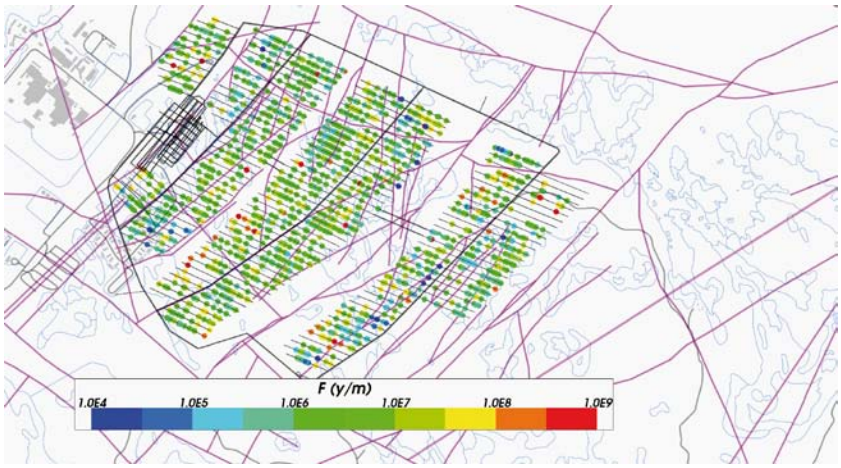

Figure 10-28. *Starting locations coloured by $\log_{10}(F)$ for particles released at 2000 AD (Q1 path) and successfully reaching the top boundary (24%). The HCD model at z = –470m (purple), roads and buildings (black) and shoreline (blue) are also shown.*

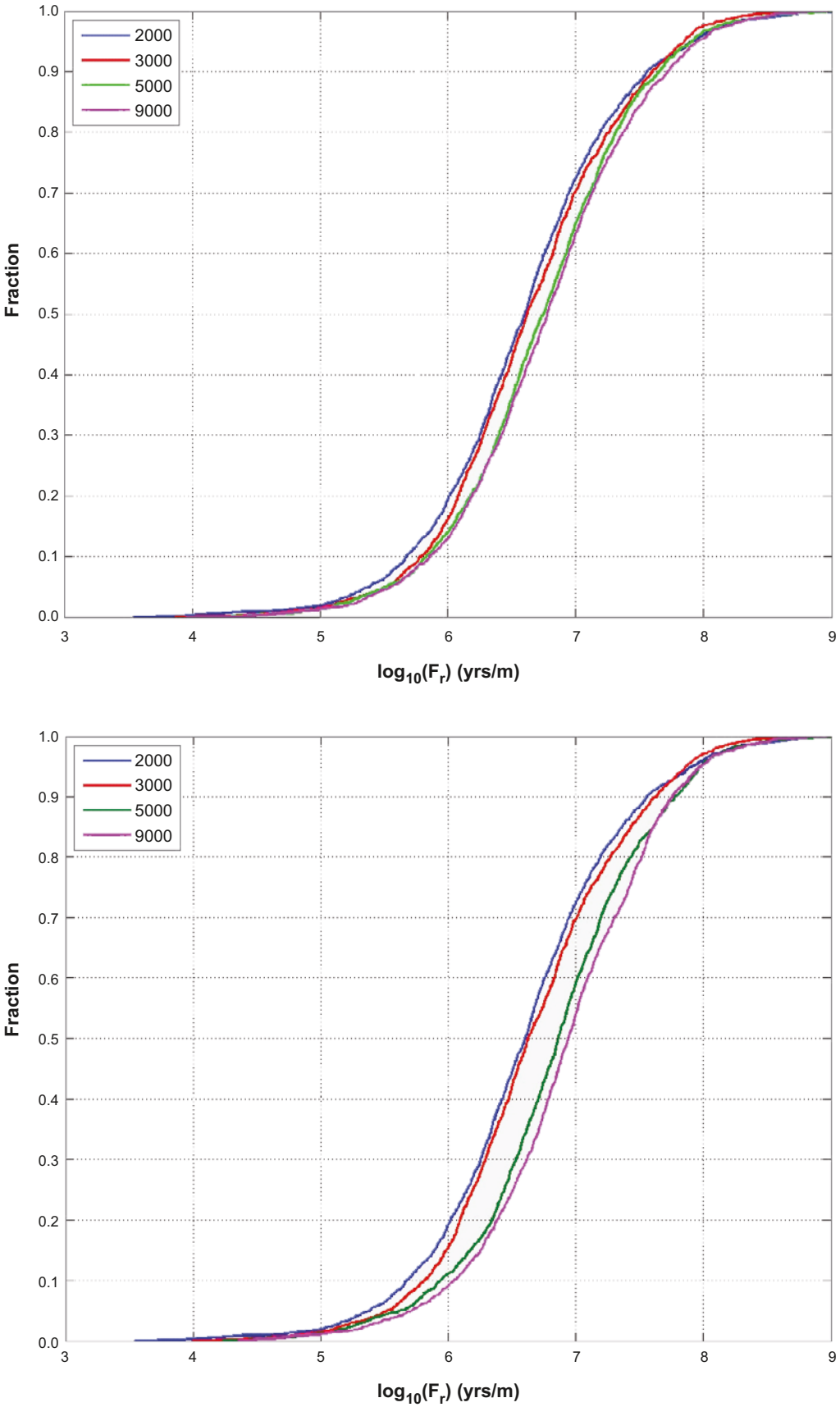

Figure 10-29. *Cumulative distribution function plots of flow-related transport resistance (F) for the Q1 path for the particles successfully reaching the model top boundary (24%) released at 2000 AD, 3000 AD, 5000 AD and 9000 AD. The top plot shows the contribution from the DFN part of the model only, whereas the bottom figure includes the contribution also from the ECPM and CPM parts.*

The definition of the flow-related transport resistance (F) is straight forward in a discrete model; in a continuum model, additional assumptions need to be made. Thus it is of interest to assess how much contribution to the overall F is accumulated in the continuum representation (ECPM+CPM) part of the domain. Figure 10-29 shows that for the later release times, the F values are shifted to somewhat higher values when the continuum representation is included. However, for the subsequent radionuclide transport calculations, only the discrete contribution is included.

As indicated in Section 5.2.2, deposition hole rejection criteria based on the Extended Full Perimeter Criterion (EFPC) are adopted within SR-Site. In Figure 10-30, the effect of the application of this criterion is illustrated for the Darcy flux in fractures intersecting deposition holes. The figure illustrates that roughly 70 percent of deposition holes do not have a flowing fracture intersecting the deposition hole. When the criterion is applied, only about 20 percent of the remaining deposition holes are intersected by a flowing fracture; i.e. the criterion leads to rejection of roughly 10 percent of the deposition holes. Also seen in the figure is that the remaining distribution is shifted towards lower Darcy flux values. Hence, the application of the criterion will have positive consequences for subsequent assessment calculations.

In the hydrogeological base case realisation, all deformation zones are assumed to have a depth trend of transmissivity, but otherwise constant properties. However, the discrete fracture network is stochastic. In additional realisations, the deformation zone properties are also assumed to be characterised by spatial variability. In Figure 10-31, box and whisker plots of the flow-related transport resistance (F) for the Q3 path are shown for the base case realisation and ten additional realisations. It is seen that the median and upper percentiles are quite stable between realisations, whereas some realisations, e.g. r1, r5 and r9, are characterised by a lower tail, i.e. a lower 5th percentile. Corresponding results are observed for the advective travel time; however, the Darcy flux is more stable between realisations. Also, for all performance measures, the Q1 path is characterised by less variability between realisations than the Q2 and Q3 paths. The reason is the large stochastic fractures intersecting the deposition tunnels and hence determining the Q2 and Q3 paths in individual realisations.

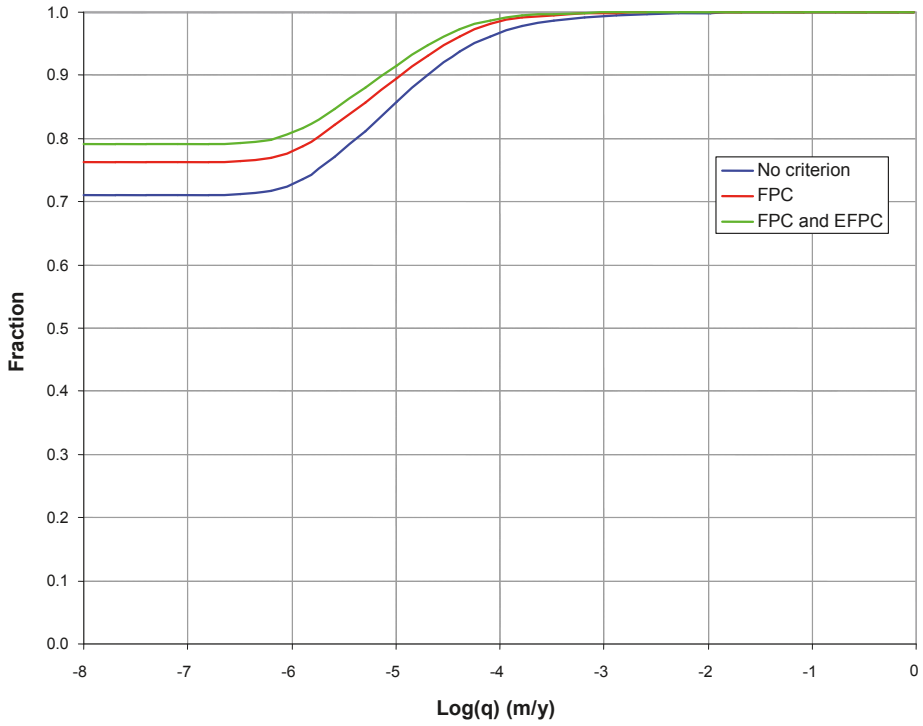

Figure 10-30. *Cumulative distribution plot of Darcy flux (q) for the Q1 path for all deposition hole positions at 2000 AD for different rejection criteria. (Modified after Figure 6-15 in /Joyce et al. 2010/).*

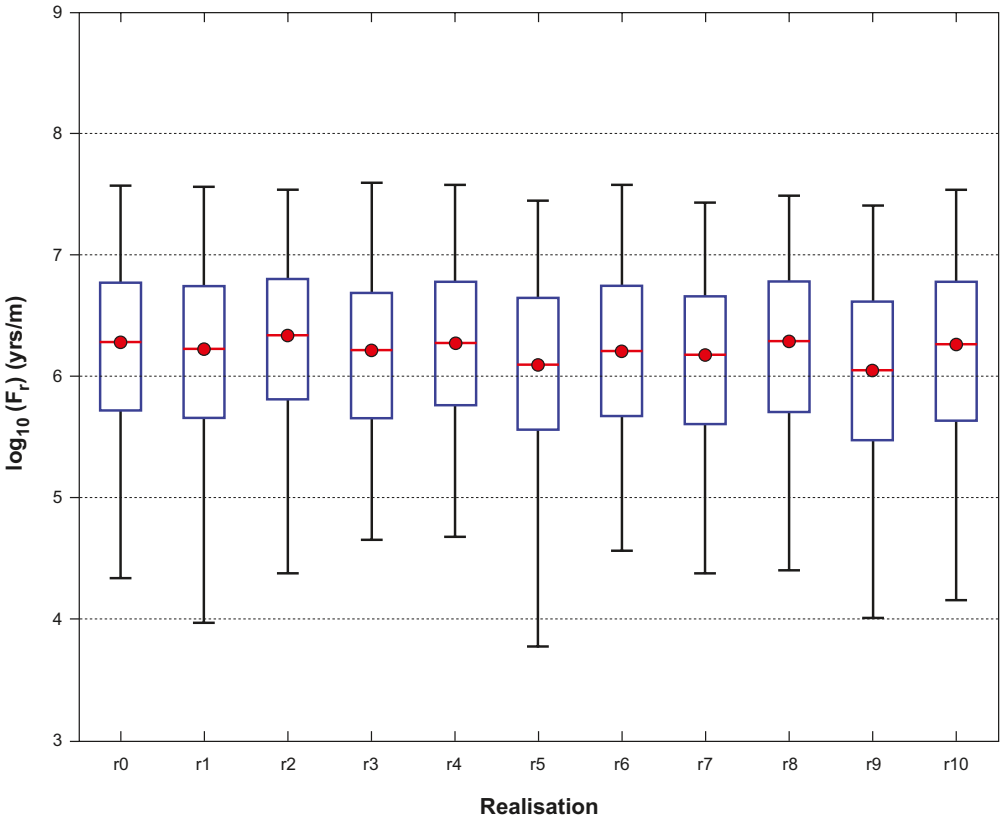

Figure 10-31. *Box and whisker plots of flow-related transport resistance (F) for the Q3 path in the hydrogeological base case realisation (r0) and the 10 stochastic realisations of the HCD and HRD (r1 to r10) for the particles successfully reaching the model top boundary released at 2000 AD. The statistical measures are the median (red), 25th and 75th percentile (blue box) and the 5th and 95th percentile (black "whiskers").*

In order to assess the effect of branching along the flow paths on the advective travel time and flow-related transport resistance, multiple particles (ten) have been released per start point in the particle tracking. Only the 25 percent of start points with highest Darcy flux were used in the comparison. The ten particles choose different flow paths due to a stochastic choice (weighted by flow rate) at each fracture intersection. The results indicate that the branching has negligible effects on the ensemble statistics of the analysed performance measures.

Penetration of dilute water

In principle, the future groundwater chemistry is provided by the regional scale groundwater flow simulation reported above. However, the regional scale simulation was terminated at 12,000 AD and, furthermore, has a fairly coarse discretisation which does not allow an assessment of the groundwater chemistry evolution on a deposition hole scale. Thus, an alternative assessment of the evolution of the groundwater chemistry, and specifically the potential for penetration of dilute water, is made since dilute groundwater may cause erosion of the buffer and the backfill.

In order to assess the potential for penetration of dilute water, a simplified approach is adopted. An injection of meteoric water along those recharge pathways that originate close to the surface within the regional-scale model is considered; it is assumed that the infiltrating water has zero salinity. Note that this is a pessimistic assumption, as discussed in Section 10.1.3. Also, in this simplified calculation, it is assumed that the matrix and fracture water salinity is in equilibrium at the start of the simulations; the relevance of this assumption is also discussed in Section 10.1.3. The flow field and recharge flow paths of year 2000 AD are used. Along the flow paths, the only mitigating process considered is the out diffusion of matrix water affecting the penetration of the meteoric water front. For each deposition hole, the time required for the groundwater salinity to fall below ten percent of the initial water concentration is calculated. Figure 10-32 shows the distribution of these times for

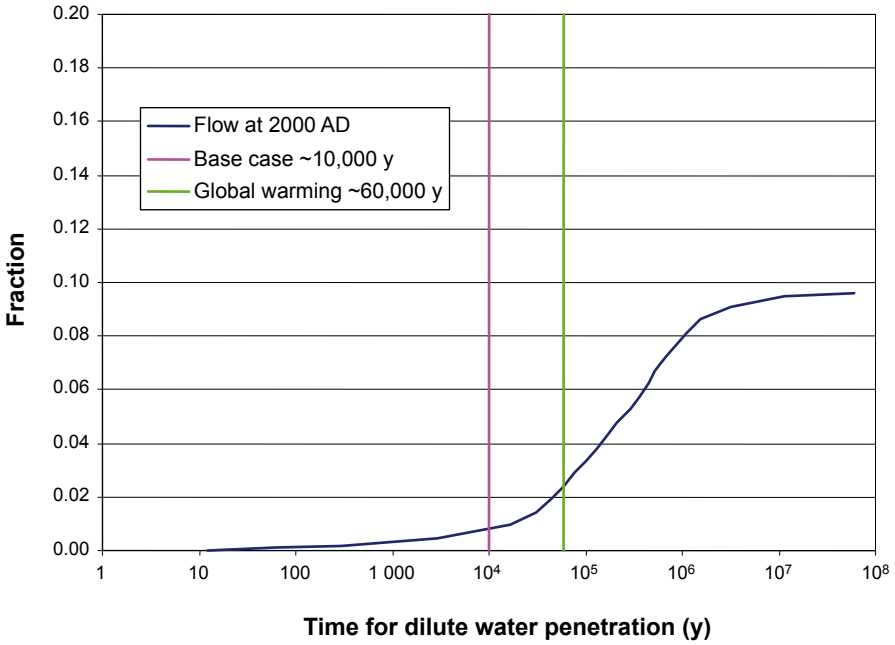

Figure 10-32. *Temporal distribution for all deposition hole positions to obtain ten percent of the initial water salinity concentration. The green line shows that slightly more than two percent of the deposition holes experience dilute conditions within the Global warming variant. The purple line shows that approximately one percent of the deposition holes experience dilute conditions during the first ten thousand years of the initial temperate period.*

all deposition hole positions. The present day salinity at the site is approximately 10 g/L; ten percent of the initial concentration thus corresponds to 1 g/L, which is well above the criterion of 0.3 g/L which is assumed to represent dilute conditions with potential buffer erosion problems, see Section 10.3.7. The vertical lines represent the assumed approximate duration of the temperate period; i.e. 10,000 years for the base case, and 60,000 years for the Global warming variant (see Section 10.6). It is observed that slightly more than two percent of the deposition hole positions experience dilute conditions within the Global warming variant, whereas approximately one percent experience dilute conditions during the first ten thousand years of the initial temperate period.

EDZ and crown space in deposition tunnels

As concluded in Section 10.2.2 there is ample evidence that a potential excavation damaged zone (EDZ) formed during excavation will be kept below the maximum allowed transmissivity as set out by the design premises. Furthermore, data suggest that a continuous EDZ will not develop at all. However, given that the occurrence of the EDZ currently can only be assessed by indirect measurements, it is justified to consider an EDZ according to the design premises, i.e. with an axial transmissivity of 10^{-8} m^2/s as a basic assumption for further analyses. Furthermore, it also seems justified to explore how transmissive an EDZ needs to be in order to significantly impact other safety functions as well as exploring the impact of no axially continuous EDZ at all.

In the hydrogeological base case model, a continuous excavation damaged zone is implemented in all tunnels (deposition, main, transport and access tunnels) under the tunnel floor. The EDZ has a transmissivity value of $T = 1 \cdot 10^{-8}$ m^2/s and a thickness of 0.3 m. In order to assess the sensitivity of performance measures to tunnel properties, four alternative cases are analysed. Two of these have higher EDZ transmissivities ($T = 1 \cdot 10^{-7}$ m^2/s and $T = 1 \cdot 10^{-6}$ m^2/s, respectively), one case has no EDZ, and the final case has the base case EDZ properties, but is combined with a crown space under the tunnel ceiling. The crown space results from a consolidation of the backfill material. In the model, the crown space is implemented as a 0.1 m thick zone with a high conductivity value ($K = 1 \cdot 10^{-3}$ m/s) and a porosity equal to unity.

The Darcy flux (q) for the Q2 path of the particles successfully reaching the model top boundary is shown in Figure 10-33. Since the Q2 path corresponds to the EDZ path, no result exists by definition for the case with the EDZ removed. The figure clearly shows, as expected, that an increase in the EDZ transmissivity implies an increase in the associated Darcy flux. The crown space, on the other hand, implies no change in the Darcy flux in the EDZ. The same holds true for the other release paths; i.e. the crown space has only a marginal influence on the estimated Darcy fluxes.

Concerning the flow-related transport resistance (F), the case with no EDZ provides the most favourable conditions. The reason is that with no EDZ present, particles tend to travel more in the fractured rock, and hence accumulate their F values (no retention is assumed in the EDZ). Conversely, with an increased EDZ transmissivity or a crown space, less favourable conditions prevail and the flow-related transport resistance distributions are shifted towards lower values. The effect of EDZ and crown space on the flow-related transport resistance is most pronounced for the Q3 path.

Effects of spalling

In Section 10.3.5 the mechanical effects of spalling in deposition holes induced by the additional stress caused by the heat from the spent fuel are discussed. The spalling also results in changed conditions for mass exchange between the buffer and the fracture intersecting the deposition hole, in the form of an altered Q_{eq} for the Q1 path. To take into account spalling in deposition hole walls, a special model was developed for use in SR-Can /Neretnieks 2006a/, with an altered equivalent flow rate for the Q1 path due to the damaged zone caused by spalling. This model has been updated for use in SR-Site /Neretnieks et al. 2010/. The altered equivalent flow rate in the damaged zone is obtained as being proportional to the square root of the flow rate in the fractures around the deposition hole, with the proportionality factor being a function of the deposition hole tortuosity (–), porosity (–), width and thickness (m) of the spalled zones, if such a zone occurs. These data are obtained from the modelling results of /Hökmark et al. 2010/ presented in Section 10.3.5 and data from experiments carried out at the Äspö HRL, as further described in the **Data report**, Section 6.5. In Figure 10-34 the effects of spalling are illustrated. The results indicate that spalling may increase the equivalent flow rate for the Q1 path by more than an order of magnitude, but the other paths are not affected.

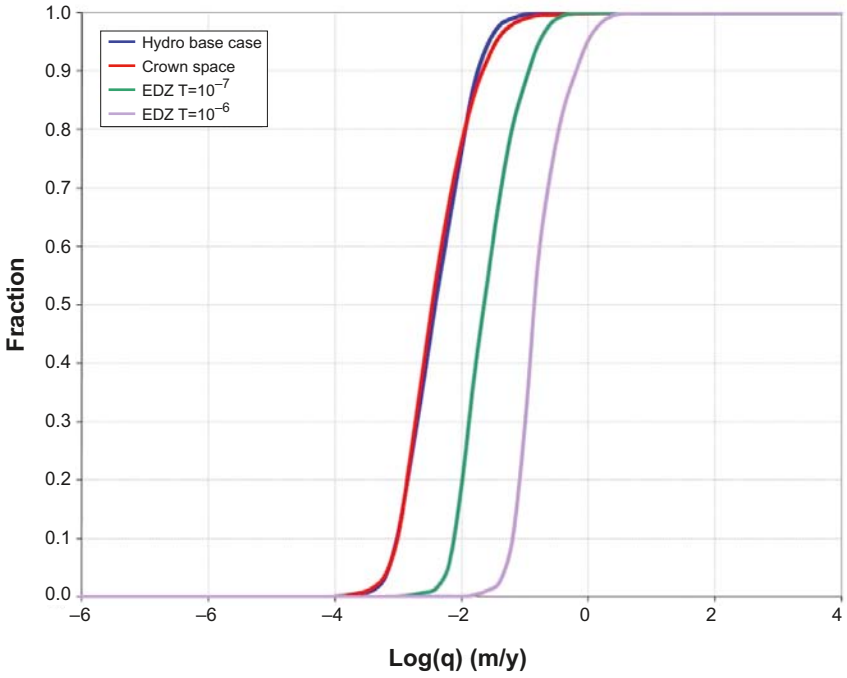

Figure 10-33. *Cumulative distribution function plot of the Darcy flux (q) for the Q2 release path for the hydrogeological base case model, the crown space model, the EDZ $T = 1{\cdot}10^{-7}$ m²/s case, and the EDZ $T = 1{\cdot}10^{-6}$ m²/s case for the deposition holes with particles successfully reaching the model top boundary, released at 2000 AD. (Modified after Figure E-49 in /Joyce et al. 2010/).*

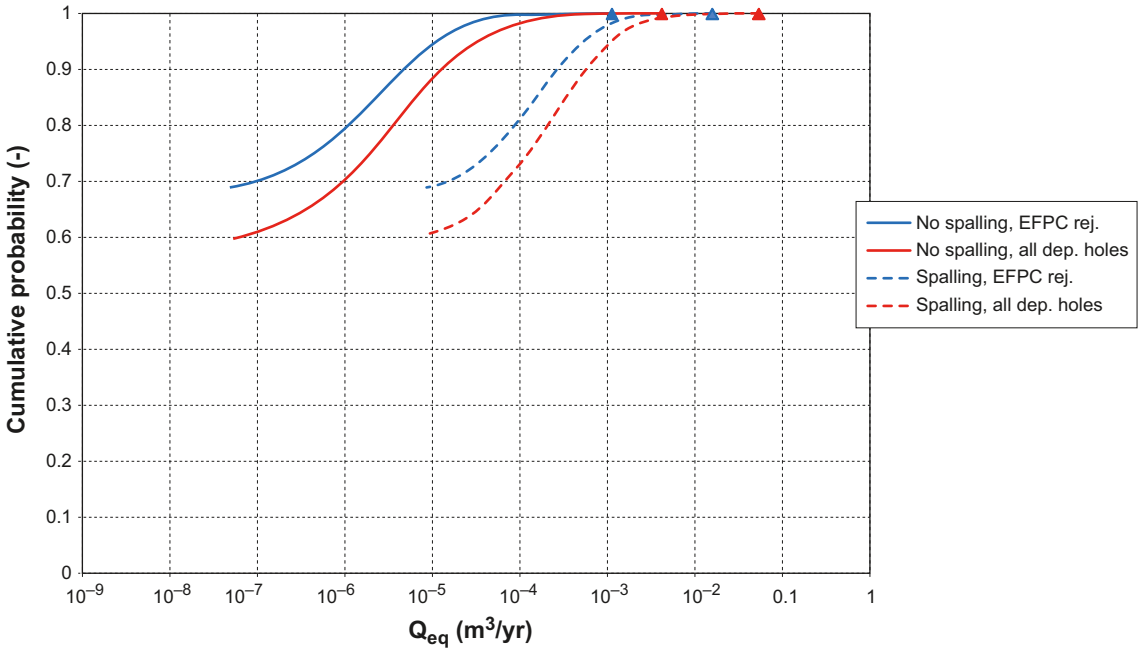

Figure 10-34. *Cumulative distribution plots of Q_{eq} for path Q1 at time 2020 AD in Forsmark for conditions with and without spalling, considering application and no application of the EFPC rejection. The triangles mark the maximum values of the distributions.*

SDM-Site related model variants

A number of variants related to site characteristics and motivated in the SDM-Site report /Follin 2008/ are also assessed within SR-Site. These are briefly summarised below.

Alternative DFN transmissivity-size relationships

The hydrogeological DFN modelling for SDM-Site /Follin et al. 2007b/ treated three kinds of transmissivity-size correlation models; fully correlated, uncorrelated and semi-correlated. It was found that the fully correlated and semi-correlated models reproduced the numbers and shape of distribution of measured specific capacities with the Posiva Flow Log reasonably well, giving a wedge shaped distribution characteristic of having some kind of transmissivity-size correlation, whereas the simulated distribution for the uncorrelated model was flatter and less representative. For this reason, the hydrogeological base case in SR-Site is based on the semi-correlated relationship between transmissivity and size as propagated by SDM-Site. However, to quantify uncertainties, the alternative relationships, i.e. the fully correlated and the uncorrelated models, are also investigated in SR-Site as variant cases, see Figure 10-35.

The particle tracking results reported by /Joyce et al. 2010/ indicate that the performance measures (Darcy flux and the flow-related transport resistance) are dependent on the chosen transmissivity-size relationship with up to about half an order of magnitude variation between variants.

Possible deformation zones

As a variant case for SR-Site, four possible deformation zones (PDZ) identified in SDM-Site were added to the HCD model and treated in the same way as the deterministically modelled deformation zones. These were combined with the corresponding realisations of the HCD and HRD fractures generated for the hydrogeological base case. Figure 10-36 shows the possible deformation zones relative to the repository structures. Some of them intersect the repository structures and may provide potential flow pathways.

The simulated exit locations for the three PDZ realisations show little variation between realisations and are similar to those for the hydrogeological base case. The modelled possible deformation zones have little effect on the performance measures.

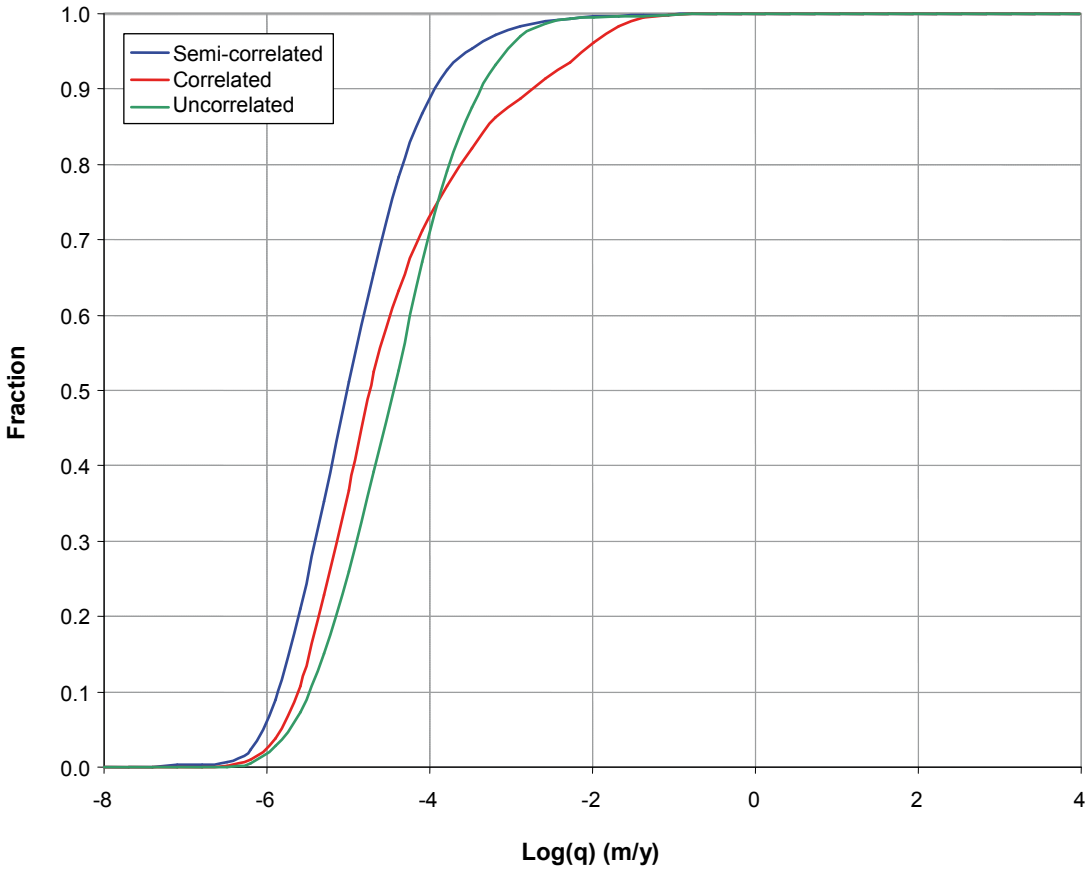

Figure 10-35. *Cumulative distribution function plots of the Darcy flux (q) for the correlated and uncorrelated transmissivity-size relationships compared to the hydrogeological base case (semi-correlated) for the Q1 release path at 2000 AD for deposition holes with particles successfully reaching the model top boundary. (Modified after Figure 6-28 in /Joyce et al. 2010/.)*

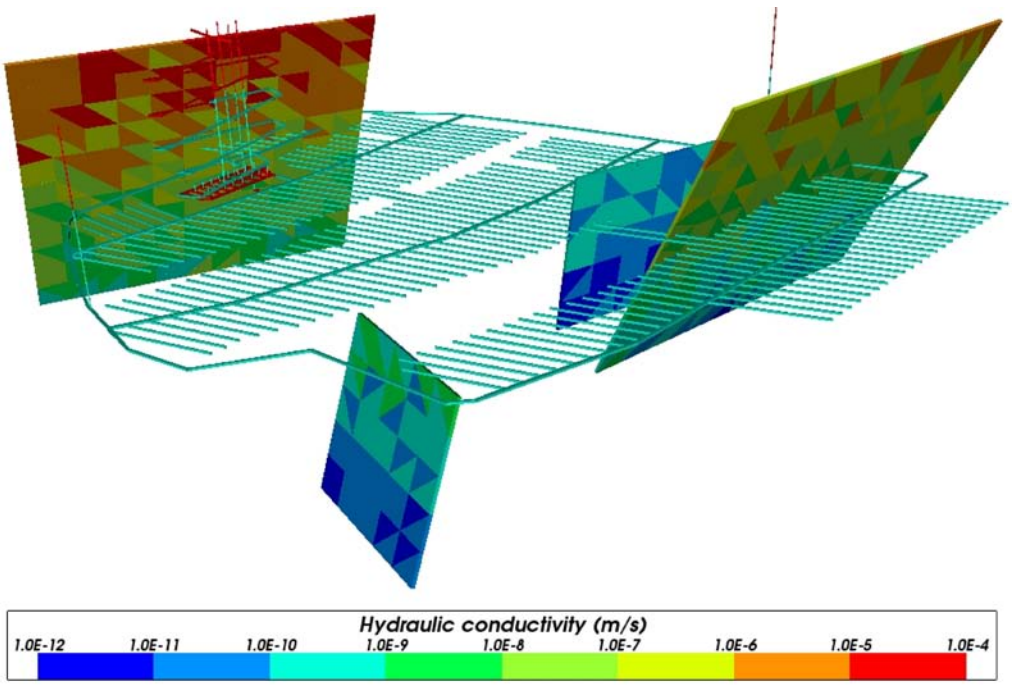

Figure 10-36. *Realisation 1 of the possible deformation zones in relation to the repository structures.*

Unmodified vertical hydraulic conductivity

During the calibration and confirmatory testing of the SDM-Site base model simulation, the vertical hydraulic conductivity of the ECPM representation of the HRD above an elevation of −400 m was reduced by a factor of ten in order to provide a better fit to chemistry and interference test data. This modification was also used for the ECPM representation in the regional and site-scale hydrogeological base case models for SR-Site. However, no corresponding change was made to the properties of the fractures in the DFN representation in the site-scale model, leading to a possible inconsistency in flows between the DFN and ECPM in the site-scale model. Therefore, as a variant case for SR-Site, the modification of the vertical hydraulic conductivity of the ECPM representation used in the regional and site-scale models was removed.

The simulated exit locations for the unmodified vertical hydraulic conductivity variant case are similar to those for the hydrogeological base case. The cumulative distribution function plots showing the Darcy flux and the flow-related transport resistance compare well with the corresponding plots for the hydrogeological base case suggesting that the site-scale model is insensitive to changes in the vertical hydraulic conductivity in the ECPM.

Extended spatial variability

The HRD model developed for SDM-Site essentially covers the repository site area. Outside this area, there was little or no information available to support any elaborated HRD modelling. Therefore, the bedrock outside the repository area was modelled as a CPM with homogeneous and isotropic properties for each depth zone. The hydrogeological base case in SR-Site is no different in this regard.

As a model variant for SR-Site, the area treated as a CPM in the hydrogeological base case was replaced by an elaborated HRD. The additional DFN data required for this variant case come from the investigations at SFR /Öhman and Follin 2010/. This information is used to provide a full ECPM representation for the regional-scale and site-scale models. In addition, the area of the DFN in the site-scale model was extended northwards beyond the Singö deformation zone, which may provide an important discharge location. Both models retain the existing HSD. The repository-scale model is not included in the analysis.

For the extended spatial variability case, more particles seem to exit closer to the repository, which is reasonable given the improved representation of discrete features (flow paths). However, the cumulative distribution function plots showing the Darcy flux and the flow-related transport resistance do not differ significantly from the corresponding plots for the hydrogeological base case, thus suggesting that the extended spatial variability case has only a moderate effect on performance measures.

Unsealed boreholes

The results indicate that the presence of an open borehole has some effect on the flow field. However, in most simulations only a small subset of released particles enter the boreholes. As a maximum, 23% of the released particles enter a borehole in one simulation.

The statistical analysis of the complete ensemble of the released particles shows that there is little change in performance measures. The change in performance measures generally stays within 20% comparing the borehole case to the hydrogeological base case. The performance measures behave as expected; the Darcy flux is slightly increased while the advective travel time and flow-related transport resistance are somewhat decreased in the borehole cases.

When the statistical analysis is performed on only the particles that enter the boreholes and the results are compared to the same subset of particles in the hydrogeological base case, the effect on the performance measures is larger. However, the changes still remain within a factor of four and in the same direction for the different performance measures as before.

Thus, it can be concluded that including a borehole in the hydrogeological base case model does not have a major effect on the performance measures even if the groundwater flow pattern is affected and the flow paths of the released particles change.

Identified uncertainties and their handling in SR-Site

General uncertainties of the results presented in this section are related to the derived hydrogeological discrete fracture network (DFN) model used in the hydrogeological base case. A comprehensive discussion of these uncertainties, including the relation between the hydrogeological DFN and geological DFN models, is presented in the **Data report**, Section 6.6. Below, specific uncertainties related to the performed analyses are discussed.

Saturation. Based on their calculations, /Svensson and Follin 2010/ conclude that it will take several hundreds of years for the repository to reach full saturation, with a relatively short period of rapid initial inflow followed by an asymptotic regime where the inflow gradually decreases. The time scale for saturation is probably overestimated in DarcyTools considering the adopted simplified handling of capillary suction /Enssle and Poppei 2010/. The saturation times reported by /Svensson and Follin 2010/ are within the range of values obtained from modelling where the hydrology of the backfill is treated in more detail and where also the buffer is included (see Section 10.3.8).

Hydrogeochemical evolution. The uncertainties related to the hydrogeochemical evolution are mainly related to the chosen initial and boundary conditions. Thus, the evolution of the proportions of individual reference waters is associated with an uncertainty comparable to the uncertainty in initial and boundary condition specification. The evolution of salinity, which depends on the reference water composition, is hence also associated with some uncertainty; however, it is argued that this uncertainty is smaller than the uncertainty related to the individual reference waters since the salinity is an integrated entity (summation of individual reference water constituents). The modelled salinity development of generally more dilute conditions during the temperate period is considered an evolution with a high degree of certainty.

Discharge locations in the biosphere. Due to the continuum representation in the outer parts of the domain where particles tend to discharge at later times, the discharge locations may be excessively dominated by the location of the shoreline. For a discrete representation, the exit locations may be more influenced by outcropping deformation zones or fractures. This issue is examined in the extended spatial variability variant case, see SDM-Site related model variants below for details.

Multiple realisations and branching. The uncertainty in performance measures is addressed both through multiple realisations and multiple particles per start location. The results indicate that branching (assessed by multiple particles per start location) implies no additional uncertainty, whereas there is some variability between realisations. Thus, multiple realisations need to be assessed in subsequent analyses.

Choice of conceptual model. The uncertainty in results due to the conceptual model chosen, i.e. a discrete representation where the parameterisation of the discrete model has been done according to the methodology developed as part of the site descriptive modelling /Follin 2008/, has been assessed by adopting a different conceptual model representation. In /Liu et al. 2010/, the channel network modelling tool CHAN3D has been applied to the temperate conditions of the Forsmark site, and the corresponding performance measures as in /Joyce et al. 2010/ have been calculated. In CHAN3D, the model is parameterised using the statistics of block-conductivity values resulting from upscaling of the original hydrogeological DFN model. The results indicate that the reported median performance measures are very similar, whereas the spread of results is smaller in CHAN3D than in the ConnectFlow application. These results are consistent with findings in an earlier assessment (SR 97) as reported by /Selroos et al. 2002/; i.e. discrete models tend to exhibit more spreading than continuum representations.

Kinematic porosity. Out of the different performance measures, only the advective travel time is dependent on porosity (or aperture in a discrete model). In /Joyce et al. 2010/ the effect of this uncertainty is considered, and a comprehensive evaluation is presented in /Selroos and Follin 2010/. The conclusion is that this uncertainty is of limited importance for the applications within SR-Site since advective travel time has only a minor impact on hydrogeochemical and radionuclide transport simulations.

Penetration of dilute water. The assessment of penetration of dilute water should be considered an approximate quantification. First, the flow field at 2000 AD is used; i.e. the temporal development in flow characteristics is not accounted for. Second, no mixing or water-rock interactions are considered, which clearly may affect the water chemistry evolution. Thus, the reported numbers should be seen as very rough estimates rather than predictions of a future evolution. However, the presented numbers of deposition holes experiencing dilute conditions are deemed appropriate for use in subsequent analyses of buffer erosion and canister corrosion as they are likely pessimistic estimates. The site understanding presented in Section 10.1.3, based on collected data, indicates that dilute waters do not penetrate to repository depth. However, as the simplified analysis conducted here indicates, it is hard to defend that not a few deposition holes could experience dilute conditions.

EDZ, crown space and spalling. The extent of the crown space is purely hypothesised. In reality, a crown space is considered unlikely or even impossible to develop with a swelling backfill, see Section 10.3.8. The implemented properties of the EDZ are also assessed to be pessimistic, see Section 10.2.2. Thus, the cases addressed are pessimistic variants, and no additional uncertainties relative to the simulations with base case repository properties are identified. However, the cases with modified repository related properties are of interest to propagate to subsequent radionuclide transport calculations since system performance is affected.

SDM-Site related model variants. The uncertainty in performance measures of the SDM-Site related hydrogeological base case parameterisation is addressed through a number of model variant simulations. Among the four variant cases studied, it is primarily the "Alternative DFN transmissivity-size relationship" variant cases that suggest any substantial additional variability (uncertainty). The results for these variant cases indicate that the performance measures of the semi-correlated relationship utilised in the hydrogeological base case model in general are more favourable than the other two correlation models. Thus it is important to propagate the other correlation models to assessment calculations. The results of the extended spatial variability variant case indicate that the effect of representing the full domain in a discrete fashion changes the discharge location pattern to a certain extent. Specifically, the incorporation of the additional discretely modelled fractures causes more particles to exit close to the repository. However, since the base case parameterisation already contains discharge locations close to the repository, it is argued that this variant does not warrant further consideration in the subsequent analyses.

In summary, the uncertainty in transmissivity-size relationship implies that all three correlation models need to be propagated for subsequent analyses of buffer erosion, canister corrosion and radionuclide transport. The other SDM-Site related variants do not warrant further consideration in the assessment.

Channeling. The calculated flow-related transport resistance (F) values can be used unmodified in subsequent radionuclide transport and oxygen penetration calculations. In SR-Can, F values were divided by a factor of ten to account for channelling. In SR-Site no such channelling factor is used based on motivations provided in the **Radionuclide transport report**. First, fracture-to-fracture variability is generally larger than within-fracture variability in aperture. Second, fluid can only enter and leave fractures on a limited area, significantly constraining the meander of flow paths. Third, substantial portions of the non-contacting fracture surface area outside of the dominant flow channels may still be accessible by diffusion within the fracture pore space and thus provide additional surface area for radionuclides to interact with the rock matrix.

The results obtained using the alternative conceptual model inherent in CHAN3D, see Choice of conceptual model above, also support the use of an unmodified flow-related transport resistance (F) value. In CHAN3D, the flow-wetted surface is not given through the discrete fractures in the model but rather estimated based on fracture frequency. Thus, similar estimates of F in both modelling tools indicate that the distribution of the flow-related transport resistance should not be modified in the discrete application.

10.3.7 Chemical evolution in and around the repository

Introduction

During the initial temperate period after closure, the infiltration of meteoric waters, the displacement of the Baltic shore line and changes in annual precipitation will influence the hydrology of the site as described in Section 10.3.6. These phenomena induce changes in the geochemical composition of groundwater around the repository.

One of the questions to be addressed for this period is whether the chemical environment will remain favourable for the containment function after repository closure. The most important parameters, as discussed in Sections 8.3 and 8.4, are redox properties (safety function R1a in Figure 10-2) and salinity (safety function R1b and R1c). Other factors to consider are the groundwater content of potassium, sulphide and iron(II), as they might affect the chemical stability of the buffer and the canister (safety function R1d) and the effect of grouting in the geosphere and cement materials in the engineered barriers that could affect groundwater pH (safety function R1e).

Modelling

Groundwater compositions are modelled through advection, mixing and chemical reactions with fracture-filling minerals. The results of the regional-scale groundwater flow modelling are used as input to a geochemical mixing and reaction model. The aim has been to obtain equivalent groundwater models for hydrogeology and geochemistry. The loose coupling of the two models also allows a description of the geochemical heterogeneity, which otherwise would be hard to attain. Indirectly the matrix diffusion effects are also accounted for because the regional-scale model considers the diffusion of salt in and out of the rock matrix see /Joyce et al. 2010/ and Section 10.1.3. This influences the fractions of end members used to assess the chemistry evolution.

The groundwater flow modelling is described in Section 10.3.6. One of the processes modelled is the transport of fractions of selected reference waters (altered meteoric, marine, glacial, brine and an older meteoric water). By this approach, the proportions of these waters may be obtained at any time for the different parts of the studied rock volume, as illustrated in Figure 10-37. The driving forces for groundwater flow during this temperate period are the topographic gradient and the density differences between overlying water bodies.

The waters of meteoric origin entering the modelled system are essentially rain, but due to their chemical reactivity these waters react quickly in the overlying soil layers, if there are any, and with the bedrock minerals in the initial few metres (perhaps some tens) of their pathways. Microbial activities contribute substantially to these processes. As a result, meteoric waters quickly obtain small amounts of solutes which may be seen for example in groundwaters sampled both at Forsmark and Laxemar in the upper ≈ 100 m of rock. This has been reflected in the composition chosen for the reference water labelled "Altered Meteoric" in the mixing calculations.

Some groundwater components behave as "conservative", that is, they do not participate to a large extent in chemical reactions, and they are mostly affected by groundwater mixing. Examples are the water isotopes such as deuterium and ^{18}O, as well as chloride, and, to some degree, sodium and calcium. However, most of the groundwater chemical components are reactive, for example Fe(II) and Fe(III), H^+, and bicarbonate. Sodium and calcium may participate in ion-exchange processes and calcium participates readily in the precipitation and dissolution of calcite, but in spite of this, the buffer capacity of the saline waters is such that these elements behave almost as conservatively. Sulphate may be reduced to sulphide under hydrothermal conditions, that is, at high pressure and temperature. At lower temperatures, as are applicable in this context, sulphate can only be reduced to sulphide by microbially mediated reactions with organic matter.

Due to the factors mentioned above, the evolution of groundwater components cannot be dealt with through calculations involving only groundwater mixing, and it has instead been modelled by using the results from the hydrogeological model as input to fully coupled chemical mixing and reaction calculations. The computer code Phreeqc /Parkhurst and Appelo 1999/ was used for that purpose. The results of this modelling are reported in the **Data report**, Section 6.1, and in /Salas et al. 2010/. The minerals calcite, quartz, hydroxyapatite and either a Fe(III) oxyhydroxide or an amorphous Fe(II) sulphide have been equilibrated with the mixtures at all points in space and time. The type

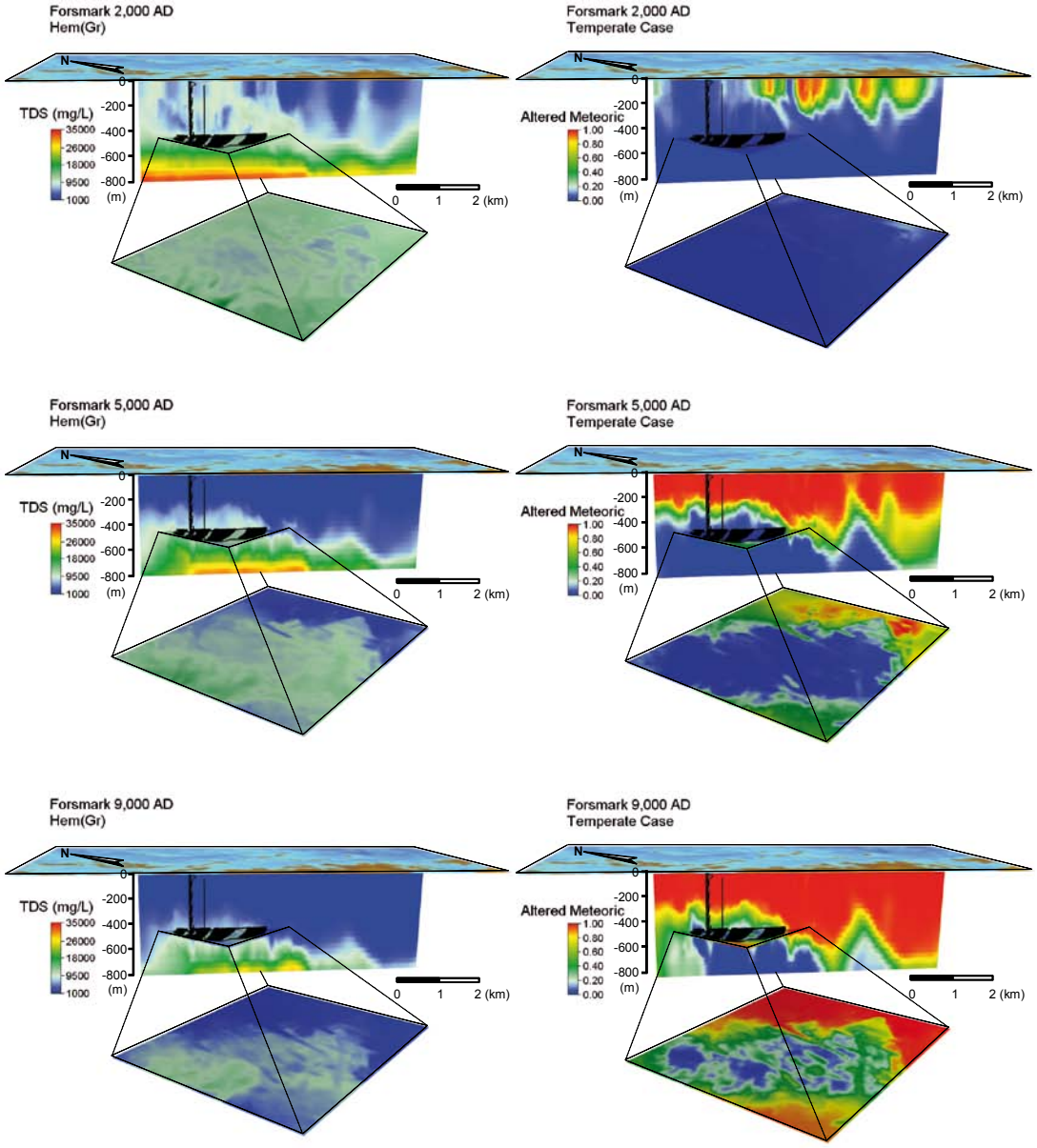

Figure 10-37. *Distribution of TDS (total dissolved solids, mg/L, left) and Altered Meteoric fraction (right) for Forsmark in vertical slices and in an enlarged horizontal slice showing the repository area at times equal to (from top to bottom) 2000 AD, 5000 AD and 9000 AD. From /Salas et al. 2010/. The figure shows the gradual inflow of Altered Meteoric water (defined in the text), and the corresponding decrease in TDS.*

of results that can be obtained using this procedure are illustrated in Figure 10-38, which shows a comparison between the calculated pH and the concentration of Ca as a function of depth with the data obtained in the site investigation programme.

Several approximations have been used in this modelling strategy. The minerals chosen to be at equilibrium with the groundwater mixtures are reasonable in that they include relatively fast groundwater/rock interactions, as in the case of calcite, or characterize the silica levels observed in the groundwaters, as in the case of quartz. However, they are a limited subset of those likely to be present. Nevertheless, even if other solid phases could be stipulated, it would not be possible to justify their selection and the minerals selected effectively represent the chemical effects observed in the reactive components discussed here. The upper part of the simulated domain, less than ≈ 100 m depth, is more affected by groundwater flow, mixing and infiltrating waters that are chemically more aggressive and the assumption of chemical equilibrium with the selected minerals is possibly less well justified than at greater depths.

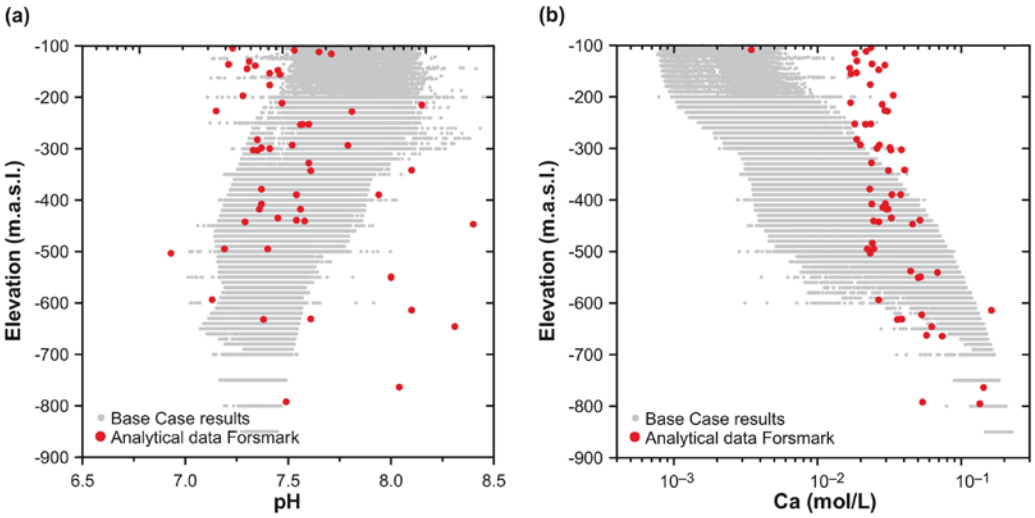

Figure 10-38. *The pH and the concentration of calcium in groundwaters sampled in boreholes at the Forsmark site (red dots) compared with values calculated using the proportions of reference waters obtained from the hydrogeological model as input for chemical mixing and reactions, including, among others, calcite dissolution and precipitation (grey dots). The groundwater data of category 3 or better /Laaksoharju et al. 2008/ have been plotted. The calculated values correspond to the vertical slice shown in Figure 10-37.*

As Figure 10-38 shows, the combination of the hydrogeological model results with the geochemical equilibrium assumption results in depth trends that do not fully correspond with the observed concentrations. The mismatch in the calcium concentrations, for example, indicates either insufficiencies in the mixing proportions obtained from the hydrogeological model, or it shows that some of the processes that have not been included in the present model, such as ion-exchange, have a significant influence in the concentration of the individual groundwater chemical components.

One of the limitations in the geochemical modelling strategy followed within SR-Site is that the composition of the marine reference water should vary with time as the waters change from a Littorina sea composition at ≈ 4000 BC to the present Baltic Sea composition, which will be further diluted in the future. This has been properly taken into account in the hydrogeological model, but for the geochemical modelling the Littorina salinity has been assumed as the reference water used in mixing calculations. This assumption is justified by the fact that less saline marine waters do not displace the Littorina component, which is denser, whereas meteoric waters displace the denser marine waters due to topographic effects.

A full propagation of uncertainties, from the hydrogeological modelling into the geochemical calculations, has not been performed. In addition, the natural variability and other uncertainties in the compositions of the reference waters used for mixing (altered meteoric, marine, glacial and brine) have not been propagated to the mineral reaction calculations. It is, therefore, probable that at any given time the real variability in the chemical compositions of groundwaters is somewhat larger than that seen in the model results presented here.

Evolution of salinity

As mentioned previously in Sections 10.2.3 and 10.2.5, the salinity distribution may initially be affected during repository operation by perturbations in the hydraulic conditions, although in the case of Forsmark this perturbation is small due to the low hydraulic conductivity. After repository closure, the backfilled tunnels will become water saturated. The modelling discussed briefly in Section 10.3.6 suggests it will take several hundred years for the repository to reach full saturation, with a relatively short period of rapid initial inflow followed by an asymptotic regime during which the inflow gradually decreases. The effects of the open repository on groundwater salinities at Forsmark, which will be minor, are expected to disappear during the resaturation period.

As explained in the introduction to this subsection, during the remaining part of the initial temperate period after repository closure, groundwaters will be affected by increasing amounts of waters of meteoric origin, see Figure 10-37. On a regional scale this corresponds to a gradual decrease of the groundwater salinity, especially in the upper part of the modelled rock volume. The salinity distribution for this time period has been calculated using the ConnectFlow model presented in Section 10.3.6. Figure 10-39 presents the calculated distribution of salinities at Forsmark at (470±20) m depth at four time steps. Towards the end of the modelled period 25% of the groundwaters in the repository volume have less than 3 g/L of dissolved salts at repository depth, whereas all the groundwaters had salinities above 6 g/L at the start of the simulation, that is, at repository closure.

In conclusion, the salinities during the first temperate period following repository closure will remain limited at Forsmark, ensuring that the swelling properties of the buffer and backfill are not negatively affected, cf. the safety function indicator R1b.

Evolution of concentrations of other natural groundwater components

The increasing proportions of groundwaters of meteoric origin will decrease the overall salt content of the groundwaters as discussed in the previous sub-section. However, the effects on the individual chemical constituents will depend on their reactivity. The evolution of the different chemical properties of groundwaters has been estimated by coupling the results from the hydrological calculations with a mixing and chemical reaction model, as described in the introduction to this section. The final objective has been to check if, during its evolution, the chemical environment around the repository fulfils at all times the safety function indicator criteria R1a to R1e. In this sub-section, the results are discussed for cations (safety function indicator R1c), potassium, sulphide and iron (R1d), and alkalinity and pH (R1e). The results for salinity (R1b) are discussed in the previous sub-section, whereas the results for redox conditions are presented in the following sub-section.

Cations

The concentration of cations (safety function indicator R1c) is important in that their presence decreases the stability of colloids (see the discussion on colloids later in this section). In groundwaters that are too dilute, colloids might enhance the transport of radionuclides. In addition, as the buffer swells into fractures, montmorillonite colloids may be released and transported away by dilute groundwaters. The criterion for the safety function indicator R1c is expressed in charge equivalents as $\sum q[M^{q+}] > 4$ mM, as available experimental data suggests that montmorillonite colloids are not stable at cation concentrations above this limit /Birgersson et al. 2009/.

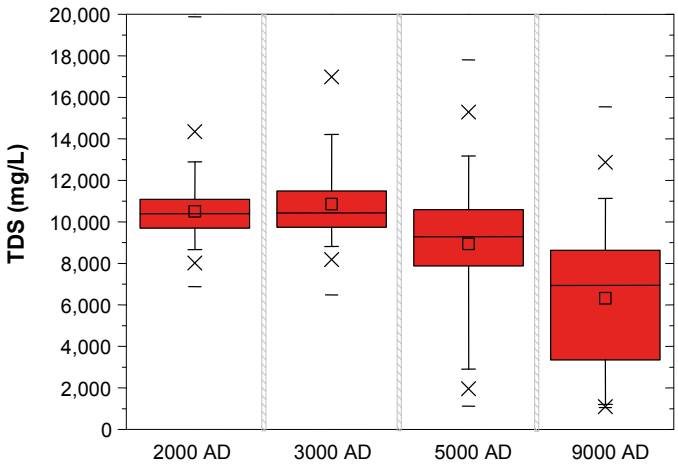

Figure 10-39. *Box-and-whisker plots showing the statistical distribution of the calculated TDS (total dissolved solids) at the Forsmark repository depth. The statistical measures are the median, the 25th and 75th percentile (box), the mean (square), the 5th and 95th percentile ("whiskers"), the 1st and 99th percentile (crosses) and the maximum and the minimum values. The figure shows the effect at repository depth of the gradual inflow of meteoric water.*

The cations contributing with the highest charge concentrations in the groundwaters at Forsmark are calcium and sodium, and to a much lesser extent magnesium and potassium. Because the concentration of calcium has double the weight of sodium in the safety function indicator, $\sum q[M^{q+}]$, calcium is the most important element in this context. The groundwaters sampled at Forsmark, Laxemar and Simpevarp show a good correlation between $\sum q[M^{q+}]$ and the total dissolved solids (TDS). The safety function indicator criterion $\sum q[M^{q+}] > 4$ mM corresponds to TDS > 0.27 g/L, that is, a salinity > 0.027% for these waters.

Calcium participates in water-rock interactions as carbonates and may be released from the weathering of feldspar. The other major divalent cation is magnesium, which is normally regulated in granitic groundwaters by the precipitation and dissolution of chlorite, a mineral that may have a wide range of compositions. In general, magnesium concentrations in groundwaters are much lower than those of calcium, and because of the low solubility of chlorites and the uncertainty in the composition of this mineral, the modelling of Mg concentrations is much more uncertain than that of Ca.

The calcium concentrations observed at present at Forsmark increase rapidly with depth in the top ≈ 100 m of the bedrock, see Figure 10-38. The selected meteoric reference water for Forsmark in the mixing and reaction calculations corresponds to groundwaters sampled at 50 to 150 m depth, which have the composition expected for a rain water that has travelled a short distance in the fractures of the granite at Forsmark.

The results of coupling the hydrogeological model results with the mixing and reaction calculations, including equilibrium with calcite, are shown in Figure 10-40, which illustrates the gradual dilution of the groundwaters at repository depth due to the inflow of superficial waters of meteoric origin. It should be noted that the Ca concentrations in groundwaters found at present in the upper 200 m vary between 0.2 and 30 mM, according to the data shown in Figure 10-38. This spread of the data is not included in the meteoric reference water used in the mixing calculations, and, therefore, the variability shown in Figure 10-40 is probably underestimated.

It may be concluded from these modelling results that for the whole temperate period following repository closure cation charge concentrations at repository depth at Forsmark will, in general, remain higher than 4 mM, that is, above to the limit where montmorillonite colloids start to become unstable. However, this analysis based on the hydrogeological simulations described in Section 10.3.6, does not consider the impact of the most extreme pathways from the surface to the repository, and additional calculations were performed to investigate this issue, see Section 10.3.6, subsection "Penetration of dilute water". As seen from the results depicted in Figure 10-32, close to one percent of the deposition holes may actually experience dilute conditions during the first ten thousand years.

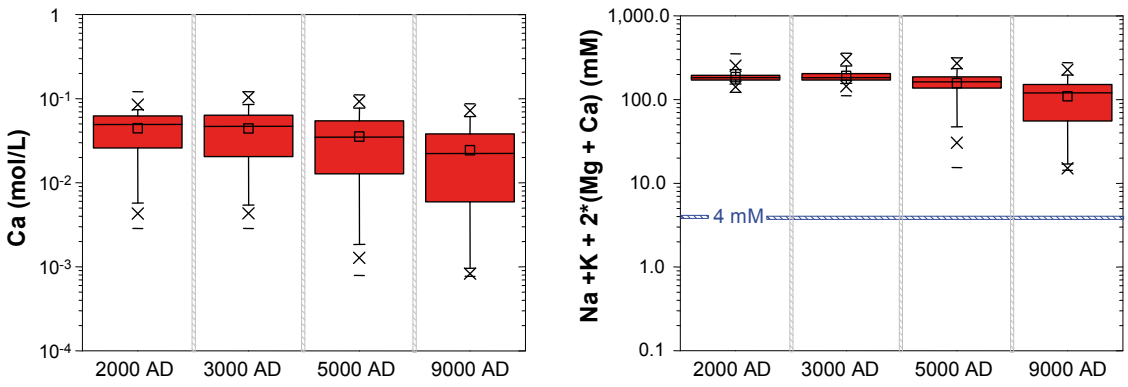

Figure 10-40. *Box-and-whisker plots showing the statistical distribution of the calculated Ca concentrations and the safety function indicator $\sum q[M^{q+}]$ for the positions located within the candidate repository volume at Forsmark. The statistical measures are the median, the 25th and 75th percentile (box), the mean (square), the 5th and 95th percentile ("whiskers"), the 1st and 99th percentile (crosses) and the maximum and the minimum values.*

Potassium, sulphide, iron, H_2, CH_4 and dissolved organic carbon

Potassium concentrations are generally low in the groundwaters sampled at Forsmark, as observed also in other Fennoscandian sites in granitic rocks. Solubility control by sericite has been proposed as a mechanism controlling the maximum concentrations of potassium /Nordstrom et al. 1989/, but ion-exchange processes cannot be ruled out. Even though the exact mechanism is not known, all available groundwater data indicate that the increased infiltration of waters of meteoric origin will not increase the potassium concentrations found at present. The reaction modelling performed within SR-Site is not well suited to constrain potassium concentrations because, as mentioned, there is not enough information available on the possible reactions that could control this element. The mixing calculations give maximum values of $[K^+]$ below 4 mM at any time for Forsmark.

The content of sulphide in groundwaters is controlled by a steady state between microbial sulphate reduction and the processes that remove sulphide: oxidation and precipitation with metals. Under oxidising conditions, for example in superficial waters, sulphide is quickly oxidised to sulphate. Under reducing conditions, dissolved Fe(II) is normally present and the maximum sulphide concentrations are regulated by the precipitation of Fe(II) sulphide according to

$$HS^- + Fe^{2+} = FeS(s) + H^+$$

with $\log_{10}K = \log_{10}([H^+] / ([Fe^{2+}] [HS^-])) \approx 3$. At a pH between 7 and 8 one obtains $\log_{10}([Fe^{2+}] [HS^-]) \approx -10$ to -11. In most groundwaters $\log_{10}[Fe^{2+}] \geq -6$ which sets the maximum $\log_{10}[HS^-]$ in the range -4 to -5.

Sulphide concentrations were analysed during the site characterisation process and during the subsequent groundwater monitoring. The data are often below the detection limit of the analysis procedure, but in some borehole sections sulphate reduction has taken place during the monitoring period and relatively high sulphide concentrations have been observed. This process has been studied and the conclusion is that accumulated organic gunge and biofilm in the standing monitoring equipment can result in microbial sulphate reduction. It is still not known why this occurs only in some of the monitored sections. When groundwater pumping is initiated for sampling during monitoring, large enough volumes of groundwater must be allowed to rinse the borehole section, tubing and standpipe in order to obtain a representative sample for the fracture groundwater. This cannot be controlled unless a time series is analysed. During monitoring a time series was rarely sampled and because of this many of the monitoring groundwater analyses are of dubious quality.

To address this problem a careful review of all sulphide data has been performed /Tullborg et al. 2010/ and in order to avoid bias due to having many samples in some borehohole sections and a few in other locations, a group of samples representing the sulphide concentrations in the different sampling points has been selected, cf. Figure 10-41. The maximum sulphide value for Forsmark is $1.2 \cdot 10^{-4}$ M from KFM01D at 343 metres depth. This is, however, an exception and, for practically all of the groundwaters, the sulphide concentration is below $1.3 \cdot 10^{-5}$ M. No correlation was found between hydrogeological information on the fractures being sampled and the sulphide data.

Because sulphide in groundwaters is mainly produced by bacterial sulphate reduction, it is essential to have data on the reductants (electron donors) to evaluate the potential for sulphide production over long periods of time. Dissolved hydrogen, H_2, methane, CH_4, and organic carbon, DOC, are potential reductants that may be used in many microbial processes, including sulphate reduction. It must be noted that the sulphide concentrations found at present in Forsmark's groundwaters, Figure 10-41, already reflect the steady state between the microbial sulphide production that is achieved with the present levels of H_2, CH_4 and DOC, and the consequent formation of sulphide minerals.

The overall reactions with methane or hydrogen are:

$$SO_4^{2-} + CH_4 \rightarrow HS^- + HCO_3^- + H_2O$$

$$SO_4^{2-} + 4H_2 + H^+ \rightarrow HS^- + 4H_2O$$

In Figure 10-42 it is seen that the maximum possible contribution to sulphate reduction from H_2 is modest, given the concentrations of this gas found in the groundwaters. If all hydrogen was quantitatively used by microbes in sulphate reduction, at most the sulphide concentration would increase to $10^{-5.6}$ M. Methane can be used by bacterial consortia to achieve sulphate reduction. Figure 10-42 shows that methane concentrations are as a rule below 10^{-5} M. The "outlier" in Figure 10-42 corresponds to borehole KFM01D at 445 metres depth. As shown in Section 10.2.5, the corrosion of iron materials

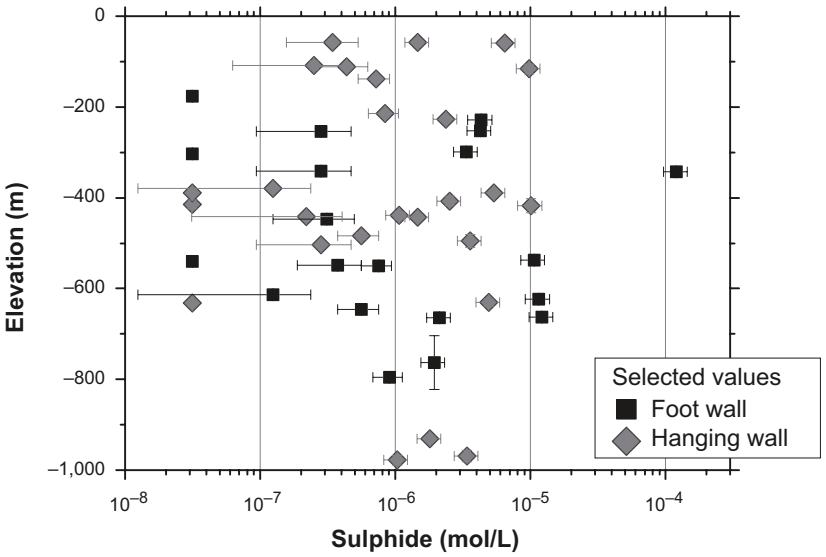

Figure 10-41. *Selected set of sulphide concentrations in contemporary groundwaters of the Forsmark area below 50 m depth /Tullborg et al. 2010/. In general only one value has been selected for any given borehole section for cases where several analyses have been reported. Data below the detection limit of the analyses, which is between $9 \cdot 10^{-7}$ and $6 \cdot 10^{-8}$ M, are shown in this diagram at $3 \cdot 10^{-8}$ M. "Foot wall" data refer to sampling points below 100 m depth and below the A2 and F1 fracture zones, while "hanging wall" are the remaining data.*

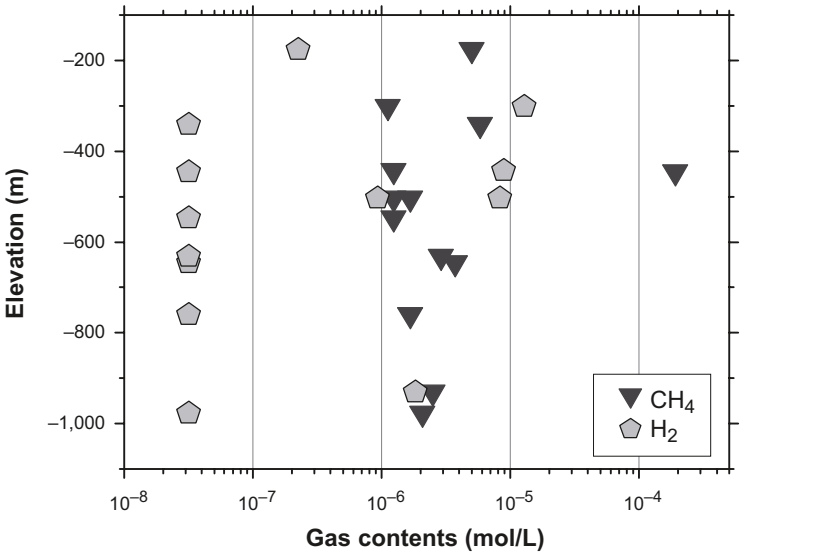

Figure 10-42. *Methane and hydrogen concentrations in contemporary groundwaters in the Forsmark area. Samples having hydrogen values below the detection limit have been plotted at $10^{-7.5}$ M.*

left in deposition tunnels is a potential source of hydrogen. However, because of the simultaneous production of Fe(II), if bacterial sulphate reduction takes place, the corrosion of Fe-materials is not expected to contribute significantly to the dissolved sulphide contents of the groundwaters around the repository.

The contribution from methane and hydrogen to microbial sulphate reduction, and hence, to the observed sulphide concentrations is deemed to be minor because the estimated flows of these gaseous species are $< 3 \cdot 10^{-10}$ mol/(m^2 yr) /Delos et al. 2010/.

Dissolved organic carbon (DOC) in groundwaters can, at least in principle, be involved in microbial processes. A large part of this carbon is relatively nonreactive in large molecules, like humates and fulvates, which have complex chemical structures. The theoretical potential for sulphate reduction,

in terms of amount of dissolved carbon, is quite large as seen in Figure 10-43. Bacterial sulphate reduction, however, preferentially uses small organic molecules such as acetate or lactate, which are only a fraction of the DOC analysed. Given the relatively large sulphate concentrations, at least in the upper ~500 m, if there was any fraction of the DOC that could be used in bacterial sulphate reduction, then that organic carbon would be quickly consumed, and it can thus be concluded that the observed DOC concentrations correspond mainly to organic matter that is not readily accessible for sulphate-reducing bacteria or to fermenting bacteria that produce the small organic acids needed by sulphate-reducing bacteria. Therefore the sulphide concentration distributions used in the copper corrosion modelling, see Sections 10.3.12 and 10.4.8, have not been increased to take into account dissolved organic carbon. The exact fraction of the DOC that will be available to sulphate-reducing bacteria over very long time scales cannot be established. As already mentioned above, the sulphide concentrations found at present in Forsmark's groundwaters, Figure 10-41, already reflect the steady state between the microbial sulphide production that is achieved with the present levels of H_2, CH_4 and DOC, and the consequent formation of sulphide minerals.

In the reaction modelling performed within SR-Site, apart from the "marine" and "deep-saline" components, the reference waters used in the mixing calculation were assumed to contain no sulphide. The marine waters infiltrating in the rock may be relatively rich in organic matter, and observations at Äspö have show that some sulphate reduction takes place in these groundwaters. Therefore, the "marine" component was assumed to be in equilibrium with solid Fe(II) sulphide.

The results of mixing the marine component with the other reference waters are shown Figure 10-44, illustrating the decrease in sulphide values as meteoric waters become increasingly dominant with time. In the calculations, equilibrium with Fe(III) oxyhydroxide has been imposed. A comparison with Figure 10-41 indicates that the mixing/reaction calculations have very limited validity for sulphide which is instead affected by microbial sulphate reduction.

From the sulphide data in Figure 10-41, from the results of the hydrogeological and geochemical modelling described above, and from the understanding of the microbial sulphate reduction processes and the data relating to it on CH_4, H_2 and DOC, it is concluded that during the initial temperate period following repository closure the sulphide concentrations in the groundwaters will remain at the levels found at present in Forsmark. Sulphide concentrations in a given fracture are expected to vary to some extent over a temperate period, but it cannot be concluded that the temporal variations will be sufficiently large that the time averaged concentration would correspond to the average of sulphide concentrations sampled at Forsmark today.

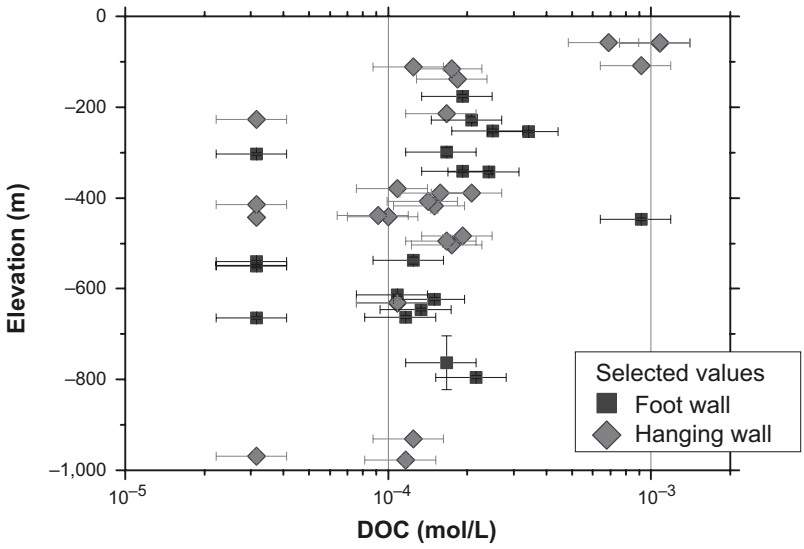

Figure 10-43. *Dissolved organic carbon in groundwaters analysed in Forsmark and obtained from below 50 m depth. Values below the detection limit have been plotted at $10^{-4.5}$ M. "Foot wall" data refer to sampling points below 100 m depth and below the A2 and F1 fracture zones, while "hanging wall" are the remaining data.*

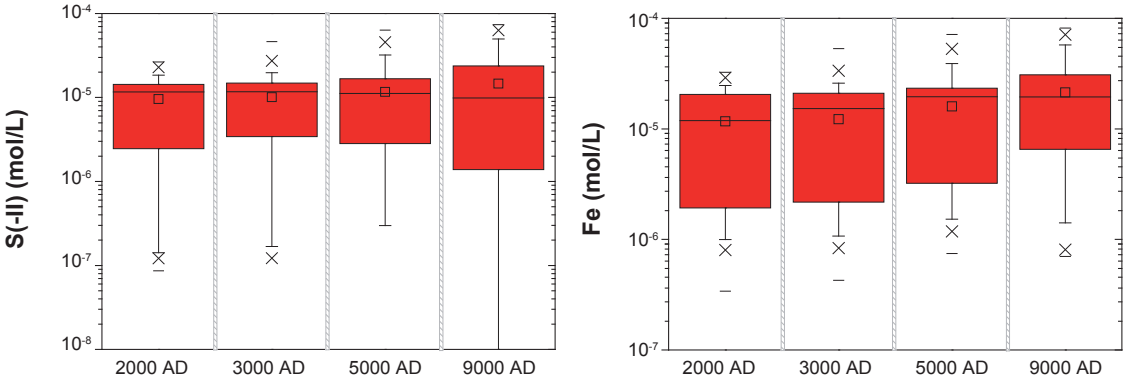

Figure 10-44. *Box-and-whisker plots showing the statistical distribution of the calculated total sulphide and total iron concentrations for the positions located within the candidate repository volume at Forsmark. The statistical measures are the median, the 25th and 75th percentile (box), the mean (square), the 5th and 95th percentile ("whiskers"), the 1st and 99th percentile (crosses) and the maximum and the minimum values.*

The conclusion reached here concerning sulphide concentrations in groundwaters is propagated in later sections of this chapter to the other time periods of the reference evolution, that is, periglacial and glacial. Although microbial sulphide production might increase during the expectedly short periods when the repository area at Forsmark is submerged under marine waters, especially at depths above ~300 m where there is at present some evidence of past infiltration of marine waters, the sulphide concentrations observed at present already reflect the enhanced sulphide production during the relatively recent Littorina sea stage. On the other hand, during the expectedly long periods when the repository area is covered by an ice sheet, the sulphide levels would decrease because of low levels of sulphate, H_2, CH_4 and DOC in the glacial meltwaters, and selecting the present sulphide concentrations during the glacial periods is judged to be a pessimistic approach.

The concentration of Fe(II) is regulated by a complicated set of reactions including the slow dissolution of Fe(II)-silicates, such as chlorite and biotite, the precipitation of Fe(II) sulphides and redox reactions. The concentrations of Fe(III) are in general negligible in granitic groundwaters, as the oxyhydroxides of Fe(III) are quite insoluble and they precipitate quickly. The results from the reaction modelling in SR-Site are displayed in Figure 10-44, which shows that the calculated Fe concentrations of groundwaters at repository level are expected to increase with time as waters of meteoric origin, assumed to have [Fe] ≈ 10^{-5} mol/L, become increasingly dominant.

In conclusion, during the initial temperate domain following repository closure, the potassium concentrations are expected to remain ≤ 0.004 mol/L, sulphide concentrations are expected to remain at the levels found at present, that is, ≤ 10^{-5} mol/L for most deposition positions with a probability that for some deposition holes the surrounding groundwaters will have sulphide concentrations as high as $10^{-3.9}$ M, as shown in Figure 10-41, and iron concentrations are expected to gradually increase but to remain below 10^{-4} mol/L.

pH and bicarbonate

Acidity, expressed as pH, is a master variable controlling most chemical processes. Too low or too high values would affect, among others, the corrosion of the canister, the dissolution of the spent fuel, the solubility limit of several radionuclides, etc. Bicarbonate, HCO_3^-, is also an important parameter that can affect spent fuel dissolution and solubility limits. For pH and bicarbonate, the mixing and reaction calculations are dominated by the precipitation and dissolution of calcite. The results show that the pH values remain approximately in the range 6.5 to 8, and that bicarbonate values increase with time being up to about 0.0075 mol/L at 9000 AD, see Figure 10-45. It may be shown that the calculated partial pressures of dissolved carbon dioxide increase with time, as it is assumed in the modelling that the infiltrating meteoric waters have a higher CO_2 content than the other waters in the system. The conclusion is that the criterion for the safety function indicator R1e (pH < 11) is fulfilled during the whole temperate period following repository closure.

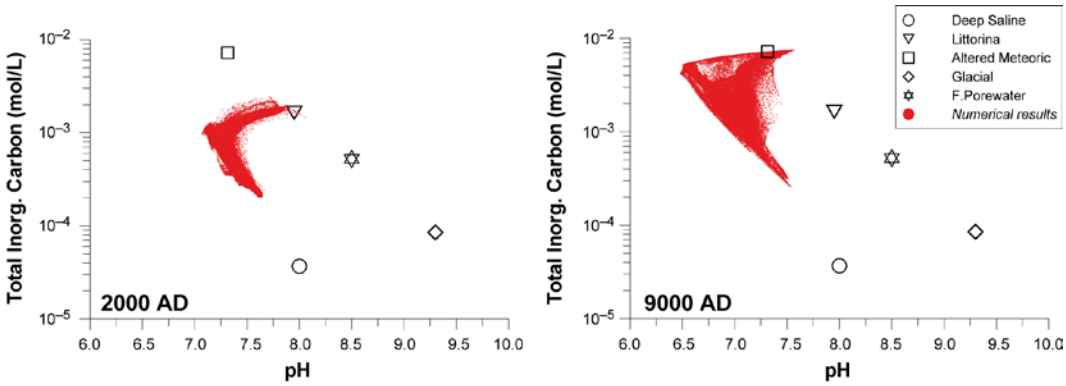

Figure 10-45. *Correlation and evolution of the calculated pH values and the concentrations of the total inorganic carbon for the positions located within the candidate repository volume at Forsmark corresponding to 2000 AD (left) and 9000 AD (right).*

Chloride and sulphate

Chloride concentrations below 2 M imply that chloride assisted corrosion of the canister can be excluded (safety function indicator R1f). Chloride concentrations are also relevant when selecting radionuclide transport properties (sorption coefficients). Sulphate is important when determining the solubility limits for radium, although not a safety function indicator. These two components behave almost conservatively, i.e. they participate in chemical reactions only to a very limited extent, and they have been modelled by mixing calculations in SR-Site. Figure 10-46 shows that the groundwater concentrations of chloride and sulphate at repository level tend to decrease with time as waters of meteoric origin become increasingly dominant. Details on these results may be found in /Salas et al. 2010/.

Colloids

Colloids may sorb irreversibly some radionuclides, and given the appropriate conditions, colloids are transported with the groundwater flow. Because of this, colloids can affect the transport of radionuclides that would otherwise be fully retained in the rock. Colloids are partly stabilised by electric repulsions between charges in their surfaces. Some of these charges arise from the dissociation of acid-base groups, and are, therefore, pH dependent. The presence of cations in the water counteracts these charge effects. The results from the modelling calculations show that colloids will not be especially stable during this temperate period, because the pH values, salinities and cation concentrations will be high enough to destabilise them. The conclusion is that colloid concentrations are expected to remain at the levels that have been measured during the site investigations, i.e. less than 200 µg/L /Hallbeck and Pedersen 2008/.

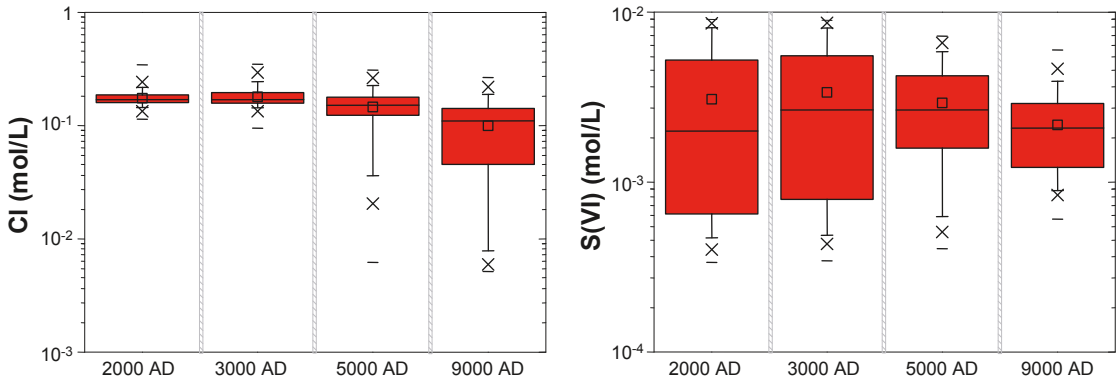

Figure 10-46. *Box-and- whisker plots showing the distribution of total chloride concentrations (left) and of total sulphate concentrations (right) in Forsmark at 400 m depth as a function of time. The statistical measures are the median and the 25th and 75th percentile (box) and the 5th and 95th percentile ("whiskers") the 1st and 99th percentile (crosses) and the maximum and the minimum values.*

Evolution of redox conditions

Redox conditions are often reported as the value for the redox potential, Eh, and this value is used when selecting radionuclide transport properties (sorption coefficients) and when calculating the solubility limit of many radionuclides. Evidence from the Äspö laboratory and other Swedish sites, shows that anoxic conditions prevail in the host rock even at a short distance from tunnel walls or from the ground surface. Air will be entrapped in the buffer and backfill, but anoxic conditions are expected to be established soon after the tunnels become resaturated, see Section 10.2.5. Even if the buffer or backfill do not become fully saturated during this period (see also the discussion in Section 10.3.8), oxygen consumption processes will take place in the partially saturated materials, as shown from the data obtained at the Febex and Prototype experiments /Jockwer and Wieczorek 2003, Eriksson 2007/.

The hydrogeological modelling described in Section 10.3.6 shows that the proportion of waters of meteoric origin at repository depth will increase with time, see Figure 10-37. This evolution is not expected to change the reducing characteristics of the groundwater, as infiltrating meteoric waters become depleted of oxygen by microbial processes in the soil layers, if there are any, or after some tens of metres along fractures in the bedrock, as shown by the data collected within the Rex experiment /Puigdomenech et al. 2001/ and from groundwaters sampled at 40 to 70 m depth during the "Redox Zone" experiment at Äspö /Banwart 1999, Banwart et al. 1999/.

The results from the hydrogeological model have been coupled with the mixing and reaction calculations, as described in the introduction to this section. The calculations included equilibrium with either an Fe(III) oxyhydroxide or with Fe(II) sulphide. The results are slightly dependent on the solid phase chosen. However, there are no geochemical arguments that can be used to postulate what mineral regulates the measured redox potentials of groundwaters, and therefore the calculated redox potentials from both options are given the same weight in SR-Site. The calculations for Forsmark including equilibrium with either an Fe(III) oxyhydroxide or with Fe(II) sulphide are presented in Figure 10-47 which shows that the redox potentials increase slightly with time but remain well below –50 mV at the end of the simulation period.

It may, therefore, be concluded that the anoxic groundwater conditions now prevailing at repository depth will continue for the whole temperate period following the closure of the repository, in spite of the increasing proportion of meteoric waters with time. The chemical environment surrounding the repository will thus satisfy the criteria for the safety function indicator R1a.

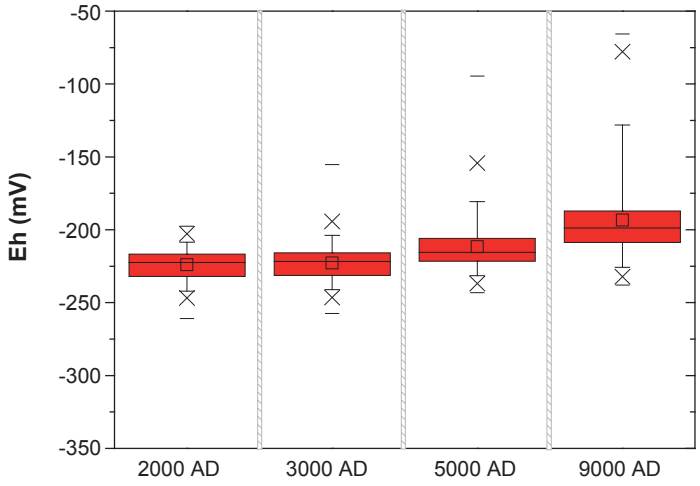

Figure 10-47. *Box-and-whisker plots showing the statistical distribution of the calculated Eh (redox potential) taking into account results using either equilibrium with Fe(III) oxyhydroxide or amorphous FeS. The statistical measures have been obtained for the positions located within the candidate repository volume at Forsmark and they are the median, the 25th and 75th percentile (box), the mean (square), the 5th and 95th percentile ("whiskers"), the 1st and 99th percentile (crosses) and the maximum and the minimum values.*

Effects of grout, shotcrete and concrete on pH

The presence of cement materials in the repository is discussed in Section 10.2.5. Cement recipes with porewaters having pH around or below 11 will be used in the vicinity of the depositon tunnels in order to avoid detrimental effects from porewater diffusing out of the cement matrix. The effect of these porewaters is much smaller than that of Standard Portland Cement paste that contains porewater that is highly alkaline (pH ≈ 12.5).

At Forsmark, it is expected that only deformation zones and a few single fractures will require grouting to avoid the inflow of groundwater into the tunnels during repository operation. These zones, however, may have a large role in model simulations of radionuclide transport. In deposition tunnels, the average amount of grout in rock fractures is expected to be less than 20 kg per metre of tunnel according to the **Underground openings construction report**, Table 4-3, while shotcrete will only be used in transport tunnels and other cavities in which deposition does not occur. It must be noted that grouting will be concentrated to a few locations in each deposition tunnel and that therefore grout will be unevenly distributed.

After repository closure, grout and shotcrete will start reacting with circulating groundwater, and a slightly alkaline plume is expected to develop downstream in the grouted fractures. A generic model has been used to illustrate this process. The 2D model, 80·40 m in size, consists of a high transmissivity fracture intersecting a deposition tunnel backfilled with crushed rock and MX-80 bentonite in a 30/70 ratio /Luna et al. 2006/. The Phast computer code /Parkhurst et al. 2004/ was used for the simulations. The results have shown that a moderately high pH plume (pH ≈ 9) can develop in grouted fractures intersected by the deposition tunnel and to a minor extent also in the backfill material. The leaching of grout material leads to the precipitation of CSH phases (calcium silicate hydrates) and calcite ($CaCO_3$) in the fracture and a corresponding decrease of the carbonate concentrations in the groundwater. Although the numerical calculations have been limited to 1,000 years, it is expected that the process will continue until all the cement has reacted. Depending on the geometry and hydrologic properties of the grouted fracture and on the amount of grout, this process could continue for up to one hundred thousand years. Note that the backfill composition in this generic model is not that to be used in the planned repository, but the general conclusions of these calculations remain unaffected.

A consequence of this process is that transport pathways for potentially released radionuclides will include groundwaters that have circulated through a grouting zone and have been modified to higher pH (≈ 9) and lower carbonate (due to increased calcium concentrations and consequent calcite precipitation). This could affect the retention properties of the transport pathways although calcite precipitation will reduce the transmissivity of the affected fractures.

The model mentioned above does not take into account changes of porosity in the fracture as CSH phases and calcite are precipitated. Experience from an experiment in Grimsel /Mäder et al. 2004/ shows that this could be an important factor in reducing the transport of highly alkaline fluids, although the experiment was conducted with solutions simulating standard cement (pH ≈ 12.5). The groundwater sampled in grouted fractures at Onkalo showed high pH values /Ahokas et al. 2006/, but the time span for these measurements is too short (some months) for conclusions to be drawn relevant to the longer timescale addressed here. There is, therefore, no experimental evidence to indicate that the model results are pessimistic.

The conclusion is, therefore, that the effect of grout in fractures will be to increase the pH in deformation zones to values ≈ 9 for relatively long periods of time, probably lasting throughout the first glacial cycle (≈ 120,000 years). pH values ≈ 9 are, however, within the criterion for the safety function indicator R1e. Radionuclide sorption data (see the **Data report**, Section 6.7) have been selected for the pH range 7 to 9, and are therefore adequate as long as "low" pH materials are used for grouting.

Degradation of grout in grouting holes

In order to be able to penetrate small fractures, the cement-based grout has to have a low viscosity. This can be achieved by using a high water/solid material ratio. A grout produced in this way will also have a high porosity and could degrade quickly. Modelling has shown that the degradation of cement-based grout in grouting boreholes is relatively slow in the hydrochemical conditions of

Forsmark groundwaters /Galíndez and Molinero 2010, Grandia et al. 2010a/. Simulated results have indicated that after 1,000 years grout material in contact with flowing groundwater can be degraded in its outmost 0.5 cm. Precipitation of calcite at the grout/granite interface would decrease the porosity, isolating the grout from the surrounding groundwater or matrix porewater.

In contrast, the natural evolution for silica sol, which is planned to be used if cement based grout is unsuitable, is to slowly recrystallise into thermodynamically more stable forms of silica, and both grouted fractures and grouting holes where silica sol have been used will, therefore, remain sealed. The conclusion is, therefore, that for modelling purposes it may be assumed that cement-based grouting boreholes are filled with a material having a high porosity. Grouting holes are, however, not included as flow paths in the flow and transport modelling in SR-Site and it is expected that their connectivity to flow paths will be limited. Small amounts of organic additives (superplasticizers) included in cement-based grouts will be gradually released during grout degradation and these substances will then be accessible for microbial processes. Their contribution to the concentration of organic carbon in groundwaters will, however, be negligible.

Identified uncertainties and their handling in the subsequent analysis

The following uncertainties are identified when considering the different chemical aspects of the evolution of the repository during the initial temperate period.

- There is a large degree of uncertainty in the detailed salinity distribution around the repository, but in general the salinity will not become so high or so low as to affect the performance of the repository during this period or when considering its future evolution. However, a fraction of a percent of the deposition holes may experience dilute conditions during the first ten thousand years, i.e. violating safety function R1c. The calculated distributions of salinity, pH and other groundwater components obtained from the modelling are used in the analysis of bentonite evolution, see Section 10.3.10 and 10.3.11, and in the radionuclide transport calculations (values for solubility and sorption) described in Chapter 13.
- There is a large degree of uncertainty in the detailed distribution of dissolved sulphide in the groundwaters around the repository. Because no dependency has been found between sulphide and other groundwater geochemical or hydrogeological parameters, the observed distribution of concentrations shown in Figure 10-41 is propagated to the analysis of canister corrosion in Section 10.3.13.

The uncertainties on other chemical aspects, such as redox, etc, have been established to be of no concern for the performance of the repository. In particular the uncertainties in the redox potential are not propagated to subsequent analyses. The anoxic groundwater conditions now prevailing at repository depth will continue for the whole temperate period following the closure of the repository, in spite of the increasing proportion of meteoric waters with time. The chemical environment surrounding the repository will thus satisfy the criteria for the safety function indicator R1a.

10.3.8 Saturation of buffer and backfill

General

The safety functions for the buffer and backfill assumes a fully water saturated state. This should mean that the buffer and backfill need to be saturated to perform properly. However, no performance is needed from the buffer as long as the deposition hole is unsaturated, since no mass-transfer between the canister and the groundwater in the rock can take place in the unsaturated stage. The water saturation process itself has therefore no direct impact on the safety functions of the buffer and backfill. It is still important to understand the water saturation process since it defines the state of the barriers in the early evolution of the repository. Finally, the ventilation of deposition tunnels during significant time spans (prior to filling of the deposition holes and the tunnels) may imply that the surrounding rock can dehydrate. This air-filled pore-space in the rock could potentially constitute a sink for the water that is associated with the buffer during installation. If a significant amount of this water were to migrate into the rock, then this could potentially cause a significant increase of peak temperatures at the canister surfaces and thus affect safety function Buff 4.

The initial state of the installed buffer and backfill is presented in Sections 5.5.3 and 5.6.3 respectively. Both the buffer and backfill are installed as compacted bentonite blocks combined with bentonite pellets. The buffer blocks will be deposited into the deposition holes with an initial water content of 17 percent (by weight).

During the early stage of the repository evolution, the deposited buffer and backfill blocks will take up water from the surrounding bedrock. The water will expand the mineral flakes and the buffer and backfill will start swelling. The swelling will be restricted by the rock wall and a swelling pressure will develop. The process is dependent on the properties of the buffer as well as on the local hydraulic conditions and the saturation state of the tunnel backfill. The saturation of the backfill is mainly dependent on its material properties and the conditions in the surrounding rock. After final saturation, the hydraulic conductivity of the buffer and backfill will be very low and the swelling pressure will be high. This section describes the general modelling of the processes together with a discussion on how this is applied to the specific sites. The following is assessed:

- Saturation of the backfill.
- Saturation of the buffer.
- Moisture redistribution in the dry rock case.
- Application to hydraulic conditions at the Forsmark site.

For SR-Site, saturation of buffer and backfill has been described in /Åkesson et al. 2010a/. The key focus has been on the evaluation of the importance of different parameters and assumptions in the modelling of the process. The modelling in /Åkesson et al. 2010a/ is generic and no data from the Forsmark site are used.

Saturation of the backfill

In /Åkesson et al. 2010a/ the saturation of the backfill was modelled for a number of different geometries and assumptions about data and boundary conditions. A summary of the investigated variations is given in Table 10-2. The primary purpose of the modelling was to analyse the time needed to saturate the backfill.

40 different cases were investigated in the primary variation, including combinations of tunnel sections, backfill representations, and fracture inflow (or boundary pressure). 25 different cases were investigated in the secondary variations using base case models and modified features including an EDZ, removal of fractures as well as modified permeabilities and retention properties. The approach with primary variations was largely an attempt to map the effects of different combinations of section areas, backfill representations, and fracture inflows (or boundary pressures) for different geometries. The secondary variations were mainly performed with 1D models with altered bentonite properties, and with large plane geometries, with or without fractures, and with altered rock properties.

Table 10-2. Summary primary and secondary variations.

Variation		
Primary	Tunnel section area	Two different tunnel sections
	Backfill representation	Two and in some cases three different representations
	Fracture distance and orientation	Two different orientations: vertical and horizontal. Two different distances for the vertical orientation
	Fracture transmissivity	Two different transmissivities
Secondary	Rock permeability	Several cases with different rock permeabilities
	Presence of EDZ	Two cases with EDZ
	Absence of fractures	Five cases with no fracture
	Water retention in the rock	Two cases with different retention curve
	Bentonite permeability	Four cases with different permeabilities
	Bentonite relative permeability	Two cases with different relative permeability
	Thermal evolution	One case with thermal evolution
	Hydromechanical processes	One case with hydromechanical processes
	Bentonite retention	Two cases with steeper retention curve
	Tunnel ventilation	One case with 10 years of RH 70%

The main result of each analysis was the time to fully saturate the backfill, where the time needed for the last node to reach 99% degree of saturation has been regarded as the saturation time. In general, either the backfill or the rock system can be regarding as the limiting factor for the rate of hydration. Hydration times of approximately 80 to 100 years, given by the one dimensional models, represent the time needed for the backfill, with free access of water, to become fully saturated. Times longer than this represent cases in which the rock system is limiting.

The different tunnel geometries that were represented were:

- One dimensional axisymmetric geometry.
- Two dimensional axisymmetric geometries with different fracture distances (6 m and 24 m).
- A two dimensional plane geometry (Figure 10-48).

The effect of uneven tunnel diameter was handled with the Maximum Fallout case, i.e. assuming the largest allowed tunnel cross section according to Figure 5-15, in which a larger proportion of pellets was included.

A selection of the calculated saturation times is compiled in Figure 10-49. The dotted lines represent the base case properties and two different fracture transmissivities. The diagram illustrates the effects of changing the bentonite properties on one hand, and the effects of changing the rock properties and fracture distance on the other. The effects of different bentonite properties and other variations are shown for a situation with free access of water in the top row. The dependence on the rock matrix permeability in a fracture-free condition is shown on the lower row, while the middle rows show results from two different fracture distances. The figure thus demonstrates that the overall influence of the rock on the hydration rate is much higher than the uncertainties related to the bentonite. The calculations for backfill with free access of water result in time-scales of approximately 80 years. A case with no fracture and a matrix hydraulic conductivity of 10^{-13} m/s result in time-scales of approximately 6,000 years. Since the rock at Forsmark is expected to contain very few water conducting fractures, typically separated by more than 100 m, it is difficult to state that any of the presented cases could be entirely ruled out. In SR-Site it is assumed that the saturation of the backfill can take anything from < 100 years to ~6,000 years depending on the location in the rock and this entire range is likely to arise at Forsmark.

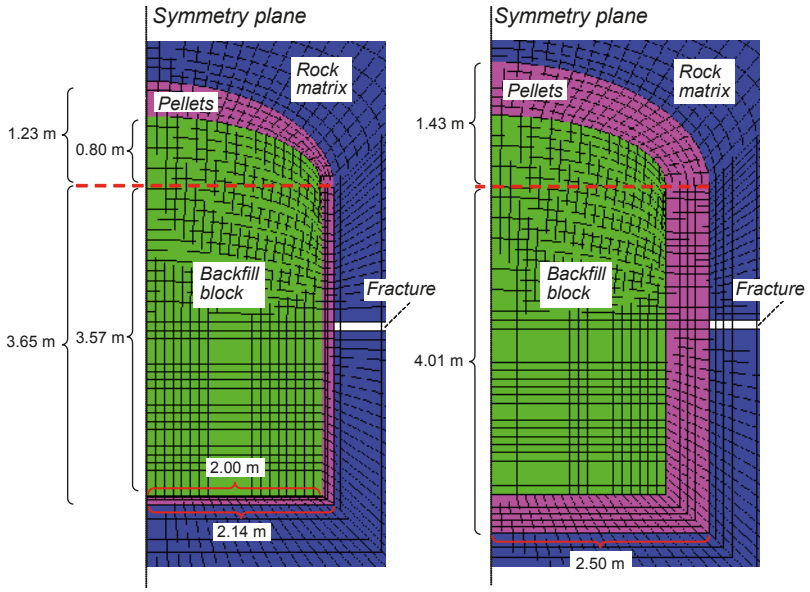

Figure 10-48. *The Geometry of 2D plane models analysed. Theoretical section (left) and maximum fallout (right) /Åkesson et al. 2010a/.*

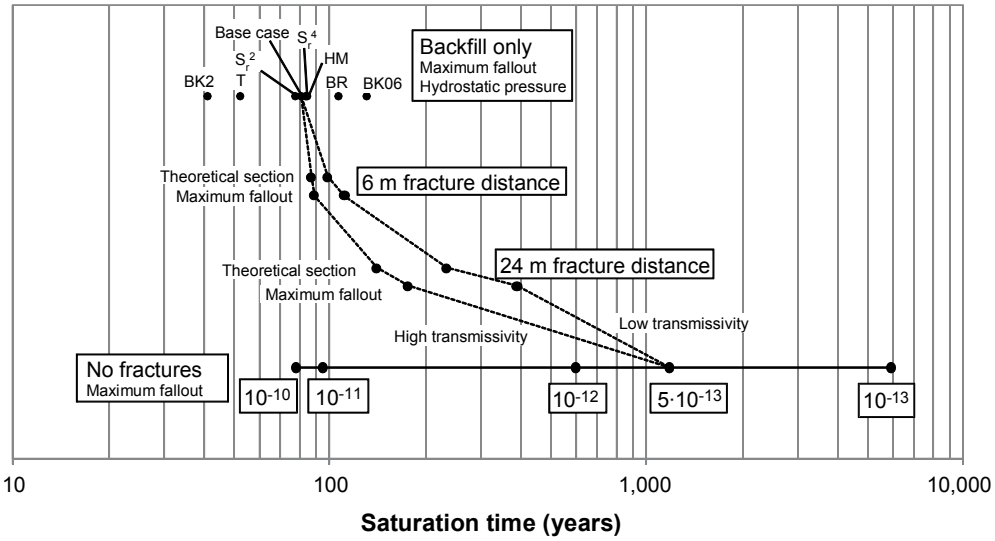

Figure 10-49. *Compilation of backfill saturation times for different geometries and cases. Results from 1D models with free access of water shown on the top row (BK2: with doubled backfill permeability; T: with thermal evolution and temperature dependence of the viscosity of water; S_r^2 and S_r^4: with square and 4th power saturation dependent backfill relative permeability relations – the base case has a cubic dependence; HM: with hydromechanical processes; BR: with steeper backfill water retention curve; BK06: with 40% lower backfill permeability). Results from 2D axisymmetric models with different fracture representations shown in the middle rows. Results from plane 2D models without fractures shown on the bottom row (numbers indicate rock hydraulic conductivity). The dotted lines represent the base case properties and two different fracture transmissivities /Åkesson et al. 2010a/.*

Saturation of the buffer

The buffer water saturation process is externally influenced by the wetting/drying from the rock and backfill and the heating from the canister. Inwards in the buffer, from the rock side, liquid water is transported by "advective" flow in the buffer and outwards, from the canister, vapour is transported by diffusion. The advective flow is driven by the water pressure gradient and the diffusive flow is driven by the vapour concentration gradient.

The transport properties are dependent on the state of the materials in terms of degree of saturation and temperature. The different retention properties of the buffer constituents (cylinder- and ring-shaped blocks and the pellet filled slot) will also influence the water transport in the buffer. The saturation of the buffer has been calculated in /Åkesson et al. 2010a/ for a number of cases with different conditions and assumptions:

- Pellets and blocks or a homogenised material.
- Unfractured rock.
- Fractured rock.
- The effect of extremely low rock permeability.
- Rock permeability dependence.
- The effect of higher water retention for the rock.
- The effect of an initially ventilated tunnel.
- The effect of altered block retention.
- The effect of altered buffer permeability.

The cases have been selected based on the identification of important parameters in the **Buffer, backfill and closure process report**.

The buffer saturation times (the time where $S_l \geq 0.99$ (liquid saturation) in the entire buffer), for all Thermo-Hydraulic (TH)-simulations of a deposition hole made in /Åkesson et al. 2010a/, are shown in Figure 10-50. The horizontal lines represent the cases indicated to the right of the line where also the "mechanical assumption", where *Homogenised* refers to an initially homogenised buffer material while *Initial state* considers the case with blocks and pellets, is indicated. The concept of using a homogenised and initial state model is to obtain two extreme solutions that are bounding the "true case" (in which mechanics, i.e. the homogenisation process, should be incorporated). Below the lower line (Init. Unfractured rock) the rock conductivity used is indicated. The hatched lines connect models with identical rock conductivities. Close to the lower line, the positions of the models where the buffer was altered are given (unfilled circles). A more detailed description of the cases can be found in /Åkesson et al. 2010a/.

As presented in Figure 10-50, the results from the calculations show:

- In general, the assumption of a homogenised buffer gives longer saturation times than when pellets and blocks are considered. The exception is when the saturation is very slow, where the homogenised buffer gives a more rapid saturation.
- For an unfractured rock, the conductivity of the rock is very important for the saturation time. For a rock conductivity of 10^{-11} m/s, the saturation time will be in the range of ~20 years, whereas it will take > 150 years for a conductivity of 10^{-12} m/s.
- Equipping the unfractured model with a horizontal fracture at either the canister mid-height (CMH) or at the tunnel wall significantly decreases the time for saturation, especially when the conductivity of the rock is low.
- To investigate the effect of a low permeability rock, the unfractured model was equipped with a low rock permeability of 10^{-20} m^2, corresponding to a hydraulic conductivity of ~10^{-14} m/s. All of the rock mass surrounding the modelled deposition hole and associated with the tunnel representation was equipped with the extremely low permeability. The water entering the backfill and buffer had to come through the rock matrix (no fractures are present) driven by the water pressure gradient. The obtained saturation times were 1,760 and 1,476 years for the block-pellet and homogenised model, respectively.
- For a high permeability rock, i.e. if the rock conductivity > 10^{-11} m/s, the calculations show that the saturation time is more or less independent of rock permeability.
- Using a higher water retention curve for the rock (larger suction given the same water degree of saturation) does not have a significant effect on the buffer saturation time.
- The effects of different relative humidity in the rock were investigated by first modelling the system without the buffer/backfill/canister and then applying the resulting pressure field as an initial condition in the model with all constituents. Two cases were investigated, a drained condition (RH = 100%) and a ventilated condition (RH = 70%). The rock permeability influences the effect of the relative humidity on the water saturation of the surrounding rock, and in extension, the saturation time of the bentonite. A low rock permeability implies a smaller volume of rock affected as well as slower resaturation. A significant effect was noted only for the ventilated case, with 70% RH, for both low and high rock permeability. The saturation times became longer, from 21 to 28 years for a rock with high permeability, and from 177 to 233 years for a rock of low permeability, considering a ventilated condition. The assumption of 70% relative humidity is, however, a very extreme case.
- The effect of block retention was also investigated. This was done by moderately altering the retention curve. At degrees of saturation higher than the initial state, the curve was lowered, while for lower degrees of saturation the curve was close to the original one. The effect of this was to increase the saturation time for high permeability rock from 21 to 26 years, while for low permeability rock the saturation time increased from 177 to 192 years.
- Changing the buffer permeabilities within a range of 0.6 to 2 times the original value did not have a significant effect on saturation time. The range of permeabilities was selected from an assessment of a relatively large number of experimental data. More about this can be found in the dedicated Data Report for the THM-modelling of the buffer, backfill and other system components /Åkesson et al. 2010b/.

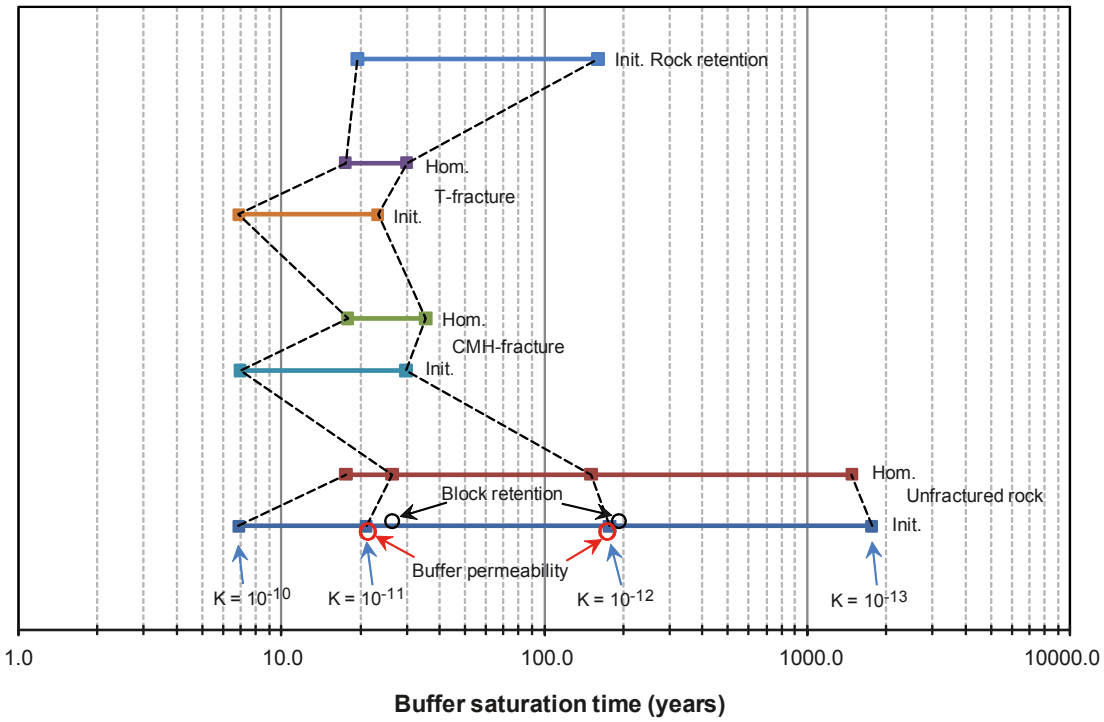

Figure 10-50. *Compilation of the buffer saturation times (the time when the liquid saturation S_l = 0.99 in the entire buffer) for all TH-simulations of a deposition hole. The text to the right of the lines indicates the representation of the rock: Unfractured rock, CMH-fracture (fracture at canister mid-height), T-fracture (fracture at tunnel) and Rock retention (changed rock water retention curve). In the three first cases (from the bottom up) the buffer has been represented as in the initial state (Init.), where blocks and pellet slot are present, and as in a fully homogenised state (Hom.) as indicated to the left of the corresponding horizontal line. In the Rock retention case only the Init. buffer representation has been used. The results obtained using the same rock conductivity, indicated below the bottom line, are connected by hatched lines. The results from changing the Buffer permeability or Block retention are indicated by red or black circles, respectively /Åkesson et al. 2010a/.*

Apart from the investigated cases there are some additional uncertainties in the description of the saturation process:

- The effect of the assumed axial symmetry, reducing the problem to two dimensions, has not been investigated.
- The inner slot (between the vertical canister boundary and the bentonite blocks), present in the buffer initially, has been omitted in the models. This effect, however, is included in the description of the thermal evolution (Section 10.3.4).
- The relation between the saturation responses for TH-models and Thermo-Hydro-Mechanical (THM)-models has only been investigated for rapid saturation processes.
- Regarding the distance to the hydraulic pressure boundary, 60 m above the repository, the strategy has been to study data on the rock properties at the Forsmark site and to develop a relevant representation. This distance is based on the distance to a more permeable part of the rock characterised at the Forsmark site.
- The importance of the mesh used in the models has only been investigated to a limited extent.

These uncertainties may influence the calculated time spans, but they are not expected to affect the conclusions and general understanding of the wetting cases.

Moisture redistribution in dry rock case

The venting of deposition tunnels during significant time spans (prior to filling of the deposition holes and the tunnels) may lead to dehydration of the surrounding rock. This air-filled pore-space in the rock could potentially constitute a sink for the water that is associated with the buffer at installation. If a significant amount of this water were to migrate into the rock, then this could potentially result in a significant increase of peak temperatures at the canister surfaces.

The moisture redistribution in a deposition hole buffer for a case with a dry surrounding rock mass was studied in /Åkesson et al. 2010a/. The main reason for the study was to investigate the effect of the water redistribution in the buffer of a dry deposition hole on the thermal conductivities in different parts of the buffer. The result of this investigation (a water saturation field translated into thermal conductivities) was used as one case in the calculations of the thermal evolution (see Section 10.3.4). While the dry conditions imply that temperature increases, these analyses show that temperatures in the buffer remain below the highest accepted value.

Application to hydraulic conditions at the Forsmark site

The study of the saturation of the buffer and backfill in /Åkesson et al. 2010a/ was made as a sensitivity study. The properties of both the engineered barriers and the surrounding rock were selected to cover a wide range of combinations. No site specific information was used.

In Section 10.3.6 an analysis of the inflow of water to tunnels with different characteristics at the Forsmark site is presented. As seen in Figure 10-24 it will take more than 50 years to saturate even a fast tunnel. However, even the slow tunnel is well within the range presented in Figure 10-49. As stated in the beginning of this section, the saturation time does not directly affect the performance of the repository and the spatial variability at the site will not affect the safety.

Identified uncertainties and their handling in the subsequent analysis

The saturation times for both backfill and buffer range from a few tens of years to several thousand years. Examples from across this entire range are likely to arise at Forsmark, since rock properties (matrix hydraulic conductivity and presence and characteristics of fractures) are the primary controls, with backfill and buffer properties only a secondary consideration.

10.3.9 Swelling and swelling pressure

The primary purpose of the buffer is to ensure that transport of species from the rock to the canister and from the canister to the rock is dominated by diffusion. The swelling pressure in the bentonite is expected to seal all gaps and ensure that there is tight contact between the rock and the buffer. It is, therefore, important that the swelling pressure is maintained. The safety function indicator criterion for ensuring tightness in the buffer is a swelling pressure of 1 MPa (Section 8.3.2), safety function indicator Buff1b in Figure 10-2. A high swelling pressure is needed for reducing microbial activity (Buff2). The required swelling pressure for preventing canister sinking is 0.2 MPa (Buff 5). On the other hand, the swelling pressure must not be higher than 15 MPa in order to limit the pressure on canister and rock (Buff6). The densities needed to meet these values are discussed in Section 5.5.3. To ensure that the buffer density is not lost by buffer swelling into the tunnel backfill, the backfill density needs to be sufficiently high (BF1), see Section 5.6 for actual values.

The two reference buffer materials MX-80 and Ibeco RWC are assumed to have a saturated density interval of 1,950–2,050 kg/m^3. The swelling pressure for the reference density (2,000 kg/m^3) will be 7.5–8 MPa for both materials, see Section 5.5. With account taken for the allowed variations in density, the swelling pressure may vary between 4.5 and ~13 MPa, provided that the buffer material is fully confined to the volume it occupies at deposition. The hydraulic conductivity will be well below 10^{-13} m/s. These values are valid for a rather large range of groundwater salinities. The present day groundwater at Forsmark has a salinity of ~0.9% or 0.15 M Cl^-.

For the backfill material with specified dry density of 1,458–1,535 kg/m^3, the swelling pressures after full water saturation should be well above 3 MPa, based on results from compressibility tests /Johannesson and Nilsson 2006/. Under these conditions, the hydraulic conductivity should be well below 10^{-12} m/s.

In short this means that if the buffer saturates and swells without loss of buffer material and without expanding into the backfill the above safety function indicators will be within the allowed values. In order to verify that the intended conditions after swelling will be reached, it is, however, necessary to assess more carefully the swelling process with focus on:

- Buffer homogenisation.
- Buffer upward expansion.
- Movement of the canister in the deposition hole.
- Homogenisation after loss of bentonite mass.

The findings of this assessment are presented in the following.

Buffer homogenisation

The initial state of the buffer after placement is unsaturated bentonite blocks and rings with much higher density than the average density for the entire hole and one empty slot at the canister surface and a pellet filled slot with very low density at the rock surface. Due mainly to friction within the material, but also due to hysteresis effects, the swelling and homogenisation that comes with the wetting of the bentonite is not complete and there will remain density differences and swelling pressure differences in the buffer.

In /Åkesson et al. 2010a/, three different analyses of the natural homogenisation process in the buffer have been carried out. In the first analysis, analytical solutions have been studied. In the second analysis, the finite element code Code_Bright has been used for studying the process in more detail. In the third analysis, the finite element code Abaqus has been used for modelling the entire deposition hole.

The important geometrical components of the models are the initial open slot between the canister and the buffer blocks, the buffer blocks themselves and the pellet filled outer slot as shown in Figure 10-51. The key phenomena investigated with the Code_Bright, was the influence on the homogenisation and swelling pressure of slot width in a section between the canister and the rock and the wetting sequence. In the study, the slot width was varied from 3 to 9 cm with the other parameters kept constant. Figure 10-52 shows the final swelling pressure in the buffer components as a function of slot width.

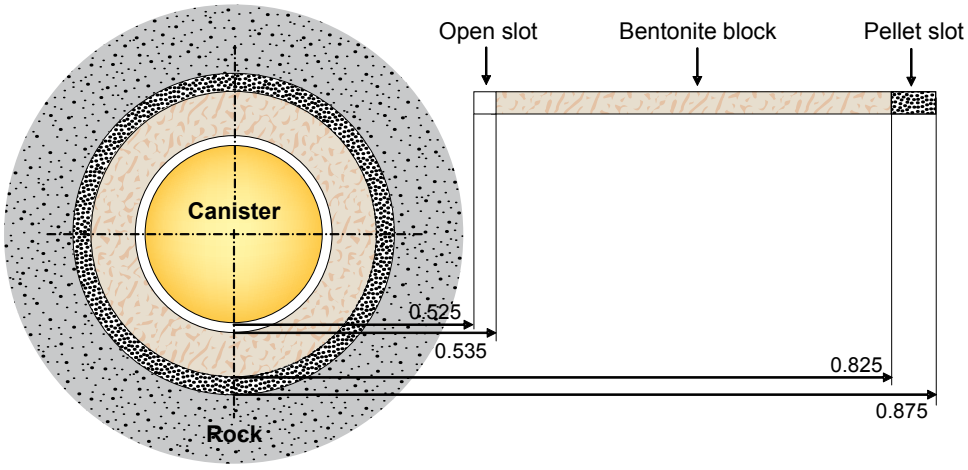

Figure 10-51. *Model geometry and constituents /Åkesson et al. 2010a/.*

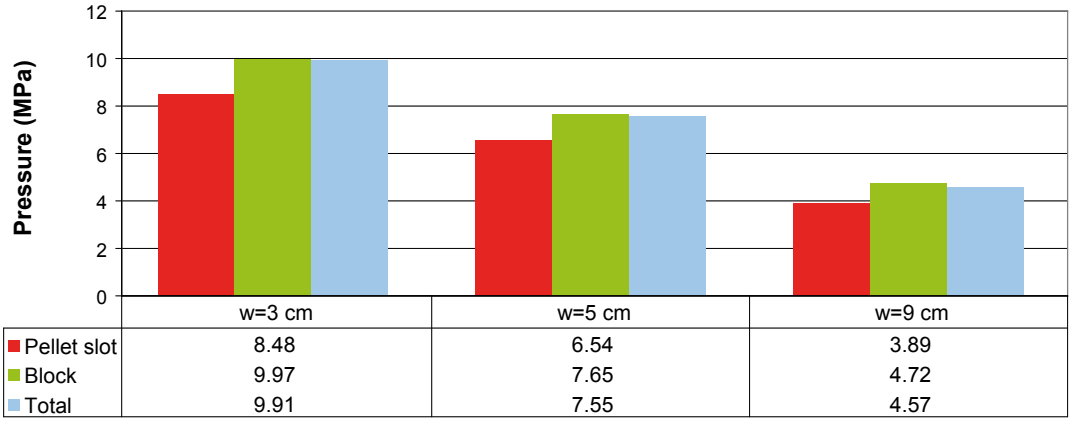

	w=3 cm	w=5 cm	w=9 cm
Pellet slot	8.48	6.54	3.89
Block	9.97	7.65	4.72
Total	9.91	7.55	4.57

Figure 10-52. *Averages of pressure for 3, 5 and 9 cm pellet slot /Åkesson et al. 2010a/.*

The effect of the wetting sequence was tested by the assumption of either entirely serial or parallel wetting. In the case of serial wetting water uptake comes from the pellet slot, while parallel wetting assumes that both components are swelling simultaneously. The results from the two models have been compared with the results obtained from the Canister Retrieval Test (CRT) /Åkesson et al. 2010a/. Compared with CRT results, pure serial wetting produces more heterogeneity in the void ratio field. The parallel wetting process produces less heterogeneity than the CRT measurements. This is illustrated in Figure 10-53.

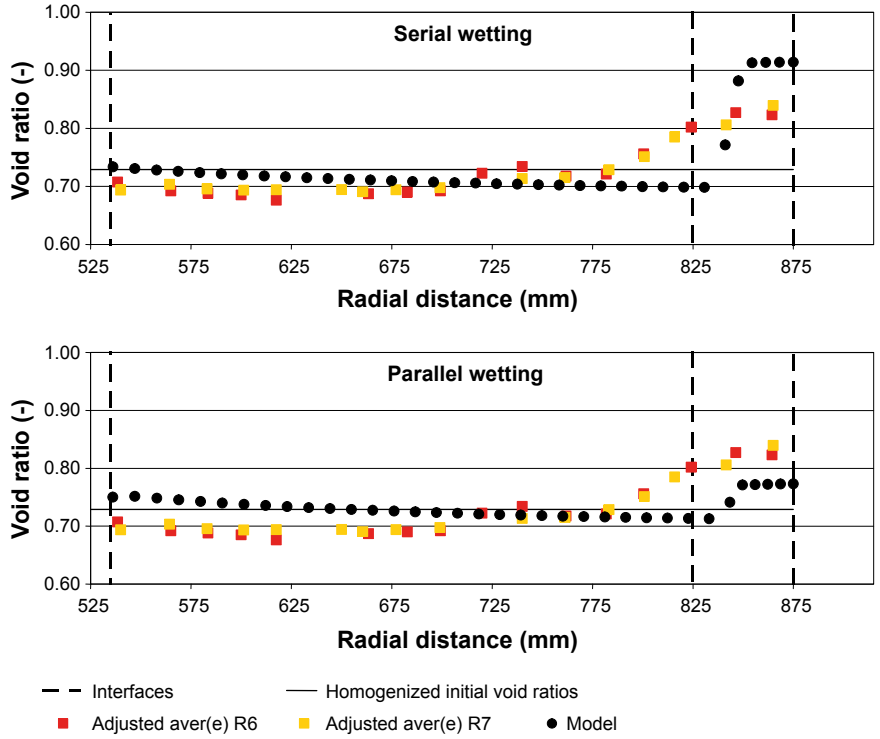

Figure 10-53. *Void ratio profiles obtained for serial and parallel wetting. Adjusted average refers to the measured average void ratio (e) for the entire periphery of ring (R) 6 and 7 in the Canister Retrieval Test /Åkesson et al. 2010a/.*

The finite element code Abaqus was used to model the homogenisation process in an entire deposition hole with identical initial conditions and boundary conditions with those in the CRT. The results shown in Figures 10-54 and 10-55 give an expected final density and stress distribution in a deposition hole covered with a backfill that is compressed about 3 cm.

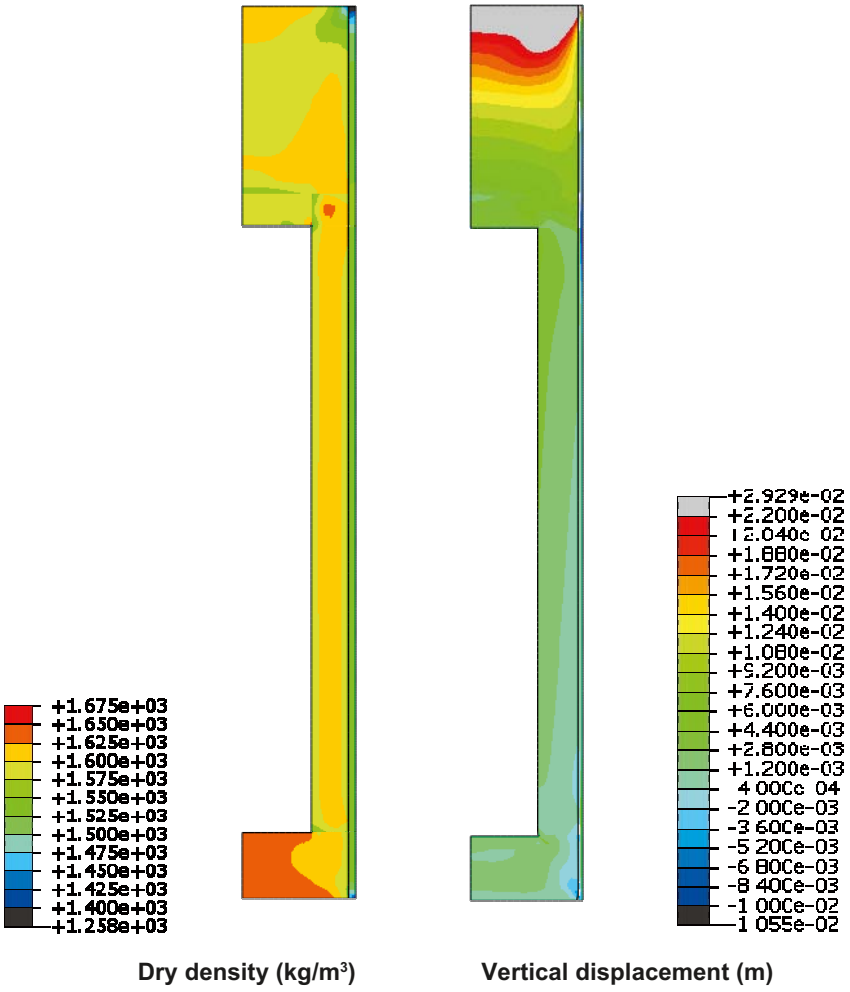

Figure 10-54. *Final state of the buffer after full saturation and completed homogenisation. The distribution of the dry density and the vertical swelling is shown /Åkesson et al. 2010a/.*

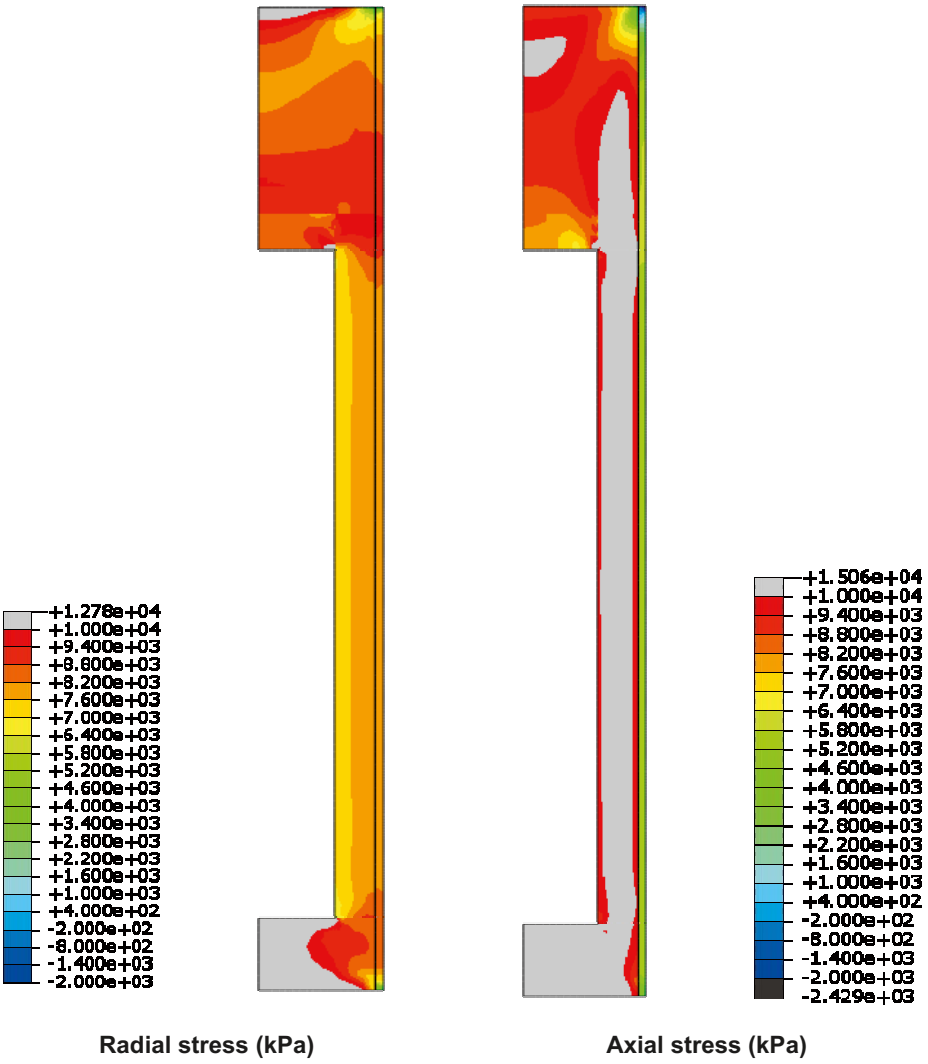

Figure 10-55. *Final state of the buffer after full saturation and completed homogenisation. The distribution of radial and axial stress is shown /Åkesson et al. 2010a/.*

The only remarkable observation is that there is no obvious density gradient (decrease in density and swelling pressure towards the backfill) in spite of there being an upwards swelling of 3 cm. This result deviates from the results of the calculations of buffer upwards swelling shown later (e.g. Figures 10-57 and 10-58), where initially completely water saturated and homogenised buffer was used.

There are several factors that in combination may explain this difference.

- The buffer material in the swelling calculations presented in the section about buffer upwards expansion, was modelled as being completely saturated and homogenised from the start. This means that the swelling pressure and the friction against the rock were fully developed from the start. This is not the case for the calculation made here where the initially low density of the pellet filling and initially unsaturated buffer blocks result in a lower friction between the rock and the buffer during a large part of the swelling process.
- The upper 75 cm was wetted later, which delayed the mobilization of the friction. The reason for this was the wetting history of CRT and the calculation was a continuation of the CRT modelling.

Modelling of the Canister Retrieval Test (CRT) and comparison with measurements confirm that the material model of unsaturated bentonite blocks and the calculation technique used are relevant for modelling the homogenisation process, since the agreement between modelled and measured density

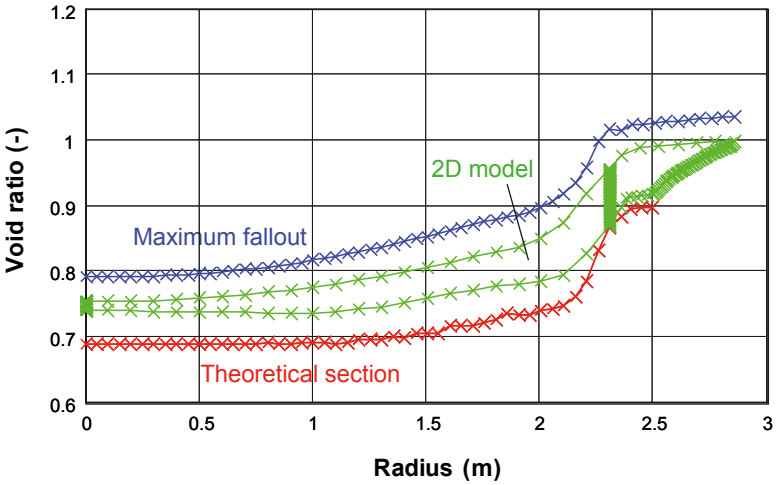

Figure 10-56. *Final void ratio distributions in 1D (blue and red crosses) and 2D models /Åkesson et al. 2010a/.*

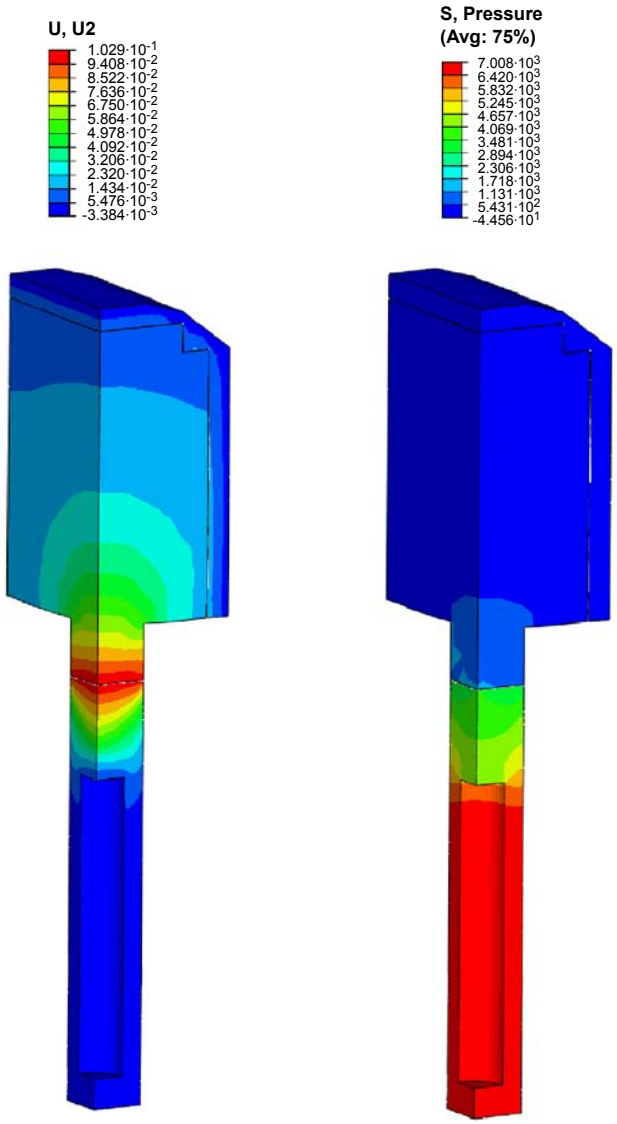

Figure 10-57. *Vertical displacements (U, m) and average stress (S, kPa) in the buffer and backfill after completed swelling (Case 1.) U2 is the direction (vertical) of the displacement U /Börgesson and Hernelind 2009/.*

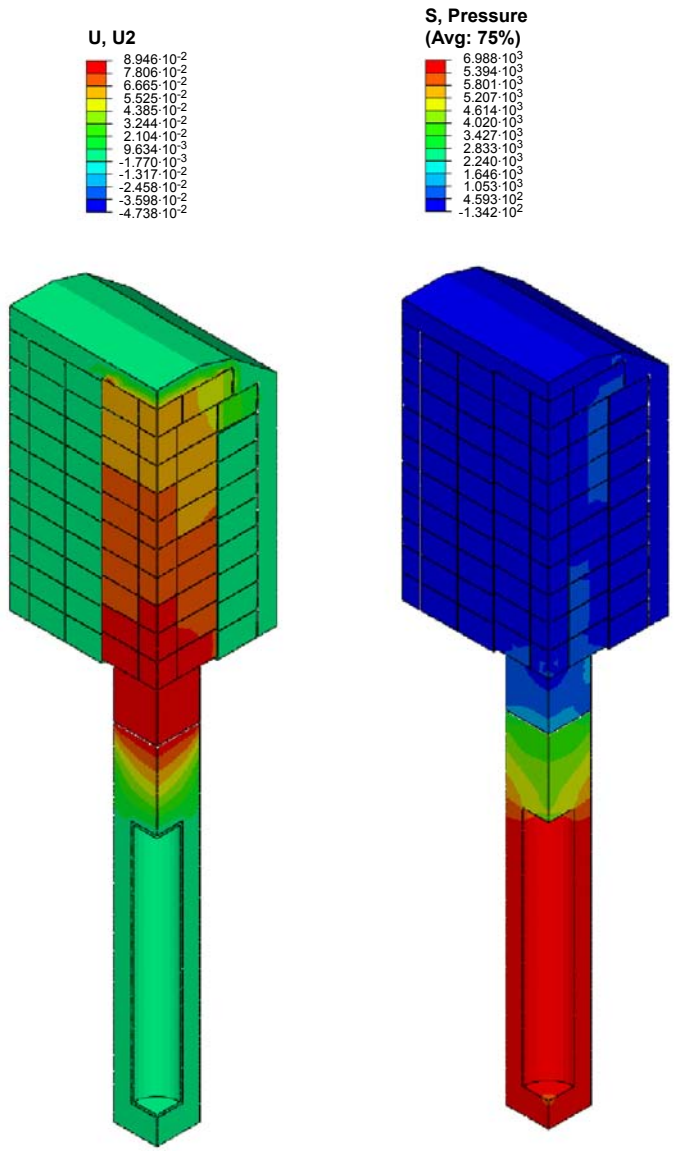

Figure 10-58. *Vertical displacements (U, m) and average stress (S, kPa) in the buffer and backfill after completed swelling (Case 2). U2 is the direction (vertical) of the displacement U /Börgesson and Hernelind 2009/.*

distribution in the buffer between the canister and the rock after full saturation and completed homogenisation was very good. The material model and calculation technique were then used to model the homogenisation process in an entire deposition hole with identical initial conditions and boundary conditions to those in CRT. The results shown in Figures 10-54 and 10-55 gave an expected final density and stress distribution in a deposition hole covered with a backfill that is compressed about 3 cm. Very similar results were reached with the Abaqus and the Code_Bright models, as well as with the analytical expression, but the entire test was only modelled with Abaqus.

The uncertainties are mainly the material models, which are very complicated, and the parameter values. Although they have been verified for the 1D case of swelling and homogenisation of the bentonite rings and pellets between the canister and the rock, the 2D case involves more degrees of freedom for the variables and more interactions like the friction between the bentonite and the rock or canister.

The results show that under expected conditions the buffer density and swelling pressure will homogenise to a situation where the relevant safety functions will be upheld.

Backfill homogenisation

The deposition tunnels will have a varying cross section. Since the ratio of backfill blocks/pellets will vary in the installed backfill, density will vary in the axial direction of the tunnel. The homogenisation of the backfill was studied by /Åkesson et al. 2010a/.

The final void ratio distributions both for 1D and 2D models are shown in Figure 10-56. A general difference between the inner and the outer parts of slightly more than 0.2 in void ratio can be noticed. This is generally in agreement with the experimental findings from the Canister retrieval test /Johannesson 2007/. It can be noticed that the distribution in the 2D model falls between the two extreme results obtained with the 1D models.

The models indicate that the backfill material will not be completely homogenised. The remaining heterogeneity is of such a degree that the difference between the inner and the outer parts is slightly more than 0.2 in terms of void ratio, and the reason for this appears to be the hysteretic effects during swelling/compression cycles. The remaining heterogeneity indicates that the final void ratio can be as high as 1.03 which corresponds to a dry density of 1,370 kg/m^3. This value is substantially lower than the lowest value in the range presented in Chapter 5 and in the **Backfill production report**, which shows that the homogenisation process needs to be considered in the design of the backfill. However, this is still higher than the dry density of 1,100 kg/m^3 that is required for the SR-Site backfill to reach a hydraulic conductivity less than 10^{-10} m/s which is stated in the **Backfill production report**.

Buffer upward expansion

One of the main design requirements of the backfill is to keep the buffer in place and prevent it from swelling upwards so that the buffer will not lose too much of its density. Some upwards swelling is expected since the backfill has a lower swelling pressure than the buffer and a certain degree of compressibility. For SR-Can, both finite element modelling and analytical calculations of this process were performed (see e.g. /Börgesson and Johannesson 2006, Börgesson and Hernelind 2006a, Börgesson et al. 2006, Johannesson and Nilsson 2006/), but the reference backfill considered in most of those calculations was an in situ compacted mixture of 30/70 bentonite/crushed rock. For SR-Site, a new reference backfill (compacted blocks and pellets of Milos backfill) compared to SR-Can is considered. This new backfill behaves very differently from the old backfill, under both dry and wet conditions.

Modelling of upwards swelling, considering different backfill properties, with both the buffer and the backfill saturated from the start has been carried out and reported /Börgesson and Hernelind 2009/. At installation both the buffer and the backfill consist of bentonite blocks with very high density and different degrees of saturation and pellets filling all remaining slots between the blocks and the rock surface. Then water enters the deposition hole and the tunnel which result in the wetting and swelling of the blocks together with wetting and compression of the pellet filling. The rate of these processes depends on the rate and location of water inflow and the actual evolution of the saturation and homogenisation of the buffer and backfill. The corresponding interaction between the buffer and backfill materials is different in every deposition hole. The complicated nature calls for simplifications in order to be able to model the process with moderate effort. The extreme cases are to assume either completely saturated (wet) or completely un-wetted (dry) conditions, which yield four cases:

1. Wet buffer and wet backfill.
2. Wet buffer and dry backfill.
3. Dry buffer and dry backfill (uninteresting).
4. Dry buffer and wet backfill.

Case 3 is obviously not interesting and is therefore not considered. In addition, case 4 is not of primary interest since there will be very little compression of the buffer blocks and rings, as the uniaxial compression strength of the blocks and rings are 3 MPa and 4 MPa respectively, which is higher than the expected swelling pressure from the backfill. This case is also not expected to occur since it takes 100 years for the backfill to be completely water saturated.

The finite element code Abaqus was used for the calculations. Abaqus contains a capability of modelling a large range of processes in many different materials as well as complicated three-dimensional geometry. In the calculations of the wet case material models simulating porous materials

(both buffer and backfill) have been used. Different cases with different degrees of homogenisation and different properties have been modelled. Since the buffer material is assumed to be water saturated from the start, the time scale only includes the time for the buffer to swell upwards. The canister has been modelled, but only as a tube of very stiff material. The calculations were carried out using some pessimistic assumptions such as:

- No swelling pressure from the backfill.
- No friction between the backfill and the rock.
- Very loose pellets filling (no homogenisation).

Figure 10-57 shows the displacements and swelling pressures in the buffer and backfill for the case when both are saturated at the start. In spite of the pessimistic assumptions, the buffer density see stays above 1,950 kg/m^3. The following can also be observed from the figure.

- The influence of the loose pellets filling on top is not very strong since it is only compressed by about 1 cm; the main reason being that the vertical stress is laterally spread and thus much smaller in the roof than in the floor above the deposition hole. However, the compression of the pellet filling is judged to be proportional to the thickness, which means that the upwards expansion may increase by two cm if the thickness is trebled.
- The expansion reaches down to the top of the canister where the displacement is about 1 cm.
- The difference in displacement pattern between the buffer and the backfill reveals that there is a rather strong friction effect between the upper buffer part and the rock surface but not in corresponding parts of the backfill. The reason is that there is a swelling pressure in the buffer that influences the friction but not in the backfill.
- There is a jump in average stress in the interface between the buffer and the backfill from about 3.5 MPa in the buffer to about 1.5 MPa in the backfill. The reason for this discrepancy is that the buffer swells and the backfill is compressed, which leads to a difference in the direction of the principal stress. It is vertical in the compressed backfill and horizontal in the swelling buffer.

For the case with a dry backfill all materials except the backfill are modelled in an identical way as for the wet case. The backfill model is complicated since the major part of the backfill consists of separate blocks. Most deformation will take place in the horizontal joints between the blocks and in the pellet filling and the properties of especially the joints between the bentonite blocks are not known. For the calculations the joints have been assumed to have the following properties (both horizontal and vertical):

- Average joint thickness: 4 mm.
- Compression properties: the joints are closed at an external pressure of 10 MPa.
- Friction angle $\varphi = 20°$.

Figure 10-58 shows the displacements and swelling pressures in the buffer and backfill for the case when only the buffer is saturated at the start. The following can be observed from the figure.

- The compression and thus also stress distribution in the backfill is limited to the block pile above the deposition hole since there is an insignificant spreading of the stress due to the vertical joints between the blocks.
- The influence of the loose pellets filling at the roof is strong since it contributes more than half of the total compression, which thus means that the compressibility of the pellet filling is important and the effect of an unfilled section is very strong.
- The expansion reaches down to the top of the canister where the displacement is about 1 cm.
- The backfill block in the top of the deposition hole is compressed very little. The block only moves upwards and opens the joint between the bottom backfill block and the floor of the tunnel.
- A similar jump in average stress as for the wet case takes place in the interface between the buffer and the backfill from about 3.5 MPa in the buffer to about 2.0 MPa in the backfill.

There is of course an influence of backfill block size and piling geometry. In the model example the blocks have been piled without individual shifting (no masonry bond). If there is a masonry bond the stress distribution will increase and the swelling decrease. On the other hand if the backfill blocks are smaller and without masonry bond the stresses will be more concentrated and the swelling larger.

In /Börgesson and Hernelind 2009/ a number of parameter variations were studied for the wet case. The calculations showed that there are three parameters that are critical for the swelling, namely the friction angle between the buffer and its surroundings, the stiffness of the backfill and the swelling pressure of the backfill. For the case of wet backfill material, only the combination of a low friction angle and a low swelling pressure in the backfill (which is not a realistic case) could lead to a significant drop of buffer density at the canister top.

Since the dry backfill case had more impact on the buffer and only one case was studied in /Börgesson and Hernelind 2009/, /Åkesson et al. 2010a/ did additional studies on the case with a wet buffer and a dry backfill. The objective was to carry out additional modelling of the dry case with some alternative geometries that were not considered in the former models and check how the final density distribution of the buffer in the deposition hole is affected by the swelling of the buffer and consequent compression of the backfill. Three calculations were done with different initial densities of the buffer and different slot heights at the roof. The results show that there will be a significant upwards swelling in the extreme case of a completely water saturated buffer material and a completely un-wetted backfill. The geometry modelled had a degree of block filling of about 76% and a pellets filled slot at the roof of 30 or 55 cm. The important results of the three calculations are summarised in Table 10-3.

The modelled cases represent an extreme wetting situation and have a rather large pellets filled slot at the roof. Most important for the upwards swelling are the horizontal joints between the backfill blocks. The properties of those joints are not known and the stress-strain relation used is estimated. The results show that there is a loss in density of the buffer above the canister but the resulting lowest density at water saturation at the canister/buffer contact for an initial density of 2,000 kg/m^3 is 1,960 kg/m^3. If the initial density is only 1,950 kg/m^3, the corresponding final density will be 1,920 kg/m^3, but the swelling pressure is still 2.1 MPa. The results also show that there may locally, in some backfill blocks on the floor, be von Mises stresses that are higher than the compressive strength and thus may cause local crushing of the blocks. This is not expected to yield any problems.

The overall picture is that the swelling pressure of the buffer and the associated safety functions will be maintained during the expansion of the buffer into the backfill for all possible combinations of buffer and backfill conditions. However, there is some uncertainty in the modelling since the buffer is modelled as completely water saturated and homogenised from the start, which may affect the results. This means that the friction force between the buffer and the rock is mobilized early in the swelling process. In the real case there is a pellet filling with very low density between the bentonite blocks and the rock, with an initially rather low swelling pressure and thus low friction force. The result of this difference is that the modelled density gradient between the canister and the backfill probably is larger than if a heterogeneous unsaturated buffer was modelled.

A comparing calculation using homogenised saturated buffer and heterogeneous unsaturated buffer showed no difference in buffer upwards swelling but the use of homogenised completely saturated buffer is nevertheless noted as an uncertainty. The homogenisation modelling in the previous section confirms that the assumptions have little impact on the results (Figures 10-54 and 10-55). The mechanical behaviour of the horizontal contacts between the backfill blocks has not been measured. The relation used assumes that there is a slot of 4 mm that is closed at the pressure 10 MPa, which is probably pessimistic. The effect of local crushing of the blocks that may occur close to the floor is not included in the model. Another uncertainty relates to how the blocks are piled. It is assumed that the blocks are not overlapping each other, which means that the there will be no lateral spreading of the pressure. The swelling is expected to be smaller if the blocks are piled with overlaps like masonry.

Table 10-3. Summary of results for the cases with slot at the roof.

Variable	Model 1	Model 2	Model 3
Density at saturation	2,000 kg/m^3	2,000 kg/m^3	1,950 kg/m^3
Pellets filled slot	30 cm	55 cm	55 cm
Max buffer upwards swelling	96 mm	102 mm	68 mm
Canister heave	4.8 mm	5.0 mm	3.2 mm
Buffer density at top of canister	1,960 kg/m^3	1,960 kg/m^3	1,920 kg/m^3
Average axial swelling pressure at top of canister	3.8 MPa	3.6 MPa	2.1 MPa

Movement of the canister in the deposition hole

One of the safety functions for the buffer is that it should prevent the canister from sinking in the deposition hole since this would render the canister in direct contact with the rock thus short-circuiting the buffer.

Canister settlement consists mainly of four different processes:

1. Consolidation/swelling caused by the canister weight.
2. Volumetric creep caused by the canister weight.
3. Deviatoric creep caused by the canister weight.
4. Stress changes caused by upwards swelling of the buffer/backfill interface
   a) Consolidation/swelling.
   b) Volumetric creep.
   c) Deviatoric creep.

The fourth process can thus be divided into the same processes as the first three processes but the consolidation and creep is caused by the swelling pressure from the buffer on the backfill instead of the weight of the canister.

The settlement of the canister has been modelled in /Åkesson et al. 2010a/. The calculations include two stages, where the first stage models the swelling and consolidation that takes place in order for the buffer to reach force equilibrium. This stage takes place during the saturation phase and the subsequent consolidation/swelling phase. The second stage models the deviatoric creep in the buffer over 100,000 years. The modeling takes into account all processes except volumetric creep, which thus may cause a slight underestimation of the canister displacement. The motive for excluding volumetric creep is that canister settlement caused by volumetric creep will not change the total mass of bentonite under the canister but will only increase the density and is thus not judged to be a problem.

The base cases in the calculations correspond to the final average density at saturation of 2,000 kg/m^3 with the expected swelling pressure 7 MPa in a buffer. In order to study the sensitivity of the system to loss in bentonite mass and swelling pressure seven additional calculations were done with reduced swelling pressure down to 80 kPa corresponding to a density at water saturation of about 1,500 kg/m^3. The results of the calculations with fixed backfill boundary and the corresponding friction angle at retained initial swelling pressure are summarized in Table 10-4. The canister settlement shown in

Table 10-4. Summary of results from the calculations with fixed buffer/backfill boundary /Åkesson et al. 2010a/.

Calculation No	Density at saturation ρ_m (kg/m^3)	Swelling pressure p (kPa)	von Mises stress at failure q_f (kPa)	Canister settlement (mm)	Friction angle at retained swelling pressure ϕ (°)[1)]	Canister settlement at corresponding friction angle and retained swelling pressure (mm)[2)3)]
1 (base case)	2,010	7,000	2,238	0.35	8.8	0.35
2	1,950	3,500	1,312	0.67	5.2	0.47
3	1,890	1,750	770	1.26	3.1	0.67
4	1,840	875	451	2.42	1.8	1.04
5	1,780	438	265	4.63	1.1	1.67
6	1,720	219	155	8.89	0.63	2.78
7	1,690 (1,640)[1)]	160	122	12.0	0.50	3.51
8	1,620 (1,470)[1)]	80	72	22.5	0.29	5.54

1) For the actual values of void ratio and density at saturation since the void ratio, e > 1.5 and Equation

$$\phi = \frac{3}{6\,p/q_f + 1}$$

2) Derived from the consolidation in the base case (0.20 mm) + the creep from respective creep calculation.

3) The total bottom buffer thickness is 500 mm.

column 5 also includes the consolidation settlement, which takes into account that the compressibility increases when the swelling pressure decreases whereas a reduced friction angle with retained swelling pressure will not have an increased compressibility. The settlements at the presented friction angles have for this reason been recalculated as the sum of the settlement of the base case and the creep from respective creep calculation (column 7).

The conclusion is thus that the expected displacement of the canister in a deposition hole from consolidation and creep during 100,000 years is very small. The sensitivity analyses with reduced swelling pressure corresponding to reduced density or reduced friction angle also show that the canister displacement is very insensitive to such phenomena since the total settlement will be less than a few cm even at a buffer density of 1,500 kg/m^3 or at a friction angle of 0.3°. The only condition when the safety function could be violated is when there is a large loss of buffer. However, if that situation would occur, many of the other buffer safety functions would be lost long before.

Homogenisation after loss of bentonite mass

Homogenisation of buffer and backfill is crucial to fulfil the safety functions related to buffer and backfill density (swelling pressure and hydraulic conductivity). The swelling properties of bentonite make the buffer and backfill material swell and close open gaps or channels to form a more homogeneous buffer. These properties are important not only for homogenising the buffer and backfill after installation of the bentonite blocks but also for limiting the potential for the long term formation of openings in the buffer and backfill. Except for the natural slots that exist after installation, which are treated in the Buffer homogenisation section, such spaces may appear for several reasons, as summarised below.

1. The postulated case of missing bentonite rings.
2. Erosion before closure of the repository caused by water inflow into deposition holes and a deposition tunnel until the water flow and high water pressure gradients are stopped by temporary plugs. If the erosion is severe, large openings of missing bentonite may locally be formed.
3. Long term erosion of bentonite by water from fractures intersecting the deposition hole or the deposition tunnel mainly caused by bentonite dispersion and subsequent colloid transportation after fresh water intrusion.

The consequences of erosion before the closure of the repository are discussed in Section 10.2.4.

Loss of buffer

The swelling and sealing of bentonite cannot take place unhindered since there is a resistance to swelling caused by friction both internally in the bentonite and between the bentonite and the surrounding fixed walls represented by the rock surface and in some cases the canister. In order to investigate how well the buffer material seals the openings resulting from the mentioned processes a number of finite element calculations with the code Abaqus have been performed /Åkesson et al. 2010a/.

The case that has been modelled represents either a huge loss of bentonite after a long time of erosion or the totally fictional case of one to three bentonite rings at the upper end of the canister, missing. The rings are 50 cm thick and are for the sake of the calculations assumed to be forgotten during the installation. This case can also represent an extreme loss of bentonite by colloid erosion. The calculations comprise cases with an empty space of 0.5 m, 1.0 m and 1.5 m. Additional calculations were also done for each case in order to investigate the influence of the friction against the rock.

Figure 10-59 shows the course of swelling for the base case (two missing rings) assuming a friction angle $\varphi = 8.69°$. After a rather long time the space is almost completely filled with bentonite but there is a small remaining final opening and the void ratio is rather high (1.7) close to that opening. The density is so low that the expected swelling pressure might very well be below 100 kPa at the position closest to the canister. For a case with low friction the lowest swelling pressure case is 300 kPa at the canister.

Variant calculations corresponding to one, two or three missing bentonite blocks were also analysed. In summary, the analyses show that in the case where large amounts of bentonite are lost from a

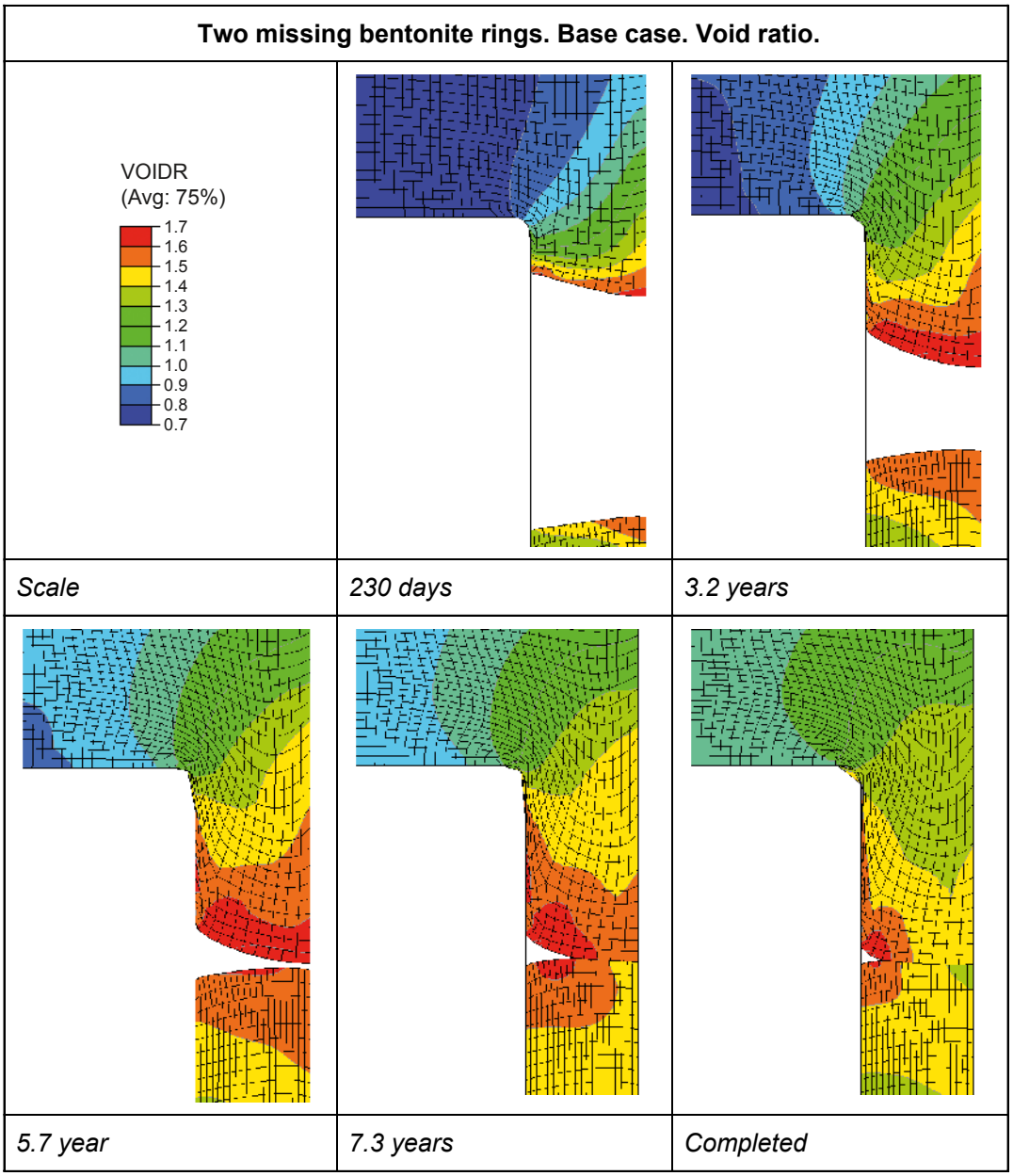

Figure 10-59. *Void ratio plotted at different times for the base case with two missing ring /Åkesson et al. 2010a/.*

deposition hole or missing from the start the remaining bentonite swells and fills the empty space but the density and resulting swelling pressure will be rather low due to the friction in the buffer and the friction against the rock surface. For a 50 cm vertical opening in a deposition hole, the resulting swelling pressure will be in average 0.5–1 MPa in almost the entire former hole. However, if the rock surface is smooth and the resulting friction against the rock is halved the swelling pressure will be above 1 MPa in a majority of the former space. For a 100 cm opening the swelling pressure will be rather low close to the canister with the pressure below 100 kPa and there may even be an unfilled part left, while the case with low friction yields a minimum swelling pressure of more than 300 kPa. If the opening is 150 cm, a large volume will have a swelling pressure below 100 kPa and may even be unfilled. However, the influence of the friction between the bentonite and the rock and canister is large and with halved friction almost the entire opening will be filled. The homogenisation is enhanced by the swelling of the bentonite above or below the canister, which is shown by comparison with results from the calculations that only consider the buffer around the canister.

Homogenisation after a loss of backfill mass

If a fracture intersects the entire perimeter of the backfilled tunnel there will be no deposition hole at that location, which means that such fractures do not intersect deposition holes. However, it is expected that there will be some such water conducting fractures crossing the tunnel close to deposition holes. If these fractures are hydraulically active they may expose the backfill to colloid erosion. /Åkesson et al. 2010a/ have investigated how much backfill can be lost before the buffer upwards swelling decreases the density in the deposition hole around the canister to a level where advective conditions have to be considered.

In the calculations, the buffer material is considered to completely have lost its sealing ability when the average swelling pressure between the canister and the rock has become lower than 100 kPa, see previous section. Since the swelling of the buffer takes place upwards into the tunnel where the backfill is lost, the swelling pressure will be lower on top of the canister than further down into the deposition hole. The criterion for loss of sealing ability will thus be when the swelling pressure on top of the canister is 100 kPa. Due mainly to friction between the buffer and the rock the swelling pressure is likely to be lower at the opening of the hole than on top of the canister. The aim of the calculations was to study how much backfill can be lost under a range of conditions where a swelling pressure of 100 kPa is still maintained on top of the canister.

A number of calculations for different assumptions and geometries were made to determine the maximum allowed loss of mass. For a bounding case where the backfill is lost directly on top of the canister and no homogenisation whatsoever is considered about 25 tonnes of backfill can be lost before the swelling pressure in the buffer on the canister top drops to 100 kPa. This case is totally unrealistic since the swelling pressures in the remaining buffer and backfill are totally neglected. It is only presented to illustrate the importance of the homogenisation and friction.

Figure 10-60 illustrates a case where both the homogenisation in the backfill in the tunnel and the friction in the deposition hole is considered. Table 10-5 summarises the maximum allowed loss of backfill for this case. Here the homogenisation and the friction in the remaining backfill and the friction in the buffer have been considered. The bevel in the deposition hole has also been considered.

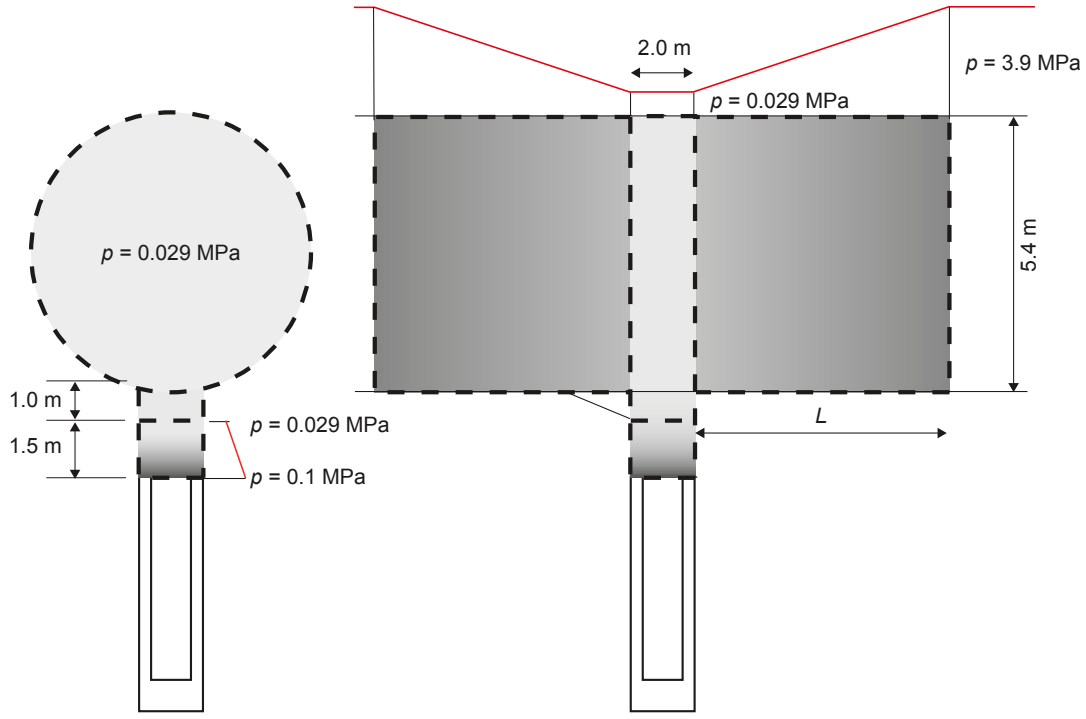

Figure 10-60. *The light grey area has lost mass to yield a swelling pressure of 29 kPa. The successive transition from dark grey to light grey illustrates the decrease in swelling pressure and density. The swelling pressure variation in the upper part of the deposition hole and in the deposition tunnel are shown by the red lines (derived from /Åkesson et al. 2010a/).*

Table 10-5. Total allowed loss for the case illustrated in Figure 10-60.

ϕ (°)	Total loss (t)
10	430
20	220
30	150

This means that the distance assumed between the canister and the backfill is 1.5 m as presented in Figure 5-16 and not the 2.5 m illustrated in Figure 10-60. It is also assumed that the friction angle is the same in the buffer and the backfill and that the mass loss in the backfill occurs directly on top of the canister and that the backfill is lost to a vertical fracture. A mass loss further away in the tunnel or to a sloping fracture would mean that additional backfill could be lost.

It is reasonable to assume that the friction angle will be about 20° for these conditions, since the swelling pressure is lower than 100 kPa /Börgesson et al. 1995/. This means that a total of 220 tonnes of backfill can be lost before the swelling pressure on top of the canister drops to 100 kPa.

Loss of backfill from erosion is important for the properties of the buffer in the deposition hole, but is not expected to have any significant importance for the transport properties itself. There will be a local volume with low swelling pressure and high hydraulic conductivity. However, the main part of the tunnel volume will be unaffected.

Potential for advective conditions

Advective conditions in the buffer can occur if the hydraulic conductivity is sufficiently high. The buffer function indicators prescribe a hydraulic conductivity of 10^{-12} m/s and a swelling pressure of 1 MPa to rule out advection in the buffer. These values do, however, have some safety margins included in them.

/Neretnieks 2006b/ calculated the conditions under which water is drawn into a deposition hole. He concluded that even for a rock fracture with a very high flow rate (transmissivity 10^{-6} m^2/s and hydraulic gradient 0.01), a buffer conductivity of around $3 \cdot 10^{-6}$ m/s suffices to prevent advection and causes the water in the fracture to flow around the buffer as if it were impervious. Such conductivity corresponds to a dry density well below 500 kg/m^3. However, to ensure that the self-sealing ability is maintained and no channels or pipes will be formed, a certain swelling pressure is also required. The minimum swelling pressure needed will be about 100 kPa. This is based on laboratory investigations in which piping has been observed at ~60 kPa /Karnland et al. 2006/. This value is most likely still pessimistic, since the gradients at the site are expected to be very low. However, the effect on the accepted mass loss will be relatively small. To ensure this for all expected groundwater compositions, a minimum dry density of 1,000 kg/m^3 is required (Figure 5-14). This corresponds to a void ratio of 1.75. As seen in Figure 10-59 this requirement is still met in almost the entire buffer diameter when two entire bentonite rings are omitted, corresponding to a dry mass loss of 2,400 kg.

For the case when the buffer erodes by colloid formation, the mass loss may be more local compared with the case in which entire blocks are omitted and it is more appropriate to consider the corresponding limit for losses over typically half the circumference, i.e. 1,200 kg, which would also cover the situation when the loss occurs closer to the centre of the canister. This value includes some pessimism since homogenisation in the horizontal direction is neglected. However, at higher mass losses, the swelling pressure cannot be guaranteed and advection in the buffer has to be considered. This is further elaborated for the case of buffer erosion in Section 10.3.11.

For the case when mass loss occurs mainly in the tunnel and only backfill material is lost, a maximum loss of 220 tonnes of backfill can be allowed before advective conditions have to be considered in the buffer in the deposition hole. However, loss of backfill by erosion does not mean that the hydraulic conductivity of the entire tunnel will be affected.

Identified uncertainties and their handling in the subsequent analysis

If the buffer and backfill is installed as envisaged by the reference design, the buffer density and swelling pressure will homogenise to a situation where the relevant safety functions will be upheld. Modelling of the Canister Retrieval Test (CRT) and comparison with measurements confirm that the material model of unsaturated bentonite blocks and the calculation technique used are relevant for modelling the homogenisation process. The uncertainties are mainly the material models, which are very complicated, and the parameter values. Although they have been verified for the one-dimensional case of swelling and homogenisation of the bentonite rings and pellets between the canister and the rock, the two-dimensional case involves more degrees of freedom for the variables and more interactions like the friction between the bentonite and the rock or canister.

The overall picture is that the swelling pressure of the buffer and the associated safety functions will be maintained during the expansion of the buffer into the backfill for all possible combinations of buffer and backfill conditions. However, in the analysis the buffer is modelled as completely water saturated and homogenised from start, which may affect the results such that the modelled density gradient between the canister and the backfill probably is larger than if a heterogeneous unsaturated buffer was modelled. The mechanical behaviour of the horizontal contacts between the backfill blocks has not been measured. The relation used assumes that there is a slot of 4 mm that is closed at the pressure 10 MPa, which is probably pessimistic, since it is reasonable to assume that blocks can be made and piled with better precision. The effect of local crushing of the blocks that may occur close to the floor is not included in the model, but this is not expected to yield any problems. Another uncertainty relates to how the blocks are piled. It is assumed that the blocks are not overlapping each other, which means that there will be no lateral spreading of the pressure. The swelling is expected to be smaller if the blocks are piled with overlaps like masonry.

The safety function for canister settlement in the deposition hole will not be violated as long as there is a reasonable amount of buffer left in the deposition hole. The only condition when the safety function could be violated is when there is a large loss of buffer. However, if that situation were to occur, many of the other buffer safety functions would be lost long before. These buffer loss cases are analysed elsewhere.

When large amounts of bentonite are lost or missing from the start, the bentonite swells and fills the empty space but the density and resulting swelling pressure is rather low due to the friction in the buffer and the friction against the rock surface. For a 50 cm opening the swelling pressure will be on average 0.5–1 MPa in almost the entire former hole in the base case. However, if the rock surface is smooth and the resulting friction against the rock is halved, the swelling pressure will be above 1 MPa in a majority of the former space. For 100 cm opening the swelling pressure will be rather low close to the canister in the base case with a pressure below 100 kPa or even an unfilled part left, whereas the low friction case yields a minimum swelling pressure of more than 300 kPa. If the opening is 150 cm corresponding to three missing bentonite rings, the base case yields that a large volume will have a swelling pressure below 100 kPa and even be unfilled. However, the influence of the friction between the bentonite and the rock and canister is large and with halved friction almost the entire opening will be filled. The homogenisation is enhanced by the swelling of the bentonite above or below the canister, which is shown by comparison with the calculations that do not include that part of the buffer.

Advective conditions in the buffer can occur if the hydraulic conductivity is sufficiently high. The buffer function indicators prescribe a hydraulic conductivity of 10^{-12} m/s and a swelling pressure of 1 MPa to rule out advection in the buffer. These values do, however, have some safety margins included in them, but a minimum dry density of 1,000 kg/m^3 is required corresponding to a void ratio of 1.75. This requirement is still met in almost the entire buffer diameter when two entire bentonite rings are omitted, corresponding to a dry mass loss of 2,400 kg.

For the case when the buffer erodes by colloid formation, further discussed in Section 10.3.11, the mass loss may be more local compared to when entire blocks are omitted and it is more appropriate to consider the corresponding limit for losses over typically half the circumference, i.e. 1,200 kg, which also would cover the situation when the loss occurs closer to the centre of the canister. This value includes some pessimism since homogenisation in the horizontal direction is neglected.

For the case when backfill material is lost, a maximum loss of 220 tonnes can be allowed before advective conditions have to be considered in the deposition hole. However, loss of backfill by erosion does not mean that the hydraulic conductivity of the entire tunnel will be affected.

10.3.10 Buffer and backfill chemical evolution

After deposition, the buffer is subjected to a thermal gradient due to the heat generation from the canister. At the same time there will be a hydraulic gradient caused by the suction in the unsaturated bentonite blocks and the hydrostatic pressure in the surrounding rock. After saturation and cooling of the near field, the interaction of groundwater with the bentonite buffer may result in an evolving distribution of some aqueous species in the bentonite porewater, as well as the redistribution of accessory minerals and the cation exchanger.

Three aspects must be considered regarding the geochemical evolution of the near field:

1. The effect of the thermal period;
2. The processes during the saturation of bentonite;
3. The interaction of the water-saturated bentonite with the local groundwater.

There are no buffer safety functions directly connected to this evolution, but an assessment needs to be made as to whether this evolution indirectly would violate the buffer safety functions. Both the MX-80 and the Ibeco RWC have been studied.

During the period of bentonite saturation (before 10, 100, 1,000 and 2,000 years, depending on the hydrological model) advection of solutes to the bentonite porewater is the main mechanism of transport between the groundwater and the buffer. The effect of solute diffusion between the inflowing groundwater and the bentonite porewater is negligible in the cases with a high rate of water saturation (10 and 100 years). In the models with low rates of saturation (1,000 and 2,000 years), the effects of the diffusion on the calculated concentrations during the period of saturation are significant. When the bentonite buffer becomes fully saturated, diffusion is the exclusive mechanism of solute transport.

Table 10-6 shows some chemical properties of the groundwaters flowing in the repository volume for different climatic conditions. The table is a summary of the results presented in Sections 10.2.5, 10.3.7 and 10.4.7, and the data are used as boundary conditions when evaluating geochemical properties of the buffer and backfill.

Table 10-6. Maximum chloride concentration, maximum and minimum Ca/Na ratio, pH and carbonate, and maximum ionic strength in the Forsmark groundwaters for all time frames /Salas et al. 2010/. The position of the ice front locations IFL 0 to V is defined in Figure 10-127 and associated text and "a" and "r" stand for ice advance and ice retreat, respectively.

	Max Cl (M)	Max Ca/Na	Min Ca/Na	Max pH	Min pH	Max carbonate (M)	Min carbonate (M)	Max Ionic Strength (M)
Temperate (2000 AD)	0.345	1.219	0.024	8.05	7.07	0.0025	0.00020	0.47
Temperate (9000 AD)	0.267	1.127	0.050	7.57	6.48	0.0075	0.00026	0.36
Glacial (IFL IIa)	0.343	1.228	0.600	8.54	6.34	0.0063	0.00026	0.47
Glacial (IFL Vr)	0.078	1.548	1.023	9.42	6.97	0.0022	0.00008	0.11
Permafrost (before onset of glaciation)	0.099	1.036	0.398	7.01	6.52	0.0067	0.00552	0.14
Submerged fresh water	0.091	1.320	1.200	8.99	7.01	0.0015	0.00006	0.13
Submerged seawater	0.276	1.230	0.024	8.03	7.22	0.0018	0.00019	0.38

Unsaturated phase and period of elevated temperatures

During the thermal period of the repository, the initially unsaturated compacted bentonite will progressively saturate due to the hydraulic pressure of the surrounding rock (Figure 10-61). Although the main transport mechanism in the low permeability compacted bentonite is diffusion, advective transport will be more important during the saturation stage due to the capillary pressure that is established during this stage.

The buffer material consists of montmorillonite and accessory minerals (see Table 5-10). In the repository environment these minerals may dissolve and sometimes re-precipitate depending on the prevailing conditions. /Sena et al. 2010/ have calculated the redistribution of accessory minerals during the early repository evolution when a thermal gradient is present and the details about the processes and mechanisms in the modelling can be found in the reference. In the calculations the following were tested:

1. The saturation time.
2. The flow rate in a fracture intersecting the deposition hole.

Under a higher flow rate regime within the fracture, the effect of the diffusion of solutes from the bentonite porewater to the granite or vice versa on the chemical conditions of the granite around the deposition hole will be rapidly buffered by the supply of unaffected granitic groundwater. Under these conditions, the geochemical changes induced by the chemical reactions taking place in the buffer will be limited to the buffer itself since any influence of these over the chemical conditions of the granite will be rapidly annulled due to granitic groundwater renewal (Figure 10-62). On the other hand, if the advective flow in the fracture is very low, diffusion will prevail and therefore, the chemical and diffusive processes occurring in the buffer will influence the chemical conditions of the fracture around the deposition hole (Figure 10-62).

In the calculations these parameters have been considered independently. However, a high flow rate would affect the saturation time. Therefore, no combinations of high flow and long saturation have been studied.

Ca-sulphates are originally present in the MX-80 bentonite mineralogy. At the beginning of the thermal period, anhydrite precipitates in the bentonite pores due to the increase of temperature, except close to the outer boundary of the buffer where the granitic groundwater (which is unsaturated with respect to this mineral) flows into the buffer. The dissolution of the primary anhydrite is more efficient for a situation when the saturation is rapid (10 and 100 years in Figure 10-63).

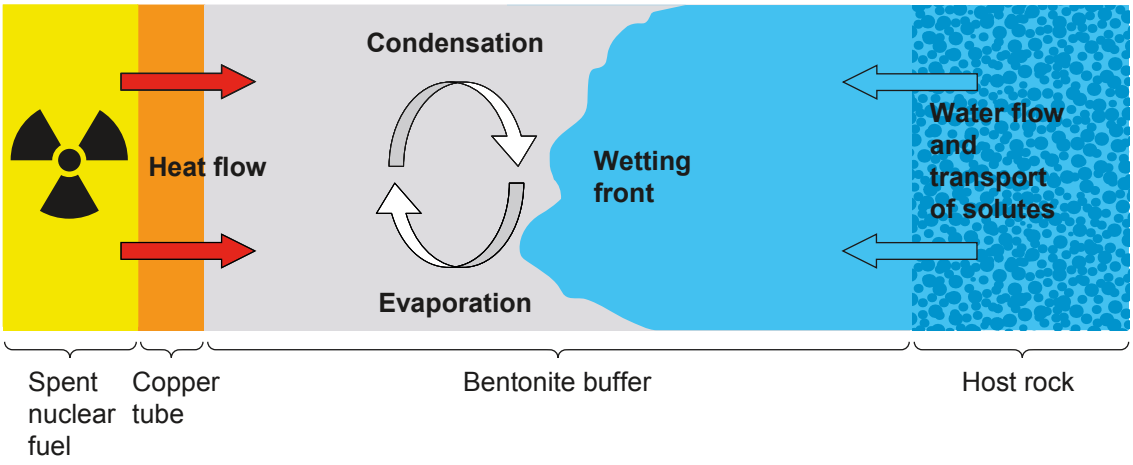

Figure 10-61. *Sketch of a vertical cross section of the near field of a KBS-3 repository showing the thermo-hydraulic and transport processes that are believed to occur during the saturation period of the bentonite buffer /Sena et al. 2010/.*

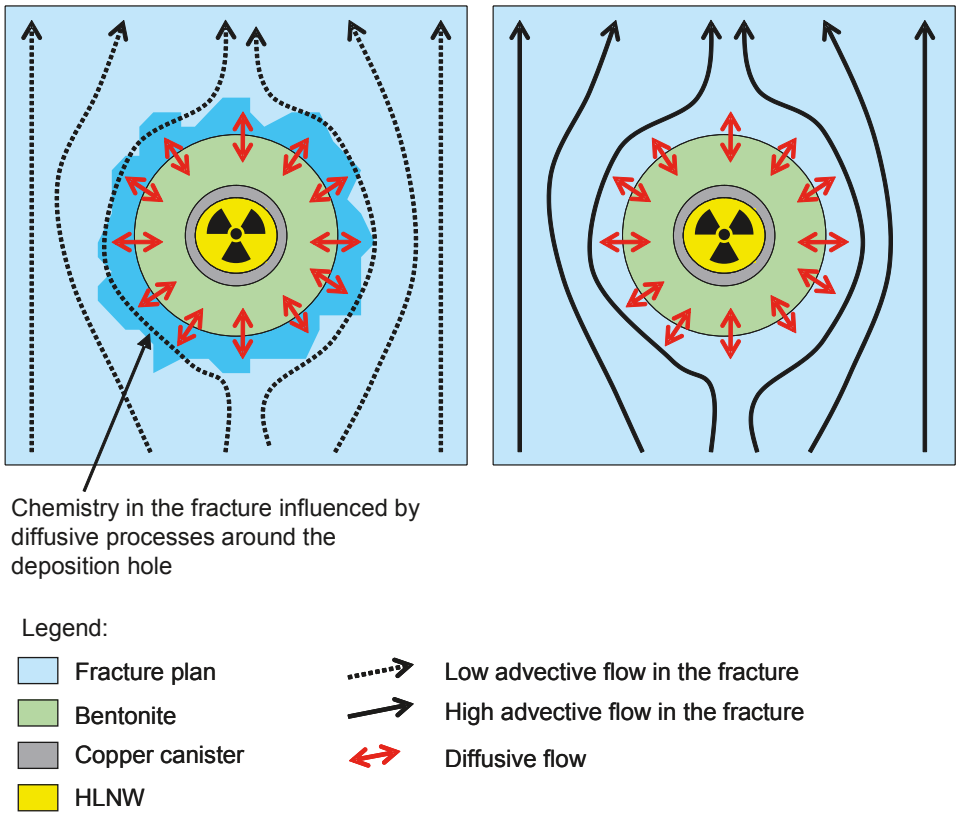

Figure 10-62. Sketch of the two different flow cases /Sena et al. 2010/.

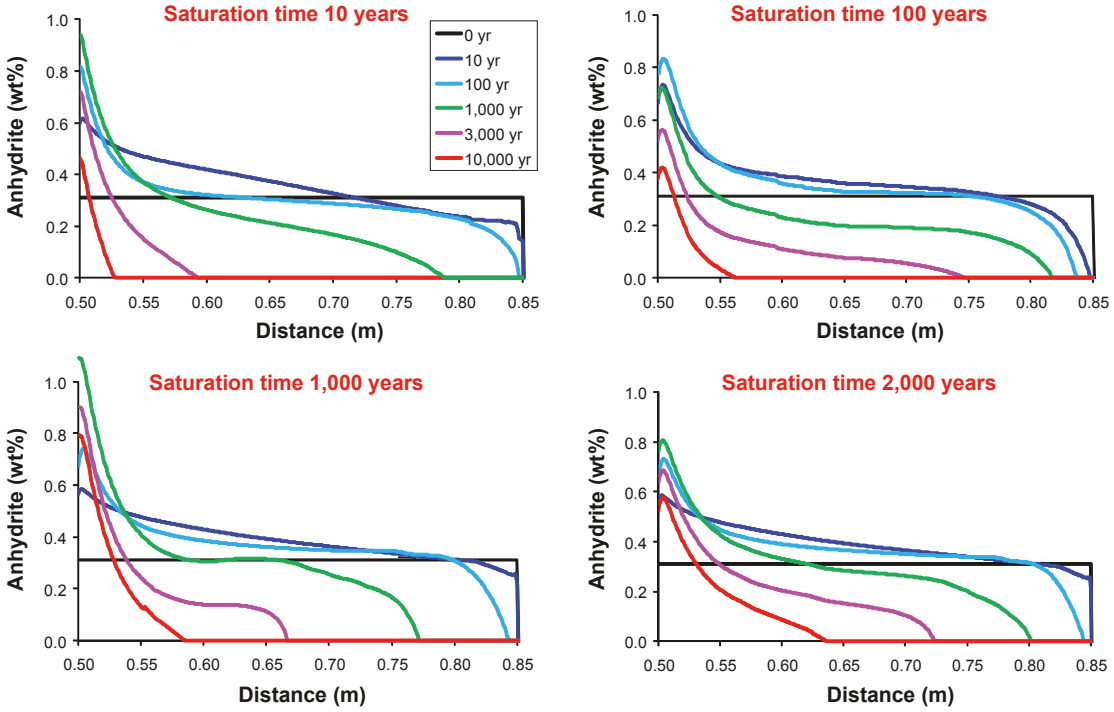

Figure 10-63. Calculated evolution of the amount of anhydrite in the MX-80 bentonite buffer as a function of buffer saturation time /Sena et al. 2010/.

SiO_2(am) is also a primary mineral of the MX-80 bentonite. The primary SiO_2(am) in the bentonite is preferentially dissolved close to the inner surface of the buffer (left side in Figure 10-64). In the case with a relatively fast saturation (10 years), a small amount of SiO_2(am) is also dissolved during the saturation period, close to the contact with the granite. Until 10 years, the SiO_2(aq) concentration progressively increases, both in the bentonite and in the granite due to the solute supply by SiO_2(am) dissolution close to the hot boundary of the system. After 10 years the aqueous SiO_2 concentration decreases due to dilution provided by the inflow of the granitic groundwater, which is depleted in SiO_2(aq) compared to the initial bentonite porewater.

In general, the calculated evolution of the composition in the montmorillonite exchanger in the MX-80 bentonite indicates that the concentration of sodium decreases with time in favour of more calcium adsorbed. The concentration of potassium and magnesium also decreases in the montmorillonite exchanger. Within the same case of advective flow in the fracture intersecting the deposition hole, the calculated evolution of the composition of the exchanger is very similar for the different cases of bentonite saturation.

The comparison between the cases with low and high advective flow in the fracture, for a saturation time of 10 years is shown in Figure 10-65. It is seen that for a high advective flow in the fracture, the final composition of the exchanger has suffered more profound changes than for the case with a low advective flow in the fracture.

The key differences between the composition of the Ibeco RWC bentonite and the MX-80 are the larger population of calcium in the exchanger and the presence of fairly large quantities of calcite and dolomite which characterise the former. In most respects the different bentonites behave in a similar manner geochemically. The difference is mainly related to the dissolution/precipitation of dolomite and calcite. In Ibeco RWC, the primary dolomite is initially dissolved, being completely

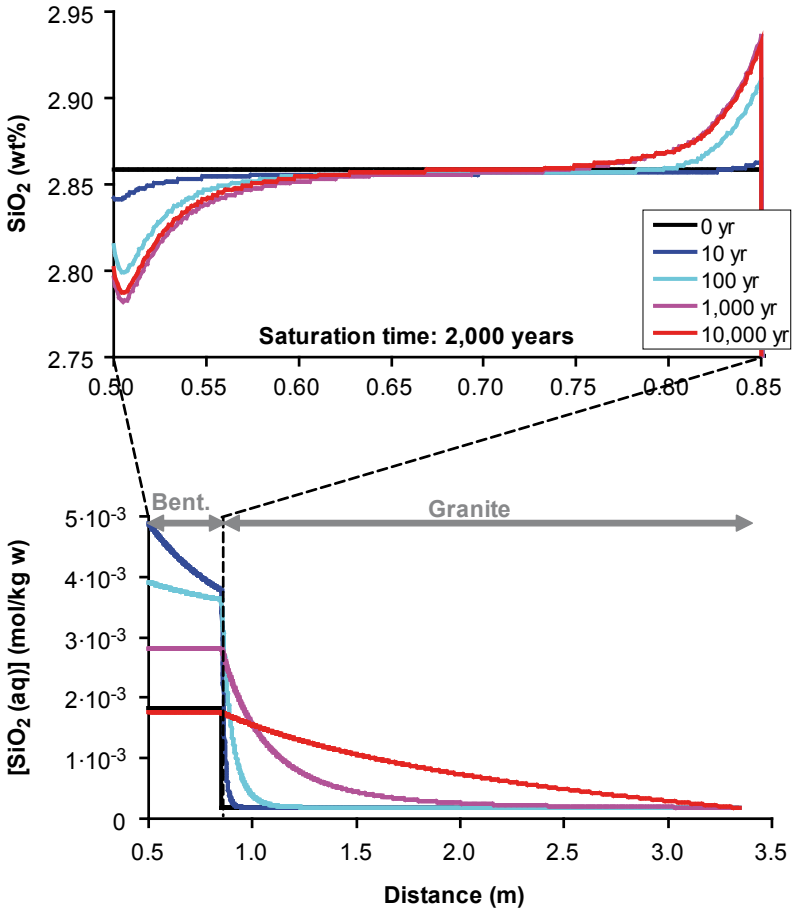

Figure 10-64. *Calculated evolution of the amount of SiO_2 in the modelled domain of MX-80 bentonite, for a saturation time of the bentonite of 10 years /Sena et al. 2010/.*

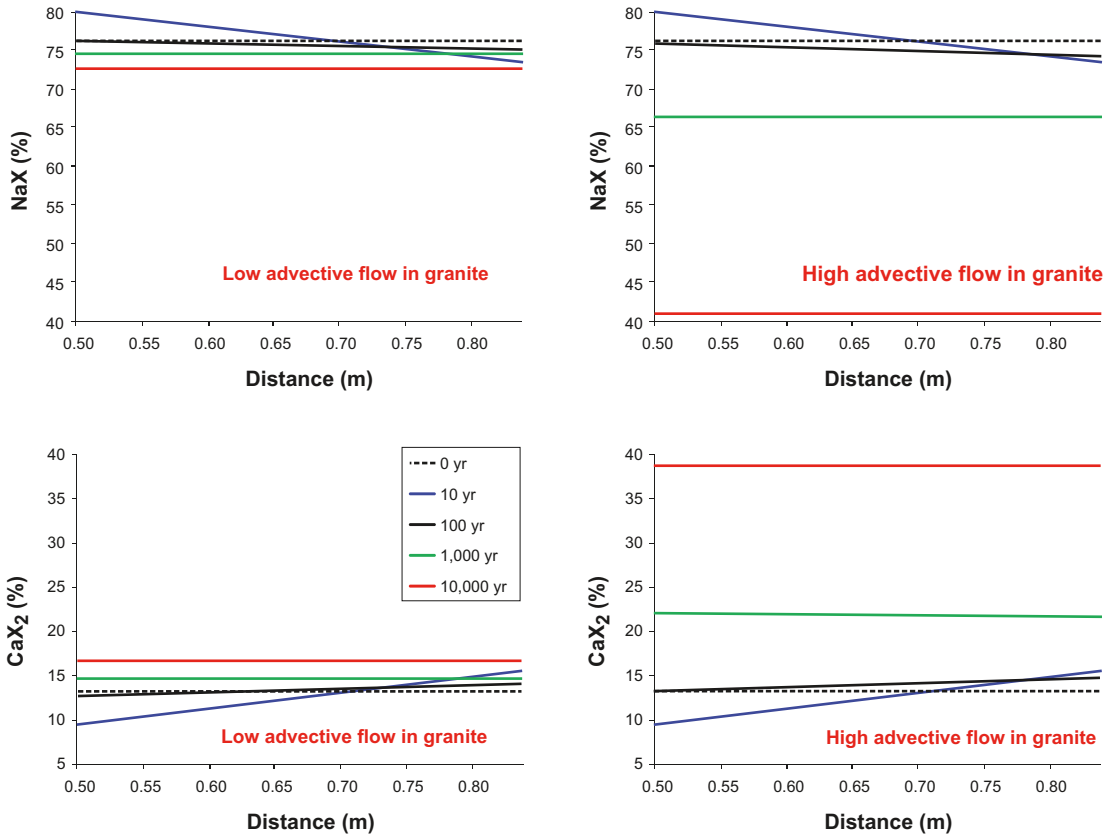

Figure 10-65. *Calculated evolution of the concentration of sodium and calcium in the montmorillonite exchanger for the case where the MX-80 bentonite is fully water saturated at 10 years, and for the two scenarios of advective flow in the fracture (low and high) /Sena et al. 2010/.*

exhausted close to the outer boundary of the buffer after 1,000 years (Figure 10-66). However, in the vicinity of the copper canister, dolomite precipitates during the warming period, being re-dissolved during the cooling stage. The amount of dolomite dissolved and/or precipitated is not very sensitive to the rate of bentonite water saturation. However, if high flow rates are considered along the deposition hole, dolomite could be exhausted in the bentonite domain before 10,000 years (Figure 10-66). Similarly to a process of loss of dolomite, secondary calcite precipitates in the Ibeco RWC bentonite (Figure 10-66). Calcite precipitation is controlled by the supply of solutes from dolomite dissolution. The exchange process is in general similar to that of MX-80. For a low flow in the rock, the ion-exchange will be limited, while for a high flow the final composition of the exchanger will be similar to that of MX-80.

As a result of the numerical simulations in /Sena et al. 2010/, it can be concluded that the main mechanisms controlling the mineralogical changes of the bentonite during the thermal period are related to:

- The dependence of the mineral solubilities on the evolution of the temperature in the near field.
- The solute transport and mass transfer between the groundwater flowing along the fracture and the bentonite porewater.

The evolution of the concentrations obtained for the bentonite porewater is a result of mixing with the local groundwater during the period of bentonite water saturation, whereas thereafter, diffusion of solutes is the dominant mechanism. Simultaneously, mineral reactions (anhydrite and carbonate dissolution and/or precipitation) and cation exchange reactions are the key mechanisms controlling

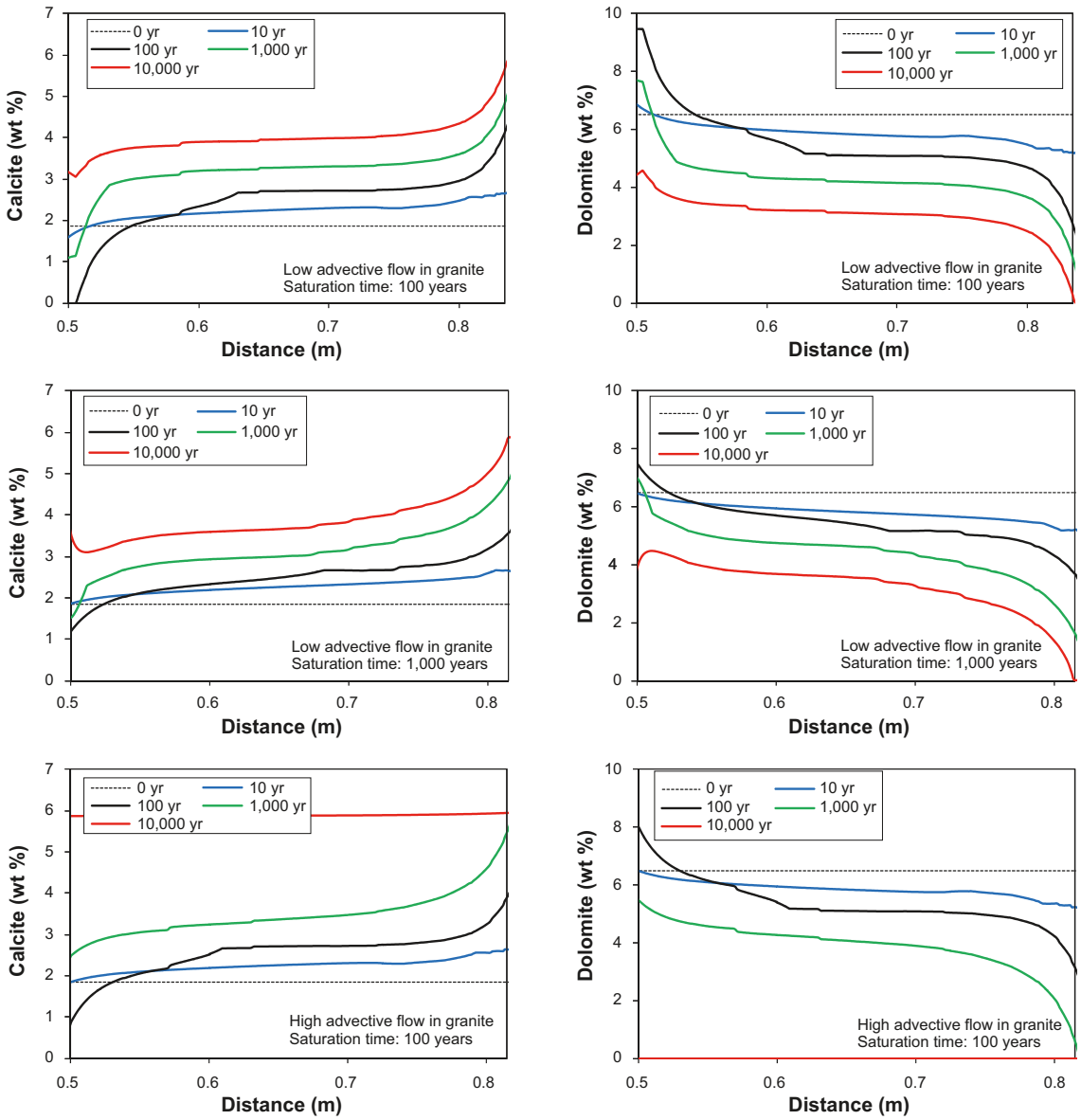

Figure 10-66. *Calculated evolution of the amount of calcite and dolomite in the IBECO RWC (Deponit CA-N) bentonite, for the case where saturation of the bentonite occurs after 100 and 1,000 years, and for the scenarios of low and high advective flow in the fracture /Sena et al. 2010/.*

the long term geochemical evolution of the buffer and its porewater. The distribution of the concentration of solutes in the granitic groundwater is a consequence of the ratio between:

- The diffusion rate through the granite-bentonite interface.
- The fluid flow rate along the fracture in contact with the deposition hole.

In this way, the results obtained considering two regimes of groundwater flow rates along the fracture intersecting the deposition hole are substantially different.

- With low flow rates along the fracture, the final composition of the bentonite porewater is different from the Forsmark groundwater. The composition of the buffer porewater has the potential to modify, by diffusion, the composition of the surrounding granitic groundwater.
- With high flow rates along the fracture, the groundwater composition is practically constant during the modelled period, maintaining the gradients of concentrations and the rates of solute transport by diffusion. Consequently, the final composition of the bentonite porewater is similar to the composition of the Forsmark groundwater.

The thermal evolution in the buffer modifies mineral solubilities (Ca-sulphates, carbonates and silica). The silica precipitation and/or dissolution in the bentonite are basically controlled by the changes of solubilities associated with the thermal evolution of the system, modifying slightly the mineralogical composition of the bentonite. The stability of the carbonate phases is the main geochemical difference between the two types of bentonite.

During the period of saturation, there will be dissolution/precipitation of accessory minerals like calcium sulphates and amorphous SiO_2, The conclusion is, however, that these effects are too small to have any impact on the long-term performance of the buffer.

Mineral transformation

The advantageous physical properties of the buffer, e.g. swelling pressure and low hydraulic conductivity, are determined by the ability for water uptake between the montmorillonite mineral layers (swelling) in the bentonite. However, montmorillonite can transform into other naturally occurring minerals of the same principal atomic structure but with less or no ability to swell in contact with groundwater. The transformation processes usually involve several basic mechanisms. At the expected physico-chemical conditions in a repository, the following possible mechanisms are identified:

- congruent dissolution,
- reduction/oxidation of iron in the mineral structure,
- atomic substitutions in the mineral structure,
- octahedral layer charge elimination by small cations,
- replacement of charge compensating cations in the interlayer.

This is discussed further in the **Buffer, backfill and closure process report**.

Transformation from smectite (montmorillonite) to illite, which is the most common alteration observed in natural sediments, is well documented in different geological formations, and has been reproduced under laboratory conditions. The main mineralogical differences being that the illites have approximately one unit charge higher tetrahedral charge, and potassium as the main charge compensating cation. Thus, potassium is a must for the montmorillonite to turn into illite. Simplified, the total illitization reaction may be expressed:

Ca^{2+}/Na^{+}-montmorillonite + K^{+} + (Al^{3+}) → Illite + Silica + Ca^{2+}/Na^{+}

High content of smectite is commonly found in old formations exposed to repository temperatures. For example, /Velde and Vasseur 1992/ studied the time-temperature space of illitization in seven deep wells in four sedimentary basins in the US, Japan and France. In all wells there was a typical reduction of smectite content with depth, which represents increase in both age and temperature (Figure 10-67).

The prerequisites for a transformation are obviously present in the sediments and time and temperature are the governing parameters. A decrease to around 60% smectite was observed in the Californian Norwal formation after 4.5 million years at a depth of 5 km, representing a final temperature increase of over 100°C. The same transformation took around 60 million years at a depth of 2 km and a temperature increase of around 70°C in the Texan Peeler sediments. The reaction rate at these repository relevant temperatures is consequently very slow in relation to the timescale of a repository.

The availability of potassium could also limit alteration rate. According to /Karnland and Birgersson 2006/ complete illitization requires approximately 850 kg of potassium per deposition hole. The concentration of potassium in the groundwater in Forsmark is low and very limited illitization would occur if the groundwater was the only source. However, the rock in Forsmark may contain a few percent of potassium /Sandström and Stephens 2009/. This means that the rock within a short distance (~metre) around the deposition hole would be able to supply sufficient potassium to convert the entire buffer to illite. The critical question is therefore whether the potassium is available for the transformation or not. Both the rate of dissolution of potassium from the granitic minerals as well as the rate of transformation of smectite to illite is very slow at the expected temperatures of the near field. Therefore, there is no need to quantify this process. No credit for limited availability of potassium is taken in SR-Site, since buffer transformation can be ruled out for other reasons.

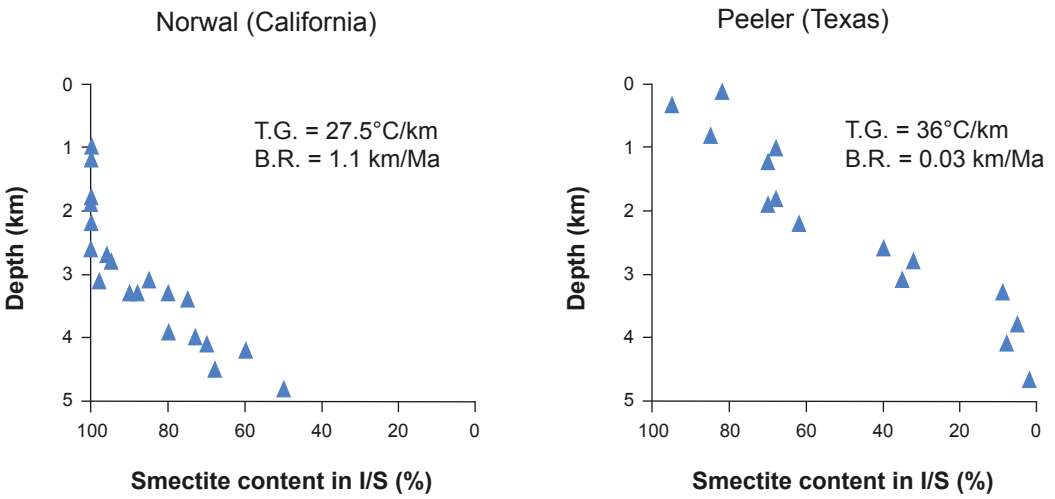

Figure 10-67. *Smectite content versus depth in smectite-illite mixed layer material in two sediments representing relatively fast burial rate (left) and slow burial rate (right). T.G. indicates the present temperature gradient and B.R. indicates the burial rate. Redrawn from /Velde and Vasseur 1992/.*

The silica solubility increases significantly at pH above 9. The tetrahedral silica in the montmorillonite consequently equilibrates at higher concentrations at pH over 9. Diffusive removal of silica or precipitation of new silica minerals thereby lead to a faster increase of the tetrahedral layer charge compared to near neutral conditions. The corresponding increase in concentration of charge compensating cations leads to a change in the interaction with water and thereby to a change in sealing properties. The layer charge may reach the critical value for collapse, which results in total loss of expandability and in principle, to the same consequences as for illitization. At pH 11 the total silica concentration is calculated to be approximately 16 times larger than at neutral pH conditions, and at pH 12.4, representing matured Portland cement, the theoretical increase in total silica solubility is more than 3 orders of magnitude higher than at near neutral conditions. The total silica concentration difference between the bentonite porewater and the groundwater increases approximately by the same factor, assuming the groundwater is in equilibrium with quartz. /Huertas et al. 2005/ studied the dissolution rate of smectite as a function of pH. Figure 10-68 plots log dissolution rate vs. pH at 25, 50, and 70°C. In alkaline solutions, the smectite dissolution rate increases as pH increases, showing a steeper slope for pH values higher than 11, which seems to be a critical value for the smectite dissolution and stability. The conclusion from /Huertas et al. 2005/ is that the results indicate that dissolution rates are strongly affected by pH and temperature. This effect is particularly important for pH values above 11.

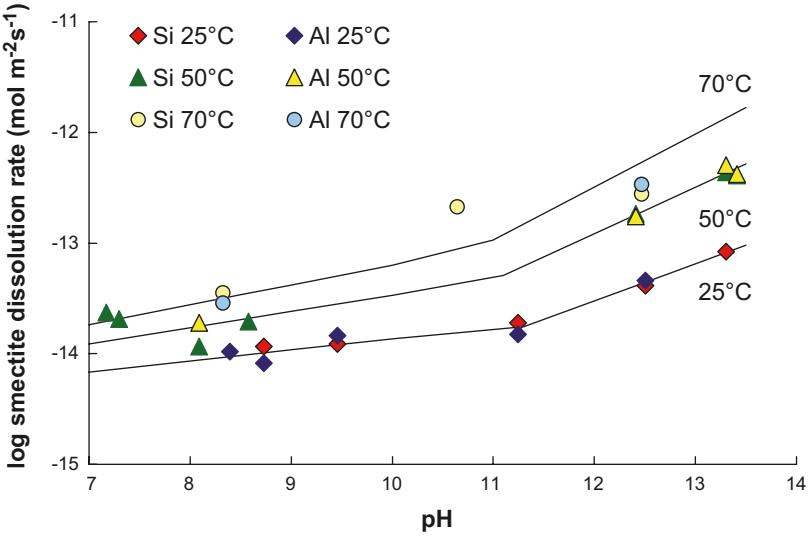

Figure 10-68. *Experimental (dots) and estimated (lines) dissolution rates /Huertas et al. 2005/.*

The effect of the alkaline plumes is especially strong for young cement waters and for high temperatures, In the KBS-3 concept any contact between cement porewater and bentonite will occur at the contact with the bottom plate, plug and fracture grouting where the temperature is relatively low and the pH is restricted to < 11. The bentonite components should therefore be much more stable.

The montmorillonite transformation in a KBS-3 repository is assumed to be small based on the following observations and arguments:

1. The timescale for significant montmorillonite transformation at repository temperatures in natural sediments is orders of magnitude larger than the period of elevated temperature in a KBS-3 repository e.g. /Velde and Vasseur 1992/.
2. The bentonite material is close to mineralogical equilibrium to start with e.g. /Fritz et al. 1984/.
3. Transformation is limited by transport restrictions /Hökmark et al. 1997/.
4. All published kinetic models, based both on natural analogues and laboratory experiments indicate that the transformation rate is very low at repository conditions e.g. /Huang et al. 1993/.

Based on this reasoning two safety function indicator criteria have been defined (see also Chapter 8). As long as the maximum temperature is below 100°C and the pH of the water in the rock is below 11 the montmorillonite in the buffer is assumed to stable for the timescale for assessment of the repository (1,000,000 years).

In the reference evolution, both the pH and the temperature in the buffer are assumed to be within the given limits and the alteration is not expected to proceed to a level where it will affect the properties of the buffer.

Effects of salinity

The salinity of the groundwater influences the vapour pressure relation and thereby the water saturation process. However, for the groundwater (Table 10-6) at the Forsmark site the effect is negligible.

Cementation

The term “cementation” has often been used in a broad sense to describe processes, which lead to specific changes in rheology and swelling properties of the buffer material. A number of quite different chemical/mineralogical and mechanical underlying processes could conceivably cause such cementation effects. The above sections which address the underlying and related processes, i.e. montmorillonite stability, ion exchange, accessory minerals alteration, diffusive transport etc. are consequently very relevant to the cementation process. There are two main concerns about the effects of cementation on the bentonite buffer; one is an increase in hydraulic conductivity, and the other is an increase of shear strength. This is discussed further in the **Buffer, backfill and closure process report**.

As described earlier in this section there is no reason to believe that there would be mineralogical changes in the buffer that would lead to substantial changes of the mechanical or hydraulic properties over the assessment timescale. The redistribution of soluble accessory minerals calculated in the previous section is rather limited and is not expected to have a significant impact on the buffer properties. However, there are experimental results that show that the mechanical properties of bentonite can be altered if the material is exposed to an elevated temperature in a saturated state /Dueck 2010/. This is observed both in field experiments over a number of years as well as in 24-hour laboratory experiments. The maximum deviatoric stress q_{max} (kPa) and corresponding strain e (%) were measured on mainly undisturbed samples as a function of bulk density ρ (kg/m^3) for a range of conditions.

Figure 10-69 shows the influence of temperature on the stress-strain behaviour for the two reference bentonites for a saturated density of about 2,000 kg/m^3. A tendency towards increasing deviatoric stress at failure with increasing temperature is seen for both MX-80 and Ibeco RWC (Deponit CA-N). However, the influence of temperature is in the same range as the difference between the two bentonites. The strain at failure is approximately the same for MX-80 and Ibeco RWC (Deponit CA-N) at the same density for any particular temperature.

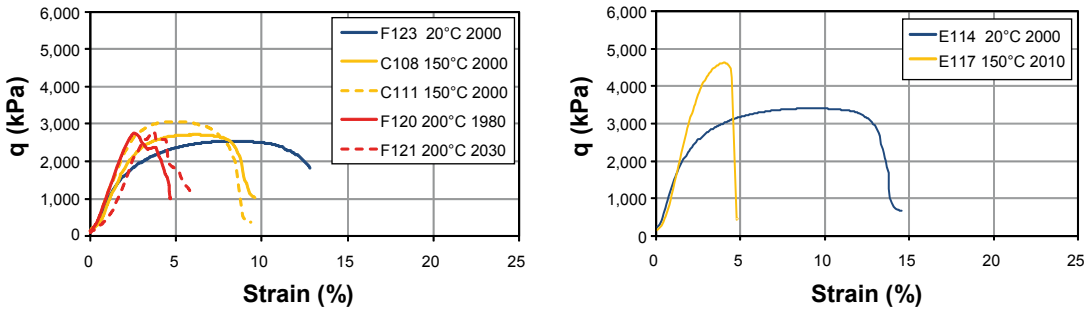

Figure 10-69. *Influence of temperature on the stress-strain behaviour of MX-80 (left) and Ibeco RWC (right) with a density about 2,000 kg/m³ /Dueck 2010/.*

Important observations from /Dueck 2010/ are that the influence of temperature on the stress/strain behaviour of bentonite can be seen after only a few hours of exposure and that milling and re-compaction after heating restored the original failure behaviour. It is evident that an increased temperature will have an effect on the mechanical properties of the bentonite. The reason behind this is still unknown. The effect is not very pronounced even at 150 degrees and does not seem to progress with time. However, this effect does have to be considered in the evaluation of shear load on the canister.

Identified uncertainties and their handling in the subsequent analysis

- The geochemical changes in the buffer during the period of saturation and thermal gradient are small and are not considered to have any significant impact on the long-term performance.
- In the reference evolution, both the pH and the temperature in the buffer are assumed to be within the given limits and mineral alteration is not expected to proceed to a level where it will affect the properties of the buffer.
- The salinity of the groundwater influences the vapour pressure relation and thereby the water saturation process, but for the groundwater at the Forsmark site the effect is negligible.
- An increased temperature will have an effect on the mechanical properties of the bentonite, but the effect is not very pronounced even at 150 degrees and does not seem to progress with time. However, this effect does have to be considered in the evaluation of shear load on the canister, see Section 10.4.5.

10.3.11 Colloid release from buffer and backfill

Extensive studies of the colloid release process have been undertaken recently. A summary of the studies and a justification of the treatment of the process can be found in the **Buffer, backfill and closure process report**. The description of the background and the development of a quantitative model is given in /Neretnieks et al. 2009/.

The uptake of water and resulting swelling of the bentonite buffer is hindered by the walls of the deposition hole, and a swelling pressure is developed in the bentonite. If fractures intersect the deposition hole, rigid swelling restrictions are not present everywhere, and localised swelling continues into the fractures until equilibrium or steady state is reached. This free swelling may lead to separation of individual montmorillonite layers (dispersion) and part of the buffer could thereby be transported away with the groundwater. This would directly affect safety functions Buff1, Buff2 and Buff5.

The maximum free swelling of the bentonite is strongly dependant on the valence and concentration of the ions in the interlayer space. At low solute concentrations in groundwater, the interlayer distance between the individual montmorillonite layers may increase enough to give the clay/water system a sol character, i.e. single or small groups of montmorillonite layers act as individual colloidal particles.

Conditions when colloid release can occur

For simple model systems such as charged spheres or parallel extended flat charged surfaces the concept of a critical coagulation concentration (CCC) is readily defined within the DLVO (Derjaguin and Landau, Verwey and Overbeek) theory as the salt/electrolyte concentration where the energy barrier for particle-particle association approaches zero e.g. /Evans and Wennerström 1999/. At the CCC and higher salt concentrations the attractive van der Waals forces dominate the system and colloidal particles will be held together and not disperse spontaneously. A CCC may be determined for monovalent systems, and used as a pessimistic concentration limit for spontaneous colloid sol formation. Governing variables are the concentration and the layer charge of the montmorillonite. For systems with only divalent counterions the CCC concept is not strictly valid, and the CCC may be considered zero, i.e. no excess ions are needed in order to prevent formation of colloidal particles as demonstrated in e.g. /Birgersson et al. 2009/ or from theoretical considerations /Kjellander et al. 1988/. For a mixed system, with both mono and divalent counter ions, one also needs to consider ion exchange equilibrium /Kahn 1958/. Thus one cannot define a CCC for Ca^{2+} for Na-montmorillonite since such a value cannot exist.

Based on the experimental studies of /Birgersson et al. 2009/, water with cation content higher than 2–4 mM charge equivalents is considered able to prevent colloidal sol formation provided that the calcium content in the montmorillonite is above 20%, irrespective of montmorillonite type. In SR-Site, the upper limit of 4 mM is selected as a pessimistic limit. This criterion is also in agreement with reported amounts of calcium salts needed to coagulate initially homoionic Na-montmorillonites /Swartzen-Allen and Matijević 1976, Hetzel and Doner 1993, Lagaly and Ziesmer 2003/. In equilibrium with a typical Forsmark water the bentonite is expected to have an approximately equal population of calcium and sodium ions in the exchanger. Ion exchange processes during the evolution of the repository may alter the counterion content relative to the initial state. This is discussed further in Section 10.3.12.

Quantification of buffer loss

Figure 10-70 shows a fracture intersecting the canister deposition hole which is filled with compacted bentonite. The bentonite, when wetted, swells out into the fracture. It has a very high swelling pressure when highly compacted but the swelling pressure decreases with decreasing bentonite density.

The smectite particles are pulled and pushed into the water that seeps in the fracture by the different forces acting on the particles. If the porewater cation concentration is below 4 mM charge equivalents, the particles at the bentonite/water interface can swell/diffuse into the moving water and be carried away. There is also a region where the gel/sol has so low a particle concentration that it is little more viscous than water and can flow away.

The loss of particles is thus influenced both by particle diffusion and by advective flow of the dilute gel/sol. For both mechanisms, the flow rate of water and gel in the fracture will set the total rate of loss.

A DLVO based force-balance model for spherical colloids /Petsev et al. 1993/ has been adapted to parallel clay layers /Liu et al. 2009, Neretnieks et al. 2009/ and used to calculate the swelling of Na-montmorillonite into fractures filled with water of low ionic strength. The force-balance model uses DLVO to describe swelling pressure and a Kozeny-Karman-like expression fitted to experimental results to describe hydraulic conductivity. The model is adjusted and tested against free-swelling experiments with results obtained through magnetic resonance imaging (MRI) /Dvinskikh et al. 2009/. Advective loss of montmorillonite is modelled by combining the force-balance model for swelling with a viscosity model for the repulsive montmorillonite gel and the Darcy equation for two-dimensional flow in a fracture intersecting the deposition hole.

The outcome of the modelling for different water velocities in a 1 mm aperture fracture is shown in Table 10-7. The “Penetration into fracture” represents the location where the smectite gel has reached the gel/water interface and from which smectite can be carried away. This is illustrated in Figure 10-71. The transient expansion is not considered. The montmorillonite release rate, $R_{Erosion}$, is found to be proportional to the water velocity, v, to the power 0.41 and directly proportional to the aperture, δ, according to

$$R_{\mathrm{Erosion}} = A \cdot \delta \cdot v^{0.41}$$

where A = 27.2 is a constant yielding the loss rate in kg/yr when the water velocity is given in m/yr and the aperture in m.

The model assumes that the bentonite consists of only montmorillonite which is converted to a pure Na-form and the buffer porewater is assumed to be depleted of Ca^{2+} ions in the fracture buffer interface. This means that Ca^{2+} ions for the prevention of colloid sol formation will not be supplied by the buffer.

Loss of bentonite material through colloid release may be significantly reduced, or even eventually stopped, by space limitations and filtering effects. Laboratory results have shown that pore-sizes smaller than 0.5 microns completely prevent the montmorillonite particles from penetrating filters, but pore-sizes of 2 microns or larger do not restrict the loss significantly. An auto healing effect may possibly be present by the clogging of fractures by accessory minerals of different grain sizes.

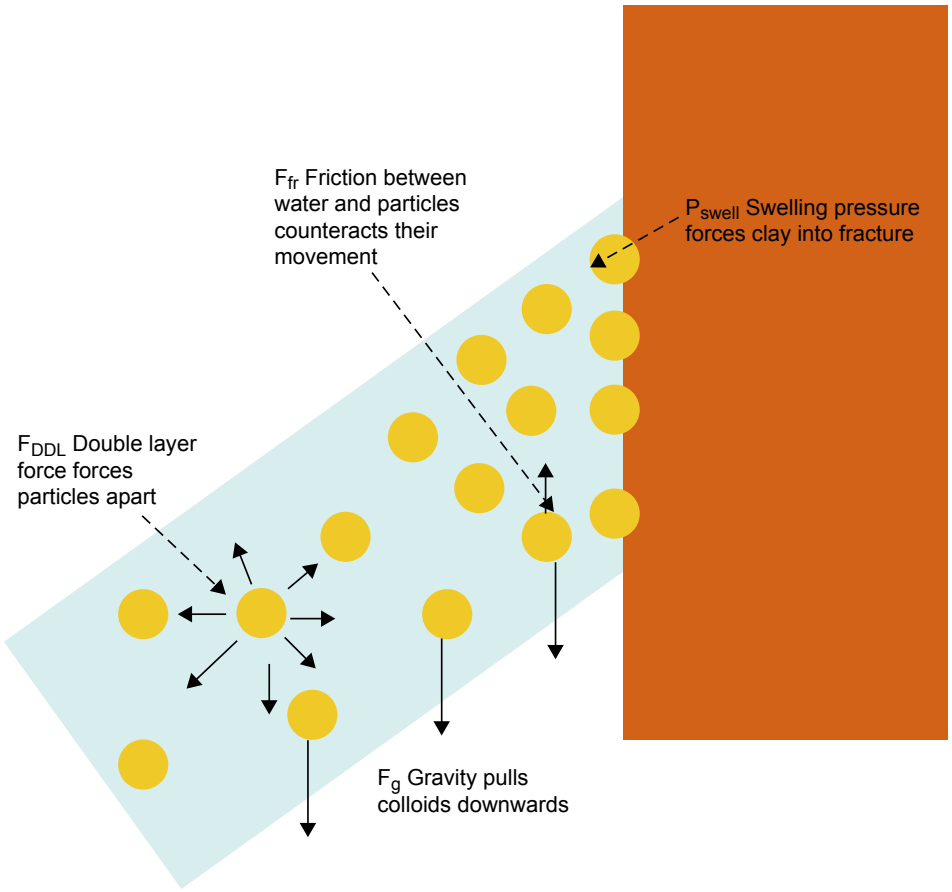

Figure 10-70. *Schematic of forces acting on the bentonite in a deposition hole and fracture (diffuse double layer, van der Waals (not shown), friction in water and forces of gravity) after /Neretnieks et al. 2009/. Friction forces against fracture surface is not shown.*

Table 10-7. Loss of smectite by advective flow /Neretnieks et al. 2009/.

Water velocity, [m/yr]	Smectite release for 1 mm fracture aperture, [g/yr]	Penetration into the fracture at the centre, [m]
0.10	11	34.6
0.32	16	18.5
0.95	26	11.5
3.15	43	7.0
31.50	117	2.1
315.00	292	0.5

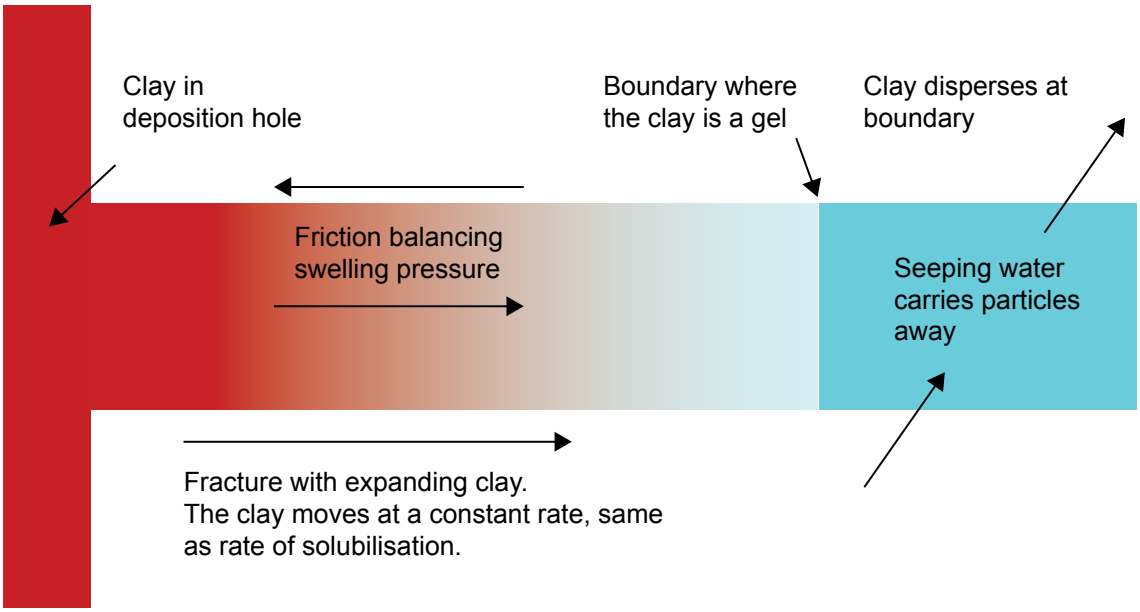

Figure 10-71. *Clay swells into a fracture. Clay disperses into the groundwater and is carried away by the water /Liu and Neretnieks 2006/.*

The route to advection in the buffer

As discussed in Section 10.3.9, a loss of 1,200 kg of buffer or 220,000 kg backfill material from one deposition hole position will lead to cases where advective transport in the buffer needs to be considered (loss of the diffusive barrier). The rate of loss can be calculated with the model described by /Neretnieks et al. 2009/ discussed above. The information needed for each canister position is:

- The duration of conditions with a groundwater composition with a positive charge of less than 4 mM, requiring a determination of the groundwater composition, in particular the concentrations of Na^+ and Ca^+.
- The water velocity around a deposition hole/tunnel.
- The fracture apertures.

As concluded in Section 10.3.7 the ionic strength of the groundwater; $\Sigma q[M^{q+}]$, could fall below –4 mM charge equivalents, i.e. violating safety indictor criterion R1c, for typically one percent of the deposition holes during the later parts of the thermal period. This means that colloid release may occur from these holes and from deposition holes, if any, located under sections of the backfill losing their density.

It should be noted that the mechanical model (Section 10.3.9) used for the determination of the buffer and backfill loss in the analyses of the swelling period, is deliberately inconsistent with the model used for the rate of loss presented in this section. The mechanical model in Section 10.3.9 is based on buffer/backfill data determined for conditions where the ionic strength of the groundwater; $\Sigma q[M^{q+}]$ is above 4 mM charge equivalent and the swelling will be restricted mainly due to friction. The model used for the rate of loss on the other hand, is based on a situation where $\Sigma q[M^{q+}]$ is below 4 mM charge equivalent and then the swelling will be sufficient for colloidal particles to form. If this latter model were to be used for the homogenisation in the deposition hole/tunnel the acceptable mass loss would be larger. It could be argued that this could be defended, since the erosion only occurs for dilute conditions. However, in SR-Site the more pessimistic values of maximum mass losses from the mechanical model have been used throughout the assessment. One important reason for this approach is the fact that the temporal variations in groundwater composition will lead to both spatial and temporal variations in the buffer porewater composition that are difficult to take into account in a strict sense in these analyses, other than through the adopted pessimistic approach.

Using the modelling approach described above and the flow rates from the semi-correlated base case of the hydrogeological DFN model (Section 10.3.6), the resulting distribution of erosion rates is seen in Figure 10-72. The figure also indicates the number of holes with advective conditions in the buffer, i.e. holes that have experienced a loss of more than 1,200 kg of buffer. It is obvious that only a small number of deposition holes will reach advective conditions, even in 10^6 years. Using the EFPC rejection criterion and assuming that "dilute" conditions occur 25% of the time, 23 deposition holes reach advective conditions. Furthermore, as indicated in Section 10.3.6 only typically one percent of the deposition hole positions are likely to have dilute conditions after 10,000 years of the initial temperate period, and as will be shown in Section 10.4.6, less than 2 percent of the deposition hole positions are likely to have dilute conditions during a glacial cycle, and they will only have these conditions a fraction of the time. Given the slow buffer erosion rate, no deposition holes are expected to reach advective conditions during the initial temperate period.

The above expression for $R_{Erosion}$ is valid when the gel/sol interface occurs in the flowing fracture. If erosion has proceeded to the extent that a sol filled cavity has formed in the deposition hole, then the erosion rate is more adequately expressed as

$$R_{\text{Erosion}} = q \cdot C_{Clay}$$

where q is the volumetric flow through the deposition hole cavity and C_{Clay} is the concentration of clay particles in the cavity, valid for most flow rates of concern here. The expression is the same as that used for the exchange of a solute in a deposition hole with a cavity, see /Neretnieks 2006b/ for details. This is a considerably higher erosion rate than that valid when the release to the groundwater occurs in the fracture. The crucial issue to evaluate is when advective conditions arise in the deposition hole, whereas the further evolution of the erosion is of secondary importance. Therefore, the development past the situation when a cavity has arisen is not further addressed here.

Further analyses of the extent of erosion, including studies of sensitivities to a number of uncertain factors are given in the buffer advection scenario, Section 12.2. Full documentation of all calculations of buffer erosion/colloid release and canister corrosion are given in /SKB 2010d/.

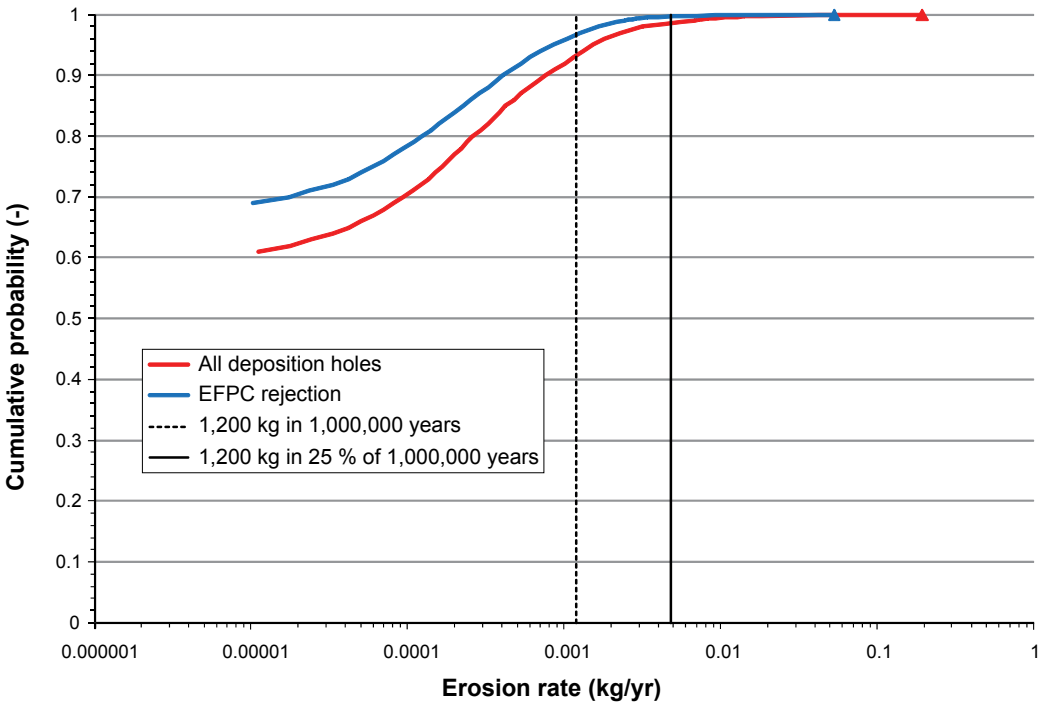

Figure 10-72. *Distribution of erosion rates for the semi-correlated base case of the hydrogeological DFN model, with the EFPC rejection criterion used and for all deposition holes. The erosion rates required to achieve advective conditions in a deposition hole are given as vertical lines, for dilute conditions all the time (dashed line) and 25% of the time (solid line) in all deposition holes. Only a fraction of a percent of the deposition holes is expected to be exposed to dilute conditions during the initial temperate period.*

Erosion of deposition tunnel backfill

The erosion rate of the deposition tunnel backfill was calculated with the same model as that used for buffer erosion with the following modification: The loss rate is increased by a factor of 2 to account for the increase in diameter of the interface between the fracture and the tunnel (diameter 5 m) compared to the deposition hole (diameter 1.75 m). The rate hence scales more slowly than linearly with the diameter /Moreno et al. 2010/.

Fracture aperture and Darcy flux data were taken from the hydrogeological calculation results (Section 10.3.6) for the semi-correlated case without EDZ, to ensure that the analysis only included "true" tunnel intersecting fractures. Water velocities were determined from the Darcy fluxes with the same procedure as used for buffer erosion /Joyce et al. 2010/. The results from the hydro analyses show the fracture apertures and water velocities for structures where particles released in the deposition tunnels immediately above each deposition hole escape to the rock. Several of these structures are in fact deformation zones that intersect the tunnel system far away from any canister position. Such data should thus be excluded from the analysis when the aim is to establish whether tunnel erosion could affect the conditions near a deposition hole.

The result of the calculation is shown in Figure 10-73. As indicated in the Figure, none of the tunnel intersecting single fractures will cause erosion to the extent that the criterion is violated, i.e. that more than 220 tonnes is lost in one million years if erosion occurs 25% of the time. For a few positions where the particle escapes to a deformation zone, potentially more than 220 tonnes could be lost, but this is not relevant from the point of view of canister integrity. For an unrealistic, bounding case of erosion occurring 100% of the time, five tunnel intersecting single fractures experience losses just above 220 tonnes in one million years. The loss of 220 tonnes of backfill indicates that advective conditions may not be excluded in the deposition hole closest to the tunnel intersecting fracture. Considering that canister corrosion is a process requiring hundreds of thousands of years to cause failure of the canister's containment for advective conditions with high sulphide concentrations, and that 220 tonnes of tunnel backfill are lost in only five positions with the unrealistic, bounding assumption of erosion 100% of the time, the contribution of loss of deposition tunnel backfill to the possible generation of advective conditions in deposition holes is considered negligible.

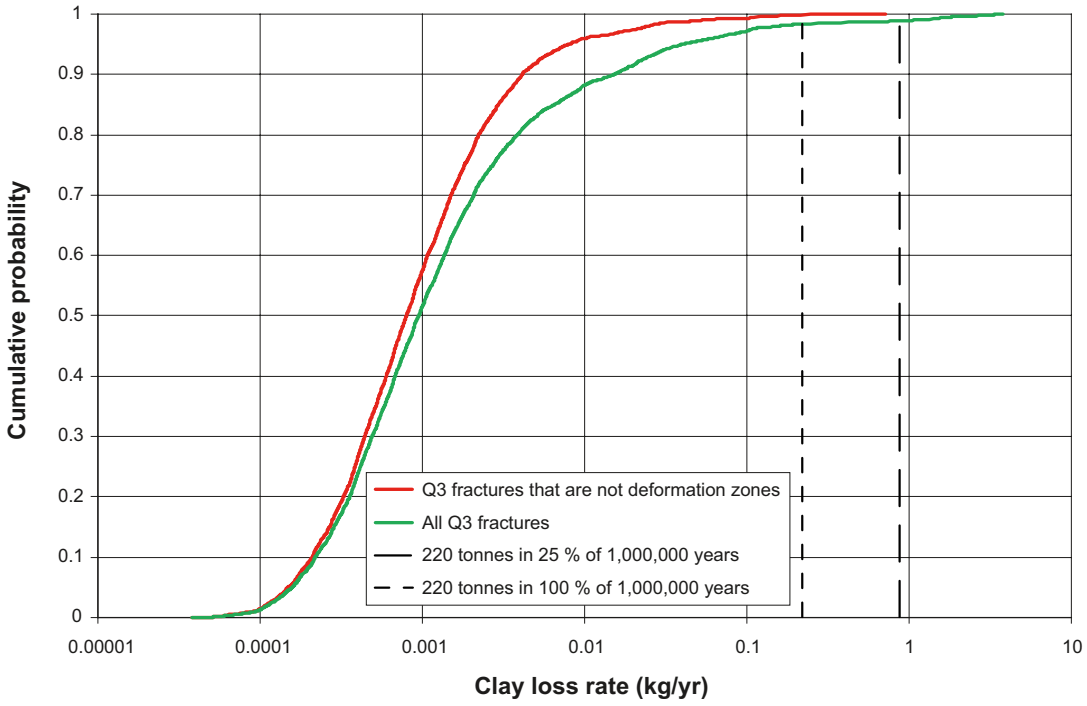

Figure 10-73. *Calculated distribution function of clay loss rate in deposition tunnels for the semi-correlated hydro case and assuming dilute conditions.*

It should also be noted that the calculated local loss of backfill does not mean that the other safety functions of the backfill are lost. 220,000 kg represents only a small part of the backfill in one deposition tunnel. Loss of backfill will lead to an open void only in a part of the tunnel while the main part will retain its hydraulic and mechanical properties (Section 10.3.9).

The saturation period

During the water filling and saturation period of the repository (Section 10.3.6), the water that enters the repository originates predominantly from the surface, either as meteoric water or water from the Baltic Sea. In the case of meteoric water it cannot be excluded that $\Sigma q[M^{q+}]$ will be below 4 mM charge equivalents. This means that the risk of erosion needs to be considered for this period. However, during this period additional factors need to be considered.

1. The buffer and backfill will be in a state of suction in this situation. The direction of the water flow will be in towards the buffer and backfill. The water uptake will compete with the clay expansion into fractures.
2. The accessory minerals in the clay will be present. The presence of calcium sulphates (gypsum), in particular, increases the cation concentration in the buffer and thus restricts the release of colloids.
3. The duration of this period is short.

Based on these arguments, colloid release is neglected during the saturation period.

Identified uncertainties and their handling in the subsequent analysis

In SR-Site, for situations when the groundwater has a total positive charge of less than 4 mM, the loss of bentonite is calculated with the model developed by /Neretnieks et al. 2009/. The model can be applied both to the buffer and to the backfill. However, there are a number of uncertainties associated with this treatment.

- The knowledge concerning colloid sol formation and colloid stability is good concerning the effects of mono- and divalent ions. However, modelling of the correlation effects caused by divalent ions is demanding. Since the model basically is based on monovalent ions the calculated loss should be pessimistic.
- The model does not consider face to edge interactions between bentonite platelets. Not considering these interactions probably leads to an overestimation of the loss.
- Filtering effects by accessory minerals could potentially limit or even eliminate the release of colloids from the buffer. However, this is disregarded in the current treatment of the process, since there is a lack of evidence that efficient filters actually do form.
- In the model, the expansion has been taken to be horizontal, thus neglecting gravity. Scoping calculations /Neretnieks et al. 2009/ suggest that gravity will give small effects as, in the model, the smectite sheets have separated into essentially individual colloid particles. For gravity to have an effect the particles must be considerably larger.
- The concentration limit for cation charge is only based on experimental observations.

Most of the uncertainties are treated with pessimistic assumptions, leading to the conclusion that advective transport conditions in the buffer, i.e. loss of safety functions Buff1, Buff2 and Buff5, does not need to be considered in any of the deposition holes during the initial temperate period.

None of the tunnel-intersecting single fractures will cause erosion to the extent that this will cause such a loss of swelling pressure above deposition holes that these in turn would enter an advective condition, even when the entire one million year assessment period is considered. For a few positions where the particle escapes to a deformation zone, potentially more than 220 tonnes could be lost, but this is not relevant from the point of view of canister integrity. Furthermore, loss of backfill will lead to an open void only in a part of the tunnel while the main part will retain its hydraulic and mechanical properties.

10.3.12 Evolution of the buffer with the bottom plate and backfill with plug after the thermal period

The barriers in the repository are designed to prevent the intrusion of groundwater into the canisters and, in case of canister failure, to retard radionuclides on their way to the geosphere. In addition to the colloid formation discussed in the previous section, groundwater interaction with the components of the barriers will modify the composition of the groundwater that will eventually reach the canister. Knowledge of its composition, especially of the master variables, is important since it may affect:

- The solubility of radionuclides in case of containment failure.
- The hydraulic and mechanical behaviour of the buffer.
- The chemical stability of the buffer.
- The corrosion of the canister.
- The sorption of radionuclides in case of isolation failure.

/Sena et al. 2010/ described the chemical evolution in the repository for a range of conditions and assumptions. The focus of the calculations has been on:

- pH.
- Amount of calcite, gypsum, dolomite.
- Concentration of calcium in the aqueous phase and in the montmorillonite interlayer.

In the study, no calculations of the evolution of either the iron system or the redox conditions have been made. The redox system is instead treated by equilibrium considerations or mass balance in SR-Site. For example, oxidation of sulphide in the buffer is pessimistically neglected and all sulphide is assumed to be available for canister corrosion (see Section 10.3.13). The details of the processes and mechanisms represented in the modelling are presented in /Sena et al. 2010/.

Furthermore, the bottom plate cannot be neglected in the long term assessment of the repository. The dissolution of the concrete may affect the buffer both chemically and mechanically and it may also be possible that a water pressure below the plate could lift the entire buffer/canister package. Also, while no performance is required from the deposition tunnel plug after closure since the transport tunnels will be backfilled, the concrete in the plug cannot be assumed to be stable over the entire assessment timeframe and therefore its degradation needs to be described.

Geochemical evolution in a buffer connected to a water conductive fracture

For a deposition hole intersected by a water conductive fracture, the geochemical evolution in the buffer was calculated for a number of cases based on the geometry presented in Figure 10-74. The geochemical simulations for the water-saturated period have been performed with the reactive transport code PHAST /Parkhurst et al. 2004/. This code is the result of coupling a transport code, and a geochemical code, PHAST is able to simulate multicomponent, reactive solute transport in three-dimensional saturated groundwater flow systems. The reference case for the sensitivity study is the bentonite composition according to Table 5-10, and a typical Forsmark groundwater.

The variations considered have been the magnitude of the water inflow and the composition of the groundwater. Figure 10-75 shows an example of a calculation of the evolution of pH in the buffer as a function of the composition of the groundwater. The variations considered were sulphate content (S(VI)), calcium/sodium ratio (Ca/Na), carbonate concentration (C(IV)) and pH.

Table 10-8 shows a summary of the main results obtained in the sensitivity analysis.

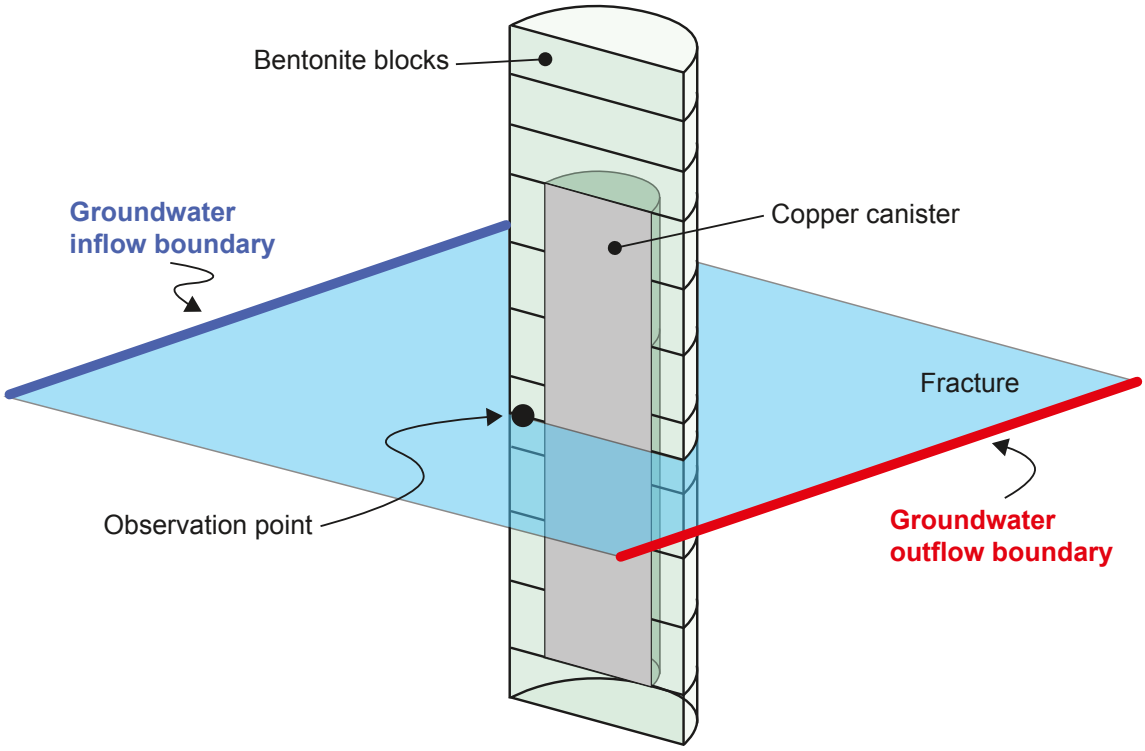

Figure 10-74. *Location of the observation point inside the buffer where the computed time evolution of selected chemical parameters has been analysed for the sensitivity cases considered /Sena et al. 2010/.*

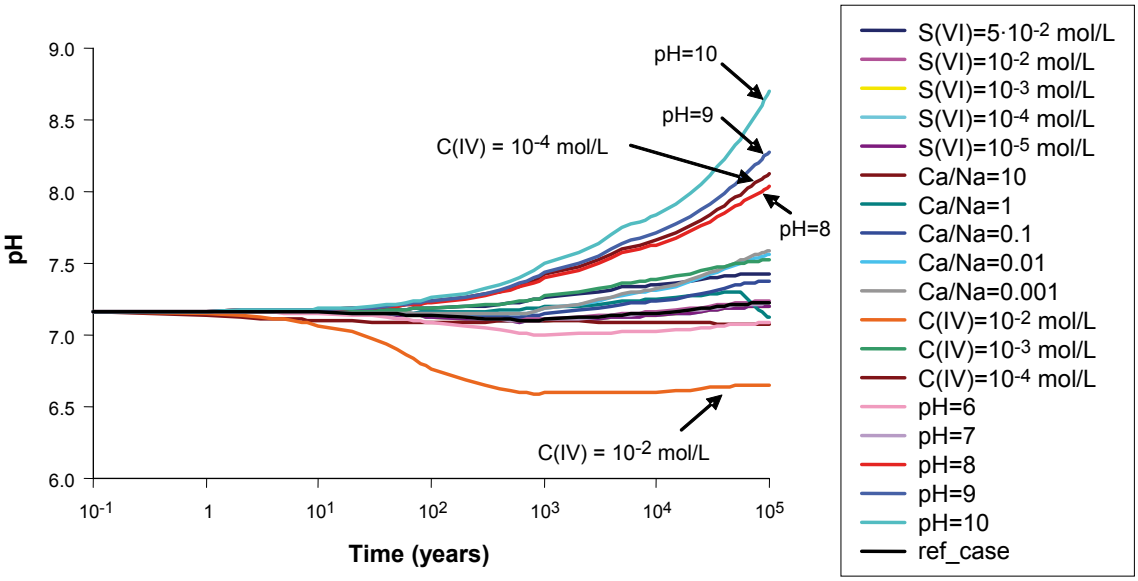

Figure 10-75. *Calculated time evolution of pH at the observation point located in the bentonite (see Figure 10-74) for nineteen inflow water compositions for a flow rate of 0.1 m^3/yr, Ibeco RWC(Deponit CA-N) bentonite /Sena et al. 2010/.*

Table 10-8. Summary of the main results obtained in the sensitivity analysis performed for the chemical composition of the groundwater /Sena et al. 2010/.

Bentonite	Flow rate (m^3/yr)	Variable	Value	Sensitivity case
MX-80	10^{-3}	Maximum pH	7.30	pH = 10
		Minimum pH	6.63	C(IV) = 10^{-2} mol/L
		Maximum amount of calcite	$3.19 \cdot 10^{-2}$ wt%	C(IV) = 10^{-2} mol/L
		Fastest gypsum exhaustion	At 50,000 yr	Ca/Na = 0.001
		Maximum amount of gypsum	1 wt%	Ca/Na = 10
		Maximum [Ca(aq)]	1 mol/L	Ca/Na = 10
		Maximum [CaX_2]	71.2%	Ca/Na = 10
		Minimum [CaX_2]	20.0%	Ca/Na = 0.001
	10^{-1}	Maximum pH	8.22	pH = 10
		Minimum pH	6.09	pH = 6
		Maximum amount of calcite	$2.79 \cdot 10^{-2}$ wt%	C(IV) = 10^{-2} mol/L
		Fastest gypsum exhaustion	At 400 yr	Ca/Na = 0.001
		Maximum amount of gypsum	5.32 wt%	S(VI) = $5 \cdot 10^{-2}$ mol/L
		Maximum [Ca(aq)]	1 mol/L	Ca/Na = 10
		Maximum [CaX_2]	84.0%	Ca/Na = 10
		Minimum [CaX_2]	7.6%	Ca/Na = 0.001
Deponit CA-N	10^{-3}	Maximum pH	7.45	pH = 10
		Minimum pH	6.53	C(IV) = 10^{-2} mol/L
		Maximum amount of calcite	25.4 wt%	Ca/Na = 10
		Fastest gypsum exhaustion	At 80,000 yr	S(VI) = 10^{-5} mol/L
		Maximum amount of gypsum	1.56 wt%	S(VI) = $5 \cdot 10^{-2}$ mol/L
		Maximum [Ca(aq)]	$6.45 \cdot 10^{-1}$ mol/L	Ca/Na = 10
		Maximum [CaX_2]	43.8%	Ca/Na = 10
		Minimum [CaX_2]	27.5%	S(VI) = $5 \cdot 10^{-2}$ mol/L
		Fastest dolomite exhaustion	At 80,000 yr	Ca/Na = 10
		Maximum amount of dolomite	16 wt%	S(VI) = $5 \cdot 10^{-2}$ mol/L
	10^{-1}	Maximum pH	8.70	pH = 10
		Minimum pH	6.65	C(IV) = 10^{-2} mol/L
		Maximum amount of calcite	25.4 wt%	Ca/Na = 10; Ca/Na = 1
		Fastest gypsum exhaustion	At 700 yr	S(VI) = 10^{-5} mol/L
		Maximum amount of gypsum	4.13 wt%	S(VI) = $5 \cdot 10^{-2}$ mol/L
		Maximum [Ca(aq)]	1 mol/L	Ca/Na = 10
		Maximum [CaX_2]	84.0%	Ca/Na = 10
		Minimum [CaX_2]	14.4%	Ca/Na = 0.001
		Fastest dolomite exhaustion	At 700 yr	Ca/Na = 10
		Maximum amount of dolomite	17.4 wt%	Ca/Na = 0.001

The overall conclusions from the sensitivity study of the geochemical evolution in the buffer were as follows.

- For higher flow rates in the fracture, more pronounced geochemical changes occur. In both bentonite types analysed, gypsum is exhausted earlier in the cases with a higher flow rate. More calcite precipitates in these cases.
- The lowest pH value computed for the MX-80 bentonite buffer is 6.10 which is reached in the case where the inflowing groundwater has a pH of 6. The computed pH drop is mainly related to the lack of carbonate minerals in this type of bentonite. On the other hand, the lowest pH value computed for the Deponit CA-N bentonite is 6.53 (see Figure 10-75) which is reached in the case where the inflowing groundwater has a high concentration of aqueous carbonate (10^{-2} mol/L).
- The highest pH value computed for the MX-80 bentonite is 8.23, which is reached in the case where the inflowing groundwater has a pH of 10, and the flow rate along the fracture is 0.1 m^3/yr. The highest pH value computed for the Deponit CA-N bentonite is 8.66 and it is reached in the

same case as for the MX-80 bentonite. The computed pH increase is mainly due to the diffusion of high-pH waters into the bentonite pores.

- When the inflowing water has a Ca/Na of 10, the excess of calcium in the bentonite buffer leads to the highest amount of calcite precipitated, and the highest concentration of calcium in the aqueous phase and in the montmorillonite interlayer.
- The population of calcium in the exchanger depends on the initial bentonite composition, the flow in the fracture intersecting the deposition hole and the relation between calcium and sodium in the groundwater. The highest calculated proportion is 84% and the lowest is 7.6%, see Table 10-8.

By comparing the results calculated for the thermal period and the water-saturated period (Figure 10-63), it is seen that the evolution of the amount of Ca-sulphate in the buffer is similar for both periods. Ca-sulphate minerals tend to dissolve due to the inflow of Forsmark groundwater. Nevertheless, during the warming period, anhydrite is predicted to precipitate close to the copper canister, but as soon as the temperature drops it will tend to dissolve. When the reference Forsmark groundwater is considered, secondary calcite precipitation in the MX-80 bentonite is predicted to be very small and temporary in both periods analysed.

Geochemical evolution in the backfill and in a buffer not connected to a water conductive fracture

The results of the calculations of the geochemical evolution in the buffer in the previous section only consider the situation when the deposition hole is intersected by a fracture with flowing water. In Forsmark many deposition holes will not be intersected by any water conducting fractures and in those positions the geochemistry in the buffer will be conditioned by the tunnel backfill. To evaluate the effect of the backfill on the geochemical evolution in the buffer, a similar sensitivity study to the one discussed in the previous section was performed /Sena et al. 2010/. The geometry and sections where the evolutions have been calculated is shown in Figure 10-76. In this case groundwater is supplied through a hypothetical fracture at the edge of the backfill.

Figure 10-77 shows the calculated pH along the backfill (Section 1 in Figure 10-76) for the same set of different groundwaters as was considered in the previous section. The initial pH of the backfill porewater is 7.16. At the end of the simulation period, almost all the cases lead to a pH profile equal or slightly higher than the initial value. Exceptions occur for two cases (Figure 10-77):

- [C(IV)] of the groundwater entering through the fracture is $1 \cdot 10^{-2}$ mol/L,
- Ca/Na of the groundwater entering through the fracture is 10.

When the carbonate content of the groundwater entering through the fracture is $1 \cdot 10^{-2}$ mol/L, the final pH in the mid-height of the tunnel is around 7. The calculated pH decrease with respect to the initial value of 7.16 is mainly due to the fact that the pH of the inflowing water is relatively low. When the Ca/Na ratio of the groundwater entering through the fracture is 10, a considerable amount of calcite is predicted to precipitate in the backfilled tunnel, and therefore, the pH of the backfill porewater decreases to 6.7 (Figure 10-77), at the end of the simulation period.

Figure 10-78 shows the pH profile along a vertical section through the backfill and buffer (Section 2 in Figure 10-76). The initial pH of the backfill and MX-80 bentonite was 7.16 and 7.19, respectively. The final pH computed along Section 2 for the case with the MX-80 bentonite, is between 6.69 and 7.29 (Figure 10-78). Although a relatively wide range of pH values (between 6 and 10) is considered for the groundwater entering through the fracture, the continuous mixing between the fracture groundwater and the backfill porewater, together with the geochemical reactions triggered by such mixing are able to buffer the pH perturbation induced by the groundwater entering through the fracture, so that the final pH of the bentonite buffer does not change much with respect to its original value.

Table 10-9 presents a summary of the main results obtained in the sensitivity analysis developed for backfill/buffer. The values are calculated for the observation point in Figure 10-74. Although a wide range of pH values, from 6 to 10, has been considered in the sensitivity analysis by /Sena et al. 2010/, the final pH in the bentonite buffer does not reach such extreme values. These results show that geochemical changes in the bentonite buffer, induced by inflows of the different groundwaters considered, are less pronounced in the case with supply through the backfill than in the case where water is supplied directly from a fracture in the rock.

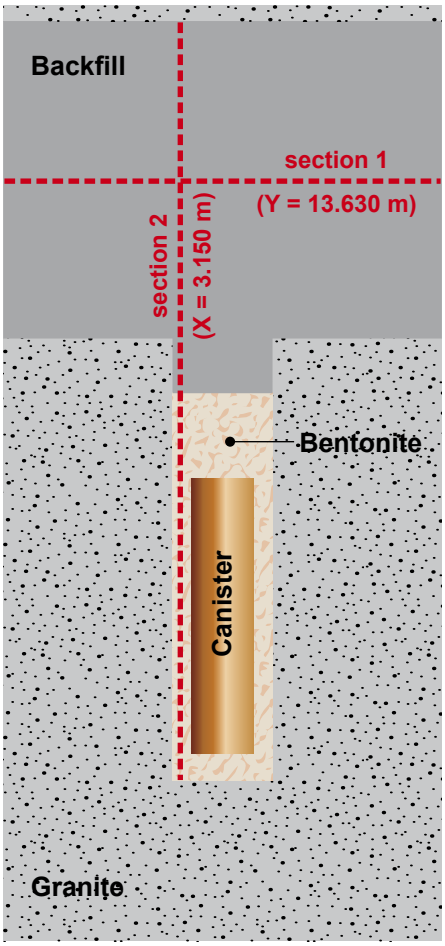

Figure 10-76. Location of the two sections of where the geochemical evolution has been calculated for the different sensitivity cases. Water enters from the left side in the backfill /Sena et al. 2010/.

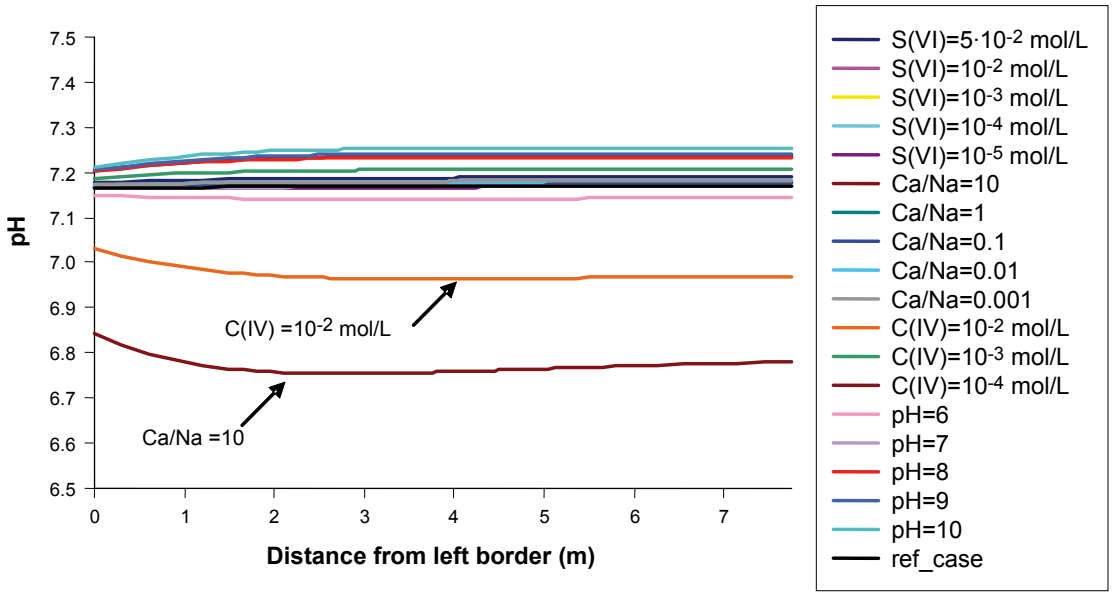

Figure 10-77. Calculated pH profiles along Section 1 (see Figure 10-76) for the sensitivity cases, at the end of the simulation period (100,000 years) /Sena et al. 2010/.

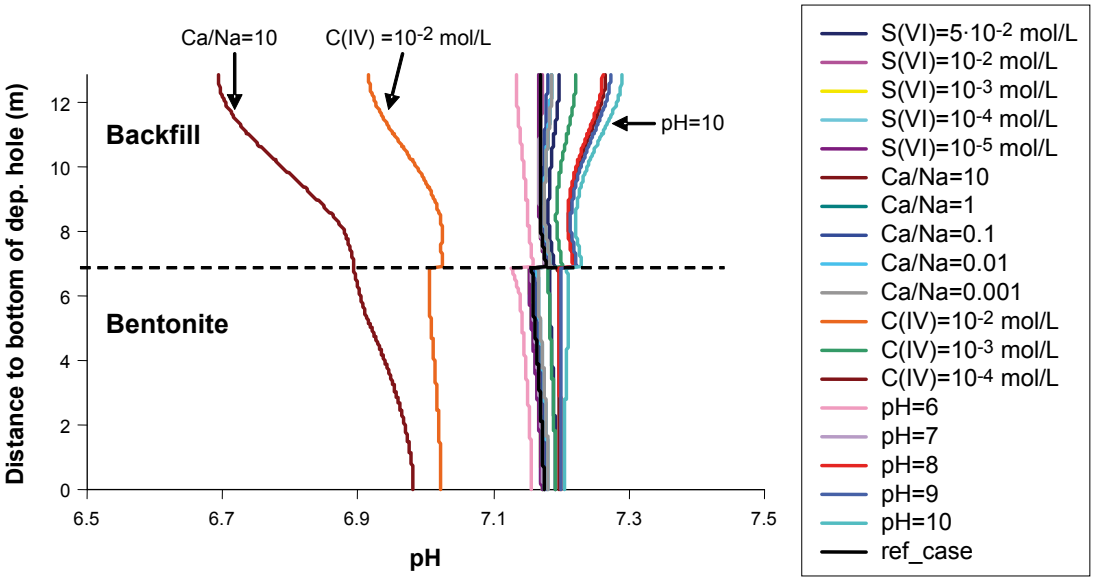

Figure 10-78. *Calculated pH profiles along Section 2 (see Figure 10-76) for the sensitivity cases, at the end of the simulation period (100,000 years), MX-80 bentonite buffer /Sena et al. 2010/.*

Table 10-9. Summary of the results of the sensitivity cases for the backfill/buffer interaction /Sena et al. 2010/.

Bentonite	Variable	Value	Sensitivity Case
MX-80	Maximum pH	7.21	pH = 10
	Minimum pH	6.91	Ca/Na = 10
	Maximum amount of calcite	$2.88 \cdot 10^{-2}$ wt%	Ca/Na = 10
	Minimum amount of gypsum	0.33 wt%	Ca/Na = 0.001
	Maximum amount of gypsum	1.85 wt%	Ca/Na = 10
	Maximum [Ca(aq)]	$9.4 \cdot 10^{-2}$ mol/L	Ca/Na = 10
	Maximum [CaX_2]	50.0%	Ca/Na = 10
	Minimum [CaX_2]	29.3%	[S(VI)] = $5 \cdot 10^{-2}$ mol/L
Deponit CA-N	Maximum pH	7.22	pH = 10
	Minimum pH	7.01	[C(IV)] = $1 \cdot 10^{-2}$ mol/L
	Maximum amount of calcite	16.4 wt%	Ca/Na = 10
	Minimum amount of gypsum	0.42 wt%	[S(VI)] = $1 \cdot 10^{-5}$ mol/L
	Maximum amount of gypsum	0.92 wt%	[S(VI)] = $5 \cdot 10^{-2}$ mol/L
	Minimum amount of dolomite	8.0 wt%	Ca/Na = 10
	Maximum [Ca(aq)]	$6.28 \cdot 10^{-2}$ mol/L	Ca/Na = 10
	Maximum [CaX_2]	32.1%	Ca/Na = 10
	Minimum [CaX_2]	29.5%	[S(VI)] = $5 \cdot 10^{-2}$ mol/L

In summary, the sensitivity cases developed for the backfill result in the following conclusions.

- The geochemical evolution of the bentonite buffer is similar to that computed for the case where water is supplied from a fracture, but it evolves at a much slower rate, since mixing of the groundwater entering through the fracture with the backfill porewater buffers the disturbing effect of the inflowing "foreign" groundwater.
- The geochemical evolution of the backfill does not change much regardless of the type of bentonite considered in the deposition hole.
- Calcite is predicted to precipitate in the backfilled tunnel in all the sensitivity cases considered. The highest amounts of calcite precipitated are computed in the cases where the inflowing water has a Ca/Na > 1. Therefore, the lowest pH computed for the backfill is 6.76, in the case where the inflowing water has a Ca/Na of 10.

- The highest concentration of calcium in the backfill ($1.4 \cdot 10^{-1}$ mol/L), at the end of the simulation period, is computed for the case with Ca/Na of 10.

Application to geochemical conditions at the Forsmark site

The various cases that are described in this section and for which the results are summarised in Tables 10-8 and 10-9 show that the backfill/bentonite is rather stable from a geochemical point of view and no dramatic changes of the geochemical conditions in the buffer can be expected. A comparison of the input data in Tables 10-8 and 10-9 with the expected geochemical evolution at the Forsmark site presented in Table 10-6 shows that the expected evolution is covered well within the cases considered.

Chemical interaction bottom plate/buffer

The concrete plate at the bottom of the deposition holes may affect the buffer chemically. Montmorillonite mineral transformations have been modelled for bentonite in contact with standard Portland cement within the Ecoclay II project /Gaucher et al. 2004/. These results show complete bentonite alteration within a distance of about 20 cm from the cement surface after a period of 100,000 years. Laboratory experiments show that the dissolution of montmorillonite is orders of magnitude slower at lower concentrations of hydroxide ions /Karnland and Birgersson 2006/. Therefore, the rate of bentonite alteration in contact with "low-pH" cement with porewaters of pH < 11 ($[OH^-]$ = 1 mM) is expected to be much slower than if it were in contact with standard Portland cement porewater, that has pH 12.5 ($[OH^-]$ = 32 mM). Concrete recipes with porewaters that prevent substantial alteration of the buffer are being developed for the concrete plates.

The interaction between the concrete in the bottom plate and the bottom of the buffer will in most respects be similar to the interaction between the plug and the backfill as described later in this section. The calculations show that, for the given composition of the cement, the pH in the bottom of the buffer may increase to pH > 11 for a short duration, but the extent of this pulse will be limited in time and is not expected to have a significant effect on the buffer properties.

No credit for any hydraulic performance of the degraded bottom plate itself is accounted for. In the transport calculations in SR-Site it is assumed that it is degraded by chemical dissolution of the binding minerals in the concrete so that the pore space becomes more permeable to water flow. /Neretnieks et al. 2010/ have explored the consequence in a case where it was assumed that the concrete has a negligible hydraulic resistance and allows water to flow through it and compared this effect to the impact of spalling, see Section 10.3.6 for an assessment of the latter. It is found that the spalling has a larger impact on Q_{eq}, and the influence of the bottom plate could thus be covered by this case. However, if spalling can be avoided and if the bottom plate is intersected by a fracture it will be the main transport path. In such a case the mass transfer resistance will much lower than in a "ideal" case where the buffer is in contact with the rock in the bottom of the deposition hole. This shows that the current design of the bottom plate requires further consideration.

Mechanical interaction bottom plate/buffer

The cement part of the bottom plate will eventually degrade and the space may be replaced by the swelling buffer. This will cause a loss of density in the buffer. The swelling has been modelled by /Åkesson et al. 2010a/. Since neither the thickness of the bottom plate nor the aggregate nor degradation products left after the cement has dissolved are known the problem is modelled in a pragmatic way. The concrete and the copper plate are made with a total thickness of 15 cm and the disintegration is simulated by stepwise displacement of the copper plate to a total displacement of 1.5 cm, 3.0 cm and 6.0 cm. After each step the bentonite is allowed to swell and homogenise and the porewater pressure equalise. Figure 10-79 shows the resulting density at water saturation in all four steps. Observe that the density scale is changed at step 4, due to local stress concentrations around the bottom corner of the canister. These stress concentrations are judged not to be realistic but are caused by the sharp corners of the modelled canister, which locally creates too high stresses and thus unrealistically large density changes. The density below the canister is reduced to about 1,970 kg/m^3, 1,950 kg/m^3 and 1,920 kg/m^3 after steps 2–4 but the density in the major part of the buffer between the canister and the rock remains at a density of 2,000 kg/m^3.

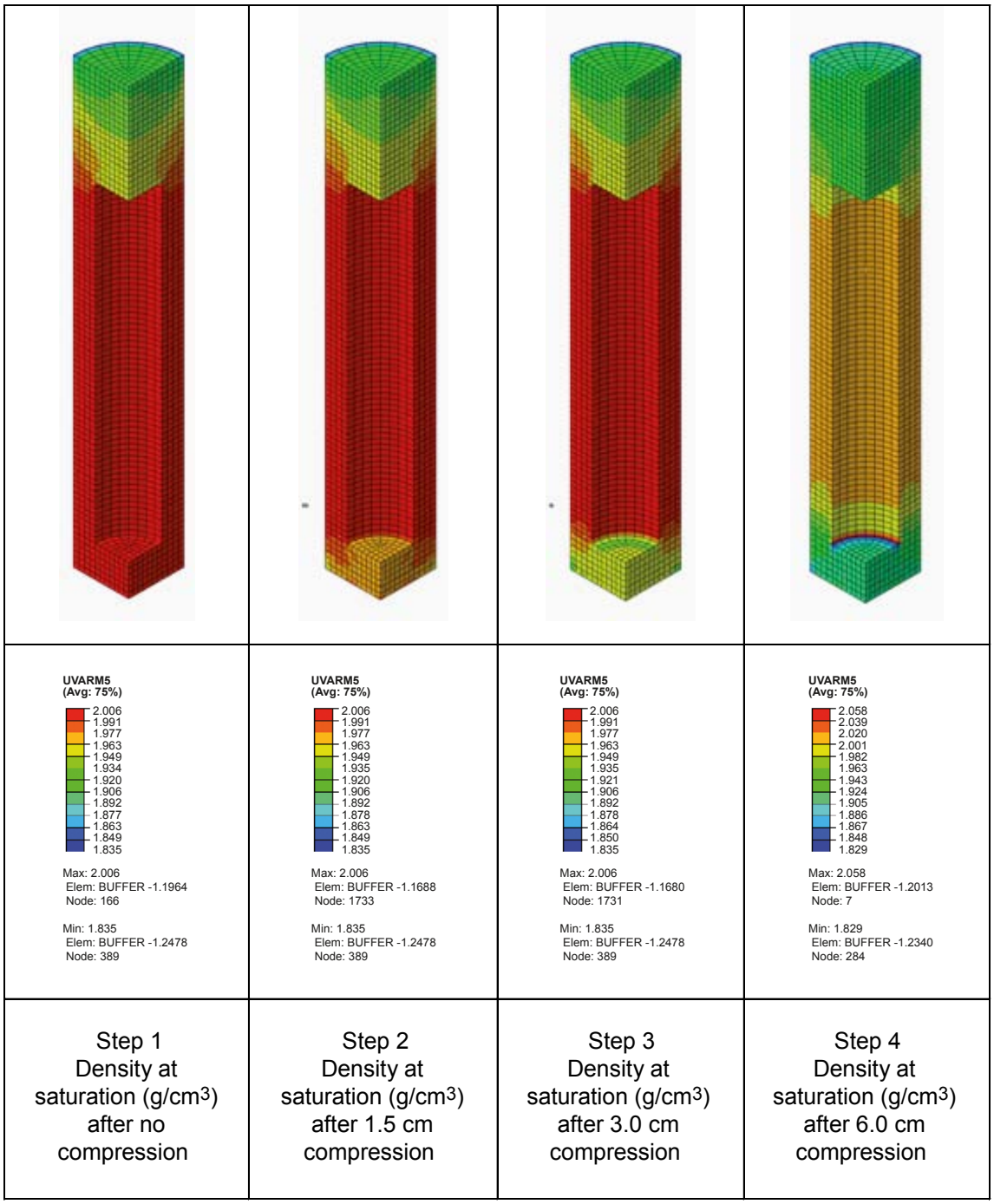

Figure 10-79. *Density at saturation in the buffer after the simulated compression of the bottom plate /Åkesson et al. 2010a/.*

Calculations of the mechanical effect of disintegration of the bottom plate show that the swelling pressure and density of the buffer beneath the canister as expected are reduced with increasing compression of the bottom plate. The density at saturation beneath the canister is reduced to about 1,950 kg/m^3 after 3 cm compression, which is within the tolerances. However, after 6 cm compression the loss of density seems to be too high, which means that the limit for allowable compression is about 3 cm. The bottom plate should thus be designed so that it will not be compressed by more than 3 cm.

Degradation of the concrete in the deposition tunnel plug

/Grandia et al. 2010b/ have evaluated the degradation of the concrete part of the plug. The conceptual description of the plug can be found in Figure 10-80.

The rock is not considered physically as a rock in the model. Instead, a flowing groundwater of Forsmark-type composition is considered. The reason behind this selection is the slow kinetics of the granite mineralogy which is not expected to undergo significant changes in spite of the diffusion of alkaline fluids from concrete alteration. Low-reactivity aggregate is predicted to be present in a defined fraction of the volume in the hydrated cement mixture. The remaining porosity is ~30%; however, this value includes all pore sizes, most of them are unconnected. Figures 10-81 and 10-82 show the calculated water composition, porosity and pH in the concrete and the backfill for 1 and 100 years of simulation.

The results from reactive transport simulations predict that the effect of low-pH concrete alteration on the stability of backfill materials is low. Dissolution of Ca-Si-hydrates (CSH phases) causes a initial hyperalkaline plume (pH > 11) penetrating ~6 cm into the backfill. This plume is transient since in a few years (< 10 y), pH decreases back to more neutral values. The main process governing geochemistry in the backfill-concrete boundary is the quick loss of porosity due to ettringite precipitation. The model predicts insignificant modifications in the geochemistry of the system from 10 years and on, since porosity has already been clogged at both concrete boundaries decreasing the diffusion between material pores. CSH phases keep replacing from Ca-rich to Si-rich intermediates. Since CSH replacement is controlled by kinetics, Si-rich CSH will form until complete equilibrium with porewater is achieved, regardless the fluid renewal. Alkaline pH does not affect the composition of the granitic groundwater, mainly because of the rate of water renewal specified in the fracture.

Backfill swelling after tunnel plug disintegration

As described in the previous section, the cement and other substances in the concrete plugs may be dissolved with time and transported away, which means that the stiffness and strength of the plugs will be dramatically reduced. This disintegration will affect the backfill material on both sides of the plug. When the plug cannot withstand the swelling pressure of the backfill it will be compressed and the backfill will swell, which leads to a loss in density and swelling pressure of the backfill. Since there is friction against the rock surface the loss in density may be significant close to the plug but will be reduced with distance from the plug. In order to understand how this affects the backfill and the location of the first deposition hole a number of finite element calculations have been carried out /Åkesson et al. 2010a/. The main purpose of the calculations was to find how much the backfill density will decrease in order to put a limit on how close to the plug the deposition hole can be located.

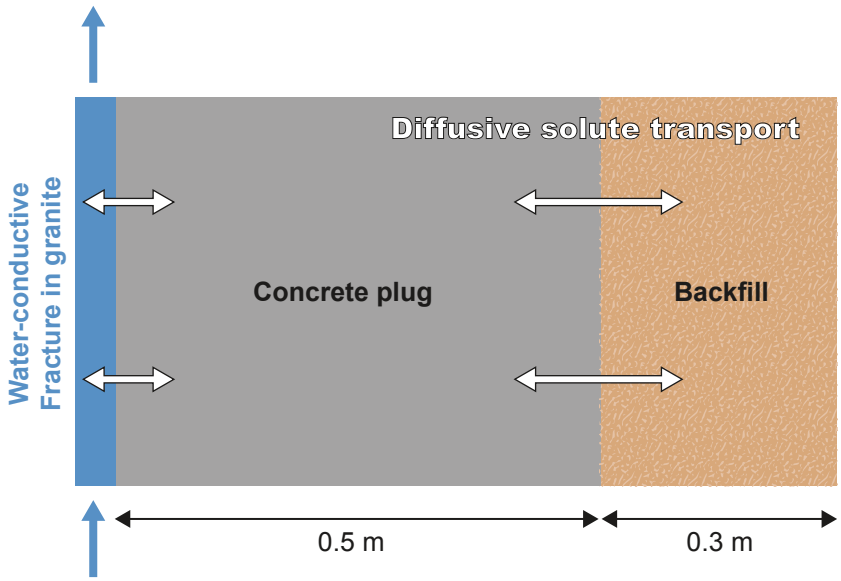

Figure 10-80. *Domain selected in the reactive transport simulations /Grandia et al. 2010b/. The actual plug design is more complex and has a tight bentonite filled seal, see Figure 5-22. However, these details are judged insignificant for the modelling.*

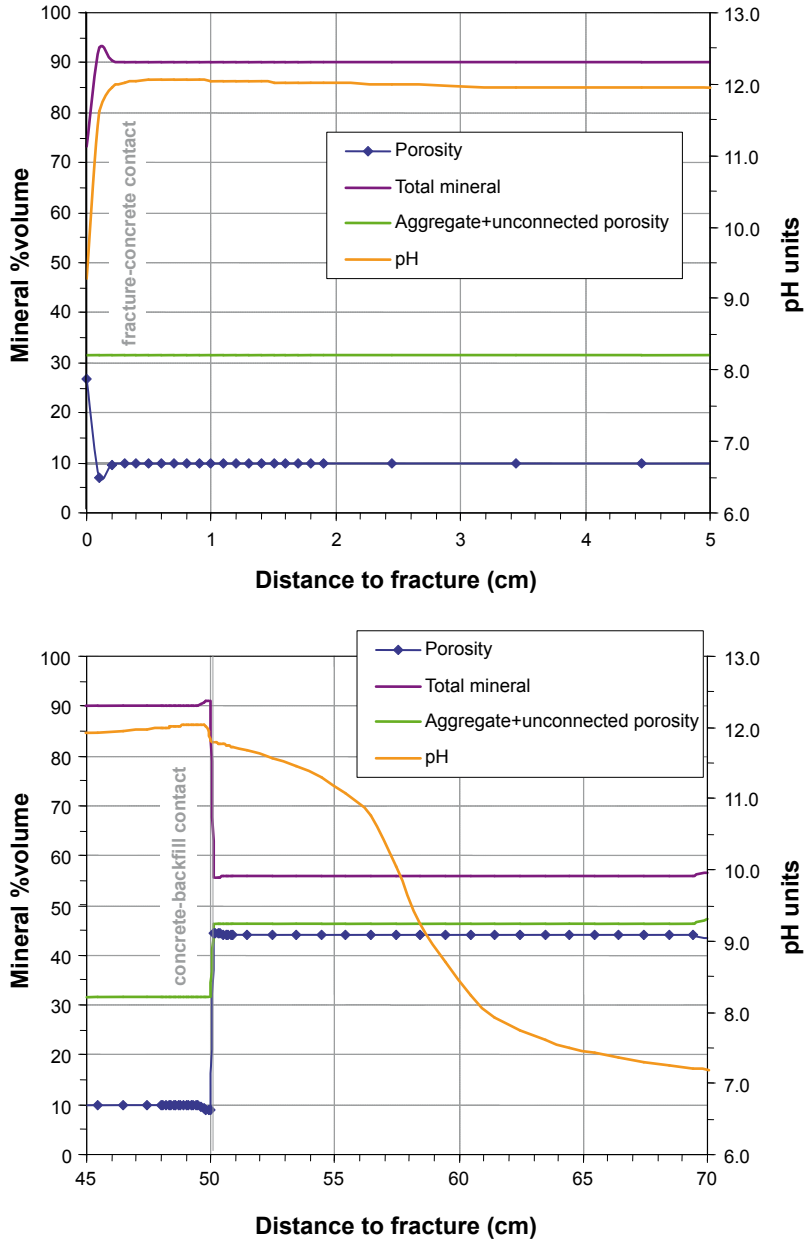

Figure 10-81. *Predicted composition of porewater, porosity and pH in concrete and backfill after 1 year of simulation in fracture-concrete and concrete-backfill contacts. Unconnected porosity and non-reactive aggregates in the concrete and backfill are plotted together /Grandia et al. 2010b/.*

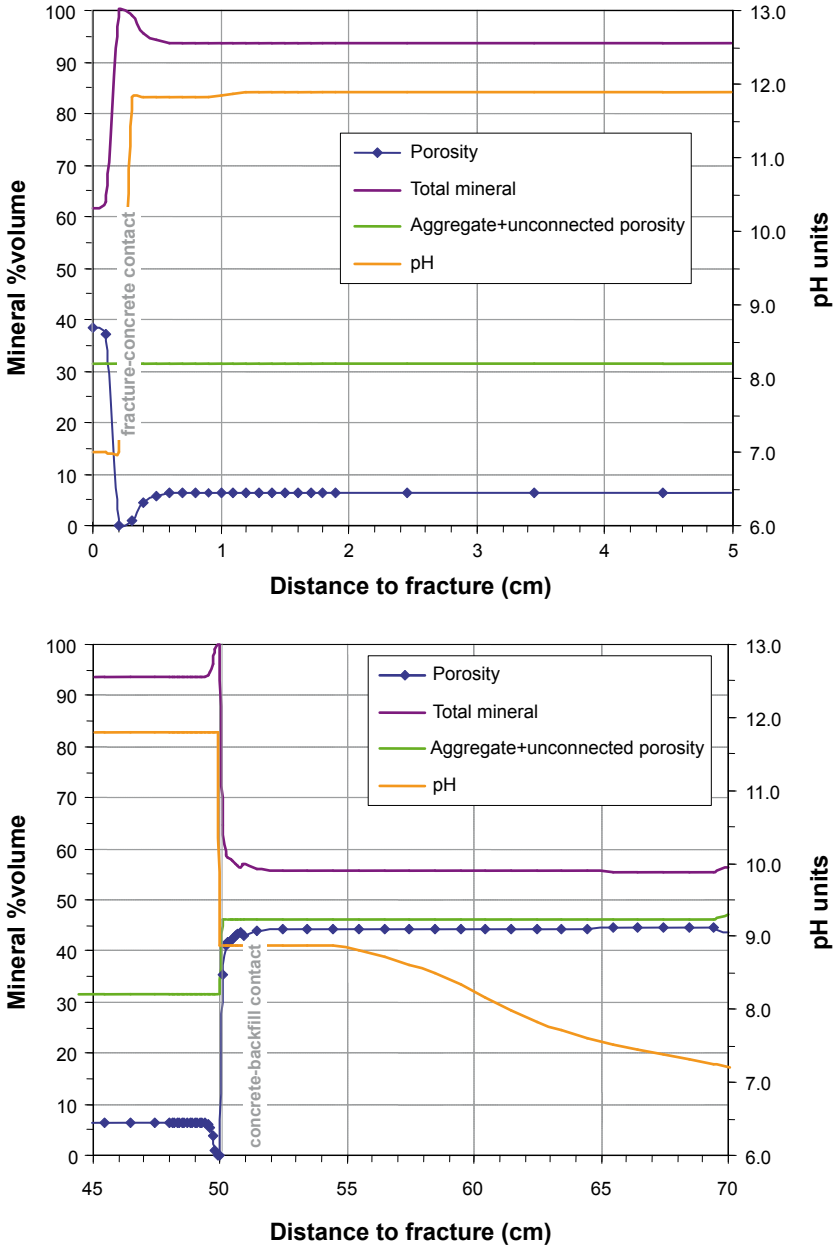

Figure 10-82. *Predicted composition of porewater, porosity and pH in concrete and backfill after 100 year of simulation in fracture-concrete and concrete-backfill contacts. Unconnected porosity and non-reactive aggregates in the concrete and backfill are plotted together /Grandia et al. 2010b/.*

Since no detailed knowledge of the plug status after disintegration is required only a very simplified model of the plug was used. The geometry used in the calculations is shown in Figure 10-83.

Different sensitivity cases, varying the E-modulus, the pressure and the void ratio have been studied /Åkesson et al. 2010a/.

A typical example of a result from the calculations can be found in Figure 10-84. The results show that case *Plug1* yields a swelling of only 7 cm, which is the smallest swelling of the investigated cases due to the low initial swelling pressure of the backfill and the high E-modulus of the plug. The entire swelling corresponds to a compression of half the plug since the same backfill is assumed to be present outside the plug. The void ratio and the swelling pressure are only changed marginally except for a small zone at the rock/plug/backfill contact.

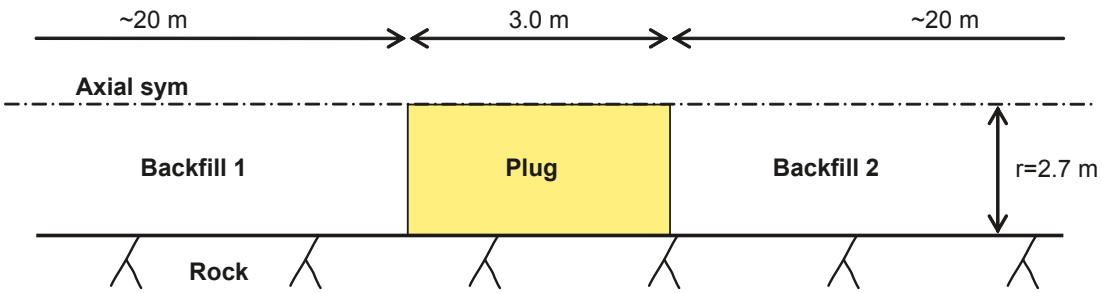

Figure 10-83. *Schematic drawing of the model. Backfill 1 is located inside the plug and Backfill 2 outside /Åkesson et al. 2010a/.*

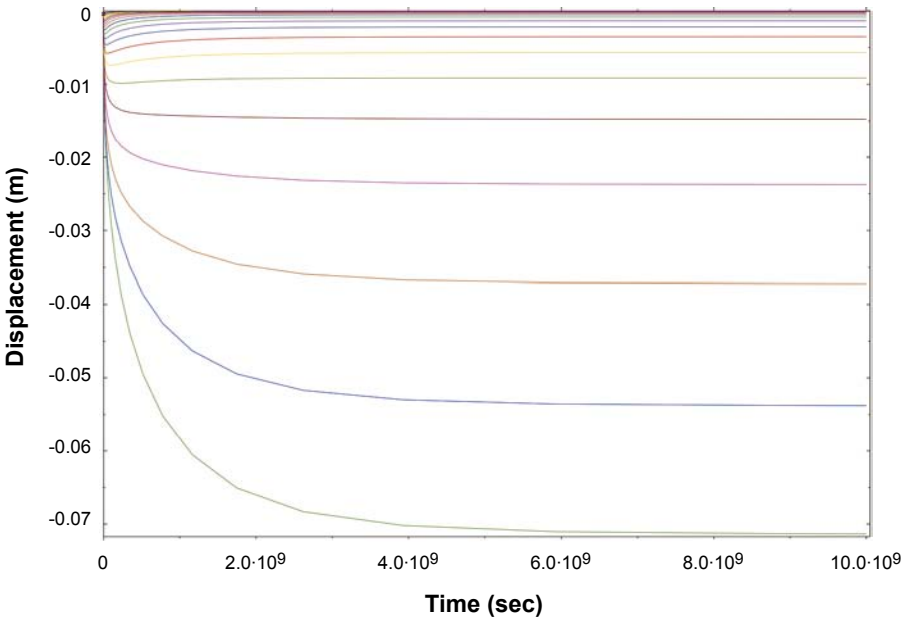

Figure 10-84. *Plug1. Axial displacements of the centre nodes in Backfill 1 as a function of time. The lowest curve represents the contact backfill/plug and the consecutive lines represent 10 cm, 20 cm, 30 cm etc. axial distance from the contact /Åkesson et al. 2010a/.*

Table 10-10 is a compilation of the most important results of the different calculations.

According to Table 10-10, the highest resulting void ratio at the backfill/plug interface is 1.2. Since this is within the limits set for the backfill above a deposition hole ($e < 1.22$) the conclusion from the calculations is that the disintegration of the plug has no detrimental effect on the backfill above the first deposition hole and no restrictions caused by plug disintegration on the location of the first deposition hole are needed.

There are of course several uncertainties particularly regarding the data applicable to the plug after disintegration. There are also uncertainties regarding the initial density and properties of the backfill. However, the properties of the plug are very pessimistically set and in spite of this the results are far from critical for the buffer in the first deposition hole.

Table 10-10. Compilation of results from the cases presented in /Åkesson et al. 2010a/. The calculations with names beginning with Plug1 have bentonite backfill on both sides of the plug while calculations with names beginning with Plug2 have crushed rock outside the plug. Suffix -2 refers to calculations with the high dry density ρ_d = 1,600 kg/m³ and high swelling pressure of the bentonite backfill, while the names without suffix refer to calculations with the low dry density ρ_d = 1,450 kg/m³ and low swelling pressure.

Calculation	Displacements (m)		Maximum void ratio	Minimum swelling pressure (MPa)	Remarks
	Backfill1/ Plug	Backfill2/ Plug			
Plug1	0.03–0.07	–(0.03–0.07)	1.0	2.0	Locally at corner
Plug1b	0.15–0.27	–(0.15–0.27)	1.1	1.3	
Plug1-2	0.08–0.17	–(0.08–0.17)	0.86	5.7	
Plug1b-2	0.30–0.58	–(0.30–0.58)	0.99	3.0	
Plug2	0.10–0.15	0.05–0.07	1.1	1.7	
Plug2b	0.35–0.50	0.20–0.28	1.2	0.8	
Plug2-2	0.24–0.32	0.13–0.17	0.98	3.0	Locally at corner
Plug2b-2	0.70–1.05	0.40–0.58	1.2	1.0	

Canister sinking

Apart from the few deposition holes losing buffer through colloid release, as assessed in Section 10.3.11, the buffer in other deposition holes will not be affected by any processes that may alter its swelling properties in a way that the swelling pressure would sink below the value needed to retain the canister in position (P > 0.2 MPa, see Section 8.3.2). Furthermore, in deposition holes loosing buffer due to colloid sol formation, creation of advective conditions would occur long before the canister sinking could happen, making this issue irrelevant also for these cases.

Osmotic effects on the buffer and backfill

According to Table 10-6, the maximum chloride concentration of any time frame is < 0.4 M at repository level in the Forsmark groundwater. As seen in Figure 5-14 this is not expected to have any impact on the properties of the buffer material. This conclusion is valid for the entire repository evolution period.

Identified uncertainties and their handling in the subsequent analysis

The various cases described in this section show that the chemical conditions in the buffer and the backfill are rather stable and no dramatic changes of the geochemical conditions can be expected. The expected conditions in the Forsmark groundwater (Table 10-6) are well within the range of of the parameters used in the sensitivity study for all future evolutions. As seen in the right side of Figure 10-65 the buffer (MX-80) is expected to have about equal populations of sodium and calcium in the exchanger for a typical Forsmark groundwater. The sensitivity study presented in Table 10-8 shows a range of 7–84% for the calcium population, but the minimum and maximum values in the range are both for Ca/Na ratios that are far away from what is expected in the Forsmark water for any condition (Table 10-6).

The effect of a degraded bottom plate on the mass transfer resistance in the near field is considered in SR-Site. However, the impact is less than the impact from assuming spalling in the deposition hole and this effect is thus covered by the assumption of spalling in all deposition holes. However, if spalling can be avoided and if the bottom plate is intersected by a fracture it will be the main transport path. In such a case the mass transfer resistance will be much lower than in an "ideal" case where the buffer is in contact with the rock in the bottom of the deposition hole. A thick, compressible bottom plate may lead to loss of density to a level below the design target of 1,950 kg/m³ in the bottom of the buffer. This shows that the current design of the bottom plate requires further consideration, see Section 15.5.10.

The model predictions indicate that the durability of backfill materials is not expected to be affected by the potential alkaline plumes developed from concrete alteration of the plug. Hence, the effect on the backfill properties will be small and can be neglected in the subsequent analysis. Also calculations show that the disintegration of the plug, which means that the backfill could then swell into the voids created, has no detrimental effect on the backfill above the first deposition hole and no restrictions on the location of the first deposition hole are needed.

10.3.13 Canister evolution

One of the main safety functions of the canister is to provide a corrosion barrier, safety function Can1 in Figure 10-2. Processes that could cause deterioration of the copper shell during the temperate phase need thus be assessed.

Thermal evolution

The thermal evolution of the buffer is analysed in Section 10.3.4 where it is shown that the buffer temperature will always stay below 100°C. This analysis can also be used to assess the temperature on the canister. For dry deposition holes the maximum temperature at the canister surface and at canister mid-height is about 2 degrees higher than the maximum buffer temperature, i.e. at the very most 102°C for a few canisters. At the canister top and bottom, the temperature is at most 100°C under these dry conditions, since there the canister is in direct contact with the buffer. If there is water in the deposition hole such that the buffer swells, there will be direct contact between buffer and canister everywhere and the temperature at the canister surface, and in the buffer, will be much lower (up to a 20 degree decrease relative to the dry case). Even for the highest temperature on the outer copper canister surface, the temperature in the iron insert will be at most 117°C (pessimistically assuming an argon-filled gap between iron and copper at the maximum tolerance and a polished copper surface, see the **Fuel and canister process report**, Section 3.2.1. This is still below the design premise of 125°C for the insert. There are thus no consequences for the integrity of the canister.

Mechanical impact of buffer swelling

After emplacement of the canister and the buffer, water will enter the deposition holes via the water conductive fractures that intersect the holes, and, to some extent, via diffusive transport of water through the rock. This leads to wetting and swelling of the buffer. After some time, the buffer will stop the water inflow through the fractures and the groundwater pressure will start to build up, which may lead to flow paths opening around the deposition holes in the superficial excavation-disturbed zone, where the flow resistance is expected to be lowest. This will tend towards a more uniform wetting of the bentonite and a more uniform pressure build-up. The size of this effect is, however, uncertain. It is, therefore, reasonable to assume that there will be inhomogeneities in the pressure build-up.

Furthermore, if the canister is slightly tilted or inclined in the emplacement hole, or if the rock is uneven, permanent pressure disequilibrium can exist in the bentonite even after water saturation. This can also occur due to swelling of the buffer at the top of the hole. Temporarily, asymmetric loads may thus occur due to uneven water saturation in the buffer. Permanent asymmetric loads may also occur due to a non-uniform density distribution of the saturated buffer caused by irregularities in the geometry of the deposition holes.

As described in Section 5.4.3, the probability that the canister would not withstand the load from uneven swelling of the bentonite is negligible. In short, buffer swelling will not pose a threat to the safety function indicators Can2 and Can3 in Figure 10-2.

Copper corrosion

A range of studies over several decades, see e.g. /King et al. 2010/ for a review, has identified the following substances as capable of corroding the copper canister material under repository conditions, after the operating period:

- Oxygen brought in from the buffer and backfill, or from the groundwater via the buffer.
- Nitric acid formed by gamma radiolysis of nitrogen compounds in moist air in the gap between canister and buffer.
- Oxidants formed by radiolysis of water near the canister, after water saturation.
- Sulphide brought in from the buffer and backfill or from the groundwater via the buffer.

The corrosion processes are marginally affected by the changes in temperature expected in the final repository. The results of corrosion are corrosion products and a change in the thickness of the copper shell.

Atmospheric corrosion and corrosion caused by oxygen initially present in the buffer and the backfill was discussed in Section 10.2.5 and the corrosion depth was shown to be less than 500 μm at the most. The chemical conditions in the repository are then expected to be reducing for the period of temperate climate, see Section 10.3.7, i.e. no further corrosion due to oxygen is expected.

During the unsaturated phase, nitric acid formed by gamma radiolysis of moist air will contribute to the corrosion attack during this period. It can be shown, however, that the amount of nitric acid formed corresponds to a corrosion depth of a few nanometre only, see the **Fuel and canister process report**, Section 3.5.4.

After water saturation, radiolysis of water near the canister will occur, leading to the formation of oxidants and hydrogen. An estimate of the maximum possible amounts of oxidised copper after c. 317 years (10^{10} s, after which time the gamma dose rate has decreased substantially), assuming that oxidants present in a 5 mm layer surrounding the canister reach and react with the copper surface, would give a corrosion depth of 14 μm. Available experimental information shows no evidence for enhanced corrosion rates caused by gamma radiation, see the **Fuel and canister process report**, Section 3.5.4.

As argued in the **Fuel and canister process report**, the influence on corrosion of chemical and mechanical conditions of the copper material (welded area, cold worked material), corrosion caused by earth currents, corrosion caused by deposition of salt on the copper surface, and stress corrosion cracking are of no importance for long-term safety.

After all the oxygen has been consumed, sulphide will be the remaining corroding agent present in the repository. The sources of sulphide would be dissolution of sulphide minerals in the buffer and backfill, sulphide formed by microbial sulphate reduction in the buffer and backfill and dissolved sulphide in the groundwater (either from dissolution of sulphide minerals in the rock or as a result of microbial reduction of sulphates in the groundwater-rock system). The corrosion of copper by sulphide will proceed with formation of copper sulphide (for simplicity written as Cu_2S even though other non-stoichiometric forms are possible) and molecular hydrogen.

$$2\ Cu + HS^- + H^+ \rightarrow Cu_2S + H_2$$

Pyrite in buffer and backfill

Corrosion due to sulphide from pyrite initially present in the buffer can be bounded by a simple mass balance estimate. If all initially present pyrite in the buffer sections surrounding the canister side attacks the canister side as sulphide, corrosion of 0.1 mm and 0.9 mm copper is obtained for MX-80 and Ibeco-RWC bentonite, respectively. The corresponding values for pyrite in the top part of the buffer attacking the canister lid are 0.4 and 2.9 mm, respectively.

More realistically the estimate of corrosion should include the dissolution of pyrite and the diffusion transport of the sulphide from the pyrite. The time required for complete depletion of this sulphide from the pyrite can be estimated with a simple transport expression involving the diffusivity and the concentration limit of sulphide in the buffer /Hedin 2004b, SKB 2010d/. The diffusivity of anions is estimated to have an upper limit of $3.0 \cdot 10^{-11}$ m^2/s /Ochs and Talerico 2004/, while the solubility of sulphide from pyrite is estimated to be $1.17 \cdot 10^{-11}$ mol/dm^3 /Duro et al. 2006/. This would give corrosion depths of less than 1 μm even for the highest allowed pyrite content in the buffer for a 10^6 year assessment period, see Table 10-11. These small corrosion depths are nearly independent of geometry, rendering the same corrosion depth at the side and the top. The depletion front penetrates less than 2 cm (even for the lowest pyrite content as in MX-80), thus only pyrite in the very close vicinity of the canister can reach the copper surface.

Both the diffusivity and the sulphide solubility are uncertain. Assuming very pessimistically a diffusivity of $1.2 \cdot 10^{-10}$ m^2/s (corresponding to uncharged H_2S, diffusing as HTO, tritium labelled water) and a solubility of $3.84 \cdot 10^{-9}$ mol/dm^3 (assuming a very low iron content in the bentontite, $1 \cdot 10^{-10}$ moles/dm^3) the bentonite at the side of the canister would be depleted of pyrite. The pyrite on top of the canister would not be depleted in one million years as the depletion front reaches at a maximum 40 cm, and thus not allowing time for any pyrite in the backfill to reach the canister. The corrosion depth would be at a maximum 114 μm, even including a factor of 3 for the deposition hole being 3 times larger than the canister top.

In conclusion, even in a million year perspective, corrosion caused by initially present pyrite in the buffer and backfill has a negligible effect on the copper thickness.

Table 10-11. Corrosion depth caused by pyrite initially present in the buffer, using a 1-D diffusion model, for different pyrite contents in the bentonite, for an assessment period of 10^6 years.

		Mx-80	Ibeco-RWC	Maximum allowed sulphide content in the buffer (Buffer production report)
		Pyrite and sulphide contents		
Pyrite (FeS_2)		0.07 weight%	0.5 weight%	
Sulphide content		0.0374 weight%	0.267 weight%	0.5 weight%
		Corrosion depth in [µm] in 1 My		
Estimated pyrite solubility, upper limit of sulphide diffusivity.		0.3 µm	0.8 µm	1.0 µm
Pessimistic case pyrite solubility at low iron content (10^{-10} mol/dm^3), and diffusivity as uncharged H_2S	canister side	9.5 µm depleted in 775 ky	28 µm	38 µm
	straight on canister top	10.4 µm	28 µm	38 µm
	also considering cylinder with width of dep. hole	31 µm	83 µm	114 µm

Sulphate reducing bacteria (SRB) in buffer and backfill

As discussed in Section 10.2.5, there are several different types of organic matter with different origins that could be degraded by microorganisms and thus be a source of energy for sulphate reducing bacteria. The largest pool of organic material in the repository at closure is the organic material in the bentonite in buffer and backfill. The character of this material is not known in detail but it probably consists to a large extent of humic and fulvic acids. Most of this material is probably very closely attached to the clay, so when the bentonite has reached its swelling pressure very little organic material will be available for dissolution into the groundwater.

The organic matter in the backfill bentonite, if all of it were to be used by sulphate reducing bacteria, would correspond to a maximum produced amount of sulphide of about 13,600 moles per canister. To assume such an amount available for corrosion is considered totally unrealistic for several reasons. First, as mentioned above, this type of organic matter would not be easily available for dissolution. Secondly, if it were dissolved, diffusion would limit the transport of either the dissolved organics or any formed sulphide. An illustration of the transport resistance in the bentonite in the backfill could be done by assuming 1D diffusion of sulphide formed at the same location as the organic matter is degraded and dissolved. Using again the simple transport expression for depletion by diffusion results in the depletion front moving 0.5 to 2.8 m in 10^6 years, depending on how the diffusivity and sulphide concentration are represented. This depletion length should be compared to the length of the adequate tunnel section (3 m, being half the distance between adjacent deposition positions) added to the bentonite on top of the canister (at least 2.5 m). This indicates that only a fraction of sulphide formed in the backfill in the case of microbial activity could reach the canister in the assessment time of 10^6 years. A simple 1D diffusion calculation can be performed to estimate the amount of sulphide that could be transported from a position in the tunnel floor to the canister lid where it causes corrosion. Assuming pessimistically that a sulphide concentration of 10^{-4} M could be maintained in the backfill (disregarding any depletion effects), and with the diffusivity set pessimistically as that for an uncharged species, this would give a corrosion depth of 2 mm if assuming corrosion on the lid and the topmost 10% of the canister height.

All other sources of organic matter in the repository are less and the amounts of sulphide that could possibly be produced are insignificant from a corrosion point of view. The organic matter in deposition tunnels and other areas /Hallbeck 2010/ excluding the bentonite organics, corresponds to about 35 moles sulphide per canister. The total organic material in the deposition hole is a factor of 5 lower than the amount in the deposition tunnels, and, again, this is totally dominated by the insoluble organics in the bentonite. Biofilms formed on the rock surfaces, assuming that no cleaning is undertaken before repository closure, would correspond to 11 moles of sulphide per canister from the deposition tunnels. Anaerobic corrosion of rock bolts and other iron components remaining in the repository gives hydrogen gas that could give sulphide via acetogens and sulphate reducing bacteria, as

described in the subsection "Effects of organic materials and microbial processes" in Section 10.2.5. The maximum amount of sulphide produced is estimated to be 353 moles sulphide per canister, by a mass balance. The sulphide is assumed to be directly available for corrosion and no account is taken of hydrogen gas diffusion to the groundwater or the reaction of sulphide with the corroded iron, forming iron(II)sulphide. Again, for illustration purposes these maximum values of possibly produced sulphide can be converted to corrosion depths, assuming evenly spread corrosion all around the canister and neglecting all transport processes. In such a comparison 350 moles sulphide per canister corresponds to a corrosion depth of 300 µm, and 35 moles sulphide corresponds to 30 µm.

The presence of sulphate-reducing bacteria (SRB) in commercial bentonite and their potential to be active after exposure to high temperature and salinity has been shown /Mazurat et al. 2010a/. In further experiments /Mazurat et al. 2010b/ the sulphide production, expressed as Cu_xS, was determined for different bentonite densities, see Figure 10-85. The effect of bentonite density and thereby the swelling pressure can clearly be seen from the experimental data. The installed buffer density in the reference design is 1,950–2,050 kg/m^3 (Section 5.5.3). At a bentonite density of 2,000 kg/m^3 the highest measured copper sulphide production was $0.034 \cdot 10^{-12}$ moles/mm^2 day, which would correspond to a corrosion depth of 0.18 mm in a 10^6 year period, while at a bentonite density of 1,800 kg/m^3 the corresponding values are a measured copper sulphide production of $0.42 \cdot 10^{-12}$ moles/mm^2 day, and a corrosion depth of 2.2 mm in a 10^6 year period. However, the experimental conditions were much more favourable for microbial activity than can be expected in the repository as lactate was added to the experiment as a source of energy and organic carbon. The formation of copper sulphide in this type of experiment has also been shown to be dominated by diffusive transport /Pedersen 2010/. In the experiments by /Mazurat et al. 2010/ it can thus not be excluded that some of the formed copper sulphide stemmed from sulphide diffusing in from the circulating groundwater, and not only from sulphide produced by microbial activity in the bentonite. The values in Figure 10-85 are thus overestimates of the sulphide production in the bentonite for several reasons. The installed density of the backfill would be only about 1,700 kg/m^3 (Section 5.6.3) and microbial sulphate reduction in the bentonite in the backfill could be somewhat higher under these conditions, but would still be very limited, as can be estimated from Figure 10-85. In total, the pessimistic estimates of corrosion caused by microbial activity in buffer and backfill would sum up to about 3 mm.

Although there are uncertainties as to the fraction of organic matter that could be used by sulphate reducing bacteria, the corrosion due to sulphide produced by microbial activity with organic matter in the repository or anaerobic corrosion of steel as energy source is considered to have negligible impact on the copper thickness, even in a 10^6 year perspective.

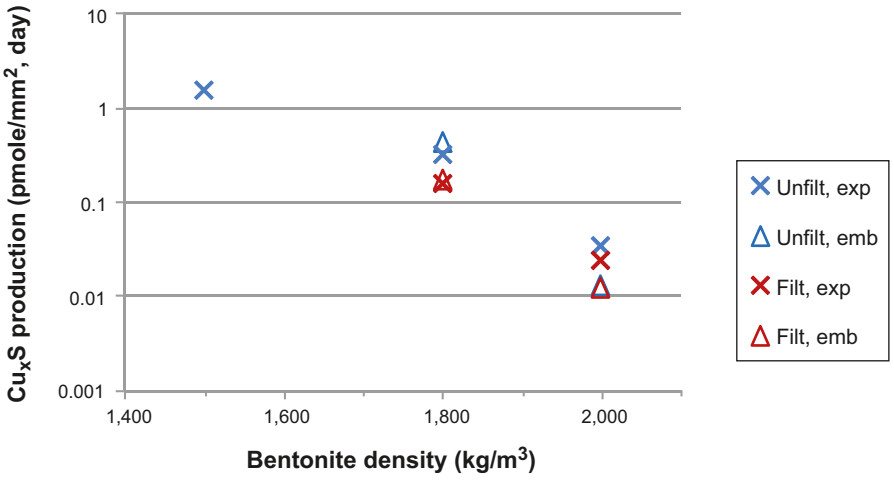

Figure 10-85. *Production rate of Cu_xS on copper test coupons buried in MX-80 bentonite and exposed to unfiltered or sterile-filtered groundwater at the Äspö HRL. The coupons had one end in contact with groundwater (exp) or were fully embedded (emb)(redrawn from /Mazurat et al. 2010b/).*

Sulphide in the groundwater – intact buffer

The hydrogeochemical assessment presented in Section 10.3.7 concludes that the anoxic groundwater conditions now prevailing at repository depth will continue for the whole temperate period following the closure of the repository, in spite of the increasing proportion of meteoric waters with time. The chemical environment surrounding the repository will thus satisfy the criterion for safety function indicator R1a.

For sulphide in groundwater, the transport of the sulphide to the canister surface determines the corrosion rate. The transport resistance consists of different parts, having different importance under different flow conditions. The concept of equivalent flow, Q_{eq}, is the main feature in the conceptual model for the transport for an intact buffer.

The mass transfer between the intact buffer and a flowing fracture intersected by the buffer is schematically depicted in Figure 10-86. The transport description depends on the existence of a thermally induced spalling zone in the rock or not as e.g. shown in Figure 10-34. In summary the transport resistance is modelled as follows. The Q_{eq} derived from the hydrogeological DFN modelling described in Section 10.3.6 is common to both cases (this transport path to/from the deposition hole is nominated Q1 in the hydrogeological modelling as well as in radionuclide transport calculations). Without spalling this resistance is in series with a geometric term taking into account the diffusion in different directions in the bentonite. With spalling, the Q_{eq} is modified such that it takes into account diffusion in the zone with higher conductivity, which reduces the transport resistance between buffer and flowing fracture. A diffusive transport resistance is then added in series to represent diffusion in the rest of the buffer. For the derivation of the equations describing the transport in mathematical terms, see /SKB 2010d/. The amount of sulphide reaching the canister is calculated from the equivalent flow and the sulphide concentration in the groundwater. The corrosion rate is then derived from the amount of sulphide acting on the surface area that is set to the cylindrical part of the canister. Due to the vertical spread of the sulphide in the buffer the sulphide will be more concentrated near the fracture. A factor of 7 (nominated buffer concentration factor, BCF, see /SKB 2010d/) is used to get the highest corrosion rate.

The transport models are then applied for the flow distributions derived from the hydrogeological DFN modelling described in Section 10.3.6. In Figure 10-87 the distribution of corrosion rates for the semi-correlated, uncorrelated and fully correlated hydrogeological base cases are shown, with and without thermally induced spalling. The sulphide concentration is set to $1 \cdot 10^{-5}$ moles/dm^3, which is the 90-percentile of the sulphide distribution measured in Forsmark, see Section 10.3.6. The highest calculated corrosion rate (for the fully correlated hydrogeological DFN base case,

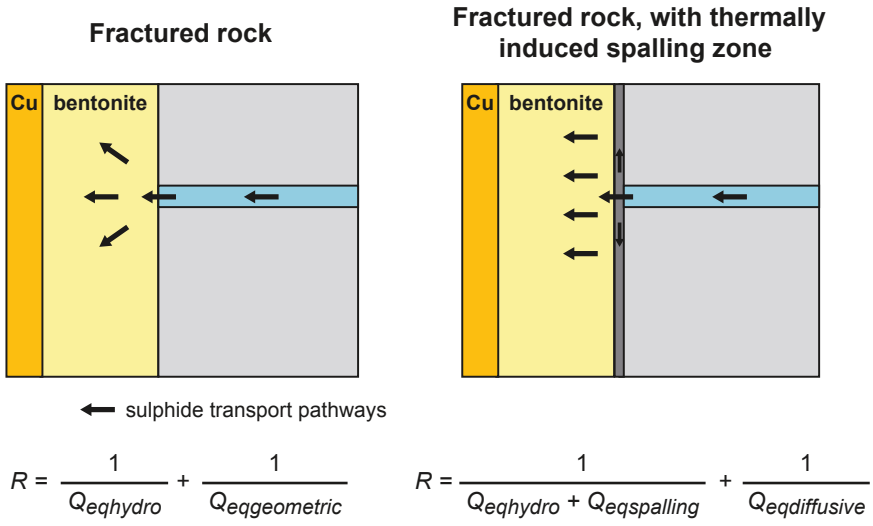

Figure 10-86. *Schematic description of the different transport resistances, for fractured rock and fractured rock with a thermally induced spalling zone.*

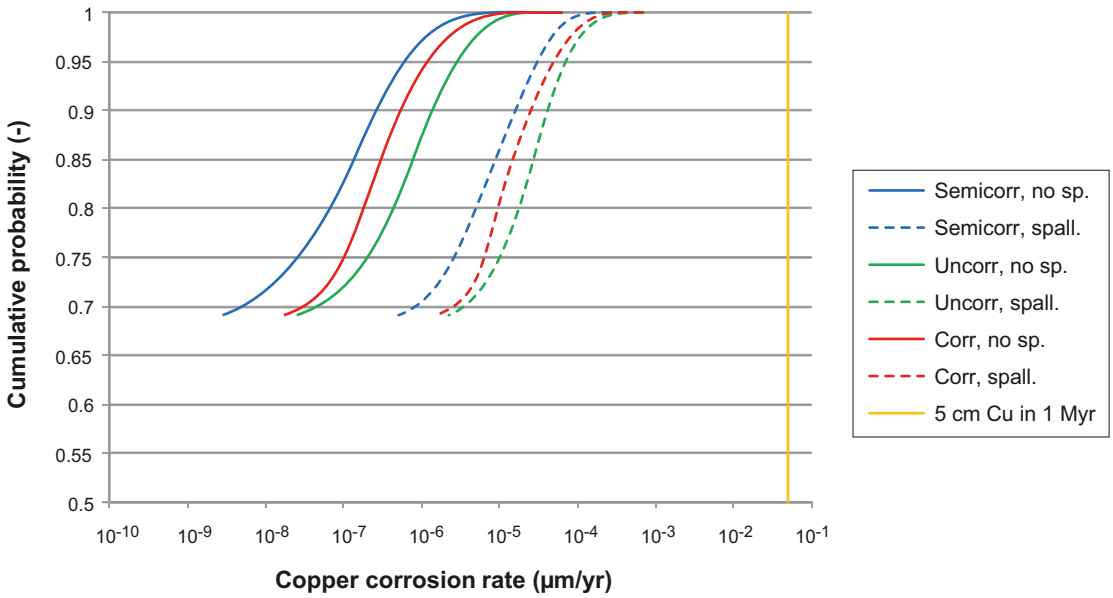

Figure 10-87. *Distribution of corrosion rates for the different Hydrogeological DFN models. The effect of a thermally induced spalling zone is shown. The sulphide concentration is set to $1 \cdot 10^{-5}$ moles/dm³, which is the 90-percentile of the sulphide distribution at Forsmark. Note that nearly 70% of the deposition holes do not have a connected Q1 fracture at all.*

including spalling) corresponds to a corrosion depth of about 0.6 mm in one million years. It must be remembered that the sulphide concentration is set constant over time in these calculations. Even if the highest measured sulphide concentration is used for all the deposition holes, the corrosion depth would be at the most 7.8 mm for the one million year assessment period. This is, however, a totally unrealistic case.

The following should also be noted.

- If several fractures intersect the deposition hole, the equivalent flow rates for these have been added, which is pessimistic since a partition between several fractures would spread the corrosion attack over the canister area.
- All fractures are assumed to intersect the part of the deposition hole where the canister is located.

Corrosion during not fully saturated conditions

During the saturation phase there will be a change from the deposited unsaturated condition to the fully saturated condition. This will cause a range of conditions in the bentonite that will vary both temporally and spatially. The microbial activity in unsaturated bentonite will be restricted by the low water activity (the ratio of the solution's vapour pressure to that of pure water; less than 0.5 at the water contents discussed in /Åkesson et al. 2010a/, which should be compared to the value of 0.96 that is required by SRBs to be active /Motamedi et al. 1996/). In the fully saturated bentonite the microbial activity is restricted by swelling pressure (see above in this subsection 10.3.13 under heading "Sulphate reducing bacteria (SRB) in buffer and backfill"). During the approach to saturation it cannot be excluded that conditions will be more favourable to microbial activity.

As discussed in the above-mentioned subsection only limited amounts of sulphide possibly formed in the backfill can reach the canister due to the limited transport capacity. That capacity would rather be lower in the unsaturated buffer than in the saturated. The phase of partly unsaturated conditions will thus not increase the maximum amount of sulphide reaching the canister. For corrosion processes bounded by mass balances of corrosive agents, there will be no addition from changed saturation conditions.

Advective conditions in the deposition hole

Corrosion under advective conditions in the deposition holes is assessed in Section 10.4.9. According to Section 10.3.11 no deposition holes will lose so much buffer mass by colloid release due to dilute groundwaters such that advective conditions must be assumed during the initial temperate period. (Even if such conditions were to occur, it is shown in Section 10.4.9, that the corrosion is not fast enough to create any failures of the copper shell during the first 100,000 years.)

Summary of copper corrosion analysis

For the corrosion processes analysed for the initial temperate period, the corrosion depth is much smaller than the copper shell thickness. This is the case also for an assessment time of 10^6 years, as illustrated in Figure 10-88. Several processes give corrosion depths less than 100 µm, and no processes give corrosion depths larger than a few mm. The corrosion depths from the different processes should not simply be summed up as their combination requires a far more detailed chemical analysis (as well as statistical analysis regarding the flow and sulphide distributions), but, even if they are cautiously added, the sum is still less than 5 mm.

Identified uncertainties and their handling in the subsequent analysis

The following conclusions are reached regarding copper corrosion during the temperate period.

- The total amount of copper corrosion during the excavation and operational phases and the first 1,000 year period can be estimated to be less than 1 mm. The largest contribution to this estimate comes from the initially entrapped oxygen.
- Copper corrosion by contaminants in the buffer, backfill or groundwater does not pose a threat to canister integrity for the initial temperate period. Even during the one million year overall assessment period, expected corrosion of the canister for an assumed temperate climate would cause corrosion depths of the order of a few millimetres, even for the most unfavourable deposition positions at Forsmark.
- No deposition holes will lose so much buffer mass by colloid release due to dilute groundwaters such that advective conditions must be assumed, meaning that corrosion under advective conditions can be ruled out during the initial temperate period.

Corrosion failure will thus not occur during the initial thermal period.

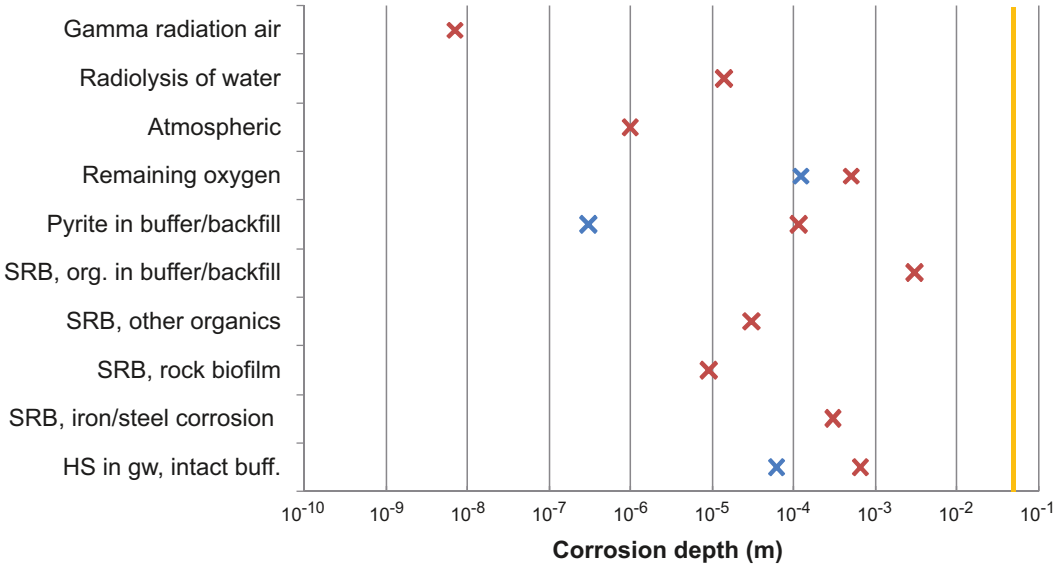

Figure 10-88. *Estimates of corrosion depth from different corrosion processes conceivable in the repository, here shown for an assessment time of 10^6 years. None of these processes causes penetration of the copper shell. Red crosses represent pessimistic assumptions, whereas blue crosses represent more realistic assumptions (where calculations are available). The yellow line indicates the copper thickness of 5 cm.*

10.3.14 Evolution of the central area, the top seal and the borehole plugs

The only function of the closure of the cavities in the central area is to occupy the space with no other design premise than to prevent substantial convergence and subsidence of the surrounding rock. The only purposes of the backfill in the upper part of the ramp and shaft are to hinder unintentional intrusion into the repository and to keep the lower backfill in place. Both these areas are filled with crushed rock with an assumed high hydraulic conductivity.

To ensure that they do not act as preferential transport paths, a number of investigation boreholes, holes drilled both from the surface and from underground openings have to be sealed, at the closure of the deep repository. The design of the borehole seals is provided in the **Closure production report** and outlined in Section 5.7.2. The basic idea is to use bentonite as a seal in the intact rock and low-pH concrete plugs where the boreholes are intersected by fractures.

Central area and top seal

For these areas, in SR-Site, only an assessment of the timescale of the saturation is done. Two different axisymmetric 2D geometries were used: with a true ramp section area and with a true ramp volume, Figure 10-89. The spiral shaped inclined ramp is simply represented with vertical cylinders. In the geometry with a true ramp section area, the section area of the cylinder in the model is the same as in the ramp (33 m^2). However, this also means that the volume of the cylinder in the model is only a tenth of the ramp volume since the ramp has a 10% inclination. A correct ramp volume is therefore represented in the second geometry in which the section area of the modelled cylinder is ten times larger than the actual section area of the ramp.

The first material to reach saturation is the crushed rock in the ramp. The crushed rock in the central area is the second, and the backfill is the last material to get saturated.

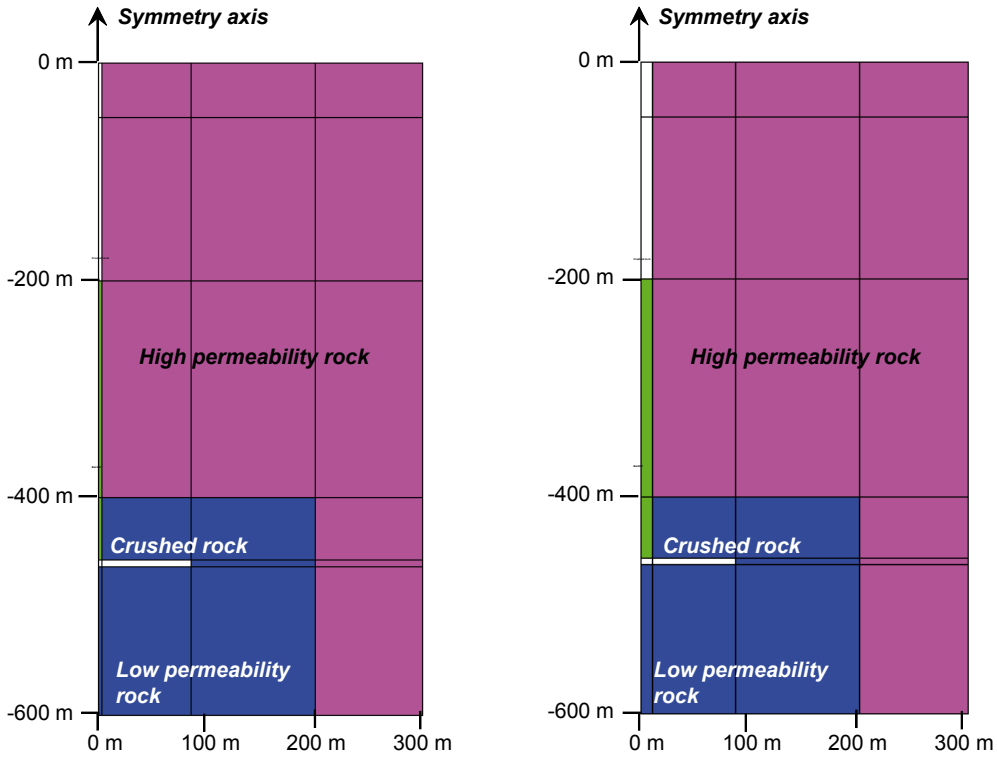

Figure 10-89. *Axisymmetric geometries for the central area and ramp showing true ramp section area (left) and true ramp volume (right) /Åkesson et al. 2010a/.*

According to the chosen approach, the true section area model is relevant for parts in which the filling material limits the inflow, since in this case the hydration is mainly governed by the properties of the filling material and the dimensions of the ramp section. In contrast, the true section volume model is relevant for parts in which the rock limits the inflow, since in this case the main process is basically the transfer of a specific water volume through a large rock volume. With this approach and the available results the following observations can be made.

- The time to saturate the crushed rock in the ramp is mainly governed by the rock. The most relevant time-scale for this is therefore given by the true section volume model, i.e. approximately 20 years.
- The time to saturate the crushed rock in the central area is also mainly governed by the rock. The most relevant time-scale for this is therefore also given by the true section volume model (although the difference is smaller) i.e. approximately 150 years.
- Finally, the time to saturate the backfill in the ramp is mainly governed by the backfill. The most relevant time-scale for this is therefore given by the true section area model, i.e. approximately 200 years.

At the Forsmark site, the timescale for saturating the central area is governed by the flow conditions in the rock, see Section 10.3.6 and Figure 10-23.

Evolution of the borehole seals

Chemical interaction concrete/bentonite

The interaction between the bentonite and the concrete in the borehole seals can be described in the same way as the interaction between the tunnel plugs and the backfill, see Section 10.3.12. The conclusion is that there will be an increase in the pH in the bentonite closest to the concrete, but the duration of the pH pulse and the penetration depth will be small. The cement part of the concrete will degrade with time, but the ballast material will remain. Thereby, the loss of bentonite to the flowing water in the fracture can be assumed to be limited.

According to Table 10-6, the maximum chloride concentration of any time frame is < 0.4 kmol/m^3 in the Forsmark groundwater. As seen in Figure 5-14 this is not expected to have any impact on the properties of the bentonite material. This conclusion is valid for the entire repository evolution period.

Analysis of time scale of borehole seal hydration

The compacted bentonite cylinders are placed in perforated copper tubes to facilitate installation. After installation of the plug, the bentonite will swell through the perforation and further out between the tube and the rock. /Åkesson et al. 2010a/ has calculated the time for water saturation of the seals as a function of the permeability of the surrounding rock. Figure 10-90 shows the saturation time at the 100 m level. At 500 m the time will be even shorter, because of the greater hydraulic pressure.

Even if the rock mass is unfractured, with extremely low permeability, the models indicate that the plug is saturated rapidly. Given that rapid saturation is desirable, the model is assessed to be rather pessimistic in the sense that the time until water saturation is probably overestimated for the lower rock conductivity. It is very unlikely that a disc with 600 m radius has such low rock permeability and is not cut by any fractures. Also, the hydraulic water pressure boundary is located quite far from the borehole (600 m). The adopted model is 1D (radially symmetric) and only radial flow is permitted. Prescribing hydrostatic pressure 600 m away from the borehole induces a very low water pressure gradient which in turn is the only driving force for saturating the borehole seal. Finally, no axial flow is allowed in the borehole, i.e. saturated parts of the seal cannot contribute to the wetting of close unsaturated parts. A less pessimistic assumption with a smaller distance to the boundary would imply faster saturation of the bentonite seal.

Homogenisation of borehole seals

The proposed design of a bentonite plug consists of cylindrical bentonite blocks that are compacted to a height of about 5 cm and placed inside a perforated copper tube. In order for the plug to function properly in a borehole the swelling ability of the bentonite must be strong enough to expand through the holes and penetrate behind the walls of the perforated tube. This expansion and penetration has been analysed with analytical solutions and the results evaluated by /Åkesson et al. 2010a/.

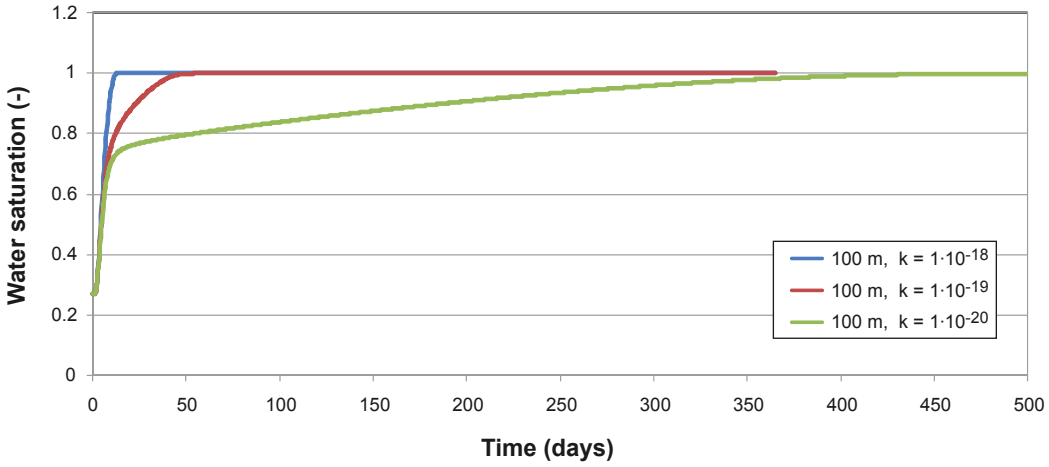

Figure 10-90. *Water saturation evolution of bentonite borehole seals for different rock permeability (m^2), 100 m depth model with a radius to water bearing boundary of 600 m.*

The bentonite will swell at first radially through the holes in the perforated copper tube and then tangentially between the copper and the rock surface (see Figure 10-91b). It is important that the swelling pressure from the bentonite inside the copper tube σ_0 can be transferred to the rock with a swelling pressure σ_1 and further through the gap behind the copper with a swelling pressure σ_2 and that these stresses must be high enough to result in good sealing.

The calculated influence of the friction angle and the radius of the perforation holes on the lowest swelling pressure between the copper tube and the rock surface is illustrated in Figure 10-92. The figure shows that a radius of 5 mm for the perforation holes yields the highest minimum swelling pressure and that the influence of the friction angle from 10 to 20 degrees is very strong, but if the density of the bentonite inside the tube is high enough to yield a swelling pressure of about 10 MPa, the drop in swelling pressure behind the tube is so small that the friction angle will not exceed 10 degrees. However, if the initial density is lower (due to e.g. loss of bentonite during installation), the friction angle may increase significantly and thus affect the resulting lowest swelling pressure.

The results show that the loss in swelling pressure is acceptable and yields a high enough density to fulfil the requirements of the plugs, provided that not too much material is lost during installation. The strength of the model is that the actual swelling can and has been tested in simulated boreholes with geometry, material and conditions that are very similar to the real ones.

Homogenisation of borehole seals after loss of bentonite

If bentonite in a section of a borehole seal is lost to such an extent that the hole will be empty along a certain length the swelling ability of the bentonite will make the adjacent bentonite swell and fill up the empty space. However, friction in the bentonite prevents complete homogenisation. /Åkesson et al. 2010a/ has calculated the homogenisation of the bentonite in a seal for a case where a part of the bentonite has been lost. Figure 10-93 describes the situation at equilibrium after bentonite over the length L has been lost and swelling and homogenisation have taken place. The path and time to achieve that equilibrium are not addressed.

The calculations show that the swelling pressure and thus the density will decrease very fast. At e.g. the distance z = 1 m (corresponding to a 2 m long empty part) the swelling pressure will, for the hole diameter of 70 mm, the original swelling pressure of 10 MPa and a friction angle $\varphi = 20°$, be $\sigma = 9 \cdot 10^{-3}$ Pa which is so low that the properties of the bentonite practically corresponds to water. If 1 kPa is set as a limit at which there is a gel, the corresponding swelling distance, the length where there will be a density gradient, will be 0.44 m. A sensitivity analysis on this limit and the friction angle shows that the swelling distance can vary between ~0.3–1 m. This means that a part of the "unaffected" borehole close to the boundary will decrease in density and a part of the "empty" borehole will increase its density. The density gradient is not linear and depends on the relation between density and swelling pressure, which has not been measured below about 10 kPa swelling pressure.

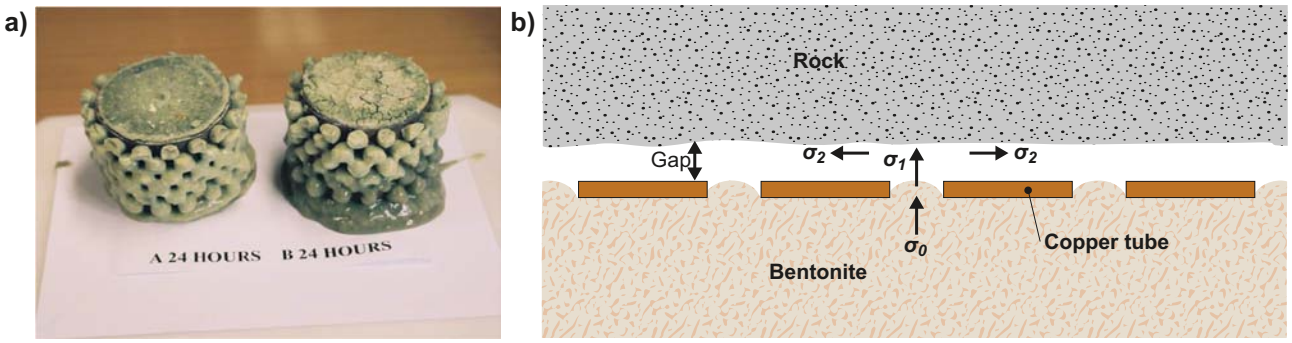

Figure 10-91. *a) Photograph of bentonite swelling through a perforated copper tube (from /Pusch and Ramqvist 2004/). b) Schematic view of the swelling of bentonite through the perforated copper tube (horizontal borehole). The original swelling pressure of the bentonite σ_0 is reduced to σ_1 when it swells through the holes to the rock and further to σ_2 when it swells behind the copper (redrawn from /Åkesson et al. 2010a/.*

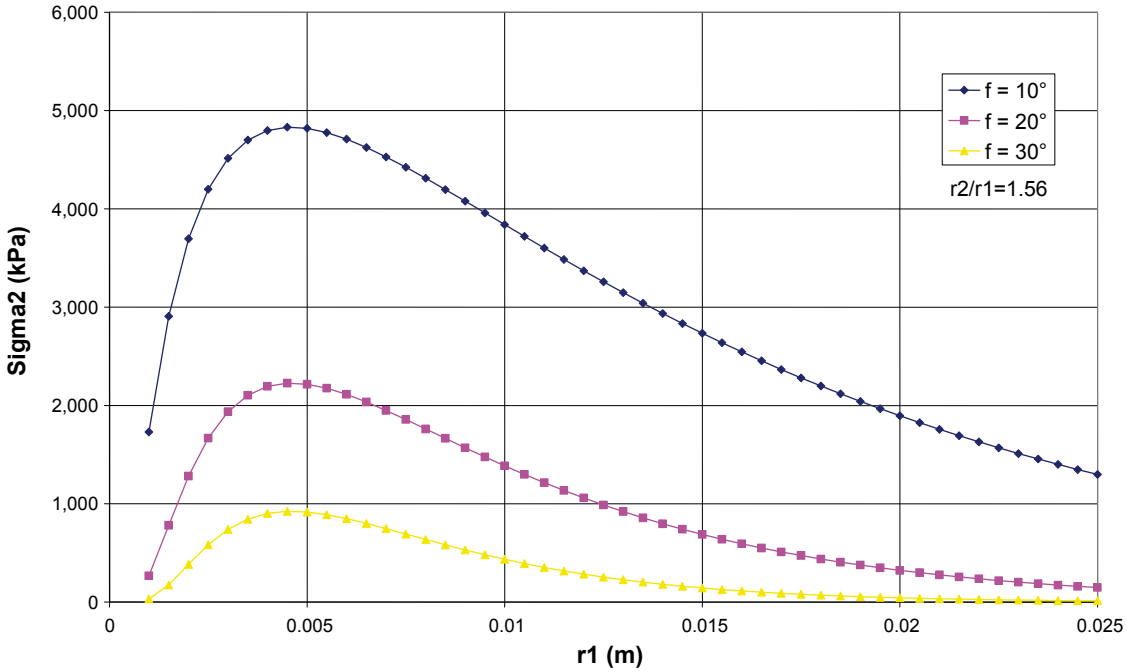

Figure 10-92. *Calculated minimum swelling pressure behind the copper tube as function of the radius of the perforation holes for different friction angles. /Åkesson et al. 2010a/.*

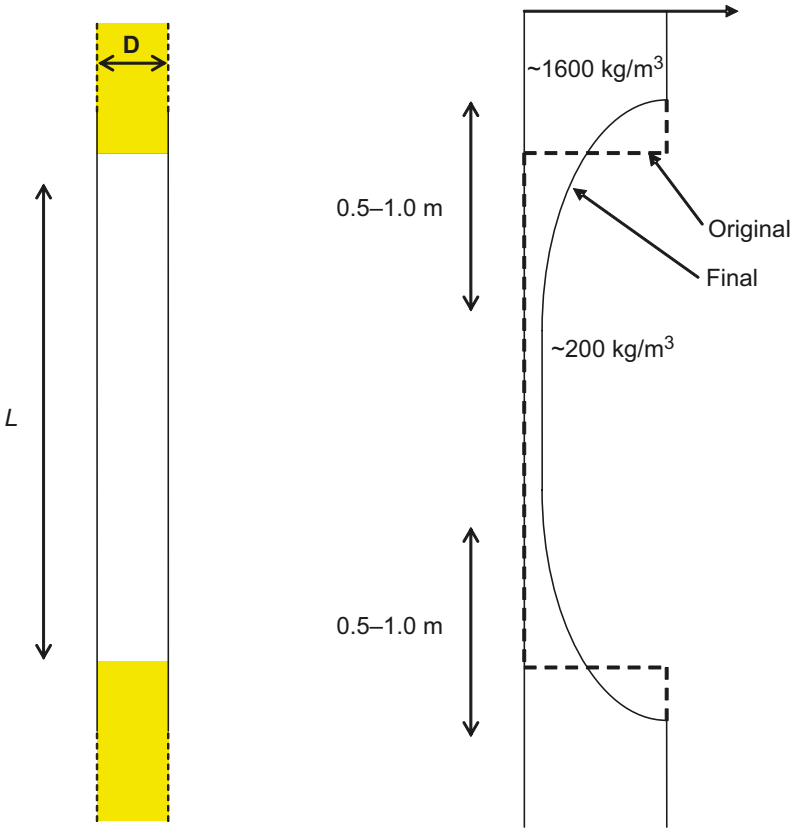

Figure 10-93. *Illustration of the density distribution in a borehole where the bentonite has been lost along the length L /Åkesson et al. 2010a/.*

A rough estimate is that 20–30% of the swelling distance *z* is taken from the "unaffected" part and the rest of the length *z* fills up the "empty" part. The remaining part of the borehole will be unfilled or filled with a very loose sol produced by down falling bentonite particles. The calculations and reasoning thus show that if a borehole sealed with bentonite loses bentonite along a length of more that 1–2 m the situation after equilibrium will be similar to the situation in the right side of Figure 10-93.

Identified uncertainties and their handling in the subsequent analysis

The saturation time for the central area and the ramp and shaft are not used further in the assessment. The aim of the calculations reported in this section was to get a reasonable estimate of the duration of the process.

The reference design of the borehole seals will perform as intended, since:

- The saturation is relatively rapid, full saturation can be expected in less than a year even in a very dry part of the rock,
- The swelling ability of bentonite cylinders is sufficient to penetrate through the perforations in the copper tube and to generate an adequate swelling pressure against the rock,
- The chemical interaction between the concrete plugs and bentonite will have limited or no effect on the integrated performance.

A loss of bentonite over a range of a few metres in the seals will lead to a total loss of performance in that section. However, the rest of the seal will be virtually unaffected.

10.3.15 Summary of the first 1,000 years after closure

The heat from the spent fuel results in a fast temperature increase in the buffer, with peak temperature occurring some 5–15 years after deposition, followed by a slow reduction of the temperature due to the decay of the heat source. The analyses presented in Section 10.3.4 show that there is an adequate margin to the peak temperature criterion for the buffer, even when the spatial variability of the rock thermal properties is taken into account and with other data essential for computing the result chosen pessimistically. This conclusion is valid provided there is thermal management of the disposal sequence, such that the influence of already deposited canisters would not unduly affect the thermal evolution of canisters deposited later, see also Section 15.5.15. Such management is judged fully feasible and there is no need to consider a situation with a buffer above the peak thermal criterion in SR-Site.

The mechanical evolution of the host rock is dominated by effects of the thermal load from the canisters and, to a minor extent, the developing swelling pressure from the buffer and the backfill. The long-term impact of the rock stress field need also to be taken into account. According to Section 10.3.5, the following conclusions concerning the mechanical evolution can be drawn.

- *Reactivation of fractures in the near field as well in the far field* due to thermal load that could affect the mechanical stability and the fracture transmissivity in the rock are excluded from further analysis since the calculated impacts on fracture transmissivity during the heating phase are small, and very local to the deposition tunnel.
- *Reactivation due to ongoing Mid-Atlantic Ridge push* that could affect the mechanical stability of the deposition holes (safety function R3a) cannot be totally ruled out even during the temperate period. According to the earthquake analysis presented in Section 10.4.5, on average between $9.3 \cdot 10^{-6}$ and $2.2 \cdot 10^{-5}$ canisters may be sheared 50 mm or more due to earthquakes within the 1,000-year time frame.
- *Fracturing of the rock, i.e. thermally induced spalling*, is likely to occur but the counter pressure exerted by bentonite pellets in the slot between buffer and rock wall, may suppress the spalling, or at least keep the spalled slabs in place and minimize the hydraulic transmissivity of the spalled damage zone. A set of distinct calculation cases, assuming no spalling or spalling in all deposition holes, are propagated for further assessment. The potential for spalling might to some extent depend on the deposition sequence and other aspects of the design, see further Section 15.5.15.
- Literature evidence suggests that there is no potential for *creep* deformation that could significantly affect deposition hole geometry, allowing the exclusion of the phenomenon from the safety assessment.

Analyses of the hydraulic evolution of the system indicate that after repository closure a rapid initial inflow is followed by an asymptotic regime where the inflow gradually decreases. It will take several hundred of years for the repository to reach full saturation.

Detailed regional and repository scale groundwater flow analyses for the saturated host rock indicate that the Forsmark site has favourable properties in terms of performance measures related to groundwater flow and transport, using either of the models. Specifically, the transport resistance of the host rock, the so called *F*-factor, ranges between 10^4 and 10^9 y/m depending on the spatial location, and about 90% of all potential deposition holes have *F* values above 10^6 y/m. Distributions of Darcy fluxes and equivalent flow rates for use in subsequent analyses have also been obtained and show favourable properties. It can be noted that at least 70% of all potential deposition holes are not connected to any water bearing fractures, which implies that the hydraulic contact with these holes primarily is by diffusion to the EDZ (if it exists) and to the deposition tunnel. The models also yield salinity distributions and handle mixing of different water types yielding concentrations of other relevant non-reacting components of the groundwater. All these results are propagated to subsequent analyses of engineered barrier performance and radionuclide transport.

The analysis of the evolution of the geochemical conditions at the site has resulted in the following conclusions.

- Anoxic conditions are expected to be re-established shortly after closure and will continue for the whole temperate period following the closure of the repository, in spite of the increasing proportion of meteoric waters with time.

- The maximum salinity is expected during operations and immediately after closure. The salt content is expected to decrease slightly during the first 1,000 years due to the progressive inflow of waters of meteoric origin.
- Cation charge concentrations at repository depth at Forsmark will, in general, remain higher than 0.004 mol/L, i.e. above to the limit where montmorillonite colloids start to become unstable, but a fraction of a percent of the deposition holes may experience dilute conditions during the first ten thousand years.
- The effect of grout in fractures will be to increase the pH in deformation zones to values ≈ 9 for relatively long periods of time, probably lasting throughout the first glacial cycle (≈ 120,000 years).

Since the rock at Forsmark is expected to contain very few water conducting fractures, typically separated by more than 100 m, the saturation of the backfill can be anything from < 100 years to ~6,000 years, the longer times being for positions far away from the flowing fractures. As for the saturation of the backfill, the time for the saturation of the buffer is strongly dependent on the local hydraulic conditions. The presence of a water conducting fracture in, or in the vicinity of, the deposition hole will lead to a relatively rapid saturation, while a position where the water is supplied solely by the rock may stay partially saturated for hundreds of years. Given the expected very low frequency of water conducting fractures at Forsmark the saturation of the buffer can be anything from < 10 years to ~1,000 years, the longer times for holes not connected to water conducting fractures. Furthermore, the moisture redistribution in the buffer in deposition holes with a dry surrounding rock mass affects the thermal conductivity of the buffer. This is considered in the assessment of the thermal evolution of the buffer.

If the buffer and backfill are installed as envisaged in the reference design, the buffer density and swelling pressure will homogenise to a situation where the relevant safety functions will be upheld. The saturation of the buffer will result in the establishment of a swelling pressure of typically 7–8 MPa. The pressure will be somewhat reduced in the upper part of the buffer, but this effect is calculated to be too small to jeopardise any of the buffer safety functions.

The geochemical changes in the buffer during the period of saturation and thermal gradient are small and are not considered to have any significant impact on the long-term performance. There will be dissolution/precipitation of accessory minerals like calcium sulphates and amorphous SiO_2.

In the reference evolution, both the pH and temperature in the buffer are assumed to be within the given limits on the basis of our assessment and the alteration in these characteristics is not expected to proceed to a level where it will affect the properties of the buffer. Alteration is therefore treated as a separate scenario.

The bottom plate in a deposition hole may degrade, which will impact on the mass transfer resistance in the near field. However, the impact is less than the impact from assuming spalling in the deposition hole and this effect is thus covered by adoption of the assumption of considering spalling to occur in all deposition holes.

The model predictions indicate that the durability of backfill materials is not expected to be affected by the potential alkaline plumes developed from concrete alteration of the deposition tunnel plug. Even if the plug was to disintegrate this has no detrimental effect on the backfill above the first deposition hole and no restrictions caused by plug disintegration on the location of the first deposition hole are needed.

The saturation time for the central area and the ramp and shaft are not used further in the assessment. The aim of calculations performed in this section was to get a reasonable estimate of the duration of the process.

The reference design of the borehole seals will perform as intended. The saturation is relatively rapid, full saturation can be expected in less than a year even in a very dry part of the rock. A loss of bentonite in the range of a few metres in the seals will lead to a total loss of performance in that section. However, the rest of the seal will be virtually unaffected.

The mechanical load on the canisters from the swelling buffer and the groundwater pressure is far too low to jeopardise canister integrity.

Canister corrosion from initially present oxygen and sulphide, from corroding agents formed by radiolysis and from sulphide in ingressing groundwater, has been found to be negligible (less than 1 mm).

10.3.16 Safety functions for the initial temperate period after closure

The following is an account of the development of all safety functions in Figure 10-2 during the initial temperate period after repository closure. Also the development during the excavation/operational period is considered where relevant.

Rock safety functions

R1. Provide chemically favourable conditions

a) Reducing conditions; Eh limited.
The analyses have lead to the conclusion that the chemical conditions will be reducing shortly after deposition in individual deposition holes and deposition tunnels and shortly after closure in the repository as a whole. This is of fundamental importance for the long-term safety of the repository and no process has been identified that challenges this conclusion during the initial temperate period after closure.

b) Salinity; TDS limited.
The salinity at the Forsmark site has, through model studies, been demonstrated to be below 12 g/L, corresponding to 0.2 M [Cl^-]. Upconing effects on salinity during the excavation/operational phase have also been studied and found to be negligible.

c) Ionic strength; $\Sigma q[M^{q+}] > 4$ mM charge equivalent.
For the whole temperate period following repository closure, the cation charge concentrations at repository depth at Forsmark will, in general, remain higher than 0.004 mol/L. However, a fraction of a percent of the deposition holes may experience dilute conditions during the first ten thousand years.

d) Concentrations of HS^-, H_2, CH_4, organic C, K^+ and Fe; limited.
During the initial temperate domain following repository closure, the potassium concentrations are expected to remain ≤ 0.004 mol/L, sulphide concentrations are expected to be $\leq 10^{-5}$ mol/L for most deposition positions, including the possible contributions from bacterial sulphate reduction using dissolved methane, hydrogen and organic carbon. Iron concentrations are expected to gradually increase up to 10^{-4} mol/L.

e) pH; pH < 11.
The effect of grout in fractures will be to increase the pH in deformation zones to values ≈ 9 for relatively long periods of time, probably lasting throughout the first glacial cycle (≈ 120,000 years).

f) Avoid chloride assisted corrosion; pH > 4 and [Cl^-] < 2 M.
The hydrogeochemical analysis shows that these safety function indicator criteria are fulfilled throughout the initial temperate period.

R2. Provide favourable hydrologic and transport conditions

a) Transport resistance in fractures, *F*; high.
The transport resistance essentially depends on the connected fracture transmissivity and the hydraulic gradient. As demonstrated in Chapter 4 there are few transmissive water conducting fractures at repository depth at Forsmark. Currently, hydraulic gradients are low since they are controlled by the very flat topography at Forsmark. This means that transport resistance is generally high although there are a few flow paths of lower transport resistance. The calculated transport resistance of the host rock ranges between 10^4 and 10^9 y/m depending on the spatial location, and about 90% of all potential deposition holes have *F* values above 10^6 y/m.

During excavation there is a potential for inducing new fractures forming an "EDZ". However, provided the blasting is well controlled, there is ample evidence that a potential EDZ formed during excavation will be kept below the maximum allowed transmissivity as set out in the design premises and data suggest that a continuous EDZ would not develop at all. It seems justified to consider an EDZ according to the design premises, but also to explore how transmissive an EDZ would need to be in order to significantly impact other safety functions as well as exploring the impact of no axially continuous EDZ at all. There is some reactivation of fractures due to thermal load but the impact on the fracture transmissivity is small and can be neglected from further analysis. As a base case it is assumed that the EDZ has a transmissivity of 10^{-8} m^2/s. Assuming no EDZ implies an increase in *F* of about half an order of magnitude. Assuming a much more transmissive EDZ (10^{-6} m^2/s) decreases *F* by about an order of magnitude.

b) Equivalent flow rate in buffer/rock interface, Q_{eq}; low.
The equivalent flow rate in the buffer/rock interface essentially depends on the groundwater flow around the deposition hole and the local geometry of the flow. The former is affected by the same things that affect the transport resistance; there is thus also a need to consider changes of the local geometry of the flow around deposition holes. It can be noted that at least 70% of all potential deposition holes are not connected to any water bearing fractures, which implies that the hydraulic contact with these holes primarily is by diffusion to the EDZ (if it exists) and to the deposition tunnel.

As for the transport resistance, it thus seems justified to consider an EDZ according to the design premises, but also to explore how transmissive an EDZ need to be in order to significantly impact other safety functions as well as exploring the impact of no axially continuous EDZ at all. Naturally, only release path Q2, i.e. through the potential EDZ, is affected by the transmissivity of the EDZ. Roughly, Q_{eq} for this release path is proportional to the square root of the EDZ transmissivity.

For assessing Q_{eq} it is also necessary to consider the impact from fracturing (spalling) in the deposition hole wall. This can occur either as a direct result of the mechanical impact resulting from the process of excavation, in which case it can be mitigated, or as a consequence of the thermal load from the spent fuel after deposition. It has been concluded that thermally induced spalling is likely to occur, but the counter pressure exerted by bentonite pellets in the slot between buffer and rock wall may suppress the spalling, or at least keep the spalled slabs in place and minimize the hydraulic transmissivity of the spalled damage zone. A set of distinct calculation cases, assuming no spalling or spalling in all deposition holes, are propagated for further assessment and must be considered in all quantitative treatments of mass transfers between buffer and rock. Spalling affects Q_{eq} only if there is a water conducting fracture intersecting the deposition hole, i.e. the migration path Q1. Spalling implies that Q_{eq} for the Q1 path increases by about a factor of 100.

R3. Provide mechanically stable conditions

a) GW pressure; limited.
The groundwater pressure is determined by repository depth for temperate climate conditions. It is hence around 4.5 MPa at the repository depth, which, from the point of view of long-term safety, is not problematic.

b) Shear movements at deposition holes < 0.05 m.
According to the earthquake analysis presented in Section 10.4.5, large seismic events are highly improbable, but cannot be totally excluded even during the thermal period. Based on the analyses presented, on average between $9.3 \cdot 10^{-6}$ and $2.2 \cdot 10^{-5}$ canisters may be sheared 50 mm or more due to earthquakes within the 1,000-year time frame, i.e. there is a chance of at most about 1 in 40,000 that one out of the 6,000 canisters will be sheared by an earthquake within 1,000 years. This frequency will be similar for the remaining part of the initial temperate period, i.e. the expected number of potentially sheared canisters scales linearly with time.

c) Shear velocity at deposition holes < 1 m/s
This criterion will always be upheld, as is further justified in Section 10.4.5.

R4. Provide thermally favourable conditions

a) Temperature > −4°C (avoid buffer freezing)

b) Temperature > 0°C (validity of canister shear analysis)

Since a temperate climate similar to the current is assumed to prevail during the temperate time period under consideration, there is no possibility that these criteria would not be fulfilled.

Buffer safety functions

Several of the buffer safety functions are related to the buffer density. The initially allowed range of saturated density of 1,950–2,050 kg/m^3 may potentially alter during the initial temperate period due to erosion related to piping during the resaturation of the buffer and backfill, upward expansion of the buffer as a consequence of swelling and colloid release in the long-term.

For the majority of deposition holes, no losses due to piping are expected since the inflow of groundwater is expected to be too low to cause piping. For holes with a significant inflow of groundwater during saturation the losses will be higher. The calculations of the swelling and homogenisation of a half torus resulting from erosion show that the swelling yields a strong decrease in density and swelling pressure in the eroded volume due to the friction in the bentonite. However, the swelling pressure after completed homogenisation is in none of the cases with torus radius varying from 3.4 cm to 13.4 cm below 1 MPa. The influence of the radius seems to be insignificant due to the long distance to the bentonite boundaries. If half a sphere is created instead of a torus the consequences are more severe, since the radius of the sphere is larger for the same amount of bentonite and thus the mass of bentonite left between the half sphere and the canister much less. However, in 2/3 of the distance between the canister and the rock the buffer has a swelling pressure higher than 1 MPa for the case corresponding to the volume of the 3.4 cm radius half torus. The conclusion is thus that about 100 kg of dry bentonite may be lost due to erosion without jeopardising the function of the buffer. The effect is strong, but the case of point erosion rather unlikely. Losses larger than 100 kg of dry bentonite are not possible since potential deposition holes with too high inflow are avoided, see Section 5.2.1, and need thus not be further assessed in SR-Site. However, the uncertainty in the assessment of the eroded volume needs to be considered when revising the design premises for acceptable inflow to deposition holes.

All deposition holes are expected to experience some loss of buffer density due to swelling and upward expansion of the buffer. This phenomenon has been analysed through a number of calculations that demonstrate that buffer density at the canister top will remain within the reference interval of 1,950–2,050 kg/m^3 after buffer swelling and expansion.

At the later part of the initial temperate period, i.e. after 10,000 years, a fraction of a percent of the deposition hole positions may experience dilute conditions such that buffer colloids are formed and released. However, given the slow erosion rate, no deposition holes are expected to reach advective conditions during the initial temperate period.

Buff1. Limit advective transport

a) Hydraulic conductivity < 10^{-12} m/s.
For deposition holes with reference design buffer density, the hydraulic conductivity criterion is fulfilled with ample margin for the range of groundwater salinities that can be expected during the initial temperate period.

b) Swelling pressure > 1 MPa.
For deposition holes with reference design buffer density, the swelling pressure criterion is fulfilled with ample margin, again for the range of groundwater salinities that can be expected during the initial temperate period.

These conclusions also hold for deposition holes affected by piping.

Buff2. Reduce microbial activity

For this safety function to be fulfilled it is required that the buffer density is high. For the initial temperate period, the analyses of possible loss of buffer mass and groundwater salinities have demonstrated that the buffer density will remain high, as long as the buffer is installed according to the reference design.

Buff3. Damp rock shear

For this safety function to be fulfilled it is required that the saturated buffer density is less than 2,050 kg/m^3. According to the reference design, 2,050 kg/m^3 is the upper allowed bound and fulfilment of this requirement is discussed in Section 5.5.3. No relevant processes that would increase the buffer density have been identified, so it is concluded that this safety function is fulfilled for all deposition holes.

Buff4. Resist transformation

For this safety function to be fulfilled, it is required that the buffer temperature is less than 100°C. It has been demonstrated that there is an adequate margin to the peak temperature criterion for the buffer, even when the spatial variability of the rock thermal properties is taken into account and with other data essential for computing the result chosen pessimistically.

Buff5. Prevent canister sinking

For this safety function to be fulfilled, it is required that the buffer swelling pressure exceeds 0.2 MPa. This is less than the fulfilled criterion (> 1 MPa) for Buff1b and the canister sinking criterion is thus fulfilled with ample margin.

Buff6. Limit pressure on canister and rock

a) Swelling pressure < 15 MPa.
With buffer and backfill selected and installed according to the reference design, the swelling pressure may vary between 4.5 and 13 MPa, with account taken for the allowed variations in density and provided that the buffer material is fully confined to the volume it occupies at deposition. Since no process is identified where the buffer material will be added during the initial temperate stage the maximum swelling pressure criterion will be upheld.

b) Temperature > −4°C.
Since a temperate climate similar to the current is assumed to prevail during the time period under consideration, there is no possibility that this criterion would not be fulfilled.

Backfill safety functions

BF1. Counteract buffer expansion

For this safety function to be fulfilled it is required that the density of the backfill material is sufficiently high. As shown in Section 10.2.4, the largest possible erosion due to piping will be 1,640 kg. Erosion in the backfill will basically mean that material is redistributed within the tunnel itself. Considering the large mass of backfill in the tunnel a redistribution of 1,640 kg can be assumed to have no impact at all on the backfill performance.

Even though dilute conditions may occur in some of the more transmissive single fractures intersecting a deposition tunnel, at the later part of the initial temperate period, these conditions will not cause erosion to the extent that this will result in such a loss of swelling pressure above deposition holes that these in turn would enter an advective condition.

Canister safety functions

Can1. Provide corrosion barrier

For this safety function to be fulfilled, it is required that the minimum copper coverage exceeds zero. This safety function will be upheld throughout the initial temperate period. The total amount of copper corrosion during the excavation and operational phases and the first 1,000 year period can be estimated to be less than 1 mm, when taking into account the contributions from residual oxygen in the repository, from corroding agents formed by radiolysis and from possible microbial sulphate reduction as well as the contribution from sulphides in the bentonite and backfill. Copper corrosion by contaminants in the buffer, backfill or groundwater does not pose a threat to canister integrity for the initial temperate period and, even during the one million year overall assessment period, expected corrosion of the canister for an assumed temperate climate would cause corrosion depths of the order only of a few millimetres, even for the most unfavourable deposition positions at Forsmark. No deposition holes will lose so much buffer mass by colloid release due to dilute groundwaters that advective conditions must be assumed, meaning that corrosion under advective conditions can be ruled out during the initial temperate period.

Can2. Withstand isostatic load

For this safety function to be fulfilled, it is required that the canister withstands isostatic loads up to 45 MPa. The fulfilment of this safety function is assured by the design of the canister, see Section 5.4.3 and the **Canister production report** for further details. It may also be noted that during the initial temperate period, the isostatic loads consist of the groundwater pressure of 4–5 MPa and the swelling pressure of the buffer that is estimated at maximally 13 MPa for the reference buffer density interval. This is considerably less than 45 MPa, i.e. no canisters will fail due to isostatic load.

Can3. Withstand shear loads

The canister is designed to withstand a fracture shearing of 50 mm, see Section 5.4.3 and the **Canister production report** for further details. As further discussed in Section 10.4.5, on average between $9.3 \cdot 10^{-6}$ and $2.2 \cdot 10^{-5}$ canisters may be sheared 50 mm or more due to earthquakes within the 1,000-year time frame.

Status of buffer/backfill after the thermal and saturation phase

The buffer and, to a lesser extent, the backfill goes through a unique transient thermal and saturation phase in the first few hundred years after deposition. The status of these components after this transient phase is not expected to change much thereafter, meaning that the initial state, in combination with the alterations occurring during the transient phase, to a large degree determine the long-term properties of the buffer and the backfill. Therefore, a specific account of the expected status of the buffer and the backfill after the thermal and saturation phase is given here.

The buffer and the backfill will be deposited as blocks and the gaps between the blocks and the rock are assumed to be filled with bentonite pellets. Water from the rock will enter into the pellets and come into contact with the blocks. The bentonite will take up water and swell. From the time of deposition, the residual heat from the waste will increase the temperature in the near field of the repository. Temperature differences of up to 20 degrees will occur across the buffer for typically 100 years. Elevated temperatures in the near field are expected for about 1,000 years. During this period, the buffer and backfill are expected to evolve as described earlier in this section. The expected final state after the thermal and saturation phase is as set out below.

- After a period of < 100 years to ~6,000 years the buffer is expected to be fully saturated. During the period over which saturation is achieved, the buffer will swell and exert a swelling pressure on the canister, the rock and the backfill. The pressure is too low to have any effect on the canister and rock, but the backfill will deform to a certain extent. This will lead to a small loss of swelling pressure in the top of the deposition holes, but the pressure exerted by the buffer around the canister is expected to remain at its initial value.
- The hydraulic gradients in the unsaturated repository may cause piping and erosion of the buffer and backfill. This may lead to a loss or redistribution of material, but the losses will not jeopardize the function of the buffer nor the backfill.
- The increased temperature in, and the thermal gradient over, the buffer may lead to redistribution of minerals. $CaCO_3$ could be enriched close to the canister. The movement of compounds of silica is expected to be negligible.
- The maximum temperature increase and the maximum duration of increased temperature are well below the limits that might cause any significant transformation of the montmorillonite.
- Groundwater from the site will enter into the buffer and mix with the original porewater. This will yield a new composition for the buffer water. Both the composition of the original bentonite and the water from the site are sufficiently well known that the new composition can be estimated.
- At the later part of the initial temperate period, i.e. after 10,000 years, a fraction of a percent of the deposition hole positions may have dilute conditions such that buffer colloids are formed and released. However, given the time it takes for such erosion, no deposition holes will reach advective conditions during the initial temperate period.
- Even if dilute conditions may occur in some of the more transmissive single fractures intersecting a deposition tunnel, at the later part of the initial temperate period, none of them will cause erosion to the extent that this will cause such loss of swelling pressure above deposition holes that these in turn would enter an advective condition. For a few positions where the fracture is connected to a deformation zone, potentially more than 220 tonnes could be lost in a million year perspective, but this is not relevant from the point of view of canister integrity.

In summary, for all identified processes occurring in the buffer and backfill during the saturation and thermal phase the consequences have been estimated. The conclusion is that none of these phenomena will jeopardize the long term performance of the buffer and backfill.

Conclusions for radionuclide transport

The following conclusions for radionuclide transport have been drawn.

1. Large earthquakes cannot totally be ruled out even for the initial temperate period. There is a chance of at most about 1 in 40,000 that one out of the 6,000 canisters will be sheared by an earthquake within 1,000 years. This frequency will be similar for the remaining part of the initial temperate period, i.e. the expected number of potentially sheared canisters scales linearly with time.
2. The EDZ developed during construction needs to be considered in the radionuclide transport analyses.
3. The hydrogeological analyses have provided distributions of F, t_w and Q_{eq} to be used in radionuclide transport calculations.
4. The geochemical assessments have provided geochemical conditions for which retention properties in the host rock for radionuclide transport can be derived.
5. The buffer assessments have provided buffer conditions for which retention properties in the buffer for radionuclide transport can be derived.
6. Spalling may affect the equivalent flow rates, Q_{eq}, in deposition holes.
7. The pH increase from cement leaching may affect geosphere retention in larger, grouted fractures.

10.4 The remaining part of the reference glacial cycle

This section presents the evolution for the remaining part of the 120,000 year long reference glacial cycle, essentially a repetition of the conditions reconstructed for the Weichselian. It is important to note that the model reconstruction of the Weichselian, constituting the reference evolution, should be regarded as one example of a credible evolution during a glacial cycle. The description is not an attempt to predict a most probable future evolution. It is a simplified 'best estimate' of the Weichselian evolution, focusing on aspects of relevance for repository safety, and used as a scientifically defensible starting point for the analysis of climate impacts on repository safety. It is complemented by additional climate cases with a potentially larger impact on repository safety, analysed in other safety assessment scenarios.

Figure 7-4 in Section 7.5 shows the assessment model flow chart, AMF, for permafrost and glacial conditions giving an overview of the modelling and other assessment studies for these periods.

10.4.1 Reference long-term evolution of climate related conditions

Model reconstructions of last glacial cycle conditions, including the Weichselian ice sheet, are chosen as reference glacial cycle and reference evolution in the SR-Site main scenario, see Figure 10-94. The rationale for this is given in Sections 6.2 and in Chapter 11. The evolution of the repository is mainly affected by the evolution of climate-related conditions e.g. shore-level variations and development of permafrost and ice sheets, whereas the climate as such at the ground surface, is of secondary importance for repository safety. On the basis of conditions and processes of importance for repository safety, three characteristic *climate domains* (see further Section 6.2.3) that can be expected to occur in Sweden in a 100,000-year time perspective were identified:

- Temperate climate domain,
- Periglacial climate domain,
- Glacial climate domain.

In addition, periods when the ground above the repository is submerged, either by the Baltic Sea or by a fresh water lake, can be expected. During submerged periods, the climate conditions can either be temperate or periglacial, the latter yielding permafrost development in areas not covered by the sea/lake. The evolution of climate-related conditions is described as time series of climate domains and submerged periods.

To first reconstruct last glacial cycle conditions, and subsequently to generate the future reference glacial cycle, three models have been used; a dynamic ice sheet model, a Global Isostatic Adjustment (GIA) model, and a permafrost model, see the **Climate report**, Sections 3.1, 3.3 and 3.4. Details and references relating to the models are found in the **Climate report**, Chapter 3 and in the **Model summary report**.

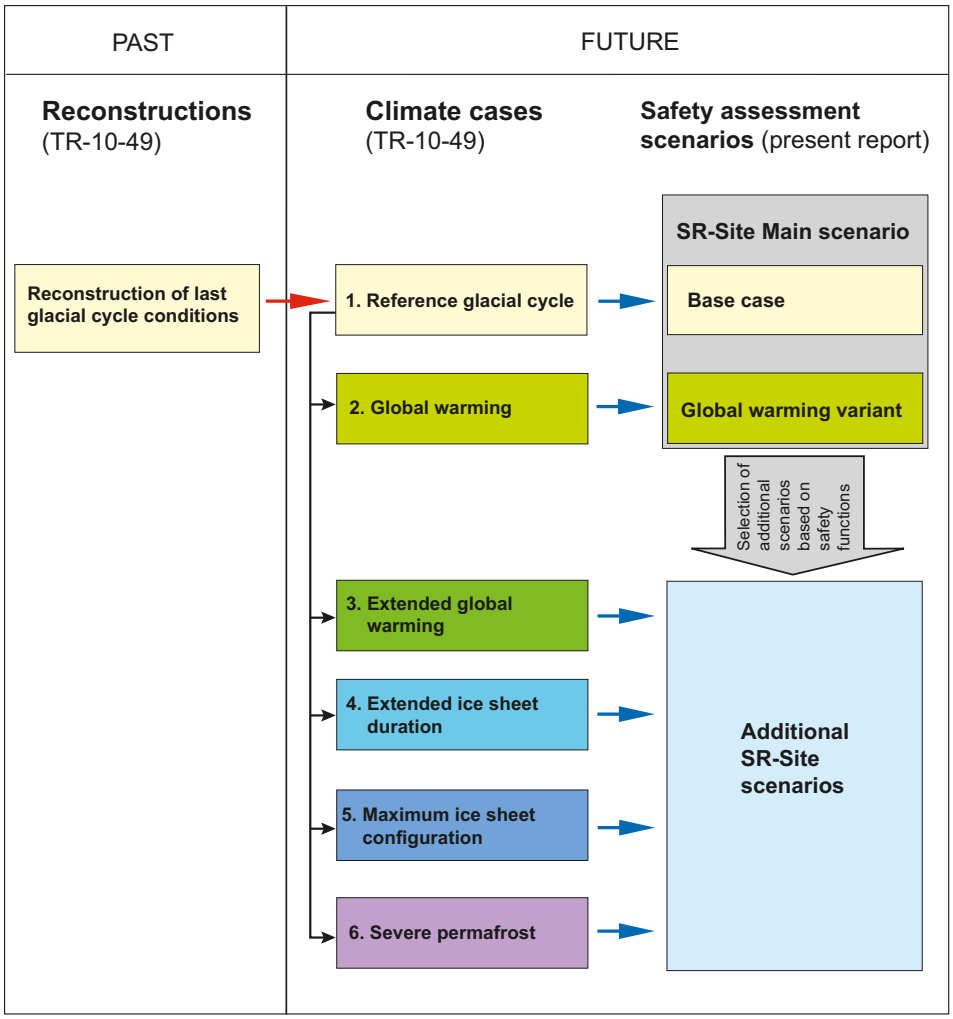

Figure 10-94. *Relationship between the reconstruction of last glacial cycle conditions, the reference glacial cycle, additional climate cases, and the corresponding SR-Site safety assessment scenarios. Figure modified from the* ***Climate report****.*

The basis for the reference evolution of climate-related conditions is a reconstruction of the evolution of the Fennoscandian ice sheet during the Weichselian, employing the ice sheet model. The generated ice sheet evolution has been used as input to the GIA model. The third main component in the modelling of the reference evolution is the permafrost model, yielding an evolution of permafrost depth given the evolution of air temperature, ice sheet extent and thickness, shore level and vegetation. The main data flows between the ice sheet, GIA and permafrost models are shown in Figure 10-95.

Ice sheet evolution and modelling

The dynamic ice sheet model (Figure 10-95) is capable of simulating realistic ice sheets that constantly are trying to adapt their size and shape to a constantly changing climate (as opposed to steady-state ice sheet models where the external climate forcing is held constant). Derived ice temperatures, together with density variations with depth, control ice viscosity and ice flow. The thermodynamic calculation accounts for vertical diffusion, vertical advection, and heating caused by internal shear. The model has been developed over an extended period /Fastook and Chapman 1989, Fastook 1994, Fastook and Holmlund 1994, Johnson 1994/ and model outputs agree with other major ice-sheet models e.g. /Payne et al. 2000/.

Inputs to the dynamic ice sheet model are:

- Topography.
- Geothermal heat flux.
- Global sea-level variations.

- Thermo-mechanical properties of the ice.
- Isostatic properties of the Earth's crust.
- Annual air temperature at sea level, and its variation over time.

For the reconstruction of the Weichselian ice sheet, the temperature pattern over the Fennoscandian model domain is changed according to a palaeo-temperature curve for the modelled time period, resulting in changes in the distributed precipitation and ice sheet mass balance. In the absence of a long-term paleo-temperature climate curve from Fennoscandia, the simulation of the Weichselian ice sheet used the temperature curve from the GRIP ice core (Figure 10-96), obtained from central Greenland e.g. /Dansgaard et al. 1993/. This is a typical method used in modelling of the Weichselian ice sheet, see the **Climate report**, Section 3.1.

The modelled ice sheet evolution starts at the end of the penultimate interglacial (the Eemian), in a situation when ice sheet extent and shore-level are assumed to have been similar to the present. The geothermal heat flow and its spatial variation has been shown to be of importance for obtaining realistic modelled basal ice temperatures and basal ice melt rates, e.g. /Waddington 1987, Näslund et al. 2005/. Basal temperatures and basal water production are in turn important for the overall ice flow and ice dynamics. A detailed dataset of geothermal heat flux, based on national measurements of gamma emission in Sweden and Finland, was therefore compiled /Näslund et al. 2005/ and used as input to the ice sheet model.

Modelled ice sheet configurations were calibrated against geological information on the Weichselian glaciation history, e.g. /Lokrantz and Sohlenius 2006/ and the **Climate report**, Section 4.2. For details on the ice sheet modelling, see the **Climate report**, Section 3.1.

The resulting evolution of ice-covered area and ice volume during the past 120,000 years are shown in Figure 10-96, together with times at which geological information was used to constrain ice sheet evolution. The modelled ice configurations for these times are shown in Figure 10-97. During the glacial cycle, the ice sheet grows progressively larger in a number of distinct growth phases. Between these phases, the ice sheet is thinner. The Last Glacial Maximum, as reflected in peak ice volume, is reached around 18,000 years before present. The overall behaviour of the ice sheet can be characterised as dynamic throughout the glacial cycle (Figures 10-96 and 10-97), as suggested also by several recent studies of the last glacial cycle /Lokrantz and Sohlenius 2006, Näslund et al. 2008, Kjellström et al. 2009, Helmens 2009, Wohlfarth 2009/ and the **Climate report**, Section 4.2 and references therein. The reconstruction of the Weichselian ice sheet is described in more detail in the **Climate report**, Section 3.1.

In the reference glacial cycle the ice sheet over Forsmark was, as expected, at its thickest at around 18,000 years ago, during the Last Glacial Maximum. The largest ice thickness over the Forsmark region was at that time ~2,900 metres. Figure 10-98 shows extracted ice thickness variations over Forsmark, when projecting the reconstructed last glacial cycle ice sheet development into the future reference glacial cycle.

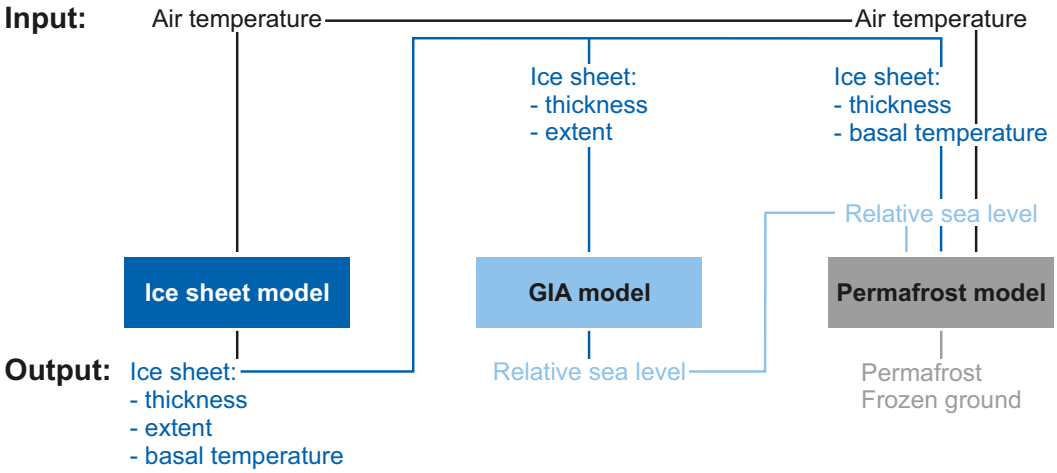

Figure 10-95. *Models used to provide data for the description and analysis of the reference glacial cycle. Only input and output data shared between the models used to generate the results are shown.*

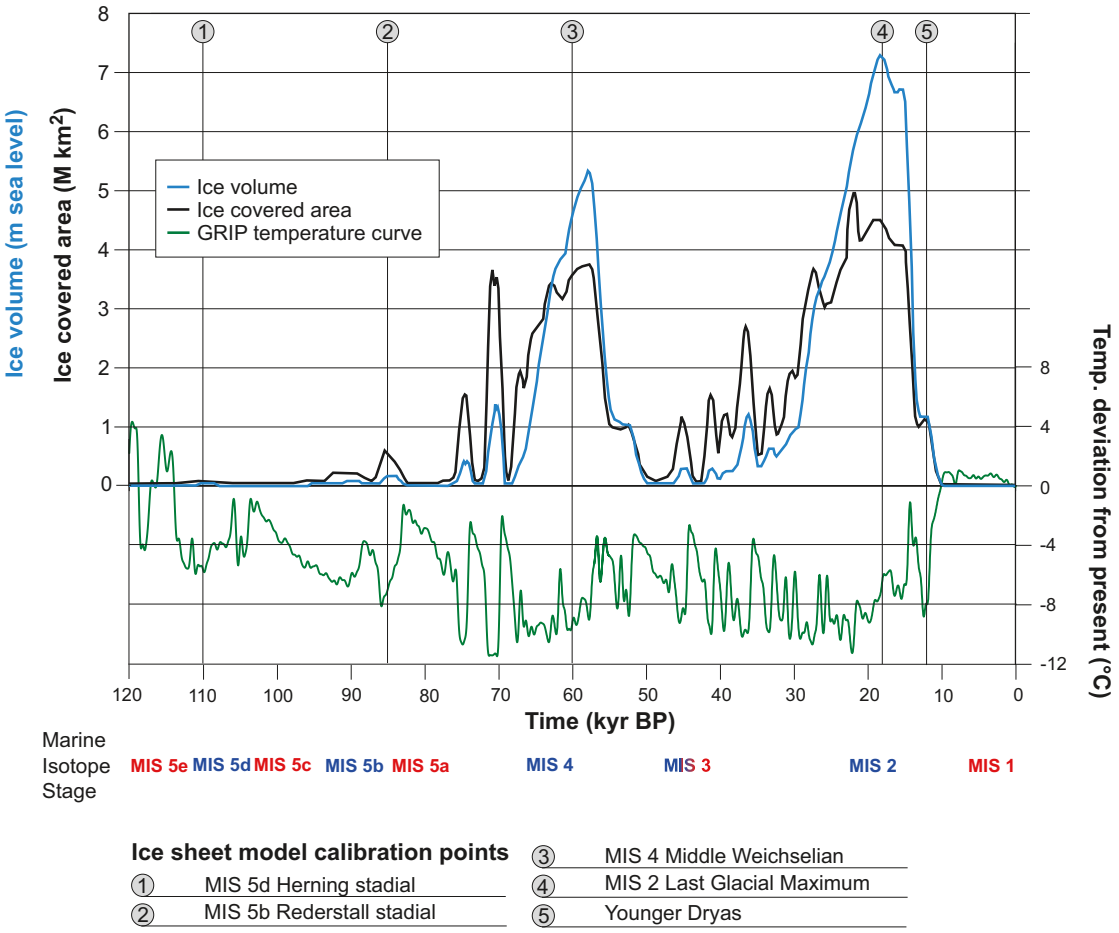

Figure 10-96. *Reconstructed ice-covered area and ice volume for the Weichselian ice sheet. The GRIP proxy temperature curve and times of model calibration are also shown, as well as Marine Isotope Stages (warm stages in red and cold stages in blue). Since the growth of continental ice sheet results in a lowering of global sea level, the changes in ice sheet volume are expressed as m sea level equivalents.*

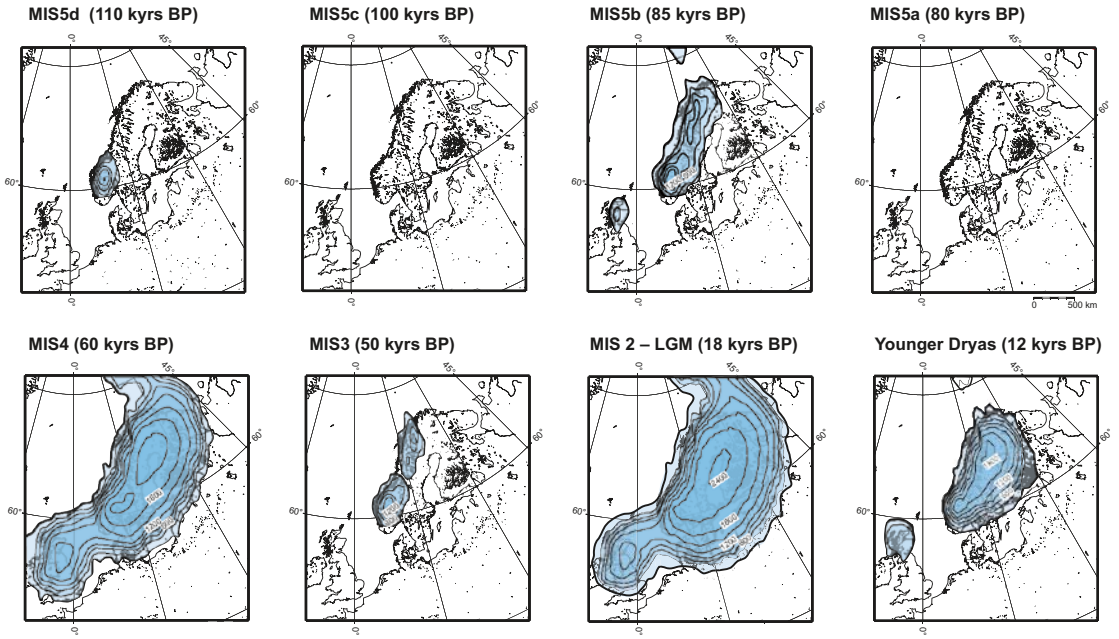

Figure 10-97. *Selected maps of modelled ice sheet configurations at major stadials and interstadials from the reconstruction of the Weichselian ice sheet. Contour lines show ice surface elevation with a 300 m interval. All maps show present day shore-line position.*

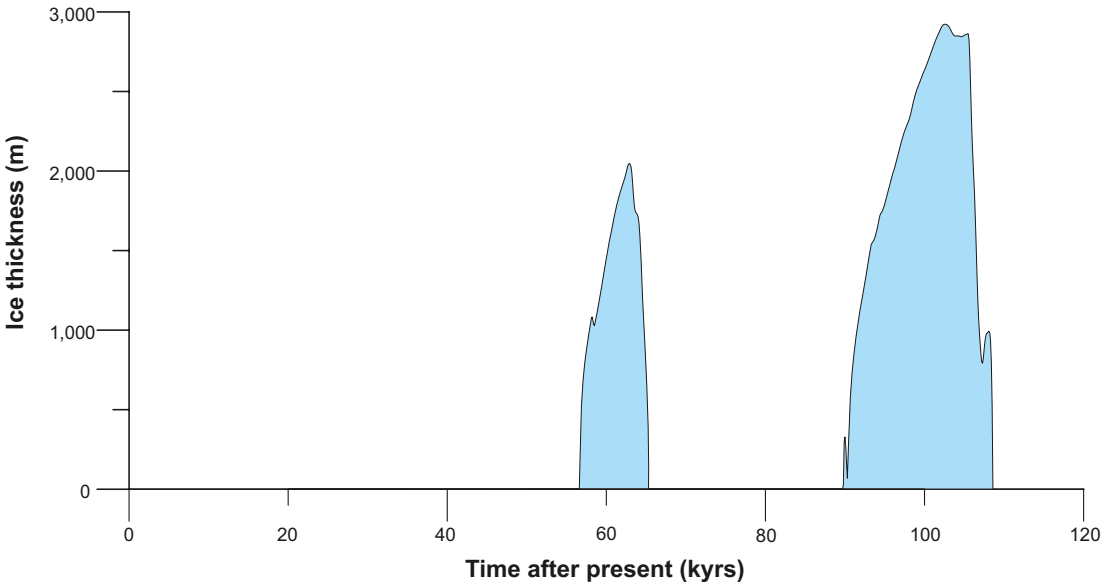

Figure 10-98. *Development of ice sheet thickness at the Forsmark site in the SR-Site reference glacial cycle. Note that even though an ice sheet is present in Fennoscandia during most of the glacial cycle, the Forsmark site, located in south-central Sweden, is not covered by the ice sheet for the majority of the time.*

The groundwater pressure at repository depth is, for non-glacial conditions, determined by the repository depth and, for glacial conditions, by the repository depth as well as an additional pressure induced by the ice load. The ice sheet thickness sets a limit on the maximum hydrostatic pressure that may occur at the ice sheet/bed interface. In the reference glacial cycle, the additional hydrostatic pressure related to the maximum thickness at Forsmark is 26 MPa. This value is listed in Table 12-2, Section 12.7.2, together with estimates of *maximum* expected ice loads and associated *maximum* expected hydrostatic pressures, discussed in Section 12.7.2.

Figure 10-99 shows a selected ice sheet surface profile modelled for the deglaciation phase of the reference glacial cycle, compared with a steeper theoretical steady-state ice sheet profile. The ice sheet profiles were used for calculations of e.g. hydraulic pressure gradients during glacial conditions /Vidstrand et al. 2010/. The hydraulic gradients associated with the steep frontal part of the theoretical profile are seen in Table 10-12.

The duration of hydraulic conditions with steep gradients depends on i) what gradients are considered as steep, ii) the assumed ice sheet profile, iii) the velocity of the ice sheet margin during advance and retreat, and iv) the size of the area of interest. For example, the theoretical profile (Figure 10-99) has been analysed together with ice sheet model data and is considered a proper representation of an advancing ice sheet over Forsmark, for details see the **Climate report**, Appendix 2. If steep gradients for instance are defined as larger than 10°, the first ~3 km of the theoretical ice sheet profile has a steep gradient (Table 10-12). If advancing ice sheet conditions similar to the last glacial cycle are assumed, the ice margin advance rate is ~50 m/a, see the **Climate report**. This results in the steep gradients in this example prevailing for ~60 years during each ice advance over any given location within the repository. However, it should be noted that at the time of ice sheet advance in the reference glacial cycle, the Forsmark site is subject to continuous permafrost conditions, see below. This indicates that the steep gradient from the ice sheet is not the only process that governs the hydrogeological conditions, see Section 10.4.6 and /Vidstrand et al. 2010/.

For a detailed description of the ice sheet profiles, and the motivation for selecting and using them in SR-Site, see the **Climate report**, Appendix 2.

Glacial hydrological conceptual model

The hydrological system of an ice sheet consist of three parts; the supraglacial system (on the ice-sheet surface), englacial system (within the ice) and subglacial system (at the bed). A schematic section through an arbitrary south western sector of a Fennoscandian ice sheet large enough to cover the Forsmark site is

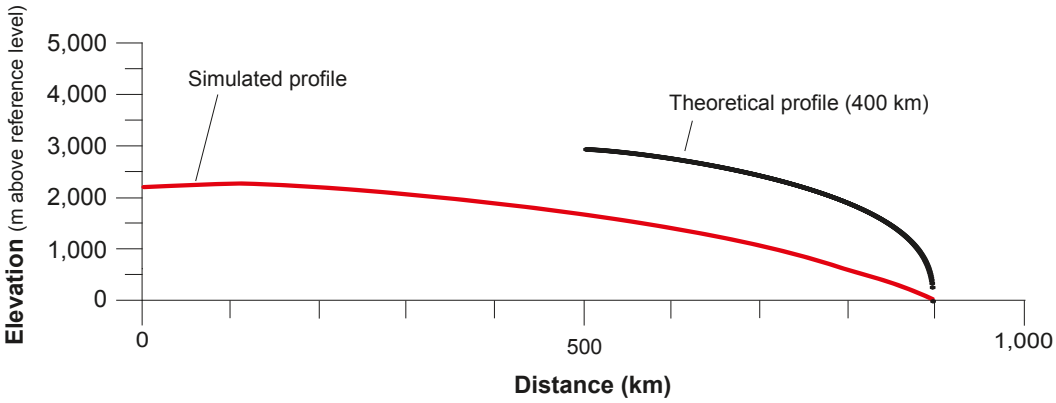

Figure 10-99. *Ice surface topography for a simulated ice profile during the last deglaciation phase of the reference glacial cycle, and a theoretical steady-state profile. For descriptions of the profiles, see the text and the* ***Climate report****, Appendix 2.*

Table 10-12. Hydraulic gradients calculated from the theoretical ice sheet profile, averaged over various distances from the ice sheet margin.

Length from margin (m)	Hydraulic gradient (m/m)	Hydraulic gradient (degrees)
100	1.49	56
200	0.96	44
400	0.62	32
1,000	0.35	19
2,000	0.23	13
4,000	0.15	8.5

shown in Figure 10-100. Water from surface melting is produced in the wet snow zone and in the ablation area, i.e. below the equilibrium line. In the ablation area, surface streams are common features during the melt season. These often end in crevasses or moulins, through which the surface water enters the en- and subglacial systems, see Figure 10-100. At the ice margin, part of the surface melt water leaves the ice sheet directly by channelized surface flow, without entering into the ice sheet.

In the conceptual model, a zone of basal melting extends some hundreds of km inward from the margin. In interior elevated parts of the ice sheet, basal ice is frozen to the bed and no basal melting occurs. One of the most important characteristics of the en- and subglacial hydrological system is that they are highly dynamic. They adjust their transport capacity to any prevailing input of melt water at the ice-sheet surface. Because of the seasonal and intra-seasonal variations in water input, and the continuously ongoing ice deformation, both the en- and subglacial conductive features experience major seasonal and intra-seasonal variations in size and capacity. For this reason, there is no limit to the transport capacity of these hydrological systems, given enough time for them to develop. Further information on the supra- sub- and englacial systems are found in the **Climate report**, Section 3.2, and in /Jansson et al. 2007, Jansson and Näslund 2009/.

Amount of water produced by melting

In the reference glacial cycle, surface melt water production for the modelled Weichselian ice sheet typically varies up to 4–8 m of water per year in the ablation area. This can be compared with observed present average ablation rates of the Greenland ice sheet of a few metres/year /Krabill et al. 2000/ up to ~10 m/year /Bøggild et al. 2004/. During the deglaciation of the Weichselian ice sheet, melt rates up to values higher than 10 m/year occurred /Humlum and Houmark-Nielsen 1994/. Basal melt rates are typically 1–10 mm/a, and can be regarded as constant over the year.

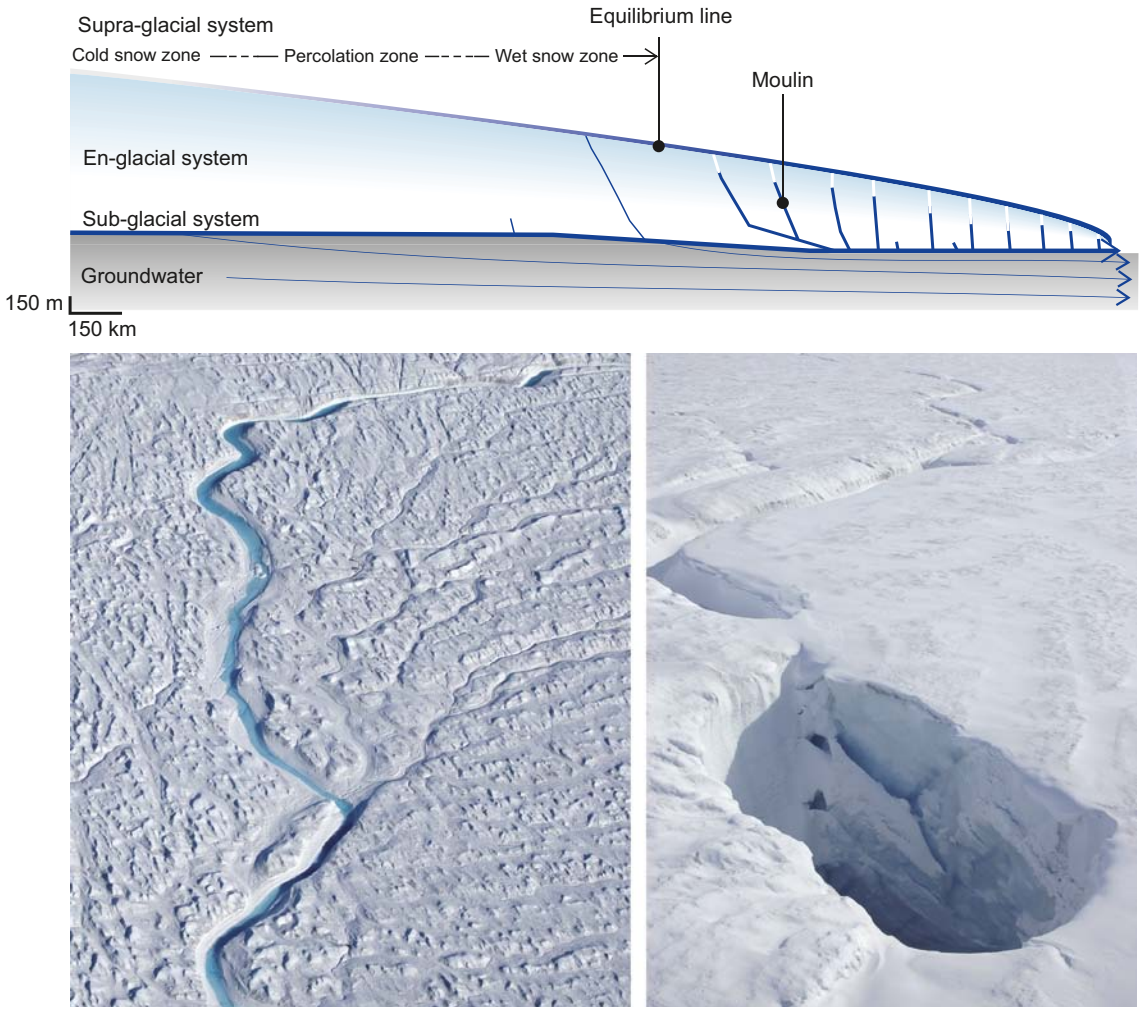

Figure 10-100. *Schematic view of the ice sheet hydrological system through an arbitrary southwestern section through a Fennoscandian ice sheet (upper panel). A supraglacial stream (lower left) and moulin (lower right) on the Greenland ice sheet photographed from the air. The active stream is 2–3 m wide, whereas the depicted moulin has a maximum diameter of c. 15 m. The pictures were taken at the end of the melting season (September), hence the moulin is no longer active.*

Subglacial hydrostatic pressures

In spring, water fluxes and hydrostatic pressures increase in the en- and subglacial hydrological system. This in turn increases the system's water transporting capacity, which in time again lowers the hydrostatic pressure. During the melting season, basal hydrostatic pressures in the area affected by surface water vary significantly diurnally and in connection to rain events e.g. /Jansson 1997/. Hydrostatic pressures in the subglacial conduits may be as low as atmospheric pressure and occasionally as high as, or even higher than, ice overburden pressure. At the end of the melting season, when the supply of surface melt water decreases, the sub-glacial system generally has a high capacity with relatively low pressures. As conduits close during winter, pressures increase. It is assumed that atmospheric pressure may occur only a few km in from the ice sheet margin, and that the sub-glacial conduits are mainly water filled further upstream.

On a glacial cycle timescale, the characteristics of the ice sheet's sub-glacial system can also be expected to change during different stages of ice-sheet advance and retreat due to varying amounts of surface melting. Furthermore, its characteristics depend on basal topography, ice thickness variations, basal temperature distribution, and hydrological properties of the substrate. Geological evidence, mainly on esker distribution, indicates that in large parts of Sweden, tunnel systems separated by several kilometres were present near and at the ice margin of the Weichselian ice sheet. It is plausible that conduits starting at moulins or crevasses at the ice sheet surface connected to channels at the ice/bed interface, and that these channels converge to larger conduits or tunnels towards the ice margin. Pressures in these tunnels prob-

ably also vary considerably during a year, ranging from atmospheric pressure close to the ice margin, to pressures up to overburden or higher during spring and summer. Very little is known about prevailing transverse pressure gradients towards such basal ice sheet conduits, for example how large the areas are that are affected over the year /Jansson et al. 2007/. Despite these uncertainties, the basic conceptual glacial hydrogeological model presented in Figure 10-100 and in the text is a good representation of the glacial hydrological systems as is understood today, see the **Climate report**, Section 3.2 and /Jansson et al. 2007, Jansson and Näslund 2009/.

Shore-level and GIA modelling

In Sweden, the evolution of the Fennoscandian ice sheet has been the principal factor governing changes in relative sea level since the last deglaciation. Hence, Glacial Isostatic Adjustment (GIA) has dominated shore-level changes during this time. GIA-induced shore-level changes depend on the following factors:

- The depth and extent of the oceans.
- The location and thickness of ice sheets over time.
- The structure and properties of the solid Earth and its response to surface loading.

The GIA model used for generating the reference glacial cycle was developed by /Mitrovica and Milne 2003/. The global ice-loading function used in the study is modified from the ICE3G deglaciation history /Tushingham and Peltier 1991/, and has been calibrated using far-field (i.e. far from the margin of the ice sheet) relative sea-level data. The near-field ice load history is taken from the ice sheet modelling described above. A eustatic curve has been used to tune the mass of ice contained within far-field ice sheets. The Earth model is based on Maxwell rheology with a 1D radial three-layer structure. For details on the GIA modelling, see the **Climate report**, Section 3.3.

During the first 1,000 years after present, and for the analysis of biosphere and hydrological evolution during the initial period with temperate climate domain, the shore-level evolution is based on observed data /Påsse 2001/. From about 8,000 years after present to the end of the reference glacial cycle, the shore-line evolution is based on the GIA-modelling. The resulting shore-line curve for Forsmark is shown in Figure 10-101.

During the initial phase of the glacial cycle, when climate is getting colder and ice sheets expand globally, sea levels fall. At the same time, the rate of isostatic rebound from the previous glaciation decreases. However, even if the rate is low, the amount of remaining uplift until the earth reaches a relaxed state is significant. In the central part of the former Weichselian ice sheet it has been estimated to be ~100 metres, and in the distal parts to be ~25 metres, see the **Climate report**, Section 4.4. The remaining uplift at Forsmark is from the GIA simulations estimated to ~70 m.

During a glacial cycle, the shore-level of the Baltic Sea is constrained by the variations in ice sheet extent and by relative sea levels at its sills. The Baltic may at times constitute a freshwater lake, with a surface level determined by the contemporary level of either the Darss sill, located in the southern Baltic between Denmark and Germany, or for the northern part of the Baltic (the Bothnian Sea), the Southern Kvark sill, located between Åland and Sweden.

In the GIA model results (Figure 10-101), the Baltic is cut off from the Atlantic and is transformed into a lake after about 9,000 years after present. However, due to the uncertainties in the GIA modelling relating to the assumption of a 2D Earth structure, Earth rheology, and ice load input, it is likely that this result underestimates the time at which isolation of the Baltic occurs in the reference evolution, see further the **Climate report**, Section 4.4. After the first major ice sheet advance over Fennoscandia, around 60,000 after present, the Baltic is re-formed during a period around 70,000 after present. This period of the reference glacial cycle corresponds to Marine Isotope Stage 3 of the Weichselian, during which the Baltic may have formed a fresh water lake /Lambeck et al. 2010/.

Later in the reference glacial cycle, following the deglaciation of the second and larger ice sheet coverage at around 110,000 years after present, the Baltic is in contact with the Atlantic and hence forms a brackish inland sea. Given that the reference glacial cycle is based on the repetition of conditions reconstructed for the last glacial cycle (including the Holocene epoch of the last c. 10,000 years), the development of the Baltic for this future post-glacial period is envisaged to follow the Holocene development, which included both saline and freshwater stages. After this deglaciation, large parts

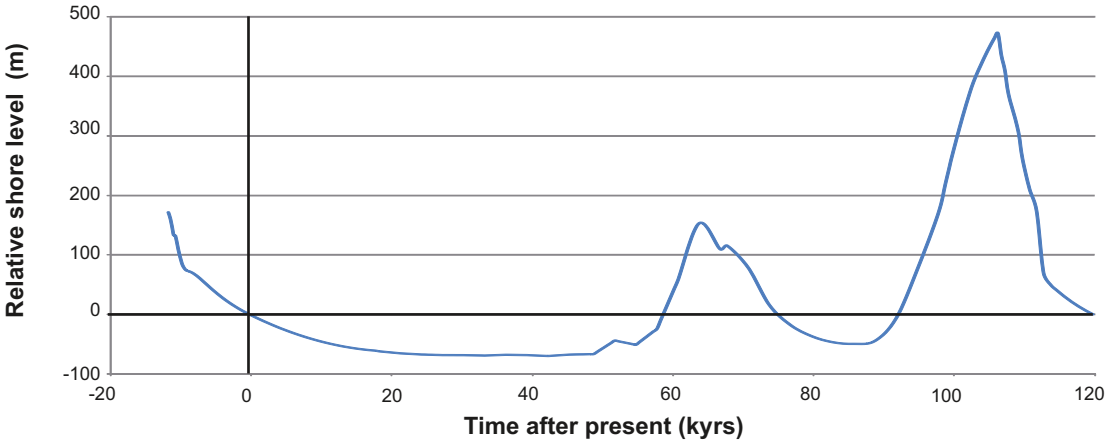

Figure 10-101. *Shore-level displacement at Forsmark for the reference glacial cycle. The figure also shows the shore-level displacement from the deglaciation of the Forsmark site up to present. The prediction for the first c. 8,000 years of the future period is based on observed relative sea level data /Påsse 2001/, whereas the following part of the curve is constructed from Glacial Isostatic Adjustment modelling. The shore-level is expressed relative to the contemporary Baltic Sea level. Positive numbers indicate that the site is submerged and vice versa. Note however, that for most of the time when the figure shows submerged conditions the site is covered by an ice sheet.*

of southern Sweden are submerged by a predominantly saline Baltic Sea. At the end of the reference glacial cycle, and as isostatic rebound proceeds, the Baltic Sea is again transformed to an inland brackish sea, similar to today's situation.

During periods of maximum salinity in the Baltic Sea, which generally develop sometime after periods of maximum glaciation, the Forsmark site is submerged. A more detailed description of the development of salinity in the Baltic Sea for this submerged period of the reference glacial cycle is found in /Lindborg 2010/.

The most important factor affecting the GIA modelled shore level migration is the Earth model and the ice loading history, primarily the near-field history. 3D GIA modelling performed for Fennoscandia, described in /Whitehouse 2009/ has shown that the assumption of a laterally homogenous earth structure over Fennoscandia, used for the construction of Figure 10-101, probably resulted in an over-prediction of the isostatic response to ice sheet load and present-day uplift rates. The relation between the Earth model structure and the ice loading history, as well as the assumption on a laterally homogenous earth structure, are further discussed in the **Climate report**, Section 3.3.

The uncertainty in modelled shore-level relates mainly to the fact that reported relative sea-level values could be too large, resulting from a overestimation of isostatic depression in response to the ice load. The size of the uncertainty varies over the modelled glacial cycle. Postulating that the ice sheet evolution is correct, the *mean* overestimation of isostatic depression, over the whole glacial cycle, may be up to 45 metres. For details on uncertainties in modelled relative shore-levels see the **Climate report**, Section 3.3.

Permafrost development and modelling

Permafrost is defined as ground where the temperature remains continuously below 0°C for more than a year while perennially frozen ground is defined as ground that remains frozen for at least two consecutive years. Therefore, the presence of permafrost does not necessarily mean that the ground is frozen. Depending on the pressure and composition of groundwater, and on adsorptive and capillary properties of ground matter, groundwater may freeze at a temperature below 0°C.

Permafrost originates from the ground surface and grows downwards as a result of a complex heat exchange across the atmosphere/ground boundary layers and the geothermal heat flow from the Earth's interior. In the reference glacial cycle, permafrost occurs in the periglacial climate domain, as well as beneath parts of the ice sheet in the glacial climate domain, see the **Climate report**, Sections 3.4.4 and

4.5. Generally, an ice sheet isolates the ground from the cold climate and therefore the presence of an ice sheet prevents the development of permafrost to great depth in cold climates. Instead, the ice sheet typically results in permafrost degradation.

The development of permafrost depends on:

- The climate conditions; mainly air temperature at the ground surface but also on precipitation and wind.
- The topography; air temperature decreases with increasing altitude and, in northern latitudes, south slopes with a southern aspect are more exposed to solar irradiation than slopes with a northern aspect.
- The presence of a soil cover and its porosity, saturation and thermal properties.
- The presence and type of vegetation.
- The presence of water bodies of substantial extent (lakes, sea, major rivers).
- The presence of ice sheets and the basal ice temperature.
- The bedrock thermal, mechanical and hydraulic properties.
- The geothermal heat flow.

As a rule, for a majority of surface covers, permafrost can build from the ground surface if the annual mean air temperature is lower than a value ranging between –9 and –1°C /Washburn 1979, Yershov 1998, French 2007/.

For the reconstruction of the last glacial cycle conditions and the construction of the reference glacial cycle, 1D permafrost modelling was performed for the repository location, see /SKB 2006c/ and the **Climate report**, Section 3.4.4. In addition, 2D permafrost modelling was performed for a section of the Forsmark site, as defined and analysed in the SR-Site biosphere programme /Lindborg 2010/, see /Hartikainen et al. 2010/ and the **Climate report**, Sections 3.4.4 and 5.5. The main objective with the 1D modelling was to study the evolution and depth of permafrost and perennially frozen ground for the full glacial cycle specifically at the repository location, whereas the 2D simulations were made to study the spatial development of permafrost and frozen ground, including talik formation, freeze-out of salt and groundwater flow along a profile over the Forsmark site. The 2D model was also used for extensive sensitivity experiments on uncertainties in subsurface- and surface conditions, as well as in climate parameters, including air temperature. Figure 10-102 shows the results when projecting the reconstructed last glacial cycle permafrost and perennially frozen ground conditions into the future reference glacial cycle. For further presentations of the results of the permafrost modelling, see Section 10.4.3, the **Climate report**, Section 3.4.4, and /Hartikainen et al. 2010/.

Permafrost growth is a progressive process, starting with sporadic permafrost at exposed areas and, if climate allows, ending with a continuous spatial coverage of permafrost. Examples of permafrost development from the reference glacial cycle along the profile investigated with the 2D permafrost model are seen in Figure 10-103. Note that heat from the repository is included in these simulations At time 8,500 yrs (8.5 kyrs) after present (Figure 10-103 upper panel), the temperature effect from the repository has a clear impact on the temperature of the surrounding bedrock.

At time 25,000 years after present, two unfrozen taliks have formed through the frozen ground beneath lakes located at ~9,000 and ~15,000 m in the profile (Figure 10-103 Second panel). Groundwater recharge and discharge may take place in the taliks but not in the surrounding frozen terrain. The size of the water body required to retain a talik was investigated by permafrost modelling. For the results of these calculations, see the **Climate report**, Section 3.4.

At time 46,000 years after present (Figure 10-103 third panel), the taliks are closed by the developing permafrost. The lower panel in Figure 10-103 shows the permafrost distribution for the situation with deepest permafrost in the reference glacial cycle. At this time, 50,000 years after present, the permafrost depth over the repository is 259 m. The perennially frozen depth is a few metres shallower, 246 m.

Some of the input data for the permafrost simulations are associated with significant uncertainties, see the **Climate report**, Sections 3.4.4 and 5.5. The largest uncertainly relates to the air temperature curve reconstructed for the Forsmark site for the last glacial cycle, which is estimated to be uncertain by up to ±6°C, see the **Climate report**, Appendix 1, the **Data report** and /Hartikainen et al. 2010/. If this uncertainty

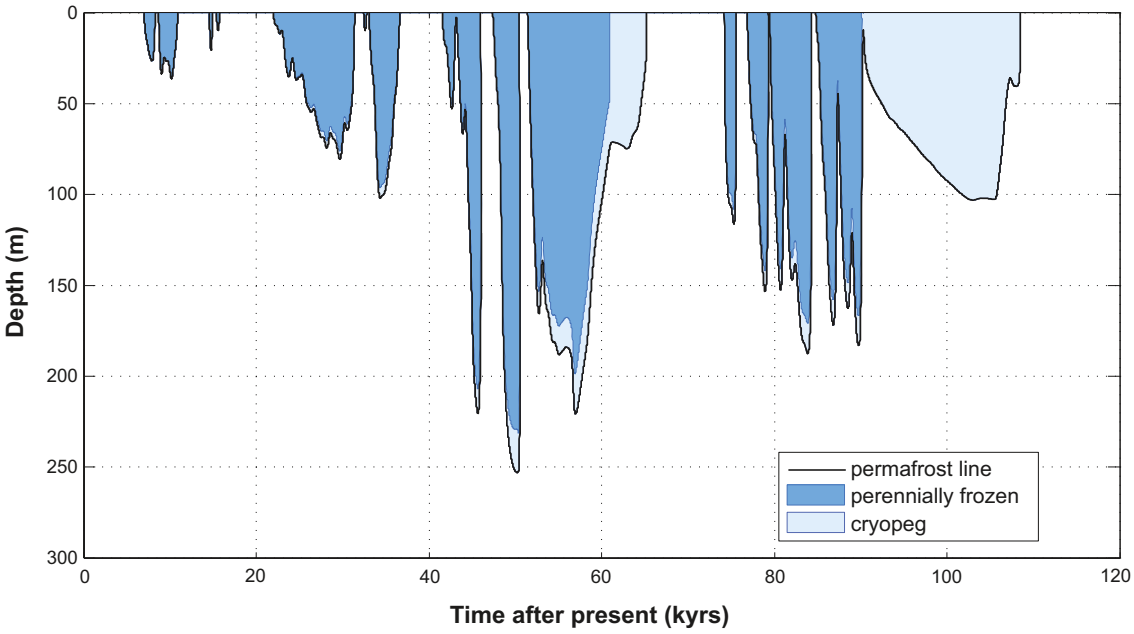

Figure 10-102. *Evolution of permafrost and perennially frozen ground depth for the reference glacial cycle. The curve shows the development specifically at the repository location, obtained from 1D modelling. Due to the high pressure, a thick unfrozen cryopeg exists within the permafrost (defined by the 0°C isotherm) for periods with ice sheet coverage around 60,000 years and 100,000 years after present. The largest permafrost depth is –260 m.*

in air temperature is combined with the uncertainty in climate humidity, the uncertainty range for the permafrost depth (e.g. 0°C isotherm depth) for the reference glacial cycle reaches a maximum depth of ~410 m, whereas the uncertainty range for the perennially frozen ground reaches ~380 m (Figure 10-104).

Uncertainties related to other surface conditions (vegetation type, surface wetness, snow cover) and subsurface conditions (thermal conductivity and diffusivity, and geothermal heat flow) have a smaller impact on the simulated permafrost results. If they all are combined with the uncertainty in climate humidity (still excluding the uncertainty in air temperature), they result in a permafrost uncertainty interval between ~170 to ~290 m depth (Figure 10-105).

With all known uncertainties (e.g. in air temperature, climate humidity, surface wetness, vegetation, snow cover, bedrock thermal conductivity and diffusivity, and geothermal heat flux) in their most extreme setting favourable for permafrost growth, the permafrost uncertainty range reaches a maximum depth of 463 m, whereas the uncertainty range for the perennially frozen ground reach a maximum depth of 422 m, see the **Climate report** Table 4-3. It must be noted, however, that this most extreme combination of uncertainties is quite unrealistic. Given that the uncertainty in the maximum depth of perennially frozen ground does not reach 450 m depth even in this most extreme unrealistic combination of all uncertainties, freezing of groundwater at repository depth is excluded in the reference glacial cycle. For a more detailed description of e.g. individual contributions of uncertainty from various parameters affecting permafrost growth, see the **Climate report**, Section 3.4.4 and /Hartikainen et al. 2010/.

Reference evolution at Forsmark

Based on the results of the ice sheet-, GIA- and permafrost modelling, the reference glacial cycle evolution of climate-related conditions at Forsmark is described as a time series of future climate domains and submerged periods (Figures 10-106 and 10-107).

The time series and the identification of main processes and conditions of importance for repository safety are the basis for the subsequent identification and construction of additional possible future climate cases for the SR-Site safety assessment (Figure 10-94).

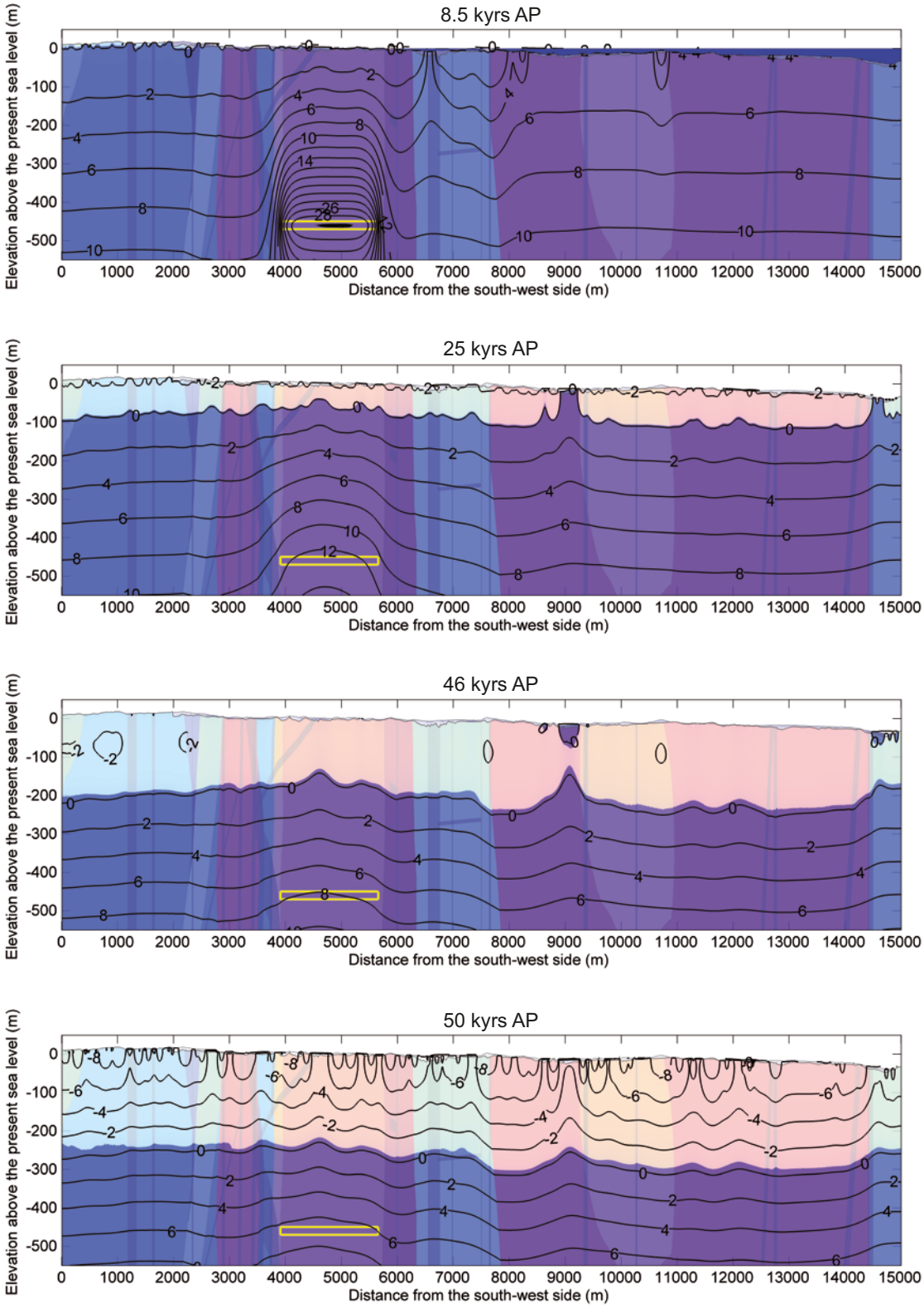

Figure 10-103. *Examples of temperature contours in (°C) and the extent of perennially frozen ground (light colour) and permafrost (0°C isotherm), obtained from 2D modelling, at times 8.5, 25, 46 and 50 kyrs after present in the reference glacial cycle. Blue colour on the top of the profile at 8.5 kyrs after present shows the Baltic Sea. The yellow rectangle indicates the location of the repository. The profile follows the general regional topographic gradient, approximately in a SW-NE direction.*

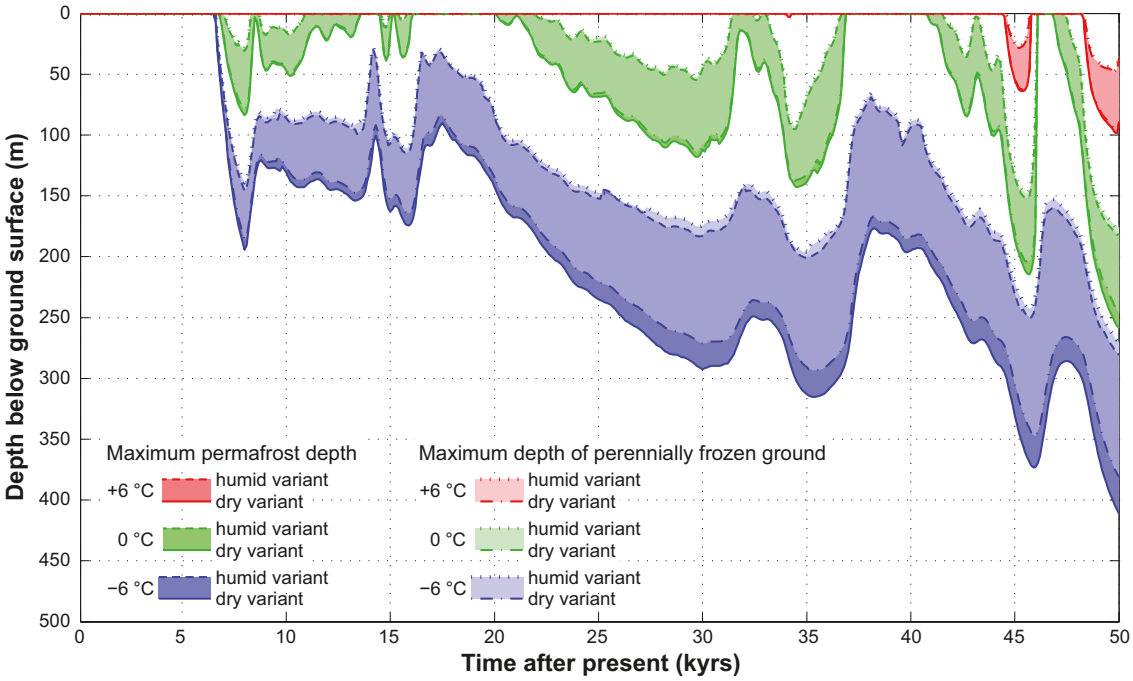

Figure 10-104. *Result of sensitivity experiment on uncertainty in air temperature and climate humidity for the first 50,000 years of the reference glacial cycle. Evolution of maximum permafrost depth (solid lines) and maximum depth of perennially frozen ground (dashed lines) over the repository location considering mean thermal properties and the air temperature curve changed by –6, 0 and +6°C. The shaded areas in blue and red represent the range when considering the dry and humid climate variants. Note that the results for permafrost and perennially frozen ground overlap to a large degree. It should also be mentioned that changes of the buffer and backfill clay properties during freezing, if freezing would occur, are reversed following thawing.*

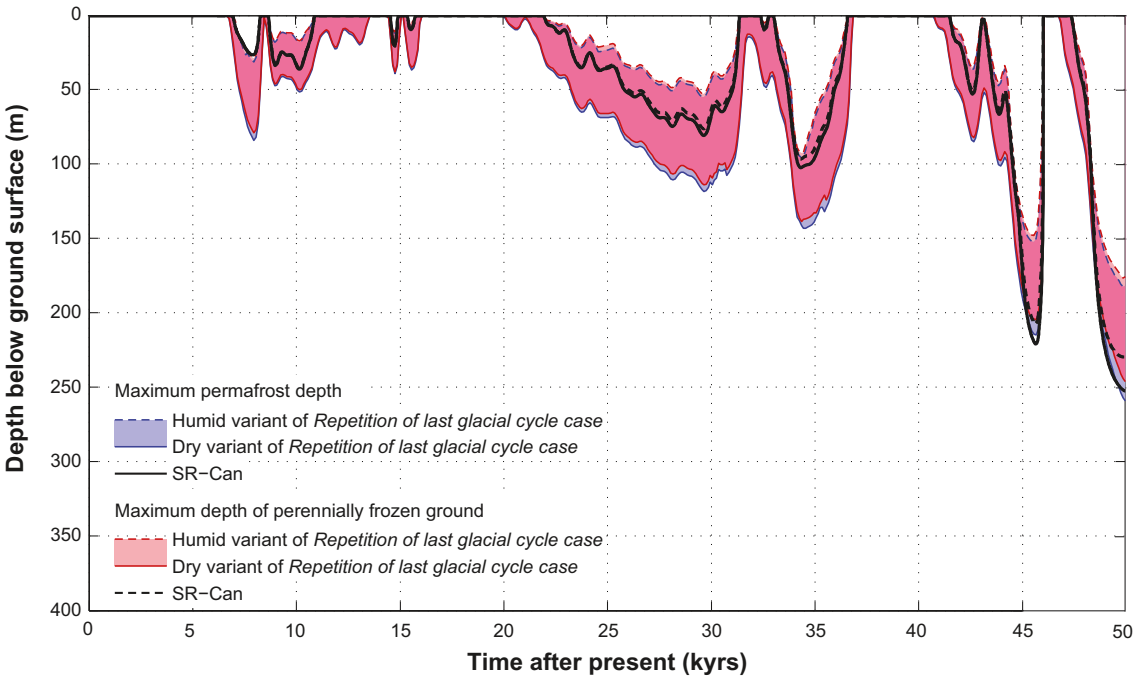

Figure 10-105. *Evolution of maximum permafrost depth and maximum depth of perennially frozen ground over the repository for the reference glacial cycle considering combined uncertainties in all surface conditions (except air temperature) and bedrock thermal properties (including geothermal heat flow). The figure shows the first 50,000 years of the reference glacial cycle as simulated by the SR-Site 2D modelling. The shaded areas in blue and red represent the range when considering dry and humid climate variants. Note that the areas overlap to a large extent (lilac colour). Corresponding 1D results from SR-Can are also shown.*

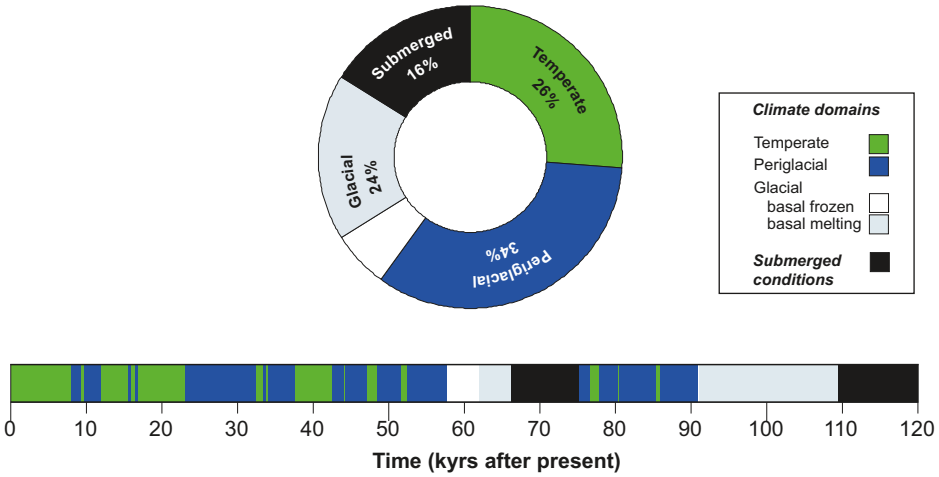

Figure 10-106. *Duration of climate domains and submerged conditions at Forsmark in the SR-Site reference glacial cycle, expressed as percentages of the total time for the reference glacial cycle. The bar below the pie chart shows the temporal development of climate-related conditions for the reference glacial cycle as a time series of climate domains and submerged periods.*

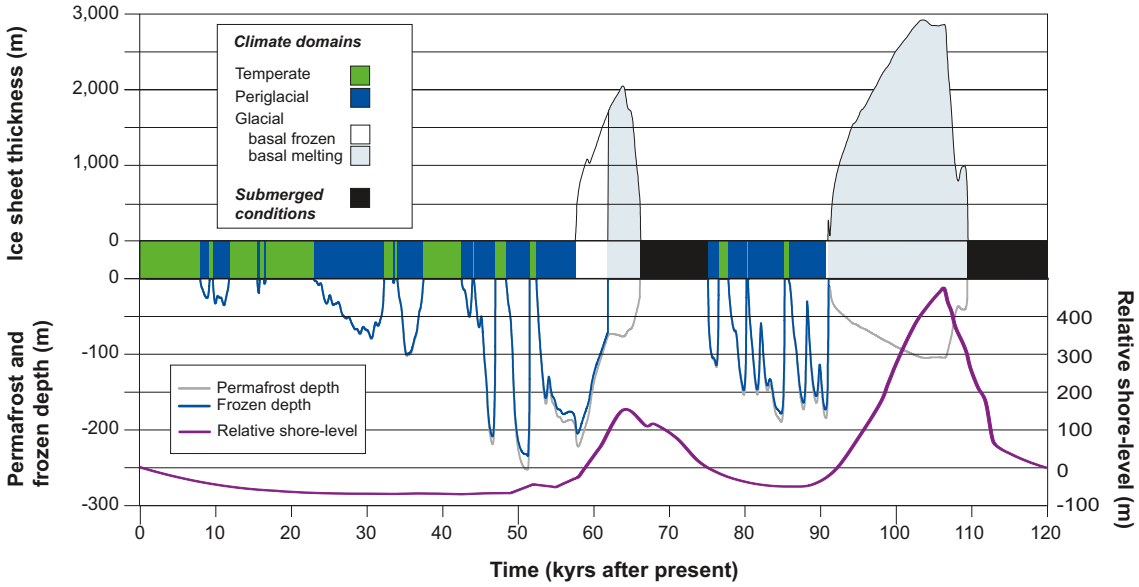

Figure 10-107. *Reference glacial cycle evolution of important climate-related variables for the Forsmark repository location.*

Periods of temperate climate domain occupy ~31,000 years of the reference glacial cycle at Forsmark. It occurs in the initial phase of the reference glacial cycle, during the interstadial between the two major ice advances, and during the interglacial period following the glacial maximum (Figures 10-106 and 10-107). During the end of the present interglacial and during following early phases of the reference glacial cycle, the periods of temperate climate domain are generally longer than those occurring during the interstadial in the later part of the glacial.

During the first 50,000 years of the reference glacial cycle, and in the interstadial period between the two glacial phases, the increasingly colder climate results in progressively longer periods of periglacial climate domain and correspondingly shorter periods of temperate climate domain (Figure 10-107). The total duration of the periglacial climate domain is ~41,000 years. The calculated permafrost depth at the repository location for the most severe permafrost period of the reference glacial cycle is ~250 m. As described in the discussion on uncertainties above, freezing of groundwater at repository depth is excluded in the reference glacial cycle.

Forsmark is exposed to two major ice advances and retreats during the reference glacial cycle, the first around 60,000 years after present and the second at around 100,000 to 110,000 years after present (Figure 10-107). Prior to both of these glaciated periods, the Forsmark site is situated above sea level with prevailing continuous permafrost conditions (more than 90% spatial permafrost coverage) when the ice sheet advances towards and over the site.

A period of basal frozen conditions, ~4,000 years long, initiates the first major stadial of glacial climate domain. During this period, there is deep sub-glacial permafrost. As the ice sheet continues to grow over the site, it insulates the subsurface from the cold climate and in time induces basal melting conditions. Also the sub-glacial permafrost starts to decay once the ice sheet has overridden the site, with very fast permafrost melting once warm-based ice sheet conditions form (Figure 10-107). The total length of periods of glacial domain in the reference glacial cycle is about 30,000 years. During this time, ice sheet basal melting conditions dominate.

Table 10-13 summarises the durations of the climate domains for the reference glacial cycle. It is again emphasized that the reference evolution is not an expected or predicted climate evolution. It is *one example* of a climate evolution covering the climate-related conditions that could occur in a 100,000 year time perspective. The example is subsequently used in the process of identifying other climate cases with a potentially larger impact on repository safety.

Climate-related factors of importance for safety

During periods of temperate climate domain, the main factor of importance for repository safety is shore-level migration and groundwater salinity. When the site is submerged, a diminished groundwater flow will be driven by prevailing differences in groundwater density, and, when not submerged, the gradients for groundwater flow will be constrained by landscape topography. During periods of periglacial climate domain, the main factor of importance for repository safety is the development of permafrost and frozen ground. Frozen ground will affect groundwater flow and composition, and cause freezing of backfill material in the ramp and shaft. If freezing temperatures were to occur at repository depth, the backfill in deposition tunnels and buffer would freeze.

The advance and retreat of an ice sheet over the Forsmark site brings about the largest climate-related change the repository will experience during a glacial cycle. The main factors of importance for repository safety in the glacial climate domain are the maximum hydrostatic pressure, the penetration of oxygen rich and/or dilute glacial melt waters to great depth, the possible up-coning of saline waters from below the repository, the alteration of rock stresses, the occurrence of glacially induced faulting and the alteration of flow properties of the bedrock.

The evolution of climate-related conditions of importance for repository safety is illustrated by the succession of climate domains in Figure 10-106 and by the evolution of important climate-related variables in Figure 10-107. In this climate succession, the temperate climate domain is always followed by the periglacial climate domain. The periglacial climate domain can either be followed by the temperate or glacial climate domain. In the reference glacial cycle, the Forsmark site is submerged by the Baltic after periods of major glaciation. The subsequent transition from submerged conditions to land can take place either during periods of periglacial climate domain, or, as at present, during periods of temperate climate domain.

Table 10-13. Duration of climate domains in the SR-Site reference glacial cycle.

Climate domain	Duration (% of reference glacial cycle)	Duration (years)
Temperate climate domain	26%	31,200
Periglacial climate domain	34%	40,800
Glacial climate domain	24%	28,200
Submerged conditions	16%	19,200

10.4.2 Biosphere

SR-Site uses a reconstruction of the last glacial cycle as a starting point for describing possible future changes in climate and climate-related processes (see Section 10.4.1). This reconstruction is used as an example of a future evolution that, in a realistic way, covers all relevant climate-related changes that can be expected in a 120,000-year perspective. The reconstruction divides the period into climate-driven process domains (in short: climate domains). In reality when looking at the entire modelled area at Forsmark, changeover from one climate domain to another is a smooth transition, see the **Climate report**, Section 4.5.4. In addition, it takes time for the environment and its predominant processes to adapt even to an abrupt change in climate (cf. Chapter 3 in /Lindborg 2010/).

For the modelled area at Forsmark it takes time for a change in environmental conditions to propagate from one end to the other. For instance, this is true for the changeover after the deglaciation, from submerged conditions to an entirely terrestrial and temperate domain. This transition is caused by shoreline displacement, which takes ~12,000 years to transfer the whole area from fully submerged just before the first islet emerges from the sea (1000 BC), until the last marine embayment is turned into a lake (around 11,000 AD). During two periods in the later part of the reference evolution, Forsmark is covered by an ice sheet (Section 10.4.1). Directly after the deglaciation of these ice sheets, the site is submerged, and thereafter the transfer from submerged conditions to an entirely terrestrial area is assumed to be repeated.

Periods of temperate climate domain

The temperate climate domain corresponds to 26% of the reference glacial cycle, Section 10.4.1. After the initial temperate period, which according to the reference glacial cycle ends around 9400 AD, a relative short period of periglacial conditions follows, and thereafter temperate conditions again dominate until c. 23,000 AD. Another temperate period lasting for about 5,000 years occurs around 40,000 AD.

During future periods of temperate conditions before the next glaciation, Forsmark is assumed to show biosphere characteristics similar to those of the later parts of the initial temperate period, i.e. the landscape will consist of terrestrial ecosystems, mainly forests and mires, with few or no lakes and no sea. Parts of the area, especially those with fine-grained sediments in central Öregrundsgrepen (see Figure 10-12), can potentially be used for long-term agriculture (cf. Chapter 4 in /Lindborg 2010/). Patches with mainly organic soils may also be cultivated for limited periods. Higher altitude areas with outcrops of bedrock will be forested with pine. Also the pattern for discharge of deep groundwater, as well as the conditions determining transport and accumulation of radionuclides in the landscape, are expected to be similar to those prevailing during the late part of the initial temperate period (cf. Chapters 4 and 5 in /Lindborg 2010/).

Periods of periglacial climate domain

Periods of periglacial conditions, which are characterised by tundra vegetation and permafrost features, correspond to 34% of the reference glacial cycle. Although the periglacial domain constitutes the largest share of the reference glacial cycle, it often occurs during relatively short periods interrupted by other climate domains. The longest uninterrupted period of periglacial conditions starts around 23,000 AD and continues for c. 10,000 years.

The vegetation period in the periglacial domain is short. Nevertheless, primary production may be high in some environments, e.g. in shallow lakes /Andersson 2010/. The terrestrial vegetation consists of sedges, herbs and shrubs. At more exposed and dryer localities, lichens dominate, whereas wet ground is dominated by mosses. The precipitation will likely be lower than during temperate conditions, due to the limited evapotranspiration transporting water to the atmosphere /Kjellström et al. 2009/. The low evapotranspiration means that wet ground is prevalent, because surplus water is unable to infiltrate into the ground /Bosson et al. 2010, French 2007/. This may result in larger areas of wetlands compared with a temperate climate, but on the other hand the peat formation rate is lower, partly because the terrestrial plant productivity is low.

Even on gentle slopes, the soil creeps downhill with the peat cover on top. Other processes typical of periglacial conditions are upward migration of stones induced by freeze-thaw processes, so called cryoturbation, causing tundra-polygons (patterned ground whose mesh is tetragonal, pentagonal or hexagonal) and thermokarsts (topographic features produced by thawing permafrost and associated settling of the ground). Thus, there are many processes disturbing the soil and also exposing it to erosion.

Taliks are unfrozen areas, often occurring under lakes or rivers in the permafrost region e.g. /Hartikainen et al. 2010/. The talik features are the only spots in the periglacial landscape where radionuclides released from the repository can be transported up to the biosphere /Bosson et al. 2010/. Given that lakes and streams often are locations for human settlement and land use, taliks can potentially be locations where humans are exposed to high radionuclide concentrations during periglacial conditions. However, the generally low productivity in the permafrost region requires utilisation of a larger area to supply the resources needed by even a small community. Therefore, even if radionuclides are discharged into a talik in such an area, this does not necessarily imply that the average concentrations in the food consumed by humans living in the area will be particularly high.

Periods of glacial climate domain

Forsmark is covered by an ice sheet during 24% of the reference glacial cycle, mainly during the later part of this cycle. On the ice surface, microbes, algae and some insects can exist. At the ice-margin, a productive aquatic community may exist, which can sustain fish populations that may be exploited by humans and by animals living on the ice (e.g. birds, polar foxes, polar bears) and in the sea (e.g. seals and whales).

Any larger vertebrates or humans living on the ice are likely to migrate over large areas due to low food production and severe weather conditions. In most cases, a human population will probably comprise occasional visitors, due to the harsh environment. The only situation under glacial conditions when humans or other biota may be exposed to high concentrations of radionuclides from the repository is when the retreating ice-front is situated near the Forsmark area and the area is submerged. Under these conditions, it is possible that a human population could be present for longer periods and live on fish taken from close to the ice margin.

During periods of glacial climate domain, no long-term accumulation of radionuclides is assumed to occur in the regolith due to the short turnover time of this potential reservoir. It is only during short periods of the glacial climate domain that radionuclides discharged from underground sources may accumulate as under periglacial conditions. However, since the Forsmark site will be depressed below the sea level during most of the glacial periods, fast water turnover in the open sea along the ice margin will probably dilute any released radionuclides and prevent the accumulation of high concentrations in sediments and organisms.

Periods with submerged conditions

In the reference glacial cycle, two periods of submerged conditions at Forsmark are present, representing 16% of the total reference glacial cycle. These periods always follow directly after the ice sheet has withdrawn as a result of the bedrock being depressed by the ice load. After the last glaciation which ended at 8800 BC in Forsmark, the first terrestrial areas appeared around 1000 BC and the last marine embayment in the modelled area is turned into a lake around 11,000 AD. This means that the submerged conditions in the modelled area may be divided into two phases; one first phase of c. 8,000 years when the whole area is submerged, and another that continues during 12,000 years when the sea gradually withdraws and the land area expands accordingly. This description of the temporal succession is not seen in the description in the reference glacial cycle (see Figure 10-107) since the latter is valid specifically for a point above the repository target area, but it gives a more realistic picture of the succession for the whole landscape (see also the section on transitions between climate domains in the **Climate report**, Section 4.5.4).

Submerged conditions are not defined as a climate domain in SR-Site, see the **Climate report**. Instead, it is a state when the processes and properties related to the marine conditions are dominant. The marine ecosystem is not expected to change dramatically from today as a result of changes in climate, except for the long-term variations in salinity. Therefore, the submerged future landscape is in SR-Site treated as corresponding to the historical and present aquatic ecosystems at Forsmark, and the prerequisites for transport and accumulation of radionuclides are assumed to be similar to those in the present marine ecosystem.

Identified uncertainties and their handling in the subsequent analysis

The main uncertainties in the landscape development during the remaining part of the reference glacial cycle are essentially the same as those dominating during the initial temperate period, i.e. 1) the configuration of the landscape, 2) the timing of different events, and 3) the composition and properties of species and communities inhabiting the future landscape (cf. Section 10.3.3). Even though it is impossible to describe in detail the landscape development during a complete glacial cycle, the systematic landscape analysis and the approach for estimating doses encompasses most of the potential future landscape configurations for the reference glacial cycle.

10.4.3 Thermal evolution

The decreasing temperature and in particular the presence of permafrost and perennially frozen ground may impact the buffer clay, backfill material and copper canister. Primarily it is safety function R4, see Figure 10-2, that may be affected, since it a) states that the temperature in the buffer should > −4°C in order to avoid buffer freezing and b) that the buffer temperature should be > 0°C to ensure the validity of the canister shear analysis. Furthermore, there is also a temperature related safety function for retention (BF2c) stating that the backfill temperature > –2°C, since this is the temperature at which it will freeze. In addition, if the buffer freezes, the pressure exerted on the canister and the rock may increase, an issue requiring separate analyses. Presence of permafrost also affects the hydromechanical conditions (potential for hydraulic jacking) as is further discussed in Section 10.4.4. It is therefore important to analyse i) the depths of permafrost, or more specifically, the depth of perennially frozen ground, ii) the depth of the isotherm corresponding to the temperature criterion used for buffer clay freezing, iii) the depth of the isotherm corresponding to the temperature criterion used for freezing of the backfill material, and iv) the freeze-out of salt that may result in a zone with higher salinity beneath the perennially frozen ground.

Permafrost development

The depth of permafrost is defined by the depth of the 0°C isotherm, see the **Climate report**, Section 3.4. However, the depth of the perennially frozen ground is often shallower, depending on the prevailing hydrostatic pressure, chemical composition of groundwater and on adsorptive and capillary properties of ground matter. These factors result in the possibility that groundwater water may freeze at temperatures below 0°C, see e.g. the **Climate report**, Section 3.4. The temperature criterion used in SR-Site for buffer freezing is −4°C, see Section 8.3.2. However, in reality it is likely that buffer clay freezes at even lower temperatures, Section 3.2.2 in the **Buffer, backfill and closure process report**. The criterion used for freezing of the backfill material is −2°C, see Section 8.4.4.

The prevailing surface conditions, such as air temperature and surface cover, are the main factors governing the spatial and temporal development of permafrost and perennially frozen ground at Forsmark, see the **Climate report**, Section 3.4.4. Subsurface conditions, such as bedrock thermal properties, geothermal heat flow, groundwater salinity and heat produced by the repository, modify the spatial and temporal development, but are of secondary importance compared to surface conditions. For a description of the development of permafrost during the reference glacial cycle, see Section 10.4.1 and the **Climate report**, Section 4.4.3.

Permafrost modelling

The evolution of permafrost and perennially frozen ground has been investigated by means of numerical modelling in 1D and 2D /SKB 2006c, Hartikainen et al. 2010/. The related mathematical models are based on the theory of mixtures and basic principles of continuum mechanics and thermodynamics considering the freezing ground as an elastic porous medium of soil or rock skeleton saturated by saline groundwater and ice. The models are capable of describing the heat- and mass transfer in a porous medium, freezing of groundwater being affected by groundwater pressure and salt concentration, and freezing-induced groundwater flow (cryogenic-suction). The numerical 2D model also describes the exclusion of salt during freezing and the density dependent groundwater flow in unfrozen and partially frozen ground. The continuum approach is adequate for modelling of permafrost and perennially frozen ground development, since these processes are primarily governed by heat conduction and only secondarily by groundwater flow /Hartikainen et al. 2010/.

The 1D modelling approach could, in certain situations, result in somewhat higher temperatures than would be calculated using a multi-dimensional model. However, a comparison between the results from the 1D model and the 2D model shows that the results from two are very similar, see the **Climate report**, Section 3.4.4. Since lateral groundwater flow has only a minor role in permafrost development, e.g. /Hartikainen et al. 2010/ it is likely that modelling including 3D groundwater flow would only contribute minor changes to the permafrost and perennially frozen depths. Furthermore, the anisotropy of thermal properties is not a problem in 1D, since one can choose a combination of thermal properties that would give lowest temperatures, or at least very close to the lowest temperatures. Therefore, it is not likely that 3D permafrost simulations would yield notably lower temperatures than the range obtained by the full series of 1D and 2D sensitivity modelling simulations that have been performed, see the **Climate report**, Section 3.4.4, and /Hartikainen et al. 2010/. A description of the 1D permafrost model is found in /Hartikainen 2004/ and the 2D model in /Hartikainen et al. 2010/.

For describing the depths of permafrost and perennially frozen ground, specifically at the repository location and for the full reference glacial cycle, the 1D modelling approach was applied /Hartikainen 2004, SKB 2006c/. The 2D modelling approach was used to simulate the temporal- and spatial (along the profile) development of permafrost and frozen ground for the first ~50,000 years of the reference glacial cycle for a section of the entire Forsmark site. This time period includes the time with deepest permafrost for the full reference glacial cycle. The 2D modelling approach was also used to perform a broad range of sensitivity experiments covering all known uncertainties in input data for the permafrost simulations, see the **Climate report**, Section 3.4.4 and /Hartikainen et al. 2010/.

The air temperature curve reconstructed for the last glacial cycle, Figure 10-108, was used to calculate ground surface temperatures using among other things assumptions regarding ground surface coverage (vegetation and snow), for details see the **Climate report**, Section 3.4.4 and /Hartikainen et al. 2010/. The influence of vegetation and surface snow cover have been considered using an empirical relationship between air and ground temperatures for different kinds of vegetation and topographic wetness index, see /SKB 2006c, Hartikainen et al. 2010/.

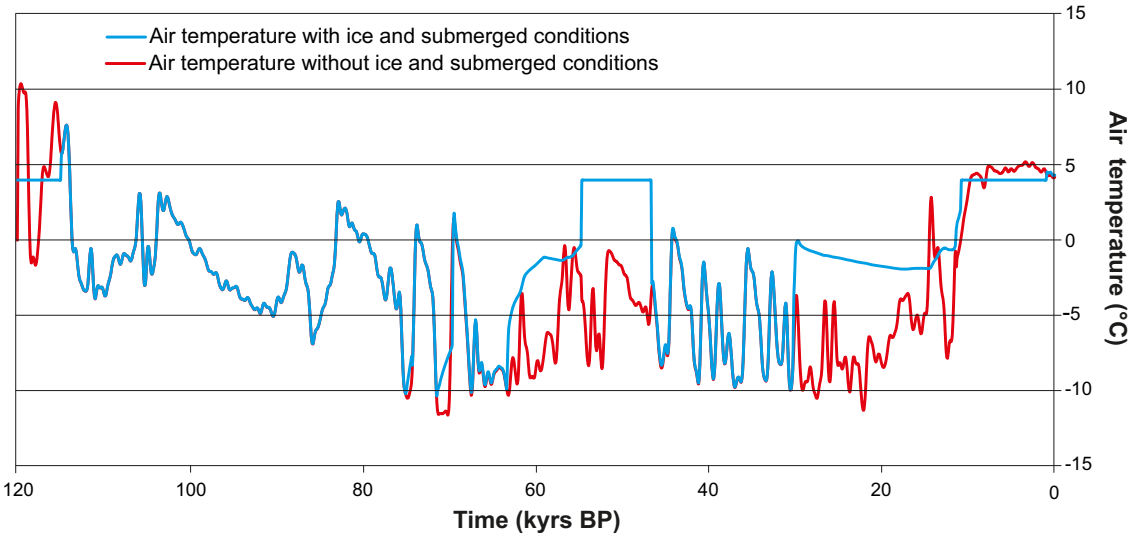

Figure 10-108. *Reconstructed air temperature curve for the Forsmark region for the past 120,000 years. The red line shows reconstructed last glacial cycle air temperatures without a presence of an ice sheet and submerged periods. The blue line includes periods of ice sheet coverage and submerged periods, i.e. it shows simulated basal ice temperatures for glaciated periods and air temperatures for ice free periods. A temperature of +4°C has been estimated for the submerged periods of the Eemian, Mid-Weichselian and Holocene. The construction of the temperature curve and its uncertainties are described and discussed in the* ***Climate report****, Appendix 1.*

For the permafrost modelling, the soil type and depth (full depth of unconsolidated Quaternary deposits), thermal and mechanical properties of rock domains and soil types, geothermal heat flow, chemical characteristics of groundwater and development of future lakes were obtained from the site descriptive models, see further /SKB 2006c, Hartikainen at al. 2010/. For examples of modelled ground surface temperatures for different stages of the reference glacial cycle (Boreal, Sub-arctic and Arctic settings), see /Hartikainen et al. 2010/.

The results of the calculations of permafrost depth (0°C isotherm) and depth of perennially frozen ground at the repository site for the full glacial cycle, projected into the future for the reference glacial cycle, are seen in Figure 10-102. The evolution of the maximum depth of the 0°C, –2°C and −4°C isotherms, as well as the perennially frozen ground, obtained from the 2D permafrost simulations are seen in Figure 10-109. The figures illustrates the first ~50,000 years of the reference glacial cycle, including the time with deepest permafrost at around 50,000 years after present. As seen in the figure, and further discussed in Section 10.4.1, the 0°C isotherm (permafrost) reaches a maximum depth of 259 m whereas the −2 and −4°C isotherms reach maximum depths of 200 m and 150 m, respectively, in the reference glacial cycle. However, these numbers do not account for all uncertainties in the input data.

As also mentioned in Section 10.4.1, the input data for the permafrost modelling have quite large uncertainties. The consequences of these uncertainties for the simulated depths of permafrost and perennially frozen ground were analysed in detail in /Hartikainen et al. 2010/. The largest uncertainty relates to air temperature. By setting *all* known uncertainties (e.g. in air temperature, climate humidity, surface wetness, vegetation, snow cover, bedrock thermal conductivity and diffusivity, and geothermal heat flux) in their most extreme setting favourable for permafrost growth, the uncertainty range for the permafrost reaches a maximum depth of 463 m and for the perennially frozen ground a depth of 422 m, see the **Climate report** Table 4-3. At the same time, the uncertainty ranges for the −2 and −4°C isotherms reach maximum depths of 388 and 316 m, respectively, see the **Climate report**, Table 4-3. This most extreme combination of uncertainties is quite unrealistic. These results conclusively show that the −4°C isotherm does not reach repository depth in the reference glacial cycle. Furthermore, since the uncertainty interval for the perennially frozen ground does not reach 450 m depth, even in this most extreme combination of all uncertainties, freezing of groundwater at repository depth is excluded in the reference glacial cycle. In this most extreme situation, the lowest temperature at the 450 and 470 m depths are approximately −0.5°C and 0°C respectively.

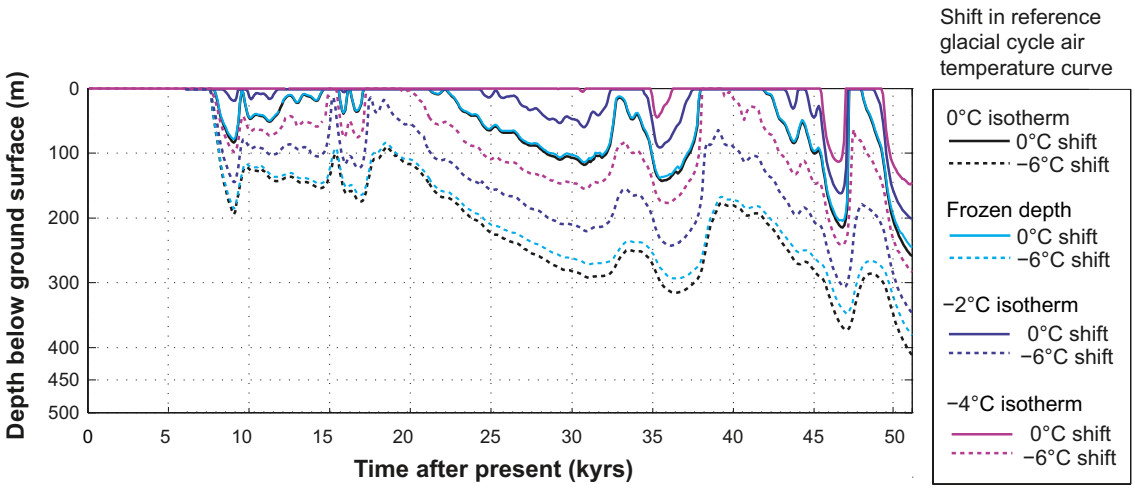

Figure 10-109. *Evolution of the 0°C isotherm (permafrost depth), perennially frozen ground, and the −2°C and −4°C isotherms at the Forsmark repository location. The results show the first ~50,000 years of the reference glacial cycle, including the period with deepest permafrost. Solid lines show reference glacial cycle. Dashed lines show the lower boundaries of the corresponding uncertainty intervals when considering the maximum uncertainty in air temperature (±6°C), see the* ***Climate report****, Appendix 1. The results are from the dry climate variant with deeper permafrost, see the* ***Climate report****, Section 3.4.4.*

In the reference glacial cycle, the maximum freezing depth is reached prior to the ice sheet overriding. This means that for this glacial cycle, glacial erosion will not reduce the repository depth so that it affects the conclusion on freezing. In addition, the total amount of surface denudation, i.e. the combined effect of surface erosion (including glacial erosion) and weathering, is expected to be within the range 1–2.6 m for the repository location in Forsmark during the reference glacial cycle, see the **Climate report**, Section 4.5.7. This amount of repository depth reduction also has an insignificant effect when considering subsequent glacial cycles.

The reconstruction of permafrost for the reference glacial cycle is described in detail in the **Climate report**, Sections 3.4.4 and 4.4.3.

Identified uncertainties and their handling in the subsequent analysis

Based on the above results, and on the buffer and backfill concept presented in Chapter 5, freezing of water, buffer clay and backfill material at repository depth does not occur in the reference evolution. Further evaluations of the uncertainties involved in this issue are given in a dedicated scenario, see Section 12.3.

10.4.4 Rock mechanics

If the buffer or backfill were to freeze under permafrost conditions, this would imply a mechanical load on the surrounding rock. However, based on the analyses in Section 10.4.3, freezing is not included in the reference evolution.

Glaciations will alter rock stresses compared with present-day conditions. The nature of glacially induced stresses depends not only on the ice-load, but also on the crust/mantle characteristics and interactions between the two. Whereas estimating the added vertical stress component is relatively straightforward, it is more complex to assess the horizontal stress components, as they will depend on the evolution and properties of the ice sheet, the thickness and mechanical properties of the crust and the properties of the viscoelastic material that the crust is assumed to rest on. However, any shear stress applied by the ice sheet at the ice-rock interface will not be significant.

The load imposed by the ice sheet on the underlying bedrock leads, on the large scale, to downwarping under the ice sheet and upwarping at the margins of the depression (forebulge). This results in an increase of compressional stresses in the crust below the ice and extensional stresses in the forebulge. On a small scale, the transient load of the ice sheet will cause an overall increase in total stresses, and an increased confinement due to the associated increase in horizontal stress. The combination of load from the ice sheet and increased pore pressures means that the effective stress is affected in two counteracting ways:

- An increase in total stress due to the mechanical loading by the ice sheet leads to an increase in effective stress, but
- an increase in pore pressure due to glaciation leads to a decrease in effective stress.

The resulting hydro-mechanical impacts will thus largely depend upon how the load of the ice sheet is transmitted to the underlying rock.

The following processes related to the glaciation cycle could have potential safety implications.

- Reactivation of fractures that could affect fracture transmissivity and transport resistance in the far field (safety function R2a) and in the near field (safety function R2b).
- Fracturing – potential for hydraulic jacking that could affect fracture transmissivity and the aperture of the deposition hole fracture interface and thus the buffer/rock interface transport resistance (safety function R2b).
- Potential for creep deformation, that could affect the geometry of the deposition holes (safety function R3), which in turn indirectly could affect several of the buffer and canister safety functions.
- Seismicity and faulting that could imply shear movement of fractures intersecting deposition holes (safety function R3b) and also increase the transmissivity of the sheared fracture (safety function R2b).

The safety implications of these processes except seismicity and faulting are assessed in the following sub-sections. Seismicity and faulting are treated in a dedicated Section 10.4.5, which also includes an assessment of the effects on the buffer and canister.

Stress changes during the glacial cycle

The continental ice sheet will increase the mechanical load on the repository, both through the additional weight of the ice itself and through the flexural response of the Earth's lithosphere. This will, on a large scale, result in a depression beneath the load, where crustal flexure will give an additional slow increase in horizontal stresses in the upper crust. Outside the ice sheet margin crustal flexure will result in an up-warping peripheral bulge in which the horizontal stresses are reduced. The magnitude of the induced bending stresses depends on the thickness of the ice sheet and on the duration the area is covered by ice. As the ice sheet retreats during deglaciation, the depressed lithosphere will experience isostatic rebound, which is a much slower process than the ice load removal process. Consequently, high horizontal stresses remain in the lithosphere for a significant amount of time after the ice sheet induced vertical stress has disappeared, resulting in increased stress anisotropy.

In addition to the glacially induced stress variations, the ice sheet will increase the water pressure in the rock below the ice or beneath an impermeable permafrost layer in front of the advancing ice. The increased pore pressure, in combination with the increased stress anisotropy, may cause the rock to fail, thereby causing disturbances ranging from increased fracture permeability to large earthquakes, such as those associated with the endglacial faults of northern Sweden e.g. /Lagerbäck 1979/.

/Lund et al. 2009/ studied how stresses induced by a realistic model of the Weichselian ice sheet evolve in time and space, and how those stresses interact with, and affect, the regional state of stress in Scandinavia. /Lund et al. 2009/ used the three-dimensional Weichselian ice sheet reported in /SKB 2006c/, which is the reference ice sheet scenario for SR-Site, in combination with both simple, horizontally layered Earth models and more complex 3D representations of the Earth. The resulting displacement fields were compared to available GPS data. In order to investigate the interaction of the glacial stresses with the background stress field the authors constructed models of the background field and showed how the combined stress field evolves. Using the combined stress field /Lund et al. 2009/ estimated how the stability of faults is affected by the glaciation, giving particular attention to the Forsmark and Laxemar sites and, for comparison, the Pärvie fault in northern Sweden, the largest of the known glacially reactivated faults.

/Hökmark et al. 2010/ use the results of /Lund et al. 2009/ to estimate the stress changes in the far field as well as the near field. Figure 10-110 shows the temporal evolution of the total principal stresses at repository depth (460 m) during the glacial phase at Forsmark. Similarly to the repository heated period of the temperate phase, the temperature changes introduced during permafrost conditions will alter the

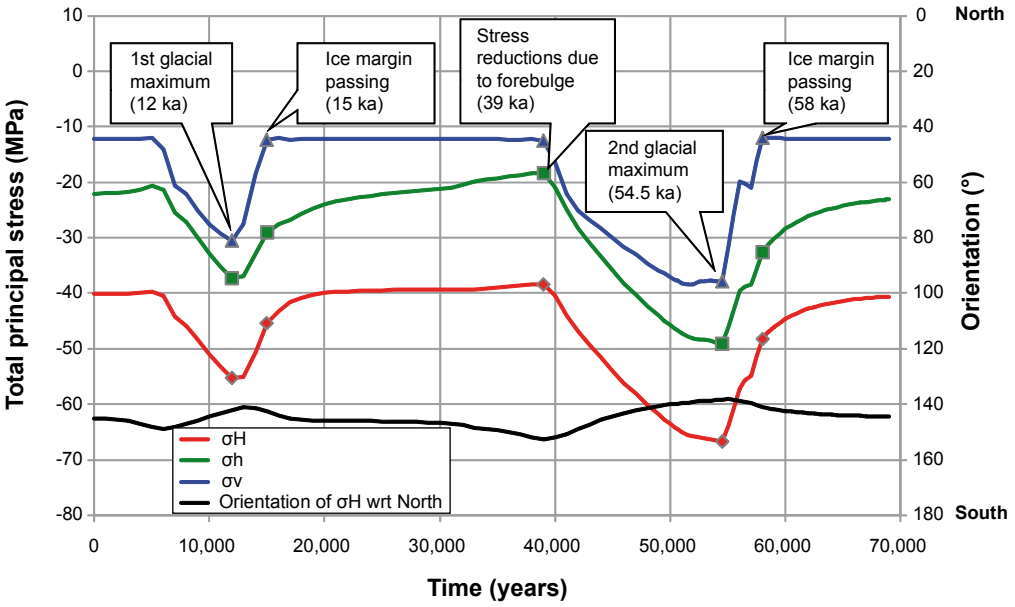

Figure 10-110. *Total principal (σH, σh, σv) stress magnitudes at repository depth during the glacial phase at Forsmark. Note that time = 0 in the figure is the time when glacial mechanical effects begin, i.e. about 50,000 AP, according to the reference glacial cycle. The orientation of major horizontal stress with respect to North is also shown. The glacially induced stresses at 500 m depth are taken from /Lund et al. 2009/. In this diagram compression is negative. From /Hökmark et al. 2010, Figure 7-14/.*

stresses in the rock mass. However, as opposed to the temperate phase the temperature reduction during permafrost conditions affects much larger volumes of the rock mass meaning that thermo-mechanical properties on a larger scale have to be considered, i.e. accounting for surrounding rock with lower stiffness and the presence of deformation zones, which will effectively reduce the deformation modulus of the rock mass. Based on estimates of the rock mass deformation modulus, in the range 40–45 GPa, suggested to be valid for large scale models of the bedrock surrounding the Forsmark site, the results from the present modelling work are scaled to an effective deformation modulus of 40 GPa. Figure 10-111 shows the resulting reduction in horizontal stress as a function of depth. Furthermore, /Hökmark et al. 2010/ make two alternative assumptions regarding the glacially induced pore pressure at different depths.

1. It is assumed to follow the hydrostatic pressure at the ice bed interface, i.e. 98% of the increase in vertical stress due to the glacier, at all times and at all depths. However, as the ice margin is passing over the site or in combination with proglacial permafrost as the ice is advancing, this approach may underestimate the excess pore pressure at large depths.
2. Estimates of the residual pore overpressure as a function of depth as the ice margin is passing over the site are established in 2D using a simplified ice sheet profile /Paterson 1994/ with the suggested ice frontal retreat rate at Forsmark /SKB 2006a/ and with depth-dependent hydraulic properties of the rock mass /Follin et al. 2007b, Vidstrand et al. 2010/. The estimate of the over-pressure that could exist under an impermeable proglacial permafrost layer is based on worst case assumptions of the permafrost melting rate, i.e. on a case that maximizes the potential jacking depth under the advancing margin /Lönnqvist and Hökmark 2010/. For the latter pore pressure estimate, the seasonal pressure variations are taken into account.

Reactivation of fractures during glacial cycle – hydraulic impacts in the far field

Using the modelling approach outlined in Section 10.3.5, /Hökmark et al. 2010/ assess the transmissivity effects for five instances in time, the first glacial maximum (12,000 years after the first mechanical impact due to the ice), ice margin passing over the site in connection with the first episode of ice frontal retreat (after 15,000 years), stress reductions due to forebulge (after 39,000 years), second glacial maximum (after 54,500 years) and ice margin passing over the site in connection with the second episode of ice frontal retreat (58,000 years after the first mechanical impact).

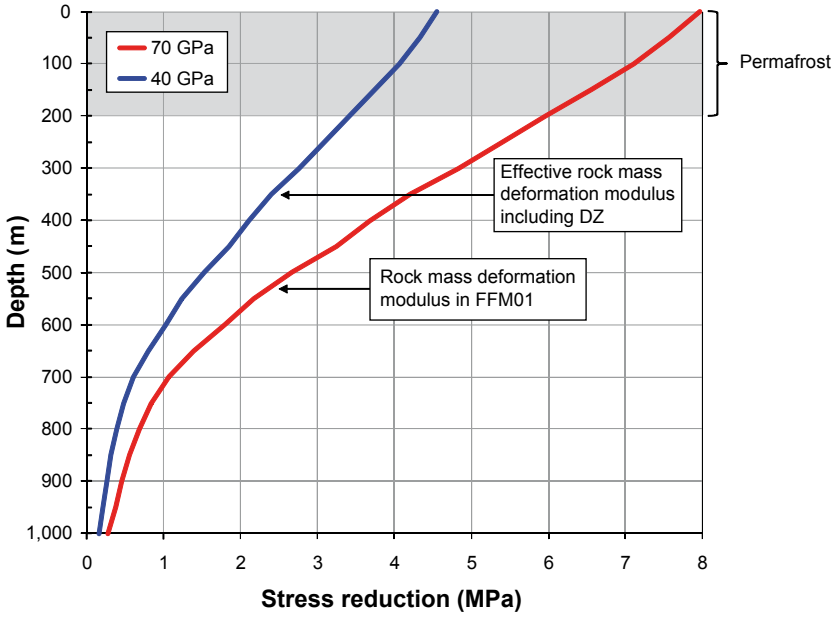

Figure 10-111. *Horizontal stress reduction (i.e. reduction of compression) during permafrost conditions. The red line is the calculation result based on a local scale rock mass stiffness of 70 GPa. For use in subsequent analyses this stress reduction is revised, shown in the blue line, such that it represent the rock mass stiffness for relevant large-scale elastic properties, i.e. a rock mass stiffness of 40 GPa. From /Hökmark et al. 2010, Figure 7-6/.*

The results are sensitive to the assumptions regarding the magnitude of the pore pressures. Two cases, described in the text above, regarding the glacially induced pore pressure are considered. In addition to variations in pore pressure, the impact of the potential reduction of the horizontal stress components by thermo-mechanical effects due to permafrost are also considered. The following is found:

- On fractures or fracture zones perpendicular to the major horizontal *in situ* stress, there are only negligible variations in relative transmissivity below a depth of around 200 m, regardless of the pore pressure assumption or potential reductions of the horizontal stress components during permafrost.
- On fractures and fracture zones oriented perpendicular to the present-day minor horizontal *in situ* principal stress, the relative transmissivity is increased during the first glacial maximum (after 12,000 years) and during the forebulge (after 39,000 years), whereas it is reduced as the ice margin passes (after 15,000 and 58,000 years) and during the second glacial maximum (after 54,500 years). This applies for both assumptions regarding the pore pressure. The maximum increase in relative transmissivity occurs during the forebulge (after 39,000 years). Without considering an increase in pore pressure due to permafrost, the relative transmissivity is increased by a factor around 2 (model A according to Figure 10-20) at shallow depths and less than 30% at repository depth and below, see Figure 10-112 (left). In combination with proglacial permafrost (after 39,000 years), the increase in pore pressure results in an increase in relative transmissivity by a factor around 2–3 (model A) at repository level and above. For model B (see Figure 10-20), no increase in relative transmissivity larger than a factor 1.6 was found. The additional reduction in the effective horizontal stresses during permafrost conditions, results in a substantial increase in relative transmissivity at shallow depths (a factor about 7) but the increase at repository level is a factor around 2.5 (model A), see /Hökmark et al. 2010, Figure 7-10/. The corresponding range for model B is 1.5–2.5.
- The effective vertical stress is unaffected or marginally increased at all times and at all depths when residual or permafrost induced pore pressures are not considered, resulting in only negligible variations in the relative transmissivity of horizontal fractures, see Figure 10-113. As the ice front is retreating (after 15,000 and 58,000 years), the maximum increase in relative transmissivity is in the range 1.5–2.1 (model A). For model B the maximum increase is less than a factor 1.4 at all depths. In combination with proglacial permafrost (39,000 years), the maximum increase in relative transmissivity is a factor 2.3 directly below the permafrost and decreases with depth (model A). For model B the maximum increase is less than a factor 1.5 at all depths.

In conclusion, the potential transmissivity increases during the glacial cycle are very moderate, especially in relation to other uncertainties in the flow model, and there seems to be little reason to assess their impacts on the groundwater flow during this period.

/Hökmark et al. 2010, Section 7–5/ also assess the potential for shearing during the glacial cycle and draw the following conclusions.

- The largest shear displacements occur in connection with the second episode of ice frontal retreat. A 100 m radius fracture with the most favourable orientation, with regard to slip, might slip at maximum about 12 mm assuming the largest possible residual pore pressure considered (about 1 MPa at repository depth). Without any residual excess pore pressure, the corresponding maximum slip is about 8 mm. Smaller fractures slip correspondingly less. The effective normal stresses are reduced but are still around 12–14 MPa for the most unstable fractures, i.e. high enough to suppress dilation. It is therefore assumed that the resulting changes in transmissivity are negligible.
- For fractures dipping more than 45°, the shear displacement is less than 2–3 mm regardless of strike. Fracture with radii larger than 100 m will move correspondingly more. The effective normal stress is significantly increased, which will mean that the resulting transmissivity is likely to be reduced rather than increased regardless of the magnitude of the displacement.

These findings should be regarded as upper bound estimates of the impact of stress changes. All results are based on numerical and analytical solutions that approximate fractures with perfectly planar slip planes. This means that, for given stress conditions, the amount of slip scales with fracture size. In reality, slip along large fractures probably would be controlled by variations in fracture orientation, large scale irregularities etc. There is, however, no defensible way of accounting for these effects and it cannot be excluded that some fractures could be close to being perfectly planar.

In conclusion, while there are some mechanical impacts on fracture transmissivity during the glacial cycle, these impacts are judge too small to require further assessment in SR-Site.

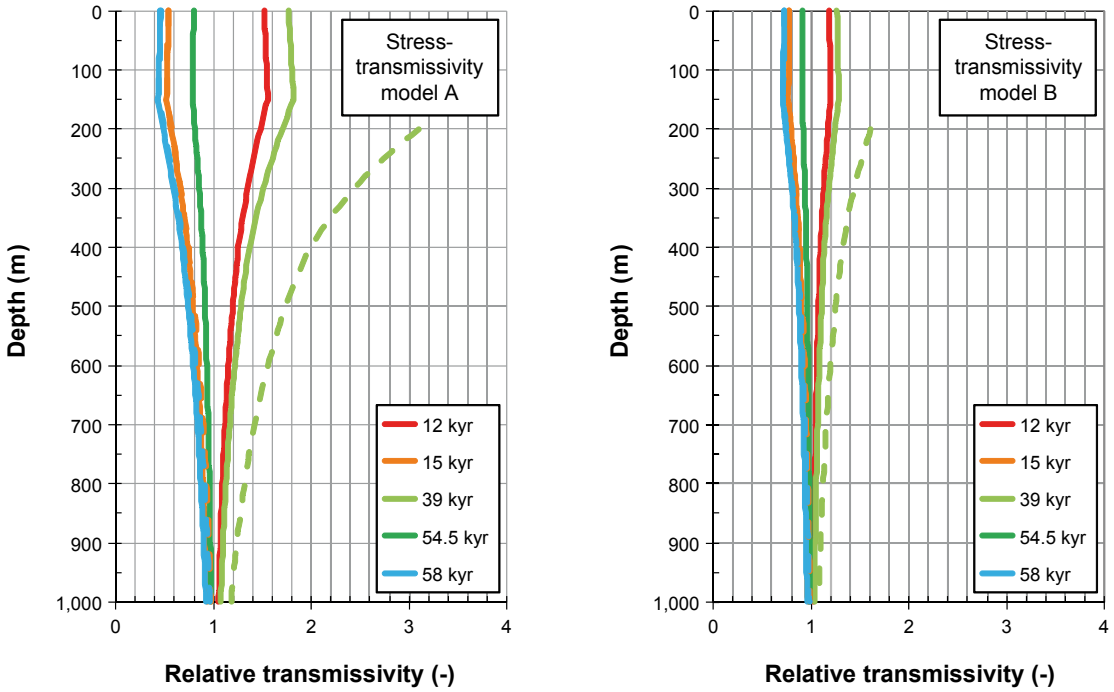

Figure 10-112. *Relative transmissivity of vertical fractures perpendicular to the present-day minor horizontal in situ principal stress, σ_h. Effects due to residual pore pressures are marked with dashed lines. From /Hökmark et al. 2010, Figure 7-9/.*

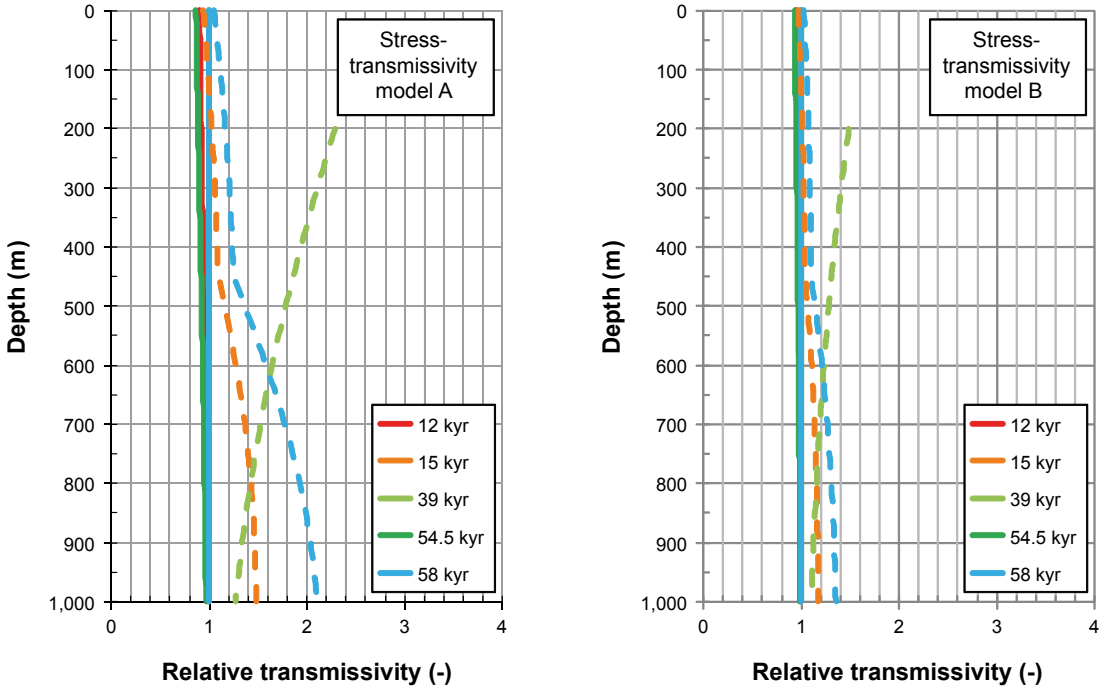

Figure 10-113. *Relative transmissivity of horizontal fractures. Effects due to residual pore pressures are marked with dashed lines. From /Hökmark et al. 2010, Figure 7-11/.*

Reactivation of fractures – potential hydraulic impacts in the near field

The transmissivity impacts discussed in the previous section also apply to the near field. However, to complement these analyses for the near-field scale, the 3DEC near-field rock mechanics analysis of /Hökmark et al. 2010/, see Section 10.3.5, explored the effects of the glacial load regarding transmissivity impacts due to variations in effective normal stress, see also Figure 10-114:

- The largest reductions in effective normal stress occur during the two glacial maxima (12,000 and 54,500 years).
- Steeply dipping fractures striking perpendicular to the deposition tunnel, and approximately to σ_H, have sufficiently high compressions that the resulting variations in relative transmissivity are only marginal.
- For other steeply dipping fractures, the changes in transmissivity could be as high as a factor of 20, but these would be concentrated in a limited region around the tunnel. The size of the fracture is not important. Note that the stress-transmissivity relation becomes very uncertain as the effective normal stress approaches zero, i.e. when the transmissivity becomes indefinite. However, /Hökmark et al. 2010/ argue that, for fractures in compression of a few MPa, the stress-transmissivity relations are relevant as upper bound estimates of the sensitivity to variations in effective normal stress.
- If the fracture is less than 2 m from the tunnel and almost parallel to the tunnel periphery, then the high-transmissivity part of the fracture may be large, i.e. extend along large distances of the tunnel. In this case, the size of the fracture will become important.
- At distances larger than approximately 2 m from the tunnel, there are only marginal changes in relative transmissivity.

Conclusions that can be drawn from the analyses of shear displacements coincide with those for the far-field fractures. However, there may be regions very close to the openings where local transmissivity effects could be significant, for instance because of shear displacements along fractures in very low compression.

- For steeply dipping fractures there are only very limited shear displacements close to the tunnel regardless of whether transient pore pressure effects during the glacial phase are considered or not. These small shear displacements are judged not to have any implications for the overall transmissivity of fractures intersecting the tunnels.
- Gently dipping fractures are more likely to shear, but the impact depends on the assumptions made on pore pressures. The amount of shearing will depend on the size of the fracture and its strike orientation. For the 50 m-radius fracture assessed by /Hökmark et al. 2010/, the maximum shear displacement was around 8–9 mm.

In summary, when taking transmissivity impacts originating from both variations in effective normal stress and shearing into account, /Hökmark et al. 2010/ concluded that the results obtained for SR-Can /Hökmark et al. 2006, Figure 5-8/ give an adequate description of the transmissivity increase of differently oriented fractures intersecting the near field. /Hökmark et al. 2006/ estimated that the transmissivity might increase by two orders of magnitude in a region of around 1–2 m from the tunnel periphery.

Fracturing – potential for hydraulic jacking

Hydraulic jacking is a phenomenon that theoretically occurs when the pore pressure in a fracture exceeds both the normal stress acting on the fracture and the fracture's tensile strength. This is the same mechanism as hydraulic fracturing, which is a standard operation in the petroleum industry carried out in wells for improving oil or gas recovery from reservoir rocks and in rock stress measurement. Hydraulic jacking could potentially be initiated during a glacial period when high pore pressures must be assumed to build up in the rock beneath the permafrost in front of an advancing ice sheet or below the ice sheet. As the ice sheet retreats at the end of the glacial phase, the pore pressure may remain high for a long time after the ice is gone. When jacking occurs, the fracture surfaces separate from each other and the fracture aperture may be very large. Jacking can be expected to continue as long as the conditions driving tensile conditions in the fracture exist. Except for horizontal or sub-horizontal fractures close to the ground surface where the overlying rock can potentially be lifted, the maximum aperture resulting from the process is limited by the deformation potential of the rock mass surrounding the dilating fractures.

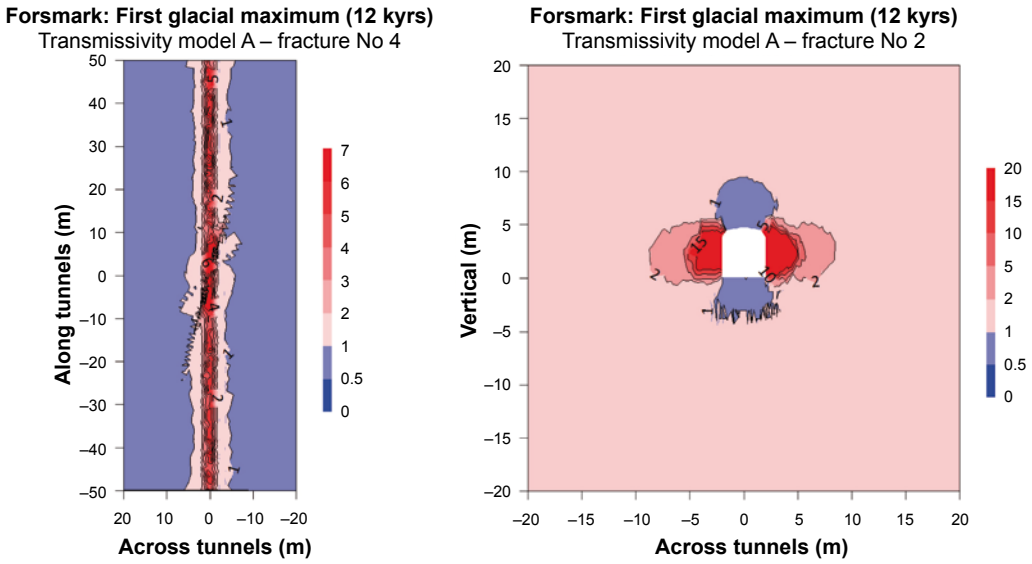

Figure 10-114. *Relative transmissivity change for at the first glacial maximum (after 12 ka) in a fracture (left) parallel to the tunnel floor and (right) a vertical fracture intersecting the tunnel with a small angle projected onto the vertical plane perpendicular to the deposition tunnel. Modified after Figures 8-16 and 8-12 in /Hökmark et al. 2010/.*

The present understanding is that the horizontal stress components due to the ice are of the same magnitude or greater than the corresponding vertical stress component and that they exist outside the ice /Lund et al. 2009/. In a reverse stress field ($\sigma_H > \sigma_h > \sigma_v$), which is the case at Forsmark /Glamheden et al. 2007/, this implies that hydraulic jacking is mainly of concern for sub-horizontal fractures.

Possible indications of hydraulic jacking events, in the form of sediment-filled fractures, have been found at Forsmark, to depths of a few tens of metres. However, hydraulic jacking may, in theory, also be initiated at substantially larger depths /Talbot 1999, Hökmark et al. 2006/. Therefore, a special study on the potential for hydraulic jacking during a glacial cycle /Lönnqvist and Hökmark 2010/ has been conducted. It shows that:

- In the absence of proglacial permafrost, hydraulic jacking in front of an advancing ice sheet is unlikely to be initiated at depths greater than about 30 m if the rock can be treated as a continuous and relatively homogeneous porous medium. The possibility that a few highly transmissive fractures in otherwise low permeable rock may transfer high pressures from large distances under the ice to the ice front and thereby cause hydraulic jacking can also be discarded. Analytical estimates indicate that in order to initiate hydraulic jacking at 400 m depth a fracture at least 7.6 km long in otherwise impermeable rock is needed. There are no indications of the existence of such fractures at Forsmark.
- For the case of proglacial permafrost in front of an advancing ice, hydraulic jacking below the permafrost could only be seen for permafrost melting rates much higher than those established for the reference glaciation cycle. Note that the pore pressure beneath the permafrost is completely determined by the pressure at the melting zone, the diffusivity of the rock and the time-frame of the frontal advance, which implies that the initial permafrost thickness will not influence the maximum jacking depth. The worst cases studied had an initial permafrost depth of 200 m with melting rates between 0.5 and 1 m/year and this condition gave maximum jacking depths of around 330–350 m. However, this depth was reduced to about 175–210 m, considering the seasonal variations in the boundary hydrostatic pressure. The reference melting rate resulted in increased pore pressure levels corresponding to jacking depths of less than 10 m. A potential occurrence of open taliks near the repository would further decrease the maximum jacking depth.
- For a retreating ice sheet, the key factors are the frontal retreat rate of the ice and the hydraulic diffusivity of the rock. The maximum jacking depth was established for two assumptions regarding the frontal retreat rate: A much faster frontal retreat rate (500 m/year) suggested by /Talbot 1999/ and the retreat rate of 300 m/year considered to be more relevant for Forsmark /SKB 2006a/. A maximum jacking depth less than 100 m results even for the fastest retreat speed. For the retreat speed relevant for Forsmark (300 m/year) the maximum jacking depth is around 50 m.

In conclusion, hydraulic jacking due to the impacts of the glacial cycle, below 200 m depth is judged highly unlikely. At more shallow depths it may happen, and the highly transmissive subhorizontal fractures near surface at Forsmark may be evidence of this occurring in the past. However, given the already very high, and potentially jacking-induced, near surface horizontal permeability, this effect is already captured in the hydrogeological models used.

Fracturing of the rock due to the glacial load

/Hökmark et al. 2010/ also assess the potential for spalling in the deposition tunnel walls due to the glacial load. The stresses at the centre of the tunnel roof will not exceed the spalling strength during the temperate phase. During the second glacial maximum (54.5 ka) the major principal stress at the centre of the tunnel roof reaches a maximum of about 95 MPa, i.e. well below the spalling threshold, but the spalling strength might be exceeded in the corners. Potentially, this can be avoided by rounding the corners, but the possibility needs to be considered as a potential mechanism for generating enhanced rock permeability near the roof.

Potential for creep deformation

As further discussed in Section 4.5 of the **Geosphere process report**, and supported by the recent study by /Damjanac and Fairhurst 2010/, creep deformation of the rock mass may be neglected for the mechanical loads that may occur during permafrost or glaciation. The process is neglected for the same reasons as for the temperate periods, see Section 10.3.5.

Identified uncertainties and their handling in the subsequent analysis

The discussion above is used to draw a set of conclusions regarding the uncertainties, and their subsequent handling in the SR-Site analyses, on the mechanical changes in the bedrock projected to occur during the remaining part of the reference glacial cycle.

- The *transmissivity increases due to reactivation of fractures* during the forebulge period of the glacial cycle are relatively moderate, especially in relation to other uncertainties, and it is judged not to be justified to assess their impacts on the groundwater flow during this period, apart from the transmissivity increase that would occur for fractures close to and parallel with the tunnel floor. However, this case is already covered by the assumptions made for the EDZ, see further the **Data report**.
- *Hydraulic jacking* below 200 m, due to the impacts of the glacial cycle is judged highly unlikely. At shallower depths it may happen, and the highly transmissive gently dipping fractures near surface at Forsmark may be evidence of this occurring in the past. Given the already very high, and potentially jacking-induced, near surface horizontal permeability, this effect is already captured in the hydrogeological models used and the phenomenon is excluded from further analysis.
- *Fracturing of the rock due to the glacial load.* During the second glacial maximum (54,500 years after first mechanical impact of the ice) the spalling strength might be exceeded in the corners of the tunnel roof. Potentially, this can be avoided by rounding the corners, but the possibility should be considered as having the potential for enhanced rock permeability near the roof. However, the permeability increase would be much smaller than the “crown space” case considered in the hydrogeological assessment, see Section 10.4.6 and there is no need for a special calculation case for assessing the importance of this effect.
- Literature evidence suggests that there is no potential for *creep deformation* that could significantly affect deposition hole geometry, allowing exclusion of the phenomenon from the safety assessment.

10.4.5 Canister failure due to rock shear movements

Introduction

One of three identified failure modes of the canister is that due to a rock shear movement across a deposition hole. The safety function Can3 in Figure 10-2 relates to the ability of the canister to withstand such loads. The buffer is designed to damp rock shear and the safety function requirement

on the buffer (Buff3) in this context is that its saturated density should be below 2,050 kg/m^3. An integrated evaluation of the response of the buffer and canister to rock shear has led to the criterion that the shear movement should not exceed 5 cm (safety function R3b), and that the shear velocity should be less than 1 m/s (safety function R3c).

Accordingly, earthquake-triggered, fast, shear movements along fractures intersecting a canister can potentially affect the containment of the spent fuel assemblies if the amount of slip exceeds 5 cm. Shear velocities higher than 1 m/s have not been observed in any of the simulations conducted to quantify seismically-induced fracture shear displacements at different distances from earthquakes of different magnitudes /Munier and Hökmark 2004, Fälth and Hökmark 2006, Fälth et al. 2010/. Therefore, the question of whether the containment of the spent fuel could also be affected by very fast shear displacements smaller than 5 cm is not relevant.

Loads other than seismic, for instance thermally-induced loads during the early temperate phase, will not produce fracture shear displacements larger than about 1cm, not even on optimally-oriented fractures of 300 m diameter, see Section 10.4.4, and /Hökmark et al. 2010/. The effects on the buffer-canister system of such minor shear displacements produced by time-continuous variations of the host rock stresses are judged to be irrelevant to the assessment of the seismic risk, i.e. the canister will withstand a 5 cm seismically-induced shear displacement, regardless of whether minor aseismic displacements occurred in the past.

In the following, the 5 cm damage threshold is pessimistically applied throughout in all assessments of the number of canisters being damaged as a result of seismically-induced shear displacements, regardless of the canister-fracture intersection geometry and the actual shear velocity. At present there is no estimate of the probability that, for instance, a 6, 7 or 10 cm random intersection geometry displacement actually would impact sufficiently that the canister should be regarded as failed. All estimates of the number of failed canisters are thus pessimistic as regards the applied damage threshold.

Sweden is located in the Fennoscandian Shield /Koistinen et al. 2004/ far from plate boundaries and active volcanism. Though its rocks bear witness of a violent tectonic past that include several orogenies and failed rifts, the bedrock is now seismically stable. However, glacially triggered faults /Kujansuu 1964, Lundquist and Lagerbäck 1976, Olesen et al. 2000/, commonly referred to as "postglacial faults" and traditionally abbreviated "PGF", occur in glaciated regions in response to changes in the glacial load, either as a result of deglaciation (crustal unloading) or glacial advance (crustal loading). Glacially induced faulting has been reported from northwest Europe (Norway, Sweden, Finland, Russia, Eire, and Scotland) and North America (eastern Canada, New England, and possibly California and Montana). To date, all examples of glacially induced faults have been recorded in regions of low to moderate seismicity, namely passive margin, failed rift, or intraplate/craton environments such as Sweden.

The postglacial faults in northern Sweden are convincing examples of glacially induced faulting. Although there have been numerous claims of such faulting in mid- to southern Sweden /Mörner 1989, 2003, 2004/, many have been questioned as to whether they are such /SKB 1990, Carlsten and Stråhle 2000, Wänstedt 2000, Lagerbäck and Sundh 2008/. Within the framework of the site investigations, /Lagerbäck et al. 2005, 2006/ investigated large areas in the vicinity of the Forsmark and the Laxemar sites and came to the conclusion that large, glacially induced earthquakes cannot be positively demonstrated. Still, /Lagerbäck and Sundh 2008/ emphasise that their findings do not exclude the possibility of smaller earthquakes having occurred, nor do they exclude the possibility of future, large earthquakes in the investigated areas.

The potential for fault weakening and/or reactivation at the sites, as a response to future glaciations has, using simulation of advancing and retreating ice sheets, been addressed in a series of reports to SKB /Lund 2005, 2006, Lund et al. 2009/ and the effect on a repository, should a large earthquake occur in the vicinity, has been investigated in a series of reports and publications by Fälth and Hökmark /Fälth and Hökmark 2006, Fälth et al. 2007, 2008/.

It is well known that underground facilities are resistant to earthquakes e.g. /Bäckblom and Munier 2002, and references therein/ and that detrimental effects of a large earthquake near the repository can be avoided or considerably lessened by adaptive design involving the use of respect distances /Munier and Hökmark 2004, Munier et al. 2008/ and deposition hole rejection criteria /Munier 2006, 2007, Hedin 2008b/.

Using the outcome of /Lund et al. 2009/, /Fälth et al. 2010/ computed stability margins of deformation zones at the Forsmark site to identify the zones most likely to reactivate during various periods of the ice sheet evolution. This, combined with deposition hole rejection criteria /Munier 2010/, was used to assess the number of critical canister positions and thereby the contribution to radiation risk at Forsmark. This is elaborated further upon below.

Probability of future large earthquakes

All tectonic plates have internal stress fields caused by their interactions with neighbouring plates and loading or unloading (e.g. sediments, ice sheets). These stresses may be sufficient to cause failure along existing fault planes, giving rise to earthquakes. Large intraplate earthquakes are rare compared to earthquakes at plate boundaries but, given the very long time frame of this safety assessment, 10^5–10^6 years, large earthquakes are anticipated in Sweden. The difficulty lies in estimating where, how large, and how many earthquakes we anticipate over the time frame considered for SR-Site.

The presence of a continental ice sheet, such as Weichsel, tends to promote fault stability /Johnston 1987, Lund et al. 2009/ while the retreat of the ice sheet is followed by rapid glacio-isostatic adjustment and is believed to be accompanied by a sudden increase in both frequency and magnitude of earthquakes. The glacially induced stress magnitudes are not large enough /Lund et al. 2009/ to initiate large ruptures on their own. However, during some periods in the glacial cycle they are large enough, aided by pore pressure disturbances, to trigger reactivation of pre-existing faults that are close to failure in the background, preglacial, stress field. Figure 10-115 displays historic and recent earthquakes in Sweden from the FENCAT /FENCAT 2007/ and SNSN /Böðvarsson 2002, 2009, Böðvarsson et al. 2006/ catalogues, respectively.

The relationship between the magnitude and total number of earthquakes in any given region and time period is given by the Gutenberg–Richter law. Prediction of future earthquakes thus essentially concerns our ability to adequately determine the parameters a and b of the Gutenberg–Richter law:

$$\log N = a - bM_L$$

in which N is the number of earthquakes with magnitudes greater than M_L.

There have been few attempts to estimate the earthquake frequency for time periods relevant to SR-Site. To our knowledge, these are restricted to the ones listed in Table 10-14.

Table 10-14. Estimated[17],[18] yearly frequency of earthquakes ≥ M5 within a 5 km radius area. These frequencies are distributed (f) along the 30 deformation zones susceptible to reactivation (see Table 10-15 and /Fälth et al. 2010/), out of the 36 deformation zones intersecting the area (Figure 10-128).

Reference	Earthquake frequency (M≥ 5/year)	
	5 km radius area	f
/Böðvarsson et al. 2006/	$2.4 \cdot 10^{-6}$	$7.8 \cdot 10^{-8}$
/La Pointe et al. 2000, 2002/	$8.7 \cdot 10^{-7}$	$2.9 \cdot 10^{-8}$
/Hora and Jensen 2005/	$2.5 \cdot 10^{-6}$	$8.3 \cdot 10^{-8}$
/Fenton et al. 2006/	$2.0 \cdot 10^{-6}$	$6.8 \cdot 10^{-8}$

The frequencies shown in Table 10-14 were, for comparative reasons, normalised by averaging the original frequencies predicted by each estimate over the area covered by each assessment and here rescaled to an area corresponding to a circle with 5 km radius. It is emphasised that estimates of

[17] The frequency estimates of /Hora and Jensen 2005/ in Table 10-14 concern earthquakes of magnitude M6 or larger. The references therein were not readily scalable to ≥ M5 but, as the slope of the logarithmic G-R relationship is close to unity /Scholz 2002/, we increased the frequencies in Table 10-14 by a factor 10 to incorporate earthquakes of magnitude M5 or larger as an approximation.

[18] In /Fenton et al. 2006/ frequency estimates ≥ M4.9 were provided and we choose to use the original values rather than rescaling to M5. This will slightly overestimate the frequency.

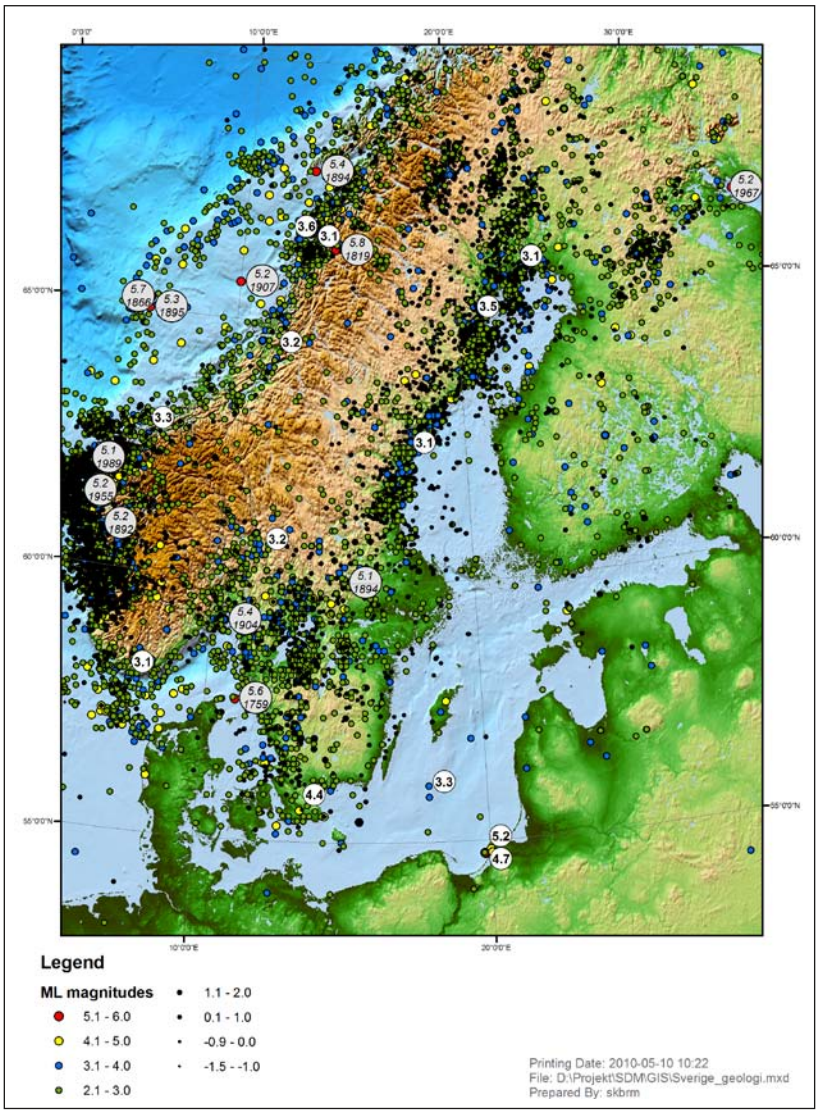

Figure 10-115. *Earthquakes measured by SNSN during the period 2002–2009 /Böðvarsson 2002–2009/ combined with the Helsinki catalogue /FENCAT 2007/.*

anticipated earthquakes at Forsmark, based on frequencies in Table 10-14, are associated with some yet unresolved uncertainties and fundamental assumptions.

A. /Lagerbäck and Sundh 2008/ note that the erosional impact of the Weichsel was quite limited, and it could not have erased remnants of post-glacial faults triggered by previous glaciations. The authors hypothesise that glaciations previous to the Weichsel did not generate faulting analogous to the ones during the Weichsel and suggest that the Weichselian ice sheet could have been anomalous in terms of permafrost-related hydraulic overpressures. Nevertheless, in the absence of further knowledge, it is cautiously assumed that the coming glaciations will have the same impact as the Weichsel in terms of fault stability.

B. The reason for the locations of all of the unequivocally identified post-glacial faults being restricted to the Lapland region is unclear. It is cautiously assumed that the estimated frequencies of large earthquakes are applicable to Forsmark. However, whether strain energy release at Forsmark will indeed be dominated by seismic or aseismic slip is an open issue. The lack of markers for large earthquakes at Forsmark is taken as an indication that faults following the retreat of Weichsel either slipped aseismically, with small magnitudes, or not at all. As aseismic slip is not anticipated to impose any threat to the integrity of the repository, the assumption is pessmistic.

C. The site proposed for the repository is located in a tectonic lens bounded by regional deformation zones (Figure 10-116) having surface trace lengths exceeding 30 km for the Singö- (ZFMWNW0001) and Eckarfjärden (ZFMNW0003) zones, respectively, and exceeding 70 km for the Forsmark (ZFMWNW0004) deformation zone (Table 10-15). It is judged probable that these zones have greater potential to attract future strains than the much smaller zones within the lens, as has been the case for the latest 1.8–1.7 Ga /Stephens et al. 2007/. In particular, these are the only zones near the repository that are large enough to host large earthquakes (up to perhaps M7.5). However, as there are no means to know which of the zones will in fact reactivate in the future, we need to pessimistically assume that all zones considered unstable during the glacial cycle have equal probability to reactivate.

D. The earthquake catalogue that forms the foundation of any estimate is very short in relation to the assessment, only about 100 years. The inter-glacial seismicity might be cyclic in nature and it is essentially unknown whether the recorded earthquakes can be regarded as representative.

E. The magnitude-frequency assessment is very much affected by the largest possible earthquake within the area for which the catalogue is defined. Very few attempts have been made to address this aspect and, using Pärvie as the largest event, published estimates of maximum magnitude range between M7 and M8.2 /Muir Wood et al. 1989, Arvidsson 1996, Johnston 1996/.

F. In the 100 years of observed seismicity there is significant spatial variation. It is unclear whether the spatial distribution of earthquakes observed during the last century is a stationary feature, or if it will vary with time. The average spatial frequency for Sweden, which is higher than the recorded frequency at Forsmark, has been pessimistically used for the assessment.

G. Although much is known about the earthquake frequency pulse following the retreat of the ice sheet /Johnston 1987, Muir Wood et al. 1989, Muir Wood 2000, Mörner 2003/ the understanding of the nature of the frequency decay with time is incomplete /Bungum et al. 2010/. The fundamental assumption that the frequency estimates used for the safety assessment represent an *average* over the glacial cycle is made. This assumption can be somewhat corroborated by checking how well the frequency-magnitude relations predict the largest events. Using the frequency-magnitude relations of /Böðvarsson et al. 2006, Section 4.4/ about 40 earthquakes ≥ M7 and about 6 earthquakes ≥ M8 during a glacial cycle are computed, when normalised to the area of Sweden. Despite the vast uncertainties, this number of events seems within an order of magnitude consistent with the number of faults that have unequivocally been designated as post-glacial faults. Additionally, this indicates that though the frequency estimates of /Böðvarsson et al. 2006/ were targeted for short time frames (≤ 1,000 years) they can be reliably extrapolated to longer time frames.

All earthquakes result in permanent strain and stress relaxation that stabilises the surrounding rock mass for a considerable amount of time. The stabilising effects reach several km from the earthquake /Fälth et al. 2010/, in agreement with observed spacing of faults as noted in /Munier and Hökmark 2004, Appendix 3/. When, or if, an earthquake occurs at Forsmark, the stress relaxation will be sufficiently efficient to encompass the nearest deformation zones at least during the same period of potential instability. Consequently, given the geometry and, in particular, the spacing of deformation zones at Forsmark (Figure 10-117), only one zone will be able to reactivate within such an episode. However, the duration of the stabilising effect is uncertain. This uncertainty relates to the strain rate, determined by large scale tectonic processes. If the tectonic strain rate is high, the background stresses may largely be restored between glacial cycles. This could lead to repeated endglacial earthquakes during following periods of glacial retreat. Intraplate strain rate estimates range between roughly 10^{-12} per year /Anderson 1986, Muir Wood 1995/ and roughly $1.5\ 10^{-9}$ per year /Slunga 1991, Sandiford et al. 2004, Scherneck et al. 2010/. However, /Slunga 1991/ argues that most of the strain energy is continuously released aseismically, meaning that only a fraction of the tectonic strain would be effective for accumulating energy and restoring stresses. This implies that the strain rate effective for local stress regeneration is much lower than the large-scale strain rate across the Fennoscandian Shield.

Assuming the average crust deformation modulus (E) to be 64 GPa /Lund et al. 2009/ for the upper 15 km, a tectonic strain rate, $\dot{\varepsilon}$, of 10^{-10} per year e.g. /Calais et al. 2005, 2006, Mazotti et al. 2005/, which is intermediate to those proposed by /Muir Wood 1995/ and /Slunga 1991/, and a stress relaxation, $\Delta\sigma$, of 3 MPa /Fälth et al. 2010/ near (< 1–2 km) the fault, then the time t required to restore the

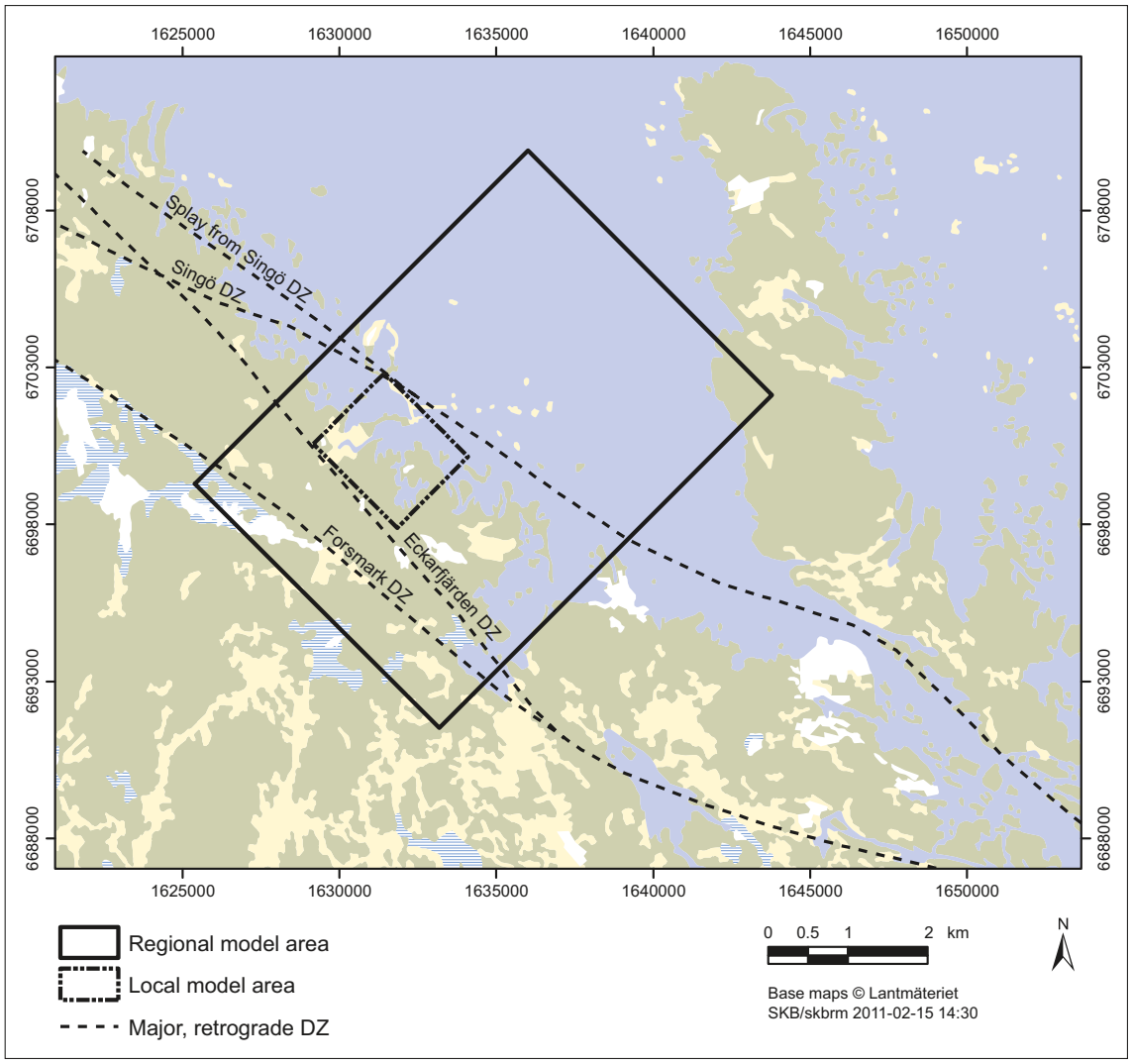

Figure 10-116. *Major deformation zones that intersect the regional model area at Forsmark (edited from /Stephens et al. 2007/).*

stress field sufficiently for a new earthquake to occur within 1–2 km is approximately t = 500,000 years according to the equation below.

$$t = \frac{\Delta\sigma}{E \cdot \dot{\varepsilon}}$$

Accordingly, at most two seismic events of magnitude ≥ M5 at Forsmark during the assessment period might be expected. It is recalled that the probability for having one large earthquake within the site is very low. The probability of having two or more earthquakes within the same area is very much smaller.

The probability of any deformation zone hosting an earthquake can be obtained by dividing the probability estimated for the circular area (Figure 10-117) by the number of deformation zones intersecting that area. Using only deformation zones modelled with intermediate to high confidence /Stephens et al. 2007/, 36 zones are identified with traces exceeding 3 km (Table 10-15 and Figure 10-117), and judged, therefore, to be able to host earthquakes of magnitude M5 or larger.

The findings of /Lund et al. 2009/ were used in /Fälth et al. 2010/ to identify which of the deformation zones at Forsmark could impact the repository during the glacial evolution. In Figure 10-118 we show the deformation zones that have any part closer than 600 m to any canister position; zones farther away have little means of jeopardising the integrity of the canisters (see next section) provided that canister position rejection criteria are applied. Of these, only five deformation zones are, due to

Table 10-15. Deformation zones intersecting an area corresponding to a 5 km radius circle centred at Forsmark. Attributes stem from /Stephens et al. 2007/. The thickness includes the fault damage zone. Maximum estimated magnitudes (M max) were obtained using regressions in /Wells and Coppersmith 1994, Table 2A/. Red = unstable, green = stable in mixed stress regime (strike-slip/reverse).

ID	Trace length (m)	Confidence	Strike	Dip	"Thickness (m) (incl. damage zone)"	M max
ZFMNW0017	**7,923**	**Medium**	**135**	**85**	**64**	**6,1**
ZFMNW0029	3,792	Medium	133	90	30	5,8
ZFMNW0805	3,694	High	134	90	10	5,7
ZFMNW0806	22,000	Medium	145	90	80	6,6
ZFMWNW0836	4,498	Medium	117	90	30	5,8
ZFMNW1200	**3,121**	**High**	**138**	**85**	**47**	**5,7**
ZFMWNW0001	30,000	High	120	90	200	6,8
ZFMWNW0004	70,000	High	125	90	160	7,2
ZFMWNW0016	8,060	Medium	123	90	45	6,1
ZFMWNW0019	8,760	Medium	116	85	45	6,2
ZFMWNW0023	7,665	Medium	111	82	45	6,1
ZFMWNW0024	7,986	Medium	124	90	45	6,1
ZFMWNW0036	11,000	Medium	123	90	55	6,3
ZFMWNW0123	**5,086**	**High**	**117**	**82**	**52**	**5,9**
ZFMWNW0809A	**3,347**	**Medium**	**116**	**90**	**25**	**5,7**
ZFMWNW1127	5,394	Medium	120	90	35	5,9
ZFMWNW0035	3,521	Medium	120	90	25	5,7
ZFMA2	**3,987**	**High**	**80**	**24**	**23**	**5,8**
ZFMA3	3,234	High	46	22	22	5,7
ZFMA4	3,641	High	61	25	37	5,7
ZFMB1	3,224	High	32	27	7	5,7
ZFMA7	3,510	High	55	23	7	5,7
ZFMENE0060A	**3,120**	**High**	**239**	**85**	**17**	**5,7**
ZFMENE0062A	**3,543**	**High**	**58**	**85**	**44**	**5,7**
ZFMEW0137	4,300	Medium	95	90	30	5,8
ZFMNE0065	4,068	High	36	70	26	5,8
ZFMNE0808A	4,080	Medium	218	80	30	5,8
ZFMNNE0828	5,932	Medium	213	80	35	6,0
ZFMNNE0842	3,157	Medium	217	80	25	5,7
ZFMNNE0860	5,922	Medium	198	80	35	6,0
ZFMNNE0929	5,203	Medium	193	80	35	5,9
ZFMNNE1133	6,284	Medium	193	80	40	6,0
ZFMNNE1134	7,284	Medium	191	80	40	6,1
ZFMNNW0823	3,273	Medium	160	90	25	5,7
ZFMNW0002	18,000	High	134	90	74	6,5
ZFMNW0003	30,000	High	139	85	53	6,8

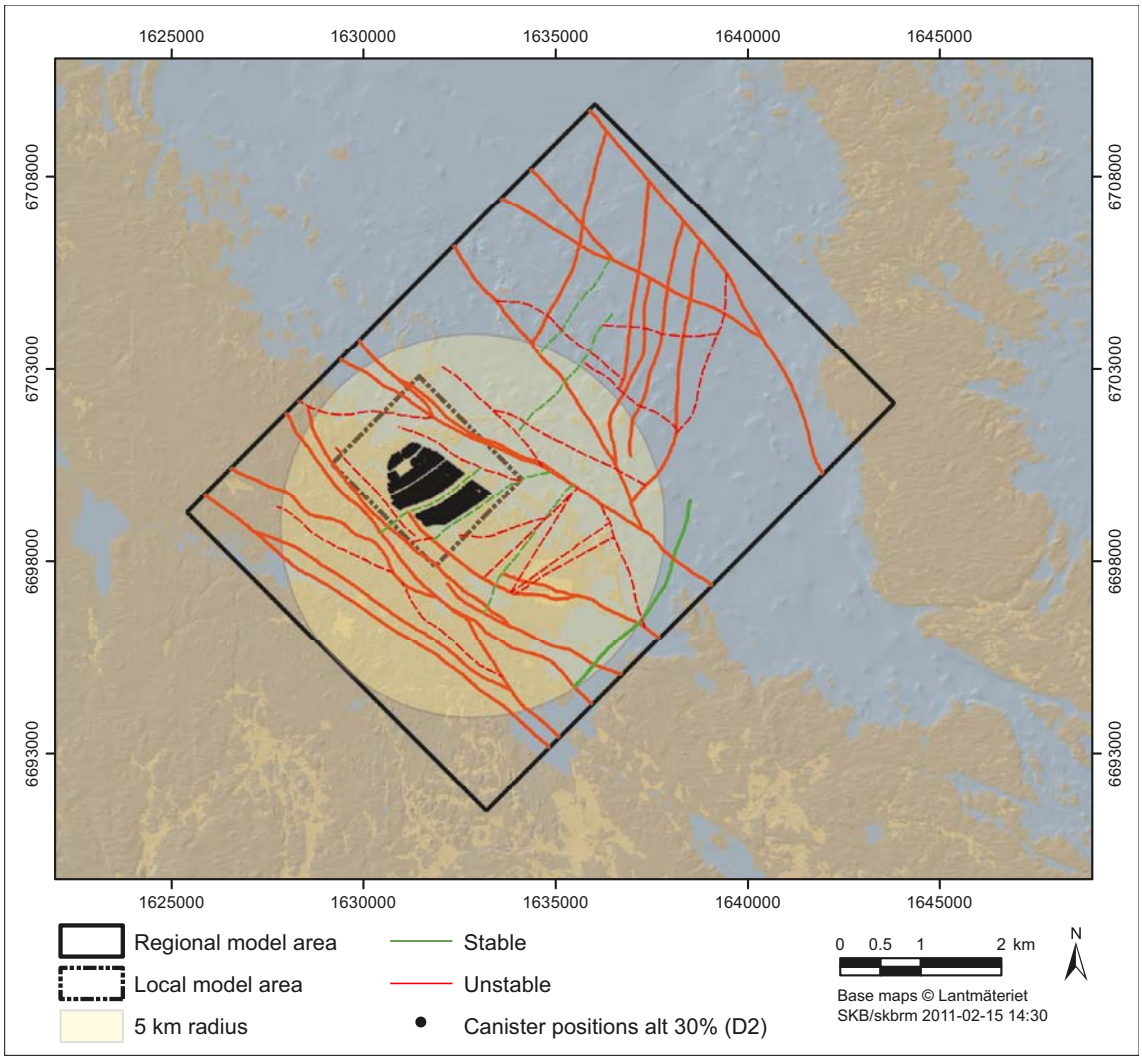

Figure 10-117. *Deformation zones at Forsmark. The circle of 5 km radius defines the area for normalisation of earthquake frequencies. Note that surface traces are truncated against the regional model boundary. The zones are classified in terms of stability in a combined strike-slip/reverse regime according to /Fälth et al. 2010/.*

their orientation with respect to stress field, amenable to reactivation /Fälth et al. 2010/ during the glacial evolution; the remaining two are judged stable. All zones classified unstable on Figure 10-118 and in Table 10-15 are judged large enough to host earthquakes of magnitudes exceeding M5 but only one of these zones, ZFMNW0017, is judged large enough to host earthquakes of magnitude up to roughly M6. In the next section we examine the impact of earthquakes on canister integrity.

Prerequisites for shear load by earthquakes

The stress evolution analysed explicitly for the Forsmark site by /Lund et al. 2009/ verifies that there is a significant increase in fault stability during periods of ice-cover, i.e. when canisters could, potentially, be subjected to high pore overpressures, i.e. to high isostatic loads. This means that shear movements across canisters such as those calculated by /Fälth et al. 2010/ will not occur in connection with high isostatic loads. At times of ice retreat /Lund et al. 2009/ predict a period of reduced fault stability, possibly resulting in end-glacial faulting along suitably-oriented deformation zones and reactivation of host rock fractures. At such times, residual pore overpressures will amount to about one MPa /Hökmark et al. 2010/. Therefore, combined effects of isostatic loads and shear movements across canisters are not taken into account.

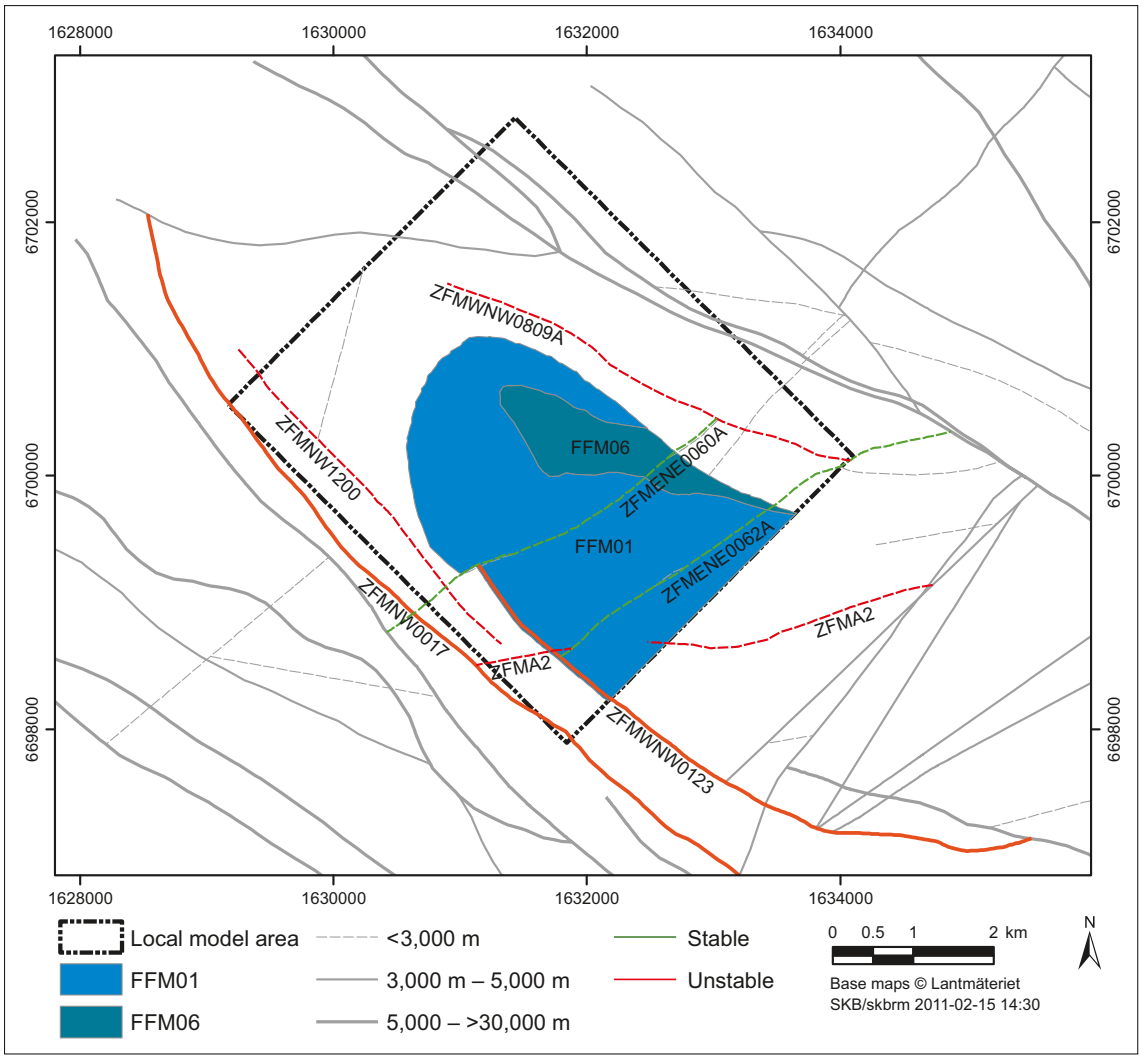

Figure 10-118. *Deformation zones (intersections at repository depth) considered in the earthquake hazard assessment.*

The canister is designed to withstand a shear movement of 5 cm. This means that if cumulative slip exceeding 5 cm along fracture planes that intersect the canisters can be avoided, earthquakes have no means to jeopardise the integrity of the canisters by shear load. As the maximum slip that can be hosted by a fracture is related to its size /Cowie and Scholz 1992b/, it must be ensured that canisters are not intersected by large fractures to warrant long term safety.

The impact of earthquakes near the repository on host rock fractures (target fractures) within the repository was addressed by /Fälth et al. 2010/, who investigated the influence of earthquake magnitude, distance to the fault and target fracture orientation on seismically induced slip on target fractures. /Fälth et al. 2010/ conclude that, provided that a distance of 600 m is kept to the boundary of deformation zones, none of the canisters within a repository will be subject to shear loads such that their integrity is jeopardised, regardless of earthquake magnitude (faults corresponding to moment magnitudes up to M7.5 were simulated). This is under the condition that fractures with radii exceeding 225 m are avoided in deposition holes. Such fractures are judged to be safely detected during underground mapping /Cosgrove et al. 2006, SKB 2010b/ and it may hence be concluded that, beyond 600 m from any deformation zone (≥ 3km), earthquakes have no impact on canister integrity.

In the interpretation of the simulation results, the deformation zones were divided into two categories: zones 3–5 km able to host minor earthquakes (≤ M5.5), and zones exceeding 5 km in trace length which are able to host large earthquakes (> M5.5). If both respect distances and rejection criteria /Munier 2010/ are applied, the canisters will avoid the impact of earthquakes even occurring on zones intersecting portions of the repository volume. For this to be valid, however, the following need to be ensured (Figure 10-119).

1. No canister is placed within the damage zone of a deformation zone (fault). The damage zone of a fault is the volume of rock within which the zone may grow /Scholz 2002, Kim et al. 2004, Kim and Sanderson 2008/. This is ensured by repository design /SKB 2009c/ and using the site descriptive models e.g. /Stephens et al. 2007, Stephens et al. 2008a, b/. The boundaries of the deformation zones will be delineated with further detail and less uncertainty during underground mapping and modelling.
2. No canister is intersected by any fracture that is mechanically connected (i.e. splay) to any deformation zone. The risk for this to occur is lessened by the use of 100 m respect distances /Munier and Hökmark 2004, Munier et al. 2008/ to the boundary of the deformation zone, defined to include the damage zone (see e.g. /Munier et al. 2003/ for details). There is an uncertainty, however, as to whether this respect distance is sufficient to include all splays. The splays are smaller than the deterministically modelled zones and ought to consist of fractures or small deformation zones with radii in the order of about 100–500 m. Hence most of them will be detected and characterised by underground investigations /SKB 2010b/. It is, however, important, during underground investigations, to ensure that such splays do not intersect any deposition hole. The work of /Cosgrove et al. 2006/ is of particular importance in this context and the ongoing detailing of the underground investigation programme /SKB 2010b/ will further specify the identification tools.
3. Deposition hole rejection criteria are applied to the rock volumes beyond the 100 m respect distance which depend on /Fälth et al. 2010/:
   a. the size of the nearest deformation zone (i.e. the maximum size of anticipated earthquake, should it occur),
   b. the distance to the deformation zone,
   c. the orientation of the fracture intersecting the deposition hole,
   d. the size of the fracture intersecting the deposition hole.

The complex task of determining the absolute size of fractures /Cosgrove et al. 2006/ can be avoided by the use of the so called FPI criteria (FPC + EFPC, see Section 5.2.2) which constitute proxies for large fractures /Munier 2010/. In practice, therefore, the critical radii of Table 10-16 are used only to obtain a quantitative estimate of the number of critical canister positions for the few cases for which the FPI criteria may fail (see next section).

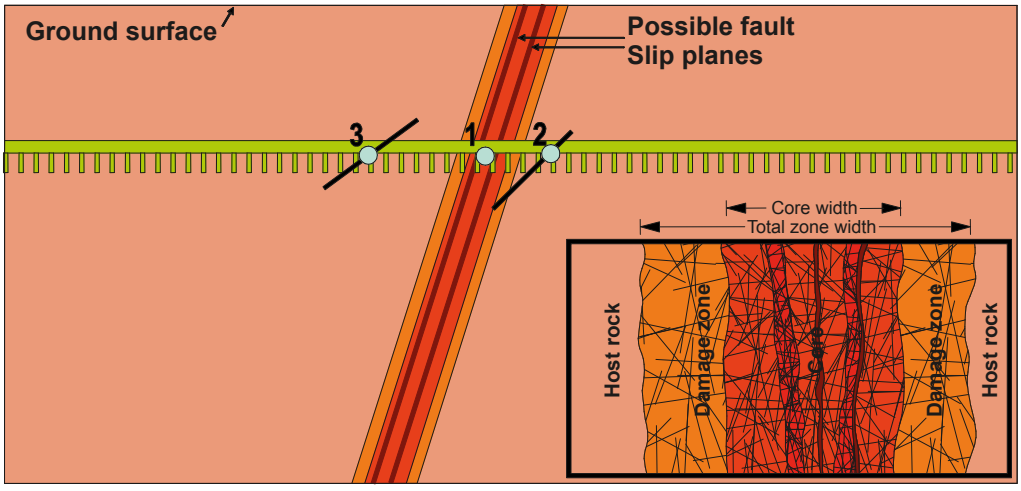

Figure 10-119. *Cases to consider regarding slip across canisters. Case #1 = the canister is intersected by a deformation zone. Case #2 = the canister is intersected by a splay from the deformation zone. Case #3 = the canister is intersected by a large fracture at some distance from, and mechanically disconnected from, the zone.*

Table 10-16. Summary of critical radii for relevant zone lengths and target fracture dips at Forsmark (from /Fälth et al. 2010/).

Zone trace length (km)	Target fracture dip (degree)	Distance from zone (m)	Critical target fracture radius (m)
> 5	0–55	100–200	62.5
> 5	0–55	200–400	125
> 5	0–55	400–600	160
> 5	0–55	> 600	225
> 5	55–90	100–200	85
> 5	55–90	200–400	170
> 5	55–90	400–600	215
> 5	55–90	> 600	> 300
3–5	0–55	100–200	75
3–5	0–55	200–400	150
3–5	0–55	400–600	235
3–5	0–55	> 600	> 300
3–5	55–90	100–200	100
3–5	55–90	200–400	200
3–5	55–90	400–600	> 300
3–5	55–90	> 600	>> 300

Cases of shear load to consider

The impact of earthquakes on the canister/buffer integrity can be avoided by the use of respect distance and deposition hole rejection criteria. In essence, SKB needs to ensure that deposition holes are not intersected by fractures large enough to host slip that may exceed the canister failure criterion. As argued by /Cosgrove et al. 2006/, the vast majority of large fractures (radii ≈ 100–500 m) are not anonymous and most display clear and interpretable characteristics. However, we need for the safety assessment a quantification of how many critical positions might escape detection. The full perimeter intersection (FPI) criteria /Munier 2010/ have been proposed as a robust proxy for large fractures. By applying the FPI criteria to the Forsmark site, we are able to provide, by simulations, a pessimistic upper estimate on the number of critical positions that may escape detection and, ultimately, an estimate of how many canisters might therefore fail as a result of nearby earthquakes.

Due to the large time spans considered in this assessment, up to 10^6 years, the effect of repeated earthquakes and hence of cumulative slip across canisters must also be considered. The concern is that though the induced slip due to an individual earthquake might be insufficient to damage the canister, the cumulative slip due to several earthquakes, on the same or different faults, might exceed the canister failure criterion of 5 cm.

There are several different cases to consider (Figure 10-120).

1) The fracture that intersects the canister is large enough to host a slip exceeding the canister failure criterion. It can either host its maximum possible slip allowed by its size (1c) or slip in smaller increments, one for each seismic event, that accumulates to a value exceeding the failure criterion (1a + 1b +…).
2) The fracture does not initially intersect the canister (2a). Triggered by nearby earthquakes (or itself hosting a small earthquake) the fracture grows into the canister position (2b), thereby enabling slip across the fracture. For large enough a growth, the fracture will eventually be able to host a slip across the canister that exceeds the canister failure criterion (2c).
3) The fracture intersects the canister position (3a), but is too small to host a critical slip. The fracture grows (3b) to a size that is able to host a critical (cumulative) slip (3c).

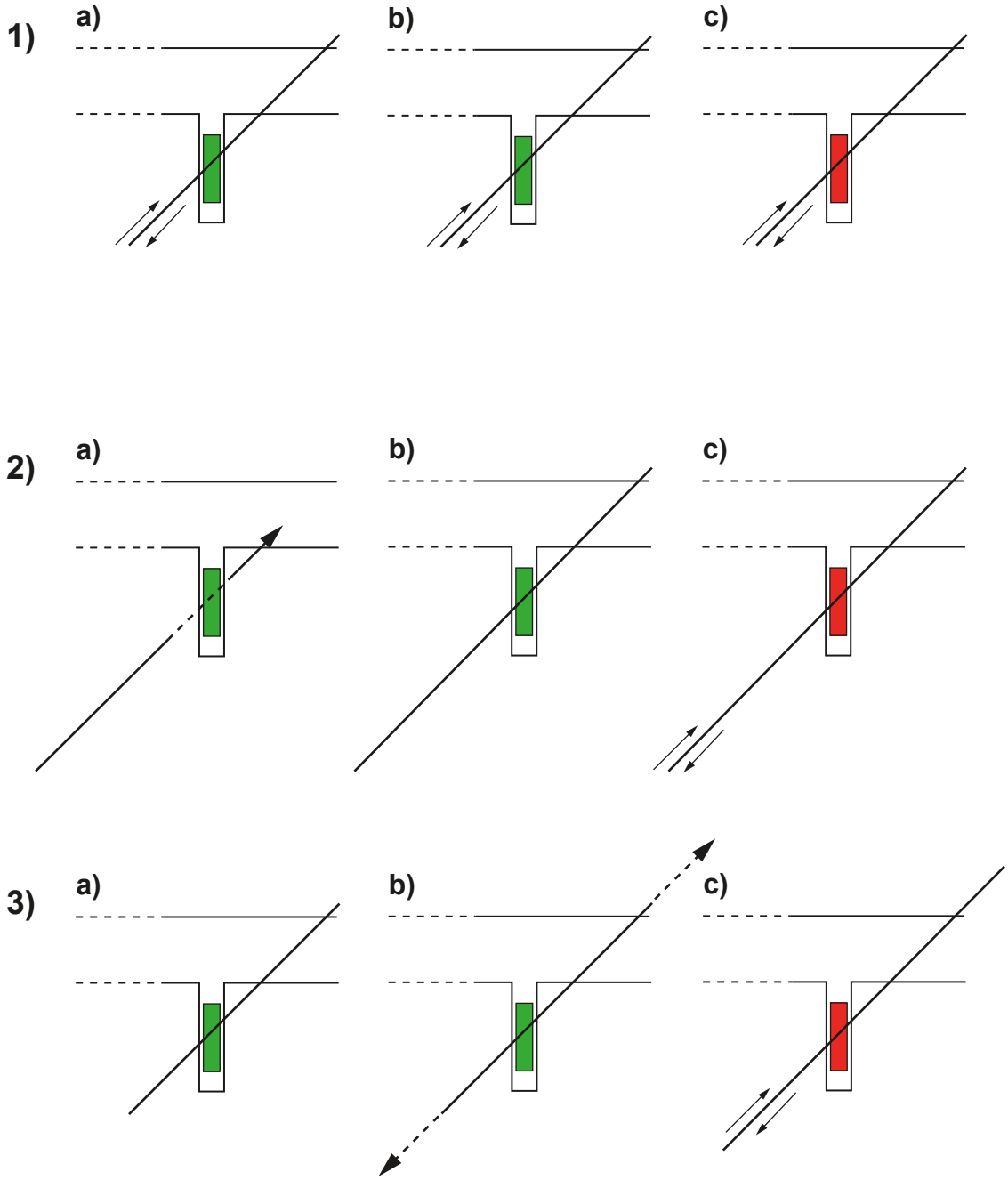

Figure 10-120. *Various cases to consider regarding slip across a canister. In "1a–c" we address the effect of cumulative slip. In 2a–c we address growth of a fracture into a deposition hole. In 3a–c we address the growth of a fracture from a subcritical size to a critical size. Red canisters could experience detrimental shear movements.*

Whether a fracture slips a distance, D, in a single event or if D is subdivided into several smaller slip distances d_1, $d_2 \ldots d_n$, is, from a purely geometric point of view, equivalent. Thus, Cases 1a+1b are equivalent to Case 1c. However, for the cumulative slip d_1, $d_2 \ldots d_n$ to equal D, slip vectors need to be perfectly parallel. This essentially requires that the same deformation zone reactivates, with essentially identical dynamics, pore pressure, etc. Additionally, the number of successive slip events is controlled by the frequency of triggering earthquakes, in practice limited to two events during the assessment period (10^6 years) as argued for earlier. Thus, only the possibility of two successive slip events on the same target fracture needs to be considered. The smallest fracture that can host a slip exceeding the canister failure criterion as a consequence of a *single* earthquake is given by Table 10-16 in terms of critical radii. For two seismic events, we need to consider the cumulative

slip of fractures with subcritical radii. The smallest fractures that can accumulate 50 mm of slip in two reactivation events have radii equal to half the critical radius of a single event, since slip scales linearly with fracture size, see the **Geosphere process report**, Section 4.3. We thus pessimistically assume that the slip vectors on the subcritical target fractures will indeed be perfectly parallel and neglect stress relaxation effects around the target fractures. Note, further, that slip velocity scales linearly with displacement as shown in Figure 10-121. We thus, pessimistically, also assume that a cumulative slip of 50 mm will have the same impact on the canister as a single, faster, slip of 50 mm. The canister failure criterion has been deduced from high shear velocities (1 m/s /Hernelind 2010/); low shear velocities have a considerably lower impact upon the canister-buffer system. It is likely that the buffer, which is sensitive to shear velocity, has sufficient time to recover between seismic events. This effect is, however, not taken into account and assuming that the cumulative effect of several smaller slip events equals a single larger event is thus additionally pessimistic.

The growth of fractures by repeated reactivation has been investigated by /Cowie and Scholz 1992a/. The authors propose that a fracture may, for each seismic event, grow in the range 0.2–2.5 percent of its size as an upper estimate, pessimistically assuming that the entire fracture surface also constitutes the faulting surface. A fracture that grows into a deposition hole, as hypothesised in Case 2, would have the canister located close to its tip. As shown by numerous authors e.g. /Walsh and Watterson 1987, 1989, Marrett and Allmendinger 1990, Dawers et al. 1993/, the displacement profiles tapers off from a maximum near the centre of the fracture to zero at its tip (Figure 10-122) where ductile deformation (e.g. growth of damage zone, propagation through damage zone, folding) takes place. For a fracture to grow to such an extent, that a canister's position is shifted from being near the tip of a fracture to a region in which slip might exceed the canister failure criterion, would require a large number of slip/growth events. For a fracture to slip 0.05 m, the canister needs to be located at the centre of a fracture with a radius of 62.5 m (strictly following simulation results), with the additional conditions that the fracture is located no farther than 200 m from a large (> 5 km) deformation zone and is gently (≤55°) dipping (see Table 10-16 from /Fälth et al. 2010/).

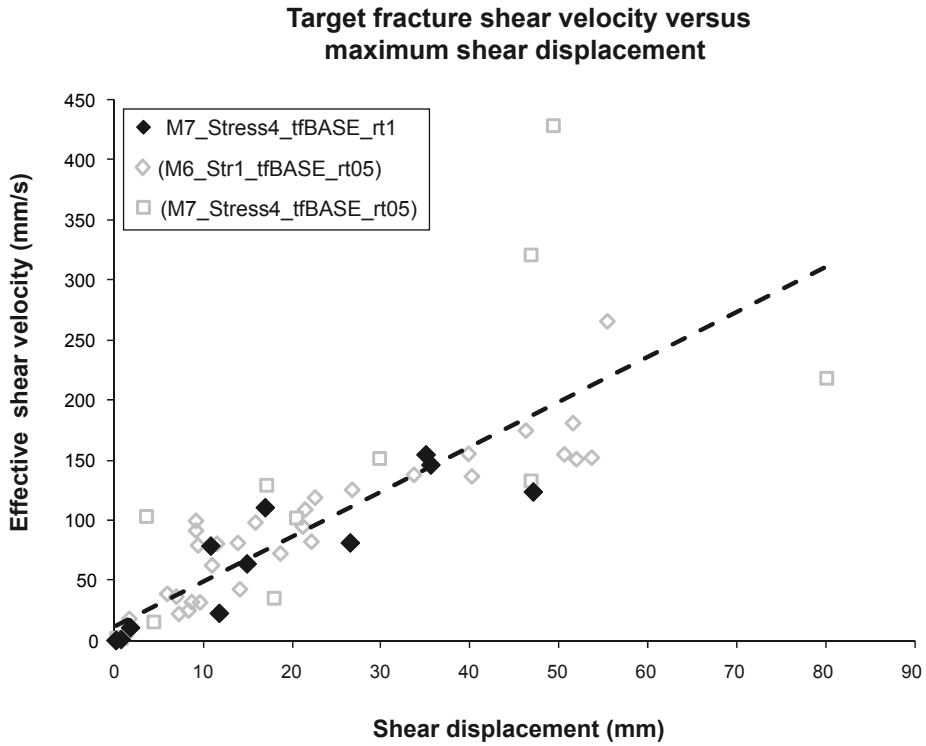

Figure 10-121. *Relation between shear velocity and shear displacement on a target fracture (from /Fälth et al. 2010/). Results are from various earthquake simulations. Unfilled plot symbols denote results from cases that were discarded in the final assessment because the source mechanism was not considered to be representative of real earthquakes.*

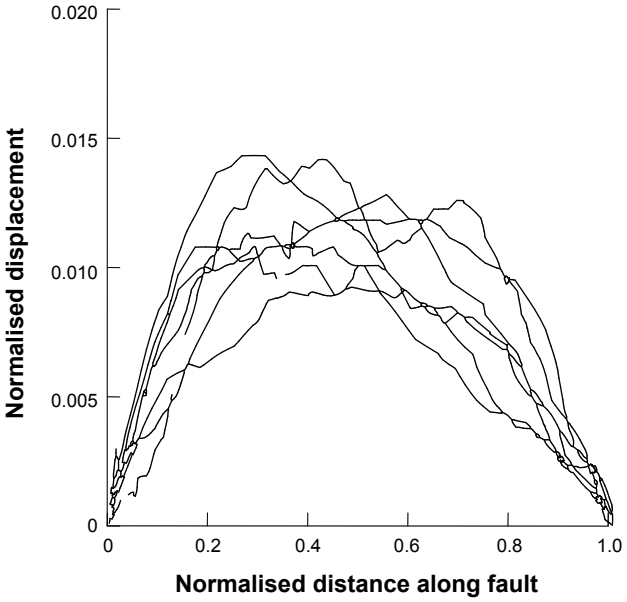

Figure 10-122. *Displacement profiles along normal faults of different size, normalised to fault size (redrawn from /Dawers et al. 1993/).*

With a growth in the range 0.2–2.5 percent for each seismic event, as proposed by /Cowie and Scholz 1992a/, it would require about 15 /Cowie and Scholz 1992a, Equation 22/ consecutive seismic events on the fracture (n.b. not necessarily triggered by a distant fault) before the canister is located in a critical position, assuming a perfectly elastic material for which Eshelby's elliptical displacement profile holds /Eshelby 1957, Munier 2010, Equation 27/. For fractures located more than 200 m from the fault, many more seismic events are required. The collage of prerequisites for Cases 2 and 3 are judged unlikely, their effects subordinate, and they are therefore not addressed further.

Number of canisters in critical positions

The detrimental effects of earthquakes on the canister-bentonite packages can be avoided by the application of deposition hole rejection criteria to the design of canister deposition locations. The maximum fracture radii allowed to intersect the deposition hole (Figure 10-123) are provided from simulations in /Fälth et al. 2010/. Applying the full perimeter intersection criteria on site-specific deformation zone and fracture models, /Munier 2010/ computed the number of canister positions that escape detection using the FPI criterion, the main results of which are presented in Tables 10-17 and 10-18 (see /Munier 2010/ for details[19]).

In short, the number of critical canisters in Forsmark, i.e. canisters that escaped the FPI rejection criteria and are thus intersected by fractures large enough to host slips exceeding 5 cm, varies between roughly $1.0 \cdot 10^{-3}$ (for DFN model "OSM + TFM" and deformation zone ZFMNW0017) and $1.1 \cdot 10^{-1}$ (for DFN model "TCM" and deformation zone ZFMA2) canisters depending on DFN model, stress regime and zone assumed to reactivate seismically (Table 10-17). The reverse stress regime (Table 10-18) only affects one deformation zone, ZFMA2, and yields a maximum of 0.11 critical canisters (using DFN model TCM). Note that ZFMA2 is judged unstable also in the mixed stress regime and that this is the zone that affects most canister positions and the maximum number of critical positions is therefore the same (0.11) for the mixed- and the reverse stress regime.

The results in Tables 10-17 and 10-18 are valid only for the case when exactly one of the deformation zones will reactivate seismically. In Figure 10-123 we display two examples of how critical radii depend on the distance to deformation zones.

[19] Since the publication of /Munier 2010/ more realisations have been added to stabilise the mean values further. As a consequence, there is small difference between the tables in /Munier 2010/ and those herein.

a)

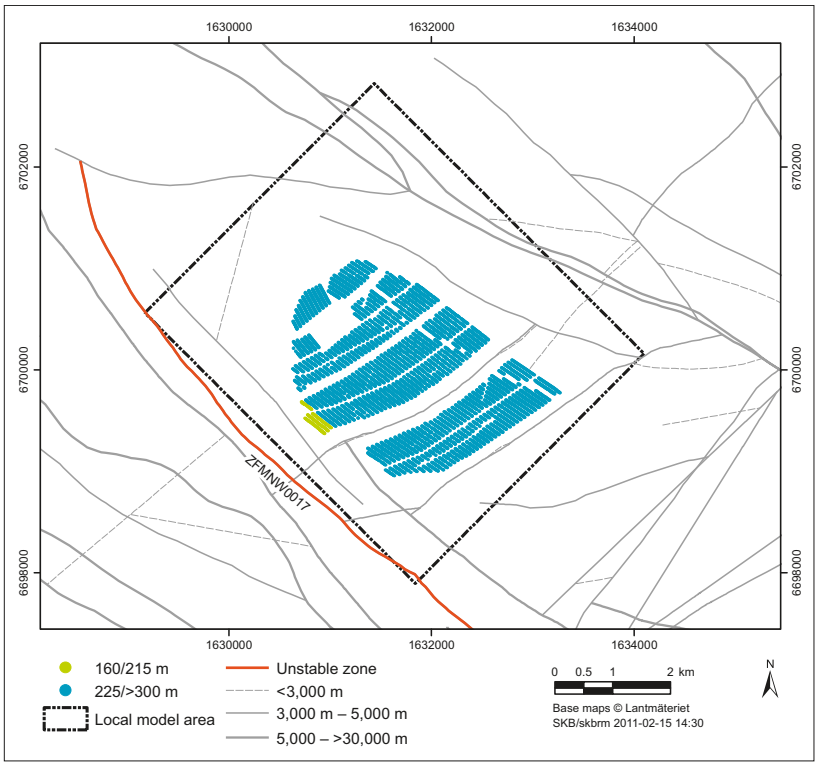

b)

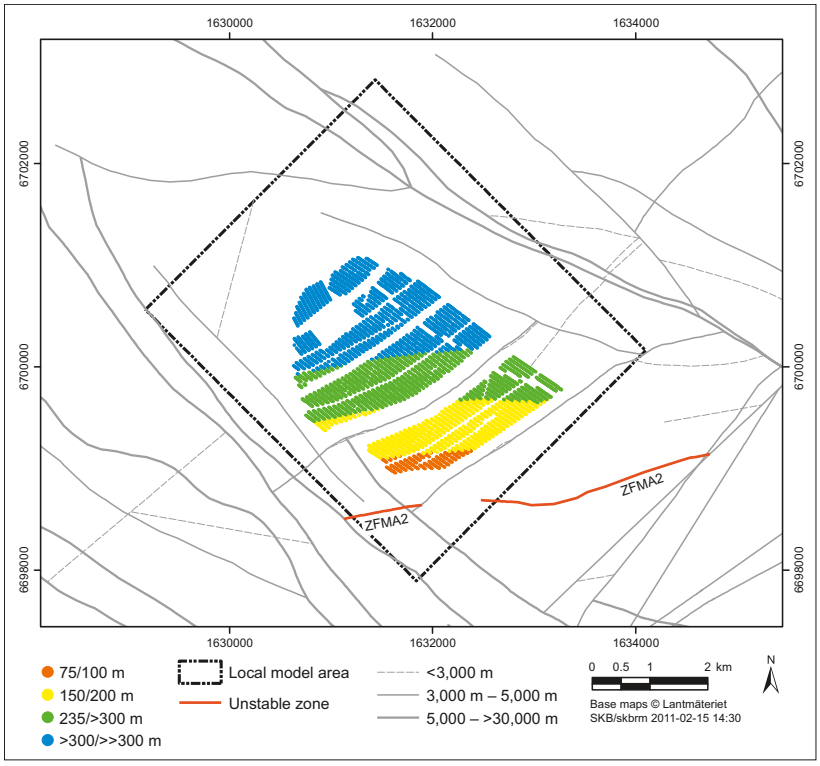

Figure 10-123. *Canister positions labelled by the largest fracture they are allowed to intersect in order not to slip in excess of the canister failure criterion (0.05m). Figure a = ZFMNW0017, Figure b = ZFMA2.*

Table 10-17. Mean number of critical canister positions for various DFN models, assuming mixed stress regime (6,000 canister repository) at Forsmark.

DFN Model	# Crit. Min	# Crit. Max
OSM+TFM	$1.0 \cdot 10^{-3}$	$6.7 \cdot 10^{-2}$
r0-fixed	$3.5 \cdot 10^{-3}$	$4.8 \cdot 10^{-2}$
TCM	$2.3 \cdot 10^{-3}$	$1.1 \cdot 10^{-1}$
Overall	$\mathbf{1.0 \cdot 10^{-3}}$	$\mathbf{1.1 \cdot 10^{-1}}$

Table 10-18. Mean number of critical canister positions for various DFN models, assuming reverse regime (6,000 canister repository) at Forsmark.

DFN Model	# Crit
OSM+TFM	$6.7 \cdot 10^{-2}$
r0-fixed	$4.8 \cdot 10^{-2}$
TCM	$1.1 \cdot 10^{-1}$

Number of potentially failed canisters by shear load

To compute the number of canisters that may fail within a certain time span, the number of critically emplaced canisters (Tables 10-17 and 10-18) is multiplied by the earthquake frequencies in Table 10-14. All earthquakes are here projected on the deformation zone ZFMA2 because:

- its geometry is similar to the geometry of the known post-glacial faults,
- it is considered unstable in both the reverse- and combined reverse+strike slip (mixed) stress regimes[20],
- it is the deformation zone that affects most canisters.

Additionally the following prerequisites apply.

- For the 1,000-year time frame, only earthquake frequencies given by /Böðvarsson et al. 2006/ are used. This work was specifically targeted towards short time frames and was therefore judged the most suitable reference in this context. Additionally, as argued for in the **Geosphere process report**, most earthquakes, at least in this time frame, occur at greater depth than is relevant to the context discussed here. Following the reasoning in the **Geosphere process report**, the frequencies are reduced by a factor of 0.5.
- For the time frame of a glacial cycle, 120,000 years, all references in Table 10-14 are used because, with the exception of /Böðvarsson et al. 2006/, they all targeted this specific time frame in their assessment. Since extrapolation of /Böðvarsson et al. 2006/ to 120,000 years produce similar frequencies, we judged it reasonable to include the results of /Böðvarsson et al. 2006/ in this time frame despite the consideration that their assessment did not target a larger time frame than 1,000 years.
- In contrast to the 1,000 year time frame, we cannot rule out the possibility of shallow, postglacial, earthquakes for the 120,000 and 1,000,000-year time frames. Hence, the frequencies have been used without adjustment for depth.
- For the 1,000,000-year time frame, a maximum of two seismic events ≥ M5 which is a consequence of an assumed strain rate of 10^{-10} year^{-1} is postulated.

Following the reasoning in the **Geosphere process report**, Section 4.3, the number of canisters that may fail is computed according to:

$$N_{failed} = 5 \cdot f \cdot t \cdot N_{crit}$$

[20] The combination of strike-slip and reverse regime (sometimes referred to as mixed regime) refers to a notion of predominantly strike-slip regime at depth (> ≈ 1 km) and reverse slip at shallower levels /Lund et al. 2009, Fälth et al. 2010/

N_{crit} is the average number of canisters in critical positions (Table 10-17), f is obtained from Table 10-14 and t is the time. The factor 5 is due to the projection of all earthquake frequencies onto ZFMA2.

For the second seismic event, applicable only to the 1,000,000-year time frame, the following expression is used (see the **Geosphere process report**, Section 4.3.1 for details):

$$N_{failed} = \frac{1}{2} \cdot \left(5 \cdot f\right)^2 \cdot \left(10^6 - T\right)^2 \cdot N_{crit,2nd}$$

in which T stands for relaxation time and $N_{crit,2nd}$ stands for the average number of canisters in critical positions (Table 10-19) using the critical radii of Table 10-16 divided by two.

The main results are summarised in Table 10-20, which should be understood as follows:

Under the assumption that a combination of strike-slip and reverse stress regime will prevail during the assessment period, on average between $9.3 \cdot 10^{-6}$ and $2.2 \cdot 10^{-5}$ canisters may fail during the 1,000-year time frame. Note that only /Böðvarsson et al. 2006/ is used for this assessment even though estimates for all references are supplied. Similarly, on average between $8.3 \cdot 10^{-4}$ and $5.7 \cdot 10^{-3}$ canisters may fail during a glacial cycle. For the 1,000,000 time frame, two seismic events are assumed and it is estimated that on average between $8.3 \cdot 10^{-3}$ and $7.9 \cdot 10^{-2}$ canisters may fail. The contribution of the second seismic event is between 20 and 50 percent of the total. Despite a much lower probability for the second event, reducing the critical radii by half dramatically increases the number of canisters in critical positions due to the powerlaw size distribution of the fractures. Since all these average numbers are well below one, the numbers, to a good approximation, are also equal to the calculated probability that canister failure has occurred in the repository at the end of the time periods under consideration.

The above results can be expressed as the frequency of canister failures as a function of time for times beyond the initial 1,000 years. This frequency will be constant during the first 500,000 years when only one large earthquake may occur, and linearly increasing between 500,000 and one million years, when also the possibility of a second earthquake must be taken into account. If, pessimistically, the highest earthquake frequencies (those by /Hora and Jensen 2005/) and the DFN model yielding the largest numbers of critically emplaced canisters (the TCM model) are used, the frequency during the first 500,000 years is $4.75 \cdot 10^{-8}$ per year (the emboldened max value for 120,000 years in Table 10-20 divided by 120,000). The frequency then increases linearly to reach $1.74 \cdot 10^{-7}$ per year at one million years, see Figure 10-124. (The latter result is obtained by the requirement that the area under the frequency curve in Figure 10-124 must correspond to the accumulated maximum number of failures from both one and two events given in Table 10-20.) This result is used as input to consequence calculations of the shear load scenario, see further Section 13.6. For the initial 1,000 years the corresponding frequency is $2.2 \cdot 10^{-8}$ per year.

Table 10-19. Number of critical canister positions (2nd seismic event) for various DFN models, assuming reverse regime (6,000 canister repository) at Forsmark.

DFN Model	# Crit. 2nd
OSM+TFM	0.7
r0-fixed	0.46
TCM	1.3

Table 10-20. Number of canisters that may fail during different time spans and using different earthquake frequencies.

Strike-slip + reverse (mixed) stress regime			Number of potentially failed canisters					
Reference	Earthquake frequency (M≥ 5/year)		1,000 years		120,000 years		1,000,000 years (2 events)	
	5 km radius area	Per zone (30)	Min	Max	Min	Max	Min	Max
/Böðvarsson et al. 2006/	$2.4 \cdot 10^{-6}$	$7.8 \cdot 10^{-8}$	$9.3 \cdot 10^{-6}$	$2.2 \cdot 10^{-5}$	$2.2 \cdot 10^{-3}$	$5.4 \cdot 10^{-3}$	$2.9 \cdot 10^{-2}$	$7.3 \cdot 10^{-2}$
/La Pointe et al. 2000, 2002/	$8.7 \cdot 10^{-7}$	$2.9 \cdot 10^{-8}$	**$3.4 \cdot 10^{-6}$**	$8.2 \cdot 10^{-6}$	**$8.3 \cdot 10^{-4}$**	$2.0 \cdot 10^{-3}$	**$8.3 \cdot 10^{-3}$**	$2.0 \cdot 10^{-2}$
/Hora and Jensen 2005/	$2.5 \cdot 10^{-6}$	$8.3 \cdot 10^{-8}$	$9.9 \cdot 10^{-6}$	**$2.4 \cdot 10^{-5}$**	$2.4 \cdot 10^{-3}$	**$5.7 \cdot 10^{-3}$**	$3.1 \cdot 10^{-2}$	**$7.9 \cdot 10^{-2}$**
/Fenton et al. 2006/	$2.0 \cdot 10^{-6}$	$6.8 \cdot 10^{-8}$	$8.1 \cdot 10^{-6}$	$1.9 \cdot 10^{-5}$	$1.9 \cdot 10^{-3}$	$4.7 \cdot 10^{-3}$	$2.4 \cdot 10^{-2}$	$6.0 \cdot 10^{-2}$

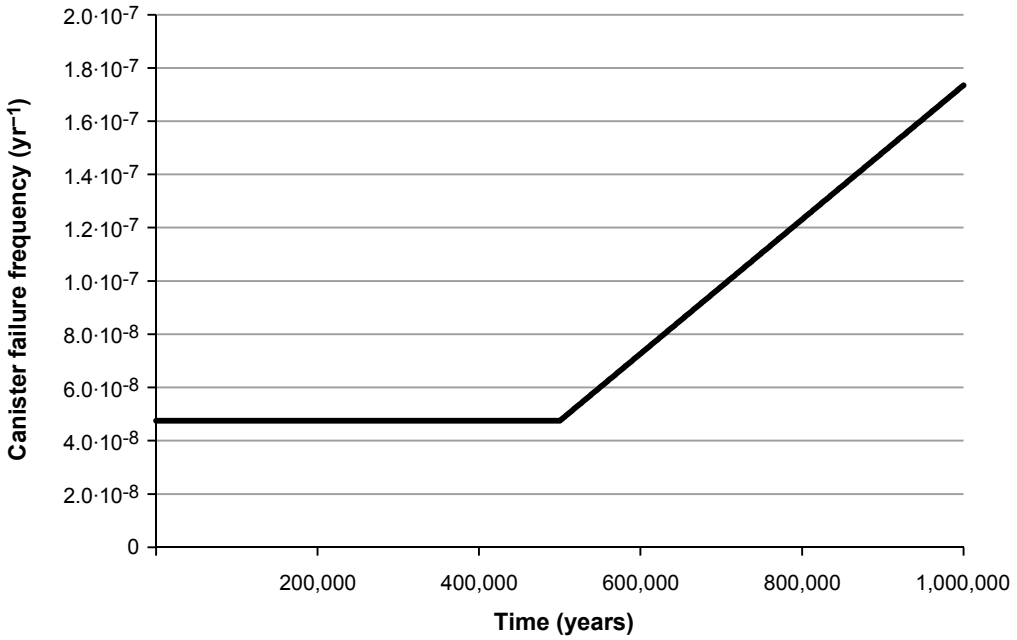

Figure 10-124. *Frequency of canister failures due to earthquake-induced shear load as a function of time. The area under the graph yields the mean number of failed canisters at one million years as 0.079, in agreement with Table 10-20.*

Modelling of buffer-canister response to shear movements

The effect on the canister of a shear movement has been assessed as a basis for the **Canister production report**, the supporting documentation being the design analysis of the canister /Raiko et al. 2010/, in turn supported by FEM-modelling of the impact of shear movements on the buffer-canister system /Hernelind 2010/ and by an analysis of damage tolerance of the canister insert when subjected to shear movements /Dillström and Bolinder 2010/.

The starting point for the canister shear analyses and the design analysis is the design premises given in /SKB 2009a/ and already cited in Section 5.4.1: For the shear movement the design premises require that the copper corrosion barrier should remain intact after a 5 cm rock shear movement at 1 m/s for buffer material properties of a 2,050 kg/m^3 Ca-bentonite. This applies for all locations and angles of the shearing fracture in the deposition hole, and for temperatures down to 0°C. The insert should maintain its pressure-bearing properties to isostatic loads after such shear movements.

The overall conclusion of these efforts is that a canister manufactured according to the reference design, production and inspection methods fulfils the design premises, as already reported in Section 5.4.3. The following account of the modelling efforts is given to demonstrate the margins to failure, and in particular to evaluate the potential of the canister to withstand a load caused by a 10 cm shearing.

There are a number of factors influencing the impact of a postulated shear movement of the buffer and canister. Table 10-21 gives an overview of such factors, their related design premises, the cases analysed as support to the **Canister production report** and their relation to the rock analyses.

The design premise of 5 cm shear is the result of a balance between achievable requirements on the canister and on the layout of the repository, given the understanding of earthquakes and secondary shear movements on the one hand and of the response of the buffer-canister system on the other. A lower design premise shear displacement would give a higher probability for shear with given layout rules, but lower requirements on the canister design and material (especially the non-destructive testing of the insert) and vice versa. In addition to the design premise shearing of 5 cm, results of analyses of 10 cm shearing are also presented in the following.

Table 10-21. Overview of factors influencing the calculated impact of a postulated shear movement on the buffer-canister system, and the relations between design premises, buffer-canister response analyses and the rock analyses.

Factor	Design premise	Cases analysed in /Hernelind 2010/ and /Raiko et al. 2010/
Shear displacement	5 cm	5 and 10 cm
Shear velocity	1 m/s	1 m/s
		Also 0.1 m/s analysed for the base case (horizontal fracture impacting at ¾ height from canister bottom, buffer density 2,050 kg/m^3)
Shear plane and angle of intersection	All angles	Shear planes: horizontal, vertical, 22.5° (to the canister axis)
Location of impact	All locations	Centred at mid height or centred on top; not-centred at a quarter of the length or diameter, see Figure 10-125.
Insert material properties	–	Material model derived from test manufacturing (iron) for different strain rates; table data are used for steel tubes
Copper shell material properties	–	Material model derived from slow strain rate testing of copper material from test manufacturing
Creep in copper shell	–	Creep model included for cases with bentonite 2,050 kg/m^3
Buffer properties – density	2,050 kg/m^3 Ca-bentonite	1,950, 2,000 and 2,050 kg/m^3 Ca-bentonite; strain-rate dependent elasto-plastic model derived from laboratory testing
Alteration of material	Temperatures down to 0°C	Iron material model from testing at 0°C.
		Temperature effects on buffer properties negligible.
Combined isostatic and shear loads	The insert should maintain its pressure-bearing properties to isostatic loads after shear movements	– Shear movement with isostatic load from ice sheet present
		– Shear movement, ice developed afterwards

Sensitivity analyses

The response of the canister to a shear movement in the rock is analysed in two steps. The first consists of FEM-modelling of buffer and canister response to an applied displacement at the outer boundary of the buffer /Hernelind 2010/. As a second step the displacements in the canister from the FEM-modelling is transferred to the damage tolerance analysis, conducted for the part of the canister with the largest displacements and only for the cases with the largest impacts on the canister /Dillström and Bolinder 2010/.

Results for the insert from the buffer-canister modelling are given in Table 10-22. The important parameters are the peak values for the equivalent plastic strain (PEEQ), the effective stress (von Mises) and the maximum axial tension stress (S33). The calculated effective strains and effective stresses all indicate that there is considerable deformation capacity left in the insert structure after shearing. The ultimate tensile strength in the BWR insert from the test manufacturing is at least 391±10 MPa, and the elongation after fracture 13.7±3.7%. The axial tension stress is important for the fracture resistance analysis.

The shear velocity for the buffer-canister system is pessimistically set to 1 m/s, which is higher than the highest velocities deduced from target fractures (0.3 m/s) in earthquake simulations /Fälth et al. 2010/. The shear velocity has only a minor impact on the strains and stresses as seen when comparing the first and penultimate cases in Table 10-22.

The analysed combinations of shear plane and angle of intersection are shown in Table 10-22. In Figure 10-125 the shear planes, angles of intersection and location of impact are illustrated as a)–f). The rock shear cases analysed:

- Shear perpendicular to the axis of the canister, at ¾ height and ½ height from the bottom, a) and b).
- With tension of the canister and a shear plane at an angle of 22.5° to the canister axis, at ¼ height and at ½ height from the bottom, c) and d).
- With a horizontal movement of a vertical plane, at a ¼ of the diameter and through the centre of the canister, e) and f).

Table 10-22. Peak values for the equivalent plastic strain (PEEQ), the effective stress (von Mises) and the maximum axial tension stress (S33) in the insert, for different shear load cases. The tabulated values should be compared to the measured elongation after fracture in the BWR insert from the test manufacturing which is 13.7±3.7%, and the measured ultimate tensile strength which is at least 391±10 MPa. All models were performed with a slip rate of 1 m/s unless indicated differently.

Model case: Impact angle Impact location Buffer density	Illustrated in part of Figure 10-125	PEEQ [%]		von Mises stress [MPa]		Maximum axial stress, S33 [MPa]	
		5 cm shear	10 cm shear	5 cm shear	10 cm shear	5 cm shear	10 cm shear
Normal ¾ height 2,050 kg/m³	a)	0.5	1.6	321	351	333	361
Normal ¾ height 2,000 kg/m³	a)	0.2	1.2	309	340	324	354
Normal ¾ height 1,950 kg/m³	a)	0.1	0.7	301	320	310	336
Normal Half height 2,050 kg/m³	b)	0.1	0.7	299	315	212	265
22.5° ¼ height 2,050 kg/m³	c)	0	0.09	290	297	126	219
22.5° Half height 2,050 kg/m³	d)	0.03	0.2	295	301	177	258
Zero (horizontal) Quarter width 2,050 kg/m³	e)	0.4	0.4	300	303	64	83
Zero (horizontal) Half width 2,050 kg/m³	f)	0.5	0.6	309	311	82	93
Normal ¾ height 2,050 kg/m³ Shear velocity 0.1 m/s	a)	0.5	1.7	312	344	327	354
Normal ¾ height 2,050 kg/m³ Creep modelling added	a)	0.4	1.5	314	347	336	365

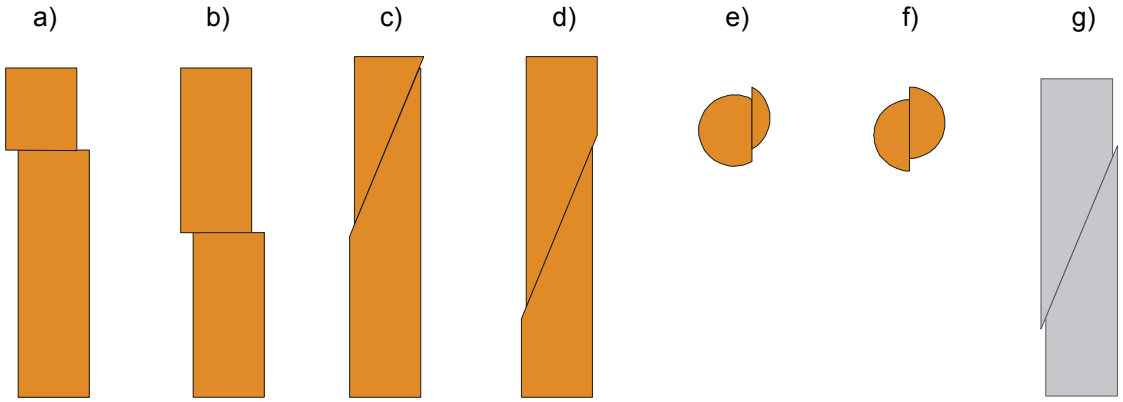

Figure 10-125. *a)–f) Shear plane, angle of intersection and location of impact for the analysed cases in /Hernelind 2010/. The normal shear mode (g) was excluded from analyses (see text for further explanation).*

Post-glacial stress conditions at 500 m depth are, as argued by /Lund et al. 2009/ to be of reverse type. Though some strike-slip component could be deduced from slip vectors on target fractures, the simulation of /Fälth et al. 2010/ show that all significant displacement on non-horizontal target fractures displayed reverse slip and that none of the target fractures displayed any normal slip. Consequently, analyses of normal faulting (deposition hole shortening) across the canister were excluded, (see g) in Figure 10-125).

The angle of 22.5° as an adverse condition was chosen based on results from previous analyses, /SKB 2006a/. With the current improved FEM modelling the copper lid fillets and the buffer are modelled more accurately /Hernelind 2010/, which causes the inclined shear to give smaller strains and stresses than the shear perpendicular to the canister axis (see Table 10-22). A horizontal shear on a vertical plane through the canister gives strains in the same range as for the perpendicular shear, but considerably smaller stresses.

For several cases with the highest density of buffer, long-term creep in copper was modelled after the fast shear displacements. The stresses and strains in the insert after this sequence are given in Table 10-22, last row. Comparing with the corresponding cases without creep in copper indicates minor effects at 5 cm displacement, as the plastic deformation occurs during the fast shearing phase. For 10 cm shear, higher stresses occur in the insert. The maximum plastic strain in the copper shell appears in fillets (besides regions containing singularities in the model). At the global level the plastic strains are much lower. Creep is thus not a concern since the copper deformation is controlled by the surrounding material, which implies small creep strain rates as soon as the final deformation has been established.

The effect of varying the bentonite density, as well as shear plane and intersection is shown in Table 10-22. The largest effects on the insert (highest strains and stresses) are obtained with shearing perpendicular to the canister axis and with an intersection point ¾ of the height from the bottom. Lowering the density to 2,000 or 1,950 kg/m^3 lessens both the strains and stresses.

All results in Table 10-22 are below the measured values of elongation and ultimate tensile strength suggesting that the integrity of the canister would not be jeopardised by such shear loads.

Alteration of the buffer material due to cementation yields small effects in the shear analyses. In the shear calculation made for SR-Can /Börgesson and Hernelind 2006b/ an 8.75 cm thick zone of the buffer material around the canister was assumed to be converted to cement like material, with no swelling pressure, with an E-modulus increased by a factor of 100 and a shear strength increased by a factor of 5 compared to the unaltered buffer. In spite of the high stiffness and strength, the change in effect of a rock shear on the canister was rather small with an increased plastic strain of about a factor of 1.5. This calculation treats much more severe cementation than the case described in Section 10.3.10. With the resulting rather small effects, no new calculations have been done for SR-Site. In addition, the material model used for the rock shear calculations covers a potential increase in strength since the shear strength values used are about 15% higher than the average measured values.

Damage tolerance analysis for the insert

For the second step of the canister shear analysis the resulting displacements are transferred from the FEM-modelling of the shear response to the damage tolerance analysis to analyse crack initiation and stable crack growth. The analysis was performed for the case with the highest impact on the canister, i.e. for shear perpendicular to the canister axis, at ¾ height from the bottom, for different bentonite densities. Four different types of crack-like defects were analysed (semi-circular and semi-elliptical; internal and surface defects).

According to the damage tolerance analyses the maximum acceptable depths of crack-like surface defects with a semi-elliptical shape is 4.5 mm (see Table 10-23). As expected, a larger shear displacement will lessen the acceptable depth, while decreasing the buffer density will increase it.

For other defect types the acceptable defect sizes are larger. E.g. for a surface defect with a semi-circular shape the acceptable depth is 8.2 mm (compare the 4.5 mm for the semi-elliptical). The insert is less sensitive to internal defects, allowing defects larger than 10 mm.

Table 10-23. Acceptable defect sizes for postulated semi-elliptical surface cracks.

Buffer density [kg/m^3]	Acceptable depth [mm]		Acceptable length [mm]	
	Shear displacement 5 cm	Shear displacement 10 cm	Shear displacement 5 cm	Shear displacement 10 cm
2,050	4.5	1.7	27.0	10.2
2,000	8.7	2.3	52.2	13.8
1,950	> 10	3.9	> 60	23.4

The importance of the acceptable depth for defects depends on the possibilities to detect the defects in the non-destructive testing (NDT) after production. In the analyses of the BWR demonstration series only clustered porosity was found in the inserts and no crack-like defects were detected. The detection limit for the NDT, using the current preliminary inspection procedures, is for artificial crack-like defects 2–3 mm for surface defects and 4–9 mm for internal defects. All defects for 5 cm shear in Table 10-23 are larger than these limits. It is also noteworthy that, for a bentonite density of 2,000 kg/m^3, the acceptable defects for a 10 cm shear are larger or comparable to the limit, for this case of highest impact on the canister. This suggests that for most fracture orientations and impact locations, even 10 cm of shear would not jeopardise the integrity of the canister. It is also noted that the derived initial state of the buffer implies a maximum bentonite density of 2,022 kg/m^3 around the canister, see Section 5.5.3. However, the detectability of real defects oriented other than in radial-circumferential directions cannot be stated as no adapted inspection techniques have been developed. As mentioned in Section 5.4.3, based on results and experiences so far, it is expected that such techniques can be implemented in production and testing. See also feedback to canister development in Section 15.5.3.

Combined isostatic and shear loads

The analyses of combined shear and isostatic loads were performed for two sequences of events:

- Shear displacements of 5 cm and 10 cm with 30 MPa isostatic load from an ice sheet present.
- Shear displacement of 5 cm and 10 cm followed by isostatic loads of 30 MPa. This case is analysed with a simplified model (for convergence reasons) where the buffer is replaced by corresponding reaction forces before applying the pressure of 30 MPa.

The results are summarised schematically in Table 10-24, for 10 cm shear. The axial stress in the insert is decreased, and the strains are decreased or only slightly increased, compared to the case with only shear load. The case with only isostatic load calculated with the same global FEM-model /Hernelind 2010/ gives no plastic strains in the insert and von Mises stress at 358 MPa, which is comparable to the values in Table 10-22. The effects on the copper shell of the combined loads are strains slightly higher locally or small changes of the already small strains at the global level (indicated by the values for strain at mid-shell). The strain (equivalent creep strain, CEEQ) in the copper shell for an isostatic load only is at a maximum very locally 16%, and about 0.1% at mid height. All the strain values should be compared to the requirements on the design parameters for the copper components that are a minimum elongation of 40 percent and a minimum creep ductility of 15 percent, and with the even higher values achieved for manufactured copper components, see the **Canister production report**.

The following is, therefore, concluded.

- A glacial load during a shear displacement does not yield a more severe impact on the canister than the corresponding case without isostatic load. Since it was concluded in the subsection “Prerequisites for shear load by earthquakes” above that large earthquakes will not occur in connection with high isostatic loads, this case is, furthermore, seen as unrealistic.
- A glacial load after a shear displacement is to be expected since several glaciations are expected in a 1,000,000 year perspective according to geological evidence and hence have been postulated in the reference evolution. It is therefore important to note that the canister integrity is not jeopardised by a 5 cm shear movement followed by a 30 MPa glacial load.

Table 10-24. The effects on the canister insert and copper shell for combinations of shear load (10 cm shear) and isostatic load. The effects compared to the case with only rock shear are indicated with arrows, ↑ and ↓, for increase and decrease, respectively. Arrows within parentheses indicate small effects.

Case	Plastic strain insert	Axial stress insert	Local strain copper shell		Maximum strain mid copper shell	
Glacial load during shear	↓	↓	(↑)	17%	↓	1.4%
Shear followed by glacial load	(↑)	↓	↑	23%	↑	2.7%
For comparison – shear only				16%		2.0%

Canister conformity to design premises

Regarding the fulfilment of the design premises for shear movements at the canister, in Section 5.4.3 the following conclusions are drawn.

- Strength calculations of the canister's resistance to shear load /Raiko et al. 2010/ verify that a canister with properties in conformity to the specification for the reference design withstands the design basis shear load.
- The results from inspections of manufactured canister components show that the specified values for fracture toughness and yield tensile strength in the manufactured series of inserts, and elongation and creep ductility in the copper shells conform to the reference design.
- The damage tolerance analysis gives acceptable defect sizes that put rigorous requirements on manufacturing and non-destructive testing (NDT) capability for the insert. Based on the results and experience so far it is expected that these additional requirements can be implemented in production and the testing methods for verification.

It is further noted that the initial state for the shear load case does not take into account PWR inserts, as representative materials data for strength and damage tolerance analysis are not yet available. However, the PWR design is more robust due to the higher material thickness in the cast insert.

Increasing the density of the bentonite and thereby its stiffness, decreases the acceptable defect size for the insert, as seen in Table 10-23. The density given in the design premise (2,050 kg/m^3) is the upper limit of the buffer density according to the design premises for the buffer. As mentioned above, the derived initial state of the buffer implies a maximum bentonite density of 2,022 kg/m^3 around the canister, see Section 5.5.3, which would increase the margins for the effects of rock shear on the canister.

The cited analyses of the response of the buffer-canister system to a shear load also suggest that if the real variability in buffer density, fracture orientation and impact location on the canister were to be taken into account, then in many cases not even a 10 cm shear movement would jeopardise the integrity of the canister. This conclusion is further corroborated by the fact that the criteria used to evaluate the modelling results concern local properties; in many cases the violation of these criteria will not lead to loss of the integrity of the copper shell.

Identified uncertainties and their handling in the subsequent analysis

Figure 10-126 displays a flowchart summarising the relevant steps in the workflow.

The largest uncertainty, and the most difficult to reduce, concerns the expected frequency of earthquakes of various sizes at Forsmark. The literature is sparse and data coverage incomplete both in time and space. However, the frequencies used herein do not underestimate the number of faults that have been unequivocally designated "post-glacial". As noted by /Lagerbäck and Sundh 2008/, the erosional effect of the latest glaciation, the Weichsel, was quite limited and could most probably not have erased remnant evidence of fault scarps from previous glaciations. Hence, the frequencies used herein seem representative of at least the latest glacial cycle. The extent, duration and impact of future glaciations are unknown but Weichselian conditions, which promote fault reactivation should sufficient strain be accumulated over time, are assumed. It is also, pessimistically, assumed that each fault will indeed host the largest possible earthquake compatible with its size (area); a single, large earthquake on a fault results in far larger dynamic effects on surrounding host rock fractures than a series of smaller earthquakes releasing the same amount of strain energy. In summary, though the uncertainties are large, cautious or pessimistic assumptions have systematically been chosen.

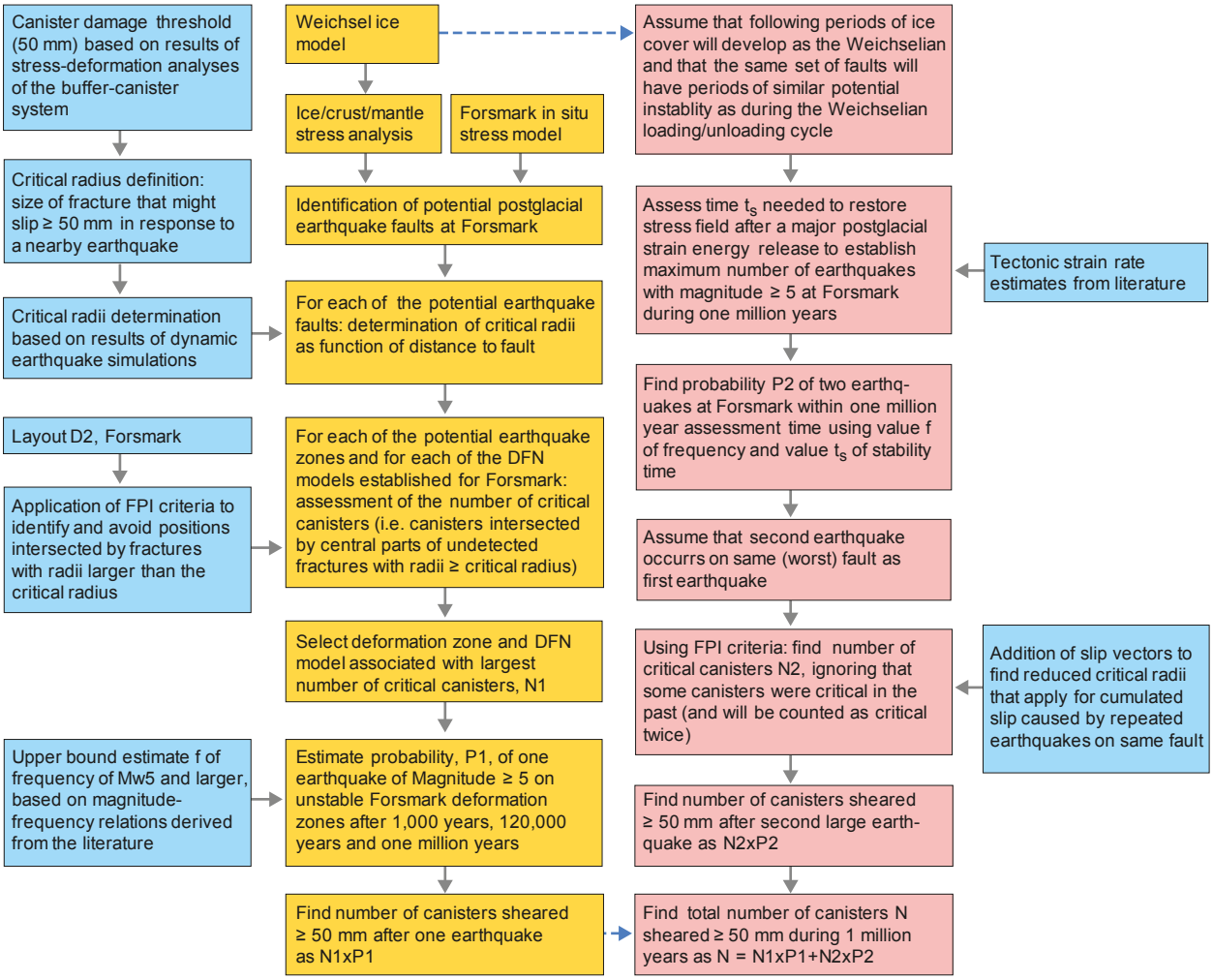

Figure 10-126. *Flow diagram showing the various steps needed for the earthquake impact assessment (Figure 4-7 in the* ***Geosphere process report****).*

Another large uncertainty concerns the properties of the deformation zones at Forsmark. Though the site has a thorough description with details on both geometry and properties of both the deformation zones and rock in-between, there is insufficient information on e.g. the strength properties of faults, to forecast the response of the deformation zones to a future deglaciation and insufficiently detailed knowledge on the process itself. Despite the lack of indications of large earthquakes at Forsmark /Lagerbäck et al. 2005, Lagerbäck and Sundh 2008/ it is pessimistically assumed that the deformation zones used for this analysis will indeed reactivate seismically.

There is a large uncertainty in the estimate of the strain rate. The strain rate governs the time necessary to build up stresses along faults and, hence, the relaxation time. The latter governs the number of successive earthquakes a fault can host within the time frame considered. Implicitly it is assumed that the strain rate (and orientation of maximum compressional stress) will remain constant for the coming 1,000,000 years. Even though the time frame is very large indeed, this is considered a reasonable assumption.

Consecutive earthquakes have been handled in the simulation of canister/fracture intersections by setting the critical radius to half the critical radius of a single event. This is a consequence of assuming that the second slip event on the target fracture occurs according to the same slip magnitude distribution as the previous one, and in the same direction. The prerequisites for this to occur are unlikely but as we do not yet possess other means to quantify the net slip this conservatism is judged appropriate. However, it needs to be emphasised that, due to the powerlaw distribution of fracture size, the number of critical fractures increases dramatically which tends to substantially overestimate the number of canisters that may fail. In addition, we do not take into account the fact that slip

velocity scales with slip magnitude. Instead, we apply the same 50 mm damage criterion for the total effects of two small low-velocity slip events separated by tens of thousands of years as for one large high-velocity slip event, hence adding further to the pessimism. However, the canister/buffer system is not particularly sensitive to slip velocity.

The number of critical canister positions is influenced by the fracture model of the Forsmark Site /Fox et al. 2007/. The uncertainties in the models are discussed thoroughly in the **Data report** and the full argumentation is not repeated here. In short, in this assessment all variants of the Discrete Fracture Network (DFN) models are propagated through all stages of this assessment to cover full uncertainty space given by the model uncertainties.

Finally, there is an uncertainty regarding the damage criterion of 50 mm. Only specific fracture/canister intersection geometries do in fact result in damage at 50 mm; other intersection geometries require larger slip magnitudes for damage to occur. Also, the failure criterion for the canister is the acceptable defect size for surface defects in the insert. The copper shell is assumed to be penetrated at the same moment as this criterion is exceeded. The strains in the copper shell are low (with the exception of model singularities) compared to copper material ductility requirements, though uncertainties arising from a copper thickness of slightly less than 50 mm are not evaluated. As the effects of different intersection geometries have been difficult to quantify and extract from the modelling and experiments on shear across the canister/bentonite package, it has pessimistically been assumed that all canisters that host slips exceeding 50 mm should count as damaged regardless of intersection geometry.

In conclusion, large earthquakes at Forsmark cannot be excluded within any of the safety assessment time frames. The impact of earthquakes, in terms of the number of canisters expected to be sheared 50 mm or more has here been quantified by using a range of earthquake frequency estimates, the Forsmark site description and by applying deposition hole rejection criteria. Using a number of numerical simulations, we identified potentially unstable deformation zones, computed critical radii of host rock fractures and the average number of canisters in critical positions. Finally, we computed the number of canisters that may be sheared 50 mm or more during the assessment time frames.

Between $9.3 \cdot 10^{-6}$ and $2.2 \cdot 10^{-5}$ canisters may be sheared 50 mm or more due to earthquakes within the 1,000-year time frame. During a glacial cycle, it is estimated that between $8.3 \cdot 10^{-4}$ and $5.7 \cdot 10^{-3}$ canisters may fail. For the 1,000,000-year time frame, at maximum two seismic events are assumed and it is estimated, using the most pessimistic way of accounting for the combined effects of both, that between $8.3 \cdot 10^{-3}$ and $7.9 \cdot 10^{-2}$ canisters may be sheared 50 mm or more. Because these expected numbers of sheared canisters are substantially less than one, they can be interpreted as the probability of one or more failed canisters being present at the end of the specified assessment time frame. The issue is further elaborated in the analysis of the scenario ‘canister failure due to shear load’ in Section 12.8.

10.4.6 Hydrogeological evolution

The primary driving force for groundwater flow at repository depth during periods of periglacial (permafrost) and glacial climate conditions is the hydraulic pressure gradient resulting from the existence of an ice sheet. The expected effects of this gradient with relevance for long-term safety are related to the groundwater chemistry, the performance measures of groundwater flow at repository depth, the advective travel time, and the flow-related transport resistance. In order to assess the magnitude of these impacts, groundwater flow simulations, based on the hydrogeological models developed as part of the **Site description Forsmark**, are performed /Vidstrand et al. 2010, Joyce et al. 2010/. The overall objective of these simulations is to assess the effects of periglacial and glacial climate conditions on site hydrogeochemical and hydrogeological conditions in the presence of a backfilled repository, i.e. safety functions R1 and R2 in Figure 10-2.

Methodology

As described in Section 10.3.6, the groundwater flow modelling conducted during temperate climate conditions by /Joyce et al. 2010/ considers the evolution between 8000 BC and 12,000 AD. To a large extent the setup of this modelling follows the specifications of the groundwater flow modelling considered in SDM-Site, which dealt with the evolution between 8000 BC and 2000 AD, a time period known as the Holocene.

In comparison, the groundwater flow modelling during periglacial and glacial climate conditions conducted by /Vidstrand et al. 2010/ is less specific with regard to time although the flow modelling as such encompasses periglacial and glacial climate conditions during a time period of approximately 19,000 years. That is, there is no particular start time associated with the flow simulations conducted to represent periglacial and glacial climate conditions. Furthermore, it is noted that /Vidstrand et al. 2010/ focus on studying the effects of a number of bounding hydraulic assumptions rather than striving for realism in every detail. Although some of the studied assumptions create overly pessimistic premises for the flow simulations, as compared to the reference evolution presented in the **Climate report**, Section 4.5, they are useful for safety assessment applications as they provide bounds on the uncertainties involved.

Based on the reference climate evolution described in the **Climate report**, the flow modelling in /Vidstrand et al. 2010/ is divided into three stages referred to as pre-LGM[21], LGM, and post-LGM. During the pre-LGM stage, the ice sheet grows and the ice sheet margin moves across the site in a forward (advancing) direction. During the LGM stage, the model domain is completely covered by ice for thousands of years. During the post-LGM stage, the ice sheet melts and its margin moves across the site in a backward (retreating) direction. Hence, the flow modelling of the three stages implies a transient top boundary condition.

It is noted that a repository is not included in the groundwater flow modelling conducted by /Vidstrand et al. 2010/. However, the influence of the hydraulic characteristics of the backfilled tunnels on the performance measures during periods with glacial climate conditions is accounted for by exporting the simulation results of /Vidstrand et al. 2010/ to be used as input (boundary conditions) in the groundwater flow modelling conducted by /Joyce et al. 2010/. The results from the simulations are presented below.

In summary, the following hydraulic conditions (assumptions) are considered in the groundwater flow modelling conducted by /Vidstrand et al. 2010/.

- **Pre-LGM stage.** Two different azimuth directions of ice sheet movement (advance from north-west and advance from north); three types of periglacial conditions (no permafrost, permafrost in front of the ice sheet margin, and permafrost in front of the ice margin as well as below the tip of the ice sheet margin); two types of permeability conditions (undistorted conditions, i.e. present-day conditions as defined in the **Site description Forsmark**, and distorted conditions, i.e. increased permeability due to hydro-mechanical deformations).
- **LGM stage.** The model domain is completely covered by a thick ice sheet for approximately 17,000 years.
- **Post-LGM stage.** One azimuth direction of ice sheet movement (retreat from southeast); submerged ground conditions in front of the ice sheet margin; undistorted permeability conditions.

The different simulations carried out by /Vidstrand et al. 2010/ may be grouped as shown in Table 10-25.

Figure 10-127 shows a map of the topography of a NW-SE orientation of the flow model domain. All structural and hydraulic properties inside the model domain are specified in /Vidstrand et al. 2010/. Inside the target volume, i.e. within the bedrock volume that hosts the repository, a DFN realisation is generated. The DFN realisation is transformed into an equivalent continuous porous medium (ECPM) approximation using the up-scaling methodology implemented in DarcyTools /Svensson et al. 2010/. Outside the region of the DFN realisation, a continuous porous medium (CPM) approximation is used.

The results of the flow simulations are reported for four ice-front locations denoted by IFL I-IV, see Figure 10-127, and five measurement localities denoted by ML 1–5, see Figure 10-128. IFL II corresponds to a situation when the ice sheet margin is right above the repository; ML 2 corresponds to a position in the centre of the repository layout. In addition to IFL I-IV, two additional ice-front locations are referred to in the flow modelling, IFL 0 and IFL V. These are both located outside the model domain shown in Figure 10-127. IFL 0 is simply the start position of the advancing ice sheet margin and IFL V is the start position of the retreating ice sheet margin. In summary, the advancing ice sheet margin starts at IFL 0 and passes IFL I-IV on its way to IFL V. At IFL V it stops and returns back to IFL 0. Conceptually, IFL 0 represents the temperate (initial) conditions at some time in the future (hence not 2000 AD), whereas IFL V coincides with the LGM.

[21] LGM is a standard acronym used to denote the glacial maximum of the last glaciation (Weichsel), cf. the **Climate report**.

Table 10-25. Overview of flow simulations in /Vidstrand et al. 2010/. The main scenarios, A and B, are divided into five cases (a)–(e). The bullets indicate the particular conditions modelled with each case considered. Case (a) constitutes the Base case in /Vidstrand et al. 2010/.

	Pre-LGM stage	LGM stage
	A. Glacial conditions without permafrost	
(a)	• Ice sheet movement from northwest. No permafrost in front of the ice sheet margin. Undistorted permeability conditions.	• Entire model domain is covered by an ice sheet. Undistorted permeability conditions. Post-LGM stages. • Submerged conditions in the ice free area. Undistorted permeability conditions.
	Variants	
	Pre-LGM stage	LGM and Post-LGM stages
(b)	• As in (a), but ice sheet movement from north.	• –
(c)	• As in (a), but distorted permeability conditions.	
	B. Glacial conditions with permafrost	
	Pre-LGM stage	LGM and Post-LGM stages
(d)	• Ice sheet movement from northwest. Permafrost in front of the ice sheet margin as well as 2 km below the tip (tongue) of the ice sheet margin Undistorted permeability conditions.	• –
	Variants	
	Pre-LGM stage	LGM and Post-LGM stages
(e)	• As in (d), but no permafrost tongue.	• –

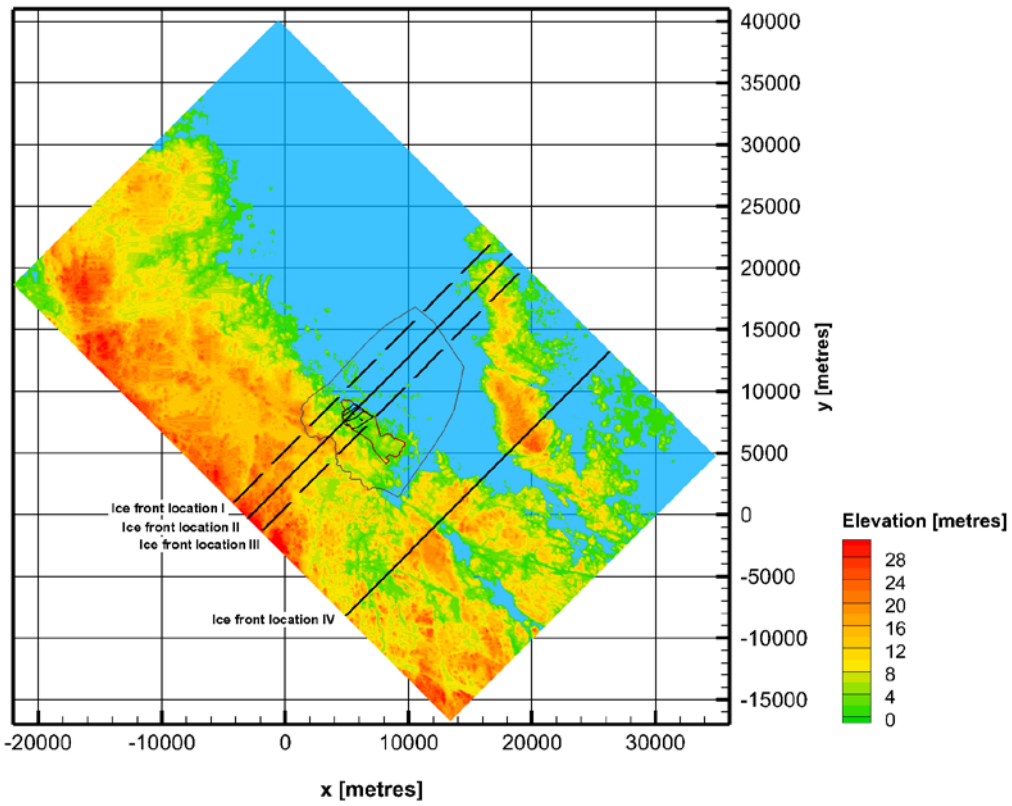

Figure 10-127. Map showing the present-day topography at Forsmark and the positions of ice front locations IFL I–IV for a NW-SE orientation of the flow model domain studied by /Vidstrand et al. 2010/. The large polygon in the centre shows the model domain used for groundwater flow modelling in SDM-Site. The small, polygon inside the large polygon shows the location of the investigated candidate area. The repository area is located in the north-western part of the small polygon. The y-axis points towards north.

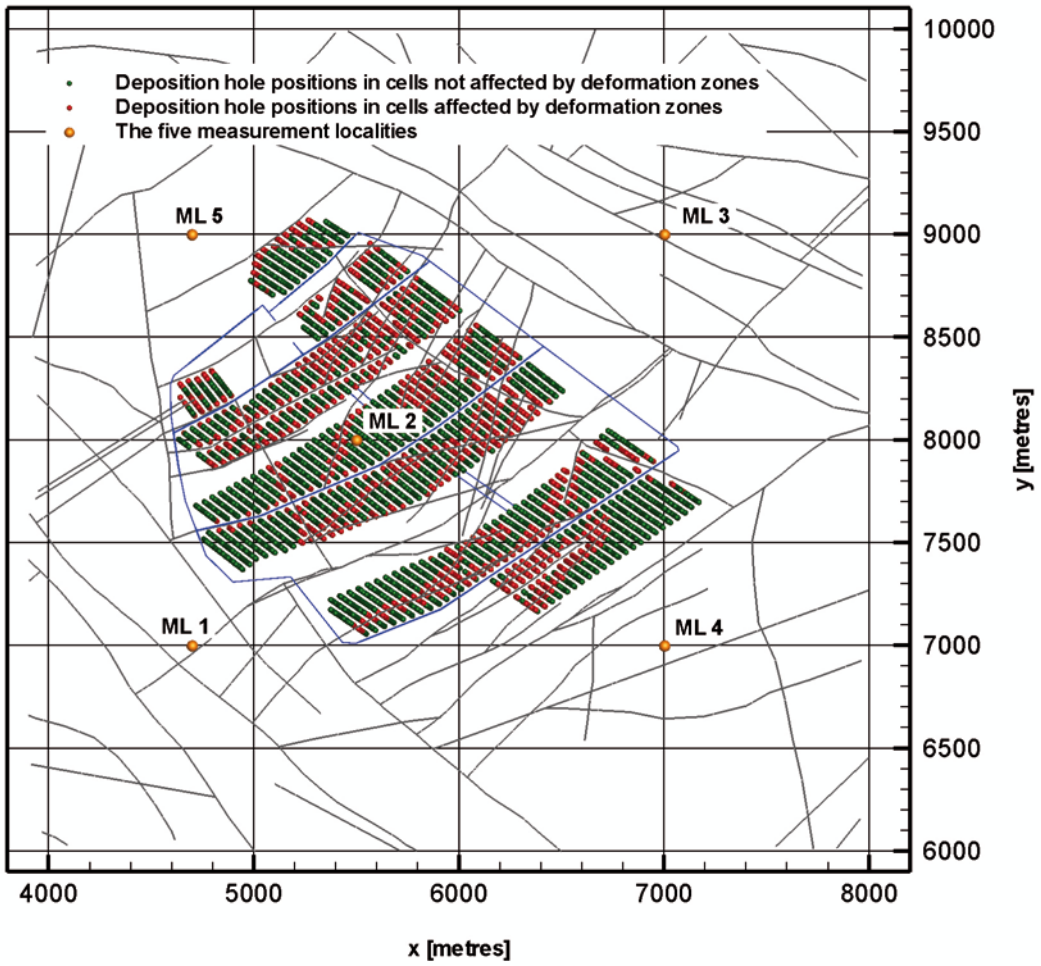

Figure 10-128. *Plane view of the repository layout at –465 m elevation (the blue lines represent major tunnels). The repository has 6,916 deposition hole positions. These are coloured according their structural location, i.e. whether the computational grid cell in DarcyTools is intersected by a deformation zone (HCD) or is fully inside the rock mass volumes between the deformation zones (HRD). (The deformation zones are shown as grey lines. It is noted that tunnels and deposition holes are not included in the model, but just shown in the figure for context.) The simulated evolution of the Darcy fluxes and the salinities is monitored at five measurement localities denoted by ML 1–5. The y-axis points towards north.*

The output parameters from the flow simulations conducted by /Vidstrand et al. 2010/ are the pressure (p [$ML^{-1}T^{-1}$]), the Darcy flux (q [LT^{-1}]) and the salinity (C [MM^{-1}]) at repository depth, i.e. at ML 1–5 for IFL I–IV. The flow simulations are accompanied by particle tracking simulations. The potential repository considered for modelling contains 6,916 deposition hole positions. One particle is released at each deposition hole position when the ice sheet margin reaches ice front locations II and IV during the pre-LGM stage simulations. All particles are tracked backwards and forwards as a means to identify their recharge and discharge locations, respectively. It is noted that the Darcy fluxes are fixed in space and time during the particle tracking, which is a simplification since the boundary conditions at ground surface change with the position of the advancing/retreating ice sheet margin. The output parameters from the particle tracking are the flow path length (L [L]), advective travel time (t_w [T]) and the flow-related transport resistance (F [TL^{-1}]).

As already mentioned, the pressure and density fields calculated by /Vidstrand et al. 2010/ are exported to the flow modelling conducted by /Joyce et al. 2010/, since the repository layout and the excavated damage zone (EDZ) are not explicitly resolved within the flow modelling conducted by /Vidstrand et al. 2010/. Thus, the flow model presented in /Joyce et al. 2010/ is also used to calculate performance measures during glacial climate conditions. These results are used as input for the far-field radionuclide transport calculations (Chapter 13). The groundwater flow results are also used as input to buffer erosion-corrosion analyses (Sections 10.4.8 and 10.4.9). Further, in the

repository-scale model of /Joyce et al. 2010/, particles are also back-tracked from the deposition hole positions in order to assess recharge pathways. The particle paths extend into the site-scale model in a corresponding manner as for the discharge pathways. Using the recharge paths and an analytical solution for solute transport, an assessment of potential for penetration of dilute waters to repository depth is made /Joyce et al. 2010, Appendix G/.

Finally, the results calculated by /Vidstrand et al. 2010/ (fracture water and matrix porewater salinities, flow path lengths, advective travel times, and flow-related transport resistances of particles travelling from the surface to repository depth) are exported to the hydrogeochemical modelling carried out by /Salas et al. 2010/ and /Sidborn et al. 2010/ to study chemical processes during periglacial and glacial climate conditions, in particular the consumption of oxygen dissolved in recharging water that could potentially reach repository depth, see Section 10.4.7.

Performed analyses and usage within SR-Site

Below, the different cases of /Vidstrand et al. 2010/ performed with relevance for the periods with periglacial and glacial climate conditions are listed. In addition, the calculations of /Joyce et al. 2010/ using boundary conditions from the glacial models are included. It is indicated where the results produced by each case are used within the subsequent analyses of SR-Site.

- **Hydrogeological evolution.** In /Vidstrand et al. 1010/, the hydrogeological evolution for the case without permafrost in front of an advancing ice sheet margin constitutes a base case for a number of other models (variant cases). Thus, results on the hydrogeological evolution for the simulated period (IFL 0 → IFL V → IFL 0) are reported for a number of different cases including a case with permafrost in front of an advancing ice sheet margin, see below. It is noted that the groundwater chemistry in all these flow models is represented by salinity alone and that the results of the simulated hydrogeochemical evolution are discussed in Section 10.4.7.
- **Recharge and discharge locations in the biosphere.** The recharge and discharge locations are identified using forward and backward particle tracking from coordinates representing the deposition hole positions within the repository footprint. The particle tracking is performed for steady-state velocity fields representing different ice front locations relative to the location of the repository. Several cases, including an ice sheet with permafrost, are presented here in a manner corresponding to the hydrogeological evolution above. The performance measures discussed below are related to these deposition hole positions and associated particle tracks. The results on discharge locations in the biosphere are used for the dose calculation in the biosphere.
- **Performance measures.** The performance measures are Darcy flux (q), advective travel time (t_w) and the flow-related transport resistance (F). The advective travel time and flow-related transport resistance are calculated for both the recharge and discharge flow paths in the super-regional scale model. Furthermore, performance measures are obtained from the combined repository-scale and site-scale model including an explicit representation of the repository structures by applying boundary conditions from the super-regional scale model /Joyce et al. 2010/. These results are used in radionuclide transport calculations, see Chapter 13.
- **Penetration of glacial meltwater.** The recharge of glacial melt water implies a gradual dilution of the originally more saline water. As dilute water has negative effects on the buffer and backfill stability, it is of interest to assess the possibilities of dilute water reaching repository depth considering the hydrogeological flow and transport conditions. This is done using the flow-related transport properties resulting from the repository-scale and site-scale models described above in conjunction with analytical transport estimates. The results are used in Section 10.4.7.
- **EDZ and crown space.** In the application of glacial boundary conditions in the repository-scale and site-scale models including an explicit representation of the repository, an assessment of modified properties of the excavation damaged zone (EDZ) is performed. Also, an assessment of the impact of a crown space in the tunnels is made. The crown space is caused by a consolidation of the tunnel backfill material. These results are used in radionuclide transport calculations, see Chapter 13.
- **Site related variants.** Some properties of the site, with specific relevance to glacial conditions, as well as the glacial conditions themselves are uncertain. The impacts of alternative parameterisations related to these issues are assessed in order to judge their importance. For example, the transmissivity of all deformation zones and fractures that strike towards northwest is changed

based on the results from the rock mechanics modelling conducted for SR-Site /Hökmark et al. 2010, Lönnqvist and Hökmark 2010/.

- **Glacial conditions with permafrost.** The reference evolution in the **Climate report** is characterised by permafrost conditions in front of an advancing ice sheet margin. The same set of analyses performed for the case without permafrost in front of an advancing ice sheet margin is repeated for this case. The most important differences are high-lighted. It is noted that boundary conditions for this case cannot be exported to the repository-scale and site-scale models of /Joyce et al. 2010/ since the hydraulic properties of the geosphere are modified due to the presence of permafrost. It is noted that the hydrogeological evolution and recharge and discharge locations of this case are commented upon above under the specific bullet points dealing with these two issues. Other aspects of this case are treated under this bullet point.
- **Comparison of the Darcy flux at different times during glaciation and deglaciation.** Various model simplifications are made in /Vidstrand et al. 2010/ and /Joyce et al. 2010/ that do not conform fully to the expected reference evolution described the **Climate report**. In order to obtain an appreciation of the evolution of groundwater flow for an advancing and retreating ice sheet margin, methods to combine all simulated "climate events" (states) are presented and exemplified. The objective is to find reasonable simplifications of the complex temporal evolution of the Darcy flux for subsequent handling in radionuclide transport calculations within the safety assessment.

Hydrogeological evolution

Figure 10-129 shows Darcy fluxes for a NW-SE vertical cross section through the potential repository area. Three cases are shown. The upper-most cross-section represents temperate conditions (IFL 0). The cross-section in the middle represents an advancing ice sheet margin at IFL II without permafrost in the periglacial area. The bottom-most cross-section represents an advancing ice sheet margin at IFL II with permafrost conditions in the periglacial area.

Figure 10-130 shows the salinity field for a NW-SE vertical cross section through the potential repository area. Three cases are shown. The upper-most cross-section represents temperate conditions (IFL 0). The cross-section in the middle represents an advancing ice sheet margin at IFL II without permafrost in the periglacial area. The bottom-most cross-section represents an advancing ice sheet margin at IFL II with permafrost conditions in the periglacial area. Figure 10-131 shows the same salinity fields but for a horizontal plane placed at –465 m through the target volume.

In summary, Figures 10-129 and 10-130 show that the hydraulic pressure at the bottom of the ice sheet distorts the temperate conditions and causes glacial meltwater to recharge and flush the advective system. In effect, the more saline water in the fractures is pushed forwards and upwards (upconing). The reason for the high salinity near the ground surface is that the permafrost hinders discharge at the top boundary (cf. the bottom most image in Figure 10-129), except where taliks (unfrozen ground) occur.

The changes in Darcy flux and fracture water salinity during the simulated period (IFL 0 → IFL V → IFL 0) are monitored at the five measurement localities ML 1–5 and expressed as ratios relative to the corresponding initial, temperate values, see Figures 10-132 and 10-134. It is recalled that the term temperate in /Vidstrand et al. 2010/ is not to be understood as 2000 AD, but rather as a time slot in the future when the ice sheet margin is close to, but still outside, the flow model domain, i.e. IFL 0.

In Figure 10-132, it is seen that the Darcy flux increases dramatically during the two ice front passages. The immediate shift to low and constant values at the start of the period of complete ice coverage is an artefact of the instantaneous shift in ice sheet gradient at the same moment. In reality, a more smooth transition is expected. For the glacial case with permafrost, slightly different shapes of the curves are obtained during glacial advance, see Figure 10-133. However, for the remaining parts of the cycle, the curves are identical to those shown in Figure 10-132 as there is no permafrost during these periods.

The normalised change in the salinity development is shown in Figure 10-134. The glacial passage during advance (pre-LGM) is characterised by an initial upconing followed by an out flushing resulting in lower salinities than during the initial temperate conditions. However, during the subsequent stage, i.e. when the site is completely covered by the ice sheet (LGM), a gradual increase in fracture water salinity at repository depth occurs. This gain of the "salt water interface" is due to an accom-

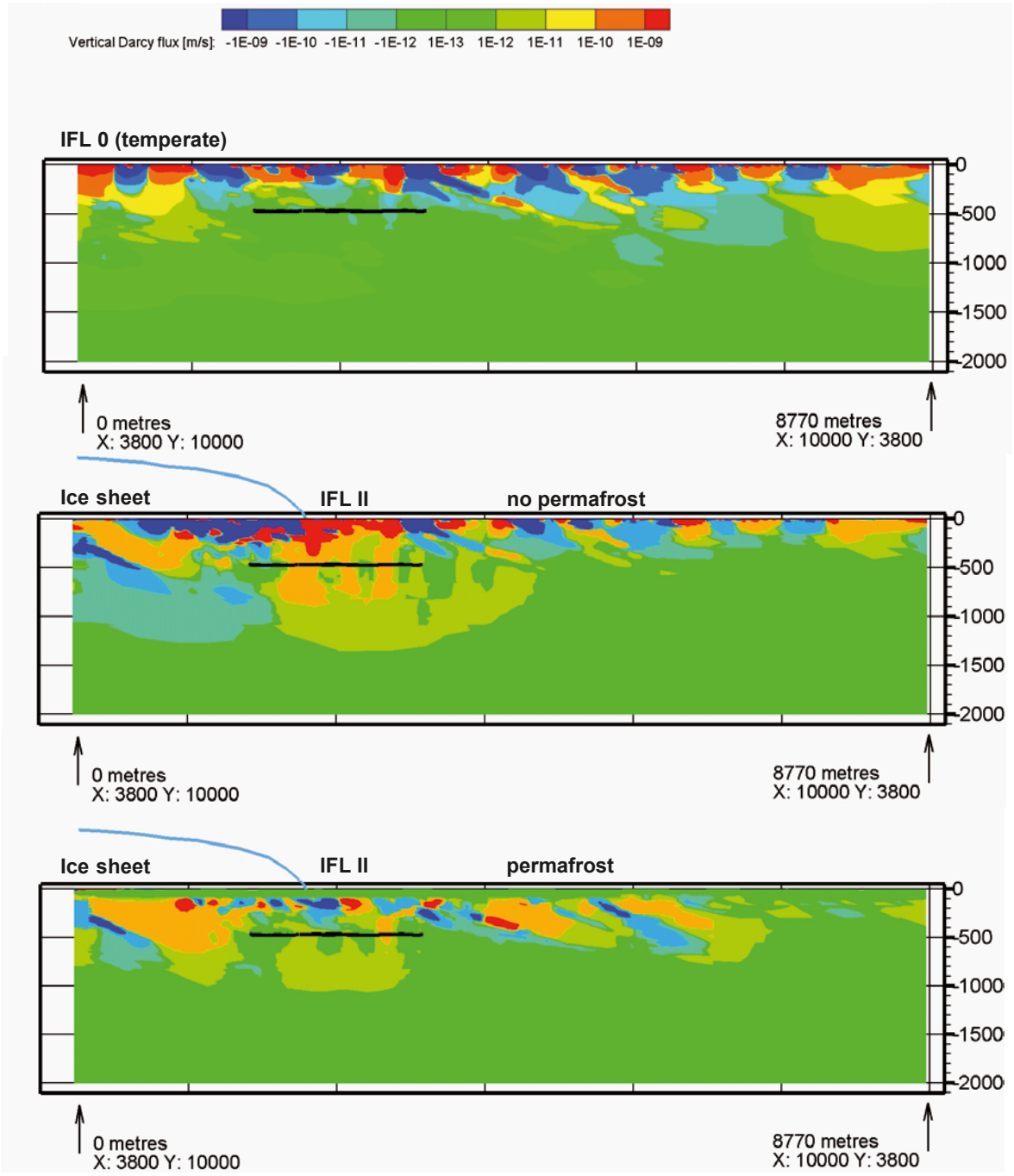

Figure 10-129. *Top: Darcy flux during temperate conditions mapped on a cross-section parallel to the direction of the ice sheet movement during glaciation. The images in the middle and at the bottom show the Darcy fluxes when the ice sheet margin is at IFL II for the glacial case without permafrost (middle) and for the glacial case with permafrost (bottom). Negative values represent downward directed fluxes. The position of the ice sheet profile is illustrated with a blue curve.*

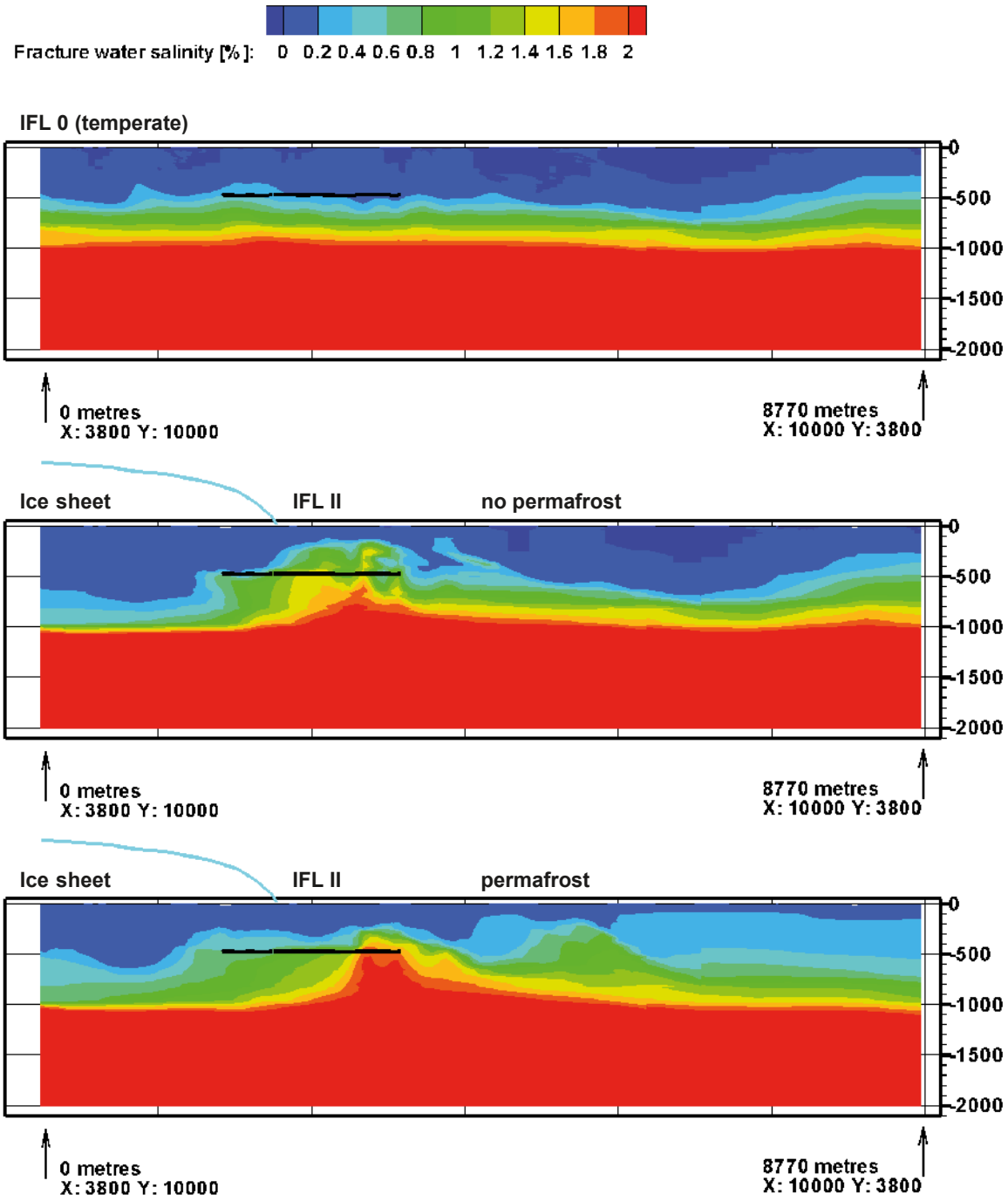

Figure 10-130. *Top: Fracture (advective) water salinity during temperate conditions mapped on a cross-section parallel to the direction of the ice sheet movement during glaciation. The images in the middle and at the bottom show the fracture water salinity when the ice sheet margin is at IFL II for the glacial case without permafrost (middle) and for the glacial case with permafrost (bottom). The position of the ice sheet profile is illustrated with a blue curve.*

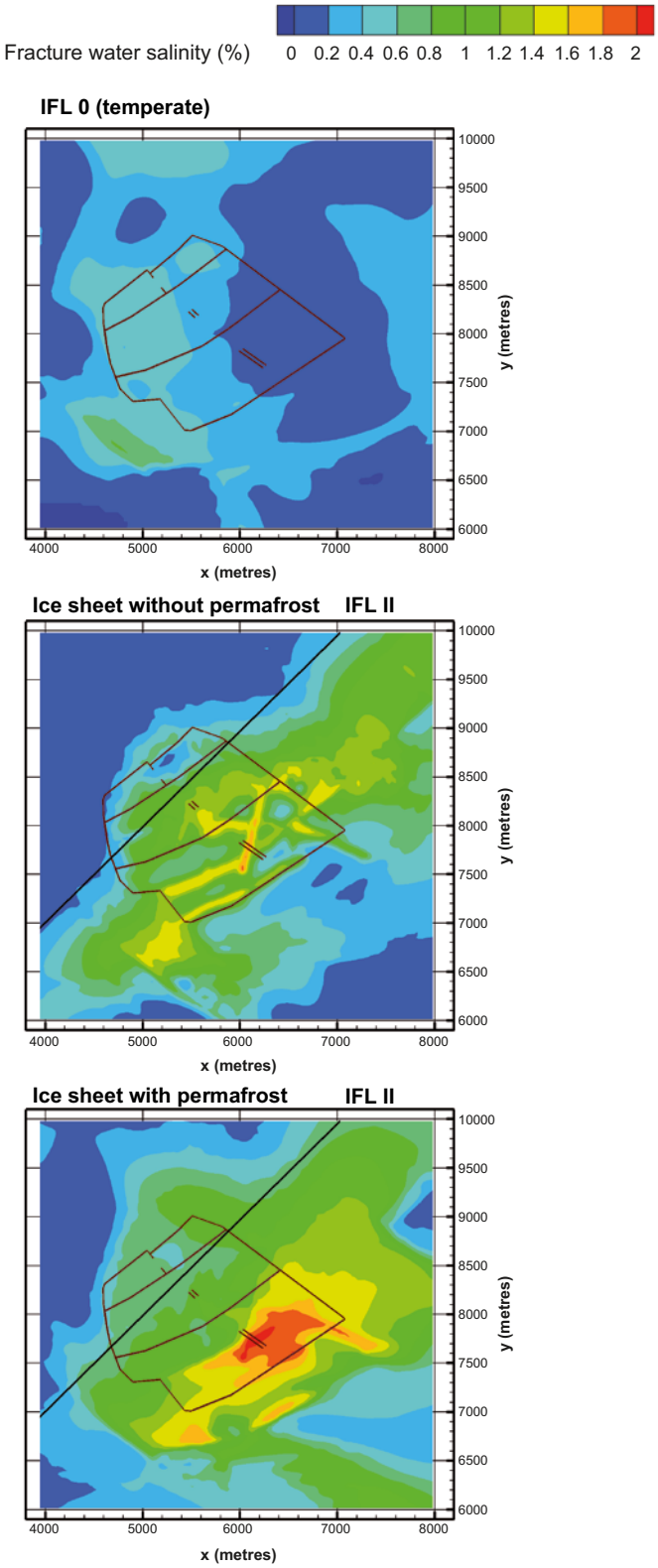

Figure 10-131. *Top: Fracture (advective) water salinity during temperate conditions mapped on a horizontal plane located at –465 m. The images in the middle and at the bottom show the fracture water salinity when the ice sheet margin is at IFL II for the glacial case without permafrost (middle) and for the glacial case with permafrost (bottom). The black thin lines represent main repository tunnels.*

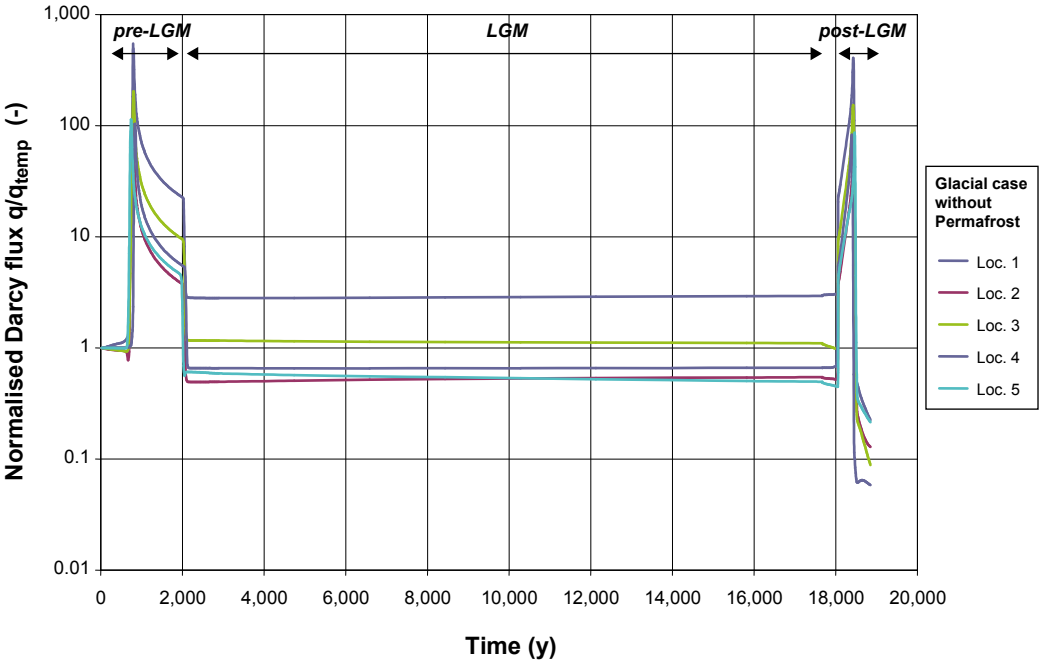

Figure 10-132. *Plot showing the normalised change in Darcy flux, (q/q_{temp}), at ML 1–5 during approximately 19,000 years for the glacial case without permafrost. ML 1 is located close to a steeply dipping deformation zone.*

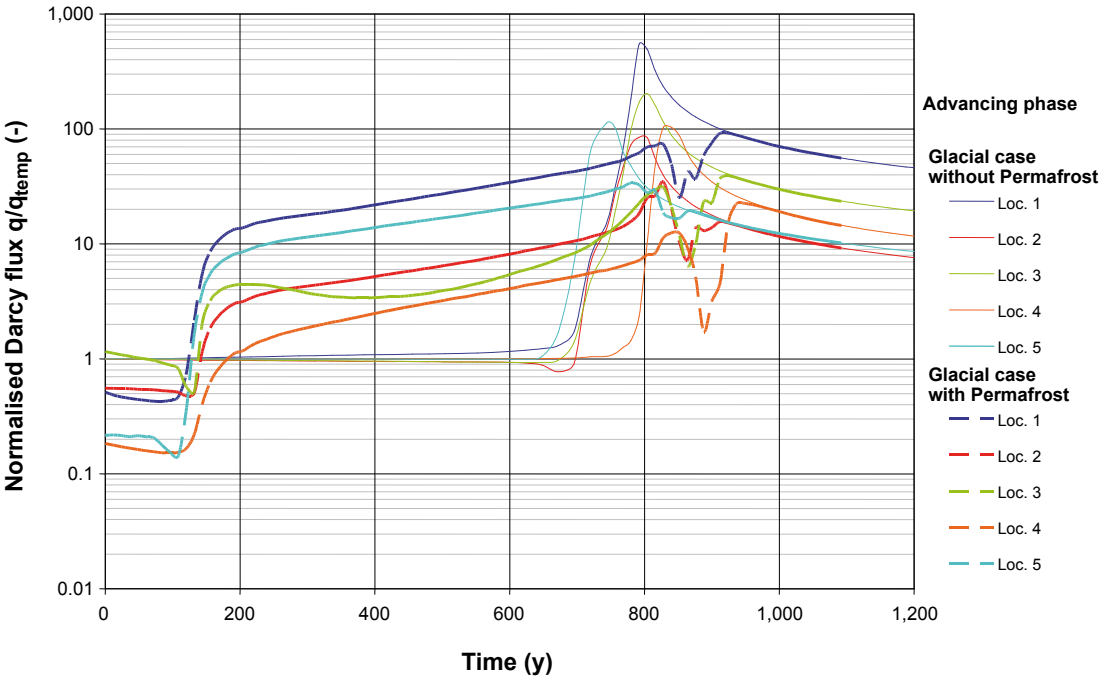

Figure 10-133. *Close-up showing the normalised change in Darcy flux, (q/q_{temp}), at ML 1–5 during glaciation (pre-LGM). In addition to the glacial case with permafrost (solid lines), the evolution of the glacial case without permafrost (dashed lines) is shown. Beyond t = 1,000 years the two cases are alike.*

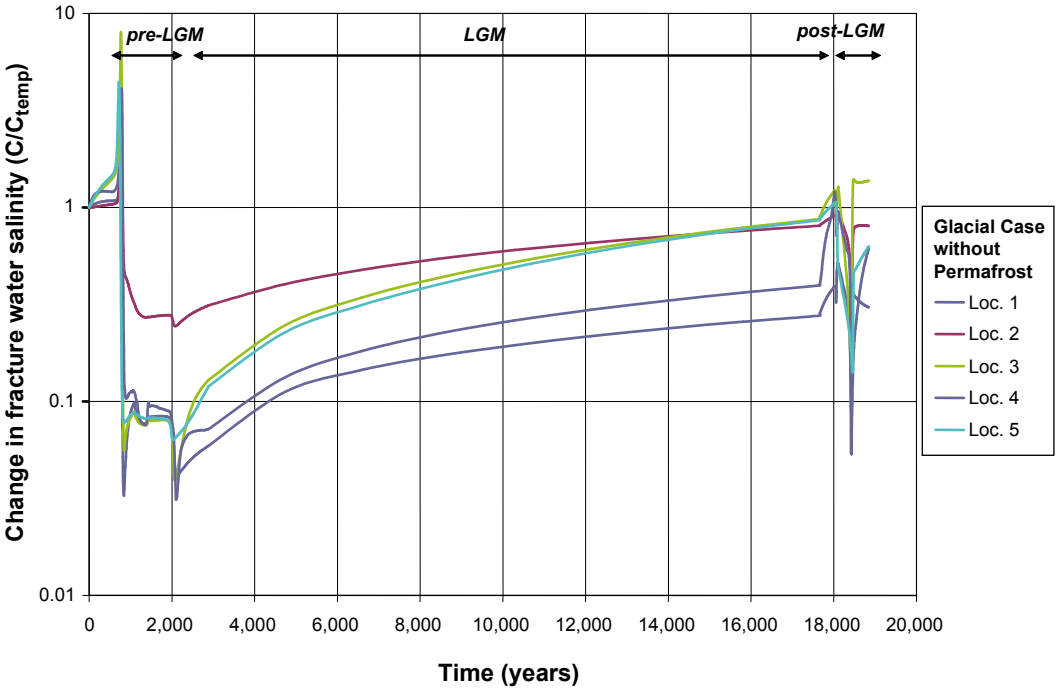

Figure 10-134. *Change in concentration, (C/C_{temp}), during a cycle of approximately 19,000 years for the glacial case without permafrost.*

modation of the buoyancy forces to the very weak top boundary condition of an almost uniform ice sheet thickness, and to the slow, but continuous advective transport of salt from below. It is recalled that the fracture water salinity at great depth is assumed to be undisturbed (fixed) at all times in the flow model. The data support for this assumption is presented in SDM-Site.

The glacial passage during retreat (post-LGM) is also characterised by an upconing and flushing event, but the effects are considerably smaller than during the advance. The reasons for this are twofold; (i) the speed of the retreating ice sheet margin is twice as fast as the speed of the advancing ice sheet margin (100 m/y versus 50 m/y), and (ii) the subglacial area in front of the retreating ice sheet margin is submerged. These conditions reduce the duration and the magnitude of the hydraulic gradient across the ice sheet margin significantly.

Figure 10-135 shows the simulated difference in flushing as a function of the average speed of the retreating ice sheet margin. A retreat speed of 300 m/y yields less flushing than a retreat speed of 100 m/y. It is noted that the average speed of the retreating ice sheet margin considered for the reference evolution in the Climate report is 300 m/y; i.e. three times the speed considered in /Vidstrand et al. 2010/. Second, the retreating ice sheet profile considered for the reference evolution in the Climate report is significantly thinner and less steep at the ice sheet margin than the ice sheet profile considered in /Vidstrand et al. 2010/, which is a theoretical maximum. Thus, the conditions considered by /Vidstrand et al. 2010/ exaggerate the impact of the ice sheet; still the results indicate that the fracture water salinities are more or less restored during the simulated period (IFL 0 → IFL V → IFL 0).

In conclusion, low fracture water salinities, i.e. dilute conditions, are mainly found in conjunction with the ice front passages. The results presented in Figure 10-134 indicate that fracture water salinities reach values below ten percent of the values in temperate conditions for a limited period of time only.

Recharge and discharge locations in the biosphere

The top image in Figure 10-136 shows the recharge and discharge locations when the ice sheet margin reaches ice-front location II for an ice sheet without permafrost, and the bottom image in Figure 10-136 shows the corresponding results for an ice sheet with permafrost. For both cases, a number of particles recharge at the upstream boundary of the model domain, which suggests that the model domain is too

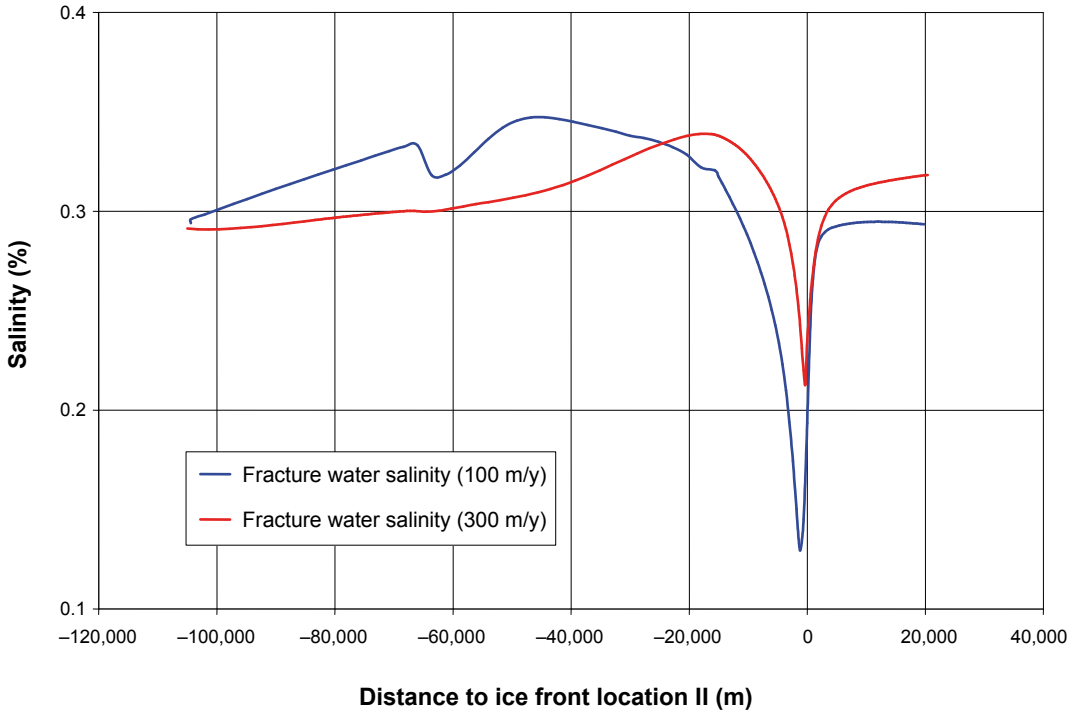

Figure 10-135. *Plot showing the difference in flushing as a function of the average speed of the retreating ice sheet margin. A retreat speed of 300 m/y yields less flushing. (The ice sheet margin moves from left to right in this plot.)*

short to give a fully undisturbed view of all recharge locations for a fixed flow field. Nevertheless, it may be concluded that the present-day topographic water divides, which play an important role in the recharge and discharge during temperate conditions, are significantly diminished in importance during glacial conditions.

In contrast, the discharge locations are predominantly found well within the physical boundaries of the model domain and often very close to the margin of the ice sheet. The differences seen in the discharge pattern between the two glacial cases are largely caused by the varying hydraulic properties and boundary conditions. For an ice sheet with permafrost, there are two centres of discharge:

- The deformation zone model that exists within the regional model domain for SDM-Site Forsmark. In this simulation approximately two percent of the released particles exit along deformation zones.
- The taliks positioned at the topographic lows in front of the ice sheet margin to the east (outside the regional model domain). In this simulation, the taliks catch approximately 98% of the released particles.

Performance measures

The performance measures of interest are the Darcy flux (and equivalent flow rate) at each deposition hole position, and the flow-related transport properties along flow paths from the deposition hole positions, i.e. the advective travel time and flow-related transport resistance. In principle, these are directly obtained from the super-regional model /Vidstrand et al. 2010/ for all ice front locations. However, the repository structures are not explicitly included in this model, and hence results for the different release paths Q1, Q2 and Q3 handled in /Joyce et al. 2010/ and presented in Section 10.3.6 are not obtained. By transferring boundary conditions from the super-regional scale model to the combined repository-scale and site-scale models of /Joyce et al. 2010/ where the repository is included, all performance measures needed for subsequent radionuclide transport calculations are obtained.

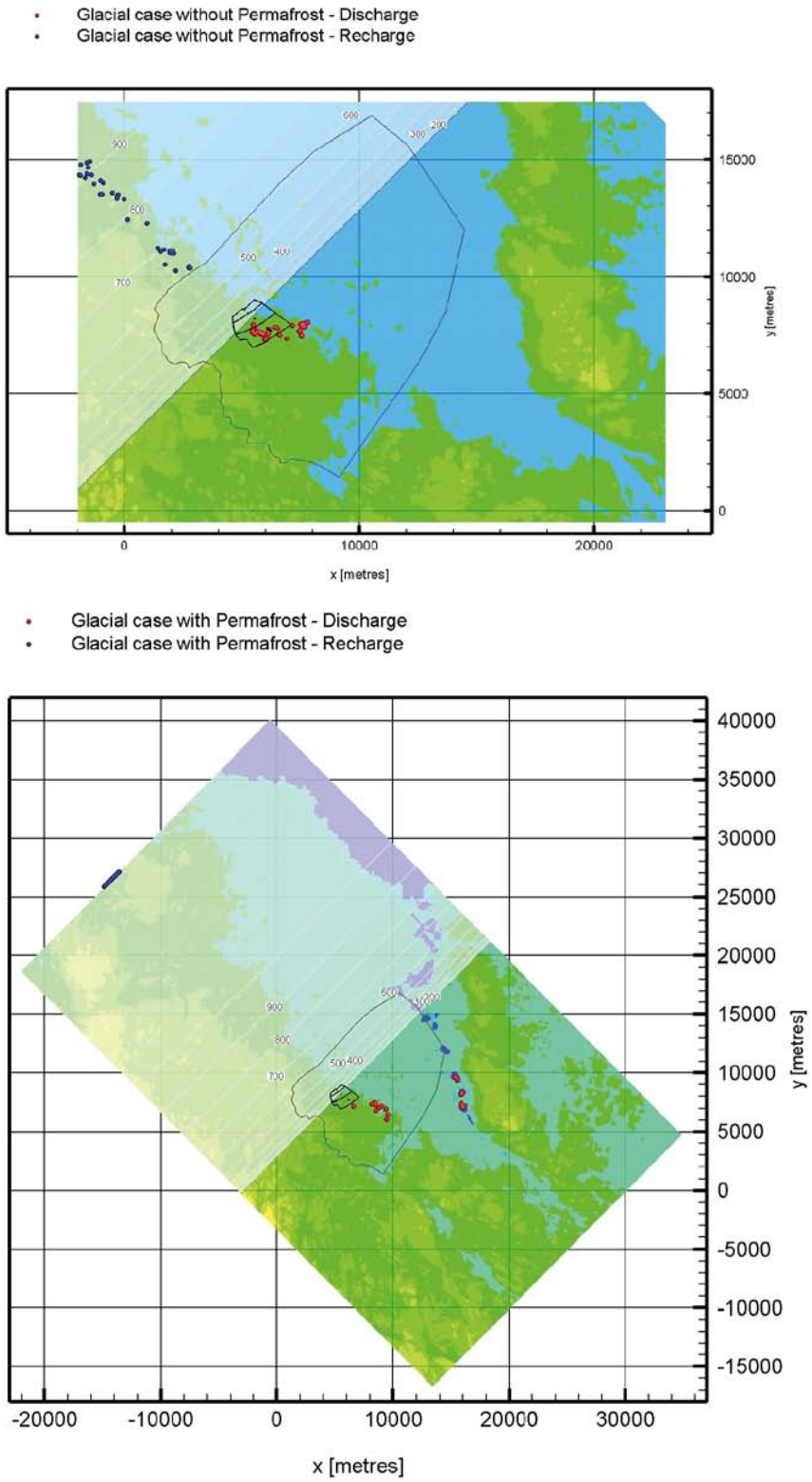

Figure 10-136. *Recharge (blue) and discharge (red) locations of the 6,916 particles released at repository depth when the advancing ice sheet margin is at ice-front location II. Top: Ice sheet without permafrost. Bottom: Ice sheet with permafrost and taliks. The taliks are positioned in the topographic lows in front of the ice sheet margin to the east (outside the polygon that indicates the SDM-Site model domain).*

In Figures 10-137 and 10-138, the Darcy flux and flow-related transport resistance are shown for the Q1 path for the case with an advancing ice sheet margin without permafrost where the ice front is in close proximity to the repository (ice-front location II). It is observed that the median Darcy flux is increased by approximately an order of magnitude. A corresponding decrease of the flow-related transport resistance is observed. Also, the results indicate that the high Darcy fluxes are more influenced by the glacial boundary conditions than the low values; e.g. the 90th percentile is shifted more than the 10th percentile. Thus, it appears that regions with low flow are relatively less affected by the high gradients induced by the ice sheet than regions with high flows.

Penetration of glacial melt water

In principle, the future groundwater chemistry, specifically salinity, is provided by the super-regional scale groundwater flow simulation reported above. However, the super-regional scale model has a fairly coarse discretisation, which does not allow an assessment of the groundwater chemistry evolution on a deposition hole scale. Thus, an alternative assessment of the evolution of the groundwater chemistry, and specifically the potential for penetration of dilute water, is made.

The combined repository-scale and site-scale models of /Joyce et al. 2010/ with boundary conditions from the super-regional scale model of /Vidstrand et al. 2010/ are used. The cases with an advancing ice sheet margin without permafrost for ice-front locations II and V are analysed. In order to assess the potential for penetration of dilute water, an injection of glacial melt water along those recharge pathways that originate close to the surface within the regional-scale model is considered for the two ice front locations. Similar simplifying assumptions as used for the temperate period calculations in Section 10.3.6 are adopted here. Along the flow paths, the only mitigating process considered is the out diffusion of salt from the matrix affecting the penetration of the glacial melt water front. It is assumed that the salt concentration of the matrix water is in equilibrium with the fracture water prior to the injection of glacial meltwater with a salt concentration of 0 g/L. The simplifying nature of these assumptions is discussed in Section 10.1.3. In Figures 10-139 and 10-140, the temporal distribution for deposition holes to obtain ten percent of the initial water concentration is shown for ice front location II and V, respectively. The initial salt concentration of the fracture water before the onset of the glacial period is estimated to be 3 g/L, see Section 10.4.7. Ten percent of the initial concentration thus corresponds to 0.3 g/L, which coincides with the value assumed to represent dilute conditions with potential buffer erosion. The vertical lines represent the assumed approximate duration of the periods. For ice front location II, i.e. an ice front in close proximity to the repository, the assumed durations are 20 and 100 years. The longer duration is an estimate for an advancing ice front, whereas 20 years is an estimate for a retreating ice front; however, all results presented in the figure are based on a flow field obtained for an advancing ice sheet. For ice-front location V, i.e. the glacial maximum case (LGM), two time durations are assumed, 20,000 and 100,000 years. It is observed that approximately two percent of the deposition holes experience dilute conditions during an advancing ice front and also during an assumed period of 100,000 years corresponding to glacial maximum conditions. The calculations provided here are bounding estimates; as shown in the results above for the temporal evolution during a glacial cycle, the salinity in the system is in fact restored at repository depth due to up-coning effects. Also, as discussed in Section 10.1.3 but not accounted for here, water-rock interactions will also modify the water chemistry. Thus, penetration of dilute water with zero concentration for an extended period of time is a pessimistic assumption.

EDZ and crown space

In the hydrogeological base case model, a continuous excavation damaged zone (EDZ) is implemented in all tunnels (both deposition tunnels and other tunnels) under the tunnel floor. The EDZ has a transmissivity value of $T = 1 \cdot 10^{-8}$ m^2/s and a thickness of 0.3 m. In order to assess the sensitivity in performance measures to tunnel properties, four alternative cases are analysed. Two of these have higher EDZ transmissivities ($T = 1 \cdot 10^{-7}$ m^2/s and $T = 1 \cdot 10^{-6}$ m^2/s, respectively), one case has no EDZ, and the final case has the base case EDZ properties, but is combined with a crown space under the tunnel ceiling. The crown space represents the effects of consolidation of the backfill material. In the model, the crown space is implemented as a 0.1 m thick zone with a high conductivity value ($K = 1 \cdot 10^{-3}$ m/s) and a porosity equal to unity.

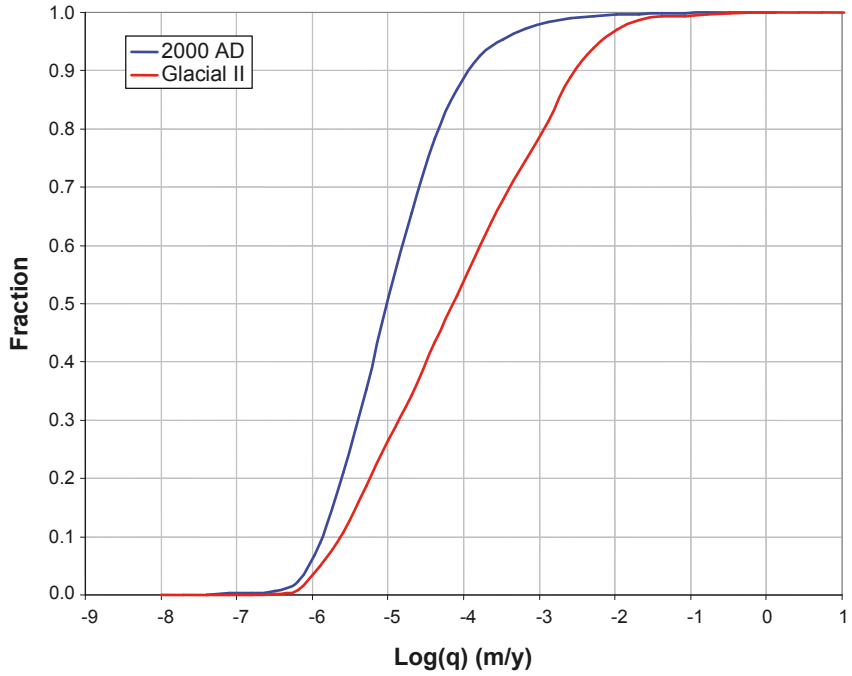

Figure 10-137. *Cumulative distribution function plots of Darcy flux (q) for the Q1 path for the hydrogeological base case simulation at 2000 AD (2000) and the glacial case without permafrost simulation at ice-front location II (glacial II) for the deposition holes with particles successfully reaching the model top boundary. (Modified after Figure E-51 in /Joyce et al. 2010/.)*

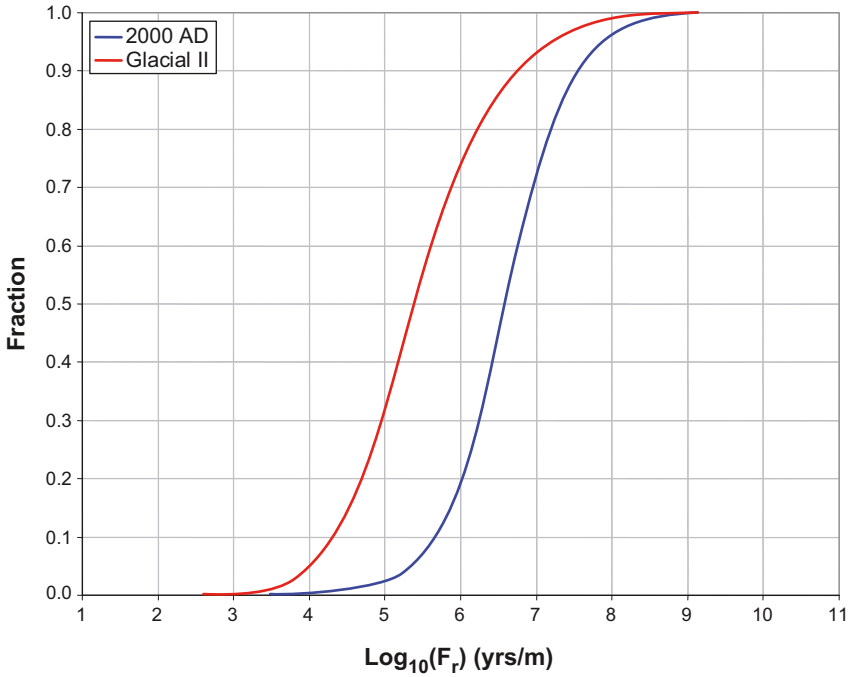

Figure 10-138. *Cumulative distribution function plots of flow-related transport resistance (F) for the Q1 path for the hydrogeological base case simulation at 2000 AD (2000) and the glacial case without permafrost simulation at ice-front location II (glacial II) for the deposition holes with particles successfully reaching the model top boundary.*

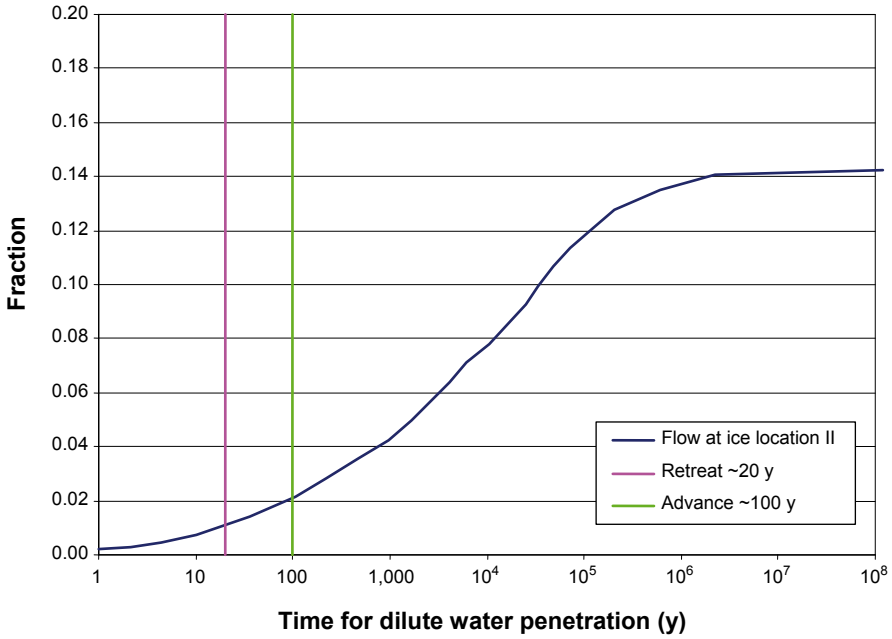

Figure 10-139. *Temporal distribution for all deposition hole positions to obtain ten percent of the initial water concentration with an ice front at ice-front location II. The green line shows that approximately two percent of the deposition holes experience dilute conditions for an advancing ice front that is assumed stationary for 100 years at IFL II.*

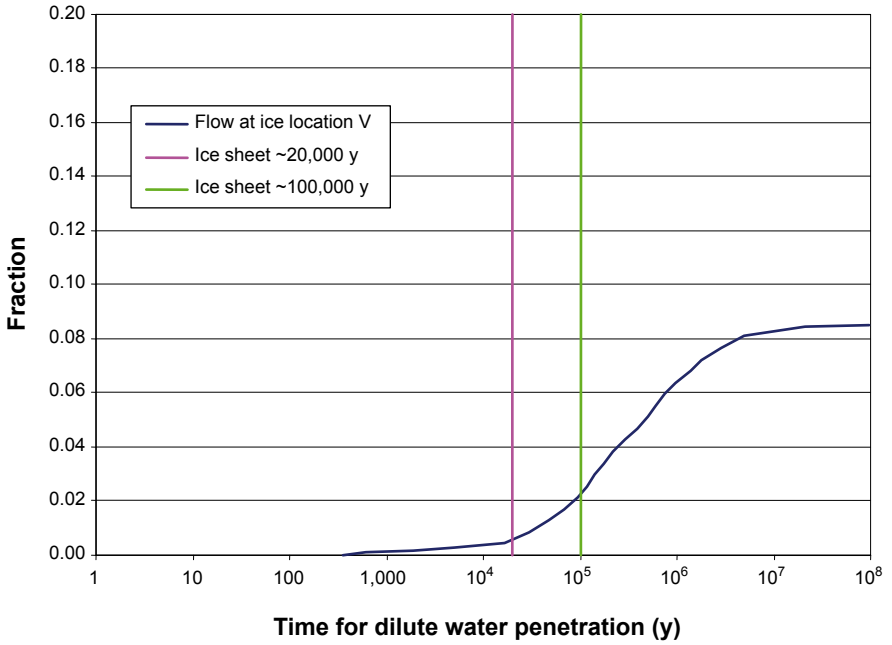

Figure 10-140. *Temporal distribution for all deposition hole positions to obtain ten percent of the initial water concentration for different assumed durations of ice-front location V (glacial maximum) conditions. The green line shows that approximately two percent of the deposition holes experience dilute conditions during an assumed duration of 100,000 years.*

The Darcy flux for the Q2 path is shown in Figure 10-141. Since the Q2 path corresponds to the EDZ path, no result exists by definition for the case with the EDZ removed. The figure clearly shows, as expected, that an increase in the EDZ transmissivity implies an increase in the associated Darcy flux in the EDZ. The crown space implies a small reduction of the Darcy flux in the EDZ; i.e. the flow is redistributed to the crown space from the EDZ.

The flow-related transport resistance of the Q3 path is shown in Figure 10-142. It is observed that more favourable results are obtained when the EDZ is removed, whereas all other cases imply less favourable conditions. The existence of a crown space is by far the most unfavourable case. Also worth noticing is that the crown space seems to have a stronger influence during glacial conditions than during temperate conditions (Section 10.3.6). This is likely due to the modified flow direction and larger flows to be accommodated during the glacial flow regime; the flow is thus preferentially directed to the high permeability crown space. With flow paths preferentially going through the crown space, less flow-related transport resistance is accumulated in the fractured rock.

Site related variants

N-S ice advance direction

Based on the historic and modelled data described in the **Climate report**, a NW-SE orientation of the model domain is conceived to be the most appropriate orientation to study for an advancing ice sheet margin. (The most appropriate retreat direction is probably somewhat more parallel to S-N.) The simulations carried out by /Vidstrand et al. 2010/ include a variant sensitivity test in which a N-S ice advance direction is used. Overall, the simulation results reported by /Vidstrand et al. 2010/ suggest minor differences of insignificant importance for SR-Site. For example, Figure 10-143 displays the Darcy fluxes at measurement localities 2 and 4 for the two different ice advance directions. The evolutions and magnitudes are similar.

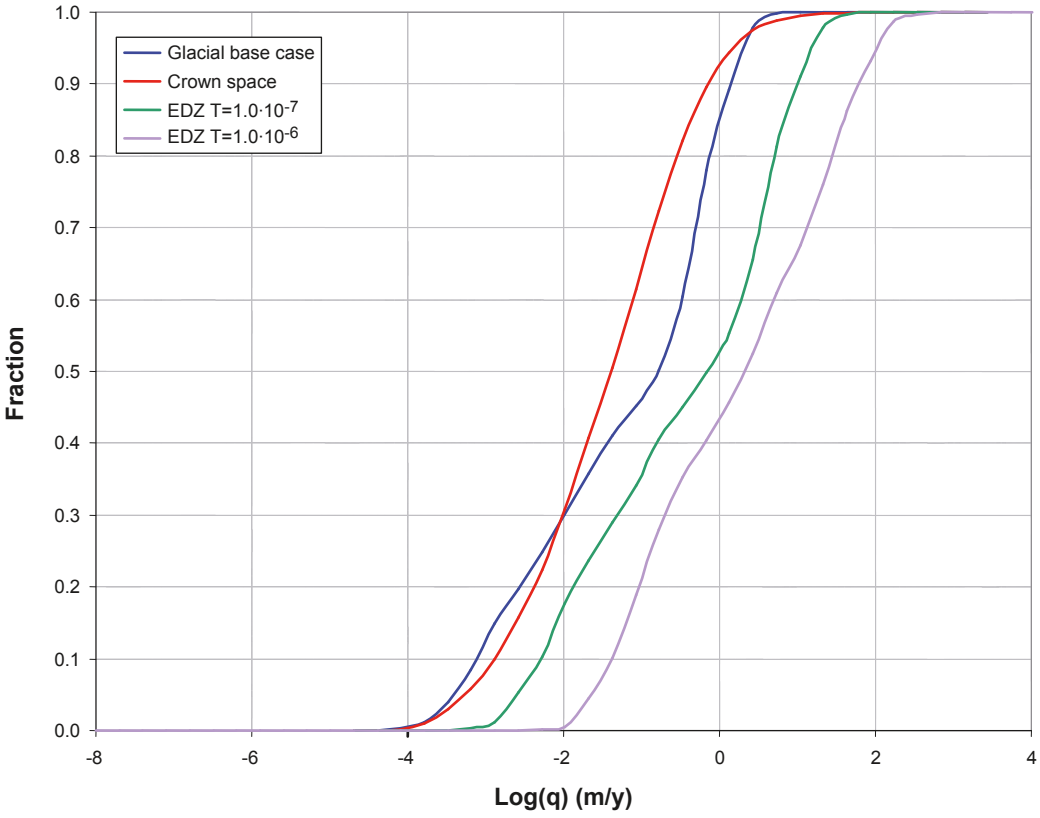

Figure 10-141. *Cumulative distribution function plots of Darcy flux (q) at glacial ice front location II for release path Q2 for the hydrogeological base case model (Glacial base case), the crown space model (Crown space), the EDZ T = 1·10^{-7} m^2/s model, and the EDZ T = 1·10^{-6} m^2/s model for the deposition hole locations with particles successfully reaching the model top boundary. (Modified after Figure E-56 in /Joyce et al. 2010/.)*

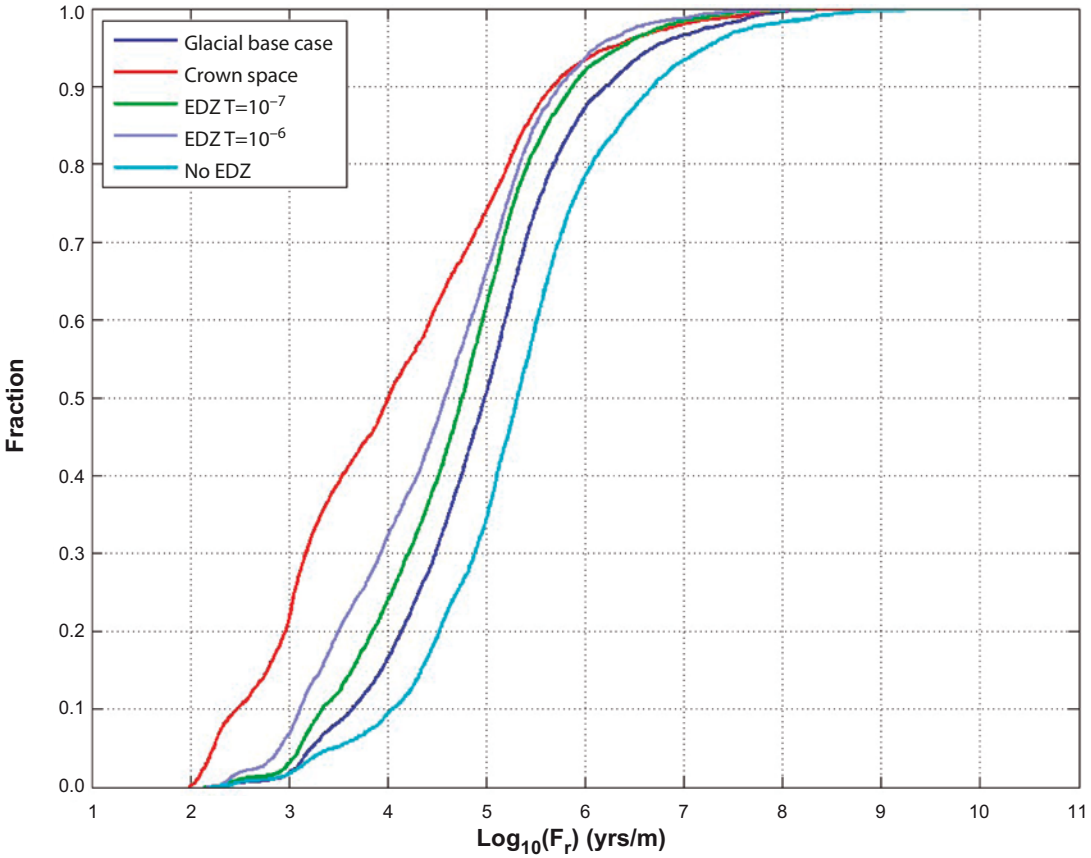

Figure 10-142. *Cumulative distribution function plots of flow-related transport resistance (F) at the glacial ice front location II for release path Q3 for the hydrogeological base case model (Glacial base case), the crown space model (Crown space), the EDZ T = 1·10^{-7} m^2/s model, the EDZ T = 1·10^{-6} m^2/s model. and the No EDZ model for the deposition hole locations with particles successfully reaching the model top boundary.*

THM properties

Isostasy is not accounted for in the study by /Vidstrand et al. 2010/ but the potential impact on groundwater flow of an uneven surface loading at the ice sheet terminus (the forebulge phenomenon) is addressed by incorporating a change in fracture transmissivity data as a sensitivity test. It is noted that the change in transmissivity applied by /Vidstrand et al. 2010/ exceeds the change suggested in the THM modelling within the SR-Site project /Hökmark et al. 2010, Lönnqvist and Hökmark 2010/, see Section 10.4.4. However, the simulation results reported by /Vidstrand et al. 2010/ suggest insignificant differences in the peak values of the Darcy flux also for these exaggerated values. As an example, Figure 10-144 displays the Darcy fluxes at measurement localities 1 to 5. Evidently, the peak values of the undistorted and the distorted simulations are alike.

Glacial case with permafrost

Permafrost is a key process to consider as it reduces the permeability of subsurface materials to water flux. Permafrost does not develop instantaneously. Its development is a transient process. /Vidstrand et al. 2010/ use a freezing algorithm to modify reported Holocene hydraulic conductivity values in a transient fashion. The input to the permafrost model was obtained from the ground surface temperature time series described in the **Climate report**, Appendix 1.

A discontinuous permafrost layer is considered. This implies that the permafrost layer may contain more or less unfrozen sections depending on the local boundary conditions and material properties. Probable locations for taliks can be estimated from the forecasted landscape development, carried out in the SR-Site project, following the shoreline displacement at Forsmark.

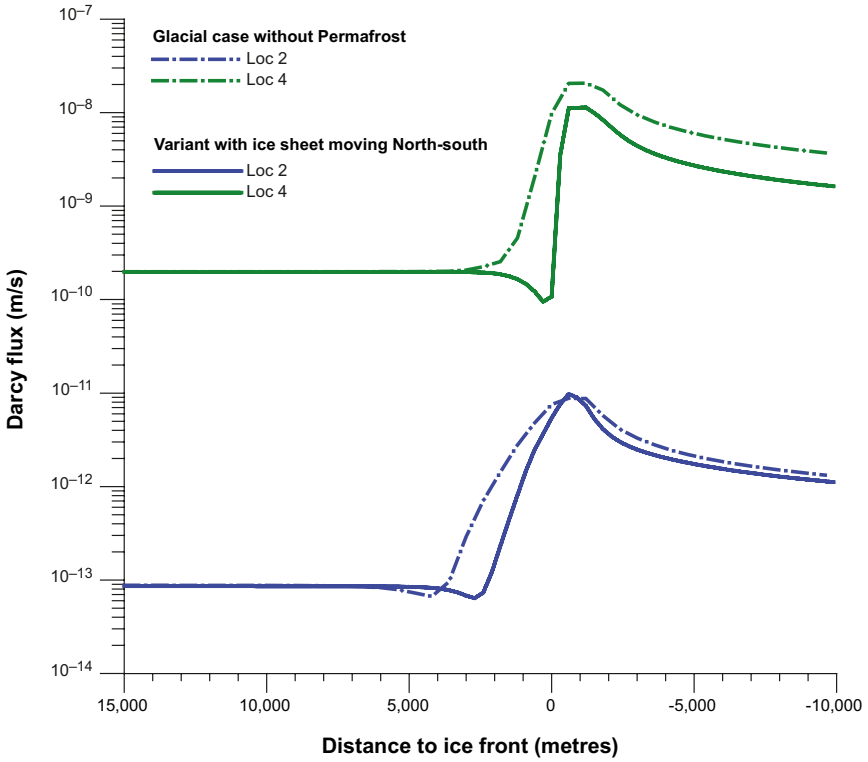

Figure 10-143. *Darcy flux at measurement localities 2 and 4 (ML 2 and ML 4) during the advance of the ice sheet margin considered in the NW-SE case (dashed lines) and the N-S case (solid lines). Positive values of "Distance to ice front" mean that the ice sheet margin has not yet arrived to the measurement locality.*

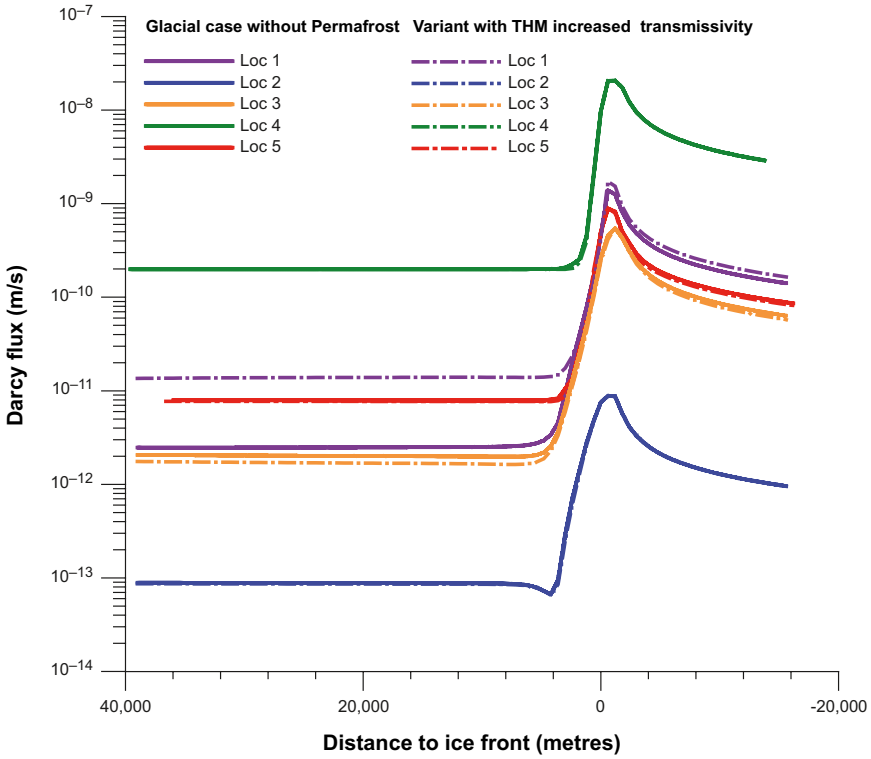

Figure 10-144. *Darcy flux at measurement localities 1–5 (ML 1–5) during the advance of the ice sheet margin considered in the undistorted case (solid lines) and the distorted case (dashed lines). Positive values of "Distance to ice front" mean that the ice sheet margin has not yet arrived at the measurement locality.*

Further, in the model the speed of the advancing ice sheet was set to 50 m/y. The ice sheet acts as a blanket that isolates the frozen ground from further influence of low surface temperatures. The speed of the advancing ice sheet is imagined to be greater than the rate of thawing of the permafrost layer, thus implying a tip (tongue) close to the ice sheet margin with trapped permafrost and cold ice base conditions. However, as a variant and sensitivity case, no permafrost under the tip close to the ice sheet margin is studied. Figure 10-145 suggests insignificant differences in Darcy flux between the two cases of permafrost conditions at the ice sheet margin. It is noted that the oscillations near the peak reflect transient effects at the top boundary due to the transient hydraulic properties of the permafrost.

Comparison of the Darcy flux at different time slots during glaciation and deglaciation

In Section 10.4.1, the expected hydrogeological evolution during a glacial cycle is described based on present day understanding of relevant processes. In the model studies described in that section, various simplifications are made that do not conform fully to the expected reference evolution. Here, an outline is provided on how the modelling results may be used for subsequent assessment calculations.

Figure 10-146 shows the minimum, median and maximum values of the Darcy flux at all deposition hole positions during the main "climate events" during the simulated period (IFL 0 → IFL V → IFL 0) of periglacial and glacial climate conditions. The main "climate events" are:

- Temperate (used to produce scaled (normalised) quantities for SR-Site).
- Glacial without permafrost.
- Glacial maximum.
- Submerged.
- Permafrost.
- Glacial with permafrost and a 2 km long tongue.
- Glacial with permafrost but no tongue.

The climate condition Glacial without permafrost provides the highest maximum as well as highest median value of all simulated climate events. Relative to the median temperate period value, the median Glacial without permafrost value is almost two orders of magnitude higher. The maximum Glacial without permafrost value is also almost two orders of magnitude higher than the maximum Temperate period value. Conditions when only permafrost prevails or when the domain is submerged provide the smallest Darcy fluxes of all climate situations. The values for these two cases are below the temperate period value.

The results presented by /Vidstrand et al. 2010/ and /Joyce et al. 2010/ are utilised in different ways in the radionuclide transport calculations presented in Chapter 13. One approach is to take the flow paths and performance measures obtained from the combined repository-scale and site-scale models, and scale the measures by factors that are obtained by scaling all different periods in Figure 10-146 with the corresponding temperate period values. A second approach is to directly use the performance measures calculated in the combined repository-scale and site-scale models utilising glacial boundary conditions from the super-regional model. However, this approach only provides results for the glacial case without permafrost for the ice front position IFL II. Thus, the second approach is used to assess the effects of glacial conditions on performance measures when different assumptions on repository properties (EDZ crown space) are made, whereas the first approach is utilized when transport calculations incorporating flow changes implied by a glacial cycle are performed.

A similar approach is used for calculations of buffer erosion and canister corrosion over a glacial cycle. Figure 10-147 shows normalised average values of the three powers of the Darcy flux that are of interest, (q, $q^{0.41}$, $q^{0.5}$), see Sections 10.4.8 and 10.4.9 for details. The desired values are obtained by averaging the values of "Glacial without permafrost" over a full glacial cycle (120,000 years) and then normalising against the corresponding temperate value, see /Selroos and Follin 2010/ for details. It is observed that for measurement location ML 2, which is inside the repository footprint, the normalised average value is about 0.8; i.e. the Darcy flux averaged over the 120,000 year glacial cycle is below the corresponding value for the temperate period.

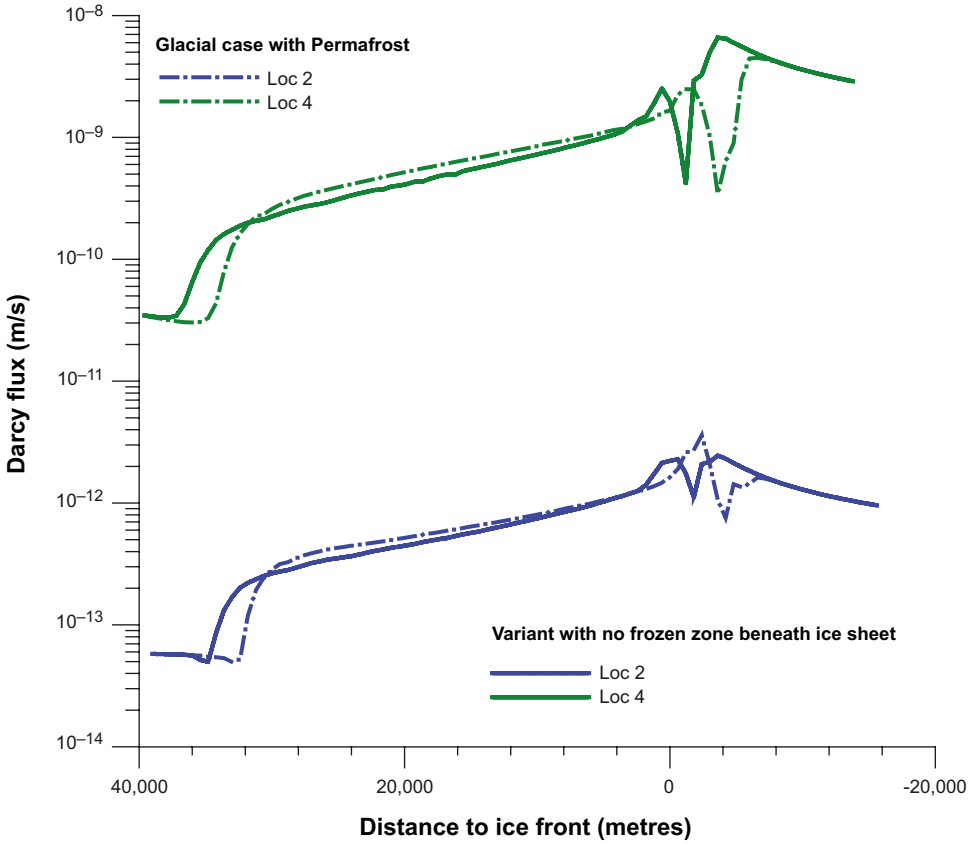

Figure 10-145. *Darcy flux at measurement localities 2 and 4 (ML 2 and ML 4) during the advance of the ice sheet margin considered in the two cases with permafrost, i.e. permafrost in front of the ice sheet margin only (dashed lines), and permafrost in front of the ice sheet margin as well as under the tip (tongue) of the ice sheet margin (solid lines). Positive values of "Distance to ice front" mean that the ice sheet margin has not yet arrived to the measurement locality.*

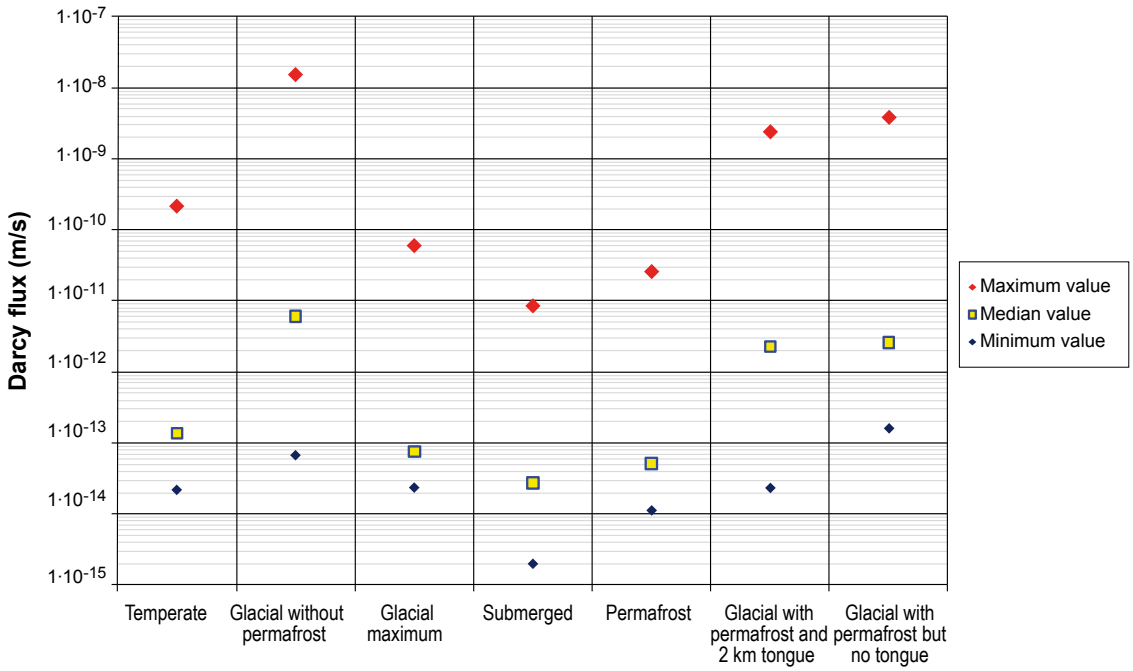

Figure 10-146. *Estimated Darcy fluxes for the main climate situations considered during the simulated period (IFL 0 → IFL V → IFL 0) of periglacial and glacial climate conditions.*

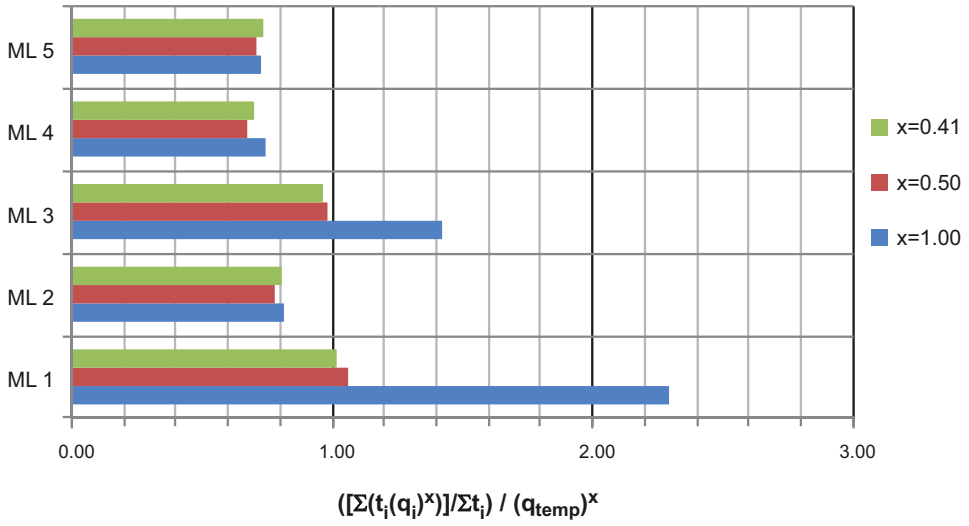

Figure 10-147. *Plot of Darcy flux to three different powers (q, $q^{0.41}$, $q^{0.5}$) averaged over a full glacial cycle and normalised against the corresponding temperate value (q, $q^{0.41}$, $q^{0.5}$)$_{temp}$. These averages are used in buffer erosion and canister corrosion calculations, see Sections 10.4.8 and 10.4.9 for details. ML = measurement locality. The glacial period within the glacial cycle is based on the glacial case without permafrost.*

Identified uncertainties and their handling in SR-Site

A general uncertainty in all models dealing with groundwater flow during periglacial and glacial conditions is the boundary condition on the top surface. /Vidstrand et al. 2010/ assume a specified head under the ice sheet, which is a common assumption in this field of science. Nonetheless, it is not clear that the water pressure at the ice-subsurface interface should be related to the ice sheet thickness under all circumstances as it implies an infinite source of water. This implies a general uncertainty of the models utilised. Another general uncertainty is in the particle tracking, which is performed for a steady state flow condition although the boundary conditions are constantly and rapidly changing in comparison to the advective travel times.

- **Hydrogeological evolution.** The importance of taking different events during a glacial cycle into account in a groundwater flow model intended for predicting the hydrochemistry in the vicinity of a repository is recognised in /NEA 1993, Bath and Lalieux 1999/. An example of an important event at Forsmark during Holocene time that is considered in SDM-Site is the Littorina Sea stage, which began at about 6500 BC and prevailed for several thousands of years. During the Littorina Sea stage, the Forsmark site was submerged by seawater that had a maximum salinity of about 1.2–1.5% by weight (approximately 12–15 g/L of TDS). According to the chemical analyses, the origin of the salt seen in the fracture water samples acquired today could be remnants from the Littorina Sea stage /Laaksoharju et al. 2008/. In comparison, little or no remnants of Littorina Sea water have been observed in the samples that represent matrix porewater from the target volume at repository depth. Furthermore, the less saline matrix porewater is not glacial meltwater but of a pre-Weichselian origin as the low contents of TDS is accompanied by high values of oxygen-18, approximately –5 to –4‰ of δ^{18}O SMOW. (Glacial meltwater is considered to be much more depleted of oxygen-18, approximately –20 to –16‰ of δ^{18}O SMOW /Laaksoharju et al. 2008/).

  In conclusion, the groundwater flow modelling considered in SDM-Site suggests that it is transients in advective flow rather than matrix diffusion that govern the fracture water salinity. This observation is supported by the modelling conducted by /Vidstrand et al. 2010/. However, as the scheme of ice sheet movement considered by /Vidstrand et al. 2010/ does not represent a full glacial cycle, the groundwater salinity after the passage of the retreating ice sheet margin cannot be expected to be equal to the groundwater salinity prior to the passage of the advancing ice sheet margin. Furthermore, water-rock interactions possibly affecting groundwater salinity are neglected, which also implies that the salinity field will not be restored in the model.

- **Recharge and discharge locations in the biosphere.** Regardless of the case studied, an ice sheet without permafrost or an ice sheet with permafrost, a number of particles recharge at the upstream boundary of the model domain, which suggests that the model domain is too short to give a fully undisturbed view of all recharge locations. Nevertheless, it may be concluded that the present-day topographic water divides, which play an important role for the recharge and discharge during temperate conditions, are significantly diminished in significance during glacial conditions. In contrast, the discharge locations are predominantly found well within the physical boundaries of the model domain and often very close to the margin of the ice sheet. The differences seen in the discharge pattern between the two glacial cases are largely caused by the alternative hydraulic properties and boundary conditions. The uncertainty in the occurrence of taliks, which may act as major discharge areas in the case of permafrost in the periglacial area in front of the ice sheet margin, is discussed in the **Climate report**.
- **Performance measures.** The same uncertainties as in the temperate simulations in Section 10.3.6 apply to the simulations based on the combined repository-scale and site-scale models used here. In addition, the transfer of boundary conditions from the super-regional model to these smaller scale models implemented in a different numerical flow code implies uncertainties.
- **Penetration of glacial melt water**. The assessment of penetration of dilute water should be considered an approximate quantification. The same uncertainties as listed for the corresponding analyses performed for temperate conditions in Section 10.3.6 apply here. Specifically, steady-state flow fields are used, and no mixing or water-rock interactions are considered. The results of the analysis of penetration of glacial melt water are propagated for further assessment.
- **EDZ and crown space.** The same uncertainties as listed above for Performance measures apply here. The results of this analysis are propagated for further assessment.
- **Site related variants.** None of the studied site related variants provide significantly different results to those of the base case, i.e. the case with a steep ice sheet profile without permafrost moving from NW to SE. It is noted that the use of the theoretical maximum ice sheet profile during the post-LGM stage is probably a considerable exaggeration compared to the reference evolution ice sheet. Furthermore, it is noted that the applied change in transmissivity in the hydro-mechanical variant case exceeds the change suggested in the THM modelling within the SR-Site project.
- **Glacial case with permafrost.** An advancing ice sheet with permafrost ahead is considered a more realistic case than an ice sheet without permafrost. However, neither of the two permafrost cases studied (cf. Table 10-25) give significantly different results from the base case, i.e. an advancing ice sheet without permafrost. It is noted that the simulations with ice sheet and permafrost combined are stopped at ice front location IV (IFL IV) to avoid numerical instabilities. These arise when the ice sheet margin gets close to the downstream boundary and the discharge at ground surface in the periglacial area is prevented due to the permafrost growth.
- **Comparison of the Darcy flux at different times during glaciation and deglaciation.** The results presented under this heading are merely a different way of illustrating the results. Thus, no additional uncertainties per se are introduced. However, the outlined methodology of using scaling factors for the performance measures representing the different climate regimes clearly is a simplification of the development depicted in the **Climate report**, and hence implies an additional uncertainty. For the subsequent assessment, an ice sheet with permafrost in front of the ice sheet margin is used for the pre-LGM stage, and a retreating ice sheet with submerged ground conditions in front of the ice sheet margin is used for the post-LGM stage. As indicated above, the climate stages of permafrost alone and submerged conditions alone also need to be included in the quantitative assessment.

10.4.7 Geochemical evolution

The successions of temperate, permafrost and glacial climate domains will affect the flow and composition of the groundwaters around the repository. The evolution between climate domains will be gradual, without a clear boundary between them. For example, during a temperate domain, temperatures may slowly decrease such that permafrost regions slowly develop within parts of the repository region.
In SR-Site the evaluation of geochemical effects is restricted to using separate specifications for the

different climatic domains. It is expected that different groundwater compositions will prevail around the repository as a result of the different types of climate domains and their corresponding hydraulic conditions. This section discusses the groundwater chemistry for periods in which the repository is *below permafrost during periglacial climatic conditions* or *under an ice sheet during glacial conditions*, whereas the conditions expected under a *temperate domain* are discussed in Section 10.3.7. In addition, this section discusses groundwater chemistry for periods in which the repository area is *submerged* either under a glacial meltwater lake, or under more or less saline seawater, such as the Littorina sea water periods in the past.

The following issues, and safety functions according to Figure 10-2, are treated for all the expected conditions during the reference glacial cycle:

- Evolution of salinity and of other relevant natural groundwater components (safety functions R1b and R1c).
- Evolution of redox conditions (safety function R1a).
- Effects of grouting, shotcreting and concrete on pH (safety function R1e).

Modelling

The modelling for the remaining part of the reference glacial cycle is similar to that performed for the initial temperate period described in Section 10.3.7. Groundwater compositions are modelled through advection, mixing and chemical reactions with fracture-filling minerals. The different components of the modelling are not fully coupled: the results of regional-scale groundwater flow modelling are used as input to a geochemical mixing and reaction model. The aim has been to obtain equivalent groundwater models for hydrology and geochemistry.

The groundwater flow modelling of the periglacial and glacial conditions is described in the previous Section 10.4.6. One of the processes modelled is the transport of salts. Contrary to the modelling of the initial temperate period, the models for the periglacial and glacial periods have not included the fractions of selected reference waters. In the geochemical models, either for the glacial scenario without permafrost or in the glacial scenario with permafrost, the rock volume initially contains a mixture of two end-member waters: a deep saline groundwater and a water of meteoric origin. The proportion of these two end-members can be obtained from the salinity at any point. With the advance and retreat of the glacier the proportion of a third mixing end-member, glacial melt-water, is calculated from the decrease in salinity at any point in space.

This strategy is used as well to describe the site submerged by a glacial melt-water lake. For periods when the candidate site is submerged under seawater, however, the results obtained using ConnectFlow /Joyce et al. 2010/, see Section 10.3.6, are used. In this case the same model is used as for the initial temperate period, and therefore the hydrogeological results include the mixing proportions of end-member waters.

A process that must be evaluated is the out-freezing of dissolved salts when ice builds up underground during periglacial periods. The groundwater flow modelling described in Section 10.4.6 considers density-driven groundwater flow and transport of salts, but the out-freezing of salts is not included. The process has instead been evaluated using a two-dimensional model set-up /Hartikainen et al. 2010/. Examples of temperature contours obtained using this model are shown in Figure 10-103 in Section 10.4.1.

Evolution during periglacial conditions

The periglacial conditions are characterised by perennial freezing of groundwaters, i.e. permafrost, and the frozen areas may be continuous or discontinuous. In any case the permafrost areas will include taliks where sufficiently large lakes are encountered. There is very little information concerning the chemical characteristics of groundwaters under permafrost. This is due to practical difficulties when drilling and sampling at ambient temperatures where freezing of drilling fluids and groundwater samples occurs.

Many geochemical characteristics or groundwaters are expected to be almost unaffected by the permafrost. The studies at the High Lake and at the Lupin Mine in N. Canada /Frape et al. 2004, Ruskeeniemi et al. 2004, Stotler et al. 2009a, b, Holden et al. 2009/ may be used to illustrate this. Geologically, the

bedrock at Lupin consists of an ancient metamorphosed sedimentary rock sequence dominated by quartz feldspar gneiss/phyllite; these were formed some 2.5 Ga, somewhat older than 1.89–1.85 Ga which was the peak of metamorphism at the Forsmark site, characterised by different types of granitoids with subordinate felsic to intermediate volcanic rocks, diorite or gabbro, pegmatite and amphibolite. Whilst the rock types are certainly not identical, they share enough properties to compare qualitatively the general hydrochemical properties at each site. The pH values for sampled groundwaters at Lupin vary between 6 and 9 and bicarbonate concentrations are found to be below $5 \cdot 10^{-3}$ mol/L. For potassium, the concentrations are higher than for the groundwaters sampled at Forsmark or Laxemar: sub-permafrost groundwaters at Lupin have $< 2.6 \cdot 10^{-3}$ mol/L. For iron, most of the groundwaters sampled at Lupin had $< 5.4 \cdot 10^{-5}$ mol/L. Thus, the concentrations and pH values found are not far from those for groundwaters sampled elsewhere, for example at Forsmark, see /Laaksoharju et al. 2008/.

Evolution of salinity and relevant natural groundwater components

It is estimated that at Forsmark the ground will be frozen to a depth of 50 m or more for around 30 percent of the time in the glacial cycle of the reference evolution, see Figure 10-106. According to these results, the permafrost will not occur over a continuous period of time, but rather thawing will occur between more or less short periods of permafrost, see also the discussion in Section 10.4.1. Some of these permafrost periods will furthermore coincide with the time when the site is covered by an ice sheet.

When water freezes slowly, the solutes present in the water will not be incorporated in the crystal lattice of the ice. During this process, salts that have been present in the surface waters and groundwaters will tend to accumulate at the propagating freeze-out front. This front is, however, not necessarily sharp, because e.g. freezing will take place over a range of temperatures, depending on the salinity, etc. The freezing process can give rise to an accumulation of saline water at the depth to which the perennially frozen front has reached. The saline waters formed in this manner within fractures and fracture zones will sink rapidly due to density gradients.

The calculations made using a two-dimensional model set-up /Hartikainen et al. 2010/ show that when the freezing is extensive (down to several hundred metres depth) a salt front is developed in the calculations. The model also shows that pockets of unfrozen groundwater with high salinity may develop in the perennially frozen rock when the freezing front advances faster than the transport of salt. These results agree qualitatively with the previous generic calculations reported in /Vidstrand et al. 2006/. It should be noted that the model used in /Hartikainen et al. 2010/ does not account for matrix diffusion, and the amounts of salts frozen out in the mobile groundwater are only a fraction of the salt contents in whole rock volume.

The concentration of the frozen out salt has been estimated in these calculations assuming that before the onset of the permafrost the salinity distribution is that found at present in Forsmark. Judging from the results in Figure 10-39, Section 10.3.7, it may be that these initial salinities are overestimated, as the groundwaters will become gradually more dilute before the start of the permafrost.

Nevertheless the results of the 2D modelling /Hartikainen et al. 2010/ indicate only a very moderate increase in salinities around the repository volume, not exceeding 1%, for the most extreme permafrost simulation, that is, for the dry variant of the repetition of the last glacial cycle with an air temperature decreased by 8 degrees. That is, even for the most extreme permafrost extent simulated, the calculated groundwater salinities in the repository volume do not exceed those found at present.

The possibility of upconing of deep saline groundwater to repository depths during permafrost conditions was addressed in /King-Clayton et al. 1997/. This may possibly occur in the vicinity of permanent discharge features such as some taliks. Such discharge features mainly occur along more extensive conductive deformation zones. In Forsmark, where the topography is quite flat, the probable location of taliks is at some distance from the candidate repository area, as estimated from the landscape development following the reference evolution shore-level displacement at Forsmark, see the **Climate report**, Section 4.5.2.

When the permafrost melts and decays there will be a release of dilute melt water from the upper highly permeable network of fractures. At this stage the low permeability matrix which has preserved (or accumulated) its salinity, especially at greater depths, will probably be more saline than

the surrounding groundwaters. The resulting chemical gradient will then cause a gradual transfer of salinity to the more permeable rock mass. In all probability this will be a relatively slow process and dilution by mixing will occur also within the more permeable rock mass. The more dilute waters will tend to stay in the top layers of the rock mass due to their lower density.

The hydrogeological calculation results obtained in /Vidstrand et al. 2010/ and described in Section 10.4.6 have produced salinity distributions for the Forsmark area under permafrost simulated by having a constant air temperature of −4.5°C. These salinities were used to calculate mixing proportions of a deep saline end-member and a meteoric water component, and these mixing proportions were then used as input to the Phreeqc code which imposed equilibrium with calcite, quartz, hydroxyapatite and either Fe(II) oxyhydroxide or amorphous iron sulphide, FeS. As a result, the detailed distribution of compositions was obtained. A full description of the procedure and the results obtained may be found in /Salas et al. 2010/.

These model results shown in Figure 10-148 indicate that during periglacial conditions, when the Forsmark site is subjected to permafrost, salinities will be limited, satisfying the safety function indicator R1b in Figure 10-2, the concentration of cations expressed as charge, $\sum q[M^{q+}]$, will be above 4 mM, satisfying the criterion R1c, the concentrations of chloride, potassium, iron and sulphide will be limited and the pH will be above 4 and below 11, in agreement with the safety function indicators and criteria R1d, R1e and R1f. In addition, colloid concentration levels are expected to remain low because sufficiently high ionic strengths are expected under these conditions.

As for the temperate period discussed in Section 10.3.7, two geochemical assumptions, namely equilibrium with respect to FeS(am) or Fe(III)-oxyhydroxide, have been simulated in order to estimate the evolution of the redox potential within the repository domain. The results shown in Figure 10-148 indicate that the redox potentials during a permafrost period should not differ substantially from those during a temperate period, shown in Figure 10-47.

Sulphide, H_2, CH_4 and dissolved organic carbon

The rate of production of sulphide due to microbially mediated SO_4^{2-} reduction could possibly decrease due to the lower temperatures. Due to freeze-out of salts, sulphate concentrations might increase as compared with those at the end of a preceding temperate period, when diluted groundwaters of meteoric origin predominate. Reducing agents are required for any sulphate reduction to take place, and under permafrost conditions the inflow of organic matter from the surface will probably decrease. However, SO_4^{2-} reduction could also be sustained by the gaseous groundwater components methane and hydrogen,

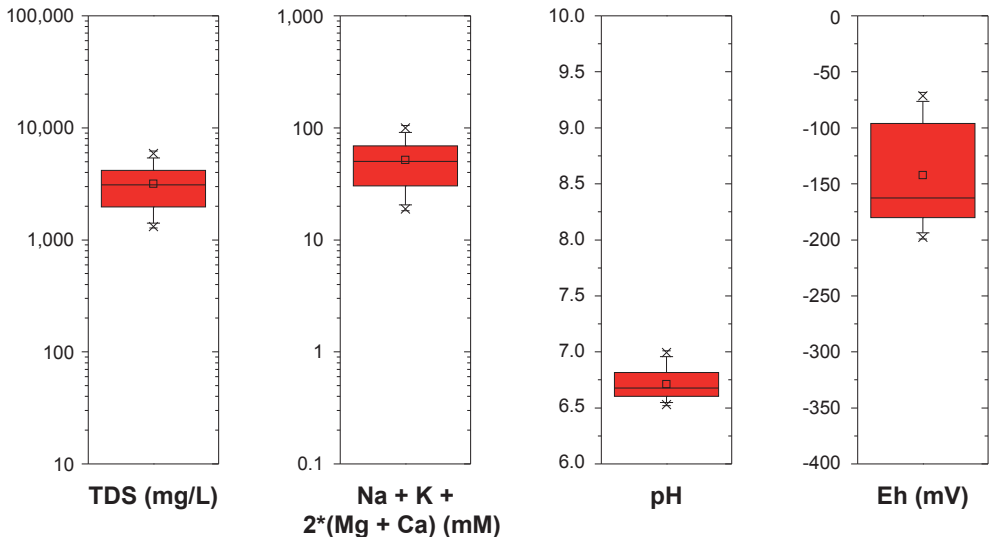

Figure 10-148. *Permafrost: Box-and-whisker plots showing the statistical distribution of the calculated TDS (total dissolved solids), $\sum q[M^{q+}]$, pH and Eh within the candidate repository volume at Forsmark. The statistical measures are the median, the 25th and 75th percentile (box), the mean (square), the 5th and 95th percentile ("whiskers"), the 1st and 99th percentile (crosses) and the maximum and the minimum values.*

see the discussion in Section 10.3.7. If microbial sulphide production occurs during this period, it will be limited by the availability of mainly CH_4 and dissolved organic carbon, as discussed in /Tullborg et al. 2010/. Fluxes and maximum production of methane and hydrogen have been estimated based on the groundwater gas content for three Fennoscandian sites: Forsmark, Laxemar and Olkiluoto /Delos et al. 2010/. There is a large uncertainty in estimating the flow of gases in Forsmark because the data are very scarce, but the estimated fluxes are $< 3 \cdot 10^{-10}$ mol/(m^2 yr) for CH_4 and H_2. The conclusion is that there is only a minor contribution from the flow of these gases to sustaining microbial sulphide production.

Although sulphide concentrations are obtained as a result of the Phreeqc modelling described in subsection "Model results" above, for the reasons outlined in Section 10.3.7, it is believed that the equilibrium solubility constraints applied cannot reflect the variability of sulphide concentrations that can be expected during periglacial conditions. Because of this the sulphide concentrations for periglacial conditions are assumed to be the same as the observed distribution of sulphide in groundwaters during the present temperate conditions, which is after a recent period of intrusion of marine sulphate-rich waters and described in Section 10.3.7. This distribution of sulphide concentrations is used to estimate canister corrosion rates during the periglacial periods. This is a cautious approach: sulphate concentrations in the groundwaters may have been reduced during a preceding long temperate period when the site is subject to the infiltration of meteoric waters, and this would reduce rates of microbial sulphide production. Although freeze-out of salts from ponds and lakes affected by sulphate-rich sea spray might induce locally an accumulation of sulphate, this should not occur at Forsmark because the Baltic Sea will be at some distance to the site during the periglacial periods. Furthermore the input of dissolved organic matter from the surface could be decreased because of the frozen ground layer, and upwards diffusion of methane or hydrogen in Forsmark is too slow. These arguments suggest that sulphide concentrations during periglacial conditions could be generally lower than those observed during the site investigations, which are used in the analysis of canister corrosion.

Given the low estimated flows of methane mentioned above in this subsection, the potential for formation of substantial amounts of methane ice can be discounted in Forsmark /Tohidi et al. 2010/.

In conclusion, although groundwaters will become progressively diluted during the temperate period following the closure of the repository, permafrost can move salts to repository depth from the upper parts of the rock. All arguments indicate that groundwaters below permafrost will not become more dilute than under temperate conditions. Rather, saline waters may move downwards within conductive fracture zones. Thus the charge concentration of cations is expected to increase during permafrost periods and satisfy the criterion concerning the safety function indicator R1c in Figure 10-2, $\sum q[M^{q+}] > 0.004$ mol/L. Regarding safety function indicator R1b, the concentration of salt at repository level due to freezing out will not become so high as to lower the swelling pressure of the buffer and the backfill, among other reasons because of the downward gravity-driven flow of saline waters. This situation will not be changed during permafrost decay as a transition to a temperate period occurs.

For major groundwater components, such as Cl, Na, Ca and other cations and sulphate the conclusion is that they will follow the trends of salinity discussed above. Other components, such as bicarbonate, potassium, iron sulphide, etc. as well as pH that are controlled by relatively fast chemical reactions are expected to remain mostly unaffected by permafrost. Therefore, the criteria concerning the safety function indicators R1d and R1e in Figure 10-2 are expected to be fulfilled, in that pH will remain < 11 and the concentrations of K and Fe will remain limited. Sulphide concentrations are generally expected to be lower than or at similar levels to those found during the temperate period preceding the periglacial conditions.

Redox conditions

The perennial freezing of rock volumes will effectively shut down the hydraulic circulation in the bedrock, at least locally. In this way, microbial populations within the rock could be isolated from the surface. Some reactive gases such as methane could be trapped as clathrates, especially in soil layers. Microbes present in the upper bedrock and soils will survive in the permafrost and will become active during the subsequent melting. No changes in redox conditions are, therefore, to be expected unless the nutrient sources become exhausted. Because of abundant biological activity in the active layer /Hallbeck 2009/ the presence of organic matter at the surface will be maintained at levels similar to those encountered during temperate conditions. All indications are that prior

to, during and following permafrost decay, groundwaters will be reducing due to a combination of microbial and geochemical reactions and processes. The results of the modelling presented in previous sections support these statements.

In conclusion, it is not expected that redox conditions will change at repository depth during the formation or decay of permafrost, remaining reducing as demanded by the safety function indicator R1a in Figure 10-2.

Effects of grouting, shotcreting and concrete on pH

The processes described in Section 10.3.7 for the temperate domain following repository closure will continue during permafrost periods. Given enough time all grout will be converted first into calcium silicate hydrates with low calcium to silica ratios, and finally into calcite and silica /Luna et al. 2006, Galíndez and Molinero 2009/. The duration of this process will depend on the velocity of the groundwaters flowing around the grouted volumes, but times of the order of 10^4 years are expected.

The conclusion reached in Section 10.3.7 is therefore still valid: the effect of grout in fractures will be to increase the pH in deformation zones to values ≈ 9 for relatively long periods of time. These values are, however, within the criteria for the safety function indicator R1e in Figure 10-2.

Glaciation

There is almost no information concerning the chemical characteristics of groundwaters in fractured rock under an ice sheet or even close to the margin of an ice sheet. This is partly due to practical difficulties when drilling and sampling at ambient temperatures where freezing of drilling fluids and groundwater samples occurs.

The composition of glacier melt waters was reviewed in /Brown 2002/. Although as expected some of these waters are extremely dilute (1 mg/L), others have gained solutes from mineral weathering reactions, reaching salinities up to 0.2 g/L. Other examples of dilute granitic waters are those sampled in Gideå (0.33 g/L) and Grimsel (0.08 g/L). Although dilute, both these waters are close to saturation with calcite. The relatively high pH values, ≈ 9, originate from the weathering of bedrock minerals.

SKB, together with NWMO (Canada) and Posiva (Finland) have started a joint project that will attempt to drill boreholes and sample groundwaters in an area close to Kangerlussuaq in Greenland. At present the evaluation of geochemical characteristics of groundwaters during a glacial period must rely almost exclusively on modelled results and, most important, chemical reasoning.

Evolution of salinity and of other relevant natural groundwater components

During the glacial cycle of the reference evolution (about 120,000 years) the Forsmark site is covered by an ice sheet during a few periods with a total duration of about 30 thousand years, see Section 10.4.1. Groundwater flow during the glacial domain has been estimated at the large regional scale including the Forsmark area /Vidstrand et al. 2010/. A full description of these calculations is given in Section 10.4.6 and in the original report. The results of that model include evaluations of the salinity distribution beneath an ice sheet, and the modelling included situations where the ice sheet advanced either over an unfrozen terrain or over an area subjected to permafrost.

For the case of advance over an unfrozen ground, a glacial period of 18,850 years has been simulated in 10 time steps, reproducing the advance and the retreat of the ice front. Three hydrological scenarios have been considered: i) when the ice front is advancing to the repository area (2,900 years, approximately), ii) when the repository is entirely covered by a warm-based ice sheet i.e. an ice sheet with basal melting (15,000 years) and, finally, iii) when the ice sheet is retreating (1,200 years) and the area is covered by a 100 m deep melt water lake.

Dilute waters of glacial origin are expected under a warm-based ice sheet. Significant changes in groundwater composition are expected as soon as the ice front advances over the repository area. The calculated results shown in Figure 10-149 indicate that salinities in the upper part of the modelled domain would usually be lower than 2 g/L. The model results also illustrate the upconing of deep saline waters under an advancing and a retreating warm-based ice sheet. The calculated salinities can

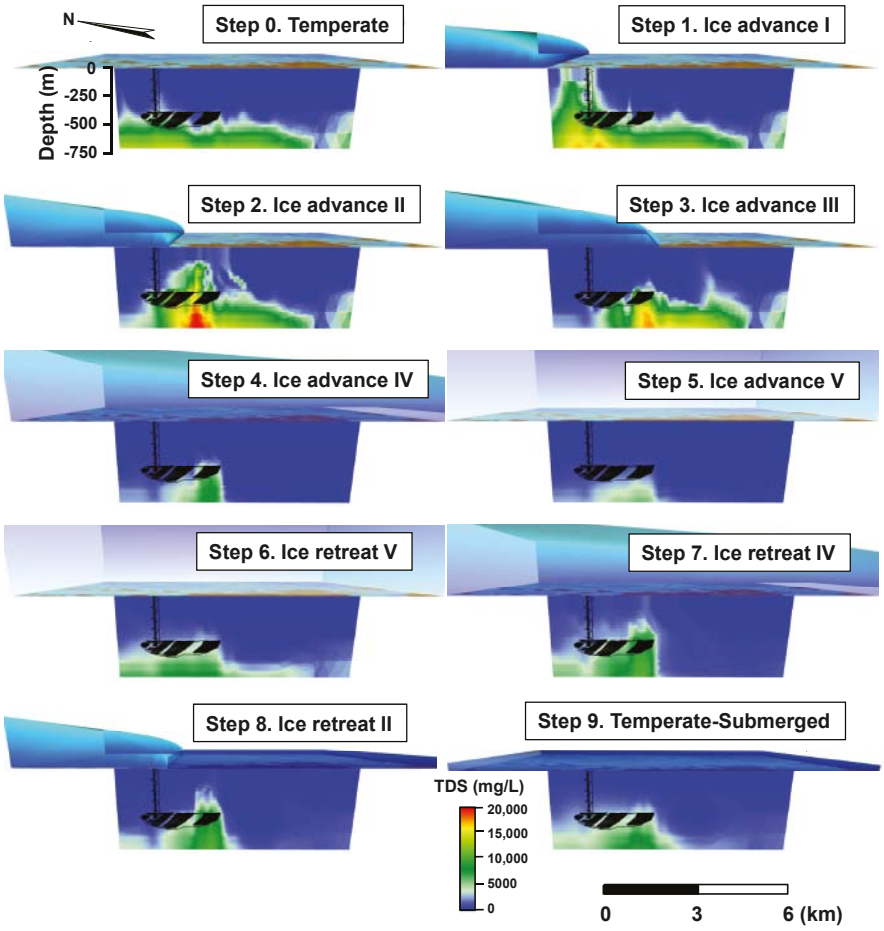

Figure 10-149. *Ice sheet advancing and retreating over unfrozen ground: Changes in the distribution of TDS (total dissolved solids, mg/L) shown in vertical slices when an ice sheet advances and retreats over the unfrozen Forsmark area. The figure shows results during the glacial sheet advance (1 to 6) and the glacial retreat (7 to 10) calculated using the model described in Section 10.4.6 /Vidstrand et al. 2010/. When the ice sheet retreats the area is covered by a 100 m deep glacial melt water lake.*

reach values up to 20 g/L in locations affected by upconing. Because the advance of the ice sheet is a relatively fast process and the retreat even more so, the high salinity conditions are predicted to last only a few centuries at most. The groundwater data sampled at Forsmark during the site investigations indicate a glacial meltwater component at repository depth /Laaksoharju et al. 2008/ qualitatively supporting the results shown in the figure.

Figure 10-150 presents the calculated changes with time of the distribution of salinities (total dissolved solids) when an ice sheet advances over unfrozen ground and retreats behind a glacial meltwater lake. The figure shows the results within the candidate repository volume at Forsmark (due to the hydrogeological grid, depths between 432 and 528 m have been included). The computed salinity is not homogeneously distributed; the calculations show groundwaters having salinities between about 0.03 g/L (during and soon after the glacial advance over the repository) and 20 g/L as a consequence of the upconing of deep saline waters when the ice front margin is located on top or the repository.

The hydrogeological calculation results obtained in /Vidstrand et al. 2010/ and described in Section 10.4.6 have produced salinity distributions for the Forsmark area during an ice sheet advance and retreat. Both an ice sheet advancing over unfrozen and permafrost ground have been modelled. The procedure used to obtain mixing proportions of end-member waters is described in the subsection “Modelling”. These mixing proportions were then used as input to the Phreeqc code which imposed equilibrium with calcite, quartz, hydroxiapatite and Fe(II) oxyhydroxide. As a result, the detailed distribution of compositions was obtained. A full description of the results may be found in /Salas et al. 2010/.

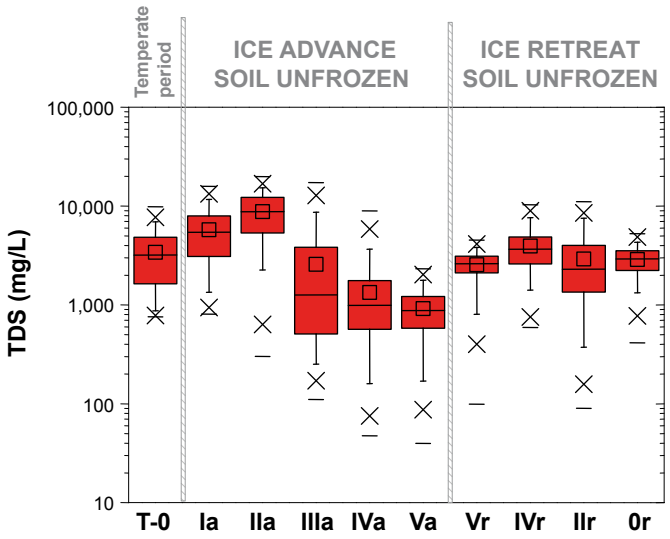

Figure 10-150. *Ice sheet advancing and retreating over unfrozen ground: Box-and-whisker plots showing the statistical distribution of the calculated TDS (total dissolved solids) within the candidate repository volume at Forsmark. The figure illustrates the steady-state temperate model (left) and the TDS distribution at different stages of the ice sheet advance over unfrozen ground (ice front locations Ia to Va) and ice sheet retreat (ice front locations Vr to 0r). The statistical measures are the median, the 25th and 75th percentile (box), the mean (square), the 5th and 95th percentile ("whiskers"), the 1st and 99th percentile (crosses) and the maximum and the minimum values.*

Only the results from one of the modelled cases in /Vidstrand et al. 2010/ of an ice sheet advancing over a permafrost area have been used for the geochemical modelling described here, namely the model in which there is a permafrost zone remaining below the ice sheet, as it advances. This zone stretches 2 km from the ice margin under the ice. Figure 10-152 shows a comparison between some of the calculation results for the ice sheet advancing over unfrozen ground and results for the advance over permafrost. Full details of the calculation results are provided in /Salas et al. 2010/. It should be noted that because there are almost no field data on the groundwater chemistry in granitic rocks under or close to an ice sheet, the model results are associated with a large degree of uncertainty.

Chemical components not participating extensively in chemical reactions, such as Cl, Na, sulphate, and possibly to some extent Ca, follow the salinity patterns under the ice sheet described above. The calculated $\sum q[M^{q+}]$ displayed in Figures 10-151 and 10-152, as well as the results shown in Figures 10-139 and 10-140, indicate that dilute melt waters, with $\sum q[M^{q+}] < 4$ mM, may occur within the candidate repository volume for some period of time during the advance and retreat of an ice sheet, violating the criterion for the safety function indicator R1c. For the glacial period, slightly less than 2% of deposition hole locations (see Figures 10-139 and 10-140) experience dilute conditions during an advancing ice front whereas only slightly more than one percent of the deposition holes experience dilute conditions during an assumed period of 100,000 years corresponding to glacial maximum conditions. The proportion of dilute conditions is somewhat larger in Figures 10-151 and 10-152 because they show all groundwaters in the rock volume close to the repository, that is, in the hydrogeological grid at depths between 432 and 528 m. Also, as seen in Figure 10-32, it would take up to 60,000 years of temperate conditions to reach dilute conditions in 1 percent of the deposition hole locations. For permafrost conditions, all arguments indicate that groundwaters below permafrost will not become more diluted than under temperate conditions. The hydrogeological model results described in Section 10.4.6, indicate that after the complete retreat of the ice sheet the salinities, shown in Figure 10-150, and the concentrations of cations, shown in Figure 10-151, are back, approximately, to the levels estimated before the onset of the glacial period, and these results are not in contradiction with the salinities observed now in Forsmark. The overall conclusion is that less than 2 percent of the deposition hole positions may be assumed to experience dilute conditions during a glacial cycle, and they will only have these conditions for a fraction of the time.

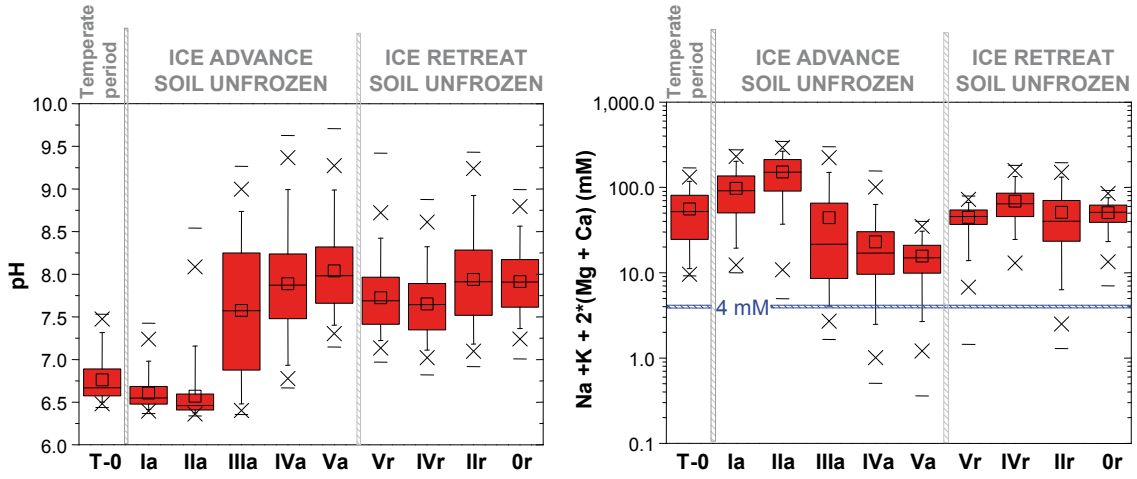

Figure 10-151. *Ice sheet advancing and retreating over unfrozen ground: Box-and-whisker plots showing the statistical distribution of calculated pH values (left) and the safety function indicator $\sum q[M^{q+}]$ (right) for the positions located within the candidate repository volume at Forsmark. The figure illustrates the steady-state temperate model (T-0 at left) and the distribution of pH or cation concentrations at different stages of the ice sheet advance over unfrozen ground (ice front locations Ia to Va) and ice sheet retreat (ice front locations Vr to 0r). The statistical measures are the median, the 25th and 75th percentile (box), the mean (square), the 5th and 95th percentile ("whiskers"), the 1st and 99th percentile (crosses) and the maximum and the minimum values.*

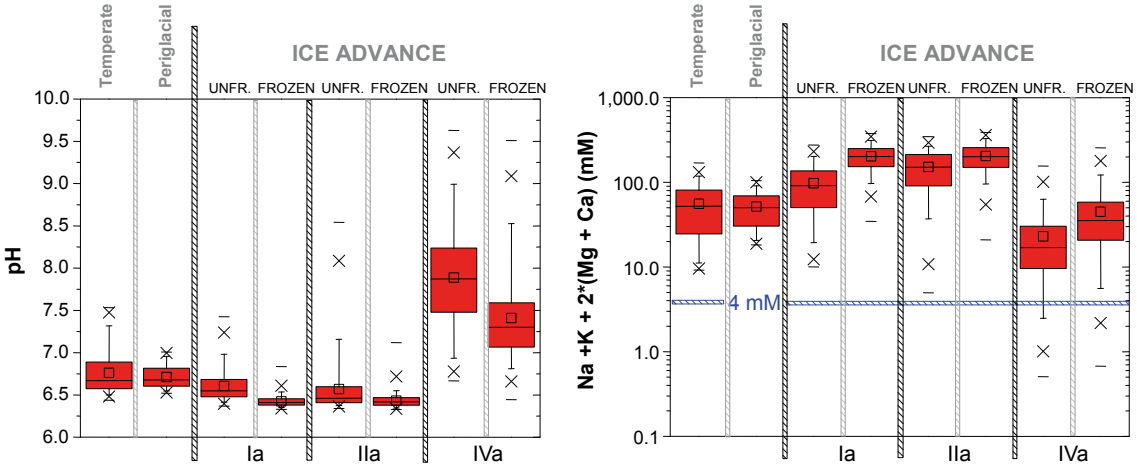

Figure 10-152. *Comparison between the advance of an ice sheet over unfrozen terrain with the advance over a permafrost area for different ice front locations: Box-and-whisker plots showing the statistical distribution of pH and the safety function indicator $\sum q[M^{q+}]$ for the positions located within the candidate repository volume at Forsmark. The figure illustrates the steady-state permafrost model (left, ice front location "0") and the pH and cation concentrations at different stages of the ice sheet advance over permafrost ground (ice front locations I to IV). The statistical measures are the median, the 25th and 75th percentile (box), the mean (square), the 5th and 95th percentile ("whiskers"), the 1st and 99th percentile (crosses) and the maximum and the minimum values.*

Other components, such as bicarbonate, iron, sulphide and pH that are controlled by relatively fast chemical reactions and reactions with minerals can also be affected by the glacial conditions to a lesser extent. The calculated pH values results shown in Figure 10-151 (and in Figure 10-152 for the advance of an ice sheet over permafrost) indicate that glacial conditions may result in a general increase of pH values, an effect which is observed for example in the Grimsel groundwaters, see for example /Degueldre et al. 1989/. The safety function criteria R1d and R1e in Figure 10-2 will be fulfilled in that pH will remain < 11 and the concentrations of K and Fe will remain limited as shown in the figures in /Salas et al. 2010/, whereas the groundwater concentrations of sulphide are discussed below.

Figure 10-152 and other results in /Salas et al. 2010/ indicate that although the calculated chemical characteristics of the groundwaters in general show a narrower range of values in the case of the ice sheet advancing over permafrost as compared with the ice sheet advancing over an unfrozen area, for a few of the modelled grid points extreme values may occur, for example there is a possibility of having lower cation concentrations in the case of the ice sheet advancing over permafrost.

As for temperate and periglacial conditions, two geochemical assumptions, namely equilibrium with respect to FeS(am) or Fe(III)-oxyhydroxide, have been simulated in order to estimate the evolution of the values of Eh (the redox potential) within the repository domain. Because the model is based on chemical equilibrium, it assumes that oxygenated waters are not present. Under equilibrium conditions any infiltrating oxygen with the glacial melt waters would react with the Fe(II) minerals included in the model.

The calculated Eh values in the case where an ice sheet advances and retreats over unfrozen ground are shown in Figure 10-153. Due to the imposed mineral equilibrium, the general variations in the pH values, shown in Figure 10-151, are reflected in corresponding variations in the calculated Eh, as these two variables are inversely related through the reaction $Fe(OH)_3(s) + 3H^+ + e^- \rightleftharpoons Fe^{2+} + 3H_2O$. Similar values of Eh are obtained from the modelling of the advancement of an ice sheet over permafrost /Salas et al. 2010/.

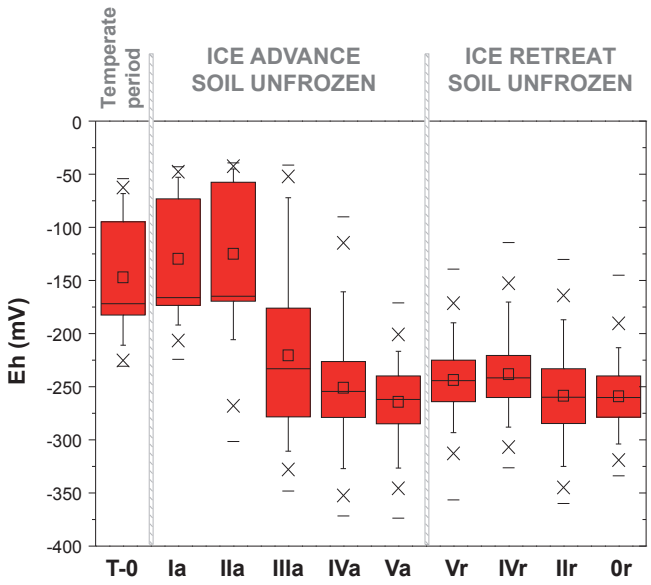

Figure 10-153. *Ice sheet advancing and retreating over unfrozen ground: Box-and-whisker plots showing the statistical distribution of calculated Eh (redox potential) for the positions located within the candidate repository volume at Forsmark. The figure illustrates the steady-state temperate model (left) and the calculated Eh values at different stages of the ice sheet advance over unfrozen ground (ice front locations Ia to Va) and ice sheet retreat (ice front locations Vr to 0r). The statistical measures are the median, the 25th and 75th percentile (box), the mean (square), the 5th and 95th percentile ("whiskers"), the 1st and 99th percentile (crosses) and the maximum and the minimum values.*

As discussed in Section 10.4.1, immediately after the retreat of an ice sheet, isostatic depression will set the ground surface at the repository site below the Baltic Sea surface level for a period of time, see Section 10.4.1. In the reference evolution, which is a repetition of the last glacial cycle, the Weichselian, the Forsmark site is expected to be below glacial melt water lakes, and sea or brackish waters during a period of time of between a few thousand years up to maybe ten thousand years.

Both the site descriptive modelling of the Forsmark site since the retreat of the last ice sheet to the present day /Laaksoharju et al. 2008/ and the SR-Site hydrogeological modelling /Joyce et al. 2010/ show a relatively fast turnover of groundwaters, in which glacial melt water is replaced by a succession of waters penetrating from the surface: the Littorina sea gradually evolving into the present day Baltic sea, and finally modern meteoric waters.

The model results presented above indicate that concerning salinity and the concentration of cations, the conditions when the site is submerged under a glacial melt water lake are similar to those found before the onset of the glaciation, see the starting steady state temperate result "T-0" and the ice front locations "0r" in Figures 10-150 and 10-151. Other more reactive groundwater components such as Eh or pH may remain affected, see Figures 10-151 and 10-153, but all groundwater characteristics are expected to satisfy the safety function indicators and criteria R1a to R1f in Figure 10-2.

The possible infiltration for relatively short periods of time of waters of marine origin after a glaciation has been modelled within SR-Site /Joyce et al. 2010, Salas et al. 2010/. Within such a period, equivalent to the Littorina sea episode that had its maximum salinity at 4000 BC, the salinity of groundwaters at repository depth could increase due to density driven groundwater flow. The detailed results of the modelled groundwater chemical characteristics are presented in /Salas et al. 2010/. The results modelled for 3000 BC show that the effects of the marine water intrusion at repository depth are delayed in time and that the proportion of Littorina waters in the repository volume is larger at present than it was then. The calculated groundwater compositions for 3000 BC show that the charge concentration of cations around the repository is well above 0.004 mol/L, corresponding to compliance with the safety function indicator R1c in Figure 10-2. As the salinities are not expected to increase above those of sea water during any period of time, the swelling capacity of the backfill will not be affected, see safety function indicator R1b.

As in the case of permafrost, the intensity of microbially mediated SO_4^{2-} reduction to produce sulphide will probably decrease under an ice sheet due to the lower temperatures. Compared with a preceding permafrost period, sulphate concentrations might increase during the short periods of upconing waters and they will decrease substantially during the longer periods of intrusion of glacial melt waters, although in Forsmark where deep saline waters have low sulphate contents, the upconing process should not increase sulphate concentrations noticeably. In any case, reducing agents are required for any sulphate reduction to take place, and under glacial conditions the inflow of organic matter from the surface will be lower. SO_4^{2-} reduction could still be sustained by the gaseous groundwater components methane and hydrogen, see the discussion in Section 10.3.7. There is a large uncertainty in estimating the flow of CH_4 and H_2 in Forsmark because the data are very scarce, but the estimated fluxes for these gaseous species are $< 3 \cdot 10^{-10}$ mol/(m^2 yr) /Delos et al. 2010/. The conclusion is that there is only a minor contribution from the flow of these gases to sustaining microbial sulphide production. Most indications suggest therefore lower sulphide concentrations during a glacial period, see also the discussion in /Tullborg et al. 2010/.

Although sulphide concentrations may be obtained by considering equilibrium with either FeS(am) of Fe(III)-oxyhydroxides, for the reasons outlined in Section 10.3.7, it is believed that the equilibrium solubility constraints applied cannot reflect the variability of sulphide concentrations that can be expected during glacial and submerged conditions. Because of this the sulphide concentrations for the glacial and submerged conditions are assumed to be the same as the observed distribution of sulphide in groundwaters during the present temperate conditions, which is after a recent period of possible intrusion of marine sulphate-rich waters and described in Section 10.3.7. This distribution of sulphide concentrations is used to estimate canister corrosion rates during the glacial and submerged periods. However, it is to be expected that glacial meltwaters will have low concentrations both of sulphate and of reductants such as DOC, methane and hydrogen, and therefore, microbial sulphate reduction during a glacial period should be more restricted than during other climatic conditions. Therefore, the use of the sulphide distribution observed during the site investigations in the analysis of canister corrosion during glacial conditions is pessimistic.

Based on the assessment presented in this subsection the following may be concluded regarding the evolution of salinity and of other relevant natural groundwater components during glacial conditions.

- Dilute melt waters, with $\sum q[M^{q+}] < 4$ mM, may occur within the repository volume for some period of time during the advance and retreat of an ice sheet, violating the criterion for the safety function indicator R1c. Upconing of deep seated saline groundwaters during the glacial period is not expected to affect the swelling capacity of the backfill, corresponding to the safety function indicator R1b.
- Major groundwater components, such as Cl, Na, sulphate, and possibly Ca, will follow the salinity trends. Other components, such as bicarbonate, potassium, iron, sulphide and pH that are controlled by relatively fast chemical reactions and mineral dissolution/precipitation are likely to be less affected by the glacial conditions. However, all the evidence points towards dilute waters with relatively high pH. The criteria concerning the safety function indicators R1d and R1e in Figure 10-2 will be fulfilled in that the pH will remain < 11 and the concentrations of K, HS^- and Fe will remain limited. Sulphide concentrations are expected to be lower than for temperate conditions.
- As indicated previously, salinity levels are expected in general to decrease during glacial periods. Colloids are known to be strongly destabilised at high ionic strengths, and at high concentrations of divalent cations (Ca^{2+}) in particular. Therefore, during periods of glaciation, with predominantly dilute groundwaters, it cannot be excluded that colloids may be generated and transported by groundwater. However, a high potential stability of colloids does not necessarily implicate a high colloid concentration. It has, for example, been shown that the granitic groundwaters at Grimsel, which are quite dilute and where colloids, if formed, are quite stable, have low concentrations of colloids (≤ 0.1 mg/L). The reason for this is not clear: there might be some unknown mechanism that removes colloids at that site, or there could be no significant generation of colloids at Grimsel. The conclusion is, therefore, that there is a potential for higher colloid concentrations in groundwaters during a glacial period, especially during the advance and retreat of an ice sheet when groundwater velocities are highest. An upper limit would be the highest colloid concentrations reported in /Birgersson et al. 2009/, about 40 g/L.

Redox conditions

As discussed in the previous section, temporal changes in groundwater conditions are expected during a glaciation cycle. Short periods of upconing of deep reducing groundwaters will be followed by longer periods with glacial melt water intruding into the rock. After some time the situation may look as in Figure 10-149, i.e. with groundwaters that originate mainly from ice melt water in large volumes of rock. Arguments have been put forward that if glacial melt waters were rich in dissolved atmospheric gases, reducing conditions might no longer prevail at repository depth, infringing the safety function indicator criterion R1a, see e.g. /Puigdomenech et al. 2001/.

Large changes in hydrogeological conditions are expected when the ice front margin passes over the repository volume as discussed in Section 10.4.6. During these periods, which will be relatively limited in time, large quantities of glacial melt water may intrude into the rock, owing to the drastic change in hydraulic head gradients. In the remainder of a glaciation cycle, the magnitude of the hydraulic head gradient over the repository volume will be much lower, with groundwater flow rates not considerably different from temperate conditions, and probably lower.

The compaction of snow into glacier ice involves the incorporation of substantial amounts of air /Martinerie et al. 1992/. Thus, recharging glacial melt water under the ice may contain dissolved carbon dioxide and oxygen at above the concentrations expected for aerated water. The oxygen concentration in pure water in equilibrium with air is temperature dependent, and approximately 0.25 mM at 20°C. For glacial melt waters, based on theoretical constraints, the maximum oxygen concentration has been estimated to be 1.4 mM /Ahonen and Vieno 1994/. However, it has been noted that much lower values are normally measured in sampled glacial melt waters in the field, in the range 0–0.16 mM /Gascoyne 1999/. It may be argued that degassing could have contributed to the observed low oxygen levels of these field samples. Also, photosynthetic and heterotrophic microbial activity on the surface of glaciers may partly be responsible for the low oxygen content /Hallbeck 2009/. Furthermore, glacial melt water reacts rapidly with sub-glacial rock minerals and debris /Wadham et al. 2010/. The amounts of sulphate found in glacial melt waters /Brown 2002, Cooper et al. 2002/

supposedly from pyrite oxidation ($4\ FeS_2 + 14\ H_2O + 15\ O_2 \rightarrow 16\ H^+ + 8\ SO_4^{2-} + 4\ Fe(OH)_3$) are sufficient to explain the low oxygen concentrations found. It may be safely concluded that a cautious oxygen concentration for infiltrating glacial meltwaters is 0.3 mM /Sidborn et al. 2010/.

During temperate conditions the top soil and the uppermost part of the rock contains relatively large amounts of organic material. Mediated by microbes the degradation of the organic substances explains the lack of oxygen below a few metres in the rock at Forsmark. During a period of glaciation, the amount of degradable organic substances is uncertain, although microbial activity is observed at the surface of most glaciers, and in glacial melt water /Hallbeck 2009/. The main reducing capacity in the absence of organic material is comprised in ferrous minerals in the rock. Biotite inside the bulk of the rock matrix and chlorite adjacent to fractures has been shown to dominate the reducing capacity in the absence of organic substances. The ferrous iron content in the bulk rock is approximately one percent by weight in the dominant rock types in Forsmark, accessible through diffusion in the pores of the matrix. Fracture minerals directly accessible in flowing fractures have even larger ferrous iron content.

The penetration of oxygen-rich glacial melt waters in fractures in granitic rocks under a warm-based ice sheet has been the subject of several modelling efforts, with an early study by /Neretnieks 1986/. /Guimerà et al. 1999/ showed that a change in the redox potential is to be expected at repository depth under certain circumstances. /Sidborn and Neretnieks 2003, 2004/ considered the possible influence of microorganisms in fractures but concluded that diffusion resistance in pores of the rock matrix eventually controls the consumption rate of oxygen.

The results from these studies along with more recent modelling efforts /Sidborn and Neretnieks 2008, Spiessl et al. 2010, Sidborn et al. 2010/ confirm that the flow-wetted surface to flow rate ratio, commonly referred to as the flow-related transport resistance (or *F*-factor) is a key parameter when studying the interaction between dissolved oxygen in the flowing water and minerals in the rock.

For relatively short times when reducing minerals are exposed to the flowing water in the fracture, a pseudo-steady state oxygen concentration profile develops to a certain distance downstream. It may also be shown /Auqué et al. 2006, Sidborn and Neretnieks 2008/ that in this case the inflow of oxygen is exactly balanced by the dissolution of reducing minerals at that distance along the flow path. Given the reducing capacity of the bedrock in Forsmark, this pseudo-steady state situation would prevail for more than 1000 years. When eventually the reducing capacity directly exposed to the flowing water along the flow path is substantially decreased, the effect of diffusion resistance in pores of the rock matrix becomes more and more prominent, limiting the rate of oxidation. When diffusion limits the oxidation reaction, the time required for oxygen to reach a certain distance along the flow path is proportional to the square of the corresponding *F*-factor /Sidborn and Neretnieks 2008/. The oxygen concentration profile for the pseudo-steady state situation with oxidation rate limited by abiotic chemical kinetics is illustrated by the blue curves in Figure 10-154 for the conditions at Forsmark /Sidborn et al. 2010/. These curves are calculated using pessimistic parameters and assumptions, as explained later in Section 12.6.2 and in /Sidborn et al. 2010/. A cautious oxygen concentration for glacial melt waters is 0.3 mM, and the corresponding pseudo steady state oxygen profile along a recharge path, using a set of other pessimistic assumptions, is shown as the blue curve in Figure 10-154-b. According to this figure, glacial melt water with a remaining oxygen concentration of 0.1µM may reach a distance along the flow-path corresponding to an *F*-factor of about 5,000 yr/m. These generic results for the pseudo-steady state oxygen concentration profiles are coupled with *F*-factors obtained from site-specific hydrogeological modelling presented in Section 10.4.6. Particle back-tracking results for various glaciation scenarios are reported in /Joyce et al. 2010/ for complete flow paths from the ground surface to each canister position. The *F*-factors are calculated using the extended heterogeneity model, see Section 12.6.2 subsection "*F*-factors". Cumulative *F*-factors for the most pessimistic glacial situation, when the ice front margin is right above the repository volume (ice front location III) are illustrated by the red curve in Figure 10-154. Only 1,184 out of 6,916 flow paths are included in the cumulative distribution in the figure. The remaining particles either did not reach the surface for the simulated time or have inflow outside the modelled domain or the deposition positions are excluded based on the FPC and EFPC criteria.

As can be seen in Figure 10-154 there is a small overlap between the oxygen concentration profile and the *F*-factors when pessimistic assumptions are made to calculate the oxygen penetration depth, indicating that a few deposition locations may be reached by oxygen at concentrations exceeding 0.1 µM under these conditions.

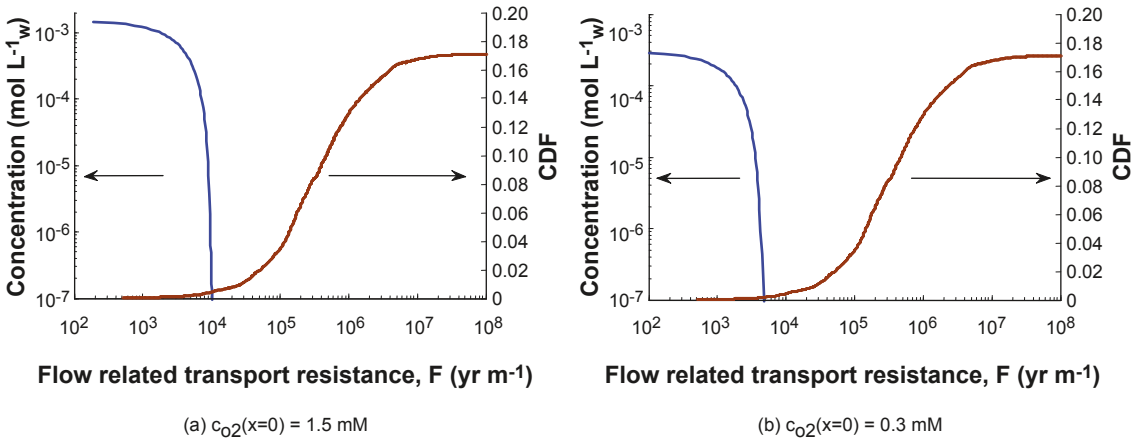

Figure 10-154. *Plots of generic pseudo-steady state oxygen concentration profiles (blue curves) and the cumulative distribution function (CDF) of the flow-related transport resistance (or F-factor) for the most pessimistic glacial situation (ice front location III). The recharge oxygen concentration in the melt water (at F = 0) is (a) 1.5 mM and (b) 0.3 mM. From /Sidborn et al. 2010/.*

It is important to note that the cumulative result (red curve in Figure 10-154) is obtained for a "snap-shot" of the most pessimistic ice front margin location. During the ice sheet advance or retreat, with a normal rate between 50 and 300 m/yr, the front margin passes over the candidate repository footprint (a few km) in less than 100 years. With such a rate for the ice front movement the hydraulic conditions change considerably according to the hydrogeological model results. The flow pattern evolves so that recharge flow paths for a given ice front location may become discharge flow paths in another, and flow rates and hydraulic gradients change in a manner such that *F*-factors for recharge flow paths reaching the repository may become orders of magnitude smaller or larger.

In a situation where the ice sheet advances over a periglacial (frozen) area, a comparison of the results obtained by the modelling described in Section 10.4.6 and in /Vidstrand et al. 2010/ shows that recharge paths in most cases have larger flow-related transport resistances (*F*-factors). The lowest *F*-values are increased at least by a factor of 3.6, depending on the ice front location considered.

If microbial activity and reducing fracture coatings are considered (in addition to an intact rock matrix and abiotic reaction rates), a lower *F*-value will yield the same oxygen consumption along the flow path. In a flow path region where the reducing minerals in the fracture walls are not yet completely oxidised, the Fe(II)-minerals are exposed to the flowing water in the fracture. In such an environment it is likely that microbe populations thrive and mediate the oxidation reaction. It is not possible however to quantify to what extent the reaction rate would increase.

The conclusion is therefore that for situations where the ice sheet advances or retreats at a continuous rate, then oxygen penetration can be discarded, because the calculated blue curve in Figure 10-154b will be shifted to the left if for example fracture filling materials and microbial processes are considered, and the *F*-values would move to the right in the situation of an ice sheet advancing when the site is affected by permafrost.

Oxygen reduction potential (ORP) measurements in soil pipes have shown that most of the oxygen under present day conditions is depleted within the first few metres at the site /Sidborn et al. 2010/ and references therein. Although no general depth trend of oxygen intrusion can be found at depths greater than a few metres, this does not exclude the possibility of greater intrusion depths in transmissive domains such as deformation zones, where only scattered samples have been taken. After the retreat of an ice sheet, during temperate conditions, the reducing conditions of the rock directly exposed to flowing groundwater are restored /Banwart 1999/, and therefore a lack of evidence of past intrusions of oxygen-rich glacial meltwaters may be expected. In addition to the investigations made at the Forsmark site, redox transition zones have been investigated in many locations in Scandinavia as well as in various sites throughout the world. Although the historical hydraulic properties at many of the investigated sites are difficult to evaluate, it is relevant to note that traces of oxygen intrusion are seldom found below 200 metres.

In conclusion, based on observations and results from pessimistic modelling, oxygen intrusion to repository depth in highly transmissive deformation zones cannot be discarded. However, the model results for a recharge oxygen concentration of 0.3 mM indicate that more than one thousand years of the worst glacial situation would be needed for oxygen at non-negligible concentrations to reach the canisters in the repository. Since such circumstances do not occur in the reference evolution, it is concluded that reducing conditions will prevail in the repository, satisfying the safety function indicator criterion R1a.

Alternative evolutions, aimed at capturing more pessimistic situations as regards oxygen penetration to repository depth are considered in the corrosion scenario, Section 12.6.2. For example if the ice front advance were to cease for a period of up to about one thousand years, then the penetration of oxygen can be discarded if the ground is frozen or if it is submerged under a melt-water lake. But if the ice sheet is stationary over the repository on unfrozen ground and if the repository area is not submerged, then calculations /Sidborn et al. 2010/ indicate that if a pessimistic value for the oxygen content in the glacial melt water is used (1.5 mM) and if several other pessimistic assumptions are made, for example microbial processes and reducing fracture infill are excluded, then oxygen could reach the deposition locations that have the smallest flow-related transport resistance (F-factor). As soon as the ice margin starts to move again, because of the shifting in the flow paths and the associated mixing, anoxic conditions are quickly reached. The consequences of an eventual oxygen intrusion for the corrosion scenario are analysed in Section 12.6.2.

Effects of grouting, shotcreting and concrete on pH

The processes described in Section 10.3.7 for the temperate domain following repository closure will continue during the glaciation periods of the first glacial cycle, although the effects will gradually decrease. Given enough time, all cement in grout will be converted first into calcium silicate hydrates with low calcium to silica ratios, and finally into calcite and silica /Luna et al. 2006, Galíndez and Molinero 2009/. The duration of this process will depend on the velocity of the groundwaters flowing around the grouted volumes, but times of the order of 10^4 years are expected.

Therefore, the conclusion reached in Section 10.3.7 is in part still valid here: the effect of grout in fractures will be to increase the pH in deformation zones for relatively long periods of time. It is expected that, with time, the pH that initially had risen to ≈ 9 will progressively homogenise with the values found in surrounding parts of the rock, and therefore remain within the criteria for the safety function indicator R1e.

Identified uncertainties and their handling in the subsequent analysis

The following uncertainties are identified when considering the different chemical aspects of the evolution of the repository during the period after the initial temperate period, that is, for the remaining part of the reference glacial cycle.

There is a large degree of uncertainty in the detailed salinity distribution around the repository. In addition, the salinities can become sufficiently low in some parts of the candidate repository volume as to affect the performance of the buffer during this period or when considering its future evolution. The calculated distributions of salinity, pH and other groundwater components obtained from the modelling are used in the analysis of bentonite evolution in Section 10.4.8 and for the selection of radionuclide transport related parameters in Chapter 13.

There is a large degree of uncertainty in the detailed distribution of dissolved sulphide in the groundwaters around the repository. Because no dependency has been found between sulphide and other groundwater geochemical or hydrogeological parameters, the observed distribution of concentrations in the Forsmark site at present is propagated to the analysis of canister corrosion in Section 10.4.9. However, it is to be expected that glacial melt waters will have low concentrations of sulphate and of reductants such as DOC, methane and hydrogen, and therefore, microbial sulphate reduction during a glacial period should be more restricted than during other climatic conditions. Therefore, the use of the sulphide distribution observed during the site investigations in the analysis of canister corrosion during glacial conditions is pessimistic.

Based on observations and results from pessimistic modelling, oxygen intrusion to repository depth in highly transmissive deformation zones during the advance or retreat of an ice sheet cannot be discarded. However, model results indicate that hundreds of years of the worst glacial situation, a situation which does not occur in the reference evolution, would be needed for oxygen to reach only a few of the canister positions in the repository. Therefore it is concluded that reducing conditions will prevail in the deposition holes of the repository, satisfying the safety function indicator criterion R1a in Figure 10-2.

10.4.8 Effects on buffer and backfill

Freezing

As concluded in Section 10.4.3, temperatures leading to buffer and backfill freezing do not occur in the reference evolution. Freezing of the upper parts of access tunnels or sealed boreholes could, however, not be excluded. Nevertheless, this section addresses the conditions when freezing may occur and how this affects the clay barriers. This information is then used in Section 12.3 when assessing consequences of more extreme future climates.

General

At temperatures below 0°C it can be anticipated that the water in the buffer and the backfill would turn into ice. This is not an issue for the materials themselves since the process is reversible and they will regain their properties after thawing /Birgersson et al. 2010/. However, the formation of ice could lead to

1. An increased pressure on the canister and rock.
2. Redistribution of material due to ice lens formation.

/Birgersson et al. 2010/ have investigated the behaviour of compacted bentonite below 0°C. It was investigated how swelling pressure (i.e. sealing properties) change with temperature and under what conditions bentonite freezes. The freezing point of a soil sample is defined as the temperature at which ice starts to form in the material. When ice formation occurs in confined bentonite a substantial pressure increase is expected due to volume expansion of water. Bentonite is a swelling material, which makes it rather unique as a soil in the sense that some of its properties are dependent on external conditions. The process of swelling, specifically, only occurs when bentonite is in contact with an external aqueous reservoir, and the concept of swelling pressure can consequently only be defined under such conditions. This means, in particular, that a bentonite component within the KBS-3 repository will be affected by freezing as soon as the groundwater in the surrounding rock freezes even though the component itself may remain unfrozen. The process of freezing bentonite in the following context therefore also includes the temperature range between the freezing point of the aqueous reservoir and the actual freezing point of the bentonite soil, in order to provide a full description of bentonite characteristics as the temperature is lowered.

There is a critical temperature below 0°C, here denoted T_c and measured in °C, at which swelling pressure is completely lost. T_c depends only on swelling pressure measured at 0°C, and not explicitly on clay specific quantities like montmorillonite content, montmorillonite layer charge or density.

/Birgersson et al. 2010/ have provided a theoretical description of the pressure response due to temperature in bentonite above T_c. From these results it can be concluded that any bentonite component of the KBS-3 repository – buffer, backfill or borehole seals – will strive to lower its pressure as the temperature drops below 0°C. The size of the equilibrium pressure drop depends, for all relevant bentonite densities, basically only on the difference in molar entropy between bulk water and ice, which at 0°C corresponds to 1.2 MPa/°C. Because the pressure drop is determined by properties not related to the clay, the same behaviour is expected independent of what specific bentonite is used. The dominating parameter that determines T_c is thus the equilibrium swelling pressure at 0°C (which of course in turn is determined by e.g. density, montmorillonite content, montmorillonite layer charge etc).

Figure 10-155 shows pressures evaluated for samples of the Ibeco RWC (Dep Can) bentonite for temperatures both below and above 0°C.

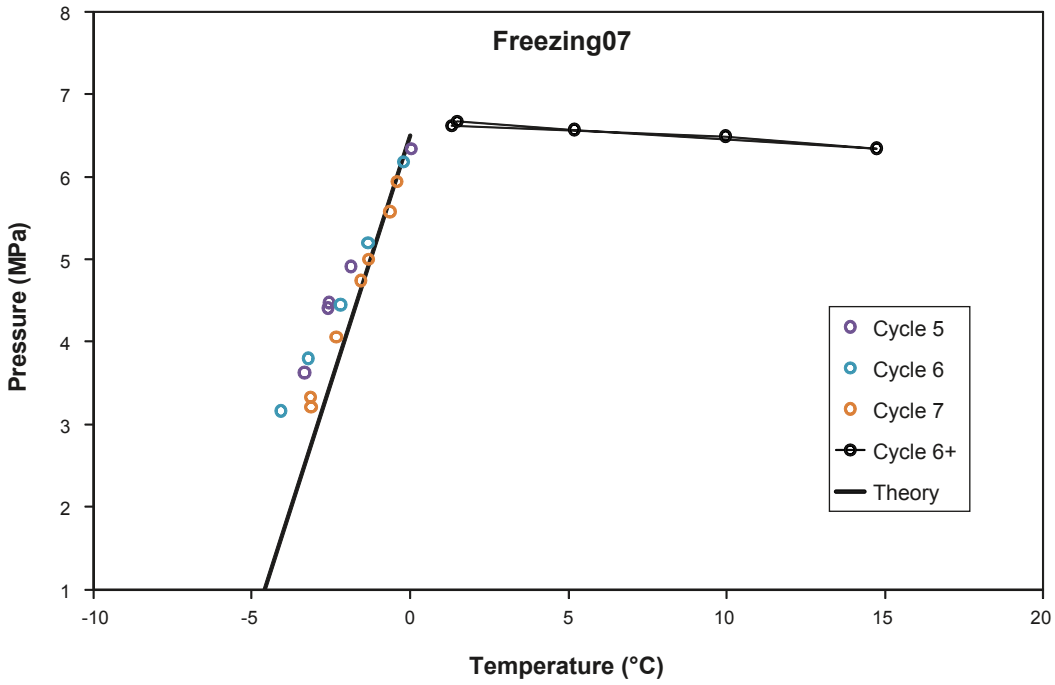

Figure 10-155. *Equilibrium pressure vs. temperature for Dep-Can (Ibeco RWC) bentonite at a swelling pressure above 0°C of ~7 MPa /Birgersson et al. 2010/. The freezing point (T_c) of the sample is below –8°C. The line labelled "Theory" shows the expected pressure response if the water saturated bentonite is treated thermodynamically equivalent to a salt solution. /Birgersson et al. 2010/.*

Confined bentonite in contact with saline ground water results in a lower swelling pressure above 0°C as compared to non-saline conditions. This effect, however, does not result in an increased freezing temperature as the freezing point of the external aqueous reservoir lowers. Actually, saline conditions lead to a lower freezing point of bentonite because salt enters the clay and contributes to lowering the chemical potential of the water. Therefore, only non-saline conditions need to be considered.

Buffer

The buffer materials in SR-Site are MX-80 and Ibeco RWC bentonites that have a mean bulk density of 2,000 kg/m^3, see Section 5.5. The corresponding swelling pressure of these materials under non-saline conditions is 7–8 MPa, which, in turn, corresponds to a T_c of approximately −6°C. Considering also the accepted density range of 1,950–2,050 kg/m^3, which gives a swelling pressure interval of 5–13 MPa /Karnland 2010/, the range for T_c is between −4°C and −11°C.

Backfill

The swelling pressure of the backfill can be significantly lower than that in the buffer. The swelling pressure of the "initial state" backfill defined in Chapter 5 is ~3 MPa, which would give a critical temperature of −2.5°C. However, this represents the average swelling pressure and as described in Section 10.3.9 there will be remaining density gradients within the backfill. The minimum density in the backfill will be 1,370 kg/m^3, which corresponds to a swelling pressure of ~1 MPa according to Figure 5-19. This would give a T_c of −0.8°C for the loosest sections of the backfill in the deposition tunnel. Furthermore, the repository closure, which, in accordance with the reference design, is similar to the backfill in deposition tunnels, is extended vertically in ramp and shafts and therefore parts of it will experience temperatures lower than those at repository level. Freezing of the backfill is not a problem per se, as the process has been demonstrated to be reversible. However, it can be imagined that freezing could occur in the backfill in a position closer to the surface when the rock surrounding the repository is frozen. This could lead to increased pressures in the repository as liquid water is "trapped" in a frozen rock matrix. Such a scenario can only occur, however, when the temperature at repository level is below 0°C.

Borehole seals

The reference density of the borehole seals is the same as for the buffer. The seals will however most likely be exposed to temperatures below T_c due to their vertical extension up to c. 100 m below surface (Figure 10-156). The borehole seal component also experiences a thermal gradient due to its vertical extent. The average value of the geothermal gradient is 0.025°C/m and at Forsmark the measured geothermal gradient in the topmost 1,000 m is below 0.020°C/m /Sundberg et al. 2009/.

During periods of permafrost, the borehole seal could connect parts of the crystalline rock in which the temperature is above 0°C to parts where ice formation occurs. Hence, this design could give frost heave effects as water is transported from locations where it is liquid to build up an ice lens, as schematically pictured in Figure 10-156. The driving force for water transport in the bentonite is a gradient in suction, and from the present study it is found that in the temperature range 0°C to T_c, this gradient is of the order 1.2 MPa/°C for a system of homogeneous density. Using the geothermal temperature gradient, the suction gradient is directly seen to be 0.03 MPa/m, or 3 m water column/m. The latter quantity can directly be put in the expression for the Darcy flux, assuming a hydraulic conductivity of $C_h = 10^{-13}$m/s /Karnland et al. 2006/ gives a flux of

$$q = -C_h \nabla \psi = 3 \cdot 10^{-13} \text{ m/s}$$

This flow puts an upper limit of the speed of a possible ice lens growth. It should be noted that with the assumptions made of a constant geothermal gradient, this limit is independent of the distance that water must travel.

Because the problem at hand in principle is one dimensional, this evaluated flux can directly be converted to an ice lens length increase rate of approximately 10 μm/yr.

From this estimate it is seen that ice lens formation will not cause a problem, as it at the most will give a build-up of 10 cm over a period of 10,000 years. Notice that since this water transport process is serial in character, it is the lowest value of hydraulic conductivity over the involved length which

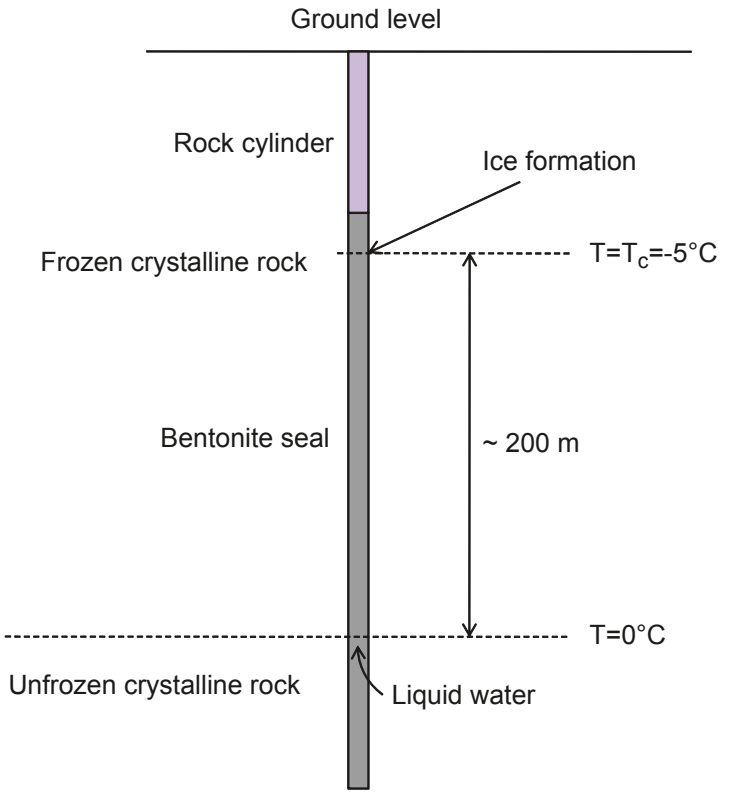

Figure 10-156. *Schematic illustration of possible ice lens formation in the bore hole seal of the KBS-3 repository assuming a geothermal gradient of 0.025°C/m and a critical temperature of the bentonite of –5°C /Birgersson et al. 2010/.*

will determine q, i.e. the section with the lowest C_h which will be rate determining. Hence, the prediction is quite robust. Furthermore, the process is only active when the temperature in the highest parts of the seal is below T_c, which will only occur during parts of a permafrost period.

Conclusions

Figure 10-109 shows the predicted evolution of the temperature in and above the repository. Based on this modelling, no component of repository will be exposed to freezing temperatures in the reference evolution. At some level, the backfill in the ramp and shaft and the borehole seals will be exposed to freezing conditions. This, however, is not expected to have any negative effects on the repository performance.

Chemical evolution of buffer and backfill for altered groundwater compositions

Intrusion of water types other that the present day deep groundwater in the repository area may modify the chemical evolution of the system. In SR-Can /SKB 2006a/ this was assessed by a geochemical simulation of an intrusion of a typical glacial melt water and a high salinity water /Arcos et al. 2006/. The conclusion from that study was that none of the waters had any significant impact on the expected performance of the system.

In SR-Site, another approach has been adopted in order to better support the conclusions from SR-Can. In SR-Site no attempt to simulate the effect of future changes of groundwater chemistry on the chemistry of the buffer and backfill has been made. Instead a sensitivity study of the importance of the groundwater components on the geochemical evolution has been made /Sena et al. 2010/. A summary of results can be found in Section 10.3.10.

Colloid release from buffer and backfill

As concluded in Section 10.4.7, the ionic strength of the groundwater; $\Sigma q[M^{q+}]$, will fall below 4 mM charge equivalent i.e. violating safety indictor criterion R1c, for some deposition holes during some part of the glacial cycle. This means that colloid release may occur from these holes and sections of the backfill similar to the situation during later parts of the temperate period, as discussed in Section 10.3.11. More specifically, it is concluded in Section 10.4.7 that less than two percent of the deposition hole positions may be assumed to have dilute conditions during a glacial cycle, and they will only have these conditions for a fraction of the time.

Regarding the duration of dilute conditions, Figure 10-32 indicates that around 10,000 years of temperate conditions are required before the first deposition holes, i.e. those with the highest flow rate, are exposed to dilute groundwater. Considering that the total duration of temperate conditions during the reference glacial cycle (Figures 10-107 and 10-108) is around 30,000 years, interrupted by permafrost episodes that are pessimistically not assumed to increase the salinity, this leaves 20,000 years of exposure to dilute groundwaters during temperate conditions. For glacial conditions, Figure 10-140 indicates that around 10,000 years of glacial conditions is required before the first deposition holes are exposed to dilute groundwater. This suggests that during the first, shorter, glacial episode, no deposition holes are exposed to dilute groundwaters and that such exposure could occur during the remaining 10,000 years of the last and longest glacial episode that has a duration of around 20,000 years. Together, these results indicate that a total exposure time of dilute ground water for the deposition holes with the highest flow rates of around 30,000 years or 25 percent of the time of the glacial cycle is a cautious assumption for the calculations of buffer erosion, although no strict exposure time can be derived from the cited results. Also, results in earlier sections indicate that the majority of deposition holes will never be exposed to dilute waters during the reference glacial cycle.

As already shown in Section 10.3.11, and illustrated in Figure 10-72, it is clear that only a small number of deposition holes will reach advective conditions, even in 10^6 years, when applying the erosion model described in Section 10.3.11 to all deposition holes. For the base case semi-correlated Hydrogeological DFN and using the EFPC rejection criterion and assuming that "dilute" conditions occur 25 percent of the time, then one deposition hole reaches advective conditions during the first 120,000 year glacial cycle (and does so after approximately 90,000 years) and 23 deposition holes reach advective conditions in 10^6 years. These positions are strongly related to those with the highest

Darcy flux. Positions with the highest fluxes are also with high likelihood among the two percent of positions exposed to dilute groundwaters. Since the 23 positions are much less than the two percent of the 6,000 positions assumed to be exposed to dilute water, further efforts to reduce the estimate of two percent being exposed to dilute groundwater would not readily yield any further reduction in the number of advective positions.

Also, assuming dilute conditions in **all** deposition holes **throughout the glacial cycle**, then 7 deposition holes are calculated to reach advective conditions in 120,000 years assuming temperate flow conditions and 4 deposition holes if the appropriate time averaged flow conditions (the mean value of $q^{0.41}$, Figure 10-147), is assumed. Therefore, it is concluded that less than one in a thousand of the 6,000 deposition holes are expected to exhibit advective conditions during the first glacial cycle.

As also found in Section 10.3.11 none of the tunnel intersecting single fractures will cause erosion of the backfill to the extent that it loses so much swelling pressure that advective conditions must be assumed in underlying deposition holes. For a few positions where the tunnel is intersected by a deformation zone, potentially more than 220 tonnes could be lost, but this is not relevant from the point of view of canister integrity since no deposition holes will be located there.

In conclusion, the quantitative evaluations of the erosion process indicate that substantial losses, affecting several of the buffer safety functions negatively, are expected to occur in less than one in a thousand of the deposition holes during the first 120,000-year glacial cycle, whereas, in a million year perspective, 23 deposition positions, i.e. less than one percent, are calculated to reach advective conditions assuming exposure to dilute groundwater 25 percent of the time. The buffer erosion calculations are integrated with the calculations of canister corrosion in a million year perspective, see Section 10.4.9, and, in the case of resulting canister failures, to calculations of radionuclide transport in Chapter 13.

Liquefaction

Liquefaction, as observed in loose clay and sand, cannot take place in a bentonite with high density, since the effective stress that holds the clay together is high due to the swelling pressure. Furthermore, the **Buffer, backfill and closure process report**, Section 3.4.2, conclusively rules out that a very high hydrostatic pressure during a reference glacial event could reduce the effective stress (swelling pressure) of the buffer to zero. Pressure increases resulting from earthquakes have been demonstrated as not being able to cause liquefaction in the buffer, see the **Buffer, backfill and closure process report**, Section 3.4.2.

Effects of saline water on buffer and backfill

Hydraulic conductivity and swelling pressure of the buffer and backfill, as affected by different groundwater salinities are presented in Section 10.3.9. The conclusion is that the hydraulic properties of the buffer will not be significantly affected by the intrusion of saline water. The conclusions in that section are valid at chloride concentrations of up to 3 M (17.5% NaCl). The highest expected value at Forsmark is a salinity of TDS = 20 g/L, i.e. about 2 percent, as a consequence of the upconing of deep saline waters when the ice front margin is located on top or the repository, see Section 10.4.7.

Mechanical effects of increased flow

For the case where there are strong hydraulic gradients in a fracture intersecting a deposition hole, it could be imagined that buffer could be lost by shearing of particles from the bentonite gel by seeping water. For physical shearing the cohesiveness of the gel has to be overcome by the friction force on the gel. The yield stress of the gel and the shear stress of the water will determine when this mechanism is active. The non-Newtonian properties, especially the Bingham yield stress must be quantified. /Neretnieks et al. 2009/ presents a model for the shear stress as a function of the hydraulic gradient and fracture aperture. Figure 10-157 shows the shear stress as a function of the hydraulic gradient based on the output from hydrogeological modelling of the glacial Base case in SR-Site, see Table 10-25 in Section 10.4.6, and aperture.

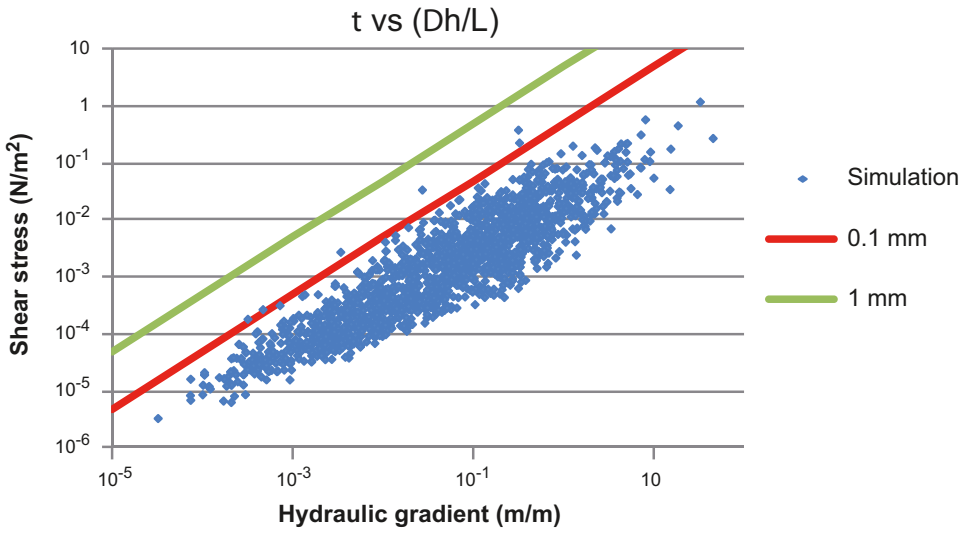

Figure 10-157. *Shear stress at gel/water interface as a function of hydraulic gradient (based on hydrogeological modelling of the glacial Base case in SR-Site, see Table 10-25 in Section 10.4.6) and aperture /Selroos and Follin 2010/.*

It is seen from the figure that that even for a gradient as high as 10% and a large fracture aperture as 1 mm, the shear stress is no more than 0.5 N/m^2 (0.5 Pa). This is a very low shear stress and is less than the yield stress of cohesive gels as found by /Birgersson et al. 2009/. They found that the shear strength of MX-80 at a water ratio of 100 (φ = 0.0037) for sodium concentrations of 10 and 100 mM is larger than 5 Pa. This is the concentration range where the gel is expected to be cohesive. Even in distilled water the shear strength is larger than 1 Pa for water ratios below 40 /Birgersson et al. 2009/. The mean aperture is also expected be much less than 1 mm.

The hydrogeological modelling of the "expanding ice front" case in SR-Site shows a similar picture to what is presented by /Neretnieks et al. 2009/. According to Figure 10-157 the calculated shear stresses are always below 5 Pa and much lower most of the time. It can thus be concluded that the loss of bentonite from shearing of particles can be neglected for all reasonable conditions.

Identified uncertainties and their handling in the subsequent analysis

In the reference evolution, no component of the repository will be exposed to freezing temperatures. At some level the backfill in the ramp and shaft and the borehole seals will be exposed to freezing conditions. This however, is not expected to have any negative effects on repository performance. Uncertainties regarding buffer freezing are further evaluated in a dedicated scenario, Section 12.3.

The quantitative evaluations of the erosion process indicate that substantial losses, affecting several of the buffer safety functions negatively, cannot be ruled out, for less than 2 percent of the deposition holes during the 120,000-year glacial cycle. These effects are propagated to calculations of canister corrosion and, in the case of resulting canister failures, to calculations of radionuclide transport.

The loss of bentonite from shearing of particles can be neglected for all reasonable conditions and such effects are therefore not propagated to further analyses.

10.4.9 Effects on canister

Canister failure due to isostatic load

The maximum expected isostatic load on the canister at the Forsmark site is 4.5 MPa hydrostatic pressure, up to 13 MPa isostatic swelling pressure from the bentonite (see Section 5.5.3) and a maximum addition of 26 MPa hydrostatic pressure from a future ice sheet in the reference glacial cycle, see Section 10.4.1. The maximum total isostatic pressure the canister will be subjected to can thus be estimated to be 43.5 MPa. This is less than the design load of 45 MPa.

As described in Section 5.4.3, the probability that the canister would not fulfil the design premises related to isostatic loads is deemed as insignificant. It can thus be concluded that no canisters will fail due to isostatic load, and the safety indicator Can2 in Figure 10-2 will not be threatened.

Canister failure due to shear loads

This failure mode is treated in Section 10.4.5.

Canister corrosion for diffusive conditions

In Section 10.3.13, it was concluded that, for an intact buffer, corrosion has an insignificant impact on the copper canister thickness in a 120,000 year perspective, if groundwater flow rates and sulphide concentrations for temperate conditions are assumed.

According to Section 10.4.7, sulphide concentrations are expected to be similar or lower for periglacial or glacial conditions compared to those for temperate conditions used in Section 10.3.13. According to Section 10.4.6, the hydrogeological entity controlling the transport of corroding species from the groundwater to the buffer, $q^{1/2}$, is, when averaged over the reference glacial cycle, less than the values for temperate conditions used in Section 10.3.13.

It is thus concluded that corrosion has an insignificant impact on the copper canister thickness in a 120,000 year perspective when variations in geochemical and hydrogeological conditions during the 120,000 year glacial cycle are taken into account.

Canister corrosion for a partially eroded buffer

The quantitative evaluations of the hydrogeological evolution presented in Section 10.4.6 indicate that exposure of the buffer to dilute groundwater such that buffer erosion must be considered may occur in the 2 percent of the deposition holes with the highest groundwater flow rates during the 120,000-year glacial cycle and for about 25 percent of the time. As demonstrated in Section 10.4.8, in a small fraction of these deposition holes, buffer may be lost to the extent that advective conditions arise. For corrosion when advection occurs in the buffer, /Neretnieks 2006b/, supplemented by the Appendix to /Neretnieks et al. 2010/ concluded that, for a very wide range of such conditions the equivalent flow rate, Q_{eq}, used for assessing the migration of corroding agents from the groundwater to the canister should be replaced by q, the water flux through the part of the fracture that intersects the deposition hole. In addition, the water flux is increased due to the lost flow resistance in the void arising from the missing bentonite. /Neretnieks 2006b/ demonstrated that this effect can be bounded by multiplying the undisturbed flow by a factor of 2.

The rate of corrosion will also depend on the geometry of the eroded buffer section, and in particular on the area of the canister exposed to groundwater, where a smaller area yields a higher corrosion rate. If buffer erosion occurs, it is also likely to continue after part of the canister surface is first exposed, meaning that the exposed area will grow with time. (Also, the erosion rate is expected to increase once a cavity is formed in the deposition hole since the outward transport of clay in solution is more efficient from a cavity than from a fracture, see Section 10.3.11.) It is cautiously assumed that the height of the exposed canister surface is equal to the buffer thickness, $d_{buff} = 0.35$ m, and that this situation does not change with time. The exposed height is set equal to the buffer thickness since buffer is lost to a fracture intersecting the deposition hole and the material for this loss is transported from all directions in the deposition hole, meaning that the eroded volume should be roughly equal in height and depth when the canister is first exposed. Furthermore, buffer loss is assumed along half the circumference of the deposition hole since the up-stream half of the fracture-deposition hole interface is most exposed to erosion. The exposed canister area, A_{corr}, is thus

$$A_{corr} = \pi \cdot r_{can} \cdot d_{buff}$$

where $r_{can} = 0.525$ m is the canister radius. For a more detailed discussion of the corrosion geometry, see /SKB 2010d/.

The copper shell thickness of 47 mm is assumed in these corrosion calculations. This is the reasonable minimum copper coverage derived from the experience of test manufacturing of the canisters.

A few canisters per thousand could though have a minimum copper coverage of 45–47.5 mm after machining, see further the **Data report**. (As mentioned in Section 10.2.5, subsection "Canister corrosion", initial corrosion by atmospheric oxygen before emplacement and from initially entrapped oxygen is expected to cause corrosion depths less than 500 µm at the most, and will thus have a negligible impact on the minimum copper coverage of the canisters.)

A distribution of sulphide concentrations for present conditions was derived in Section 10.3.7 and it was argued that this distribution can be expected to persist during temperate conditions. The values include the potential contribution from methane and hydrogen as nutrients for sulphate reducing bacteria. The dissolved organic carbon is not expected to influence the sulphide concentration in the groundwater.

As described in Section 10.4.7 there could be factors influencing, and in general lowering, the sulphide concentration during other climate conditions but these are difficult to quantify. The overall conclusion is that it is pessimistic to use present day sulphide concentrations for other climate conditions. The observed distribution of sulphide concentrations at the Forsmark site at present is thus used in the corrosion calculations, see Figure 10-41.

As stated in Section 10.4.6, the time averaged flow, q, over the reference glacial cycle is about 80 percent of the values for the temperate period. This is pessimistically disregarded in the erosion/corrosion calculations, where temperate flow rates are used throughout.

Erosion and subsequent corrosion is modelled probabilistically, using distributions of groundwater flow conditions from the hydrogeological DFN modelling and the sulphide distribution for temperate conditions. The corrosion rate distribution for the semi-correlated base case of the hydrogeological DFN model and assuming advective conditions in all deposition holes remaining after rejection according to the EFPC criterion, is given in Figure 10-158. Here, a sulphide concentration of 10^{-5} M is assumed in all deposition holes and all incoming sulphide is assumed to attack the exposed canister surface. Also the result when disregarding EFPC rejection is shown in the figure.

In the combined erosion/corrosion calculations the time to canister failure is calculated by adding the corrosion time to the erosion time for each deposition hole with its specific flow and for a sulphide concentration randomly sampled from the sulphide distribution. The central output is the mean number of failed canisters at one million years and a list of failure times and canister positions resulting from the combination of canister specific flow rates with the sampled sulphide concentrations.

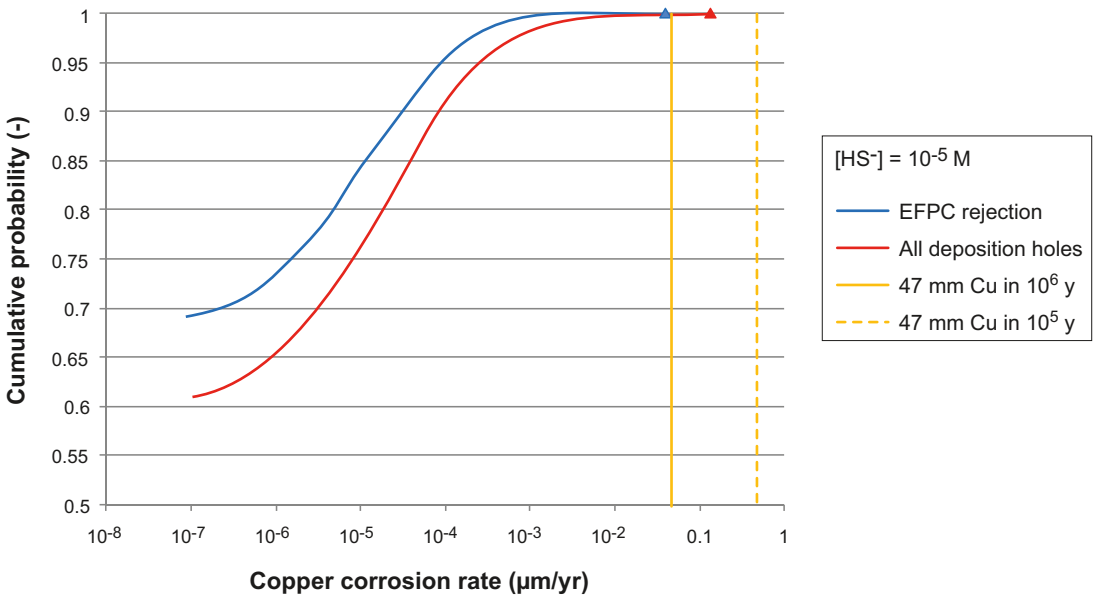

Figure 10-158. *Distribution of corrosion rates for the base case semi-correlated hydrogeological DFN model assuming advective conditions. The vertical lines indicate the corrosion rates that correspond to corrosion of 47 mm copper in 10^5 (dashed line) and 10^6 (solid line) years respectively.*

In a base case calculation, the semi-correlated base case of the hydrogeological DFN model, deposition hole rejection according to the EFPC criterion, the sulphide concentration distribution for temperate conditions and the cautious corrosion geometry are used. This yields a mean number of failed canisters of 0.087 at one million years when the sulphide distribution is randomly combined with the flow rates for all the deposition holes. Only four deposition holes have sufficiently high flow rates for failure to occur within one million years and for all four, the highest concentration of sulphide in the set of discrete values, $1.2 \cdot 10^{-4}$ M, is required.

Table 10-26 shows the erosion and corrosion times for the four canister positions that could fail within 10^6 years for the base case calculation. It can be seen from the table that the erosion and corrosion times are comparable for this highest sulphide concentration. For lower sulphide concentrations the corrosion times will increase, and thus largely determine the failure times.

If all ten available realisations of the semi-correlated hydrogeological DFN model are evaluated, on average 0.12 canisters fail within one million years. The same calculation with the five realisations of the uncorrelated and correlated hydrogeological DFN models yield on average 0.65 and 0.57 failed canisters, respectively. It is also noted that assuming advective conditions initially in all deposition holes leads to increases of less than a factor of two in the mean number of failed canisters, i.e. uncertainties in the extent of erosion cannot lead to significantly increased occurrences of corrosion failures. For e.g. the semi-correlated hydrogeological DFN model, the mean number of canister failures is 0.17 if advective conditions are assumed initially in all deposition holes.

More extensive corrosion calculations, including sensitivities to additional factors are given in the corrosion scenario, Section 12.6.2. Full documentation of all calculations of buffer erosion/colloid release and canister corrosion is given in /SKB 2010d/.

In conclusion, on average less than one canister may fail due to dilute groundwater causing advective conditions in the deposition holes over the entire 10^6 year assessment period. Further assessments of corrosion, including additional sensitivity analyses are made in the corrosion scenario, Section 12.6.

Canister corrosion due to oxygen penetration

As discussed in Section 10.4.7, reducing conditions will prevail in the deposition holes of the repository, during the entire glacial cycle. There is thus no further corrosion caused by oxygen.

Identified uncertainties and their handling in the subsequent analysis

In addition to failure caused by shear movements on fractures intersecting deposition holes, see Section 10.4.5, the only reason for canister failure during the remaining part of the glacial cycle is by corrosion due to dilute groundwater causing advective conditions in deposition holes. Up to around one canister may fail over the entire 10^6 year assessment period for this reason. The results from the erosion/corrosion calculations are further transferred to the radionuclide transport calculations, giving the time needed for erosion and corrosion specifically for each deposition hole and for each sulphide concentration.

Table 10-26. Flow rate, erosion, corrosion and failure time for the 4 canister positions, that fail within 10^6 years, for the base case of the semi-correlated hydrogeological DFN model and after applying the EFPC criterion. The figures are model data output, with the possible failures sorted with the earliest time on top. In this case, failures within 10^6 years only occur for the highest sulphide concentration in the distribution, $1.2 \cdot 10^{-4}$ M.

Dep. hole ID in DFN hydro model	Flow rate [m³/yr]	Erosion time [yr]	Corrosion time [yr]	Failure time [yr]
1978	0.144	90,820	109,967	200,786
411	0.161	119,733	98,482	218,215
6875	0.084	110,655	188,485	299,140
401	0.026	278,678	607,395	886,073

10.4.10 Evolution of other parts of the repository system

Except for freezing of the ramp, shaft and borehole seals, see Section 10.4.8, other repository components are not expected to be affected by the conditions imposed by the remaining part of the reference glacial cycle.

10.4.11 Safety functions at the end of the reference glacial cycle

The following is an account of the development of all safety functions in Figure 10-2 during the reference glacial cycle.

Rock safety functions

R1. Provide chemically favourable conditions

a) Reducing conditions; Eh limited.
The reducing conditions during the initial temperate period are expected to continue to exist throughout the reference glacial cycle. The only identified challenge to this conclusion concerns the possible penetration of oxygenated glacial melt water to repository depth for glacial situations with enhanced groundwater flow. Based on observations and results from pessimistic modelling efforts, oxygen intrusion to repository depth in highly transmissive deformation zones cannot be discarded. Model results indicate that hundreds of years of the worst glacial situation would be needed for oxygen to reach the canisters in the repository. Therefore it is concluded that reducing conditions will prevail in the repository throughout the reference evolution.

b) Salinity; TDS limited.
For temperate domains during the reference glacial cycle, the salinity is not expected to exceed that of the initial temperate period, i.e. the salinities are well within the ranges where the buffer and backfill have favourable properties.

For permafrost conditions, freeze out of salt above the repository may increase the groundwater salinity at repository depth, but the concentration of salt at repository level due to out-freezing will not become high enough to lower the swelling pressure of the buffer and the backfill, among other reasons because of the downward gravity-driven flow of saline waters. This situation will not be changed during permafrost decay as a transition to a temperate period occurs.

Upconing of deep saline groundwaters during the glacial period is not expected to affect the swelling capacity of the backfill. The highest expected value at Forsmark is a salinity of TDS = 20 g/L, i.e. about 2 percent, as a consequence of the upconing of deep saline waters when the ice front margin is located on top or the repository.

c) Ionic strength; $\Sigma q[M^{q+}] > 4$ mM charge equivalent.
For the glacial period, slightly less than 2 percent of deposition hole locations could experience dilute conditions during an advancing ice front whereas only slightly more than one percent of the deposition holes could experience dilute conditions during an assumed period of 100,000 years corresponding to glacial maximum conditions. Also, as seen in Figure 10-32, it would take up to 60,000 years of temperate conditions to reach dilute conditions in 1 percent of the deposition hole locations. For permafrost conditions, all arguments indicate that groundwaters below permafrost will not become more diluted than under temperate conditions. Rather, saline waters may move downwards within conductive fracture zones. Thus the charge concentration of cations is expected to increase during permafrost periods. Finally, the hydrogeological analysis indicates that salinities are more or less restored during a glacial cycle. The low salinities, i.e. dilute conditions, are mainly found in conjunction with glacial passages. This means that less than 2 percent of the deposition hole positions may have dilute conditions during a glacial cycle, and they will only have these conditions for a fraction of the time.

d) Concentrations of HS^-, H_2, CH_4 organic C, K^+ and Fe; limited.
Other components, such as bicarbonate, potassium, iron sulphide, etc. that are controlled by relatively fast chemical reactions are expected to remain mostly unaffected by permafrost. These components will also be less affected by glacial conditions, although all the evidence points towards more dilute waters and hence lower concentrations of these components. Therefore the concentrations of K, HS^- and Fe will remain limited. This means that the potassium concentrations are expected to remain

≤ 0.004 mol/L, sulphide concentrations are expected to be $\leq 10^{-5}$ mol/L for most deposition positions and iron concentrations are expected to gradually increase up to 10^{-4} mol/L. Dissolved organic carbon, methane and hydrogen during periglacial periods will remain at the same levels as during temperate conditions, but they are expected to decrease during a glacial period due to the overall dilution by melt waters depleted in these components. For the same reason sulphide concentrations and microbial sulphate reduction will be lower during a glacial period, but they are expected to return to the levels observed now at Forsmark after a short submerged period under brackish marine waters.

e) pH < 11.
pH is controlled by relatively fast chemical reactions and expected to remain mostly unaffected by permafrost and will also be less affected by the glacial conditions, although all the evidence points towards dilute waters with relatively high pH. The effect of grout in fractures will be to increase the pH in deformation zones for relatively long periods of time. It is expected that, with time, the pH that initially had risen to ≈ 9 will progressively homogenise with the values found in surrounding parts of the rock.

f) Avoid chloride assisted corrosion; pH > 4 and $[Cl^-] < 2$ M.
The hydrogeochemical analysis shows that these safety function indicator criteria are fulfilled throughout the assessed period.

R2. Provide favourable hydrologic and transport conditions

The analyses of mechanical evolution for the reference glacial cycle have not given rise to any results that imply any significant change of fracture transmissivity or new fracturing at repository depth. The transmissivity increases due to reactivation of fractures during the forbulge period of the glacial cycle are relatively moderate, apart from the transmissivity increase that would occur for fractures close to and parallel to the tunnel floor. However, this case is already covered by the assumptions made for the EDZ. Hydraulic jacking below 200 m, due to the impacts of the glacial cycle is judged highly unlikely. At shallower depths it may happen, and the highly transmissive gently dipping fractures near surface at Forsmark may be evidence of this occurring in the past. Given the already very high, and potentially jacking-induced, near surface horizontal permeability, this effect is already captured in the hydrogeological models used and the phenomenon is excluded from further analysis.

Pessimistically, it is also assumed that if a fracture shears more than 5 cm in a deposition hole, i.e. potentially causing a canister failure, that fracture is assumed to have such large transmissivity that its transport resistance can be neglected.

While changes to the fractures are relatively small during the glacial cycle, there are dramatic effects from the changes of boundary conditions. The Darcy flux increases dramatically, some orders of magnitude, during the ice front passages during advance and retreat, while the flux is generally below the temperate value during the phase when the repository is covered by ice. Darcy flux is lower, or at the same magnitude as for temperate conditions, during permafrost. For submerged conditions, very low flows are expected.

a) Transport resistance in fractures, F; high.
Due to changing boundary conditions during the glacial cycle, the transport resistance decreases dramatically, some orders of magnitude, during the ice front passages during advance and retreat, while it is generally above the temperate value during the phase when the repository is covered by ice. It is higher, or at the same magnitude as for temperate conditions, during permafrost. For submerged conditions, the transport resistance in fractures will be high.

b) Equivalent flow rate at the buffer/rock interface, Q_{eq}; low.
No significant changes of the fracturing close to deposition holes are expected during the glacial cycle, but the equivalent flow rate will change due to the changing flow boundary conditions during the glacial cycle. It increases dramatically, up to between one and two orders of magnitude, during the ice front passages during advance and retreat, while it is generally below the temperate value during the phase when the repository is covered by ice. It is below, or at the same magnitude as for temperate conditions, during permafrost. For submerged conditions, very low flows are expected.

R3. Provide mechanically stable conditions

a) GW pressure; limited.
For temperate domains during the reference glacial cycle, the groundwater pressure is expected to be similar to that of the initial temperate period, i.e. around 4.5 MPa at repository depth at Forsmark.

For permafrost, ice-free conditions, the same groundwater pressure as for temperate conditions is expected.

For glacial conditions, the maximum groundwater pressure is determined by the thickness of the overlying ice sheet. In the reference glacial cycle, the maximum thickness at Forsmark corresponds to an increase in groundwater pressure of 26 MPa, yielding a total groundwater pressure of around 30 MPa. Furthermore, it is pessimistic to assume that the full ice burden is translated into groundwater pressure.

b) Shear movements at deposition holes < 0.05 m.
Large earthquakes at Forsmark cannot be excluded within any of the safety assessment time frames. The impact of earthquakes, in terms of the number of canisters expected to be sheared 50 mm or more has here been quantified by using a range of earthquake frequency estimates, the Forsmark site description and by applying deposition hole rejection criteria. During a glacial cycle, it is estimated that between $8.3 \cdot 10^{-4}$ and $5.7 \cdot 10^{-3}$ canisters may fail. For the 1,000,000-year time frame, we assume at maximum two seismic events and estimate, using the most pessimistic way of accounting for the combined effects of both, that between $8.1 \cdot 10^{-3}$ and $6.9 \cdot 10^{-2}$ canisters may be sheared 50 mm or more. As the numbers of failed canisters are substantially less than one, they can be interpreted as the probabilities of a canister failure occurring over the cited time frames.

c) Shear velocity at deposition holes < 1 m/s
This criterion is upheld, as is further justified in Section 10.4.5.

R4. Provide thermally favourable conditions

For temperate domains during the reference glacial cycle, the rock temperature is envisaged to be similar to that of the initial temperate period, i.e. well above 0°C at Forsmark. As shown in Section 10.4.3, the 0°C isotherm reaches a maximum depth of 250 m while the −4°C isotherm reach a maximum depth of ~150 m in the reference glacial cycle. If also considering a quite unrealistic and most extreme combination of uncertainties, the uncertainty range for the perennially frozen ground reach a maximum depth of ~420 m and at the same time, the uncertainty range for the −4°C isotherm reach a maximum depth of ~320 m. These results conclusively show that the −4°C isotherm does not reach repository depth in the reference glacial cycle and since the uncertainty interval for the perennially frozen ground does not reach 450 m depth, even in this most extreme combination of all uncertainties, freezing of groundwater at repository depth is excluded in the reference glacial cycle. In this most extreme situation, the lowest temperature at the 450 and 470 m depths are approximately −0.5°C and 0°C respectively. For periods with glacial conditions, the ice sheet acts to insulate the bedrock from the low air temperatures, meaning that permafrost depths are smaller than for periglacial conditions.

a) Temperature > −4°C (avoid buffer freezing)
The thermal modelling shows that this safety function is fulfilled for the reference glacial cycle.

b) Temperature > 0°C (validity of can shear analysis)
When not considering the uncertainties related to permafrost growth, the bedrock temperature is well above 0°C for the reference glacial cycle. In the case of the most extreme, and quite unrealistic, combination of uncertainties related to permafrost growth, the bedrock temperature at repository level may have a temperature marginally below 0°C. However, since this case is considered unrealistic it is anyway judged that the safety function is upheld for the reference glacial cycle. Furthermore, during the first glacial cycle after deposition the residual heat in the spent fuel implies that the temperature in the buffer and inside the canister will be higher than in the rock for at least the first 100,000 years, see e.g. Figure 10-16.

Buffer safety functions

For the initial temperate period, it was concluded that the saturated buffer density in deposition holes where piping does not occur will be in the interval allowed for the initial state, ie. 1,950–2,050 kg/m^3 around the canister.

Up to 2 percent of deposition hole positions may experience dilute conditions during a glacial cycle, although only for a limited part of the time. Assuming that these positions coincide with the positions of the highest flow, only one out of 6,000 deposition holes is calculated to also lose buffer mass to the extent that advective conditions must be assumed during the 120,000 year reference glacial cycle.

Buff1. Limit advective transport

a) Hydraulic conductivity < 10^{-12} m/s
For deposition holes within the initially allowed buffer density range, the hydraulic conductivity criterion is fulfilled with ample margin, also for groundwater salinities that can be expected during the reference glacial cycle, see Section 10.4.8. For a deposition hole that has experienced loss of buffer mass due to erosion/colloid release and to the extent that advective conditions prevail, this safety function can, however, not be guaranteed.

b) Swelling pressure > 1 MPa.
For deposition holes within the initially allowed buffer density range, the swelling pressure criterion is fulfilled with ample margin, also for groundwater salinities that can be expected during the reference glacial cycle, see Section 10.4.8. For a deposition hole that has experienced loss of buffer mass due to erosion/colloid release and to the extent that advective conditions prevail, this safety function can, however, not be guaranteed.

Buff2. Reduce microbial activity

For this safety function to be fulfilled it is required that the buffer density is high.

For deposition holes within the initially allowed buffer density range, this safety function is fulfilled.

For a deposition hole that has experienced substantial loss of buffer mass due to erosion/colloid release, this safety function can, however, not be guaranteed.

Buff3. Damp rock shear

For this safety function to be fulfilled, it is required that the saturated buffer density is less than 2,050 kg/m^3. 2,050 kg/m^3 is the upper allowed bound of the initial density and as no relevant processes that would increase the buffer density have been identified, it is concluded that this safety function is fulfilled for all deposition holes.

Buff4. Resist transformation

For this safety function to be fulfilled, it is required that the buffer temperature is less than 100°C. The peak buffer temperature will occur a few tens of years after deposition. At the start of the reference glacial cycle (10,000 years after deposition), the buffer temperature will be similar to that of the ambient, natural rock temperature. There is thus no conceivable way in which the buffer temperature could exceed 100°C during the reference glacial cycle.

Buff5. Prevent canister sinking

For this safety function to be fulfilled, it is required that the buffer swelling pressure exceeds 0.2 MPa. For deposition holes within the initially allowed buffer density range, the swelling pressure criterion is fulfilled with ample margin, see above. For a deposition hole that has experienced loss of buffer mass due to erosion/colloid release and to the extent that advective conditions prevail, this safety function cannot be guaranteed. However, if advective conditions prevail, the fact that the canister sinks is of secondary importance.

Buff6. Limit pressure on canister and rock

a) Swelling pressure < 15 MPa
Since no process is identified where the buffer material will be added during the next glacial cycle, this maximum swelling pressure criterion will be upheld.

b) Temperature > −4°C.
As mentioned regarding the rock safety function R4 above, the criterion is expected to be fulfilled with ample margin for the reference glacial cycle.

Backfill safety functions

BF1. Counteract buffer expansion

For this safety function to be fulfilled it is required that the density of the backfill material is sufficiently high. As shown in Section 10.2.4, the largest possible erosion due to piping will be 1,640 kg. Erosion in the backfill will basically mean that material is redistributed within the tunnel itself. Considering the large mass of backfill in the tunnel a redistribution of 1,640 kg can be assumed to have no impact at all on the backfill performance.

Even if dilute conditions occur in some of the more transmissive single fractures intersecting deposition tunnel, during the next glacial cycle, none of them will cause erosion to the extent that this will result in such loss of swelling pressure above deposition holes that these in turn would enter an advective condition. For a few positions where the fracture is connected to a deformation zone, potentially more than 220 tonnes could be lost, but this is not relevant from the point of view of canister integrity.

Canister safety functions

Can1. Provide corrosion barrier

The only reason for canister failure due to corrosion during the remaining part of the glacial cycle is by corrosion for advective conditions in the deposition holes, caused by erosion of the buffer when exposed to dilute groundwaters. Up to around one canister may fail over the entire 10^6 year assessment period for this reason. The results from the erosion/corrosion calculations are further transferred to the radionuclide transport calculations, giving the time needed for erosion and corrosion specifically for each deposition hole and for each sulphide concentration.

Can2. Withstand isostatic load

For this safety function to be fulfilled, it is required that the canister withstands isostatic loads above 45 MPa. The fulfilment of this safety function is assured by the design of the canister, see Section 5.4.3 and the **Canister production report**. It may also be noted that the maximum expected isostatic load on the canister at the Forsmark site is 4.5 MPa hydrostatic pressure, up to 13 MPa isostatic swelling pressure from the bentonite and a maximum additional 26 MPa hydrostatic pressure from a future ice sheet in the Weichselianreference evolution. The maximum total isostatic pressure to which the canister will be subjected can thus be estimated to be 43.5 MPa.

The probability for local canister insert damage at 44 MPa over-pressure is vanishingly small, as demonstrated by probabilistic calculations, see Section 5.4.3. Furthermore, the criterion for failure is that a global collapse occurs, which is not expected for pressures below 100 MPa, see further Section 5.4.3. As a consequence, no canister failures are expected at the maximum over-pressure that could be experienced at the Forsmark site in the reference evolution.

Can3. Withstand shear loads

Canister failures due to future earthquakes are avoided through the use of respect distances and acceptance criteria for deposition holes, adapted to the ability of the canister to resist loads from fracture shear movements. However, it cannot be fully ruled out that such failures will occur, see discussion of rock safety function R3b for estimates of the likelihood of such failures.

Conclusions for consequence calculations

The following conclusions for radionuclide transport can be drawn.

1. The only causes for canister failure that has not been ruled out for the reference glacial cycle are corrosion in a deposition hole with advective conditions and shearing due to a large earthquake. The likelihood of either of these types of failure during the first glacial cycle is low.
2. As for the initial temperate period, the EDZ developed during construction needs to be considered in the RN-transport analyses.
3. The hydrogeological analyses have provided distributions of F, t_w and Q_{eq} to be used in radionuclide transport calculations for temperate periods of the glacial cycle. For other climate periods, estimates of these quantities, in many cases as stylised examples, have been derived.
4. The geochemical assessments have provided geochemical conditions for which retention properties in the host rock for radionuclide transport can be derived.
5. The buffer and backfill assessments have provided buffer conditions for which retention properties in the buffer for radionuclide transport can be derived.
6. The effect of a partially eroded backfill needs to be evaluated in radionuclide transport calculations.
7. Spalling may affect the equivalent flow rates, Q_{eq}, in deposition holes.
8. pH increase from cement may affect geosphere retention in larger, grouted fractures, potentially throughout the glacial cycle.

10.5 Subsequent glacial cycles

For the reference climatic evolution, the first glacial cycle is simply assumed to be repeated until the end of the one million year assessment period. This is also in line with suggestions given in SSM's General Guidance. With a cycle period of around 120,000 years, this means about seven repetitions of the initial Weichselian glacial cycle, i.e. a total of eight such cycles.

Reversible phenomena like the thermal, hydrogeological and geochemical evolution of the bedrock are essentially expected to follow the cyclic variations of external conditions controlling them, see e.g. the discussion in Section 10.4.6 on the evolution of salinity during a glacial cycle and in Section 10.4.7 on the evolution of redox conditions during a glacial cycle. This is also the case for biosphere development at the site.

Irreversible phenomena like buffer erosion, canister corrosion and possibly earthquake-induced effects are essentially expected to occur to an extent eight times greater than that during the initial glacial cycle. Particular implications of this are listed below.

- Buffer erosion caused by dilute groundwater that could be a significant phenomenon during the initial glacial cycle, has to be considered for subsequent glacial cycles. Essentially, eight times more erosion could be expected at the end of the one million year assessment period.
- The evaluations of canister corrosion for the initial glacial cycle indicate that, for an unaltered buffer, corrosion would not cause canister failures even in a million year perspective. For a buffer that has been partially eroded to the extent that advective conditions must be assumed in the deposition hole on average less than one canister may fail over the entire 10^6 year assessment period for this reason.
- The analysis of canister failures due to earthquakes for the initial glacial cycle is extended to one million years. During a glacial cycle, it is estimated that between $8.3 \cdot 10^{-4}$ and $5.7 \cdot 10^{-3}$ canisters may fail. For the 1,000,000-year time frame, using the most pessimistic way of accounting for the combined effects of multiple earthquakes, it is estimated that between $8.1 \cdot 10^{-3}$ and $6.9 \cdot 10^{-2}$ canisters may be sheared 50 mm or more.

There are also phenomena like ion exchange in the buffer that could require millions of years to equilibrate with the average ionic contents of the groundwater over a glacial cycle. Furthermore, the residual power will affect the thermal conditions in the rock only during the initial glacial cycle. Thereafter, the thermal evolution is determined by naturally occurring phenomena.

10.5.1 Safety functions at the end of the assessment period

The following is an account of all safety functions in Figure 10-2 at the end of the one million year assessment time, often as a comparison to the situation after the initial glacial cycle reported in Section 10.4.11.

Rock safety functions

R1. Provide chemically favourable conditions

a) Reducing conditions; Eh limited
No challenges to the conclusion for the initial glacial cycle, that reducing conditions will prevail, have been identified. It is, therefore, concluded that reducing conditions will prevail throughout the assessment period.

b) Salinity; TDS limited.
Repetitions of the same pattern of variations as for the initial glacial cycle are expected, meaning that salinity levels will remain limited.

c) Ionic strength; $\Sigma q[M^{q+}] > 4$ mM charge equivalent.
Repetitions of the same pattern of variations as for the initial glacial cycle are expected, meaning that additional periods of temperate and glacial conditions where this safety function indicator is not fulfilled must be assumed.

d) Concentrations of HS^-, H_2, CH_4 organic C, K^+ and Fe; limited.
Repetitions of the same pattern of variations as for the initial glacial cycle are expected, meaning that concentrations of K and Fe will remain limited and that sulphide concentrations are expected to be $\leq 10^{-5}$ mol/L for most deposition positions averaged over the time period.

e) pH; pH < 11.
Repetitions of the same pattern of natural variations as for the initial glacial cycle are expected, meaning that pH is not expected to exceed 10. Possibly, continued releases of leach water from grout, shotcrete and cement may exhibit pH-values of around 9 even after the initial glacial cycle.

f) Avoid chloride assisted corrosion; pH > 4 and $[Cl^-] < 2$ M.
Repetitions of the same pattern of natural variations as for the initial glacial cycle are expected, which means that these safety function indicator criteria are fulfilled throughout the period.

R2. Provide favourable hydrologic and transport conditions

a) Transport resistance in fractures, F; high
Repetitions of the same pattern of variations of gradients and small alterations of fracture transmissivity for different glacial loads as for the initial glacial cycle are expected. This means that the variation in groundwater flow and thus in transport resistance of the initial glacial cycle will also be applicable for the subsequent glacial cycles.

b) Equivalent flow rate in buffer/rock interface, Q_{eq}; low.
Repetitions of the same pattern of variations of gradients and small alterations of fracture transmissivity for different glacial loads as for the initial glacial cycle are expected. This means that the variation in groundwater flow and thus in equivalent flow rate of the initial glacial cycle will also be applicable for the subsequent glacial cycles However, in deposition holes where advective conditions need to be assumed, Q_{eq} should be replaced by the flow in the fracture intersecting the deposition hole, as further discussed in Section 10.4.9.

R3. Provide mechanically stable conditions

a) GW pressure; limited.
Repetitions of the same pattern of variations as for the initial glacial cycle are expected, meaning that increased pressures will occur for glacial conditions. As for the initial glacial cycle, this yields maximum total groundwater pressures of around 30 MPa.

b) Shear movements at deposition holes < 0.05 m.
For the 1,000,000-year time frame, using the most pessimistic way of accounting for the combined effects of multiple earthquakes, between $8.1 \cdot 10^{-3}$ and $6.9 \cdot 10^{-2}$ canisters may be sheared 50 mm or more.

c) Shear velocity at deposition holes < 1 m/s.
As for the initial glacial cycle it is shown that shear velocities will stay below the 1 m/s limit.

R4. Provide thermally favourable conditions

Repetitions of the same pattern of variations as for the initial glacial cycle are envisaged. For the first glacial cycle it was shown that the −4°C isotherm reaches a maximum depth of ~150 m and if also considering a quite unrealistic and most extreme combination of uncertainties, the uncertainty range for the perennially frozen ground reach a maximum depth of ~420 m and at the same time, the uncertainty range for the −4°C isotherm reach a maximum depth of ~320 m. These results conclusively show that the −4°C isotherm does not reach repository depth in the reference glacial cycle and since the uncertainty interval for the perennially frozen ground does not reach 450 m depth, even in this most extreme combination of all uncertainties, freezing of groundwater at repository depth is excluded in the reference glacial cycle. In this most extreme situation, the lowest temperatures at the 450 and 470 m depths are approximately −0.5°C and 0°C, respectively. For periods with glacial conditions, the ice sheet acts to insulate the bedrock from the low air temperatures, meaning that permafrost depths are smaller than for periglacial conditions.

a) Temperature > −4°C (avoid buffer freezing).
This safety function is fulfilled, even considering that the maximum permafrost depths for the reference glacial cycle may increase by up to 37 m, see the **Climate report**, Section 4.5.3, when the residual power from the fuel does not counteract the development of permafrost after the initial glacial cycle.

b) Temperature > 0°C (validity of can shear analysis).
When not considering the uncertainties related to permafrost growth, the bedrock temperature is well above 0°C during the first and all following safety assessment period glacial cycles. In the case of the most extreme, and quite unrealistic, combination of uncertainties related to permafrost growth, the bedrock temperature at repository level may have a temperature marginally below 0°C. However, since this case is considered unrealistic it is anyway judged that the safety function is upheld for the entire assessment period of 1 million years.

Buffer safety functions

As for the initial glacial cycle, quantitative evaluations of the buffer erosion process indicate that substantial losses, affecting several of the buffer safety functions negatively, cannot be ruled out, potentially for a fraction of the deposition holes during the one million year assessment period. These potential losses would be higher than for the initial glacial cycle.

This influences the evaluation of several of the buffer safety function indicators, as discussed below.

Buff1. Limit advective transport

a) Hydraulic conductivity < 10^{-12} m/s.
For deposition holes within the accepted range of buffer density, the hydraulic conductivity criterion is fulfilled with ample margin, also for groundwater salinities that can be expected during the reference glacial cycle, see Section 10.4.8. For a deposition hole that has experienced loss of buffer mass due to erosion/colloid release and to the extent that advective conditions prevail, this safety function can, however, not be guaranteed.

b) Swelling pressure > 1 MPa.
For deposition holes within the accepted range of buffer density, the swelling pressure criterion is fulfilled with ample margin, also for groundwater salinities that can be expected during the reference glacial cycle, see Section 10.4.8. For a deposition hole that has experienced loss of buffer mass due to erosion/colloid release and to the extent that advective conditions prevail, this safety function can, however, not be guaranteed.

Buff2. Reduce microbial activity

For this safety function to be fulfilled it is required that the buffer density is high.

For deposition holes within the accepted range of buffer density, this safety function is fulfilled.

For a deposition hole that has experienced substantial loss of buffer mass due to erosion/colloid release, this safety function can, however, not be guaranteed.

Buff3. Damp rock shear

For this safety function to be fulfilled, it is required that the saturated buffer density is less than 2,050 kg/m^3. Since 2,050 kg/m^3 is the upper bound of the accepted initial state and as no relevant processes that would increase the buffer density have been identified, it is concluded that this safety function is fulfilled for all deposition holes.

Buff4. Resist transformation

For this safety function to be fulfilled, it is required that the buffer temperature is less than 100°C. As for the initial glacial cycle, there is no conceivable way in which the buffer temperature could exceed 100°C during the assessment period.

Buff5. Prevent canister sinking

For this safety function to be fulfilled, it is required that the buffer swelling pressure exceeds 0.2 MPa.

For deposition holes within the acceptable buffer density range, the swelling pressure criterion is fulfilled with ample margin, see above.

For a deposition hole that has experienced loss of buffer mass due to erosion/colloid release and to the extent that advective conditions prevail, this safety function cannot be guaranteed. However, if advective conditions prevail, the fact that the canister sinks is of secondary importance.

Buff6. Limit pressure on canister and rock

a) Swelling pressure < 15 MPa.
Since no process is identified where buffer material will be added during the future glacial cycles, this maximum swelling pressure criterion will be fulfilled.

b) Temperature > −4°.
As mentioned regarding the rock safety function R4, the criterion is expected to be fulfilled with ample margin.

Backfill safety functions

BF1. Counteract buffer expansion

Even though dilute conditions may occur in some of the more transmissive single fractures intersecting deposition tunnels, during the 10^6 years assessment period, none of them will cause erosion to the extent that this will result in such loss of swelling pressure above deposition holes that these in turn would enter an advective condition. For a few positions where the fracture is connected to a deformation zone, potentially more than 220 tonnes could be lost, but this is not relevant from the point of view of canister integrity.

Canister safety functions

Can1. Provide corrosion barrier

The only reason for canister failure due to corrosion during future glacial cycles is by corrosion for advective conditions in the deposition holes, caused by to erosion of the buffer when exposed to dilute groundwaters. On average less than one canister may fail over the entire 10^6 year assessment period for this reason. The results from the erosion/corrosion calculations are further transferred to

the radionuclide transport calculations, giving the time needed for erosion and corrosion specifically for each deposition hole and for each sulphide concentration.

Can2. Withstand isostatic load

Since repetitions of the maximum loads experienced during the initial glacial cycle are expected for the remainder of the assessment period, it is concluded that this safety function will be upheld also for the one million year assessment time.

Can3. Withstand shear loads

Canister failures due to future earthquakes are avoided through the use of respect distances and acceptance criteria for deposition holes, adapted to the ability of the canister to resist loads due to fracture shear movements. However, it cannot be fully ruled out that such failures will occur, see discussion of rock safety function R3b for estimates of likelihoods of such failures.

Conclusions for consequence calculations

The following conclusions for radionuclide transport can be drawn.

- One cause for canister failure that has not been ruled out for the one million year assessment period is an earthquake caused by changes in the glacial load. The likelihood of this type of failure is low, even when the entire assessment period is considered.
- Failure due to corrosion for advective conditions in a partially eroded buffer must be also considered for the one million year assessment time. On average less than one canister may fail due to this cause.
- All other conclusions regarding consequence calculations drawn for the initial glacial cycle, see Section 10.4.11, are also considered to be valid for repeated cycles.

10.6 Global warming variant

10.6.1 External conditions

There is a large range of potential future climate developments when the combined effect of natural and anthropogenic climate change is considered. One such case is described in the present *Global warming variant*. This variant describes a future climate development influenced by both natural climate variability and climate change induced by anthropogenic emissions of greenhouse gases, with the latter resulting in weak to moderate global warming. In order to cover a reasonably broad array of future climate developments based on present knowledge, a case of *Extended global warming* is also included in the SR-Site safety assessment, describing a situation with stronger and longer-lasting global warming.

In SR-Site, there are two main reasons for analysing cases of climates warmer than the reference glacial cycle; i) modelling studies of the climate response to increased greenhouse gas emissions, mainly CO_2, indicate that global temperatures will increase in the future under such conditions, e.g. /IPCC 2007, Kjellström et al. 2009a/, and ii) natural long-term climate cycles are believed be driven mainly by changes in solar insolation, see the **Climate report**, Section 2.2, and the coming 100,000 year period is initially characterised by exceptionally small amplitudes of insolation variations /Berger 1978/, suggesting that the present interglacial may be exceptionally long. By considering the known future changes in insolation, /Loutre and Berger 2000/ and /Berger and Loutre 2002/ suggest that the interglacial may end ~50,000 years after present. Given this insolation forcing, the results suggest that a growth of the Greenland-, Eurasian- and North American ice sheets would not start until after 50,000 years after present even without increased CO_2 levels. The global warming variant handles these future variations in insolation, as well as the effect of low to moderate global warming from an anthropogenic increase of atmospheric CO_2 levels.

In the global warming variant, peak air temperatures are reached within the first hundreds to thousands of years as a result of the greenhouse gas emissions. Mean annual air temperatures several degrees warmer than at present then occur in central Sweden and Forsmark. Subsequently, following the reduction in e.g. CO_2 emissions, temperatures are envisaged to slowly decline for the rest of the long initial period with temperate climate conditions, in response to the slow decline in atmospheric CO_2.

In line with the results of /Berger and Loutre 2002/, it is assumed for the global warming variant that the present temperate climate domain, albeit with higher initial air temperatures, will prevail for another 50,000 years before the relative mild onset of the next glacial cycle. After that, the first 70,000 years of the reference glacial cycle is assumed to follow. This development is also in broad agreement with results simulated for two global warming cases within the BIOCLIM project /BIOCLIM 2003/.

Due to the near-coastal location of Forsmark, the surface conditions at the site are sensitive to changes in sea level and shore line position. Such changes could be caused by effects of future global warming climates on the present glaciers and ice sheets. At present, there are major uncertainties in the estimates of future sea-level rise due to global warming. A major part of this uncertainty relates to the response of the cryosphere to increased temperatures. The Greenland ice sheet is more sensitive to increases in air temperature than are the Antarctic ice sheets, especially the East Antarctic ice sheet, see the **Climate report**, Section 5.1.3 subsection *Ice sheets and sea level*.

In some studies, the decay of the Greenland ice sheet under global warming is a relatively smooth function of the temperature increase /Huybrechts and de Wolde 1999/. However, many recent studies have highlighted that the response of the Greenland ice sheet to climate change is a complex process, involving internal ice sheet processes as well as interactions between the cryosphere, atmosphere and ocean, see the **Climate report**, Section 5.1.3, subsection *Ice sheets and sea level*. According to /Gregory and Huybrechts 2006/ an increase in annual temperature of 4.5±0.9° or more over Greenland, corresponding to a global temperature increase of 3.1±0.8°, could result in an irreversibly collapsing Greenland ice sheet. In the most pessimistic CO_2 scenario of /IPCC 2007/, with a 4° global climate warming by the year 2100 (compared to the period 1980–1999), with a likely range of 2.4°–6.4°, the warming would in the long run be sufficient to lead to complete Greenland ice sheet collapse and eventually a global mean sea-level rise by 7 m, see the **Climate report**, Section 5.1.3, subsection *Ice sheets and sea level*.

The maximum contribution to future global sea-level change from melting glaciers and ice caps (i.e. excluding the Greenland and Antarctic ice sheets) is considerably smaller, no more than 0.5 metres (corresponding to the total volume of water stored in glaciers and ice caps at present).

For the purpose of the present assessment, it is adequate to assume that the Greenland ice sheet completely melts away at a linear rate during the coming 1,000 years, resulting in 7 m of global sea level rise. Due to gravitational effects these 7 m are not distributed evenly over the global seas, e.g. /Milne et al. 2009/.

The effects of this sea-level rise on the development of the Baltic shore level were investigated by Global Isostatic Adjustment (GIA) modelling, see the **Climate report**, Section 3.3.4. The relative shore level curve from the GIA modelling was combined with observed shore level data /Påsse 2001/ in order to produce the global warming variant evolution of shore level seen in Figure 10-159. As can be seen in Figure 10-159, the rise of global sea levels due to the melting of the Greenland ice sheet is of negligible importance for the development of the shore level at Forsmark. This is due to a counterbalancing gravitational effect associated with the removal of the mass of the Greenland ice sheet, see the **Climate report**, Section 5.1.3 and /Milne et al. 2009, Whitehouse 2009/. Therefore, the isostatic rebound is larger than the rise of sea level. It should be noted, however, that there are large uncertainties in the GIA modelling and in the present knowledge as to global sea level rise resulting from global warming, see the **Climate report**, Section 5.3.1. In addition to the uncertainties introduced by the uncertain response of the cryosphere to raised air temperatures, uncertainty also relates to the long-term response from thermal expansion of ocean water (thermosteric sea-level rise). The rate of global sea-level rise from thermal expansion of ocean water would initially be low and then increase. The IPCC estimates the total sea-level increase due to thermal expansion in year 2300 to be 0.3–0.8 m (A1B emission scenario), and to be 0.5–2 m in year 3000 AD compared to year 2000 AD /IPCC 2007/. Because of the large heat capacity of the ocean, thermal expansion would continue for many centuries after a warmer climate had stabilised /IPCC 2007/. The final maximum contribution to sea-level change from thermal expansion would thus be considerably larger than at the time of peak climate warming.

Yet another uncertainty relates to a collapse of the West Antarctic ice sheet. By using the traditional value of an ice volume in West Antarctica corresponding to 5 m of global mean sea-level rise, /Mitrovica et al. 2009/ estimated that a collapse of the West Antarctic ice sheet would result in a sea-level rise around Fennoscandia of 5±1 m, with gravitational effects included. However, using a new value of the West Antarctic ice sheet volume, corresponding to 3.3 m of global mean sea-level rise, /Bamber at al. 2009/ showed that a full collapse of the West Antarctic ice sheet gives a sea-level rise around Fennoscandia of around 3 m (also taking gravitational effects into account).

Due to these uncertainties it is possible that, in contrast to what is shown in the figure, there might be initial periods of transgressions at the Forsmark site in the global warming variant. Such situations are described in /Brydsten et al. 2009/. However, after an early phase with these large uncertainties in the global warming variant, the results of the isostatic modelling suggest that in the long run the Forsmark site will be situated above sea level until the end of the 120,000 year period (Figure 10-159).

The global warming variant of the reference evolution is shown in Figures 10-160 and 10-161. Given the assumption of a long initial period of temperate climate conditions, the temperate climate domain is dominant. Temperate conditions prevail for ~78,000 years (65% of the time), permafrost conditions for ~28,000 years (23% of the time), glacial conditions for ~11,000 years (9% of the time) and submerged conditions prevail for ~3,000 years (~3% of the time).

At the Forsmark site, the climate is dominated by an initial ~60,000 year long period with temperate climate conditions. The variation in air temperature and precipitation is considerable within this temperate period, starting with air temperatures and precipitation rates that are considerably higher than at present in the early phase due to global warming. In time these temperatures and precipitation rates slowly decrease. During this initial long warm period, it is likely that climate within the temperate domain will vary significantly, with a range that is larger than that during the preceding parts of the Holocene. The length of the initial period of temperate domain in the SR-Site global warming variant should not be taken as a prediction or statement on future climate change. Under a future warming climate, this period could be shorter or longer than that described here. One alternative case with a longer duration is described in the extended global warming case, see the **Climate report**, Section 5.2.

Between ~60,000 years after present and more than 100,000 years after present, periods of periglacial conditions with permafrost occur and get progressively more severe. The first major ice sheet advance occurs after 100,000 years after present. The maximum ice sheet thickness, around 2,000 m, occurs at around 115,000 years after present.

As exemplified in the global- and regional climate modelling performed by /Kjellström et al. 2009/, a global warming climate may result in the Forsmark region experiencing a mean annual air temperature increase by ~3.5°C and an increase in mean annual precipitation by ~20% a few thousand years after present, as compared to the climate during the reference period 1961–2000. These results are in line with several other climate model simulations assuming similar future atmospheric greenhouse gas concentrations /Kjellström et al. 2009, BIOCLIM 2003, Rummukainen 2003/. For further details on the modelled global warming climate for Forsmark, see the **Climate report**, Section 5.1.7, and /Kjellström et al. 2009/.

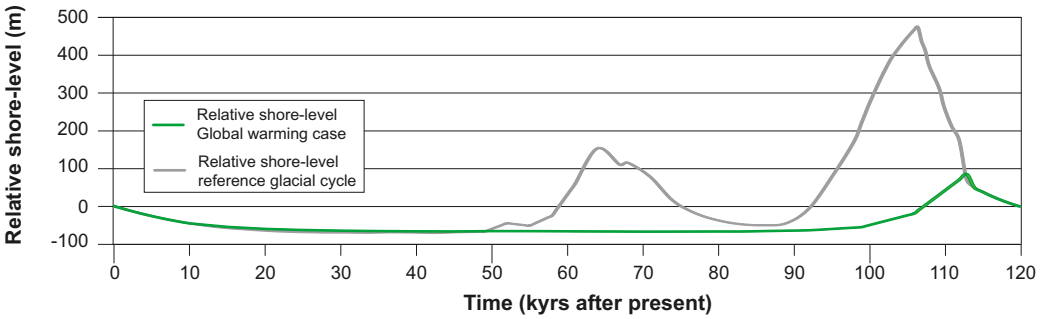

Figure 10-159. *Shore level evolution at Forsmark for the global warming variant of the reference evolution. For comparison, the shore level evolution for the reference glacial cycle (Section 10.4.1) is also shown. Negative numbers indicate that the area is situated above the contemporary sea-level. Uncertainties in future shore level are discussed in the text.*

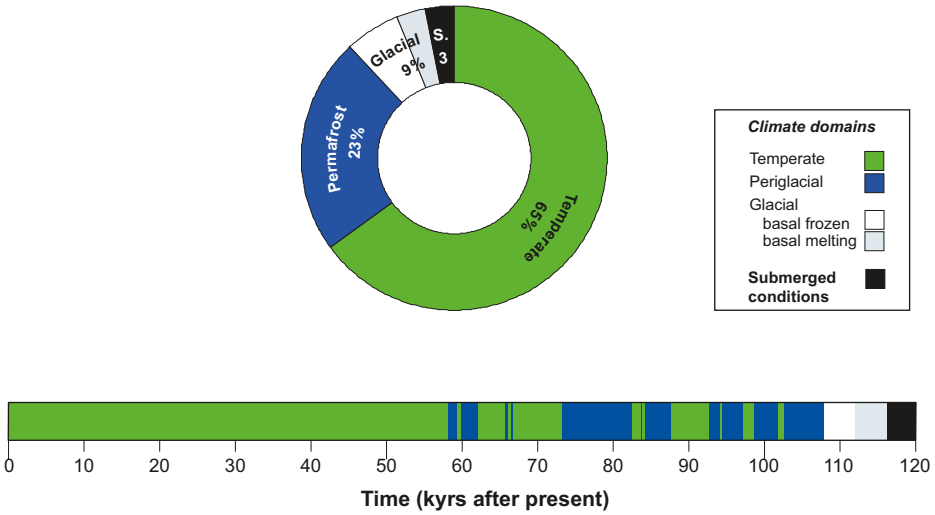

Figure 10-160. *Duration of climate domains at Forsmark, expressed as percentages of the total time for the global warming variant of the reference evolution. The bar below the pie chart shows the development as a future time series of climate domains and submerged periods.*

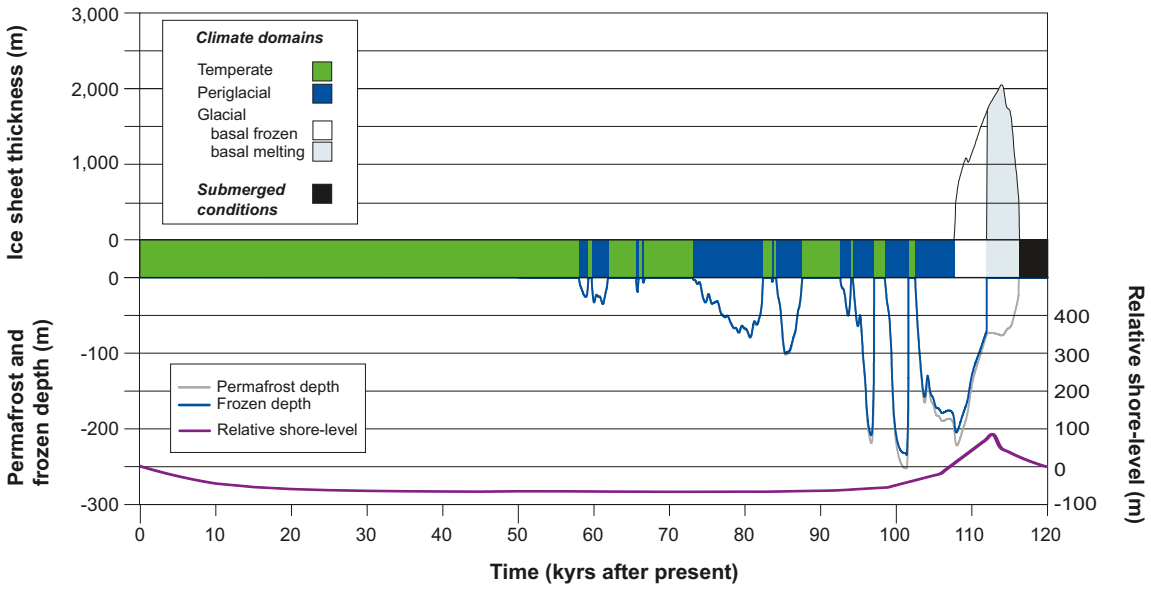

Figure 10-161. *Evolution of climate-related conditions at Forsmark as a time series of climate domains and submerged periods for the global warming variant of the reference evolution.*

Another possible course of events within a generally warming climate due to an increased greenhouse effect, is that the thermohaline circulation in the North Atlantic is reduced or shut-down e.g. /Wu et al. 2004, Schlesinger et al. 2006, IPCC 2007/. This would result in less heat being transported towards Fennoscandia by the North Atlantic Drift sea current, which in turn would lead to a regional cooling over Fennoscandia. However, it is believed that the general warming would be considerably larger than such a cooling effect, resulting in net warming in Fennoscandia /IPCC 2007, Kjellström et al. 2009/. Nevertheless, a case with a more severe permafrost development than in the reference glacial cycle is investigated in the Buffer freezing scenario, see Section 12.3 and the **Climate report**, Section 5.5.

During the second half of the global warming variant (Figures 10-160 and 10-161), climate varies within the same range as during the first part of the reference evolution, and consequently the climate-related processes will act in the same way as in the reference evolution. The global warming variant reduces the effects of climate-related processes of importance for repository safety that are related to cold climate conditions, i.e. in the periglacial- and glacial climate domains.

In a warming climate due to an increased greenhouse effect, the warmer temperatures at the ground surface would not affect repository safety functions. If precipitation increases, this would not affect groundwater formation significantly, since, on a regional scale, the major part of the groundwater aquifer is filled already by present-day precipitation rates. However, low groundwater salinity due to persistent infiltration of meteoric water during the initial prolonged temperate period in the global warming variant may have a potential effect on the function of the clay buffer, investigated in Section 10.6.3.

10.6.2 Biosphere

Climate change or variability due to increased greenhouse gas-induced warming over the coming 1,000 years, considered in the global warming variant of the reference evolution, is also expected to influence important parameters in the biosphere such as the hydrological cycle, the sea level, and the seasonal vegetation period.

Increased precipitation predicted in the global warming variant (see Section 10.6.1) may lead to higher runoff /Bosson et al. 2010/, even if partly balanced by increased evapotranspiration due to higher temperatures. The expected changes of sea levels will reduce, stop or, at least for limited periods, even reverse the shoreline displacement and thus maintain the site close to the sea, see the **Climate report**. In that case, water turnover rates close to the repository may be affected by the vicinity of the sea for extended periods. As the areas for discharge of groundwater from the repository are temporally varying and, to some extent, move with the moving shoreline /Joyce et al. 2010/, this means that discharge areas near the repository may receive potentially released radionuclides for extended periods, compared with the base case. The predicted increase in runoff to the northern parts of the Baltic Basin will probably decrease salinity in the Bothnian Sea /Gustafsson 2004/.

Due to higher winter temperatures (see the **Climate report**, Section 5.1.7) and longer vegetation period, there may be a shift in species composition, especially in the terrestrial ecosystem where deciduous trees may be more common. Such changes may also suggest higher biomasses and similar or slightly higher productivity. However, this is not necessarily the case and there are studies from freshwater ecosystems indicating that increased temperatures may disfavour primary producers on lake bottoms, even if total lake productivity remains unaltered, cf. /Andersson 2010/. Moreover, data describing peat accumulation suggest that the peat accumulation decreases with a warmer temperate climate as it changes from a boreal to a nemoral climate state, cf. /Löfgren 2010/. In summary, the prerequisites for transport and accumulation of radionuclides in the biosphere during temperate periods of the global warming variant are assumed to be similar to those in the initial temperate period of the reference evolution.

10.6.3 Repository evolution

Geochemistry

For the global warming variant, which described a situation with low to moderate global warming, atmospheric CO_2 levels increase, temporarily, up to around 750 ppm before starting to decline, see the **Climate report**, Section 5.1, which is approximately three times the pre-industrial value of 280 ppm. Higher levels of atmospheric CO_2 concentrations, and thus stronger global warming, are envisaged for the extended global warming climate case, see the **Climate report**, Section 5.2. In this case, peak atmospheric CO_2 concentration could temporarily be above 1,000 ppm. The consequences of the increased acidity and sulphate contents of superficial waters on a granitic aquifer were analysed in /Wersin et al. 1994b/, where it was concluded that several tens of thousands of years would be necessary to exhaust the calcite present in fracture-filling minerals. In addition, silicate weathering and ion-exchange processes also contribute to neutralise the increased inflow of carbonic acid in infiltrating waters while sulphate is removed by microbial reduction to sulphide. It may thus be concluded that the groundwater conditions will be similar to those of the reference evolution, with the difference that a longer period of exposure to groundwaters of meteoric origin is expected to have some influence at repository depth. The composition of the waters is, however, not expected to vary substantially during the temperate period, as shown by the hydrogeological modelling results for Forsmark discussed in Section 10.3.6 and the results in /Wersin et al. 1994b/.

In Forsmark, which has a low topographic gradient, the influence of the infiltration of meteoric waters down to the repository volume, that is, below ~400 m, is expected to be minor, even for a long period of temperate conditions. For example, the groundwaters in the candidate volume at present show no influence of either glacial melt waters or marine waters, even though the driving forces for

the infiltration of these waters were relatively large. In fact the influence of the last Littorina Sea is evident at Forsmark at shallower depths, above ~300 m, and south-east of the candidate repository area where the higher overall rock hydraulic conductivity has allowed the infiltration of these marine waters driven by density gradients. Nevertheless, as mentioned in Section 10.3.7, when considering the impact of the most extreme pathways from the surface to the repository in the hydrogeological simulations depicted in Figure 10-32, it cannot be excluded that a fraction of the deposition holes may experience dilute conditions during this long temperate period. As shown in the figure, approximately 2 percent of deposition hole locations experiences dilute conditions after the 60,000 years of temperate conditions assumed within the Global warming variant. Considering temperate conditions over the entire 1,000,000 years this fraction would still lie well below 10 percent.

The conclusions are, therefore, similar to those presented in Sections 10.3.7 and 10.4.7. For the whole first temperate period following repository closure, anoxic groundwater conditions will prevail at repository depth, in spite of the increasing proportion of meteoric waters with time, thus satisfying the criterion for the safety function indicator R1a in Figure 10-2. Salinities during this period will be limited, ensuring that the swelling properties of the buffer and backfill are not negatively affected, cf. the safety function indicator R1b in Figure 10-2. Cation concentrations, expressed as charge, $\sum q[M^{q+}]$, will be in general well above 0.004 mol/L in the candidate repository volume, although it cannot be excluded that for a fraction of deposition holes the cation concentrations will be below the limit where montmorillonite colloids start to become stable.

The concentration of sulphide, which is another important parameter, is expected to remain at the levels found in the Forsmark groundwaters at present. For colloids, concentrations are also expected to remain at the levels that have been measured during the site investigations, i.e. less than 200 μg/L /Hallbeck and Pedersen 2008/.

Buffer and deposition tunnel backfill

The buffer and deposition tunnel backfill will not be significantly affected by the different evolution in the global warming variant. The main difference is that the temperate period will be longer and glacial conditions will occur later, which will have an effect on the groundwater chemistry, etc. However, as shown in Section 10.3.11, even if "dilute" conditions persist all the time, still less than 7 percent of the deposition holes will reach advective conditions in a million year perspective.

Canister

An initial 100,000 year long warm period will have negligible impact on canister performance. The prolonged period before the first occurrence of permafrost is expected to lead to a longer period of exposure to groundwaters of meteoric origin, with some influence at repository depth, but the groundwater conditions will be similar to those of the reference evolution. The concentration of sulphide is expected to remain at the levels found in the Forsmark groundwaters at present.

The canister corrosion analyses presented in Section 10.4.9, for canister failure due to a partially eroded buffer also covers these cases. A somewhat longer period of dilute conditions in the first glacial cycle, than the 25% of the time in the reference evolution, has a very minor effect on the average number of failed canisters. This is further elaborated in the sensitivity analyses in Section 12.6.2.

The reduced ice-sheet thickness will lead to a lower mechanical load on the canister during the first glacial cycle. This may also lead to a lowering of the risk for the occurrence of larger earthquakes, but as discussed in Section 10.4.5 it is not trivial to adapt the earthquake frequency estimates to the occurrence of glaciations. This means that the earthquake probability, and the potential shearing of canisters, is cautiously assumed to be the same for the global warming variant, as for the reference glacial cycle.

10.6.4 Safety function indicators for the global warming variant

Based on the contents of Section 10.6.3, the status of the safety function indicators at the end of a prolonged period of temperate climate can be expected to be very similar to those reported for the initial temperate period in Section 10.3.16. Therefore, no detailed account of the safety function indicators is given here.

10.7 Conclusions from the analysis of the reference evolution

Conclusions regarding all the identified safety functions, related to their indicators have been given in Section 10.2.7 for the excavation/operational period, in Section 10.3.16 for the initial period of temperate climate, in Section 10.4.11 for the first glacial cycle and in Section 10.5.1 for the entire assessment period for the base case of the reference evolution. Brief conclusions regarding the global warming variant of the reference evolution are provided in Section 10.6.4. These are not repeated in detail here.

Results and uncertainties related to containment

A number of uncertainties relating to containment have been identified and evaluated in the analysis of the reference evolution, and these are summarised under the headings "Identified uncertainties and their handling in the subsequent analysis" throughout the chapter. Table 10-27 provides an overview of these uncertainties. Issues labelled "red" in the table may affect one or several safety functions related to containment, indicated in the rightmost column of Table 10-27. When relevant, these issues are propagated to analyses of subsequent parts of the reference evolution as also indicated in the table. For example, uncertainties related to groundwater flow during the temperate period are propagated to evaluations of buffer erosion and canister corrosion.

If propagated uncertainties are found to be insignificant in all their impacts on subsequent parts of the reference evolution, they are not qualified as uncertainties to be considered in the scenario selection as a result of the analysis of the reference evolution.

Most of the uncertainties propagated to subsequent parts of the analyses do have significant impact on the resulting evaluation of containment in the reference evolution. This is e.g. the case for uncertainties related to groundwater flow and in particular the three different fracture transmissivity-size relationships, through their impact on buffer erosion and canister corrosion, ultimately leading to uncertainty in the number of failed canisters in the reference evolution. These uncertainties are propagated to the analyses of scenarios and calculation cases in the subsequent chapters of the report.

The uncertain issues that need to be propagated to scenario analyses are essentially connected within two groups: issues related to canister failure due to corrosion (safety function Can1) and issues related to canister failure due to shear loads (safety function Can3), whereas canister failures due to isostatic load (Can2) are ruled out according to the assessments in the reference evolution.

The issues relating to canister failure due to corrosion are as follows.

- Groundwater flow over the glacial cycle.
- Groundwater salinity over the glacial cycle.
- Buffer erosion, determined by groundwater flow, fracture apertures and salinity and the assessment of which is also affected by the incomplete conceptual understanding of buffer erosion.
- Groundwater sulphide concentrations over the glacial cycle.
- Canister corrosion under advective conditions, requiring buffer erosion to the extent that advective conditions arise in the deposition hole, and then determined by groundwater flow and sulphide concentrations.

The issues relating to canister failure due to shear load are as follows.

- The occurrence of earthquakes of a sufficient magnitude to cause secondary shear movements in fractures intersecting deposition holes.
- The extent of detrimental secondary shear movements given sufficiently large earthquakes.
- The impact of secondary shear movements on the buffer/canister system.

Table 10-27. Summary of issues potentially affecting safety functions and findings from the evaluation made in this chapter. The following colour code is used: Green: Analysis results indicate either favourable or insignificant conditions with respect to risk allowing the exclusion of the phenomenon in question from further analyses. Yellow: Results propagated with no significant uncertainties. Red: Results and uncertainties propagated as distributions, range(s) of values or several distinct cases. The rightmost column lists uncertain issues that are assessed to contribute to canister failures in the reference evolution and that are hence of particular importance in the subsequent scenario analysis.

Subject, section	Issue	Further assessed in analyses of	Canister safety function affected
Excavation/Operational phase			
M-rock 10.2.2	EDZ	Groundwater flow	
	Excavation induced spalling		
	Reactivation of fractures		
	Induced seismicity		
H-rock 10.2.3	Infiltration of shallow water and upconing of saline water		
	Inflow to the repository		
HM-buffer/backfill 10.2.4	Piping/erosion		
C-rock, backfill, buffer 10.2.5	Salinity (upconing effects)		
	Redox conditions		
	Effects of grout, shotcrete and concrete on pH		
	Precipitation/dissolution of minerals		
	Effects of organic materials and microbial processes		
	Oxygen consumption in backfill		
	Colloid formation		
Initial temperate period			
T 10.3.4	Near-field temperature	Buffer mineral alteration, Canister corrosion	
M-rock 10.3.5	Thermally induced spalling (cases with and without)	Groundwater flow	
	Reactivation of fractures –hydraulic impacts		
	Creep		
	Reactivation of fractures (potential for shearing)	Canister shear failure	Can3
H-rock 10.3.6	Groundwater flow − DFN transmissivity-size relationship − EDZ and crown space cases − Cases with and without thermally induced spalling	Salinity, erosion, corrosion	Can1
	Time for saturation	Buffer saturation	

	Branching migration paths Choice of conceptual model Channelling		
C-rock 10.3.7	Salinity – potential for dilute groundwater	Erosion	Can1
	Concentrations of sulphide	Corrosion	Can1
	Redox conditions		
	Effects of grout, shotcrete and concrete on pH		
	Degradation of grout in grouting holes		
HMC-buffer, backfill 10.3.8 10.3.9 10.3.10 10.3.11 10.3.12 10.3.14	Saturation		
	Moisture redistribution	Near field temperature	
	Swelling – if no loss of buffer due to erosion/ colloid formation		
	Chemical evolution and effects of salinity		
	Mineral alteration		
	Cementation due to increased temperatures	Canister shear failure	Can3
	Canister sinking		
	Degradation of bottom plate – covered by spalling assumption		
	Degradation of deposition tunnel plug		
	Erosion/colloid formation	Corrosion	Can1
	Saturation time for the central area and the ramp and shaft		
	Saturation and swelling of borehole plugs		
Canister 10.3.13	Corrosion		
Remaining part of the reference glacial cycle			
T-rock 10.4.3	Permafrost		
M-rock 10.4.4 10.4.5	Jacking		
	Reactivation of fractures – Hydraulic impacts		
	Fracturing of the rock due to the glacial load		
	Earthquakes – Shearing		Can3
H-rock 10.4.6	Groundwater flow – DFN transmissivity-size relationship – EDZ and crown space cases – Cases with and without thermally induced spalling	Salinity, erosion, corrosion	Can1
	Shape of ice profile. Existence of permafrost		
C-rock 10.4.7	Salinity (“glacial upconing” effects)		
	Redox conditions		
	Effects of grout, shotcrete and concrete on pH		
	Degradation of grout in grouting holes		
	Salinity – potential for dilute groundwater	Erosion	Can1
	Concentrations of sulphide	Corrosion	Can1
Buffer backfill borehole seals 10.4.8	Freezing of closure material	12.4	
	Erosion/colloid formation	Corrosion	Can1
	Erosion due to high hydraulic gradients		
Canister 10.4.9	Corrosion		Can1
	Canister shear failure		Can3
	Isostatic loads		
Global warming variant			
M-rock 10.6.3	Earthquakes – Shearing	Canister shear failure	Can3
H-rock 10.6.3	Groundwater flow	Erosion, corrosion	Can1
C-rock 10.6.3	Salinity – potential for dilute groundwater	Erosion	Can1
	Concentrations of sulphide	Corrosion	Can1
	Redox conditions		
	Effects of grout, shotcrete and concrete on pH		
	Degradation of grout in grouting holes		
Buffer, backfill 10.6.3	Chemical evolution		
	Erosion/colloid formation	Corrosion	Can1
Canister 10.6.3	Corrosion		Can1
	Canister shear failure		Can3

Results and uncertainties related to retardation

A number of results, with their uncertainties, are relevant for the evaluation of the secondary safety function of the repository, i.e. its retarding potential. These include the following.

- Biosphere conditions and groundwater discharge locations during a glacial cycle, providing input to the derivation of release-to-dose conversion factors.
- Groundwater flow in the geosphere over a glacial cycle, providing direct input to the modelling of radionuclide transport in the geosphere.
- Geochemical conditions in the geosphere over a glacial cycle, providing input to the determination of solubilities of radioelements in the repository near field and of sorption properties in buffer and the geosphere.
- Transport conditions in the near field, e.g. the flow conditions and the relevant properties of the buffer and at the wall of the deposition hole.

These are propagated and further evaluated in the assessment of the retarding potential of the repository in Chapter 13.

Uncertainties related to external conditions

By definition, the external conditions for the reference evolution are constrained either to a development compatible with a repetition of the Weichselian glacial cycle (the base case) or to one compatible with the global warming variant. There are uncertainties within these constraints, leading to uncertainties within the reference evolution. There are also significant uncertainties due to the fact that external conditions other than those defining the Weichselian base case or the global warming variant can be conceived. The former uncertainties are addressed in the same way as other uncertain factors relating to the reference evolution and the latter are handled in the analyses of additional scenarios in Chapters 12 and 13.

Design issues and feedback to repository engineering and to R&D

A number of issues regarding design options have emerged from the analysis of the reference evolution. Issues specifically mentioned in the conclusions from the various sections of the reference evolution are the following.

- Deposition hole rejection criteria. It is of interest to explore both the effect of variants of the geometric criterion applied in the layout for SR-Site and the impact of potential criteria based on inflow.
- The consequences of alternative excavation techniques in terms of associated differences in EDZ properties affecting the flow conditions in the repository.

Additional conclusions concerning e.g. feedback to repository engineering, to needs of research and development etc. could to some extent be developed based on the findings in the reference evolution. This discussion is, however, postponed to the development of final conclusions in Chapter 15 where a fuller account, also based on results of consequence calculations and of the analyses of additional scenarios, can be given.